Physicochemical Problems of Mineral Processing

Volume 51, Issue 2

June 1, 2015

Instructions for preparation of manuscripts
It is recommended that the following guidelines be followed by the authors of the manuscripts:
- original papers dealing with principles of mineral processing and papers on technological aspects of mineral processing will be published in the journal which appears twice a year (January 1 and June 1)
- the manuscript should be sent to the journal via manuscript management system available at http://www.editorialsystem.com/ppmp
- only manuscripts written in English are accepted
- contributors whose native language is not English are urged to have their manuscript competently edited prior to submission
- the manuscript should not exceed 10 pages
- there is a 105 EUR fee for publishing and printing the paper
- additional correspondence regarding the journal should be sent to either jan.drzymala@pwr.edu.pl or przemyslaw.kowalczuk@pwr.edu.pl.

Physicochemical Problems
of Mineral Processing

Volume 51, Issue 2, June 1, 2015

CONTENTS

OPTIMIZATION OF PURE BORAX PENTAHYDRATE EXTRACTION FROM CALCINED TINCAL

Yuksel ABALI[*], Salih Ugur BAYCA[**], Gokhan EDGUNLU[*]

[*] Celal Bayar University, Science and Arts Faculty, Chemistry Department, 45030 Muradiye, Manisa
[**] Celal Bayar University, Soma Vocational School, Soma, 45500 Manisa, Turkey, salihbayca@gmail.com

Abstract: In this study, conditions for the calcination process of tincal were investigated and the optimum calcination conditions for boron extraction from tincal were determined. The experimental parameters were dissolution temperature, solid-to-liquid ratio, dissolution time and stirring speed. The optimum dissolution parameter levels were determined to be temperature 80 °C, solid-to-liquid ratio 10 g/dm^3, stirring speed 250 rpm and dissolution time 5 min.

Introduction

The optimization of dolomite ore dissolution in hydrochloric acid solutions was studied by Abali et al. (2011). The dissolution of roasted zinc sulphide concentrate in sulphuric acid solutions was investigated in an optimization study by Copur et al. (2004). Behnajady et al. (2012) found the optimum conditions for the dissolution of lead from zinc plant residues in NaCl–H$_2$SO$_4$–Ca(OH)$_2$ media by the Taguchi method. Ekinci et al. (2007) studied optimization and modeling of boric acid extraction from colemanite in water saturated with carbon dioxide and sulfur dioxide gases. Yesilyurt (2004) found that the boric acid extraction efficiency from colemanite ore was 99.66%. Kucuk (2006) found that the dissolution percentage of ulexite in NH$_4$Cl solution was 98.37%. In the study of Bese et al. (2010) the Taguchi method was applied to determine the optimum conditions of dissolution of metals in the Waelz sintering waste in HCl solutions. The orthogonal array (OA) experimental design was chosen as the most suitable method to determine the experimental plan, L$_{25}$ (5^5), five parameters, each with five values. Keles et al. (2009) reported that silver cementation from nitrate containing solution using the Taguchi method was studied to understand and optimize silver cementation yield by considering design and rotation rate of the impeller, temperature and pH of the solution.

Tincal is best represented by formula $Na_2B_4O_5(OH)_4\cdot 8H_2O$, with 2 moles of water existing as hydroxyl groups and 8 moles as crystal water (Gerhartz, 1985). The largest known tincal deposit in the world is in Kirka, some 220 km to the west of Ankara, Turkey (Abali et al., 2006; Smith and Mcbroom, 1992). The commercially produced calcined tincal has 52% B_2O_3 with particle size of -6 mm and borax pentahydrate which has 47.76 % B_2O_3 with particle size of -1 mm (Etimaden, 2013).

A robust design method was developed in order to reduce cost and improve the dissolution of calcined tincal in water. In the experiments, an L_{16} orthogonal array was employed to determine the effect of four process parameters on the dissolution efficiency of calcined tincal. For each factor, four levels were chosen to cover the wide region of variation. The parameters selected in this study, dissolution temperature, solid-to-liquid ratio, stirring speed and dissolution time, can potentially affect the dissolution efficiency of calcined tincal in water. The experimental factors and their levels, were determined by preliminary tests. Since four parameters were investigated in the research, four levels of each parameter were considered. Therefore, an L_{16} orthogonal array (L_{16} 4^4) was selected for this study. The total of 16x4 = 64 data values in the layout of this L_{16} OA were collected for analysis in the study.

The quantitative design is used in the Taguchi method to optimize the process with multiple performance characteristics. The orthogonal array (OA) experimental design was chosen as the most suitable method to determine the experimental plan, L_{16} (4^4), with four parameters for each of four values. In order to observe the effects of noise sources on the dissolution process, each experiment was repeated twice under the same conditions at different times. The performance characteristics were chosen as the optimization criteria. There are three categories of performance characteristics, the larger-the-better, the smaller-the-better and the nominal-the-best. The performance statistics was evaluated by using Eq. 1 (Phadke, 1989; Pignatiello, 1988).

For the larger-the-better approach

$$SN = -10\log\left(\frac{1}{n\Sigma}\frac{1}{Y^2}\right) \tag{1}$$

where the larger-the-better is performance characteristics, n is the number of repetitions performed for a given experimental combination, and Y is the performance value of the ith experiment. Detailed information on the Taguchi method is given by Abali et al. (2011).

The aim of the present study was to investigate the optimization of the dissolution of tincal dissolved in large amounts in hot water in order to obtain pure borax pentahydrate, using the Taguchi method. The each experiment was repeated twice under the same conditions at different times to observe the effect of noise sources on the dissolution process. After optimum calcination conditions for the extraction of boron from tincal were determined, the optimum water dissolution conditions for maximizing the boron oxide contents of the dissolution solution were determined by

the Taguchi experimental design method, and then the dissolution experiments were carried out according to this design method. An *F* test was carried out on the dissolution results to determine the most effective and least effective parameters. Signal-Noise (*SN*) graphs were drawn for each of the parameters to determine the optimum conditions. The maximum dissolution performance of calcined tincal was predicted by calculation at the optimum conditions.

Materials and methods

The tincal used in the present experiments was obtained from Kirka, Eskisehir, Turkey. The ore was initially crushed by jaw crusher, and then the sample was placed in a porcelain crucible. Calcination of tincal was carried out using a muffle furnace. The solubility of borax decahydrate and borax pentahydrate in water is shown in Table 1.

Table 1. Solubility of borax decahydrate and borax pentahydrate in water (Jansen, 1999)

Temperature ^{o}C	Solubility, wt % in water	
	Borax decahydrate $Na_2O \cdot 5B_2O_3 \cdot 10H_2O$	Borax pentahydrate $Na_2O \cdot 5B_2O_3 \cdot 5H_2O$
0	1.18	
10	1.76	
20	2.58	
25	3.13	
30	3.85	
40	6.00	
50	9.55	
60	15.90	16.40
70		19.49
80		23.38
90		28.37
100		34.63

Particle size in the sample was -1.25 mm after crushing and screening. The boron oxide content of the tincal sample was determined as 23.2% B_2O_3, whereas tincal theoretically contains 36.5% B_2O_3. This can be explained by the fact that the ore used in the experiment contained 63.38% tincal mineral and 36.62 % impurities. Alp et al., (2004) reported that the impurities in tincal ore were calcite, dolomite, montmorillonite minerals.

The dissolution experiments were carried out in a 250 cm^3 three necked glass reactor equipped with a mechanical stirrer with a digital controller unit and timer, a

thermostat and a cooler. The experimental parameters and their levels are given in Table 2.

Table 2. Parameters and their values corresponding to their levels

	Parameters	Parameter levels			
		1	2	3	4
A	Dissolution temperature, °C	20	40	60	80
B	Solid-to-liquid ratio, g/dm^3	10	20	50	100
C	Stirring speed, rpm	250	350	450	600
D	Dissolution time, minutes	5	10	20	45

The temperature of the reaction medium could be controlled to within ±0.5 °C. In the dissolution process, 100 cm^3 of water was introduced into the reactor. After the desired dissolution temperature was reached, a predetermined amount of the sample was added to the solution while the content of the vessel was stirred at a certain speed. At the end of the experiment, the contents of the vessel were filtered using a blue filter paper and the filtrate solution was analyzed volumetrically for B_2O_3 (Koklu et al, 2003). The chemical composition of the calcined tincal was determined by volumetric and gravimetric methods.

The dissolution efficiency of B_2O_3 was Y percent

$$Y = \frac{M_1}{M_o} \cdot 100 \tag{2}$$

where M_o is the amount of B_2O_3 in the original sample (g) and M_1 is the amount of B_2O_3 in the solution after dissolution (g).

Results and discussion

Calcination of tincal

Results obtained from tincal calcination showed that the percentage of boron oxide increased with increasing calcination temperatures and with increasing calcination times.

The calcination reaction of tincal is given in Eq. 3.

$$Na_2B_4O_5(OH)_4 \cdot 8H_2O_{(s)} \xrightarrow{\text{Heat}} Na_2O \cdot 2B_2O_{3(s)} + 10H_2O. \tag{3}$$
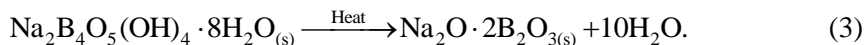
When tincal is completely calcined, anhydrous borax is formed. Anhydrous tincal theoretically contains 69.19% B_2O_3. The results are given in Fig. 1.
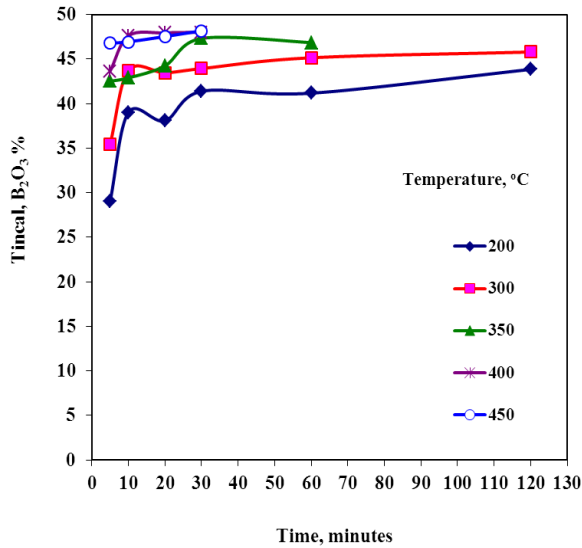
Fig. 1. The effects of calcination temperature and time on boron oxide

Calcination at 450 $^{\circ}$C for 30 minutes was selected. The boron oxide content of calcined tincal was found to be 48.19% B_2O_3. Tincal calcination at 400 $^{\circ}$C and 450 $^{\circ}$C gave similar results. However, 450 $^{\circ}$C was selected in order that the calcination should be homogeneous. The boron oxide value (48.19% B_2O_3) was much lower than the theoretical boron oxide value for anhydrous borax (69.19% B_2O_3). This can be explained by the tincal not being completely calcined. This boron oxide value is very close to the boron oxide value (47.8% B_2O_3) of borax pentahydrate. The calcination reaction is given by

$$Na_2B_4O_5(OH)_4 \cdot 8H_2O \longrightarrow Na_2O \cdot 2B_2O_3 \cdot 5H_2O + 5H_2O. \qquad (4)$$
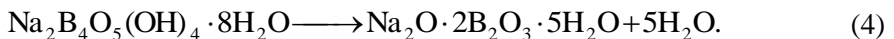
Thus, the product resulting from the calcination of tincal in this study may be called borax pentahydrate.

Dissolution of calcined tincal

The dissolution of calcined tincal in water was investigated to determine the optimum conditions. The dissolution reaction of calcined tincal in water can be described by the following equation

$$Na_2O \cdot 2B_2O_3 \cdot 5H_2O_{(s)} + H_2O_{(l)} \longrightarrow 2Na^+{}_{(aq)} + B_4O_5(OH)_4{}^{2-}{}_{(aq)} + 4H_2O_{(l)}. \qquad (5)$$
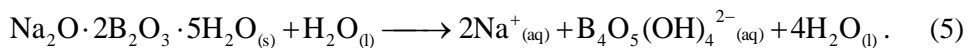
The reaction between calcined tincal and pure water results in sodium ions and tetraborate ions. Kotz et al. (2006) reported that tetraborate anions [$B_4O_5(OH)_4{}^{2-}$] occur in borax in solution in water. This pregnant leach solution was crystallized at

room temperature and borax decahydrate crystals were obtained.   Tincal was completely dissolved in hot water (95 $^{\circ}$C) and this solution contained maximum 36.5% B_2O_3.

Statistical analysis

An L_{16} orthogonal array with five columns and 16 rows was used in this study. Each dissolution parameter was assigned to a column, and 16 dissolution-parameter combinations were possible. Therefore, only 16 experiments were required to study the entire parameter space using the L_{16} orthogonal array. The experimental layout for the five dissolution parameters using the L_{16} orthogonal array is shown in Table 3.

Table 3. The experimental plan, parameters and results

Exp. No.	Temperature ($^{\circ}$C)	Solid-liquid ratio (g/dm^3)	Stirring speed (rpm)	dissolution time (min)	Experimental results		
					Y_1	Y_2	$Y_{average}$
1	20	10	250	5	65.98	66.18	66.08
2	20	20	350	10	43.96	43.93	43.95
3	20	50	450	20	30.29	25.79	28.04
4	20	100	600	45	4.98	6.17	5.57
5	40	10	350	10	70.77	74.23	72.50
6	40	20	250	20	63.01	52.63	57.82
7	40	50	600	45	41.36	24.11	32.74
8	40	100	450	5	8.14	10.57	9.36
9	60	10	250	20	91.54	81.15	86.34
10	60	20	350	45	64.69	65.58	65.14
11	60	50	450	5	43.78	45.17	44.48
12	60	100	600	10	10.22	11.60	10.91
13	80	10	450	45	94.75	95.54	95.14
14	80	20	600	5	88.08	100.00	94.04
15	80	50	250	10	37.90	52.43	45.17
16	80	100	350	20	12.89	13.48	13.19

F-ratios of the factors were calculated and are given in Table 4. The F test is a tool to determine which process parameters have a significant effect on the dissolution value. The results show that solid-to-liquid ratio parameters were significant on the calcined tincal dissolution rate.

The F-value for each process parameter is simply the ratio of the mean of the squared deviations to the mean of the squared error. Usually, the larger the F-value, the greater the effect on the dissolution value due to the change of the process parameter. The optimum combination of process parameters can be predicted using the dissolution efficiency characteristics and ANOVA analyses.

Table 4. The results of variance analysis (ANOVA) and F tests

	Parameters	Degree of freedom DOF	Sum of Squares SS	Mean Squares MS	Test Statistic F
A	Temperature	3	1506.587	502.196	0.922
B	Solid/liquid ratio	3	11569.957	3856.652	7.084
C	Stirring speed	3	1997.544	665.848	0.145
D	Dissolution time	3	236.729	78.910	1.223
	Error	3	1633.203	544.401	
	Total	16	13677.614		

In order to determine the optimum dissolution rate, the larger-the-better dissolution efficiency characteristic in Eq. (1) was taken for the dissolution efficiency of B_2O_3, and the SN ratios for the larger-the-better dissolution efficiency were calculated. The level which had the higher value determined the maximum level of each factor. For example, level five for temperature had the highest *SN* ratio value.

The effects of dissolution temperature on the performance statistics for calcined tincal are given in Figure 2. The results showed that the dissolution efficiency of B_2O_3 increased with increasing dissolution temperature. Abali et al. (2007) reported that the dissolution rate of tincal in phosphoric acid solution increased with increasing temperature. Dissolution efficiency was 51.72% at a temperature of 60 $^{\circ}$C, but reached 61.88% efficiency at 80 $^{\circ}$C. Therefore a dissolution temperature of 80 $^{\circ}$C was chosen.
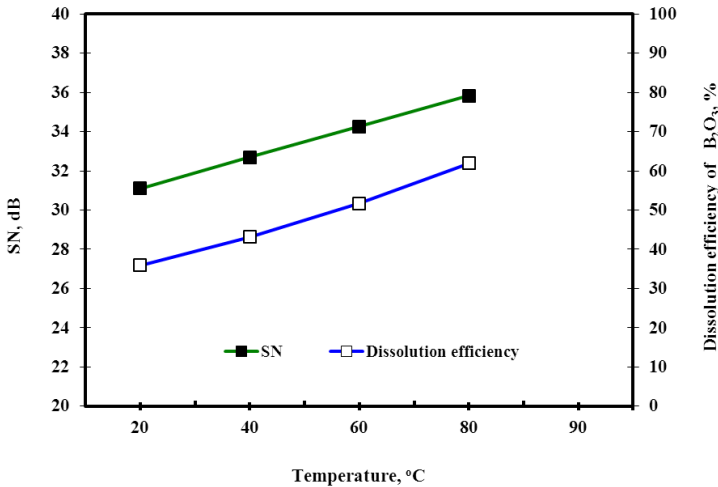
Fig. 2. The effect of dissolution temperature on the performance statistics for calcined tincal

As seen in Figure 3, the dissolution efficiency decreased with an increasing dissolution solid-to-liquid ratio. As the amount of reagent (water) per unit of solid

(tincal) in the suspension increased at low solid to liquid ratio, the reaction rate increased. This might be attributed to the fact that the amount of reagent compensation to every particle decreases with increasing amounts of solid in the suspension. Similar results were found by Abali et al. (2006) for tincal in oxalic acid solutions. Maximum dissolution efficiency was achieved with 10 g/dm^3 solids and the dissolution efficiency was 80.02%. Therefore, a solid-to-liquid ratio of 10 g/dm^3 was chosen.
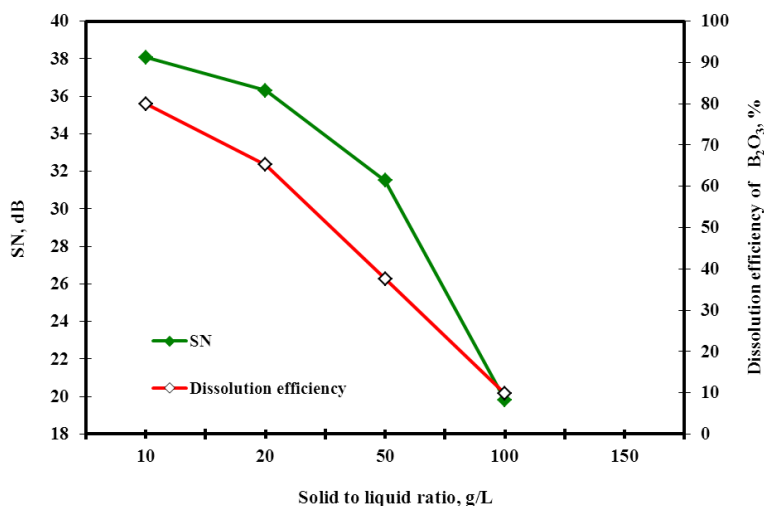
Fig. 3. The effect of solid-to-liquid ratio on the performance statistics for calcined tincal
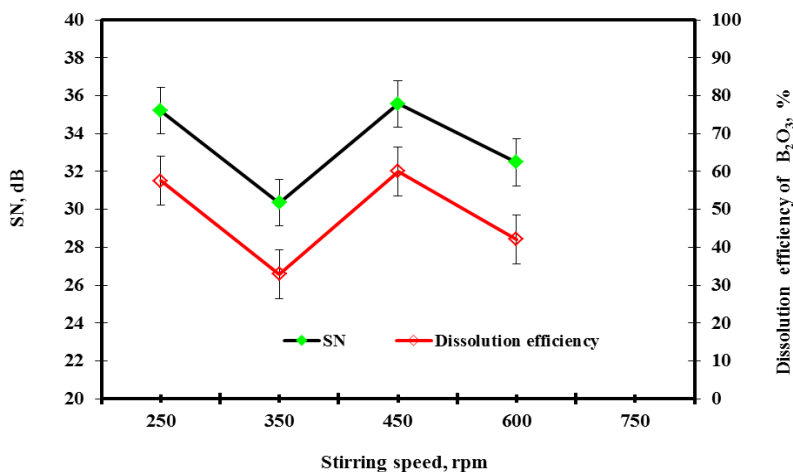
Fig. 4. The effect of stirring speed on the performance statistics for calcined tincal

The effect of stirring speed on the performance statistics for calcined tincal is shown in Fig. 4. Dissolution efficiency was 57.58%, 32.91%, 60.04% and 42.08% at stirring speeds of 250, 350, 450 and 600 rpm, respectively. There was a fluctuations of the results. This fluctuating behaviour was observed in previous studies by Copur et al. (2004) in studying the effect of sulphuric acid solutions on zinc sulphide. A stirring speed of 250 rpm was chosen.

Figure 5 shows that the dissolution efficiency fell within 5-10 minutes of reaction time, but rose slowly after 20-45 minutes. The maximum dissolution efficiency was reached at 5 minutes of leaching time. Therefore, a leaching time of 5 minutes was chosen.
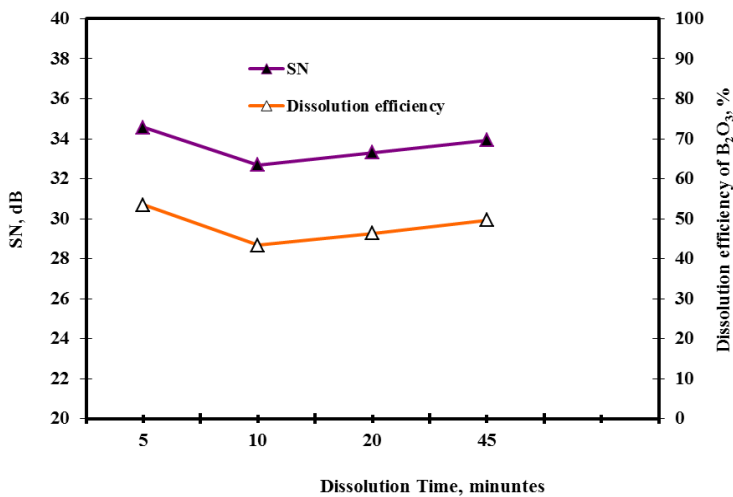
Fig. 5. The effect of dissolution time on the performance statistics for calcined tincal

The optimum dissolution conditions for B_2O_3 production were selected according to conditions of maximum amount, as shown in Table 5.

Table 5. Optimum working conditions predicted dissolution of tincal

Parameters	Case 1	Level	Case 2	Level
Temperature, ^oC	60	3	80	4
Solid/liquid ratio, g/dm^3	10	1	10	1
Stirring speed, rpm	250	1	250	1
Dissolution time, min	5	1	5	1
Predicted dissolution efficiency of B_2O_3, %	98.35		100	

The optimum process conditions were selected as A_4, B_1, C_1, and D_1. The predicted dissolution efficiency using optimum SN conditions was calculated.

Conclusions

Calcination of tincal at 450 $^{\circ}$C for 30 minutes resulted in a product of borax pentahydrate.

The optimum conditions for borax extraction from calcined tincal by water dissolution can be determined by using the Taguchi experimental design method with a small number of experiments. In the optimization study, sixteen experiments were carried out and each experiment was repeated twice. A total of 32 experiments were performed.

It was found that the dissolution efficiency increased with decreasing solid-to-liquid ratio and increasing temperature, and that the most significant parameter affecting the dissolution of calcined tincal was the solid-to-liquid ratio. The least significant parameter affecting the dissolution of calcined tincal was the stirring speed. The optimum reaction conditions were determined as A_4, B_1, C_1, D_1 and a dissolution temperature of 80°C, a solid-to-liquid ratio of 10g/dm^3, a stirring speed of 250 rpm, and 5 minutes for dissolution time. The dissolution efficiency of calcined tincal in water was estimated to be 100% under optimum conditions with 95% confidence level.

Pure borax pentahydrate crystals were obtained by dissolving tincal in hot water at these optimum conditions.

Borax pentahydrate is highly soluble in hot water. Borax pentahydrate solution can be divided by solid-liquid separation insoluble material. When the solution is cooled, borax pentahydrate crystals precipitated. The Taguchi method can be applied to produce the compounds of borax on a large scale.

The optimum conditions of this laboratory-scale study were determined by the statistical analysis method. This statistical method permits scientists observing more than one independent variable at a time.

In the dissolution study discussed in the paper, researchers working in this field helped to interpret the scientific data. The results of this study can be very useful for designing plant operating on an industrial scale.

References

ABALI, Y., BAYCA, S.U., MISTINCIK, E., 2006. *Kinetics of oxalic acid leaching of tin*cal. Chemical Engineering Journal, 123, 25–30.

ABALI, Y., BAYCA, S.U., ARISOY, K., VAIZOGULLAR, A.I., 2011. *Optimization of Dolomite Ore Leaching in Hydrochloric Acid Solutions*. Physicochemical Problems of Mineral Processing, 46, 253-262.

ABALI, Y., BAYCA, S.U., GULER, A.E., 2007. *The dissolution kinetics of tincal in phosphoric acid solutions*, International Journal of Chemical Reactor Engineering, 5, 1–10.

ALP, I., DEVECI, H., OZDAG, H., 2004. *Processing Tincal Ores using Ultrasonic Waves,* 2. International Boron Symposium, 23-25 September 2004 Eskisehir Turkey, pp: 59-64.

ATA, O.N., COLAK, S. COPUR, M., and CELIK, C., 2000. *Determination of the Optimum Conditions for Boric Acid Extraction with Carbon Dioxide Gas in Aqueous Media from Colemanite Containing Arsenic*, In*d. Eng. Chem. Res., 39,* pp 488–493

BEHNAJADY, B., MOGHADDAM, J., BEHNAJADY, M.A., RASHCHI, F., 2012. *Determination of the Optimum Conditions for the Leaching of Lead from Zinc Plant Residues in NaCl–H_2SO_4–Ca(OH)$_2$ Media by the Taguchi Method*. Ind. Eng. Chem. Res., 51, 3887–3894.

BESE, A.V., BORULU, N., COPUR, M., COLAK, S., ATA, O.N., 2010. *Optimization of dissolution of metals from Waelz sintering waste (WSW) by hydrochloric acid solutions*, Chemical Engineering Journal 162 () 718–722

COPUR, M., OZMETIN, C., OZMETIN, E., KOCAKERIM, M.M., 2004. *Optimization study of the leaching of roasted zinc sulphide concentrate with sulphuric acid solutions*. Chemical Engineering and Processing: Process Intensification, 43, 1007–1014.

EKINCI, Z., SAYAN, E., BESE, A.V., ATA, O.N., 2007. *Optimization and modeling of boric acid extraction from colemanite in water saturated with carbon dioxide and sulphur dioxide gases*, International mineral processing 82, 187 – 194.

ETIMADEN, (2013). http://www.etimaden.gov.tr.

GERHARTZ, W., 1985. *Ullmann's Encyclopedia of Industrial Chemistry*, vol. A4, Germany.

KELES, O., 2009. *An optimization study on the cementation of silver with copper in nitrate solutions, by Taguchi design*, Hydrometallurgy 95, 333–336.

KOKLU, M., OZYETIS, O., MARASLIOGLU, D., YAVUKLU, E., CELEN, B., TUFAN, T., GUNDUZ, M., 2003. *Developments in analyzes of calcium borate (in Turkish)*, 18 International Mining Congress and Exhibition of Turkey, 10 – 13 June, Antalya. 141 – 146.

KUCUK, O., 2006. *Application of Taguchi method in the optimization of dissolution of ulexite in NH_4Cl solutions*, Korean J. Chem. Eng., 23, 21 – 27.

KOTZ, J.C., TREICHEL, P.M., WEAVER, G.C., 2006. *Chemistry and Chemical Reactivity*, Thomson Learning, Canada.

PHADKE, M.S., 1989. *Quality Engineering Using Robust Design*. Prentice Hall: New Jersey. 61–292.

PIGNATIELLO, *J.J.,* 1988. *An overview of strategy and tactics of Taguchi*. I.I.E. Transactions. 20, 247 – 254.

SMITH, R.A., MCBROOM, R.B., 1992. *Encyclopedia of Chemical Technology*, vol. 4, John Wiley, Canada.

YESILYURT, M., 2004. *Determination of the optimum conditions for the boric acid extraction from colemanite ore in HNO_3 solutions*, Chemical Engineering and Processing, 43, 1189–1194.

RECOVERY MECHANISMS OF SERICITE IN MICROCRYSTALLINE GRAPHITE FLOTATION

Hongqiang LI[*], Leming OU[**], Qiming FENG[**], Ziyong CHANG[**]

[*] College of Resource and Environmental Engineering, Wuhan University of Technology, Wuhan 430070, PR China

[**] School of Mineral Processing and Bioengineering, Central South University, Changsha 410083, PR China, olm@mail.csu.edu.cn

Abstract: Sericite is the main contaminant of concentrate in commercial microcrystalline graphite ore flotation. It was necessary to identify its recovery mechanisms so that the appropriate solution can be selected. In this study, the influence of sericite on flotation selectivity of microcrystalline graphite ore and its recovery mechanisms were investigated. Artificial mixtures flotation test suggested that sericite seriously reported into concentrate leading to poor flotation selectivity of microcrystalline graphite ore. However, the aggregation/dispersion behavior of artificial mixtures indicated that a large repulsive energy existed between sericite and microcrystalline graphite particles at pH 7.4, and sericite was not likely to report into graphite concentrate by slime coating. The results obtained from contact angle measurements and a technique of Warren showed that the floated sericite reached the froth via a combination of both entrainment and entrapment mechanisms, not via true flotation.

Keywords: microcrystalline graphite, sericite, flotation, entrainment, entrapment

Introduction

Natural graphite forms from the metamorphism of organic carbon or carbonaceous rocks and is found in three commercial varieties: crystalline flake, microcrystalline, and crystalline vein (Crossley, 1999). Some microcrystalline graphite deposits usually have a high air dried basis fixed carbon content (FC_{ad}) ($FC_{ad} > 80$ wt.%), and can be marketed after selective mining and a minimum processing. However, the average FC_{ad} of some European deposits is as low as 55 wt.% (Simandl and Kenanl, 1997) while in China the FC_{ad} of some microcrystalline graphite deposits is 50-70 wt.%. So far, a number of research projects have been undertaken to purify those low-grade microcrystalline graphite ores, flotation and chemical purification are commonly used. Chemical purification is an effective beneficiation method, including alkali roasting,

hydrofluoric acid treatment and chlorination roasting, but it easily leads to environment pollution while flotation is a low cost and environment friendly method compared with chemical purification (Dong, 1997).

For commercial microcrystalline graphite ore with FC_{ad} of 60-70wt.%, it can only be upgraded to 80-88wt.% (FC_{ad}) by flotation (Ji, 1991; Xia et al., 1996; Dong, 1997), and the primary contaminant of concentrate is sericite, which is a fine grained muscovite mica. Sericite also occurs in many base metal ore bodies, and it is often recovered strongly into the final flotation concentrate (Silvester, 2011). It has been hypothesized that liberated sericite may be collected in the froth product by true flotation due to surface hydrophobicity (Blaskett, 1960) or slime coating (He, 2009). A wide range of sericite depressants or dispersants has been tried over the years, but it does not appear to respond readily to those conventional reagents, and mostly ends up as a significant diluent in the final concentrate, which suggests that the mechanism of sericite recovery is not properly understood. Before the best mean for preventing liberated sericite recovery can be selected, it is necessary to determine how the sericite is actually being recovered.

In this study, in order to simulate the flotation process of microcrystalline graphite ore, batch flotation test of artificial mixtures in -30 μm size fraction was carried out. To demonstrate how sericite particles were reaching the froth phase, and determine which class of sericite particles (floating particles due to hydrophobicity, hetero-coagulation particles or entrained particles) was the most important contributor to sericite recovery in froth flotation, contact angle measurements, zeta potential measurements, and a technique of assessment of true flotation and entrainment of mineral have been applied (George et al., 2004).

Materials and methods

Materials

The sericite used for all experiments was obtained from Xiangyang, Hubei Province, China. The sample was dry ground and screened, and the -97 μm size fraction was collected and used in the experiments. X-ray fluorescence (XRF) analysis indicated that it contains 8.877 wt.% K_2O, 0.69 wt.% Na_2O, 36.59 wt.% Al_2O_3, and 47.11 wt.% SiO_2. The software Jade 5.0 was used to analysis X-ray diffraction pattern. Figure 1(a) is the X-ray diffraction pattern of sericite, which indicated that the purity of the sericite is 92 wt.%.

The microcrystalline graphite was obtained from the Hunan Lutang Graphite Mine located in the Beihu district of the Chenzhou city. It was processed using the same method as sericite. The results of proximate analysis (volatile matter, fixed carbon, and ash) of microcrystalline graphite revealed that the air dried basis volatile matter (V_{ad}) was 3.25 wt.%, the air dried basis ash content (A_{ad}) was 6.63wt.%, and the FC_{ad} was 90.12 wt.%. Figure 1(b) shows the X-ray diffraction pattern of the microcrystalline graphite sample. Based on the results of proximate analysis and X-ray

diffraction, it can be concluded that the purity of graphite sample obtained was 93 wt.%.
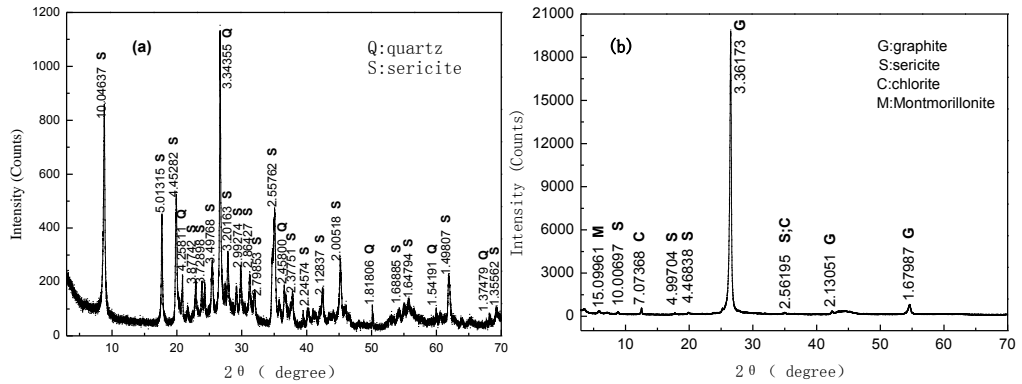
Fig. 1. XRD patterns of single minerals (a) sericite (b) microcrystalline graphite

Particle size distributions of test samples were determined by a Mastersizer 2000 particle size analyzer, and the results are seen in Table 1 and Fig. 2. kerosene used as a collector was emulsified in a high-speed blender at a concentration of 1 g/dm^3. The median size of the kerosene droplets emulsified with addition of surfactants was below 4 μm and the droplet size was also determined by Mastersizer 2000 particle size analyzer. Additionally, methyl isobutyl carbinol (MIBC) was used as a frother.

Table 1. Particle size distribution of single minerals

Single mineral	D_{10} (μm)	D_{50} (μm)	D_{90} (μm)	Average diameter (μm)
Microcrystalline graphite (-97 μm)	2.729	34.375	90.207	46.736
Sericite (-97 μm)	2.016	20.379	76.296	30.739
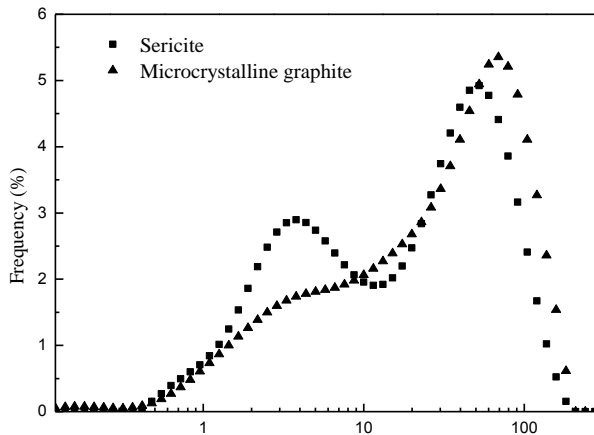
Fig. 2. Particle size distribution of single minerals

Methods

Contact angle measurements

These experiments were implemented to determine the hydrophobicity of sericite at different kerosene dosages. The assessments of hydrophobicity of sericite powder were carried out on GBX MiniLab ILMS using the Washburn technique (Chibowski and Perea-Carpio, 2002). The flotation tests were conducted in water, thus the reference liquid was water. The results were checked by the sessile drop on polished surface of sericite block. The data were the average value of five separate determinations. The experimental error of the contact angle measurements was within ±10%.

Batch flotation tests of artificial mixtures of microcrystalline graphite–sericite

These tests were carried out to assess the influence of sericite recovery on flotation selectivity of microcrystalline graphite. Based on the vast difference of floatability between hydrophobic graphite and hydrophilic sericite, the recovery of sericite was determined when all of the microcrystalline graphite was recovered into the concentrate. The tests were conducted in an XFD-type laboratory flotation machine (1 dm^3), and the flotation experimental error was within ±5%. The artificial mixtures slurry was composed of 2.5wt.% sericite and 15 wt.% graphite. Both sericite and microcrystalline graphite were in the same size fraction (-30 µm).

Firstly, the original weight of tap water (W_0) was recorded, the slurry in flotation cell was prepared by adding artificial mixtures of microcrystalline graphite (W_g)– sericite (W_s) to tap water followed by adding the collector kerosene (1.3 kg/Mg) and frother MIBC (100 g/Mg) to the slurry. Then, the flotation froth was scraped into the plastic basin every 10 s for 12 min, all of the graphite was scraped out at this point, the froth depth was controlled at about 20 mm through adding tap water, and the plastic basin with concentrate (W_{c1}), and tap water left (W_1) should be weighed. Finally, the tailing left in flotation cell was collected and filtrated, the filtrated tailing and the plastic basin with concentrate were dried at 80 ^{o}C in an oven, weighed and recorded as (W_t) and (W_{c2}). The recovery of water and sericite can be calculated by Eqs. 1 and 2

$$R_w = \frac{W_{C1} - W_{C2}}{W_0 - W_1} \cdot 100\% \qquad (1)$$

where
R_w – recovery of water (%)
W_0 – original weight of tap water (g)
W_1 – weight of tap water left (g)
W_{c1} – wet weight of plastic basin with concentrate (g)
W_{c2} – dry weight of plastic basin with concentrate (g)

$$R_s = \left(1 - \frac{W_t}{W_s}\right) \cdot 100\% \quad . \tag{2}$$

R_s – recovery of sericite in graphite concentrate (%)
W_t – dry weight of tailing (g)
W_s – dry weight of sericite in feed (g).

Zeta potential measurements

The zeta potential measurements were performed using a ZetaPALS zeta potential analyzer, the experimental error of zeta potential measurement was within ±10%. To prepare the stock suspension, 1 g of the mineral (- 4 μm) was added to a 1 dm^3 volumetric flask containing 10^{-2} mol/dm^3 KNO$_3$ solution. For each zeta potential measurement, 10 cm^3 of the stock mineral slurry was withdrawn and diluted with 90 cm^3 of 10^{-2} mol/dm^3 KNO$_3$ solution, adjusted to appropriate pH using NaOH or HCl, and then treated by desired reagents. A very small amount (about 2 cm^3) of this conditioned particle slurry was transferred to the plastic sample cell of the ZetaPALS for zeta potential measurement. The zeta potential measurement was carried out from low pH upwards, when a test was finished, another 10 cm^3 of the stock mineral slurry was withdrawn for zeta potential of a higher pH.

Assessment of true flotation and entrainment of sericite

These tests were used for determination of true flotation and entrainment of sericite in the presence of microcrystalline graphite. This technique, proposed by Warren, assumes that particle entrainment does not take place in a dry froth (Warren 1985). A series of experiments were conducted, and the rate of water recovery was varied by changing the rate of froth removal or froth depth. A regression line for the relationship between total solids recovery and water recovery was extrapolated to a zero water recovery. The mass of solids recovered at this point is the recovery by true flotation alone. This technique could be summarized as seen in Eq. 3:

$$R_m(t) = F + R_E = F + e \times R_w(t) \tag{3}$$

$R_m(t)$ – total recovery of solids by true flotation and entrainment (%)
F – recovery of solids due to true flotation (%)
R_E – recovery of solids due to entrainment (%)
$R_w(t)$ – recovery of water (%)
e – degree of entrainment
where, e is equal to the slope of $R_m(t)$ versus $R_w(t)$. A schematic representation of this technique is shown in Fig. 3.

The tests were conducted, and the rate of water recovery was varied by changing froth depth as 10 mm, 20 mm, and 30 mm, and the Jg was fixed at 3.3 dm^3/min for each test. The artificial mixtures slurry was composed of 6.6 wt.% sericite and 13.4 wt.% graphite. The dosages of kerosene and MIBC were chosen as 1300 g/Mg and

100 g/Mg, respectively. The impeller speed was kept constant at 1080 rpm. Time t=0 was taken as the instant the froth overflowed into the first froth collecting tray, the froth was removed at a constant, controlled rate of 6 scrapes per minute. Timed samples were obtained at cumulative flotation times of 0.5, 1, 1.5, 2, 3, 4, and 8 min, and the flotation experimental error was within ±5%.
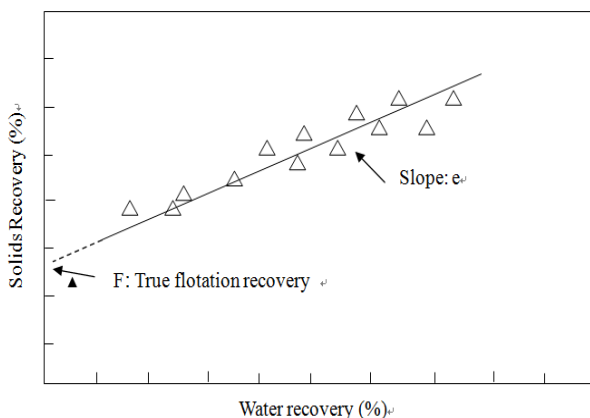
Fig. 3. Determination of true flotation by the Warren method

Theoretical background

Hetero-coagulation, which leads to slime coating between valuable mineral and gangue, is usually described by the DLVO theory (Adamczyk, 1999), the colloidal forces considered include the electrostatic double-layer force and the Van der Waals force.

Electrostatic double-layer (EDL) interaction

The model used to describe the Electrostatic Double-Layer (EDL) interaction energy is based on the Poisson–Boltzmann equation, which describes the electrostatic potential in an ionic solution as a function of position relative to the particle surface, and has been found to be accurate down to separations of a few nanometers (Mitchell et al., 2005). The interaction energy at constant surface potentials is often used, and can be described by Eq. 4:

$$V_E = \frac{\pi\varepsilon_0\varepsilon_r R_1 R_2}{(R_1 + R_2)}(\psi_1^2 + \psi_2^2)\cdot\left\{\frac{2\psi_1\psi_2}{(\psi_1^2 + \psi_2^2)}\cdot\ln\left[\frac{1+\exp(-\kappa H)}{1-\exp(-\kappa H)}\right] + \ln[1-\exp(-2\kappa H)]\right\} \quad (4)$$

where the average radius of sericite particle R_1 was 15.37 μm (Table 1), the average radius of microcrystalline graphite particle R_2 was 23.37 μm (Table 1); $1/\kappa$ is the electrical double layer thickness in which $\kappa = 0.10$ nm^{-1} (Wan, 1997); ε_0, ε_r represent the vacuum dielectric constant and the relative dielectric constant of continuous phase, respectively. The given value of $\varepsilon_0 \cdot \varepsilon_r$ was $6.95 \cdot 10^{-10}$ C$^{-2} \cdot$(J·m)$^{-1}$, H represents the

distance between particles, ψ_1 and ψ_2 are the surface potential. When contact time between the particles is very short, the assumption of constant surface charge is appropriate (Nguyen, 2002).

Van der Waals interaction

The Van der Waals interaction energy is calculated using Eq. 5:

$$V_w = -\frac{A}{6H} \cdot \frac{R_1 R_2}{(R_1 + R_2)} \ .$$ (5)

The Hamaker constant (A) for sericite/water/graphite is not available in literature. For mica, the value of the Hamaker constant acting through vacuum was $9.86 \cdot 10^{-20}$ J (Bergstrom 1997). Sericite is fine grained mica, thus the Hamaker constant of sericite (A_{11}) could be chosen as $9.86 \cdot 10^{-20}$ J. The Hamaker constant of graphite in vacuum is $23.8 \cdot 10^{-20}$ J (Maurer et al., 2001), because microcrystalline graphite is fine grain graphite, the Hamaker Constant of microcrystalline graphite (A_{22}) could be chosen as $23.8 \cdot 10^{-20}$ J. The Hamaker constant (A_{123}) for two different materials (1 and 2) interacting through medium 3 is (Eq. 6):

$$A_{132} = (\sqrt{A_{11}} - \sqrt{A_{33}})(\sqrt{A_{22}} - \sqrt{A_{33}}).$$ (6)

When medium 3 is water ($A_{33} = 3.7 \times 10^{-20}$ J), a value of the Hamaker constant of $4.45 \cdot 10^{-20}$ J was calculated for the sericite/ water/ microcrystalline graphite system on the basis of Eq. 6, and this value was used in this study.

Results and discussion

Influence of sericite recovery on flotation selectivity of microcrystalline graphite ore

During the multistage cleaning processes of commercial microcrystalline graphite ore, the enrichment ratio (E_r) decreased sharply, especially when the FC_{ad} of feed was above 85 wt.%, it was difficult to upgrade further by flotation. This was illustrated in previous literature clearly (Li, 2014). To simulate flotation process of commercial microcrystalline graphite ore, artificial mixtures with the same FC_{ad} (85 wt.%) should be selected.

For the purpose of assess the effect of sericite recovery on the enrichment ratio in artificial mixtures flotation and it was supposed that FC_{ad} of microcrystalline graphite single mineral was 100 wt.%, the equivalent FC_{ad} ($FC_{ad}*$) of artificial mixtures feed could be calculated by Eq. 7:

$$FC_{ad}* = \frac{C_g}{C_g + C_s} \cdot 100\%$$ (7)

FC_{ad}* – equivalent FC_{ad} of artificial mixtures, ignoring the ash and volatile of
    graphite, wt.%
C_g – sub-concentrate of microcrystalline graphite in slurry, wt.%
C_s – sub-concentrate of sericite in slurry, wt. %.

In this section, artificial mixtures (FC_{ad}*=85.72 wt.%) was selected. The artificial
mixtures slurry was composed of 2.5 wt.% sericite and 15 wt.% graphite.

E_r could be calculated with Eq. 8, (100-FC_{ad}^*) was the content of sericite in feed,
(100-R_s) represented the amount of sericite that was rejected as tailing:

$$E_r = \frac{\beta}{\alpha} = \frac{FC_{ad}*+(100-FC_{ad}*)(100-R_s)/100}{FC_{ad}*} = 1 + \frac{(100-FC_{ad}*)(100-R_s)}{100 \cdot FC_{ad}*} \quad (8)$$

β – grade of concentrate, wt.%
α – grade of feed, wt.%
FC_{ad}* – equivalent FC_{ad} of feed, wt.%
E_r – enrichment ratio
R_s – recovery of sericite, %.

The commercial microcrystalline graphite ore was usually ground to more than
90% or even 100% pass through -30 µm sieve to liberate graphite from gangue
minerals, thus, artificial mixtures in -30 µm size fraction was selected.

The FC_{ad}^* of feed after one stage flotation was 85.70%. FC_{ad}^* of the concentrate
was only 87.5% due to 88.02% of sericite recovered in graphite concentrate, and the
enrichment ratio was only 1.02. These results suggested that the serious misreport of
sericite led to poor flotation selectivity when microcrystalline graphite ore was fine
ground.

There are several mechanisms which have been proposed by which liberated
gangue particles may be collected in the concentrate:

- via true flotation if the conditioning step applied makes the minerals hydrophobic,
- via aggregation with the valuable mineral,
- via entrainment or entrapment.

In order to determine mechanisms by which liberated sericite may be collected into
the concentrate in artificial mixtures flotation, three sets of experiments were carried
out.

Effect of kerosene dosage on wettability of sericite

Kerosene is widely used as a collector in graphite flotation (Salgado, 2001). In order
to assess the effect of kerosene dosage on the hydrophobicity of sericite, the contact
angle of sericite powder at different kerosene dosages was measured. The results are
presented in Table 2.

It can be seen from Table 2 that the contact angle of sericite powder was 16.78° in
the absence of kerosene, indicating that sericite was almost a hydrophilic mineral,

which was in agreement with earlier observation (Gao et al., 2007). As the kerosene dosage increased from 0 to 2000 g/Mg, the average contact angle of sericite powder was not changed. The result indicated that kerosene did not improve the surface hydrophobicity of sericite, and sericite would not report into concentrate by true flotation when kerosene was used as the collector.

Table 2. Contact angle of sericite powder at different kerosene dosages

Kerosene dosage (g/Mg)	Contact angle (°)
0	16.78
250	17.20
500	16.55
750	16.05
1000	17.09
1500	16.85
2000	17.05

Aggregation/dispersion behaviors of microcrystalline graphite and sericite particles

The aggregation/dispersion behaviors of gangue mineral and valuable mineral particles were usually evaluated from particle interaction energy, particle interaction energy in aqueous solution is commonly described through application of DLVO theory, which allows quantitative prediction of the interaction energy. If particle interaction energy was negative, hetero-coagulation (slime coating) was unavoidable.

The zeta potential values of the sericite and microcrystalline graphite are shown in Figs. 4(a) and (b), respectively.
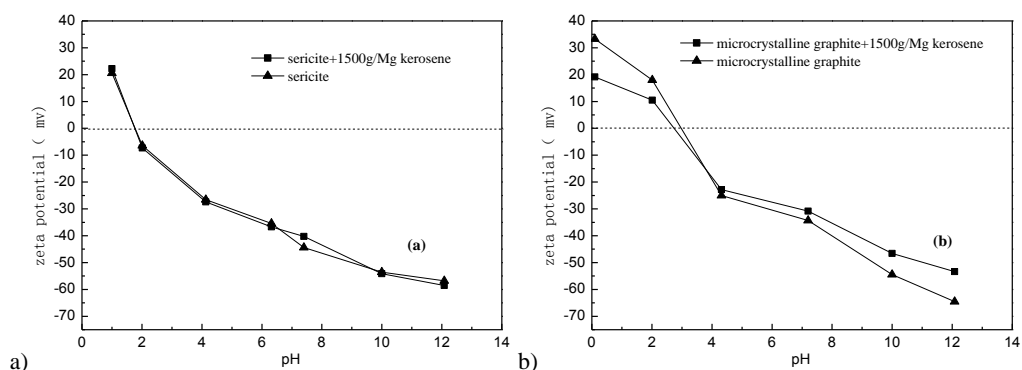
Fig. 4. Zeta potential of (a) sericite (b) microcrystalline graphite as a function of pH
in the absence and presence of kerosene

In the absence of kerosene, the zeta potential value of sericite at pH 7.4 was -44.38 mV, and that of the microcrystalline graphite was -34.32 mV. When kerosene dosage

was 1300 g/Mg, the zeta potential of sericite was -45.45 mV, that is almost the same as that of original sericite. The results indicated that kerosene did not adsorb on sericite surface, which agreed with the results of the contact angle measurements. Different from sericite, when kerosene dosage was 1300 g/Mg, the zeta potential of microcrystalline graphite changed to -30.83 mV from -34.32 mV. The absolute value of the zeta potential of microcrystalline graphite decreased in the pH value range of 0-12 because of the adsorption of kerosene on the mineral surface.

The total interaction energy V_T^D was calculated by replacing the relative data using Eqs. 4 and 5, and the results are shown in Fig. 5. The maximum value of total interaction energy V_T^D was 38.07×10^{-18} J when the particle distance was 4.24 nm indicating that sericite and microcrystalline graphite particles must overcome this large repulsive energy to form aggregates. It is suggested that aggregates between sericite and microcrystalline graphite particles did not form during artificial mixtures flotation, sericite was not likely to report into graphite concentrate by slime coating (sericite-microcrystalline graphite aggregates).
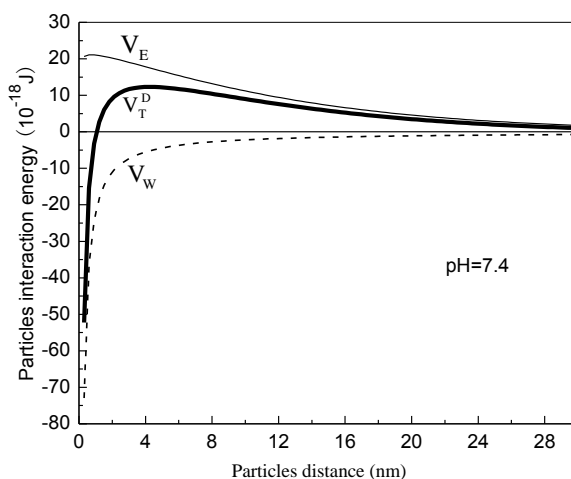
Fig. 5. Interaction energy between sericite and microcrystalline graphite particles
in the presence of 1300 g/Mg kerosene at pH=7.4

Determination of true flotation and entrainment of sericite

To evaluate the quantity of sericite recovered by true flotation and entrainment in flotation of microcrystalline graphite, the technique proposed by Warren (1985) was applied.

The interval entrainment factor $e(t)$ and cumulative entrainment factor $e^c(t)$ in a given time could be calculated by Eqs. 9 and 10, respectively:

$$e(t) = \frac{R_S(t)}{R_W(t)} \tag{9}$$

$R_s(t)$ – recovery of sericite in a given time (%)
$R_w(t)$ – recovery of water in a given time (%)
$e(t)$ – interval entrainment factor in a given time

$$e^c(t) = \frac{R_s^c(t)}{R_w^c(t)} \tag{10}$$

$R_{sc}(t)$ – cumulative recovery of sericite in a given time (%)
$R_w^c(t)$ – cumulative recovery of water in a given time (%)
$e^c(t)$ – cumulative entrainment factor in a given time.

Table 3. Correlation (e) between solid recovery and water recovery during the batch flotation tests

Froth depth （mm)	Time interval (min)	$R_w^c(t)$ （%)	$R_s^c(t)$ （%)	$e(t)$	$e^c(t)$
	0~0.5	9.32	10.29	1.10	1.10
	0.5~1.0	20.30	20.12	0.90	0.99
	1~1.5	27.87	25.23	0.67	0.91
10	1.5~2	32.85	29.31	0.82	0.89
	2~3	36.44	29.77	0.13	0.82
	3~4	38.31	30.31	0.29	0.79
	4~8	40.70	30.79	0.20	0.76
	0~0.5	4.31	5.07	1.18	1.18
	0.5~1.0	10.59	12.49	1.18	1.18
	1~1.5	15.83	17.23	0.90	1.09
20	1.5~2	21.06	20.84	0.69	0.99
	2~3	27.86	24.16	0.49	0.87
	3~4	35.28	24.97	0.11	0.71
	4~8	41.03	26.49	0.26	0.65
	0~0.5	7.38	9.52	1.29	1.29
	0.5~1.0	12.97	16.12	1.18	1.24
	1~1.5	19.86	22.53	0.93	1.13
30	1.5~2	27.04	27.11	0.64	1.00
	2~3	33.99	29.82	0.39	0.88
	3~4	40.13	31.51	0.28	0.79
	4~8	43.75	31.93	0.12	0.73
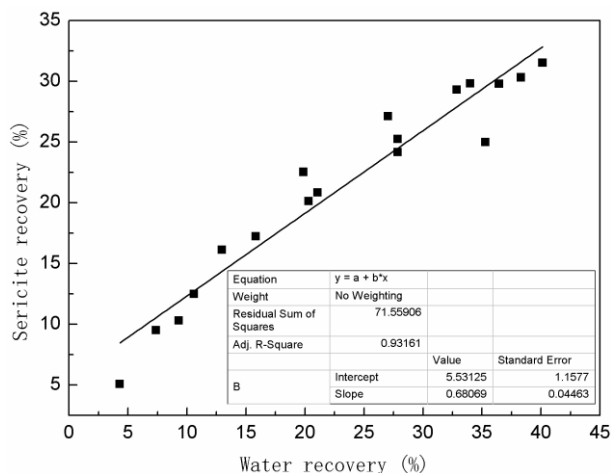
Fig. 6. Recovery of sericite versus water recovery obtained using the technique of Warren

Warren (1985) found that the correlation (entrainment factor) between solid recovery and water recovery normally deteriorated with time. As shown in Table 3, e of sericite decreased with the increase of the flotation time. When the froth depth was 30 mm, e of sericite was 1.29 over the first 0.5 min and it decreased to 0.12 over the last 4 min. Therefore, this method should ideally be applied over a flotation time that is just long enough for the recovery of most, but not all, of the easily floatable solids. In this section, the proper time interval was chosen between 0 and 4 min.

A plot of the recovery of sericite versus water recovery is seen in Fig. 6. The procedure of Warren assumes that entrainment occurs when particles are transported in the interstitial liquid. When the line of best fit was extrapolated to zero water recovery, the intercept was about 5.5%, the overall recovery of sericite was about 32%, indicating that around 17% of all recovered sericite was captured by true flotation, and about 83% of all floated sericite was recovered by entrainment. However, as the kerosene dosage increased from 0 to 2000 g/Mg, the average contact angle of sericite powder ranged from 16.05° to 17.20° and it was impossible for sericite to be recovered by true flotation. In all of the tests, $e(t)$ of sericite was greater than one over the first 0.5 min, as shown in Table 3, similar results was found in literature of (Wang and Peng, 2013). Zheng et al. (2006) claimed that if the entrapment was an additional mechanism for the recovery of liberated silica particles, it was possible in practice for the calculated entrainment factor (e) value to be greater than 1. It is suggested that entrapment may be an additional mechanism for sericite recovery.

In well-drained froths, entrained particles and water drain from the froth rapidly near the pulp-froth interface, but the entrained particles become entrapped between the bubble films at increased heights in the froth. It is therefore reasonable to postulate that as the bubble films grow thinner with increasing height in the froth (as a result of drainage), the probability of entrained particles becoming trapped in these films will

increase. Over the first 0.5 min, *e* of sericite was 1.10 when the froth depth was 10 mm, *e* of sericite increased to 1.29 with the increasing of the froth depth to 30 mm. It was shown that the quantity of sericite reporting to concentrate by entrapment increased with the increase of the froth depth.

The results obtained by the technique of Warren and the contact angle measurements showed that while the majority of sericite was recovered into the concentrate as a result of entrainment, part of sericite was recovered into the concentrate by entrapment, and no sericite was recovered via true flotation.

Conclusions

In this study, the recovery mechanisms of sericite and their effect on microcrystalline graphite flotation were investigated. The following conclusions were drawn from the above observations.

The batch flotation tests of artificial mixtures indicated that the poor flotation selectivity of commercial microcrystalline graphite ore was attributed to the serious misreport of sericite into concentrate.

The aggregation/dispersion behaviors of microcrystalline graphite and sericite particles suggested that sericite was not likely to report into graphite concentrate by slime coating.

Sericite was a hydrophilic mineral, and kerosene did not change its surface hydrophobicity therefore it was impossible for sericite to be recovered by true flotation in microcrystalline graphite flotation.

From the results obtained by the technique of Warren and the contact angle measurements it can be concluded that the majority of sericite was recovered into the concentrate as a result of entrainment and a part of sericite was recovered by entrapment.

Acknowledgements

References

ADAMCZYK Z., WERONKI P., 1999, *Application of the DLVO theory for particle deposition problems*, Advances in Colloid and Interface Science, 83(1-3), 137-226.

BERGSTROM L., 1997, *Hamaker constants of inorganic materials,* Advances in Colloid and Interface Science, (70), 125-169.

BLASKETT K.S., 1960, *Some effects of depressants in the flotation of a lead ore*, Proc. 5th Int. Mineral Processing Cong., 409-429.

CROSSLEY P., 1999, *Graphite—High-tech supply sharpens up*, Industrial Minerals, (386), 31-47.

DONG F.Z., 1997, *A study on flotation of a cryptocrystalline graphite ore*, Conservation and Utilization of Mineral Resources, (1), 15-17.

CHIBOWSKI E., PEREA-CARPIO R., 2002, *Problems of contact angle and solid surface free energy determination*, Advances in Colloid and Interface Science, 98(2), 245-264.

GAO H.M., YUAN J.Z., WANG X., GUAN J., ZHANG L., JING Z., MAO Y.L., 2007, *Mechanism of surface modification for sericite*, Journal of Wuhan University of Technology--Materials Science Edition, 22(3), 470-472.

GEORGE P., NGUYEN A.V., JAMESON G.J., 2004, *Assessment of true flotation and entrainment in the flotation of submicron particles by fine bubbles*, Minerals Engineering, 17(7-8), 847-853.

HE M., 2009, *The influence of adsorbed polymer on clay and copper mineral particles' interactions*, Doctoral Dissertation, Applied Science, University of South Australia, Brisbane, 2-3.

JI G.C., 1991, *Continuous flotation experiment of microcrystalline graphite*, Non-metallic Mines, (2), 16-18.

LI H.Q., FENG Q.M., YANG S.Y., OU L.M., LU Y., 2014, *The entrainment behaviour of sericite in microcrystalline graphite flotation*, International Journal of Mineral Processing, (127), 1-9.

MITCHELL T.K., NGUYEN A.V., EVANS G.M., 2005, *Heterocoagulation of chalcopyrite and pyrite minerals in flotation separation*, Advances in Colloid and Interface Science, 114–115227–237.

NGUYEN A.V., EVANS G.M., JAMESON G.J., 2002, *Approximate calculations of electrical double-layer interaction between spheres*. Encyclopedia of surface and colloid science. H. AT. New York, Marcel Dekker.

MAURER S., MERSMANN A., PEUKERT W., 2001, *Henry coefficients of adsorption predicted from solid Hamaker constants*, Chemical Engineering Science, 56(11), 3443–3453.

SALGADO M.R., 2001, *Upgrading the graphite by flotation at Bogala Mines in Sri Lanka*, J. Cent. South Univ. Technol., 8(3), 193-196.

SILVESTER E., 2011, *The recovery of sericite in flotation concentrates*, Mineral Processing and Extractive Metallurgy, 120(1), 10-14.

SIMANDL G.J., KENANL W.M., 1997, *Microcrystalline graphite*, British Columbia Geological Survey Geological Fieldwork, 240-241 240-244.

WAN Q.H., 1997, *Effect of electrical double-layer overlap on the electroosmotic flow in packed-capillary columns*, Analytical Chemistry, 69(3), 361-363.

WANG B., PENG Y., 2013, *The behaviour of mineral matter in fine coal flotation using saline water*, Fuel, 109309-315.

WARREN L.J., 1985, *Determination of the contributions of true flotation and entrainment in batch flotation tests*, International Journal of Mineral Processing, 14(1), 33-44.

XIA Y.K., REN Z.M., CHEN H.X., GUAN F.T., 1996, *A noval flotation flowsheet of microcrystalline graphite and its industrial application*, Non-metallic Mines, 19963.

ZHENG X., JOHNSON N.W., FRANZIDIS J.P., 2006, *Modelling of entrainment in industrial flotation cells: Water recovery and degree of entrainment*, Minerals Engineering, 19(11), 1191-1203.

CHANGES IN THE FLOTATION KINETICS OF BITUMINOUS COAL BEFORE AND AFTER NATURAL WEATHERING PROCESSES

Wencheng XIA*, Yaoli PENG*, Chuancheng REN**, Guangyuan XIE*, Chuan LIANG***

* Key Laboratory of Coal Processing and Efficient Utilization (Ministry of Education), School of Chemical Engineering and Technology, China University of Mining and Technology, Xuzhou 221116, Jiangsu, China
** Dezhou University, Dezhou 250323, Shandong, China
***Shandong Energy Linyi Mining Group Co., Ltd., Linyi 276017, Shandong, China
w.xia.cumt@gmail.com (W. Xia), peng_yaoli@163.com (Y. Peng)

Abstract: Natural weathering processes can make coal surface more hydrophilic due to the increase of content of hydrophilic functional groups (C-O, C=O, and COOH) and the decrease of content of hydrophobic functional groups (C-C and C-H) on coal surface, and hence the flotation recovery of fine coal is reduced. In this paper, a series of flotation tests were conducted in order to investigate the changes in the flotation kinetic of bituminous coal before and after natural weathering processes. Additionally, XPS was used to indicate the changes in surface properties of bituminous coal. In the investigations the flotation kinetic was changing. The classical first-order rate constant (k) of bituminous coal flotation was reduced after the natural weathering processes. A relationship between the classical first-order rate constant (k) and the hydrophilicity ability (HA) was given.

Keywords: flotation kinetic, classical first-order rate constant, natural weathering processes, XPS, contact angle

Introduction

The surface properties of coal can be changed by the weathering/oxidation processes. The obvious changes are due to the increase of oxygen containing functional groups on coal surface which are hydrophilic groups (Pietrzak and Wachowska, 2003; Pilawa et al., 2002; Kozłowski et al., 2002; Grzybek et al., 2002, 2006). Natural weathering processes usually make coal surface more hydrophilic, and hence the flotation recovery of fine coal is reduced. In most cases, it is difficult to float the oxidized coal

using the common oily collectors such as kerosene and diesel oil (Xia and Yang, 2013; Wang et al., 2013; Xia et al. 2013, 2014a).

It is necessary to seek the useful ways for improving the flotation recovery of oxidized coal. In the literature, the ultrasound treatment, premixing treatment, grinding treatment, and surface attrition treatment have been considered and they can remove the oxidized layer from oxidized coal surface (Ozkan, 2012; Feng and Aldrich, 2005; Piskin and Akgun, 1997; Sokolovic et al., 2012a, 2012b; Xia et al., 2012). Microwave pretreatment could improve the floatability of oxidized coal through reducing the moisture content of coal samples (Xia et al., 2013). Besides these treatments before the flotation processes, the efficient collectors and promoters were also found to enhance the flotation of oxidized coal. Oxidized coal could be well floated by the new collectors or surfactants. For example, blending of hydrocarbons and non-hydrocarbon collectors such as copolymers, long chain amines, and fatty acid amides could improve the floatability of oxidized coal (Polat et al., 2003; Ahmed and Drzymala, 2012).

Although the flotation recovery of oxidized coal could be enhanced or improved by pretreatments, new collectors and surfactants, the flotation kinetic of coal before and after natural weathering processes have been little investigated. In this paper, bituminous coal was used as coal samples and XPS was used to indicate the changes in surface properties of bituminous coal before and after natural weathering processes. A series of flotation tests were conducted in order to investigate the changes in the flotation kinetic of bituminous coal before and after natural weathering processes. The classical first-order rate constant (k) of flotation of bituminous coal before and after natural weathering processes was investigated.

Experimental method and procedure

Materials and experiment design

Bituminous coal sample was obtained from Shanxi Province of China. The coal sample was dry-ground in a laboratory mill to pass a 0.5 mm sieve. Natural weathering processes of bituminous coal were conducted on the roof. The weathering times were three and six months. Bituminous coal underwent the breakdowns from the sun, wind, and water. The oxidation processes occurred under natural environment.

The coal samples used in this study were three types: $Coal_1$ (fresh coal), $Coal_2$ (coal was oxidized for 3 months), and $Coal_3$ (coal was oxidized for 6 months). The proximate analyses of three coal samples are presented in Table 1, where M_{ad} is the moisture content, V_{ad} the volatile matter content, FC_{ad} the fixed carbon content, and A_{ad} is the ash content on an air dry basis.

Table 1 shows that the moisture content and ash content of the coal samples increased after the weathering processes while the volatile matter content and fixed carbon content reduced. This clearly indicates that natural weathering processes should change both the chemical and physical properties of bituminous coal.

Table 1. Proximate analysis of fresh and oxidized coals (air dried, wt. %)

Coal types	M_{ad}	V_{ad}	FC_{ad}	A_{ad}
Coal$_1$	2.91	16.54	58.32	22.23
Coal$_2$	3.60	16.27	56.55	23.58
Coal$_3$	5.14	15.79	52.03	27.04

XPS and contact angle measurements

Before the XPS experiments, coal samples were pressed into plates. Three plates were obtained from three types of coal samples. Then, these plates were moved to the test room. The XPS experiments were carried out at room temperature in an ultra high vacuum (UHV) system with the surface analysis system (ESCALAB 250Xi, America). The base pressure of the analysis chamber during the measurements was lower than 1.0×10^{-9} mbar. Al Ka radiation ($hv = 1486.6$ eV) from a monochromatized X-ray source was used for XPS. For all analyses, the take-off angle of the photoelectrons was 90° and the spot size was 900 μm. The spectra of survey scan were recorded with the pass energy of 100 eV while the energy step size was 1.00 eV. High resolution spectra were recorded with the pass energy of 20 eV and the energy step size was 0.05 eV. The data processing (peak fitting) was performed with XPS Peak fit software, using a Smart type background subtraction and Gaussian/Lorentzian peak shapes. The binding energies were corrected by setting the C1s hydrocarbon (-CH_2-CH_2-bonds) peak at 284.6 eV.

Before the contact angle measurement, the coal samples were also pressed into plates. Three plates were also obtained from three types of coal samples. The plates of coal samples were subjected contact angle measurements in a JC2000D analyser putting a water droplet on the surface of coal plates in air.

Flotation tests

In these tests, the coal samples were pre-wetted in a flotation cell for 3 min at the impeller speed of 1910 rpm. After the pre-wetting process, the collector was added into the flotation pulp, and the pulp was conditioned for 3 min. At last, 2-octanol frother was added, and the pulp was conditioned for another 1 min.

The collector and frother dosages were chosen 800 g/Mg and 300 g/Mg, respectively. The flotation tests were conducted in a 1.5 dm^3 XFG flotation cell using 100 g of coal. The flotation rate tests were conducted, i.e., the whole flotation processes were divided into five stages from the beginning to the end, and the time lengths of five stages were 0.5, 0.5, 1.0, 1.0, and 2.0 min, respectively. The flotation concentrate was analyzed for combustible matter recovery and concentrate ash content. Equation (1) was used to calculate the combustible matter recovery:

$$\text{Combustible matter recovery (\%)} = [M_C (100 - A_C) / M_F (100 - A_F)] \times 100 \qquad (1)$$

where M_C is weight of the concentrate (%), M_F weight of the feed (%), A_C the ash content of the concentrate (%), and A_F is the ash content of the feed (%).

Results and discussion

XPS and contact angle analysis

Figure 1 shows the C1s peaks for bituminous coal surface before and after natural weathering processes. Peaks at binding energies of 284.6 eV, 285.6 eV, 286.6 eV, and 289.1 eV correspond to the following groups: C-C or C-H, C-O, C=O, and O=C-O (Xia and Yang 2013; Wang et al. 2013). The contents of these groups can be calculated (Table 2). The content of C-C and C-H groups decreased from 55.31% to 8.79% while the content of O=C-O group increased from zero to 8.77% after natural weathering processes (from $Coal_1$ to $Coal_3$). Meanwhile, the content of C-O increased from 38.74% to 50.99% and the content of C=O increased from 5.95% to 31.45% after natural weathering processes (from $Coal_1$ to $Coal_3$). The C-C and C-H groups can be oxidized to C-O groups. Then, C-O group can be oxidized to C=O group, and C=O group can be oxidized to COOH group. At last, COOH group can be further oxidized, and release some gas components (CO_2, CO) and water. The functional groups are changing by the process of the natural weathering (Xie et al., 2014; Nie et al., 2013; Wang et al., 2014).
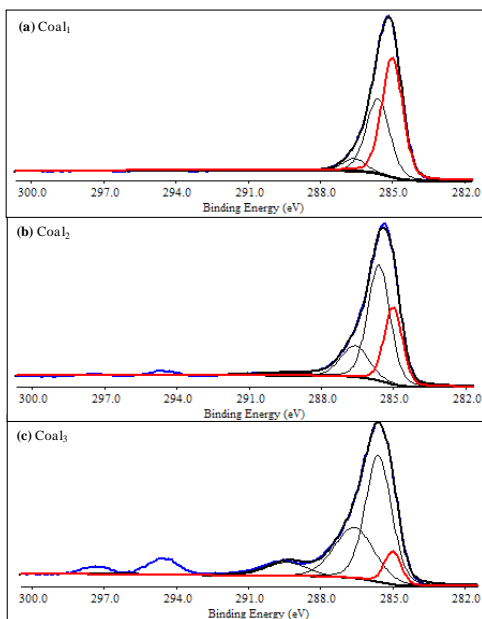
Fig. 1. C1s peaks for bituminous coal surface before
and after natural weathering processes

Table 2. Fraction of C on bituminous coal surface before and after
natural weathering processes (relative % of C1s)

Coal types	C-C, C-H (%)	C-O (%)	C=O (%)	O=C-O (%)
$Coal_1$	55.31	38.74	5.95	0.00
$Coal_2$	27.80	50.94	18.83	2.42
$Coal_3$	8.79	50.99	31.45	8.77

The primary hydrophilic functional groups are C-O, C=O, and O=C-O, and the primary hydrophobic functional groups are C-C and C-H (Xia et al., 2014a; Cinar, 2009). A hydrophilicity index involving the values of absorption intensity for carboxyl, hydroxyl, aliphatic CH, and aromatic CH groups has been developed to determine the hydrophobic/hydrophilic balance at the coal surface (Yuh and Wolt, 1983; Painter et al., 1983; Ye et al., 1988). The value of hydrophilicity index is obtained based on the results of FTIR which is usually a very common testing technology before the 1980s. The XPS technology has been developed in recent years. Considering the testing accuracy of FTIR in the determination of hydrophilicity index is lower than that of XPS. Meanwhile, XPS is used to the surface testing while FTIR focuses on both surface and interface. Therefore, this paper used XPS to determine the hydrophobic/hydrophilic balance at the coal surface by using a new index, such as hydrophilicity ability (HA). The hydrophilicity ability (HA) may be calculated using the ratio of the content of hydrophilic functional groups to the content of hydrophobic functional groups as shown in Eq. (2).

$$\text{Hydrophilicity Ability} = [(C-O)+(C=O)+(O=C-O)]/[(C-H)+(C-H)] \qquad (2)$$

where *C-O*, *C=O*, *O=C-O*, *C-O* and *C-H* are the contents of functional groups shown in Table 2.

The HA value of $Coal_1$ surface is 0.81, HA value of $Coal_2$ surface is 2.60 while HA value of $Coal_3$ surface is 10.38. The HA value of coal surface is increased by the natural weathering processes. It indicates that the hydrophilicity of bituminous coal is increased while the hydrophobicity of bituminous coal is reduced after the natural weathering processes.

The hydrophilic functional groups on coal surface are usually wetted by water easier than the hydrophobic functional groups since the hydrophilic functional groups may be bonded with water by hydrogen bond. After the natural weathering processes, the content of hydrophilic functional groups is increased while the content of hydrophobic functional groups is decreased. Figure 2 is the representative pictures of contact angles of three coal samples. Each contact angle was obtained using the average of three measurements. After the average calculating operation, the contact angle of $Coal_1$ is about 68°, the contact angle of $Coal^2$ is about 47°, while the contact angle of $Coal_3$ is about 35°. It indicates that the contact angle of coal surface is

reduced after natural weathering processes. The results of contact angle match well with the results of XPS.

<div style="text-align:center">(a) $Coal_1$ (b) $Coal_2$ (c) $Coal_3$</div>
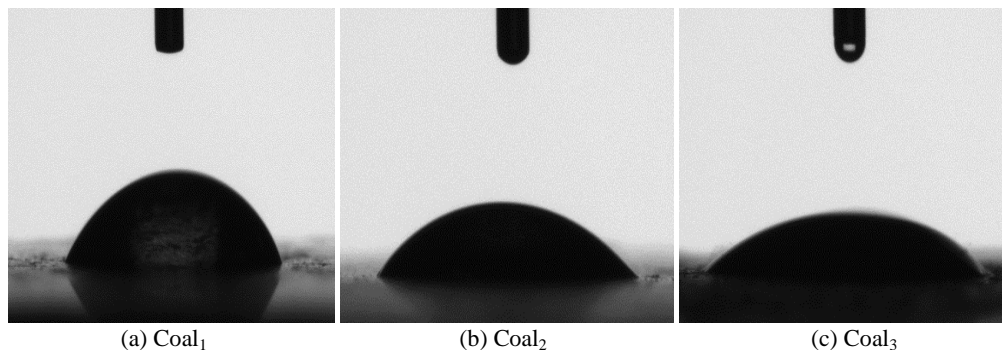
Fig. 2. Contact angles of three coal samples

Flotation results

Figure 3 illustrates the relationship between cumulative combustible matter recovery and flotation time. The combustible matter recovery increases with the increase of floatation time. As shown in Eq. (3), the classical first-order rate constant (k) of bituminous coal flotation can be obtained using the curve fitting (Sokolovic et al., 2012b; Wen and Sun, 1981; Fuerstenau et al., 1983).

$$\varepsilon_e = e_w(1 - e^{-kt}) \tag{3}$$

where e_w is the maximum combustible matter recovery (%) while k is classical first-order rate constant and t is the flotation time.

As shown in Fig. 3, the classical first-order rate constant (k) is 3.7 for $Coal_1$, 2.5 for $Coal_2$ and 1.2 for $Coal_3$. The k value is reduced by the natural weathering processes. Furthermore, the flotation recovery obviously decreased since the natural weathering processes reduced the hydrophobicity of bituminous coal but increased the hydrophilicity of bituminous coal. After the natural weathering processes, bituminous coal was difficult to float with common oily collectors. Figure 3 also indicates that the flotation behavior of $Coal_3$ is the worst and the flotation behavior of $Coal_1$ is the best. The flotation behavior of $Coal_2$ is between $Coal_1$ and $Coal_2$. The longer the natural weathering process is, the worse the flotation behavior of bituminous coal is.

Figure 4 illustrates the relationship between product ash content and flotation time. The product ash content increases with the increase of floatation time. The product ash content of $Coal_3$ is the highest. The product ash content of $Coal_1$ is similar to that of $Coal_2$. It indicates that mild oxidation processes may have very little effect on the product ash content but the long weathering processes may increase the product ash content obviously.
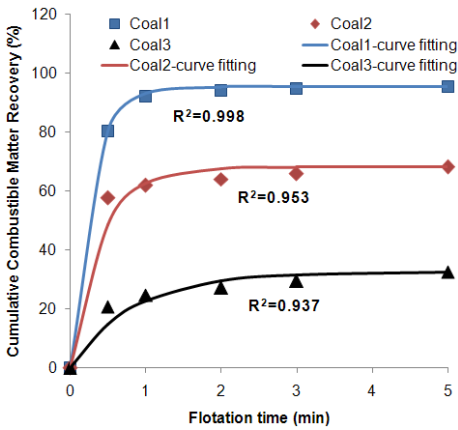
Fig. 3. Cumulative combustible matter
recovery changes with flotation time
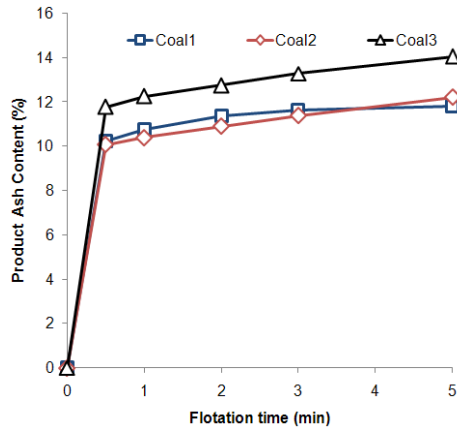
Fig. 4. Product ash content changes
with flotation time

Figure 5 illustrates the relationship between the classical first-order rate constant (k) and the hydrophilicity ability (HA). The relationship between the classical first-order rate constant (k) and the hydrophilicity ability (HA) is:

$$k = -0.97\ln(HA) + 3.471. \tag{4}$$

The k value decreases with the increase of HA value. Since the oxidation processes occur on the coal surface during the natural weathering processes, more and more hydrophilic functional groups are produced and the hydrophobicity of coal surface is reduced.
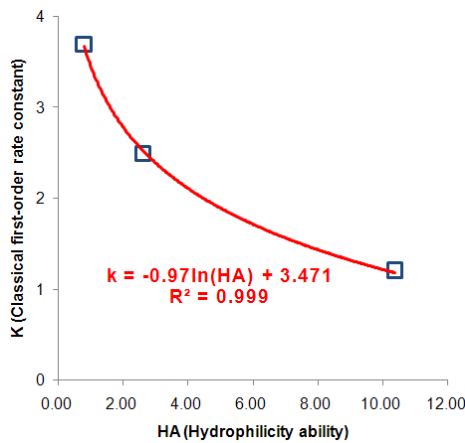
Fig. 5. Relationship between classical first-order rate constant (k)
and hydrophilicity ability (HA)

The HA value of coal surface is greatly increased after the natural weathering processes. After the natural weathering processes, the content of the primary hydrophilic functional groups (C-O, C=O and O=C-O) is increased and the content of the primary hydrophobic functional groups (C-C and C-H) is reduced. Therefore, the natural weathering processes make bituminous coal surface more hydrophilic and difficult to float with common oily collectors. The whole combustible matter recovery of $Coal_1$ is much higher than that of $Coal_2$ or $Coal_3$. The natural weathering processes not only reduce the hydrophobicity of coal surface and the combustible matter recovery but also reduce the value of classical first-order rate constant (k). Hence, the classical first-order rate constant (k) is 3.7 for $Coal_1$, 2.5 for $Coal_2$ and 1.2 for $Coal_3$. It indicates that the natural weathering processes make bituminous coal surface less hydrophobic (Xia et al. 2014b, 2014c).

Conclusions

- Natural weathering processes can reduce the content of hydrophobic functional groups (C-H and C-C) but increase the content of hydrophilic functional groups (C-O, C=O and O=C-O) on bituminous coal surface. Therefore, the natural weathering processes make bituminous coal surface more hydrophilic.
- The hydrophilicity ability (*HA*) value of bituminous coal surface is greatly increased by the natural weathering processes. The *HA* value is 0.81 for $Coal_1$ surface, 2.60 for $Coal_2$ surface and 10.38 for $Coal_3$ surface.
- Natural weathering processes not only reduce the whole combustible matter recovery but also reduce the value of classical first-order rate constant (k). The classical first-order rate constant (k) is 3.7 for $Coal_1$, 2.5 for $Coal_2$ and 1.2 for $Coal_3$.
- The relationship between the classical first-order rate constant (k) and the hydrophilicity ability (*HA*) meets the Equation $k=-0.97\ln(HA)+3.471$. The k value decreases with the increase of *HA* value.

Acknowledgements

References

AHMED H.A.M., DRZYMALA J., 2012, *Upgrading difficult-to-float coal using microemulsion,* Minerals & Metallurgical Processing, 29, 88-96.

CINAR M., 2009, *Floatability and desulfurization of a low-rank (Turkish) coal by low-temperature heat treatment,* Fuel Processing Technology, 90(10), 1300-1304.

FENG D., ALDRICH C., 2005, *Effect of preconditioning on the flotation of coal,* Chem. Eng. Comm., 192, 972-983.

FUERSTENAU D. W., ROSENBAUM J. M., LASKOWSKI J., 1983, *Effect of surface functional groups on the flotation of coal,* Colloids and Surfaces, 8(2), 153-173.

GRZYBEK T., PIETRZAK R., WACHOWSKA H., 2002, *X-ray photoelectron spectroscopy study of oxidized coals with different sulphur content,* Fuel Processing Technology, 77, 1-7.

GRZYBEK T., PIETRZAK R., WACHOWSKA H., 2006, *The influence of oxidation with air in comparison to oxygen in sodium carbonate solution on the surface composition of coals of different ranks,* Fuel, 85(7), 1016-1023.

KOZLOWSKI M., PIETRZAK R., WACHOWSKA H., YPERMAN J., 2002, *AP–TPR study of sulphur in coals subjected to mild oxidation. Part 1. Demineralised coals,* Fuel, 81(18), 2397-2405.

NIE B., WANG L., LI X., WANG C., LI, L., 2013, *Simulation of the interaction of methane, carbon dioxide and coal,* International Journal of Mining Science and Technology, 23(6), 919-923.

OZKAN S. G., 2012, Effects of simultaneous ultrasonic treatment on flotation of hard coal slimes. Fuel, 93, 576-580.

PAINTER P.C., STARSINIC M., SQUIRES E., DAVIS A.A., Concerning the 1600 cm^{-1} region in the spectrum of coal. Fuel, 62 (6), 742–744.

PIETRZAK R., WACHOWSKA H., 2003, *Low temperature oxidation of coals of different rank and different sulphur content,* Fuel, 82(6), 705-713.

PILAWA B., WIECKOWSKI A. B., PIETRZAK R., WACHOWSKA H., 2002, *Oxidation of demineralized coal and coal free of pyrite examined by EPR spectroscopy,* Fuel, 81(15), 1925-1931.

PISKIN S., AKGUN M., 1997, *The effect of premixing on the floatation of oxidized Amasra coal,* Fuel Processing Technology, 51, 1-6.

POLAT H., POLAT M., CHANDER S., 2003, *Physical and chemical interactions in coal flotation,* International Journal of Mineral Processing, 72, 199-213.

SOKOLOVIC J., STANOJLOVIC R.R., MARKOVIC Z.S., 2012a, *Activation of oxidized surface of anthracite waste coal by attrition*, Physicochemical Problems of Mineral Processing, 48(1), 5-18.

SOKOLOVIC J., STANOJLOVIC R.R., MARKOVIC Z.S., 2012b, *The effects of pretreatment on the flotation kinetics of waste coal,* International Journal of Coal Preparation and Utilization, 32(3),130-142.

WANG B., PENG Y., VINK S., 2013, *Diagnosis of the surface chemistry effects on fine coal flotation using saline water*, Energy & Fuels, 27, 4869-4874.

WANG G., WANG K., REN T., 2014, *Improved analytic methods for coal surface area and pore size distribution determination using 77K nitrogen adsorption experiment,* International Journal of Mining Science and Technology, 24(3), 329-334.

WEN W. W., SUN S. C., 1981, *An electrokinetic study on the oil flotation of oxidized coal,* Separation Science and Technology, 16(10), 1491-1521.

XIA W., YANG J., ZHAO Y., ZHU B., WANG Y., 2012, *Improving floatability of taixi anthracite coal of mild oxidation by grinding,* Physicochemical Problems of Mineral Processing, 48 (2), 393-401.

XIA W., YANG J., 2013, *Reverse flotation of Taixi oxidized coal,* Energy & Fuels, 27(12), 7324-7329.

XIA W., YANG J., LIANG C., 2013, *A short review of improvement in flotation of low rank/oxidized coals by pretreatments,* Powder Technology, 237, 1-8.

XIA W., YANG J., LIANG C., 2014a, *Investigation of changes in surface properties of bituminous coal during natural weathering processes by XPS and SEM,* Applied Surface Science, 293, 293-298.

XIA W., XIE G., REN C., ZHANG Z., LIANG C., GE X., 2014b, *Effect of natural weathering processes on size and density compositions of bituminous coal,* Energy & Fuels, 28 (7), 4496–4500.

XIA W., XIE G., LIANG C., YANG J., 2014c, *Flotation behavior of different size fractions of fresh and oxidized coals,* Powder Technology, 267, 80-85.

XIE W., SUN Z., XIONG Y., LI L., WU T., LIANG, D., 2014, *Effects of surface chemical properties of activated coke on selective catalytic reduction of NO with NH$_3$ over commercial coal-based activated coke,* International Journal of Mining Science and Technology, 24(4), 471-475.

YUH S.J., WOLT E.E., 1983, FTIR studies of potassium catalyst treated gasified coal chars and carbon. Fuel, 62, 252–255.

YE Y., JIN R., MILLER J.D., Thermal treatment of low rank coal and its relationship to flotation response. Coal Preparation, 6, 1–6.

PRODUCTION OF ZINC POWDER FROM Co-Zn PLANT RESIDUE USING SELECTIVE ALKALINE LEACHING FOLLOWED BY ELECTROWINNING

Hossein KAMRAN HAGHIGHI*,*****, Davood MORADKHANI*, Mohammad Hadi SARDARI***,****, Behzad SEDAGHAT***

*   Department of Mining and Metallurgical Engineering, Amirkabir University of Technology, Tehran, Iran, h.kamran.h@aut.ac.ir
**   Faculty of Engineering, University of Zanjan, Zanjan, Iran
***   Research & Engineering Co. for Non-ferrous Metals, Zanjan, Iran
****   Department of Mineral Processing, Faculty of Engineering, University of Sahand Technology, Tabriz, Iran
***** University of Applied Science and Technology, Calcimin Branch, Zanjan, Iran

Abstract: Annually, gigagrams of cobalt residues, called hot filter cake (HFC), are produced from the Co neutralization step at Iranian zinc plants. With respect to the composition of HFC (i.e., 15-25% Zn, 0.5–1.5% Co, 3–8% Mn), it can be used as a secondary source of zinc, cobalt and manganese. In the present study, for the first time, treatment of HFC for separation and recovery of zinc has been studied. The residue was treated by employing selective alkaline leaching, in order to recover the maximum amount of zinc, followed by zinc electrowinning process. As a results, a solution was obtained from alkaline leaching under the optimum condition of 75 °C, sodium hydroxide of 8 M, solid-to-liquid ratio dm^3 of 1:10, and stirring speed of 600 rpm, having zinc recovery of 88.5 %. In the following step, the electrowinning process, under the optimum working conditions being current density 350 A/m^2 and time 10 hours, was carried out to produce a zinc powder with high purity of 99 percent. Finally, a simple and effective conceptual flow diagram was proposed for the process.

Introduction

A part of zinc is recovered from different secondary resources, namely zinc ash, zinc dross, flue dusts of electric arc furnace and brass smelting, automobile shredder scrap, rayon industry sludge etc., which contain different levels of impurities depending on their sources. These secondary metal resources could be used to extract metallic values or it may be disposed of. However, the disposal of such materials is now becoming expensive because of increasingly stringent environmental protection regulations.

Furthermore, the chemical nature of these dust particles is such that they are classified as hazardous wastes (Safarzadeh et al., 2009). Therefore, the extraction of metallic values from these resources instead of their disposal seems to be economical.

In the zinc production plant Zanjan in Iran, because of the chemical composition of the ores, removal of some impurity such as cobalt is necessary to recover zinc product (Safarzadeh et al., 2009). The solid residue of the cobalt precipitation step, known as hot filtercake (HFC), is obtained after filtration of pulp. This residue, with the composition of 15-25% Zn, 0.5-1.5% Co and 3–8% Mn, can be considered as a secondary resource of zinc in Iranian zinc plants.

This paper is the first work in which the HFC waste containing Co and Zn and the other heavy metals was treated to recovery and produce metals. Therefore, the emphasis of this paper is on treating the Co-waste produced in zinc plants. The hot filter cake (Co-waste), that was a waste is now is a potential and considerable source of zinc, cobalt etc. The hazardous high-cobalt composition of the filter cake, poses unavoidable risk to human health and environment. Metal content extraction from the HFC and controlling the hazard of it, is a great concern among Iranian researchers not only for environmental reasons but also for economic aspects (Safarzadeh et al., 2008, 2009). Therefore, a cost-effective process is necessary to extract the metals from the waste sources such as HFC by hydrometallurgical treatment.

Some studies have been carried out in the world to recover valuable metals from zinc plant residues (ZPR). The extraction of zinc, cobalt and manganese from the Iranian HFC of National Iranian Lead and Zinc Company (NILZ) by solvent extraction has been reported. In such solvent extraction routs, the separation of zinc, manganese and cobalt was accomplished using 20% D2EHPA+5% TBP in kerosene, 298 K and at O:A ratio of 1:1and pH of 1.5-2 (Eivazi et al., 2008ab; Jha et al., 2001). Despite the recovery of zinc from acidic media, zinc leaching from ZPR in alkaline medium has been developed. Alkaline agents such as sodium hydroxide, ammonium hydroxide, and sodium carbonate can selectively bring the desired metal into solution, leaving Fe and other metals such as Ni and Mn. Alkaline leaching of zinc-carbon batteries has been reported in literature (Kim et al., 2008; Shin, 2008). Kim et al. reported the alkaline leaching of zinc-carbon batteries in 4 M NaOH and obtained a solution with recovery of 64% Zn and 0.1% Mn (Kim et al., 2008). This solution can be followed by electrowinning (EW) of alkaline leaching solution to produce zinc powder with 99.9% purity (Gurmen and Emre, 2003). Zhao and Stanforth (2000) also investigated alkaline treatment of smithsonite ores followed by zinc powder production. In some investigations, different alkaline leaching techniques were tested in order to dissolve zinc present in an electric arc furnace (EAF) steel dust (Dutra et al., 2006). Furthermore, alkaline leaching of sphalerite by feeding lead carbonate, illustrates leaching zinc out as $Na_2Zn(OH)_4$ (Chenglong and Youcal, 2009). The alkaline leaching of metals from various resources in different investigations has been summarized in Table 2. Among the reports summarized in Table 2, no research has been done on selective extraction of zinc from cobalt waste followed by EW.

Furthermore, as seen in this table, the novelty is the usage of a specific material (EAF dust, ores etc.) that leaching has been carried out on it. For example, in one of the latest investigations carried out by Mohapatra et al. (2014), a flowsheet has been developed for extraction of zinc from spent catalyst by alkaline leaching as the flowsheet of this study developed for zinc extraction from HFC. This research shows that developing a process for metal recovery from various resources is currently attractive. Therefore, one of the differences of this paper from the others is usage of HFC in an advanced process in which some products were obtained. Using this advanced process, a main product (zinc powder) and a by-product (Co-Mn concentrate) have been produced.

In our previous research, selective zinc alkaline leaching optimization and cadmium sponge recovery by electrowinning from residue obtained from Ni-Cd neutralization step (cold filter cake, CFC) was carried out (Moradkhani et al., 2012). In the present study, selective leaching of zinc from the hot filter cake by using sodium hydroxide (NaOH) was conducted. Through this method, zinc leaves most of the impurities such as Co, Mn, Ca etc. largely unaffected in the residue. As the scope of the present work, the effective leaching parameters such as caustic soda (NaOH) concentration (M), temperature (°C), liquid to solid ratio (L/S) and stirring rate (rpm) were investigated and the optimum condition were obtained. After leaching HFC with caustic soda, a strongly alkaline filtrate solution was obtained and stored. Finally, zinc was recovered as an active powder from this solution by alkaline electrolysis.

Experimental methods

Materials and reagent

The investigation was carried out involving hot filter cake (HFC) residue sampled from a disposal site of Iranian Zinc Mine Development Company (IZMDC). The filter cake was dried at 110 °C for 24 h and then was comminuted to a size below 100 μm. The composition of the sample was analyzed by the atomic absorption method and the result was shown in Table 1. Furthermore, the characterization of minerals was performed by X-ray powder diffraction (XRD) under the condition of Cu Kα at 40 kV and 30 mA. Sodium hydroxide with the purity of 98% from Merck (Germany) was used in leaching experiments.

Table 1. Chemical composition of filter cake produced in cobalt purification step

Elements	Zn	Co	Mn	Ca	Cd	Ni	Fe
wt,%	17.51	1.06	6.33	11	0.13	0.04	0.6

Table 2. A brief summary of alkaline leaching of metals from various materials

Research	Reagents	Material	Aim	Ref.
Leaching of oxidized zinc ore in various media	Sodium hydroxide	Oxidized zinc ore	The extraction of zinc from oxidized zinc ore	Frenay, 1975
Extraction of antimony from sulfide ores	Sodium hydroxide	Sulfide ores	Extraction of antimony	Olper, 1997
Caustic soda leach of electric arc furnace dust	Sodium hydroxide	Electric arc furnace	The extraction of zinc and lead from electric arc furnace dust	Mordodan et al. 1999
Production of Zn powder by alkaline treatment of smithsonite Zn–Pb ores	Sodium hydroxide	Smithsonite Zn–Pb ores	Production of Zn powder	Zhao and Stanforth, 2000
Pressure oxidative leaching of molybdenite in alkaline media	NaOH–NH$_4$OH or NaOH–NaOCl	Molybdenite	Recovery of molybdenum from molybdenite	Mirvaliev and Inoue, 2001
Leaching and cementation of heavy metals from electric arc furnace dust in alkaline medium	Sodium hydroxide	Electric arc furnace	The extraction of zinc from electric arc furnace dust	Orhan, 2005
Oxidative alkaline leaching of americium from simulated high-level nuclear waste sludge	Sodium hydroxide	Nuclear waste sludge	Leaching of americium	Reed et al., 2005
Alkaline leaching of zinc from electric arc furnace steel dust	Sodium hydroxide	Electric arc furnace steel dust	Zinc recovery from the EAF dust	Dutra et al., 2006
Separation of zinc from spent zinc-carbon batteries by selective leaching	Sodium hydroxide	zinc-carbon batteries	Separation of zinc from spent zinc-carbon batteries	Shin, 2008
Preparation of Mn–Zn ferrite from spent zinc–carbon batteries by alkali leaching, acid leaching and co-precipitation	Sodium hydroxide	zinc–carbon batteries	Preparation of Mn-Zn ferrite	Kim et al., 2008
Mechanochemical leaching of sphalerite in an alkaline solution containing lead carbonate	Mechanochamical leaching by Sodium hydroxide	Sphalerite	The extraction of zinc from sphalerite	Chenglong and Youcai, 2009
Alkaline leaching Zn and its concomitant metals from refractory hemimorphite zinc oxide ore	Sodium hydroxide	Refractory hemimorphite zinc oxide ore	Separation of zinc and silica	Chen et al., 2009
The kinetics of gibbsite dissolution in NaOH	Sodium hydroxide	Gibbsite	Al dissolution	Pereira et al., 2009

Metal extraction from spent sulfuric acid catalyst through alkaline and acidic leaching	Sodium hydroxide	Spent sulfuric acid catalyst	Vanadium extraction	Ognyanova et al., 2009
Pretreatment of copper anode slime with alkaline pressure oxidative leaching	Sodium hydroxide	Copper anode slime	Prepare a sample for acidic leaching	Liu et al., 2014
Desilication from titanium–vanadium slag by alkaline leaching	Sodium hydroxide	Titanium–vanadium slag	Desilication from titanium–vanadium slag	Chen et al., 2013
Ligand mediated eco-friendly leaching of zinc from spent catalyst in alkaline media	NaOH and EDTA	Spent catalyst	The extraction of zinc from spent catalyst	Mohapatra et al., 2014

The results of XRD analysis revealed that $CaSO_4 \cdot 2H_2O$, $ZnSO_4 \cdot H_2O$, $CoSO_4 \cdot 4H_2O$ and $Ca_3Mn(SO_4)_2$ were the major mineralogical phases in the filter cake (Fig. 1).
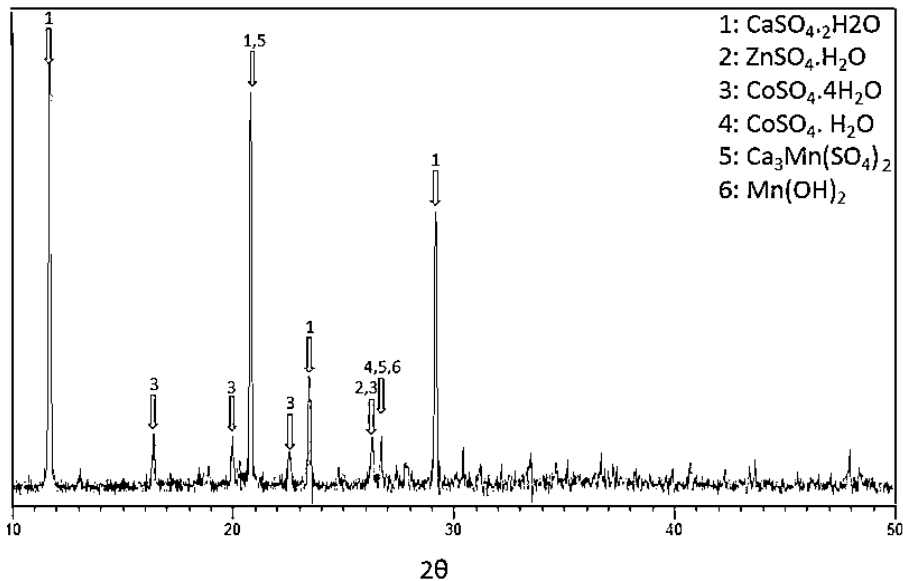
Fig. 1, X-ray diffraction analysis of hot filter cake (HFC)

Experimental procedure

As mentioned, the comminuted HFC was used in the experiments of this work. In order to separate zinc from other impurities, two-step alkaline leaching followed by electrowinning were proposed. In these experiments, the solution was heated to the desired temperature. Then, HFC sample was added to the alkaline solution. The mentioned pulp was stirred for one hour. For chemical analysis, some samples were taken from the pulp at different time intervals. The samples were immediately

vacuumed filtered, diluted and analyzed for zinc and other elements. The obtained filtrate from the optimum condition experiment was stored for electrowinning experiments. All the experiments of this study were conducted in triplicate and 95% confidence interval (CI) was used to calculate the experimental error bar in each figure. In other words, the responses are the mean ± 95% confidence intervals of three independent experiments.

First alkaline leaching tests

Alkaline leaching experiments were carried out in a beaker in thermo-controlled water bath equipped with a mechanical stirrer. The effects of sodium hydroxide concentration (M), liquid to solid ratio (L/S), temperature (°C) and stirring rate (rpm) on these leaching experiments were studied. In order to carry out the leaching experiments the desired amount of HFC was added to specific volume of caustic soda solution at the desired temperature and stirring rate (with respect to the designed parameters). The condition of parameters applied in the alkaline leaching experiments is illustrated in Table 3. In order to obtain and store the solution for the next step, an experiment was performed under the optimum condition. Hence, 50 g solid residue was dissolved in 0.5 dm^3 of 8 M sodium hydroxide (L/S of 10:1) at 75 °C and 600 rpm for one hour. After completion of the leaching, the hot slurry was filtered. The concentrations of Zn^{2+}, Mn^{2+} and Co^{2+} in the leaching filtrate and solid residue were characterized by the atomic absorption analysis.

Table 3. The parameter values for alkaline leaching of cobalt filter cake

Parameter	Value
NaOH concentration (M)	4, 6, 8, 10
Temperature (°C)	25, 50, 60, 90
Phase ratio (v/w)	4, 6, 8, 10
Steering speed(rpm)	400, 600, 800, 1000

Second alkaline leaching tests

The aim of second alkaline leaching is to reduce the amount of zinc in residue as much as possible and increase the overall zinc recovery (Moradkhani et al., 2012). Under optimum conditions obtained in the first alkaline leaching experiments, the solid residue obtained from the first stage containing 3-5% Zn was again treated with NaOH solution. In the second alkaline leaching experiments, 50 g solid residue was dissolved in 0.5 dm^3 of 8 M sodium hydroxide at 95 °C and 600 rpm for 1 h. The concentration of Zn^2, Co^{2+} and Mn^{2+} in the leaching liquor and solid residue were characterized by atomic absorption analysis. It is noteworthy that in lab-scale experiments, the first alkaline leaching solid residue is treated with fresh NaOH solution. However, in the larger scale operations, the spent electrolyte of zinc alkaline electrowinning process is

recycled to the second leaching step to recover the remaining zinc of the residue. Furthermore, in pilot-scale operations the alkaline filtrate obtained from the second leaching step is also recycled to the first alkaline leaching step. Therefore, the second alkaline leaching filtrate solution is contacted with HFC in the first alkaline leaching tank. At the end of the laboratory experiments, the zinc alkaline solution is stored for next studies.

Electrowinning experiments

Based on the reported investigations (Gurmen and Emre, 2003; Kim et al., 2008; Zhao and Stanforth, 2000), zinc present in the highly alkaline filtrate solution can be recovered in an active powder form by zinc alkaline electrowinning. Alkaline electrowinning has many advantages versus sulfate electrowinning such as lower electricity consumption and production of a highly active zinc powder (Moradkhani et al., 2012). In order to perform the electrowinning experiments, the first and second alkaline leaching were combined. In this step, under the optimal conditions, the zinc powder was produced with high purity. Stainless steel electrodes formed the anode and cathode in this study. Finally, the deposited zinc metal powder could easily be removed from the electrode. It was then washed with warm distilled water and dried at 50°C, weighed and analyzed.

Result and discussion

Alkaline leaching experiment and recovery of zinc

Alkaline leaching with sodium hydroxide can be exploited in separating cations, since only certain metal oxides such as zinc oxide and aluminum oxide show amphoteric behavior and dissolve in it (Moradkhani et al., 2012). With respect to this behaviour, sodium hydroxide was chosen as the selective alkaline agent because it thermodynamically leaches zinc from the solid state. However, it cannot dissolve nickel and cadmium under atmospheric condition. In this study, the effects of NaOH concentration, leaching temperature, L/S, leaching time and stirring rate on the alkaline leaching extraction of zinc were investigated. As mentioned before, the zinc content of highly alkaline filtrate solution can be recovered in the active powder form by zinc alkaline electrowinning. In order to perform the electrowinning experiments, the first and second alkaline leaching were combined. In the subsequent steps, a filtrate solution obtained from the first alkaline leaching step containing about 20 g/dm^3 Zn was electrolyzed to recover zinc in an active powder form.

Effect of concentration of sodium hydroxide

In order to investigate the effect sodium hydroxide, four concentrations (4, 6, 8, and 10 M) were used in the experiments. The metal recovery percentage and its concentration leached out into solution vs. sodium hydroxide concentration were

showed in Fig. 2. It is noteworthy that the recovery of impurities such as cobalt and manganese due to approximately zero recovery of them is not shown in the figures of this study.
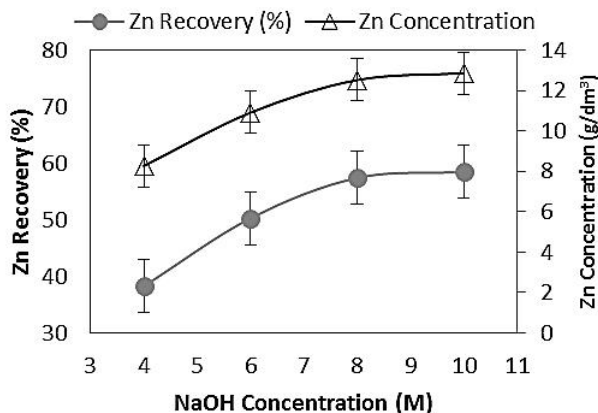
Fig. 2. Effect of sodium hydroxide concentration on metal leaching extraction in the first step (leach cond. temperature 25 °C, L/S 10:1, rpm 600, time 1 h)

The results showed that the zinc dissolution depends on NaOH concentration and increases with its enhancement. This result indicate high selective alkaline leaching of Zn over Co and Mn. This was because in the highly alkaline media, zinc exists in solution as a complex anion of ZnO_2^{2-}. Nevertheless, NaOH cannot bring Co and Mn from solid state to the solution and form water-soluble complexes.

Based on the experimental result, the zinc extraction efficiency after 1 h at different sodium hydroxide concentrations in the first leaching step was found to be 38.2, 50.6, 57.4 and 58.4%, respectively. Therefore, the NaOH concentration of 8 M is selected as the optimum condition. Furthermore, with respect to the result obtained in the second alkaline leaching under the condition applied in the first leaching, the overall zinc extraction efficiency of two steps was found to be 88.5 %.

Effect of L/S

Figure 3 shows the zinc recovery as a function of L/S at 25 °C, NaOH concentration of 8 M, rpm of 600 for 1 h. These results showed the obvious effect of L/S ratio on the zinc leaching recovery. In other words, with increasing ratio of NaOH solution to solid in the sample, dissolution of zinc can be facilitated. As shown in this figure, the zinc recovery enhanced from 38.8% at L/S of 4 to 57.4% at L/S of 10. Therefore, L/S=10:1 with the maximum zinc recovery is considered as the optimum phase to liquid ratio.
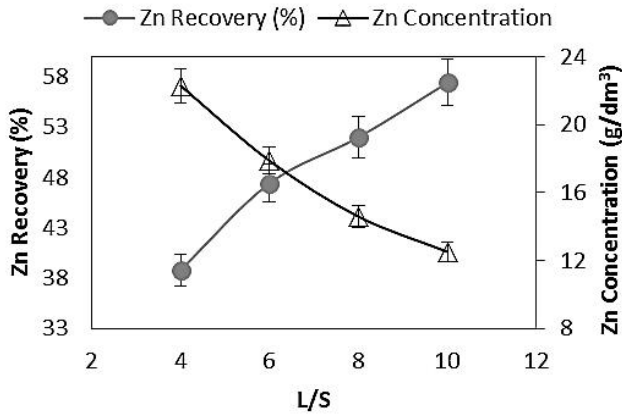
Fig. 3. Effect of L/S on Zn leaching recovery (leaching conditions: temperature 25 °C, NaOH concentration 8 M, time 1 h)

Effect of leaching temperature

The plot of the temperature vs. metal dissolution is illustrated in Fig. 4. As seen in this figure, the recovery of zinc increased as the temperature increased from 25 to 95°C. These results show that the temperature has strong effect on the Zn leaching recovery. The Zn leaching recovery increased from 57.4% at 25 °C to 88.5% at 95 °C. Despite the high recovery of zinc at 95°C, some amount of impurities such as Co is dissolved. Therefore, to prevent them entering the electrowinning process, 75°C was chosen as the optimum temperature of the first leaching step. Furthermore, the solution at 95 °C is more viscose to such extent that filtration of slurry is difficult and slow (Moradkhani et al., 2012).
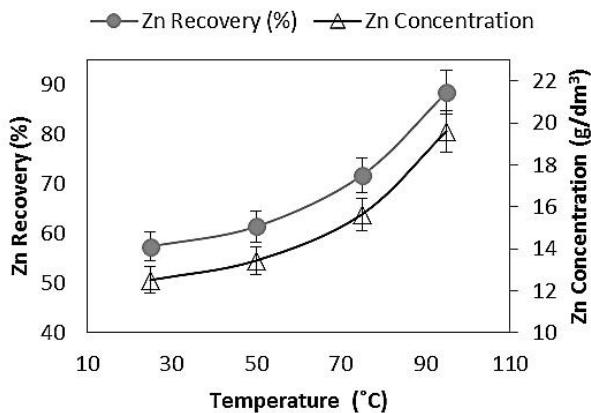
Fig. 4. Effect of temperature on Zn leaching recovery (leach conditions: NaOH concentration 8 M, L/S 10:1, rpm 600, time 1 h)

Effect of stirring rate

In order to evaluate the effect of stirring speed on the zinc leaching, a series of experiments were carried out under the condition: NaOH concentration 8 M, temperature 95°C, time 1 h and L/S 10:1. The effect was studied at four levels; 400, 600, 800 and 1000 rpm. The obtained results are shown in Fig. 5. As shown in this figure, the stirring rate had not considerable effect on zinc dissolution. On the other hand, zinc leaching recovery and concentration was enhanced from 85.1% and 18.7 g/dm^3 at 400 rpm to 88.6% and 19.8 g/ dm^3 at 600 rpm, and no significance changes occurred between 600 rpm (88.5% recovery) and 1000 rpm (89.1% recovery). Therefore, 600 rpm was selected as the optimum stirring speed to confirm enough pulp mixing. Hence, with respect to the results of pervious sections, the optimum conditions of alkaline leaching are found to be sodium hydroxide concentration 8 M, temperature 95°C, time 1h, stirring rate 600rpm and L/S 10:1, with the zinc leaching recovery of 88.5%.
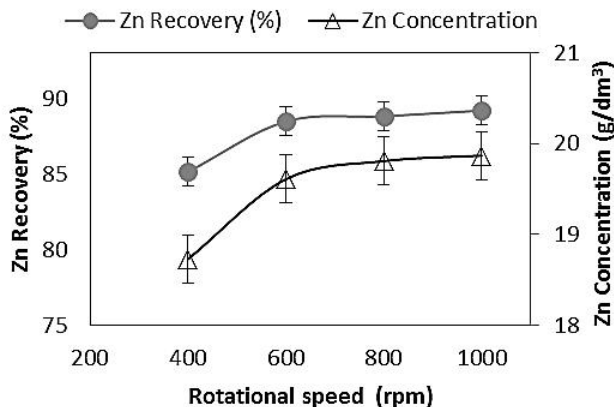
Fig. 5. Effect of stirring rate on Zn leaching recovery (leach conditions: temperature 95°C, NaOH concentration 8 M, time 1 h, L/S 10:1)

Thermodynamic aspects of zinc dissolution

Some researches, reported that a concentrated NaOH solution could selectively dissolve zinc from solid state and leave behind iron and manganese in the leach residue (Cusanelli et al., 1973; Eacott et al., 1984; Merrill and Lang, 1965; Shin, 2008; Valdez and Dean, 1975). Thermodynamic data (ΔG of -62,76 kJ at 75°C) showed the dissolution of zinc from zinc oxide occurs due to reaction:

$$ZnO + 2NaOH = 2Na^+ + ZnO_2^{-2} + H_2O. \qquad (1)$$
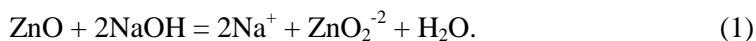
This equation was also used in the Eh-pH diagrams of this study. Figure 6 illustrates the Eh-pH diagrams for the zinc-water system to show the effect of

temperature. As seen in this figure, at 25°C the lines related to the species of $ZnOH_2$ and ZnO_2^{2-} shifts to the right side meaning the need for a higher pH or concentrated NaOH to dissolve a high concentration of zinc(II) in the form of ZnO_2^{2-} ions (Shin, 2008). The same results have been reported by Shin et al. (2009).
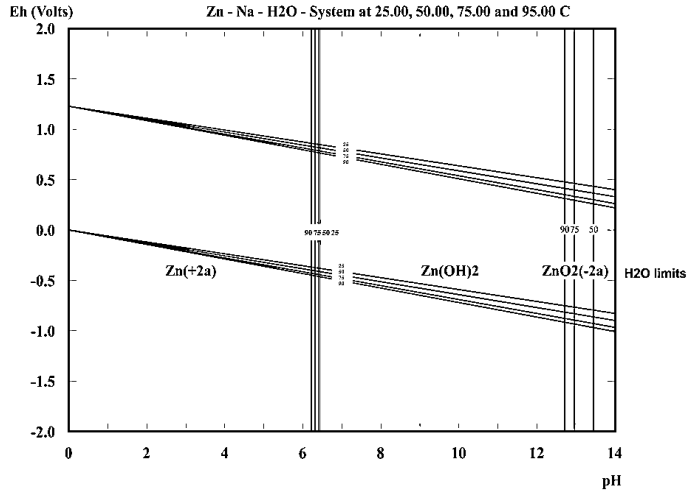
Fig. 6. Potential-pH diagram for zinc-water system in the temperature range 25–95 °C, {Zn} 0.3 M and {NaOH} 8 M (HSC 5.1 software)
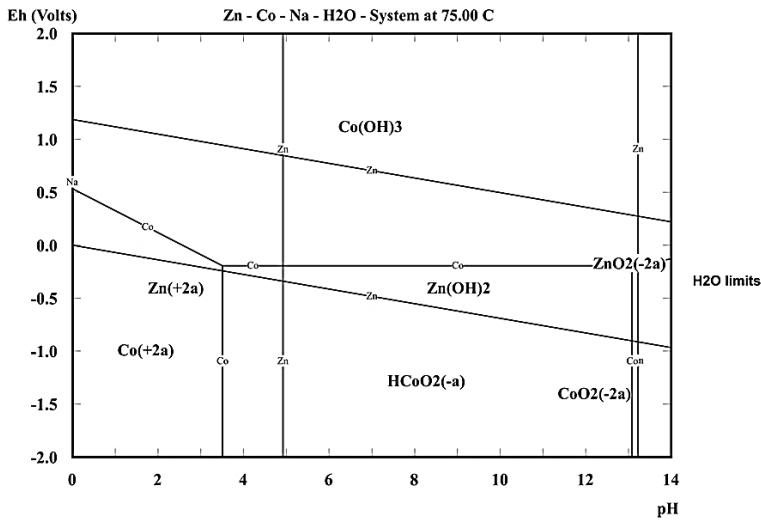
Fig. 7. Potential-pH diagram for zinc-cobalt-water system at 75°C and {Zn} 0.3 M, {Co} 0.01 M and {NaOH} 8 M (HSC 5.1 software)

With respect to Fig. 6, the enhancement of the temperature shifts the aforementioned lines to the left side. This shifting means that at relatively low pH values, dissolving of ZnO as ZnO_2^{2-} can easily occur. Furthermore, in order to prove

that the complete dissolution of the impurities such as cobalt, manganese etc. is not possible, the Eh-pH diagram of Zn-Co system in alkaline water was also constructed (Fig. 7). It is noteworthy that because of ignoring the complexity of diagrams and similar results, the cobalt-zinc system was only plotted. As seen in Fig. 7, a very thin area has been dedicated to CoO^{2-} at high pH values indicating a low possibility of cobalt dissolution at 75°C. The same result was obtained for the manganese-zinc system.

Zinc electrowinning

Some studies have been carried out on alkaline zinc electrowinning by Gurmen and Emre (2003) as well as St-Pierre and Piron (1986). They showed that electrowinning of zinc from alkaline solution is economical. In this study, a series of experiments was performed to investigate the electrolysis of zinc from alkaline solution obtained from two-step alkaline leaching. With respect to the aforementioned discussions, due to very low solubility of the metals except zinc in NaOH, the concentrations of the impurities entering the electrowinning cell are in their standard limits. Hence, there was no specific problem in the EW cell.

Figure 8 illustrates the effect of the electrolysis time on Zn(II) concentration in the spent electrolyte of the EW cell. As seen in this figure, the concentration of zinc in the solution falls down indicating that zinc ions deposit on the cathode. Thus, the deposition of zinc was approximately completed within 10 h at 350 A/m^2 for the electrolyte solution containing 19.6 g/dm^3 Zn. Under his condition spongy and powdery zinc deposits was obtained with high purity (over 97%) on the cathode. Subsequently, it was removed easily from the cathode by scraping the metal. The main impurity of this powder is Na_2O resulting from the NaOH usage. To increase the purity of zinc (to over 99%) in the obtained powder, the product was washed in distilled hot water. The aforementioned composition of the zinc powders meets the industrial standards and can be used for gold and silver cementation.
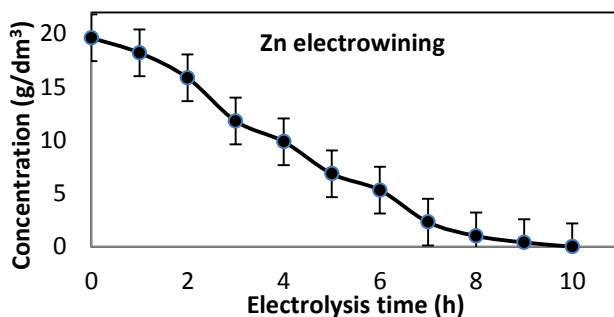
Fig. 8. Concentration versus electrolysis time

Finally, with respect to the stages developed in this study, a simplified flow diagram (Fig. 9) was proposed for the production of zinc powder from the cobalt-zinc plant residue (Co-ZPR), showing the sequential stages according to the conditions obtained in each stage.

Fig. 9. Flow diagram for recovery of zinc from Co filter cake of zinc plant residues

Conclusion

In this study, the production of zinc powder from a Co-Zn plant residue (Co-ZPR) using selective alkaline leaching followed by electrowinning was investigated. With respect to the results of the leaching steps, 88.5% of zinc was selectively leached out in two steps, leaving Co and Mn intact in the solid residue. The condition under which the high leaching recovery of zinc occurred was found to be NaOH concentration 8 M, temperature 75 °C, leaching time 1 h, L/S 10 and rpm 600. Furthermore, a thermodynamic evaluation showed that zinc was leached as an anionic complex (ZnO_2^{2-}) in caustic solution. As a result, the alkaline filtrate solution obtained from the leaching steps could be electrolyzed to produce zinc in a powder form. Therefore, the deposition of zinc was approximately performed in 10 h at 350 A/m^2 with an electrolyte containing 19.6 g/dm^3 Zn. Under this condition, spongy and powdery zinc deposits were obtained. The high purity (over 99%) of zinc powders was obtained after washing the powders. Finally, with respect to the stages developed in this study,

a simplified flow diagram was proposed for the production of the zinc powder from the Co-Zn plant residue.

References

CHEN, A., ZHAO, Z.W., JIA, X., LONG, S., HUO, G., CHEN, X., 2009, *Alkaline leaching Zn and its concomitant metals from refractory hemimorphite zinc oxide ore*. Hydrometallurgy 97, 228–232.

CHEN D.-s., ZHAO L.-s., QI T., HU G.-p., ZHAO H.-x., Li J., WANG L.-n., 2013, *Desilication from titanium–vanadium slag by alkaline leaching.* Transactions of Nonferrous Metals Society of China 23, 3076-3082.

CHENGLONG, Z., YOUCAI, Zh., 2009, *Mechanochemical leaching of sphalerite in an alkaline solution containing lead carbonate.* Hydrometallurgy 100, p. 56.

CUSANELLI, D.C., COFFIN, L.D., RAJCEVIC, H.P., 1973, *U.S. Patent 3, in: 743 (Ed.)*, p. 501.

EACOTT, J.G., ROBINSON, M.C., BUSSE, E., BURGENER, J.E., BURGENER, P.E., 1984, *Technoeconomic feasibility of zinc and lead recovery from electric arc furnace bag-house dust.* Can. Min. Metall. Bull 77 75–81.

DUTRA, A.J.B., PAVIA, P.R.P., TAVARES, L.M., 2006, *Alkaline leaching of zinc from electric arc furnace steel dust. Miner.* Eng. 19, 478–485.

EIVAZI, A.R.H., ALAMDARI, E.K., MPRADKHANI, D., 2008a, *Dissolution kinetics of zinc from zinc plant residue, in: In: Young, C.A. (Ed.)*, Proceedings of the 6th International Symposium: Hydrometallurgy 2008, Vancouver, Canada, pp. 196-200.

EIVAZI, A.R.H., MOEADKHANI, D., ALAMDARI, E.K., DARVISHI., D., 2008b, *Solvent extraction separation of zinc, manganese and cobalt in sulfate solutions by D2EHPA.,* Int. Solvent Extraction Conference, pp. 233-238.

FRENAY, J., 1985, *Leaching of oxidized zinc ore in various media.* Hydrometallurgy 15, 243–253.

GURMEN, S., EMRE, M., 2003, *A laboratory-scale investigation of alkaline zinc electrowinning.* Miner. Eng. 16, 559-562.

JHA, M.K., KUMAR, V., SINGH, R.J., 2001, *Review of hydrometallurgical recovery of zinc from industrial wastes.* Resour. Conserv. Recycl. 33, 1–22.

KIM, T.H., KANG, J.G., SOHN, J.S., RHEE, K.I., LEE, S.W., SHIN, S.M., 2008, *Preparation of Mn-Zn ferrite from spent zinc-carbon batteries by alkali leaching, acid leaching and co-precipitation.* Met. Mater. Int. 14, 655-658.

LIU W., YANG T., ZHANG D., CHEN L., LIU Y., 2014, *Pretreatment of copper anode slime with alkaline pressure oxidative leaching.* International Journal of Mineral Processing 128, 48-54.

MERRILL, C.C., LANG, R.S., 1965, *USBM Report,* p. 6576.

MIRVALIEV, R., INOUE, K., 2001, *Pressure oxidative leaching of molybdenite in alkaline media.* J. Min. Mater. Process. Inst. Jpn. 117, 72–76.

MOHAPATRA M., NAYAK B., SANJAY K., SUBBAIAH T., MISHRA B.K., 2014, *Ligand mediated eco-friendly leaching of zinc from spent catalyst in alkaline media.* Journal of Industrial and Engineering Chemistry 20, 2217-2223.

MORDODAN, H., i EK, T., I IK, A., 1999, *Caustic soda leach of electric arc furnace dust.* Turk. J. Eng. Environ. Sci. 23, 199–207.

MORADKHANI, D., RASOULI, M., BEHNIAN, D., ARJMANDFAR, H., P., A., 2012, *Selective zinc alkaline leaching optimization and cadmium sponge recovery by electrowinning from cold filter cake (CFC) residue.* Hydrometallurgy 115-116, 84–92.

ORHAN, G., 2005, *Leaching and cementation of heavy metals from electric arc furnace dust in alkaline medium.* Hydrometallurgy 78, 236–245.

OGNYANOVA, A., OZTURK, A.T., MICHELIS, I.D., FERELLA, F., TAGLIERI, G., AKCIL, A., VEGLIÒ, F.,2009, *Metal extraction from spent sulfuric acid catalyst through alkaline and acidic leaching.* Hydrometallurgy 100, 20–28.

OLPER, M., 1997, *Extraction of antimony from sulfide ores by alkaline leaching, recovery of elemental sulfur and electrowinning antimony from fluoborate solution.* European Patent Application, Appl. num. 97201300.7.

PEREIRA, J.A.M., SCHWAAB, M., DELL'ORO, E., PINTO, J.C., MONTERIO, J.L.F., 2009, *The kinetics of gibbsite dissolution in NaOH.* Hydrometallurgy 96, 6–13.

REED, W.A., GARNOV, A.Y., RAO, L., NASH, K.L., BOND, A.H., 2005, *Oxidative alkaline leaching of americium from simulated high-level nuclear waste sludge.* Sep. Sci. Technol. 40, 1029–1046.

SAFARZADEH M.S., MORADKHANI D., ILKHCHI M.O., GOLSHAN N.H., 2008, *Determination of the optimum conditions for the leaching of cd–ni residues from electrolytic zinc plant using statistical design of experiments.* Separation and Purification Technology 58, 367-376.

SAFARZADEH, M.S., MORADKHANI, D., ATASHI, P., 2009, *Recovery of zinc from Cd–Ni zinc plant residues.* Hydrometallurgy 97, 67–72.

SHIN, S.M., 2008, *Separation of zinc from spent zinc-carbon batteries by selective leaching with sodium hydroxide.* Hydrometallurgy 96, 349–353.

ST-PIERRE, J., PIRON, D., 1986, *Electrowinning of zinc from alkaline solutions.* J Appl Electrochem 16, 447-456.

VALDEZ, E.G., DEAN, K.C., 1975, *USBM Report*, p. 8000.

ZHAO, Y., STANFORTH, R., 2000, *Production of Zn powder by alkaline treatment of smithsonite Zn–Pb ores.* Hydrometallurgy 56, 237–249.

DESIGN AND EXPERIMENTS USING A SPIRAL-LIQUID-SOLID FLUIDIZED BED SYSTEM

Jie SHA, Long LIANG, Bo LIU, Guangyuan Xie, YAOLI PENG

Key Laboratory of Coal Processing and Efficient Utilization (Ministry of Education), School of Chemical Engineering and Technology, China University of Mining and Technology, Xuzhou 221116, Jiangsu, China, e-mail: xgywl@163.com; peng_yaoli@163.com.

Abstract: Liquid-solid fluidized bed (LSFB) has been widely known and used for separation of coarse coal particles (normally larger than 0.25 mm). The process of separation by LSFB needs fluidization water from the bottom to the top of LSFB. The fluidization water is formed by the water addition at the bottom of the LSFB. Normally the quantity of water addition is very large, which increases the burden of water treatment in coal preparation processes. In this investigation, a spiral unit was introduced into the conventional LSFB and the new separation equipment was named S-LSFB. The spiral unit could provide an upward force for the upward movement of coarse low density coals into the concentrate, and hence the quantity of water addition for fluidization water may be reduced. Samples of 0.5-0.25 mm size fraction coal were used to investigate the difference in separation performance between S-LSFB and LSFB. It was found that the separation performance of S-LSFB was nearly equal to that of LSFB. S-LSFB may be beneficial to coarse coal separation in coal preparation plant since the burden of water treatment can be reduced by the application of S-LSFB.

Keywords: liquid-solid fluidized bed, spiral unit, coal separation, water quantity

Introduction

Fine coal (<0.5 mm) is usually beneficiated by flotation. However, the size fraction of 0.5-0.25 mm may be difficult to float since these coals have relative high weight (Jameson, 2010; Kohmuench et al., 2012). The size fraction of 0.5-0.25 mm can also considered as coarse coal slime in coal preparation industry. The coarse coal is usually difficult to separate by both gravity separating equipment (jig and dense medium cyclone) and flotation equipment (flotation cell and flotation column) (Li, 2008; Fan et al., 2010). As a result, Knelson concentrator, spiral concentrator, small diameter cyclone and liquid-solid fluidized bed (LSFB) are used in coarse coal separation (Uslu et al., 2012; Mukherjee and Mishra, 2007; Sha et al., 2012). Liquid-solid fluidized bed

(LSFB) is created based on the fluidization technique and used to separate coarse coal particles ranging from 0.2 to 2 (1) mm. The separation process of coarse coal particles in the liquid-solid fluidized bed has been observed by many researchers (Chu et al., 2012; Ganguly, 1986; Mukherjee and Kumar, 2009; Sha et al., 2011). Computational fluid dynamics (CFD) simulation technologies have been used to investigate the separation performance of particles in the liquid-solid fluidized bed and also the flow behavior in fluidized bed has also been investigated (Zhang et al., 2012; Wang et al., 2012). Meanwhile, the changes in size, density and ash content of coal particles on the column axis have been observed (Li et al., 2013). Usually, a wide size range of coal particles in LSFB may worsen the separation process (Li, 2008; Sha et al., 2012; Galvin et al., 2010). The separation process in LSFB needs the fluidization water to form a separation density. The fluidization water is formed by the water addition at the bottom of LSFB. Normally the quantity of water addition is very large, which may increase the burden of water treatment in coal preparation processes. As a result, coal preparation plant makes many efforts into the dewatering of coal products and the treatment of water slurry since water should be reused in coal separation processes. Especially, water should be economized in some arid and semiarid areas. The water addition in the separation process of LSFB may be antinomy to water conservation.

The upward fluidization water, which is the main force of coarse coal particles separation in LSFB, is required to be uniform in both axial and radial directions. Usually, it is easy to provide a more even radial fluidization water with a water distributor (Maharaj et al., 2007). However the uniform of axial direction is hard to implement because of the change of solid volume concentration in the axial direction, which cause a reduction in the force to particles in the top area of the cell and thus not enough flow. Recently, a lot of attempts of changing the structure to overcome the non-uniform of axial were observed to improve the separation effect, such as using jigging water (Galvin et al.,2002), combining flotation and fluidization (Sarkar et al., 2008; Das et al., 2009), and joining a series of inclined plate (Galvin et al., 2010; Iveson et al., 2014).

In this investigation, a spiral unit was introduced into the conventional LSFB and the new separation equipment was named S-LSFB. The spiral unit could provide an upward force for the upward movement of coarse low density coals into the concentrate, and hence the quantity of water addition for fluidization water may be reduced. The separation performance of S-LSFB will be compared with that of LSFB and some constructive suggestions will be obtained throughout this paper.

Materials and experimental procedure

Materials

Samples of 0.5-0.25 mm size fraction coal were used to investigate the difference in separation performance between S-LSFB and LSFB. The results of the float-sink tests are shown in Table 1. Table 1 is a summary of the cumulative floats at a specific

density. It indicates that a clean coal with yield of 86.02% and 11.89% ash content can be obtained at a separation density of 1.8 g/cm^3. The theoretical clean coal yield is 79.10% with ash content of 9.36%. The coal samples contain many low density and ash coal particles. In addition, the yields of near-gravity materials at gravities of 1.5 to 1.7 g/cm^3 range from 15.65% to 6.92%. It shows that the coal samples are easy to separate.

Table 1 Float-sink test results of 0.5-0.25 mm size fraction

Gravity range (g/cm^3)	Float		Cumulative floats		Cumulative sinks	
	Weight (%)	Ash (%)	Weight (%)	Ash (%)	Weight (%)	Ash (%)
<1.30	31.57	3.24	31.57	3.24	100.00	19.76
1.30-1.40	31.88	8.80	63.45	6.03	68.43	27.37
1.40-1.50	9.42	19.05	72.87	7.71	36.55	43.58
1.50-1.60	6.23	28.57	79.10	9.36	27.13	52.10
1.60-1.80	6.92	40.84	86.02	11.89	20.90	59.11
>1.80	13.98	68.15	100.00	19.76	13.98	68.15

Experimental system

Figure 1 is a picture of the LSFB. The LSFB is 100 mm in the diameter and 810 mm in the height. The coal slurry was fed into LSFB from the feed inlet. The upward water quantity was fixed at 400, 500, 600 and 700 dm^3/h from the bottom of the liquid-solid fluidized bed. The pulp taken from concentrate and tailings was collected, filtered, dried and analyzed by the float-sink tests.

Figure 2 is the picture of S-LSFB. S-LSFB is 100 mm in the diameter and 700 mm in the height. The coal slurry was fed into S-LSFB from the feed inlet. The upward water was fed into S-LSFB by a tube and the quantity of water was adjusted by a valve. The upward water quantity was fixed at 100, 150 and 200 dm^3/h from the bottom of the liquid-solid fluidized bed. A spiral unit was introduced into the conventional LSFB. The diameter of spiral blade is 96 mm and the pitch is 100 mm. The blade has a thickness of 2.5 mm. The revolution speed of spiral blade was adjusted by a motor with a power of 1.5 kW. The direction of rotation was at a counterclockwise direction. The revolution speed was fixed at 247, 261 and 276 rpm. The feed density of LSFB or S-LSFB is 300 g/dm^3. The pulp taken from concentrate and tailings was collected, filtered, dried and analyzed by the float-sink tests. Both the results of LSFB and S-LSFB are obtained by dozens of measurements (in a period of 30 min) and representative and reproducible.
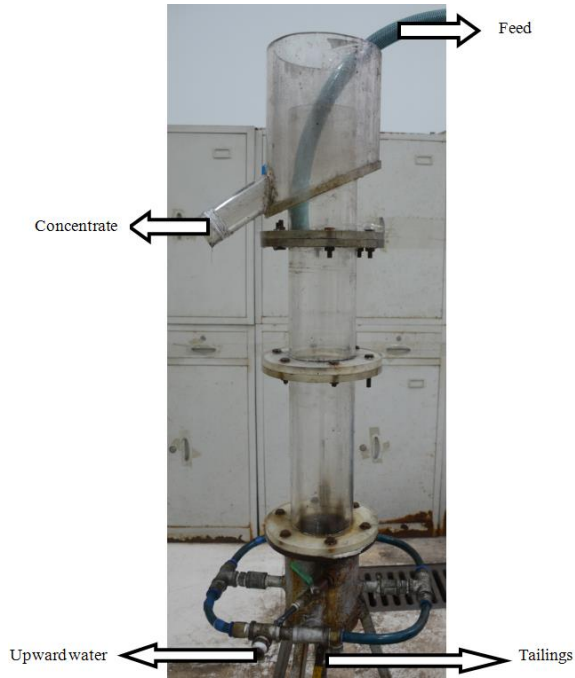
Fig. 1. Picture of liquid-solid fluidized bed (LSFB)
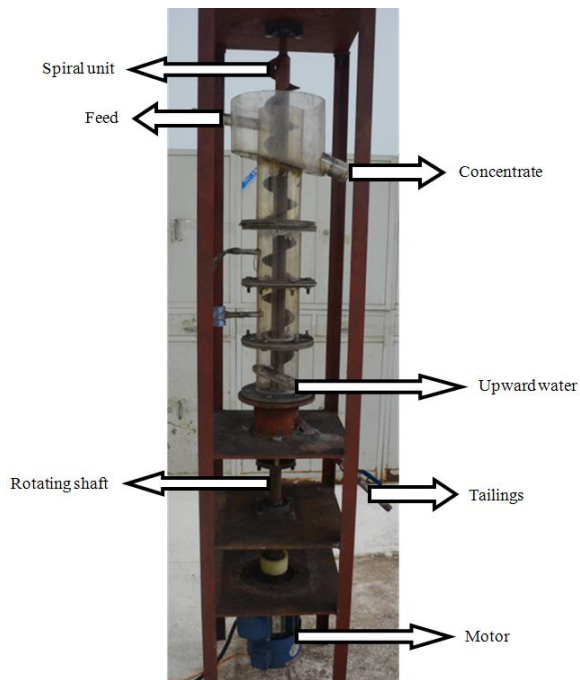
Fig. 2. Picture of spiral-liquid-solid fluidized bed (S-LSFB)

Results and discussion

Separation of LSFB

As shown in Table 2, both the concentrate yield and concentrate ash increase with the increase of upward water quantity. The organic efficiency is also increased. In this investigation, the concentrate ash should be controlled below 10%. Therefore, the concentrate obtained at the upward water quantity of 600 dm^3/h is used as the result at the optimum operating condition. The upward water flow velocity increases with the increase of upward water quantity. Higher flow velocity can lift more coal particles (especially, low density coal particles). It means that high upward water flow velocity can produce a high separation density (Wang et al., 2009). The separation efficiency of liquid-solid fluidized bed is affected by many factors, such as particle size, yield of near-gravity materials and particle density distribution (Mukherjee and Mishra, 2007). In some cases, some larger particles with low density are lost in tailings while some smaller particles with high density are carried into concentration. This causes a mismatch of both tailings and concentration. However, the separation efficiency in this investigation is very high compared with other liquid-solid fluidized beds in the literature (Sha et al., 2011; Li, 2008). The high separation efficiency in this investigation is due to the size composition of coal samples is 0.5-0.25 mm which is a narrow size range. A narrow size range is suitable and easy to separate compared with wide size range (Mukherjee et al., 2009).

Table 2. Separation results of coal samples in liquid-solid fluidized bed (LSFB)

Upward water quantity (dm^3/h)	Concentrate		Tailings		Organic efficiency (%)
	Ash (%)	Yield (%)	Ash (%)	Yield (%)	
400	7.09	55.37	35.47	44.63	78.65
500	8.57	63.86	39.52	36.14	83.58
600	9.96	68.77	41.32	31.23	84.59
700	11.07	78.19	50.89	21.81	92.65

Separation of S-LSFB

Table 3 shows the separation results of coal samples in spiral-liquid-solid fluidized bed (S-LSFB). Both the concentrate yield and concentrate ash increase with the increase of revolution speed at the same upward water quantity. A higher revolution speed produces a higher upward water flow, and hence more coal particles (especially, low density coal particles) can be lifted into the overflow. Meanwhile, both the concentrate yield and concentrate ash increase with the increase of upward water quantity at the same revolution speed. It indicates that a higher quantity of upward water can also increase both the concentrate yield and concentrate ash. The best result can be obtained at the upward water quantity of 150 dm^3/h and the revolution speed of 247 rpm since the concentrate ash should be controlled below 10% in this investigation.

In this investigation, a spiral unit was introduced into the conventional LSFB. The spiral unit can produce a lift force for the upward moving of coal particles. Duan et al. (2014) used an inflatable unit to produce bubbles for improving the separation efficiency of liquid-solid fluidized bed. The bubbles could increase the lift force for particles into the concentration and save the upward water quantity. The upward water is needed in the separation process of LSFB, which increase the burden of water treatment in coal preparation processes. Therefore, the water used in coal preparation processes should be controlled to save both the water resource and the economy.

Table 3. Separation results of coal samples in spiral-liquid-solid fluidized bed (S-LSFB)

Upward water quantity (dm³/h)	Revolution speed (r/min)	Concentrate		Tailings		Organic efficiency (%)
		Ash (%)	Yield (%)	Ash (%)	Yield (%)	
100	247	8.31	54.35	35.77	45.65	71.98
100	261	8.95	56.43	36.27	43.57	72.35
100	276	10.41	63.57	39.07	36.43	77.06
150	247	9.89	67.27	43.38	32.73	83.15
150	261	10.22	69.10	44.63	30.90	84.37
150	276	12.03	73.40	45.18	26.60	85.06
200	247	11.29	73.15	46.90	26.85	86.47
200	261	13.37	83.46	58.58	16.54	93.88
200	276	13.91	85.03	60.26	14.97	94.69

Comparison of LSFB and S-LSFB

Table 4 shows the best results from LSFB and S-LSFB. It indicates that the organic efficiency of LSFB is 84.59% which is a little higher than that of S-LSFB (83.15%). Even though the organic efficiency of S-LSFB is a little lower than that of LSFB, the upward water quantity for S-LSFB is a lot lower than that of LSFB. The upward water quantity for LSFB is four times as large as that of S-LSFB. It is believed that the burden of water treatment using LSFB is much higher than that using S-LSFB. However, an additional energy input is given into the separation process of S-LSFB. Maybe the comprehensive benefits of using S-LSFB instead of LSFB should be considered further.

Table 4. Comparison of the best results from LSFB and S-LSFB

Separation system	Upward water quantity (dm³/h)	Revolution speed (r/min)	Concentrate		Organic efficiency (%)
			Ash (%)	Yield (%)	
LSFB	600		9.96	68.77	84.59
S-LSFB	150	247	9.89	67.27	83.15

Conclusions

A spiral unit was introduced into the conventional liquid-solid fluidized bed (LSFB) and the new separation equipment was named spiral-liquid-solid fluidized bed (S-LSFB). The spiral unit can produce the upward water flow, which may reduce the burden of water treatment in the conventional LSFB. A comparison of separation performance of LSFB and S-LSFB was conducted. It was found that the separation performance of S-LSFB was nearly equal to that of LSFB. The organic efficiency of LSFB is 84.59% which is a little higher than that of S-LSFB (83.15%).

With a similar concentrate ash, the upward water quantity for LSFB is four times as large as that of S-LSFB. It indicates that using S-LSFB can reduce the burden of water treatment in the conventional LSFB. The burden of water treatment using LSFB is much higher than that using S-LSFB. However, an additional energy input is given into the separation process of S-LSFB. Maybe the comprehensive benefits of using S-LSFB instead of LSFB should be considered further.

Acknowledgements

References

CHU, Z.F., XIE, J.X., LI, Y. F., 2012, *Effect of properties of materials on solids distribution in a binary mixture liquid-solid fluidized bed,* Journal of China University of Mining and Technology 41(4), 620-623.

DAS, A., SARKAR, B., MEHROTRA, S.P., 2009, *Prediction of separation performance of floatex density separator for processing of fine coal particles,* International Journal of Mineral Processing, 91, 41-49.

DUAN, C.L., ZHAO, Y.M., WU, L.L., SHENG, C., ZHOU, C.Y., CAI, L.H., 2014, *Research on separation of waste printed circuit boards by an inflatable liquid-solid fluidized bed,* Journal of China University of Mining and Technology 43(5), 915-919.

FAN, M.M., TAO, D., HONAKER, R., LUO, Z.F., 2010, *Nanobubble generation and its applications in froth flotation (part IV): Mechanical cells and specially designed column flotation of coal,* Mining Science and Technology, 20(5): 641-671.

GALVIN, K.P., CALLEN, A.M., SPEAR, S., 2010, *Gravity separation of coarse particles using the Reflux Classifier*, Minerals Engineering 23, 339-349.

GALVIN K.P., ZHOU J., WALTON K., 2010, *Application of closely spaced inclined channels in gravity separation of fine particles,* Minerals Engineering, 23:326-338.

GALVIN, K.P., PRATTEN, S.J., LAMBERT, N., CALLEN, A.M., LUI, J., 2002, *Influence of a jigging action on the gravity separation achieved in a teetered bed separator,* Minerals Engineering; 15, 1199–1202.

GANGULY, U.P., 1986, *Elutriation characteristics of solids from liquid-solid fluidized bed systems; part iii: a study of the possible causes of non-linearity in the elutriation of fine particles from fluidized beds,* Canadian Journal of Chemical Engineering 64(1), 171-174.

IVESON, S. M., MASON, M., GALVIN, K.P., 2014, *Gravity separation and desliming of fine coal: pilot-plant study using reflux classifiers in series,* International Journal of Coal Preparation and Utilization 34, 239-259.

JAMESON, G. J., 2010, *New directions in flotation machine design,* Minerals Engineering, 23(11-13): 835-841.

KOHMUENCH, J.N., MANKOSA, M.J., 2012, *Christodoulou L. Practical and proven methods for improving ultrafine and coarse particle recovery,* Separation Technologies for Minerals, Coal, and Earth Resources, 447-456.

LI, Y.F., 2008, *Study on the separation mechanism and application of liquid-solid fluidized bed coarse slime separator,* Xuzhou: China University of Mining and Technology.

LI, Y., ZHAO, W., XU, S., XIA, W., 2013, *Changes of size, ash and density of coal particles on the column axis of a liquid–solid fluidized bed,* Powder Technology, 245:251-254.

MAHARAJ, L., POCOCK. J., LOVEDAY. B.K., 2007, *The effect of distributor configuration on the hydrodynamics of the teetered bed separator,* Minerals Engineering 20,1089-1098.

MUKHERJEE, A. K., KUMAR, A., 2009, *Liquid/solid fluidization its role and limitation in fine beneficiation-A review,* Mineral Processing and Extractive Metallurgy Review 30(3), 280-306.

MUKHERJEE, A.K., MISHRA, B.K., 2007, *Experimental and simulation studies on the role of fluid velocity during particle separation in a liquid–solid fluidized bed,* International Journal of Mineral Processing 82, 211-221.

MUKHERJEE, A. K., MISHRA, B. K., KUMAR, R. V., 2009, *Application of liquid/solid fluidization technique in beneficiation of fines,* International Journal of Mineral Processing, 92(1), 67-73.

SARKAR, B., DAS, A., MEHROTRA, S.P., 2008. *Study of separation features in floatex density separator for cleaning fine coal,* International Journal of Mineral Processing. 86,40-49.

SHA, J., XIE, G., WANG, H., LIU, J., TANG, L., 2012, *Effect of the column height on the performance of liquid-solid fluidized bed for the separation of coarse slime,* International Journal of Mining Science and Technology 22(4), 585-588.

SHA, J., XIE, G.Y., PENG, Y.L., SHI, B.X., 2011, *Hydrodynamics of Coarse Coal Slime and Quartz Particles in a Liquid-Solid Fluidized Bed Separator,* Mechanics, Solid State and Engineering Materials, Advanced Materials Research, 279, 350-355.

WANG, X., JIN, B., ZHONG, W., XIAO, R., 2009, *Modeling on the hydrodynamics of a high-flux circulating fluidized bed with Geldart group A particles by kinetic theory of granular flow,* Energy & Fuels, 24(2), 1242-1259.

WANG, S., GUO, S., GAO, J., LAN, X., DONG, Q., LI, X., 2012, *Simulation of flow behavior of liquid and particles in a liquid-solid fluidized bed,* Powder Technology 224, 365-373.

USLU, T., SAHINOGLU, E., YAVUZ, M., 2012, *Desulphurization and deashing of oxidized fine coal by Knelson concentrator,* Fuel Processing Technology 101, 94-100.

ZHANG, K., WU, G., BRANDANI, S., CHEN, H., YANG, Y., 2012, *CFD simulation of dynamic characteristics in liquid–solid fluidized beds,* Powder Technology 227, 104-110.

NEODECANOIC ACID AS EXTRACTANT OF SELECTED NON-FERROUS METALS

Leszek GOTFRYD, Grzegorz PIETEK, Zbigniew SZOŁOMICKI, Ksawery BECKER, Justyna PIWOWONSKA

Institute of Non-Ferrous Metals, Hydrometallurgy Dept., Sowińskiego 5, 44-100 Gliwice, Poland, leszekg@imn.gliwice.pl

Abstract: The paper presents results of studies on extracting properties of neodecanoic acid (Versatic 10) solutions. Neodecanoic acid was diluted in Exxsol D80 AZ to three concentrations: 7.5, 15, and 30 % ($^v/_v$). Tests were conducted using sulphate(VI) solutions of six ions: Zn(II), Ni(II), Cu(II), Co(II), Cd(II), Mn(II) and a nitrate(V) solution of Pb(II). All the aqueous solutions were prepared as 0.1 M concentration. For all combinations of the used solutions (organic and aqueous), direct methods of measuring and recording the pH of the biphasic mixture have been applied. The degrees of ions extraction, depending on equilibrium pH were also presented in the paper. Extraction and stripping isotherms of selected ions and organic phase were plotted for 7.5 and 30 % ($^v/_v$) of extractant solutions and Zn(II), Ni(II) and Cu(II) ions.

Introduction

Neodecanoic acid is a commercial mixture of organic acids with common formula $R_1R_2CH_3CCOOH$, where R_1 and R_2 are hydrocarbon chains with number of carbon atoms equal to seven. The extractive properties of neodecanoic acid (Versatic 10) have been known for years (Net 1, 2014; Net 2, 2014; Preston and Du Preez, 1985). It is a well-known reagent in petrochemical and chemical industries due to its organic acid nature. It is used as a solvent or active reagent (especially in a form of its esters, salts, acid chloride etc.) (Net 1, 2014; Net 2, 2014). A highly branched structure of Versatic 10 results in high stability, that is resistance to oxidation, hydrolysis etc. These features are also beneficial for application as solvent in extraction processes.

Initially, the extractant was suggested for use for either zinc extraction, especially from chloride solutions (Sanuki et al., 1982 and 1983) or directly for organic solution in zinc leaching from powdery secondary materials in parallel with Versatic 911 (Jha

et al., 2001). The extractive properties of Versatic 10 for nickel(II) extraction from highly contaminated (Mg) solutions after leaching lateritic ores were recognized in 70's of the last century (Preston, 1983; Preston and du Preez, 1995). The neodecanoic acid is still within the scope of interest of researchers (Cheng et al., 2010, Sinha et al., 2012). Versatic 10 is also an interesting extractant because of its special properties in mixtures with other extractants (e.g. Cyanex 272, LIX 63, oximes, esters) (Preston, 1983; Preston and du Preez, 1995). The mixture components interact synergistically with each other and provokes better selectivity of nickel extraction. Some of these two-extractant systems inhibit transfer of calcium to stripped solution, which prevents gypsum precipitation (du Preez et al., 2007; Preez et al., 2004; Preston et al., 2000), while the well-known extraction systems using DEHPA and Cyanex 272 for nickel(II) separation (Gharabadhi et al., 2013), even from zinc(II) and cobalt(II), do not solve gypsum precipitation problem (Gotfryd, 2005).

Aim of the work

In this paper the objective of interest was the extractive property of Versatic 10 diluted with hydrocarbon Exxsol D80 AZ solvent. The aim of the work was to recognize the dependency of extraction degree on pH, extraction and stripping isotherms and the practical time of extraction of both extractive processes for selected inorganic cations. A novel direct method of measurements of extraction time and stripping time was used. The neodecanoic acid reacts with several metals cations. The obtained compounds are highly soluble in organic phases and weakly soluble in aqueous phases. Their stability during extraction and stripping processes was the object of interest. The maximum extraction capacities of the saturated organic phase for a given cations were tested. Also viscosity of obtained saturated organic phases was the matter of concern.

Materials used for testing

The organic phases were Versatic 10 (Momentive, Poland) solutions having concentrations of 7.5, 15 and 30 % ($^v/_v$). They were diluted in hydrocarbon solvent Exxsol D80 AZ (Brenntag, Polska / ExxonMobil). The aqueous phases were 0.10 M sulphate(VI) solutions of zinc(II), nickel(II), copper(II), cobalt(II), cadmium(II) and manganese(II) and 0.10 M solution of lead(II) nitrate(V). Additionally, standard solutions of 5.0 M sodium hydroxide (for pH correction), 2.0 M and 10.0 M sulphuric acid as well as 4.0 M and 14.4 M nitric acid (for stripping) were used in the investigations.

Experimental

Extractive procedures

All extractive procedures were performed at ambient temperatures using mechanical

800 rpm stirring with a typical laboratory glass propeller. After mixing and/or attaining expected pH, the samples of reacting phases were divided using either a separation funnel and/or filter paper and analysed for metal ion content.

Procedure I (degree of extraction versus equilibrium pH)

Organic (O) and aqueous (A) phases at initial volumetric proportion of 400/400 cm^3/cm^3 were mixed together until a stable pH was observed (typically after 10 minutes). Then, equal aliquot volume samples (50 cm^3) of each phase were separated and analysed for metal ion concentration. The rest of reacting mixture (350/350 cm^3/cm^3) was next treated in the similar way with NaOH solution. This procedure was repeated several times and each time 2.0 cm^3 portion of 5.0 M NaOH was added. The degree of extraction [% E] was calculated as:

$$[\%E] = 100 \cdot \frac{Me(O)}{Me(O) + Me(A)}, \tag{1}$$

where *Me(O)* is the metal ion concentration in the organic phase while *Me(A)* is the metal ion concentration in the aqueous phase.

Procedure II (extraction isotherms at constant pH)

Organic phase and aqueous phase (metal salt solution) were mixed together at different ratios (e.g., A:O from 1:6 to 2:1) with portions of 5.0 M NaOH gradually added until expected equilibrium pH was reached.

Procedure III (stripping isotherms)

Step I - saturation of organic solution with specific cation: it was performed according to procedure II at O:A proportion 1:1. Step II (stripping): saturated organic phase (O) from step I was filtered and mixed with 1.00 M H_2SO_4 solution (A) with different volume proportions (typically O:A = 1:10 to 10:1) for 10 minutes.

Procedure IV (time of extraction)

Aqueous (feed) and organic phase (stripped regenerated extractant) were mixed together while keeping the continuity of the aqueous phase (at volumetric proportion 1:1). The reaction advance was controlled by continuous measurements of pH. The 0.500 cm^3 portions of 5.0 M NaOH were being added several times during the mixing to increase step by step the equilibrium pH value. The total time of reaction, after each portion of added NaOH solution, was determined basing on the measurements of the individual graph peak widths (from sodium hydroxide addition point until pH stabilization point - see Fig. 5). The mentioned consecutive times of reaction were plotted on a new graph (reactions times versus hydroxide consumption - cumulative dose of NaOH solution).

Procedure V (time of stripping)

Saturated organic phase (see procedure III, step I) and distilled water were mixed together at O:A = 100:100 cm^3/ cm^3, keeping the continuity of the aqueous phase. The pH of reactions mixtures were measured (as in procedure IV). The reaction was performed by adding to the mixture a small amount (1.0 cm^3) of 10.0 M H$_2$SO$_4$, or in case of Pb(II) 14.4 M HNO$_3$ solution (90-95% of stoichiometric quantity). The reaction (stripping) time was read from the graph in the same manner as in the extraction time measurement procedure.

Viscosity measurements

The viscosities of saturated organic phases are important factors in solvent extraction. The measurements were performed using apparatus Rheotec RC01 - R, with a spindle R2. Following the procedure described in the manual, one can obtain directly displayed values of dynamic viscosity (in cP).

Analytical methods

After phases separation and filtration using tissue paper, metal ion concentration of both phases (organic and aqueous) were analysed. The samples of aqueous phases were analysed directly and the organic phases samples were stripped twice with either 2.0 M H$_2$SO$_4$ solution or 4.0 M HNO$_3$ solution (the last only for Pb(II)) at a volume ratio O:A = 2:1. After stripping both aqueous phases were combined and then analysed. The standard procedure was complexometric titration with 0.05 M EDTA solution to determine the Me(II) concentration.

Results and discussion

Degree of extraction versus equilibrium pH

Three sets of results were obtained according to procedure I, each for a particular concentration of the extractant (Fig. 1.).
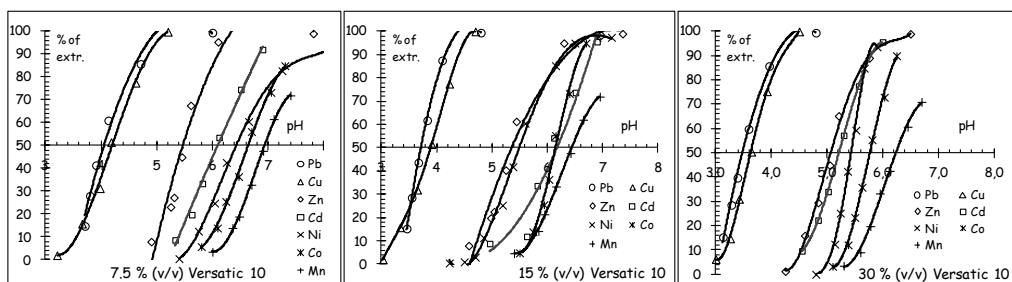
Fig. 1. Degree of extraction versus equilibrium pH for Pb(II), Cu(II), Zn(II), Ni(II), Cd(II), Co(II), Mn(II) at 7.5, 15 and 30 % ($^v/_v$) Versatic 10 / Exxsol D80 AZ

Extraction isotherms

Procedure II (limited to Zn(II), Ni(II), Cu(II) and 7.5 and 30 % ($^v/_v$) extractant) led to a data set of extraction isotherms shown in Fig. 2.
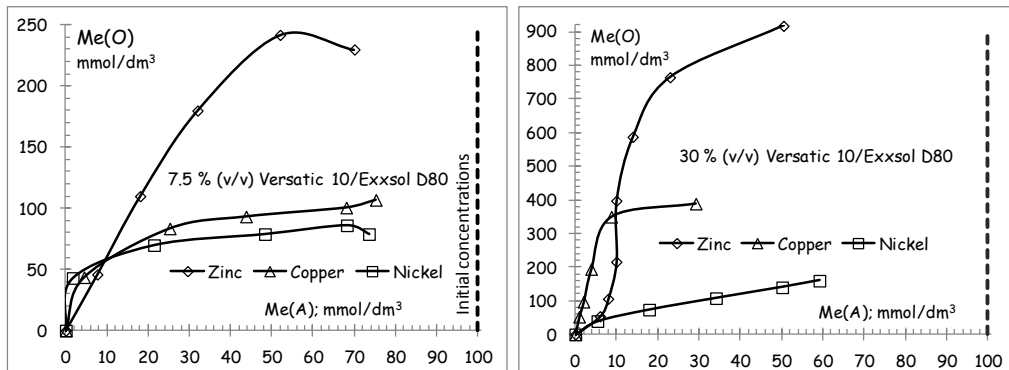
Fig. 2. Extraction isotherms of Cu(II), Zn(II) and Ni(II) (7.5 and 30 % ($^v/_v$) solutions of Versatic 10); Me(O) - cation concentration in organic phase, Me(A) - cation concentration in aqueous phase

For comparison of extraction isotherm results the data were expressed in molar concentrations (mmol dm^{-3}). Most of data were determined at optimum equilibrium pH levels (Table1).

Table 1. Optimum equilibrium pH value and level of saturation

	7.5 % ($^v/_v$) Versatic 10		30 % ($^v/_v$) Versatic 10	
	pH	Saturation level (g/dm^3)	pH	Saturation level (g/dm^3)
Zinc	5.80	15.8	5.95	60.0
Copper	4.50	7.0	4.60	26.0
Nickel	7.20	5.6	5.80	10.4

Nickel(II) extraction with 30 % ($^v/_v$) of Versatic 10 is a special case, which was carried out at pH 5.8 which is less than optimal, due to the tendency to form emulsions at higher values of this parameter.

Stripping isotherms

In Fig. 3 the results of measurements of the stripping isotherms carried out according to procedure III are presented. Initial saturation levels of the organic phases with cations are marked with vertical lines.
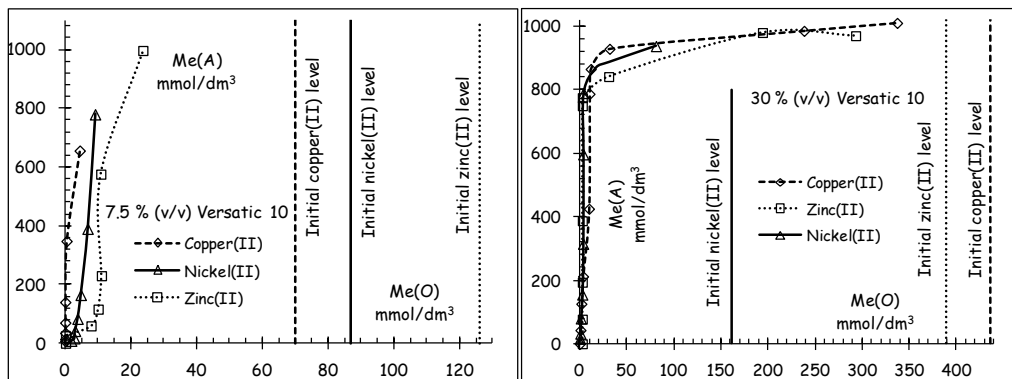
Fig. 3. Stripping isotherms of copper(II), zinc(II) and nickel(II) at 7.5, 30 % ($^v/_v$) Versatic 10

In all three cases Zn(II), Ni(II), Cu(II), at the extractant of 30 % ($^v/_v$) concentration, a complete neutralization of the acid was observed. The same seems to be possible for 7.5 % ($^v/_v$) Versatic 10, after application of the higher proportion of the organic to aqueous phases (more than 10:1).

Time of extraction

The direct method for recording pH changes as a function of time was used. The measurements started when the first dose of 5.0 M sodium hydroxide was added. The typical "waveforms" are presented in Figure 4 and 5.
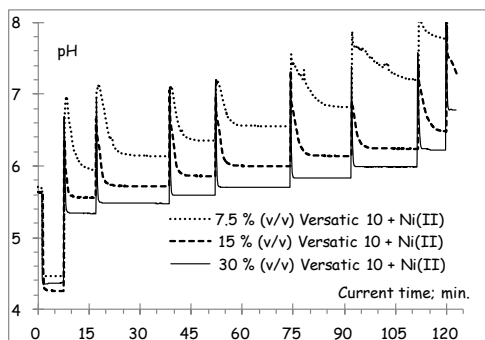
Fig. 4. pH changes for Ni(II) extraction (response to 0.5 cm^3 5.0 M NaOH portions added; Versatic 10 versus 0.10 M NiSO$_4$)
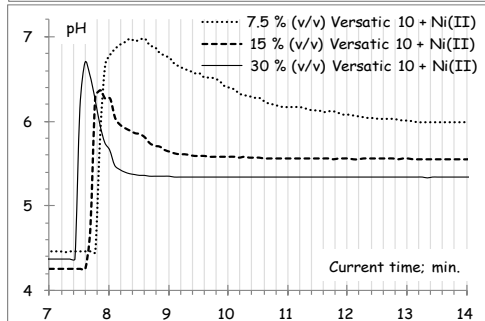
Fig. 5. Direct measurements of extraction time (close-up view of a fragment of Fig. 4)

The width of each peak represents time required for NaOH solution consumption (time of extraction). The changes in these values versus sum of used NaOH solution portion are presented in Fig. 6.
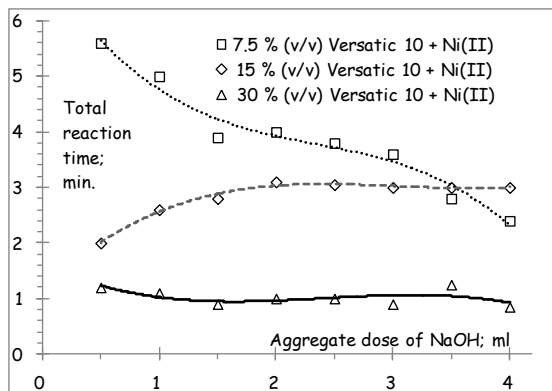
Fig. 6. Time of reaction versus sum of NaOH solution portions for (Ni(II) extraction. Extractant: Versatic 10. Neutralizing agent: 5.0 M NaOH

For other studied systems (extractions of other ions), similar data were collected. The extraction times are inversely proportional to the extractant concentration for all tested ions. When the extractant is more concentrated, shorter extractions times were observed. In some cases (7.5 %, $^v/_v$) extractant reacts 2-3-fold slower than the 30 % ($^v/_v$) one (Table 2). The lowest extractions times for 30 % ($^v/_v$) extractant were about 1 to 1.5 min (extraction of Zn(II), Ni(II) and Cu(II)). The highest measured extraction time for 7.5 % ($^v/_v$) extractant was about 5 to 5.5 min for Ni(II) and from 4 to 4.5 min for Cu(II) extraction. The extraction times at the beginning, in the middle course and at the end of the process are often different. The cadmium(II) extraction time (from 0.5 to 2.5 min) was the lowest of all measured ones. The same pattern was observed for lead(II) in nitrates(V) environment. In the cases of Co(II) and Mn(II) extraction, there were very strong interferences associated with the catalytic activity of these cations (especially for 7.5 % ($^v/_v$) extractant).

Table 2. Time of extraction

Cation	Versatic 10, % ($^v/_v$)		
	7.5	15	30
	minutes		
Zn(II)	2.3-3.1	1.55-2.6	1.0-1.45
Ni(II)	2.8-4.0	2.6-3.1	0.90-1.25
Cu(II)	2.80-4.9	1.6-2.7	1.3-1.6
Co(II)	0.80-1.3	0.40-0.90	0.75-1.65
Cd(II)	1.4-2.5	0.80-1.45	0.60-0.85
Mn(II)	0.30-1.0	0.80-1.9	3.0-6.6
Pb(II)	2.1-2.6	0.55-0.85	0.50-0.73

Time of stripping

The investigation was carried out using a technique similar to the extraction time measurements. The portions of either 10.0 M H_2SO_4 or 14.4 M HNO_3 (90% of the stoichiometric amount) were the impulses for pH changes. Graphical shapes of system responses quite often were perfect, as observed for stripping lead from either 7.5 or 15 % ($^v/_v$) Versatic 10 (Fig.7). Some cases needed further investigation.
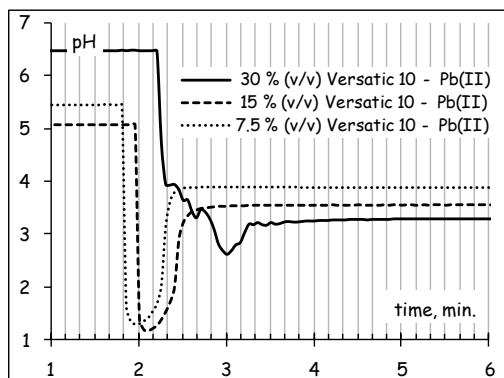
Fig. 7. Direct measurements of stripping time of lead(II)

Reactions times read from the stripping graphs, as a total duration of interference, are summarized in the Table 3.

Table 3. Initial saturation level, dynamic viscosity and time of stripping reaction

V. 10; % ($^v/_v$)	7.5	15	30	7.5	15	30	7.5	15	30
	Initial Me(II) saturation			Dynamic viscosity			Stripping time		
Cation Me(II)	mol/dm^3			cP			minutes		
Pure extractant	0.000	0.000	0.000	2.3	2.5	3.2	*not applicable*		
Zn(II)	0.116	0.113	0.112	2.3	3.0	3.2	-	3.60	≥ 4.0
Ni(II)	0.095	0.104	0.100	2.5	2.6	3.4	-	2.10	3.75
Co(II)	0.080	0.080	0.084	2.5	2.8	3.2	-	-	-
Cu(II)	0.104	0.102	0.103	2.3	2.6	3.4	0.75	0.90	1.03
Cd(II)	0.102	0.097	0.110	2.1	2.5	3.0	-	1.35	1.85
Mn(total)	0.089	0.082	0.086	2.5	2.8	3.4	2.00	-	1.35
Pb(II)	0.103	0.103	0.103	2.3	2.6	3.4	0.70	0.85	1.10

Some of the saturated organic phase samples, especially containing Co(II), but also samples of Mn(II) in a solution of 15 % ($^v/_v$) Versatic 10 were degraded in a natural manner during storage (probably by autocatalytic oxidation). Excessive amounts of a free extractant in organic solutions seems to be the reason for the delayed (slower) stripping from richer solution of the extractant. It appears in the form of slightly higher viscosities of more concentrated extractants (saturated or not).

Viscosities

Dynamic viscosities of organic phases saturated with cations to the level of ≤ 0.1 M were measured before stripping time experiments. The results have already been shown in Table 3 and Fig. 8.
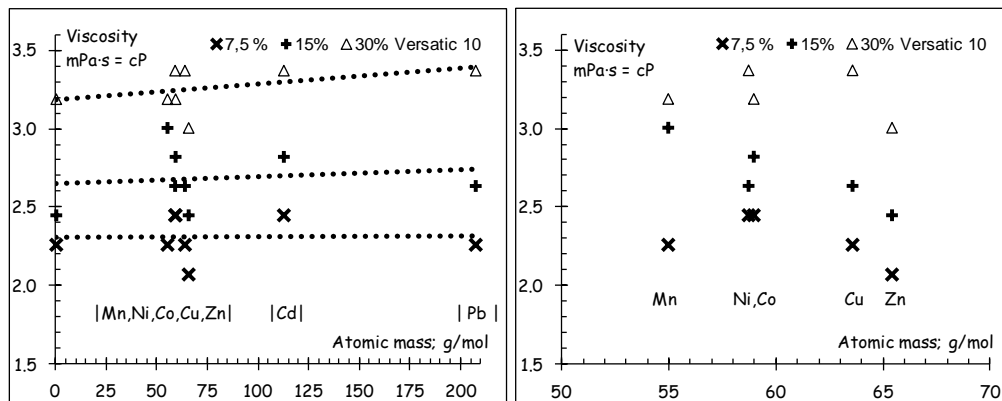
Fig. 8. Viscosities of organic phases containing Versatic 10 and metal ions

Organic phases, much more saturated with ions, show also stronger increase of their viscosities as it is shown in Table 4.

Table 4. Viscosities of selected saturated organic phases (Versatic 10/Exxsol D80 AZ)

	Versatic 10	Cation concentration		Dynamic viscosity
Zn^{2+}	7.5	8.0	0.122	2.6
	30	26.0	0.398	4.8
Cu^{2+}	7.5	4.5	0.071	2.8
	30	28.0	0.441	5.1
Ni^{2+}	7.5	6.0	0.128	2.8
	30	18.5	0.315	5.0
	% ($^v/_v$)	g/dm^3	mol/dm^3	mPa·s

Summary and conclusions

The extraction and stripping characteristics of Versatic Acid 10 extractant (neodecanoic acid) were investigated. The behavior of the extractants was examined at three concentrations of 7.5, 15 and 30 % ($^v/_v$) in hydrocarbon solutions (Exxsol D80 AZ). All tests were carried out with non-ferrous 0.10 M metal salts solutions, not only for Zn(II) and Ni(II), but also for Cu(II), Co(II), Cd(II), Mn(II) (sulphates) and Pb(II) (nitrate). The basic parameters of extraction and stripping (times of reactions, isotherms of extraction and stripping and saturations levels) for selected cations were obtained. A direct current continuous control method of the extraction process was

developed and practically applied during the research. It involves also direct pH measurements in biphasic reacting mixtures.

It can be stated that:
- Versatic 10 shows extraction abilities for all tested non-ferrous metal cations in the following order on the pH scale: Pb(II), Cu(II) (pH ≤ 4.0); Zn(II) and Cd(II) (pH 5.5-6.0); Ni(II), Co(II) and Mn(II) (pH ≥ 5.5-6.0),
- selectivity of cation extractions slightly increases with decreasing extractant concentration; this is especially true for Ni(II) extraction, which is most delayed,
- a modified method for extraction and stripping direct observation and control has been tested and confirmed. It consists of measuring and recording the pH of reacting two-phase mixture directly in the mixing chamber,
- the pH real-time measurement and registration method in a biphasic reaction medium is useful either in measuring the total times of extraction (from aqueous to organic phase) or (under certain conditions) during the stripping processes,
- mixing time, necessary to accomplish extraction reaction, under established conditions, never exceeds a few minutes and tends to be shorter with the increase of the extractant concentration,
- average time of cation extraction is the shortest for Co(II) and Cd(II) (0.6 to 1.2 min), next are Zn(II) (1.2 to 2.1 min) and Pb(II) (0.6 to 2.4 min), then Ni(II) (1.1 to 3.4 min) and Cu(II) (1.5 to 3.8 min),
- higher concentration of the extractant causes longer times of stripping reaction.

The investigations will be continued for Al(III), Mg(II) and Fe cations using presented above method.

References

CHENG, C.Y., BODDY, G., ZHANG, W., GODFREY, M., ROBINSON, D.J., PRANOLO, Y., ZHU, Z., WANG, W., 2010, *Recovery of nickel and cobalt from laterite leach solutions using direct solvent extraction: Part I - selection of a synergistic SX system*, Hydrometallury 104, 45-52.

GHARABAHDI, M., IRANNAJAD, M., AZADMEHR, A.R., 2013, *Separation of nickel and zinc ions in a synthetic acidic solutions by solvent extraction using D2EHPA and Cyanex 272*, Physicochemical Problems of Mineral Processing, 49, 233-242.

GOTFRYD, L., 2005. *Solvent extraction of nickel(II) sulphate contaminants,* Physicochemical Problems of Mineral Processing 39, 117-128.

JHA, M.K., KUMAR, V., SINGH, R.J., 2001, *Review of hydrometallurgical recovery of zinc from industrial wastes*. Resources, conservation and recycling 33, 1-22.

Net 1 - http://www.momentive.com/Products/TechnicalDataSheet.aspx?id=6018 (accessed July 2014).

Net 2 - http://www.team-well.com/upload/1194241441890.pdf (accessed July 2014).

DU PREEZ, A.C., PRESTON, J. S., 2004, *Separation of nickel and cobalt from calcium, magnesium and manganese by solvent extraction with synergistic mixtures of carboxylic acids*, SAIMM Journal, 2004, 333-338.

DU PREEZ, R., KOTZE, M., NEL, G., DONEGAN, S., MASIIWA, H., 2007, *Solvent extraction test work to evaluate Versatic 10/NICKSYN™ synergistic system for nickel-calcium separation*, Proc. of The Fourth Southern African Conference on Base Metals; Swakopmund, Namibia; 23-25 July 2007, 193-210, The Southern African Institute of Mining and Metallurgy.

PRESTON, J. S., DU PREEZ, A. C., 1995, *The solvent extraction of nickel and cobalt by mixtures of carboxylic acids and pyridinecarboxylate esters*, Solv. Extr. Ion Exch, 13, 465-494.

PRESTON, J. S., DU PREEZ, A. C., 2000, *Separation of nickel and calcium by solvent extraction using mixtures of carboxylic acids and alkylpyridines*, Hydrometallurgy, 58, 239-250.

PRESTON J.S., 1983, *Solvent extraction of nickel and cobalt by mixtures of carboxylic acids and non-chelating oximes*, Hydrometallurgy 11, 105-124.

PRESTON, J.S., 1985, *Solvent extraction of metals by carboxylic acids*, Hydrometallurgy, 14, 71-188.

SANUKI, S., IZAKI, T., MAJIMA, H., 1982, *Studies on the solvent extraction of Zn^{2+} with Versatic Acid 10*, Journal of the Japan Institute of Metals, 46, 591-597.

SANUKI, S., IZAKI, T., MAJIMA, H., 1983, *Extraction of Pb^{2+}, Cu^{2+} and Zn^{2+} from sodium chloride solutions with Versatic Acid 10*; Journal of the Japan Institute of Metals, 47; 301-307.

SINHA, M. K., SAHU, S.K., MESHRAM, P., PANDEY, B.D., KUMAR, V.; 2012, *Solvent Extraction and Separation of Copper and Zinc from a Pickling Solution*, International Journal of Metallurgical Engineering 1(2), 28-34.

APPLICATION OF POLYMER INCLUSION MEMBRANES DOPED WITH 1-HEXYL-4-METHYLIMIDAZOLE FOR PERTRACTION OF ZINC(II) AND OTHER TRANSITION METAL IONS

Malgorzata ULEWICZ*, Elzbieta RADZYMINSKA-LENARCIK**

* Department of General Building Engineering and Building Physics, Faculty of Civil Engineering, Czestochowa University of Technology, 42-201 Czestochowa, Akademicka 3, Poland, e-mail: ulewicz@onet.eu
** Department of Inorganic Chemistry, University of Technology and Life Sciences, 85-326 Bydgoszcz, Seminaryjna 3, Poland, e-mail: elaradz@utp.edu.pl

Abstract: Transport of Zn(II) from unary aqueous chloride solutions and from solutions which contain mixtures of Cd(II), Co(II) and Ni(II) ions in source phases ($c_{Me} = 0.001$ mol/dm^3, pH = 6.0) across polymer inclusion membranes (PIMs) doped with 1-hexyl-4-methylimidazole as ion carrier was studied. The use of 1-hexyl-4-methylimidazole enables the separation of 98.5% Zn(II) from a unary solution and 96.9% from a quaternary solution of Zn(II)-Cd(II)-Co(II)-Ni(II) after running the process for 24 hours. Using that ion carrier, the metals are transported in the following order: Zn(II) > Cd(II) > Ni(II) > Co(II), and the selectivity coefficients of Zn(II)/Cd(II), Zn(II)/Ni(II), and Zn(II)/Co(II) are 12.9, 23.4 and 40.8, respectively. Findings of atomic force microscopy (AFM) examinations as well as thermograms of a polymer inclusion membrane containing 1-hexyl-4-methylimidazole are also presented. A membrane with 1.0 mol/dm^3 of carrier has a porosity of 15.8%, and roughness of 6.6 nm. The membranes remain thermally stable at temperatures up to 200°C. The findings were compared with earlier-reported results for 1-hexylimidazole.

Keywords: polymer inclusion membrane, PIM, metal ions separation, zinc(II), transition metal ions, imidazole derivatives

Introduction

A variety of techniques are known for non-ferrous metal ion separation from aqueous solutions in commercial facilities or in a bench scale. Such techniques include liquid-liquid extraction, ion exchange, ion flotation and sorption on polymer resins. The choice of the suitable technique depends on the scope of concentrations of the

components in the solution and on the properties of the compounds to be separated. Apart from conventional methods for the separation of metal ions, much attention has been paid for some time to the processes of transport across liquids membranes. A liquid membrane is a hydrophobic organic liquid which separates two aqueous phases, i.e., the feed solution and the receiving solution. Regardless of their type, liquid membranes have one feature in common: the steps of extraction and re-extraction run concurrently (pertraction process). This enables the process to be carried out in a continuous manner, without any intermediate operations. The pertraction process selectivity depends on the structure of the membrane and its physicochemical properties, on the properties of the substances to be separated, as well as on the nature of their interactions with ligands which carry the ions (Bartsch and Way, 1996; Kislik, 2010; Araki and Tsukube, 1990; Sastre et al., 1998; Noble and Stem, 1995; Nghiem et al., 2006, Walkowiak and Kozlowski, 2009).

The efficiency of metal-ion transport across liquid membranes largely depends on the right choice of carrier. The metal-ion carriers used in the transport across liquid membranes are usually the same organic compounds as those used in extraction processes, that is, organic acids, tertiary amines, quaternary ammonium salts, or macrocyclic compounds (Nghiem et al., 2006; Ulewicz, 2011; Walkowiak et al., 2002, 2009). In the commercial practice, a majority of extractants which have been used in the laboratory scale as metal-ion carriers in the transport across liquid membranes enable the efficient separation of non-ferrous metal ions only. In addition, their selectivity is low, especially for metal ions with similar physico-chemical properties. Therefore, their application is rather limited. At present, a number of research works have been dedicated to searching new organic compounds which have highly efficient separation properties and which are applicable as metal-ion carriers in the transport across liquid membranes. The studies are dedicated to the use of such compounds as imidazole derivatives, for instance, imidazole derivatives of aza- and azothiocrown ethers, for that purpose (Ulewicz et al., 2007[a,b], 2009; Luboch et al., 2006).

Imidazole and its alkyl derivatives, have also been useful in the solvent extraction of such metals as Co(II), Ni(II), Cu(II), Zn(II), Fe(III) and Cd(II) (Gheaedi et al., 2008; Radzymińska-Lenarcik, 2008[a], du Preez et al., 2004; Lenarcik et al., 1989, 1999; Lenarcik and Kierzkowska, 2004[a,b], 2006; Lenarcik and Rauckyte, 2004; Lenarcik and Ojczenasz, 2004) and in the process of transport of nonferrous metal ions across liquid membranes (Ajji and Ali, 2010; Ulewicz and Radzyminska-Lenarcik, 2011, 2012[a,b]; Radzyminska-Lenarcik and Ulewicz, 2012, 2014). Alkyl derivatives of imidazole are a convenient group of bases in which the complex-forming properties in respect of transition metals may be predicted and programmed in order to differentiate their extraction properties so as to improve the selectivity of recovery of selected metals (Radzymińska-Lenarcik, 2007[a,b], 2008; Lenarcik and Rauckyte, 2004, Gheaedi et al., 2008; Lenarcik and Kierzkowska, 2006; Lenarcik et al., 1999).
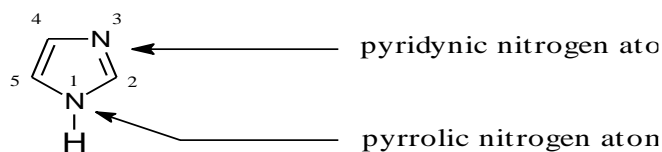
Fig. 1. Molecule of imidazole

Table 1. Comparison of the stability constants β_n of Co(II), Ni(II), Cu(II), and Zn(II) complexes with
1-hexylimidazole, 1-hexyl-2-methylimidazole, and 1-hexyl-4-methylimidazole
at 25°C, ionic strength 0.5 mol/dm^3 (KNO$_3$)

Ligand	Metal ions	log β_1	log β_2	log β_3	log β_4
1-hexylimidazole	Co(II) [2]	3.47	5.64	7.14	8.38
	Cu(II) [3]	4.15	7.57		
	Zn(II) [4]	3.36	5.87	8.07	
pK$_a$ = 7.30[1]	Ni(II) [5]	3.29	5.34	7.07	7.95
1-hexyl-2-methylimidazole	Co(II) [6]	1.96	2.18	3.02	5.61
	Cu(II) [7]	3.52	6.63	8.98	
	Zn(II) [8]	3.48	5.80	8.30	10.10
pK$_a$ = 8.32[1]	Ni(II) [9]	2.08	4.62		
1-hexyl-4-methylimidazole	Co(II) [10]	1.40	2.04	3.02	5.61
	Cu(II) [11]	3.72	4.55	6.53	
	Zn(II) [12]	2.95	5.60	6.30	
	Cd(II) [10]	2.20	3.93	5.11	5.81
pK$_a$ = 8.01[1]	Ni(II) [10]	1.74	3.00	3.92	

data from: (1) Lenarcik and Ojczenasz, 2002; (2) Lenarcik and Ojczenasz, 2004; (3) Radzyminska-Lenarcik, 2007b; (4) Lenarcik and Kierzkowska, 2004a; (5) Lenarcik and Rauckyte, 2004; (6) Radzyminska-Lenarcik and Witt, 2014; (7) Radzyminska -Lenarcik, 2007a; (8) Lenarcik and Kierzkowska, 2006; (9) Lenarcik et al., 1999; (10) Lenarcik et al., 1989; (11) Radzyminska-Lenarcik, 2010; (12) Lenarcik and Kierzkowska, 2004b

Although a weaker base than ammonia, imidazole (Fig. 1) (pK$_a$ = 7.12 (Sundberg and Martin, 1974)) forms more stable complexes with transition metal cations due to back-donation, therefore, it is classified as a soft base according to the HSAB theory (Pearson, R.G., 1968). Its basicity and complex stability with metal ions may be somewhat improved by substituting an alkyl group in position 1 (Lenarcik and Ojczenasz, 2002). On the other hand, when introduced in position 2 or 4, even small alkyl group will increase the basicity of a pyridine nitrogen atom by as much as one order of magnitude but will also reduce the contribution of the $\pi_{M \leftarrow L}$ bond component. When placed in such positions, the alkyl groups constitute a steric hindrance making it difficult to form a stable coordination bond with metal cations (Radzyminska-Lenarcik, 2007a, 2008a,b, 2009, 2010; Lenarcik and Kierzkowska, 2004b, 2006; Lenarcik et al., 1986, 1999; Lenarcik and Barszcz, 1980). As a result of the two effects, the 6-coordination (octahedral) complexes with 2 or 4 substituted

alkylimidazoles have lower stability constants (Table 1). The phenomenon is observed especially for metal cations with a rigid, octahedral structure of the coordination sphere which is hard to deform, for instance Ni(II).

The steric effect much less hinders the formation of tetrahedral complexes of 1-alkyl-2-methylimidazoles and 1-alkyl-4-methylimidazoles with cations which have an ability to change the shape of a coordination polyhedron from an octahedron to a tetrahedron (Eqs. 1 and 2) (Radzyminska-Lenarcik, 2007a, 2008a, 2010; Lenarcik and Kierzkowska, 2004b, 2006; Lenarcik et al., 1986, 1999):

$$[M(H_2O)_6]^{2+} + nL + 2A^- \leftrightarrow [M(H_2O)_{6-n}L_n]A_2 + nH_2O \qquad (1)$$

$$[M(H_2O)_6]^{2+} + nL + 2A^- \leftrightarrow [M(H_2O)_{4-n}L_n]A_2 + (n+2)H_2O \qquad (2)$$
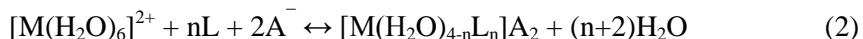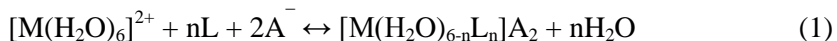
where L denotes the carriers molecule.

The reactions, described by Eq. 2 and involving a change in the coordination number, are typical for Zn(II), Cd(II), Cu(II) and Co(II), especially for the fourth stage of complexation (n=4) (Radzyminska-Lenarcik, 2007a, 2008a,b, 2010; Lenarcik et al., 1986, 1999; Lenarcik and Kierzkowska, 2004b, 2006). In such cases, configuration equilibria are established (Equation 3) between ML_n complexes, which have different coordination sphere structures, for instance:

$$[M(H_2O)_2L_4]^{2+} \leftrightarrow [ML_4]^{2+} + 2H_2O. \qquad (3)$$
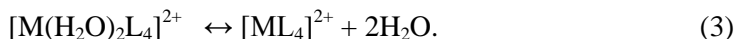
The occurrence of configuration equilibria in the n-th stage of complexation will lead to higher values of its corresponding stability constant, β_n (Table 1), because it is a sum of the stability constant of the tetrahedral complex, β_t, and the octahedral complex β_o ($\beta_n = \beta_t + \beta_o$) (Radzyminska-Lenarcik, 2008a; Lenarcik and Kierzkowska, 2004b, 2006; Lenarcik et al., 1986).

There was a decrease in the stability of all the metal complexes due to steric hindrance, which in turn, depends on the kind of the central ion.

As seen in Table 1 the stability constants for 1-hexylimidazole complexes with all metal ions are the highest. Stability constants of the Cu(II) complexes are considerably higher than those for Co(II), Ni(II), and Zn(II). This may be explained in terms of a larger contribution of the $\pi_{M \rightarrow L}$ back donation to interaction of Cu(II) with the imidazole ring (Radzyminska-Lenarcik, 2007a,b, 2008a).

Phenomena which change the structure and the values of stability constants of metal complexes may affect the process of competitive transport of metal cations through PIM (Radzyminska-Lenarcik and Ulewicz, 2014; Ulewicz and Radzyminska-Lenarcik, 2012a,b).

In this work, the authors present the results of investigation of the competitive transport of nonferrous metal ions as zinc(II), cobalt(II), cadmium(II) and nickel(II) ions across polymer inclusion membranes doped with 1-hexyl-4-methylimidazole from dilute chloride solutions. The results were compared with results previously

published for the transport of Zn(II), Co(II), and Ni(II) ions across PIM doped with 1-hexylimidazole (Radzyminska-Lenarcik and Ulewicz, 2014).

Experimental

Reagents

The inorganic chemicals, i.e., zinc(II), cadmium(II), nickel(II), cobalt(II) chlorides and tetramethylammonium hydroxide, were of analytical grade and were purchased from POCh (Gliwice, Poland). The organic reagents, i.e., cellulose triacetate (CTA), *o*-nitrophenylpentyl ether (*o*-NPPE) having a density 1.098 g/cm^3 and dichloromethane were also of analytical grade and were purchased from Fluka and used without further purification. 1-hexyl-4-methylimidazole (formula in Table 1) was synthesized according to a method reported in the literature (Pernak et al., 1987).

Preparation of polymer inclusion membranes and its characterization

The polymer inclusion membranes were prepared according to the procedure reported in the previous paper (Ulewicz and Radzyminska-Lenarcik, 2011, 2012a,b; Radzyminska-Lenarcik and Ulewicz, 2012). A solution of cellulose triacetate as the support, plasticizer and 1-hexyl-4-methylimidazole as ion carrier in dichloromethane was prepared. The plasticizer used was *o*-nitrophenylpentyl ether, which penetrates into the polymer molecules and neutralizes the polar groups of the polymer with its own polar groups, thus making the membrane more flexible. A specified portion of the solution was poured into a membrane mould composed of a 9.0 cm diameter glass ring fixed on a glass plate with a cellulose triacetate-dichloromethane glue. After a slow evaporation of the solvent overnight, the resulting polymer inclusion membrane was peeled off from the glass plate by immersion in cold water. Then the polymer inclusion membrane was soaked for 12 hours in distilled water to achieve its homogeneity.

Two samples of the PIM membranes (containing 15.8% CTA, 42.1% carriers and 42.1 plasticizer) were cut from the same membrane film for duplicate transport experiments. A surface characterization study of the polymer inclusion membranes was performed by atomic force microscopy (AFM) according to the procedure described in our earlier paper (Ulewicz et al., 2007a). The analysis of surface pore characteristics of the polymer membrane was made using the NanoScope v.5.12 AFM image processing program, which enabled the calculation of two parameters: roughness (R_q) and porosity (ε).

Transport studies

The transport experiments were carried out in a permeation module cell described in our earlier paper (Ulewicz and Radzyminska-Lenarcik, 2012, 2014; Radzyminska-

Lenarcik and Ulewicz, 2012a,b). The membrane film (having a surface area of 4.9 cm^3) was tightly clamped between two cell compartments. Both the source and the receiving aqueous phases (45 cm^3 each) were mechanically stirred at 600 rpm. The receiving phase was double distillated water (conductivity 5 μS/m). The PIM transport experiments were carried out at a temperature of 20±0.2^{o}C. Metal concentration was determined by withdrawing small samples (0.1 cm^3 each) of the aqueous receiving phase at different time intervals and analysing by atomic absorption spectroscopy (AAS Spectrometer, Solaar 939, Unicam). The source phase pH was kept constant (pH = 6.0) using tetramethylammonium hydroxide and controlled by pH meter (pH meter, CX-731 Elmetron, with a combination pH electrode, ERH-126, Hydromet, Poland). The permeability coefficients (P, m/s) of metal ions across polymer membranes was described by the following equation (Danesi, 1984-85):

$$\ln\left(\frac{c}{c_i}\right) = -\frac{A}{V} \cdot P \cdot t \tag{4}$$

where c is the metal ion concentration (mol/dm^3) in the source aqueous phase at some given time, c_i is the initial metal ions concentration in the source phase, t is the time of transport (s), V is volume of the aqueous source phase (m^3), and A is an effective area of membrane (m^2).

A linear dependence of ln(c/c$_i$) in the source phase versus time was obtained and the permeability coefficients was calculated from the slope of the straight line that fits the experimental data. The initial flux (J$_i$) was determined as equal to:

$$J_i = P \cdot c_i . \tag{5}$$

The diffusion coefficient D_o (cm^2/s) of the metal-complex across the organic phase can be determined in the case of absence of diffusion resistances in the aqueous layer source phase/membrane by the following equation (Danesi, 1984-85):

$$c = c_i - \frac{[L]_o \cdot A \cdot t}{n \cdot V \cdot \Delta_o} \tag{6}$$

where $\Delta_o = d_o/D_o$ (s/cm) is the resistance of transport by diffusion across the membrane, d_o (cm) is the thickness of the membrane, n - is the number of moles of the carrier in the complex (in our case $n = 1$), $[L]_o$ is the initial concentration of the extractant in the organic phase (mol/dm^3). Plotting [Me^{2+}]$_i$-[Me^{2+}]$_t$ vs. time gives a slope equal to ([L]$_o$·A)/(Δ$_o$·V) and allow access to the diffusion coefficients D_o of the metal complex species in the membrane phase.

To describe the efficiency of metal removal from the source phase, the recovery factor (RF) was calculated:

$$RF = \frac{c_i - c}{c_i} \cdot 100\% \; . \tag{7}$$

The reported values correspond to the average values of three replicates, with a standard deviation within 5%.

Results and discussion

Findings on the transport of non-ferrous metal ions from chloride solutions, across polymer inclusion membranes containing 1-hexyl-4-methylimidazole as ion carrier are discussed below. The concentration of the ion carrier in the membrane was 1.0 mol/dm^3 (relative to the plastifier) since earlier studies (Radzyminska-Lenarcik and Ulewicz, 2014) indicate that the concentration is optimum for that group of compounds. The studies were carried out using single- or multi-component solutions, containing each metal at a concentration of 0.001 mol/dm^3. The initial flux values and selectivity coefficients for the metal ion transport across the PIMs are shown in Table 2.

Table 2. Initial fluxes, selectivity order and selectivity coefficients for the competitive transport of nonferrous ions across PIM containing 1.0 mol/dm^3 of 1-hexyl-4-methylimidazole

Solutions	Metal ions	J_i, µmol/m^2·s	$S_{Zn(II)/Me(II)}$
I	Zn(II)	4.37	-
II	Zn(II)	3.85	Zn(II) > Cd(II)
	Cd(II)	0.41	9.4
III	Zn(II)	3.73	Zn(II) > Cd(II) > Co(II)
	Cd(II)	0.38	9.8 24.9
	Co(II)	0.15	
IV	Zn(II)	3.64	
	Cd(II)	0.29	Zn(II) > Cd(II) > Ni(II) > Co(II)
	Co(II)	0.01	12.9 23.4 40.8
	Ni(II)	0.16	

It follows from the data shown in Table 2 that the initial flux value for Zn(II) ion transport from a unary solution is higher than that from multi-component solutions. For a quaternary mixture, the initial fluxes of metal ions transport across PIMs containing 1-hexyl-4-methylimidazole decrease in the following order: Zn(II) > Cd(II) > Co(II) > Ni(II). This is similar to earlier results, obtained for membranes containing 1-decyl-4-methylimidazole and discussed by these authors in (Ulewicz and Radzyminska-Lenarcik, 2014). On the other hand, selectivity coefficients obtained for Zn(II)/Cd(II), Zn(II)/Ni(II) and Zn(II)/Co(II) during the transport across PIMs containing 1-hexyl-4-methylimidazole are higher, compared with those for 1-decyl-4-methylimidazole as ion carrier, for which the respective values were 11.6, 24.8 and 33.8. Shown in Table 3, for comparison, are earlier-reported values of initial fluxes,

selectivity order and selectivity coefficients for competitive transport of Zn(II), Co(II), and Ni(II) ions across PIM doped with 1-hexylimidazole (Radzyminska-Lenarcik and Ulewicz, 2014).

Table 3. Initial flux, selectivity order and selectivity coefficients for competitive transport of Zn(II), Co(II), and Ni(II) ions across PIM doped with 1-hexylimidazole[*]

membrane: 2.6 cm^3 o-NPPE /1g CTA and 1.0 M carriers calculated on plasticizer

Carrier	Metal ions	J_i, μmol/m^2·s	$S_{Zn(II)/Me(II)}$	
1-hexyl-imidazole	Zn(II)	1.79	Zn(II) > Cd(II) > Co(II)	
	Cd(II)	0.19		
	Co(II)	0.15	7.4	9.3

(*) data from Radzyminska-Lenarcik and Ulewicz, 2014

From comparison of the data in Tables 2 and 3, it follows that, in the case of 1-hexyl-4-methylimidazole as ion carrier, the initial fluxes value for Zn(II) ions is twice as high as that for a membrane doped with 1-hexylimidazole, and selectivity coefficients are considerably higher.

After 24 hours, 98.5% of Zn(II) ions was separated from the unary solution, compared with 97.2 and 97.0%, respectively, from Zn(II)-Cd(II) and Zn(II)-Cd(II)-Co(II). The degree of separation from the quaternary solution is 96.9% for Zn(II) ions, 25% for Cd(II) ions, while those of Co(II) and Ni(II) ions are below 12%.

Using alkyl derivatives of imidazole, substituted in positions 1 and 4, the degree of recovery of Zn(II), Co(II) and Ni(II) is higher, compared with membranes doped with 1-hexylimidazole (Radzyminska-Lenarcik and Ulewicz, 2014), for which the degree of recovery was 72%, 30% and 24%, respectively, for Zn(II), Co(II) and Ni(II).
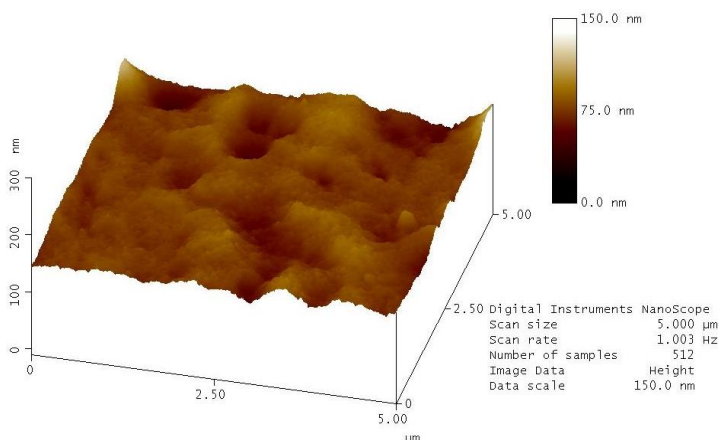
Fig. 2. 3D-view atomic force microscopy for PIM with 1-hexyl-4-methylimidazole

The AFM image of PIM in a two-dimensional form in the format 5.0 x 5.0 μm is shown in Fig. 2. The porosity (ε) and roughness (R_q) of the polymer inclusion membrane were calculated using atomic force microscopy (AFM) data and were equal to 15.8% and 6.6 nm, respectively. The effective pore size was 0.06 μm; thickness membrane 30 μm. The distribution of the carrier in the investigated membrane after evaporation of dichloromethane is homogeneous over the entire surface. The tortuosity of the PIM doped with 1-hexyl-4-methylimidazole was determined also from the relationship developed by Wolf and Strieder (1999) and was found to be equal to 2.85.
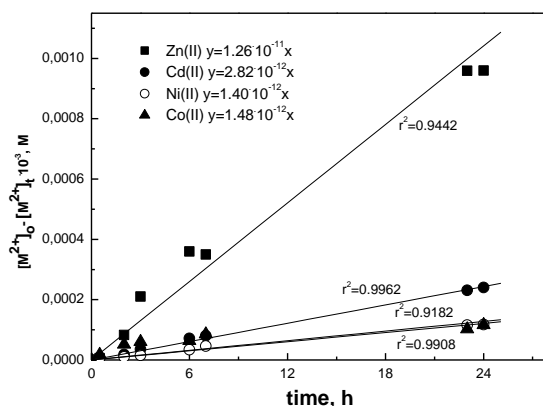
Fig. 3. Relation of $[Me^{2+}]_i$-$[Me^{2+}]_t$ plotted vs. time for Zn(II), Cd(II), Co(II) and Ni(II) transport across PIM membrane doped with 1.0 mol/dm^3 1-hexyl-4-methylimidazole

In Fig. 3, the correlation graphs of $[Me^{2+}]_i$-$[Me^{2+}]_t$ versus time of metal ions transport across PIM doped with 1-hexyl-4-methylimidazole are presented. The diffusion coefficient of Me(II) was calculated, substituting $D_o = d_o / \Delta_o$, where d_o is the thickness of the membrane (0.003 cm) and Δ_o could be evaluated by plotting $[Me^{2+}]_i$-$[Me^{2+}]_t$ vs. time. The corrected (normalized) membrane diffusion coefficient $D_{o,n}$, which considers the morphological features inside the membrane (ε - porosity and τ - tortuosity), was calculated from equation (Salazar-Alvarez et al., 2005): $D_{o,n} = D_o \cdot (\varepsilon / \tau)$. The obtained values of diffusion coefficients are presented in Table 4.

Table 4. Diffusion coefficients normalized for competitive transport of Zn(II), Cd(II), Co(II), and Ni(II) ions through PIM with 1-hexyl-4-methylimidazole

Metal ions	Δ_o, s/m	D_o, cm^2/s	$D_{o,n}$, cm^2/s
Zn(II)	$10^{5.64}$	$6.94 \cdot 10^{-09}$	$3.85 \cdot 10^{-10}$
Cd(II)	$10^{7.23}$	$1.56 \cdot 10^{-10}$	$8.66 \cdot 10^{-12}$
Ni(II)	$10^{7.54}$	$7.71 \cdot 10^{-11}$	$4.28 \cdot 10^{-12}$
Co(II)	$10^{7.57}$	$8.16 \cdot 10^{-11}$	$4.53 \cdot 10^{-12}$

Values of diffusion coefficient determined in this study are comparable with data presented in literature for different membranes. They are in the range 10^{-6} to 10^{-12} cm^2/s and show that limiting step of the process is the transfer of metal complex across membrane barrier. The value of the diffusion coefficient of Me(II)-carrier species of $3.85 \cdot 10^{-10} - 4.28 \cdot 10^{-12}$ cm^2/s is smaller than the value of $1.5 \cdot 10^{-7}$ cm^2/s reported for the lead complex with the D2EHPA in PIM reported by (Salazar-Alvarez et al., 2005).

The values of normalized diffusion coefficients (considering membrane porosity and tortuosity) of Me(II)-carrier complexes, obtained in the process of transport across PIMs containing 1-hexyl-4-methylimidazole from the solution Zn(II)-Cd(II)-Co(II)-Ni(II) are in the range $3.85 \cdot 10^{-10} - 4.28 \cdot 10^{-12}$ cm^2/s. Thus, the rate of transport of non-ferrous metal ions across PIMs doped with 1-hexyl-4-methylimidazole is determined by the diffusion rate of the complexes Me(II)-carrier across the membrane.
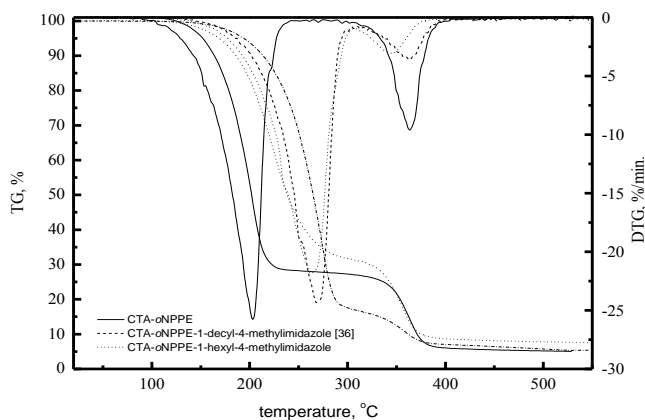
Fig. 4. TGA thermograms of CTA-*o*-NPPE and CTA-*o*-NPPE-carrier:
1-hexyl-4-methylimidazole and 1-decyl -4-methylimidazole

In the final stage of the studies, the thermal stability of the PIM doped with 1-hexyl-4-methylimidazole was determined. Literature reports (Arous et al., 2004; Gherrou et al., 2004, 2005) indicate that degradation of a CTA membrane proceeds in two steps. The first step occurs at temperatures in the range 292-320°C while the second (carbonization) occurs in the range 450-476°C. The membrane thermal stability changes after addition of a plastifier and ion carrier (Gherrou et al., 2004, 2005; Benosmane et al., 2009). Figure 4 shows the thermograms of the membrane CTA-*o*-NPPE–carrier. The diagram indicates that degradation of the membrane made of CTA–*o*-NPPE with 1-hexyl-4-methylimidazole (carrier) proceeds in two steps. In the first step, at 220.1°C, the weight loss is 80.57%, in the second at 327.0°C the weight loss is 5.88%. At a temperature of 547.6°C, the residue is 3.43%. The first and second steps of degradation of a membrane doped with 1-hexyl-4-methylimidazole occur at temperature lower by 10°C, compared with the membrane which contains 1-

decyl-4-methylimidazole, for which the results were reported in (Ulewicz and Radzyminska-Lenarcik, 2014). The first step of degradation of the membrane studied in this work occurs at temperatures higher by 10°C, compared with that of the membrane doped with 1-hexylimidazole (211.3°C) – the relevant findings were reported in (Radzyminska-Lenarcik and Ulewicz, 2012), while the second step does at temperatures lower by 33°C (360.7°C). The findings obtained lead to the conclusion that PIMs doped with 1-alkyl-4-methylimidazole are thermally stable up to temperatures just below 200°C.

Conclusions

In the case of alkyl derivatives of imidazole, shown in positions 1 and 4 as ion carriers in PIMs, the initial flux for Zn(II) ions is twice as high as that for a membrane doped with 1-hexylimidazole. Also the selectivity coefficients and degrees of recovery are significantly higher for Zn(II), Co(II) and Ni(II), compared with the membranes doped with 1-hexylimidazole. Polymer inclusions membranes doped with 1-alkyl-4-methylimidazole are thermally stable up to temperatures just below 200°C.

Zinc(II) cations can be removed effectively from aqueous chloride solutions in the hydrometallurgical process of supported and polymer inclusion membrane transport with 1-hexyl-4-methylimidazole as ion carriers. The use of the ion carrier enables the separation of 98.5% Zn(II) ions from a unary solution and of 96.9% from a quaternary solution of Zn(II)-Cd(II)-Co(II)-Ni(II) after running the process for 24 hours. Competitive transport of metal ions across PIM doped with 1-hexyl-4-methylimidazole showed the following preferential selectivity order: Zn(II) > Cd(II) > Ni(II) > Co(II). The selectivity coefficients of Zn(II)/Cd(II), Zn(II)/Ni(II), and Zn(II)/Co(II) obtained during transport across the polymer membranes are 12.9, 23.4 and 40.8, respectively. Moreover the values of diffusion coefficient of Me(II)-carrier complexes, obtained in the process of transport across PIMs containing 1-hexyl-4-methylimidazole are in the range 10^{-10} to 10^{-12} cm^2/s and show that limiting step of the process is the transfer of metal complex across membrane barrier.

References

AJJI, Z., ALI, A. M., 2010, *Separation of copper ions from iron ions using PVA-g-(acrylic acid/N-vinyl imidazole) membranes prepared by radiation-induced grafting*, J. Hazardous Materials 173, 71-74.

ARAKI, T., TSUKUBE, H., (ed.)., 1990, *Liquid membranes: Chemical applications*, CRC Press: Boca Raton, FL.

AROUS, O., AMARA, M., KERDJOUDJ, H., 2004, *Synthesis and characterization of cellulose triacetate and poly(ethylene imine) membranes containing a polyether macrobicyclic: Their application to the separation of copper(II) and silver(I) ions*, J. Appl. Polym. Sci. 93, 1401-1410.

BARTSCH, R.A., WAY, J.D., 1996, *Chemical separation with liquid membranes,* ASC, Washington DC.

BENOSMANE, N., HAMDI, S.M., HAMDI, M., BOUTEMEUR, B., 2009, *Selective transport of metal ions across polymer inclusion membranes containing calix[4]resorcinares*, Sep. Purif. Technol. 65, 211÷219.

DANESI, P. R., 1984-85, *Separation of metal species by supported liquid membranes*, Sep. Sci. Technol. 19, 857-894.

Du PREEZ, J. G. H., GERBER, T.I.A., EGDE, W., MTOTYWA, V.L.V., van BRECHT, J.A.M., 2001, *Nitrogen reagents in metal ion separation. XI. The synthesis and extraction behavior of a new NS imidazole derivative*, Solv. Extr. Ion Exch., 19, 143-154.

GHEAEDI, M., NIKNAM, K., SHOKROLLAHI, A., NIKNAM, E., GHEADI, H., SOYLAK, M., 2008, *A solid extraction procedure for Fe^{3+}, Cu^{2+} and Zn^{2+} ions on 2-phenyl-1H-benzo[d] imidazole loaded on Triton Z-100 coated polyvinyl chloride*, J. Hazardous Materials 158, 131-136.

GHERROU, A., KERDJOUDJ, H., MOLINARI, R., SETA, P., DRIOLI, E., 2004, *Fixed sites plasticized cellulose triacetate membranes containing crown ethers for silver(I), copper(II) and gold(III) ions transport*, J. Membr. Sci. 228, 149-157.

GHERROU, A., KERDJOUDJ, H., MOLINARI, R., SETA, P., 2005, *Preparation and characterization of polymeric plasticized membranes (PPM) embedding a crown ether carrier application to copper ions transport*, Mat. Sci. Eng. 25, 436-443.

KISLIK, V.S., (ed.), 2010, *Liquid membranes. Principles and application in chemical. separation and wastewater treatment*, Elsevier, UK.

LENARCIK, B., ADACH, A., RADZYMINSKA-LENARCIK, E., 1999, *The influence of steric effect and alkyl chain length on the extraction of the complexes of Co(II), Ni(II), Cu(II), Zn(II), and Cd(II) with 1-alkyl-2-methylimidazole*. Pol. J. Chem. 73, 1273-1281.

LENARCIK, B., BARSZCZ, B., 1980, *Stability and Structure of Transition Metal Complexes with Azoles in Aqueous Solutions. Part XXI. A Comparison of Complex-Forming of 1,2-Dimethylimidazole with that of Other 1,3-Diazoles*, J. Chem. Soc. Dalton Trans. 24-28.

LENARCIK, B., KIERZKOWSKA, A., 2004a, *The influence of alkyl length on stability constants of Zn(II) complexes with 1-alkylimidazoles in aqueous solutions and their partition between aqueous phase and organic solvent*, Solv. Ext. Ion Exch. 22, 449-471.

LENARCIK, B., KIERZKOWSKA, A., 2004b, *The influence of alkyl chain length and steric effect on stability constants and extractability of Zn(II) complexes with 1-alkyl-4(5)-methylimidazoles*, Sep. Sci. Technol. 39, 3485-3508.

LENARCIK, B., KIERZKOWSKA, A., 2006, *The influence of alkyl chain length and steric effect on extracttion of zinc(II) complexes with 1-alkyl-2-methylimidazoles*. Solv. Extr. Ion Exch. 24, 433-445.

LENARCIK, B., KURDZIEL, K., CZOPEK, R., 1986, *Search for optimum conditions of extraction of metal complexes with alkylimidazoles. III. Structure – extractability relationships for 1,4-dimethylimidazole complexes of Co(II), Ni(II), Cu(II), Zn(II), and Cd(II)*, Solv. Ext. Ion Exch. 4, 165-182.

LENARCIK, B., OJCZENASZ, P., 2002, *The influence of the size and position of the alkyl groups in alkylimidazole molecules on their acid – base properties*, J. Heterocycl. Chem. 39, 287-290.

LENARCIK, B., OJCZENASZ, P., 2004, *Investigation of the stability constants of Co(II) complexes with a homologous series of 1-alkylimidazoles in aqueous solution by using a partition method with several solvents*, Sep. Sci. Technol. 39, 199-226.

LENARCIK, B., RAUCKYTE, T., 2004, *The influence of alkyl length on extraction equilibria of Ni(II) complexes with 1-alkylimidazoles in aqueous solution/organic solvent systems*, Sep. Sci. Technol. 39, 3353-3372.

LUBOCH, E., WAGNER-WYSIECKA, E., FAINERMAN-MELNIKOVA, M., LINDOY, L.F., BIERNAT, J.F., 2006, *Pyrrole azocrown ethers. Synthesis, complexation, selective lead transport and ion-selective membrane electrode studies*, Supramol. Chem. 18, 593-601.

NGHIEM, L.D., MORNANE, P., POTTER, I.D., PERERA, J.M., CATTRALL, R.W., KOLEV, S.D., 2006, *Extraction and transport of metal ions and small organic compounds using polymer inclusion membranes (PIMs)*, J. Membr. Sci. 281, 7-41.

NOBLE, R.D., STEM, S.A., (ed.), 1995, *Membrane separation technology*, Elsevier, New York.

PEARSON, R.G., 1968, *Hard and Soft Acids and Bases, HSAB, Part I. Fundamental principles*, J. Chem. Edu. 45, 581-586.

PERNAK, J., KRYSINSKI, J., SKRZYPCZAK, A., 1987, *Bakterizide Wirkung von Iminiumverbindungen*, A. Tenside Surfact. Det. 24, 276-286.

RADZYMINSKA-LENARCIK, E., 2007a, *Effect of alkyl chain length on the extraction of copper(II) complexes with 1-alkyl-2-methylimidazoles*, Sep. Sci. Technol. 42, 2661-2675.

RADZYMINSKA-LENARCIK, E., 2007b, *The influence of the alkyl chain length on extraction equlibrium of Cu(II) complexes with 1-alkylimidazoles in aqueous solution/ organic solvent systems*, Solv. Extr. Ion Exch. 25, 53-64.

RADZYMINSKA-LENARCIK, E., 2008a, *Search for the possibility of utilizing the differences in complex-forming capacities of alkylimidazoles for selective extraction of some metal ions from aqueous solutions*, Polish J. Chem. Technol. 10, 73-78.

RADZYMINSKA-LENARCIK, E., 2008b, *Influence of the steric hindrance, ligand hydrophobicity and DN of solvents on structure and extraction of Cu(II) complexes of 1-alkyl-2-ethylimidazoles*, Sep.Sci. Technol. 43, 794-814.

RADZYMINSKA-LENARCIK, E., 2009, *The influence of alkyl chain length in 1,2-dialkylimidazoles on the extraction capacity and structure of their copper(II) complexes*, Sep. Sci. Technol. 44, 954-970.

RADZYMINSKA-LENARCIK, E., 2010, *The influence of steric effect, alkyl chain length and donor number of solvent on the extraction of copper(II) complexes with 1-alkyl-4-methylimidazoles*, Solv. Ext. Ion Exch. 28, 636-652.

RADZYMINSKA-LENARCIK, E., ULEWICZ, M., 2012, *Selective transport of Cu(II) across a polymer inclusion membrane with 1-alkylimidazole from nitrate solutions*, Sep. Sci. Technol. 47, 1113–1118.

RADZYMINSKA-LENARCIK, E., ULEWICZ, M., 2014, *The use of 1-alkylimidazoles for selective separation of zinc ions in the transport process across a polymeric inclusion membrane*, Physicochem. Probl. Miner. Process. 50, 131-142.

RADZYMINSKA-LENARCIK, E., WITT, K., 2014, *The influence of alkyl chain length and steric effect on stability constants and extractability of Co(II) complexes with 1-alkyl-2-methylimidazoles*, Sep. Sci. Technol. *in press*

SALAZAR-ALVAREZ, G., BAUTISTA-FLORES, A. N., SAN MIGUEL, E.R., MUHAMMED, M., de GYVES, J., 2005, *Transport characterization of a PIM system used for the extraction of Pb(II) using D2EHPA as carrier*, J. Membr. Sci. 250, 247-257.

SASTRE, A.M., KUMAR, A., SHUKLA, J.P., SINGH, R.K., 1998, *Improved techniques in liquid membrane separations: an overview*, Sep. Purifi. Meth. 27, 213-298.

SUNDBERG, R.J., MARTIN, R.B., 1974, *Interactions of Histidine and other Imidazole Derivatives with Transition Metal Ions in Chemical and Biological System*. Chem. Rev. 74, 471-517.

ULEWICZ, M., 2011, *Separacja jonów metali nieżelaznych w procesie transportu przez ciekłe membrany zawierające związki makrocykliczne*, Wydawnictwo WIPMiFE PCz, Czestochowa.

ULEWICZ, M., RADZYMINSKA-LENARCIK, E., 2011, *Transport of metal ions across polymer inclusion membrane with 1-alkylimidazole*, Physicochem. Probl. Miner. Process. 46, 199-130.

ULEWICZ, M., RADZYMINSKA-LENARCIK, E., 2012a, *Supported liquid (SLM) and polymer inclusion (PIM) membranes pertraction of copper(II) from aqueous nitrate solutions by 1-hexyl-2-methylimidazole*, Sep. Sci. Technol. 47, 1383–1389.

ULEWICZ, M., RADZYMINSKA-LENARCIK, E., 2012b, *Application of supported and polymer membrane with 1-decyl-2-methylimidazole for separation of transition metal ions*, Physicochem. Probl. Miner. Process. 48, 91-102.

ULEWICZ, M., RADZYMINSKA-LENARCIK, E., 2014, *Application of polymer and supported membranes with 1-decyl-4-methylimidazole for pertraction of transition metal ions*, Sep. Sci. Technol. *in press*

ULEWICZ, M., SADOWSKA, K., BIERNAT, J.F., 2007a, *Facilitated transport of Zn(II), Cd(II) and Pb(II) across polymer inclusion membrane doped with imidazole azocrown ethers*, Desalination 214, 352-364.

ULEWICZ, M., SADOWSKA, K., BIERNAT, J.F., 2007b, *Selective transport of Pb(II) across polymer inclusion membrane using imidazole azocrown ethers as carriers*, Physicochem. Probl. Miner. Process. 41, 133-143.

ULEWICZ, M., SZCZYGELSKA-TAO, J., BIERNAT, J.F., 2009, *Selectivity of Pb(II) transport across polymer inclusion membranes doped with imidazole azothiacrown ethers*, J. Membr. Sci. 344, 32-38.

WALKOWIAK, W., KOZLOWSKI, C.A., 2009, *Macrocycle carriers for separation of metal ions in liquid membrane processes - a review*, Desalination 240, 186-197.

WALKOWIAK, W., ULEWICZ, M., KOZLOWSKI, C., 2002, *The application of crown ethers for metal ions removal and separation*, *an overview*, Ars Sep. Acta 1, 87-98.

WOLF, J. R., STRIEDER, W., 1999, *Tortuosities for a random fiber bed: overlapping, parallel cylinders of several radii*, J. Membr. Sci., 49 103-115.

IMPACT OF PHYSICAL AND MECHANICAL PROPERTIES OF ROCKS ON ENERGY CONSUMPTION OF JAW CRUSHER

Tomislav KORMAN, Gordan BEDEKOVIC, Trpimir KUJUNDZIC, Dalibor KUHINEK

University of Zagreb, Faculty of Mining, Geology and Petroleum Engineering, Pierottijeva 6, Zagreb, Croatia
gordan.bedekovic@rgn.hr

Abstract: The aim of this paper was to determine the impact of physical and mechanical properties of rocks on the electricity consumption of a jaw crusher during crushing. This paper presents a different approach to determine the energy consumption during comminution. The energy required for crushing rocks was obtained by direct measurement of crusher's motor power during the crushing of samples. Laboratory tests were used to determine the following physical and mechanical properties of the tested samples: bulk density, compressive strength, tensile strength, hardness, and fracture toughness. After that, the laboratory jaw crusher crushing tests were conducted. In the first part of the study, the individual rock samples were crushed one by one. In the second part of the test, multiple samples were crushed simultaneously. By measuring the energy consumption for crushing rocks with different physical and mechanical properties, we explored the dependence of energy required for crushing on individual mechanical properties of rocks and the simultaneous effect of the properties. Using statistical analysis of the influence of individual mechanical properties we found that the greatest influence on energy consumption for crushing was compressive strength. Fracture toughness and tensile strength of the rocks had a significant impact on the crushing energy. The effect of bulk density was not large while for the hardness could not be stated that it had influence. By the analysis of deviations of specific crushing energy calculated using equations obtained by multiple regression analysis of simultaneous influence of multiple mechanical properties of rocks and from the measured values, it was found that the dependence obtained on the basis of all investigated properties showed the smallest deviation and dependence obtained by compressive strength, fracture toughness, and hardness showed significantly smaller deviation. By examining the influence of mechanical rock properties on particle size of crushed material it was found that the increase in compressive strength increased the proportion of larger particles while other properties showed no effect.

Keywords: mining, crushing, physical and mechanical properties of rocks, energy, crushed stone, jaw crusher

Introduction

Comminution is a process in which larger pieces of ore or rock form smaller pieces under exposure of mechanical forces, i.e. there is a change in dispersed state of solids which is uniquely determined by grain size composition. There are many reasons for using comminution: achieving the release of useful minerals from useless minerals as preparation for concentration, attaining certain size and shape of grain in producing concrete and asphalt, increasing the grain surface and thus its reactivity, changing structural and chemical characteristics i.e. mechanical activation (Salopek and Bedekovic 2000). All these make grinding an integral part of almost every process in mineral processing, and its importance and significance arise from the fact that it is highly energy demanding and also very inefficient and as such will always be an interesting area to explore. According to (Sadrai et al. 2011), "the energy efficiency of comminution equipment can be defined as the ratio of surface energy change to the mechanical energy input". According to this, grinding efficiency varies between 0.1% and 1% (Furstenau and Abouzeid 2002). Crushing efficiency is slightly higher beween 2% and 3% (Sadrai et al. 2011). According to Rittinger (1867) the energy required for comminution is proportional to the newly created (free) surface area. According to Kick (1885) the specific energy consumption during grinding is proportional to reduction in the diameter of the observed particles. According to Bond (1952) the energy is inversely proportional to the square root of the newly created surface area, which is a sort of compromise between "Rittinger's area" and "Kick's diameter." Kick's "law" gives good results for crushing, Bond's for grinding and Rittinger's for fine grinding.

Based on a large number of tests, Bond introduced a working index or comminution parameter that represents the resistance of the material to crushing and grinding. Characterization of rocks for selection of crusher can be done in different ways, and the most commonly used is Bond work index (Tavares and Carvalho 2007).

Holmes (1957) proposed a modification of Bond's equation with the additional coefficient that depends on the properties of rock.

There are several methods for the determination of resistance to crushing, however, two most commonly used methods are pendulum and falling weight tests. For the determination of the resistance to crushing, Bond's index is determined based on the average comminution energy for individual samples using a device with a double pendulum (Donovan 2003). Numerous authors have conducted tests of resistance to crushing by considering physical and mechanical properties.

Bearman (1991) conducted an extensive research on the impact of physical and mechanical properties of rocks on the performance of crushers. Based on these studies, the most important characteristics that affect crushing energy are fracture toughness, tensile strength, and point load index.

On the basis of the falling pendulum tests, Narayanan and Whiten (1988) developed a straightforward *t10* parameter that describes the distribution of classes in

the grain-size composition of the crushed material. This parameter represents the proportion of fragmented particles smaller than 1/10 of the input grain sizes. The tests established the link between the specific comminution energy and the parameter *t10* (Napier–Munn et al. 1996).

Donovann (2003) analyzed the influence of individual characteristics on the performance of jaw crusher, and found that of all of the surveyed properties fracture toughness had a greatest impact on crushing energy.

Kujundzic et al. (2008) found that the energy required for crushing igneous rocks was higher compared to the crushing of sedimentary rocks. It was also found that the hardness showed no significant influence on the crushing energy. Olaleye (2010) found that the increasing uniaxial compressive strength increased the time required for crushing. Toraman et al. (2010) conducted tests on laboratory jaw crusher and found a link between the crushing index and the impact strength index.

Tosun and Konak (2014) developed a model to predict the energy consumption of primary and secondary crushers. According to this model, the specific energy of crushing depends on the specific consumption of explosives and uniaxial compressive strength. From an energy consumption viewpoint, it is clear that blasting with the intention of decreasing the Bond work index (*Wi*) will produce large energy savings (Workman and Eloranta 2003).

In the previous research the specific crushing energy was determined indirectly based on the pendulum or falling weight tests. None of these ways of testing simulates the motion of the jaw crusher's jaw. In this study, the effect of certain mechanical properties of rocks on crushing energy of jaw crusher was determined using direct measurement of the power on the jaw crusher motor.

Materials and methods

For the purposes of laboratory tests we collected samples of igneous and sedimentary rocks of different physical and mechanical characteristics from seven surface mines of crushed stone: Ivanec, Belaj, Spica, Kremesnica, Jelenje vode, Brensberg, and Zervanjska. All quarries are located in Croatia: "Ivanec" and "Jelenje vode"near Zagreb, "Belaj" near Karlovac, "Špica" near Ljubeščica, "Kremešnica" near Lasinja, "Brensberg" and "Žervanjska" near Orahovica. The sampling was carried out in such a way that the pieces of rocks had any visible cracks selected from the blasted rock mass. The previous studies have showed that the energy requirements for comminution depend on the size of the material and its distribution (Stamboliadis 2002), and that "shape of rocks and its contacts with the jaws may have considerable effect on the comminution energy" (Refahi et al. 2007). Therefore, in the laboratory from the larger pieces of rock by coring samples for crushing were obtained, then the determination of the physical and mechanical properties was performed in accordance with the methods recommended by ISRM. Thus, the laboratory testing consisted of

two parts: the determination of physical and mechanical properties of samples and measuring electricity consumption during the crushing.

According to the test methods proposed by ISRM the following properties were determined: bulk density, tensile strength, hardness, and fracture toughness. Compressive strength tests were conducted on the samples in the form of a cube with the length of each side d=5cm. It is known that the value obtained in such a way is higher than in the testing of samples according to the recommendations of ISRM. Therefore, the values were calculated using the empirical relation (Eq. 1) proposed in ASTM:

$$\sigma_{c1} = \frac{\sigma_c}{0.788 + \dfrac{0.222}{\left(\dfrac{h}{d}\right)}} \tag{1}$$

where:

σ_{c1} compressive strength of samples with ratio $h/d = 1$

σ_c compressive strength of samples with ratio $h/d > 1$

d diameter of samples that are in the form of a core or length of edge if samples are in the form of a cube

h height of the sample.

Calculated values of compressive strength were obtained with the ratio h/d=2.5. The second part of the tests included the measurement of the specific crushing energy in a laboratory jaw crusher Loro & Parisini. The feed size of the opening was 250 mm × 190 mm, and the granulation aperture size could be controlled in the range of 35 mm to 65 mm. During the tests, the opening was set to a minimum value of 35 mm. The technical characteristics of the other jaw crusher are presented in Table 1.

Table 1. Technical characteristics of the laboratory jaw crusher Loro & Parisini

Nominal voltage	380 V
Nominal power	5.5 kW
Nominal current	11.7 A
Frequency	50 Hz
$\cos\Phi$	0.84
Engine speed	1440 min^{-1}
Jaw speed	280 min^{-1}

The measurement of the specific crushing energy was conducted in two phases. In the first phase five individual samples from each quarry were crushed, and in the second phase in each individual test three samples were simultaneously crushed. The crushing tests were conducted in two phases in order to determine whether the specific energy depends on the quantity of the material being crushed.

Due to the fact that the average time for crushing one sample was about 3 s, the measurement system was designed (Fig. 1), which enabled the recording of data on the current power used by the electric engine that drives the jaw crusher at the rate of 20 readings per second. On the diagram of the time-power dependence, energy is represented by the area under the power curve. The energy required for the crushing of individual samples was obtained indirectly, by measuring electrical power. For this purpose, the measuring transducer MI 400 with a measuring range of voltage up to 500 V and currents up to 5 A, which was set to measure apparent, active and reactive power was converted to DC voltage in the range of ± 10 V on three separate analog outputs. The output voltage is proportional to the power consumed by the motor. Mains voltage was about 400 V, and the voltage clamp of transducer MI400 were connected directly to the phase conductors of the network while the current exceeded the value of 5 A. The measurement was performed indirectly using a current transformer MSZ1576 that can measure AC currents from 15 A to 600 A which converts them into the current of up to 5 A at secondary.
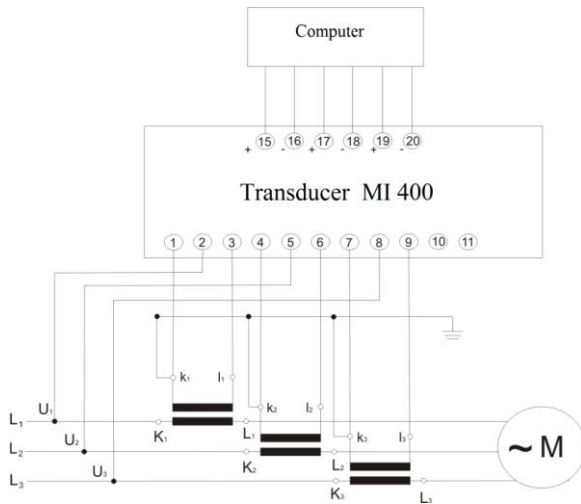
Fig. 1 Electrical diagram of the system for measuring power

The measuring transducer was connected to the data acquisition card NI PCI 6024 in the computer, and it was controlled using LabVIEW. In LabVIEW a program was created to collect 100 samples at each of the three channels with a sampling rate of 2000 S/s. The collected blocks of 100 samples were averaged in order to reduce the noise of the useful signal which yields effective 20 S/s on each of the three channels. The measured values were shown in the power-time graphs, and were recorded in the corresponding file. After the setting system the control of the work was carried out in the conditions similar to those expected during the measurement. The active power was changing depending on the load. The reactive power was almost constant, only little changed during the load changes. The apparent power was changing as it

depends on the vector sum of active and reactive power. Although to us the most interesting was the active power that is performing the work, it was decided to use apparent power for the analysis to take into account the small but existing changes in reactive power load in the comparisons.

When the motor was started and reached the full rotation speed it consumed a certain power from the electric network. After the increasing the load, the consumed power increased and after the crushing the sample returned to the original level, the idle power. The energy used for the crushing of the individual sample equals the total energy consumed minus the energy in idle crusher from the moment of increasing load until the moment of the fall of the power level to idle power. The principle is shown in Fig. 2 where the energy consumed for the crushing is represented by the area under the power curve and above the idle power. From the display of measurement data (as in Fig. 2) we can also read the start time of the crushing t_p and end time of the crushing t_k.
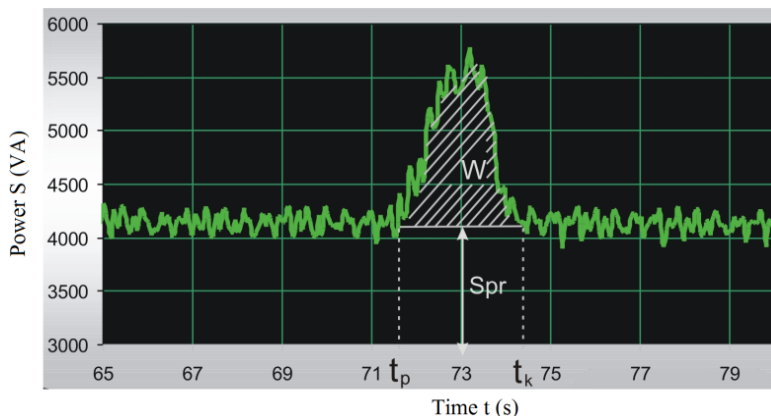
Fig. 2. Dependence of apparent power on time during crushing of individual sample

In Fig. 2, it can also be observed a change of power in the idle crusher (influence of noise in the measurement system), accordingly for each measurement mean values of idle power were calculated. Crushing energy W was calculated as the area with the use of numerical integration of the expression (Eq. 2):

$$W = \sum_{i=t_p}^{t_k} \frac{1}{2} \left[(S_i - S_{pr}) + (S_{i+1} - S_{pr}) \right] \cdot (t_{i+1} - t_i) \tag{2}$$

where:
    W – crushing energy (VA)
    t_p – start of crushing (s)
    t_k – end of crushing (s)
    S – apparent power (VA)

S_i – apparent power in i-th point (VA)
t_i – time in i-th measurement point (s)
S_{pr} – average idle power (VA).

A jaw crusher is a device that crushes only 50% of the time, and the crushing occurs only when a movable jaw is approaching the stationary jaw while when the movable jaw is leaving the stationary jaw the discharge of the crushing area is performed. Therefore, crushing of one sample requires more cycles of crushing i.e. approaching the moving jaw to the stationary jaw (Fig. 3).
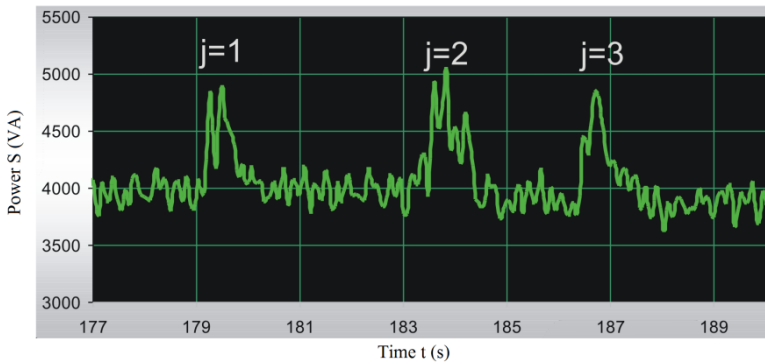
Fig. 3. Crushing sample in more cycles sample

Therefore, it is necessary to add up all the cycles according to Eq. 3 to determine the total energy required for crushing of one sample.

$$W = \sum_{1}^{j} \left(\sum_{i=t_p}^{t_k} \frac{1}{2} \left[(S_i - S_{pr}) + (S_{i+1} - S_{pr}) \right] \cdot (t_{i+1} - t_i) \right) \qquad (3)$$

where j is the number of crushing cycles for the individual sample.

Upon the completion of the crushing the grain size analysis of crushed material was conducted. The statistical analysis of the measured energy determined the influence of individual mechanical properties of rocks on the crushing energy.

Results and discussion

The results of laboratory determination of mechanical properties of rocks are presented in Table 2. The data obtained by analyzing the results from the consumption of energy and time for the crushing of individual samples in the laboratory crusher are shown in Table 3. When comparing Tables 2 and 3, it is evident that the energy consumed for grinding samples varies depending on the type of rock. The samples of igneous rock spilite and diabase from the quarries of Kremesnica, Brensberg,

Zervanjska and Jelenje vode showed much higher crushing energy consumption compared to the samples of limestone from the quarry of Belaj and Spica, and the lowest energy was spent for dolomite samples from the quarry of Ivanec. The samples used for the crushing were of different sizes; hence the crushing energy and time are expressed per unit mass of the crushed sample kJ/kg or s/kg.

The data obtained by direct measurement of specific crushing energy as described in this paper are not available in literature. In other papers, the crushing energy was not measured directly on crusher's motor. Donovan (2003) calculated the specific crushing energy from high energy crushing test. According to the results presented by Donnovan, the specific crushing energy for igneous rocks (granite, diabase, metabasalt) is in the range of 0.828-1.980 kJ/kg. For the sedimentary rocks (Siltstone) the specific crushing energy is approximately 1.26 kJ/kg.

Tosun and Konak (2014) measured power consumption of jaw crusher during crushing of limestone rocks. The specific crushing energy for the limestone rocks ranged between 1.012-3.298 kJ/kg. According to Refahi et al. (2009), the specific crushing energy for igneous rocks (granite) was around 1.5 kJ/kg while it was less for limestone, i.e. around 1.0 kJ/kg. Besides the measuring, the specific energy consumption was determined using numerical simulations. Refahi et al. (2009) also used a discrete element method to model the crushing behavior of some rocks with different mechanical properties in a laboratory jaw crusher. According to the authors, there is a difference between the Bond and wall energy varying from 2.7% for the lowest-strength rock (spherical limestone rock) to 26.5% for the hardest rock (spherical biotite rock) and from 37.8% for the lowest-strength cubic rock to 56.7% for the hardest cubic rock. Consequently, the Bond equation does not seem to be a suitable method for estimating fracture energy of a single cubic and/or a single spherical rock.

In this paper, the specific crushing energy for diabase ranged between 2.56-4.09 kJ/kg while lower values of the specific energy were obtained for sedimentary rocks ranging between 1.16-1.93 kJ/kg (Table 3).

Table 2. Results of laboratory tests of physical and mechanical properties of rocks

Open pit	Type of rock	Bulk density (kg/m^3)	Compressive strength (MPa)	Tensile strength (MPa)	Schmidt hardness	Fracture toughness II (MN/m$^{1.5}$)
Ivanec	Dolomite	2810	127.00	6.31	61.00	2.23
Belaj	Limestone	2650	135.20	7.01	59.00	2.35
Spica	Limestone	2660	122.20	10.62	53.00	3.02
Kremesnica	Spilite	2870	178.60	11.36	62.00	3.24
Jelenje vode	Diabase	2910	178.06	12.83	63.00	4.14
Brensberg	Diabase	2930	189.90	13.11	60.00	4.12
Zervanjska	Diabase	2940	199.80	14.62	61.00	4.28

Table 3. Results of laboratory tests of crushing energy and time

Crushing of individual samples				
Quarry	Type of rock	Total mass of samples (kg)	Total crushing time (s)	Specific crushing time (s/kg)	Specific crushing energy E_c (kJ/kg)
Ivanec	Dolomite	5.04	15.47	3.06	1.16
Belaj	Limestone	4.94	18.95	3.82	1.93
Spica	Limestone	4.83	12.25	2.53	1.65
Kremesnica	Spilite	5.55	19.70	3.55	3.45
Jelenje vode	Diabase	5.46	27.59	5.04	2.56
Brensberg	Diabase	5.15	21.34	4.21	3.51
Zervanjska	Diabase	4.34	19.34	4.55	4.09
Crushing of multiple samples simultaneously				
Quarry	Type of rock	Total mass of samples (kg)	Total crushing time (s)	Specific crushing time (s/kg)	Specific crushing energy E_c (kJ/kg)
Ivanec	Dolomite	6.07	17.07	2.82	1.09
Belaj	Limestone	6.10	12.83	2.10	1.64
Spica	Limestone	-	-	-	-
Kremesnica	Spilite	-	-	-	-
Jelenje vode	Diabase	5.91	15.72	2.64	1.52
Brensberg	Diabase	-	-	-	-
Zervanjska	Diabase	8.12	8.67	1.06	4.25

Due to the fact that the specific energy was calculated on the basis of crushing energy of individual samples, the measurements were repeated by crushing larger number of samples simultaneously. Test results obtained by measuring the crushing energy of larger number of samples are also shown in Table 3. As can be seen from Table 3 that the specific energy is approximately equal in crushing of individual samples and in crushing of several samples simultaneously while the specific crushing time reduced with the higher number of samples. This confirms that the specific energy does not depend on the amount of material that is crushed but on physical and mechanical properties of rocks.

The statistical analysis of the results determined the empirical dependence of crushing energy on certain mechanical properties of rocks (Table 4). From the statistical analysis it can be concluded that the specific crushing energy depends mostly on the compressive strength. Namely, the principle of comminution depends on the crusher construction; we can observe more crushing modes, one of which is predominant (Slokan 1969). In the jaw crusher the main mechanism of comminution is pressure, i.e. the comminution comes primarily from squeezing. Therefore it is logical to expect that compressive strength will have the greatest influence on crushing energy.

Table 4. Empirical dependence of specific energy of crushing on mechanical properties of rocks

Mechanical properties	Regression equation	Coefficient of determination	Maximum deviation (%)
Bulk density ρ_v (kg/m^3)	1. $E_c = 0.0065\rho_v - 15.778$	$R^2 = 0.541$	117.95
Uniaxial compressive strength σ_c (MPa)	2. $E_c = 0.032\sigma_c - 2.568$	$R^2 = 0.900$	30.29
Tensile strength σ_V (MPa)	3. $E_c = 0.2949\sigma_v - 0.5744$	$R^2 = 0.713$	55.99
Fracture toughness K_{IIc} (MN/m$^{1.5}$)	4. $E_c = 1.024K_{IIc} + 0.799$	$R^2 = 0.651$	39.03
Hardness determined by Schmidt hammer H	5. $E_c = 0.1378H - 5.624$	$R^2 = 0.171$	139.6

Table 4 shows that fracture toughness and tensile strength also significantly affect the crushing energy. Some authors (Bearman 1991; Donovan 2003) also concluded that the above properties have a significant influence on the crushing energy. In addition, it is evident that the hardness has only a slight effect and bulk density has not such a significant impact. It was expected that the bulk density would indicate a greater impact since it is known that it is directly related, not only with the mineral composition but also with porosity and the number of cracks and voids in the material. The mineral composition has a greater role in influence of bulk density while cracks and voids within the samples did not play a major role due to the fact that the samples for testing were obtained by coring.

Since it is evident from the performed analysis that there is a considerable influence of a number of tested physical and mechanical properties on crushing energy, a multiple regression analysis of simultaneous influence of multiple properties was conducted.

Table 5 shows the results of the analysis for the combination of properties that provide the largest and smallest maximum absolute deviation of the specific energy, calculated using regression equations from the measured values. It appears from the indicators of reliability of multiple regression analysis that on the specific crushing energy the biggest common effect is provided by all the tested physical mechanical properties of rocks (Table 5, regression Eq. 12). Additionally, this dependence showed the smallest maximum deviation from measured values of specific energy (1.3%). However, testing dependence of the specific energy on the combination of three studied properties of rocks already yielded a significantly small maximum deviation of the calculated energy from the measured values. The smallest maximum deviation of specific energy calculated using the three studied properties of rocks was obtained using equation on dependence of the energy on the uniaxial compressive strength, fracture toughness and hardness (5.4%). That is also evident from Fig. 4 which shows the highest and lowest maximum deviation from measured values of the specific crushing energy calculated according to the regression equations shown in Tables 4 and 5.

Table 5. Multiple regression analysis of dependence of crushing energy E_c on physical and mechanical properties of rocks

Regression equation	Regression summary for dependent variable: Specific energy, E_c (kJ/kg)	Maximum deviation (%)
6. $E_c = -15.37 + 0.0082\rho_v - 0.086H$	$R=0.757$; $R^2=0.573$; Adjusted $R^2=0.359$; F(2,4)=2.68; $p<0.183$; Std. Error of estimate: 0.877	107.5
7. $E_c = 1.758 + 0.0375\sigma_c - 0.087H$	$R=0.97$; $R^2=0.943$; Adjusted $R^2=0.914$; F(2,4)=32.82 $p<0.0033$; Std. Error of estimate: 0.321	16.0
8. $E_c = -6.06 + 0.001\rho_v + 0.829K_{IIc} + 0.033H$	$R=0.827$; $R^2=0.683$; Adjusted $R^2=0.367$; F(3,3)=2.159 $p<0.272$; Std. Error of estimate: 0.871	48.2
9. $E_c = 4885 + 0.059\sigma_c - 0.733K_{IIc} - 0.156H$	$R=0.996$; $R^2=0.992$; Adjusted $R^2=0.985$; F(3,3)=128.94 $p<0.001$; Std. Error of estimate: 0.136	5.4
10. $E_c = -7.977 - 0.0002\rho_v + 0.7\sigma_v - 1.608K_{IIc} + 0.148H$	$R=0.917$; $R^2=0.841$; Adjusted $R^2=0.522$; F(4,2)=2.64 $p<0.293$; Std. Error of estimate: 0.756	25.6
11. $E_c = 6.138 - 0.0009\rho_v + 0.06\sigma_c - 0.674K_{IIc} - 0.141H$	$R=0.997$; $R^2=0.994$; Adjusted $R^2=0.981$; F(2,4)=78.722 $p<0.013$; Std. Error of estimate: 0.151	4.5
12. $E_c = 4.397 - 0.001\rho_v + 0.053\sigma_c + 0.17\sigma_v - 1.108K_{IIc} - 0.095H$	$R=0.9997$; $R^2=0.9994$; Adjusted $R^2=0.996$; F(5,1)=326.796 $p<0.042$; Std. Error of estimate: 0.066	1.3

where:
R Pearson correlation coefficient
R^2 coefficient of determination
Adjusted R^2 : adjusted coefficient of determination
F(2,4) F-distribution
p probability value.

Table 6. Results of grain size analysis of crushed samples

Class (mm)	Average share of class (%)						
	Ivanec	Belaj	Spica	Kremesnica	Brensberg	Zervanjska	Jelenje vode
+32	8.11	0.00	4.46	4.45	3.52	4.88	0.98
32/16	46.56	52.18	46.90	53.73	57.67	56.54	59.06
16/8	24.93	26.02	26.21	24.39	20.89	20.22	21.62
8/4	9.06	8.90	9.49	7.44	6.65	6.78	7.68
4/2	5.52	5.95	6.30	4.63	4.48	4.70	4.83
2/1	2.86	3.25	3.21	2.22	2.63	2.72	2.64
-1	2.96	3.70	3.42	3.15	4.16	4.16	3.20

Upon the completion of the crushing, grain size analysis was conducted on the crushed samples with sieve size openings of 32, 16, 8, 4, 2, and 1 mm. From Table 6, it is evident that the share of each class varies depending on the type of rock. It can be seen that the share of larger classes (+32 mm and 32/16 mm) is higher in igneous rock (Kremesnica, Brensberg, Zervanjska, Jelenje vode) in comparison to the sedimentary limestone and dolomite (Ivanec, Belaj, Spica), and in the middle classes (16/8, 8/4 and 4/2 mm) it is the other way around. The share of smaller classes is more or less uniform for all rock types. Jaw crusher crushes materials by squeezing (pressure), and compared to other crushers due to friction effects of the jaw, gives a slightly higher proportion of dust.
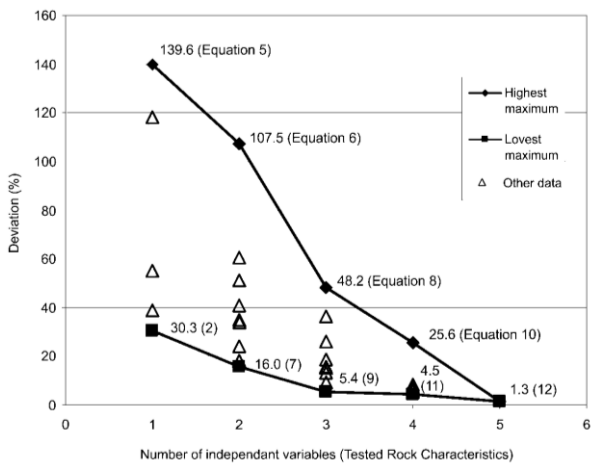

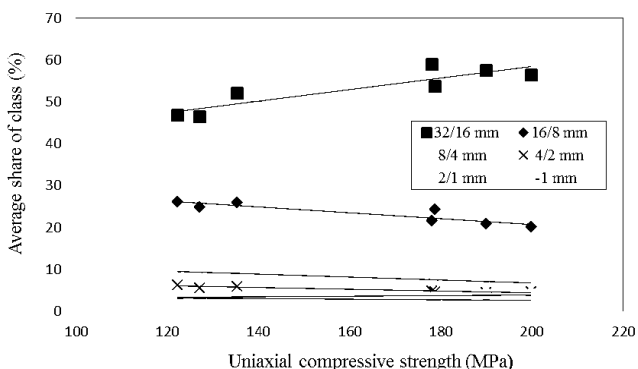Fig. 4. Calculated specific energy deviation from measured values analysis

Fig. 5. Dependence of share of classes on uniaxial compressive strength

Figure 5 shows the dependence of share of classes on the uniaxial compressive strength. The diagram shows that the increasing uniaxial compressive strength increases share of the class 32/16 mm, and reduces the share of class 16/8 mm, 8/4

mm and 4/2 mm while in class 2/1 mm and -1 mm there is no noticeable dependence on pressure strength. Considering the fact that the jaw crusher gives a larger proportion of dust due to its crushing mode (squeezing and abrasion), i.e. smaller classes compared to the other crusher, the mass proportion of small classes (2/1 mm and -1 mm) is approximately the same and varies ranging from 5.37 % to 6.95 %. Other properties of the rocks showed no significant effect on the share of each class. Thus, rocks with a higher uniaxial compressive strength are "harder" to crush resulting in an increased share of larger particles and the need to use more energy for crushing.

Conclusions

In this paper, a measuring system was developed, which enables a direct measurement of power of the jaw crusher electromotor. The specific crushing energy was determined based on the difference of the energy used in crushing samples and energy used by the idle jaw crusher. According to the test results, obtained by crushing the individual samples and crushing multiple samples at the same time, the influence of the quantity of material that is crushed is negligible. Accordingly, it can be concluded that the quantity of material does not affect the specific crushing energy and that the power consumption for crushing in the jaw crusher depends on the mechanical and physical properties of the crushed material. The energy used for crushing depends on the type of rock, and is higher for igneous rocks than for limestone and the lowest is for dolomite.

Based on the empirical dependence of the energy on the individual properties of rocks further conclusions are summarized as follows:
- specific crushing energy depends mostly on the compressive strength,
- fracture toughness and tensile strength also significantly affect the crushing energy,
- the impact of bulk density is not large while hardness has only a minor impact.

Due to the fact that the effect of the tested properties of rocks on the specific energy of rock crushing was observed, a multiple regression analysis of their simultaneous influence was carried out. Using the obtained regression equations, we performed an analysis of the deviation of the specific crushing energy obtained by computation from the measured values. The smallest maximum deviation was obtained for the equation of dependence of the specific energy on all investigated properties of rocks while a significantly little deviation was obtained by expressing dependence on only three examined properties i.e. uniaxial compressive strength, fracture toughness and hardness.

By exploring the dependence of the particle sizes of crushed samples on the mechanical properties of rocks it was found that the increasing uniaxial compressive strength of crushed material increases the proportion of larger particles, while other properties have no effect.

Acknowledgements

References

A.S.T.M., 1942, *Tentative method of test for compressive strength of natural building stone*, A.S.T.M.: Designation: C170-41T, A.S.T.M. Standards – Part 2, 1102-1104.

Bearman R. A., 1991, *The application of rock mechanics parameters to the prediction of crusher performance,* Doctoral dissertation, University of Exeter.

Bond F.C., 1952, *The third theory of comminution*, Trans. AIMF, 193, 484.

Donovan J. G., 2003, *Fracture toughness based models for the prediction of power consumption, product size, and capacity of jaw crushers*, Doctoral dissertation, Virginia Polytechnic Institute and State University.

Fuerstenau D.W., Abouzeid A-Z.M., 2002, *The energy efficiency of ball milling in comminution*, Int. J. Miner. Process. 67, 161-185.

Holmes J.A., 1957, *A contribution to the study of comminution*, Trans. Inst. Chem. Eng., 35, 125-156.

ISRM, 1978, *Suggested Methods for Determining Hardness and Abrasiveness of Rocks*, Int. J. Rock Mech. Min. Sci. & Geomech. Abstr. 15, 89-98.

Kick F., 1885, *Das Gesetz des proportionalen Widerstands und Seine Anwendung*, Felix, Leipzig.

Kujundzic T., Bedekovic G., Kuhinek D., Korman T., 2008, *Impact of rock hardness on fragmentation by hydraulic hammer and crushing in jaw crusher*, The Mining-Geological-Petroleum Engineering Bulletin, 20(1), 83 – 90.

Napier-Munn T. J., Morrell S., Morrison R. D., Kojovic T., 1996, *Mineral Comminution Circuits Their Operation and Optimisation*, Julius Kruttschnitt Mineral Research Center, Australia.

Narayanan S.S., Whiten W.J., 1988, *Determination of comminution characteristics from single-particle breakage tests and its application to ball-mill scale-up*, Transactions of IMM, 7, Section C, 115-124.

Olaleye B. M, 2010, *Influence of some rock strength properties on jaw crusher performance in granite quarry*, Mining Science and Technology (China), 20(2), 204-208.

Refahi A., Rezai B., Mohadesi J.A., 2007, *Use of rock mechanical properties to predict Bond crushing index*, Miner. Eng., 20, 662-669.

Refahi A., Mohadesi J.A., Rezai B., 2009, *Comparison between bond crushing energy and fracture energy of rocks in a jaw crusher using numerical simulation*, J. South. Afr. Inst. Min. Metall., 109, 709-717.

Sadrai S., Meech J.A., Tromans S., Sassani F., 2011, *Energy efficient comminution under high velocity impact fragmentation*, Miner. Eng., 24, 1053-1061.

Salopek B., Bedekovic G., 2000, *Fragmentation – First Stage in Enrichment Process of Mineral Raw Materials*, The Mining-Geological-Petroleum Engineering Bulletin, 12(1), 83-88.

Slokan K., 1969, *Crushing*, Tehnička enciklopedija, 3, 395-401, Leksikografski zavod Miroslav Krleža" (in Croatian).

Stamboliadis E. Th., 2002, *A contribution to the relationship of energy and particle size in the comminution of brittle particulate materials*, Miner. Eng., 15, 707-713.

Tavares L.M., Carvalho R.M., 2007, *Impact work index prediction from continuum damage model of particle fracture,* Miner. Eng. 20, 1368-1375.

Toraman O. Y., Kahraman S., Cayirli S., 2010, *Predicting the crushability of rocks from the impact strength index*, Miner. Eng., 23(9), 752-754.

Tosun A., Konak G., 2014, *Development of a model estimating energy consumption values of primary and secondary crushers*, Arabian Journal of Geosciences, 1-12.

Von Rittinger P.R, 1867, *Lehrbuch der Aufbereitungskunde*, Ernst and Korn, Berlin.

Workman L., Eloranta J., 2003, *The effects of blasting on crushing and grinding efficiency and energy consumption*, Proc 29th Con Explosives and Blasting Techniques, Int Society of Explosive Engineers, Cleveland OH, 1-5.

FLOCCULATION/DISPERSION OF HEMATITE WITH CAUSTIC DIGESTED STARCH

Min TANG, Shuming WEN

State Key Lab of Complex Nonferrous Metal Resources Clean Utilization, 650093, China and Department of Mineral Processing, Kunming University of Science and Technology, Yunnan, China, 650093, mtang-kmust@foxmail.com

Abstract: Selective flocculation of hematite with starch is a process well-known in practice. However, the separation of hematite from other minerals depends strongly on the methods of starch digestion performed either as heating-digestion or alkali-digestion (different type and dosage of alkali). The purpose of this study is to identify possible influence of the alkali-digested starch on flocculation of ultra-fine hematite when the starch was digested at different concentrations of sodium hydroxide at room temperature. Adsorption of starch digested with sodium hydroxide at different concentration on hematite was investigated by abstraction and co-precipitation tests. Turbidities tests, settling rates, flocculation/dispersion measurement and Fourier transform infrared spectroscopic analysis (FTIR) have also been conducted. Based on the results of the above mentioned tests it is suggested that the flocculating power of caustic digested starch towards fine particles may be significantly weakened, while its dispersing ability starts to play a role instead, if the concentration of sodium hydroxide is high enough in starch digestion. When the weight ratio of NaOH /starch is lower than 2, incomplete gelatinization of starch granules may lead to coagulation of fine particles of hematite mostly due to non-selective electrostatic attraction. The weight ratio of NaOH /starch from 2 to 4 helps to flocculate mineral surfaces selectively and efficiently, assuring a complete digestion of starch granules and a small amount of acidic functional products on the starch chain. However, much smaller and homogenous short-chain granules resulting from higher concentration of sodium hydroxide (the weight ratio of NaOH /starch is more than 4) used to digest starch may weaken the flocculating capacity of the caustized starch for hematite and lead to its dispersion.

Keywords: starch, alkali-digestion, flocculation, dispersion

Introduction

The common methods to prepare starch solution for use in mineral flotation are alkali-digestion using sodium hydroxide at room temperature (Iwasaki and Lai, 1965; Peres and Correa, 1996; Pavlovic and Brandao, 2003; Tomasik and Schilling, 2004) and heating-digestion at certain temperature (Afenya, 1982; Khosla et al., 1984;

Subramanian and Natarajan, 1988). Table 1 provides the application of starch as flocculant in flotation of hematite, indicating that selective flocculation on fine iron oxides is obtained with starch digested using traditional methods like alkali or heating, which may contribute to different flocculating results partly even under similar reagent condition and particle size.

Table 1. Selected literature data on application of starch as a flocculant for hematite

Mineral depressed	scale	Reagents, pH	Separation results	Reference
Hematite	Lab	Polyacrylic acid as flocculants; pH=3-9	Selective flocculation	Drzymala and Fuerstenau, 1981
Iron ore tailings	Lab	Starch as flocculants; Sodium silicate or sodium hexametaphosphate as dispersant; pH=10.5	64.8% grade and 80% recovery of Fe	Rao and Narasimhan, 1985
Hematite	Lab	Starch/amylose/amylopectin as flocculants; pH=10.0	Less than 10% floatability of hematite when 10 mg/l starch (amylose/amylopectin ~40/80)	Pinto et al., 1992
Ultrafine Hematite	Lab	Wheat Starch as flocculants; pH=10.5	Selective flocculation	Weissenborn et al., 1994; Weissenborn et al., 1995
Fine hematite	Lab	Sodium oleate as collector; Starch as depressant; pH=9-9.5	60% recovery with adding $1 \times 10^{-4} mol/dm^2$ oleate	Shibata and Fuerstenau, 2003
Fine hematite	Lab	Tetradecylammonium chloride as collector; Starch as depressant; pH=7.5	80% recovery of hematite when adding $7.0 \times 10^{-4}M$ collector.	Montes and Atenas, 2005
Iron ore slimes	Pilot	Amine as collector; Starch as depressant; pH=10.7	80.5% recovery of Fe and 23.9 of Gaudin's selectivity index	Rocha et al., 2010
Hematite in waste-water	Lab	Polyalumiun chloride (PAC)/ferric chloric (FA)=3:7 as coagulant; Polyacrylamide (PAM) as flocculant; pH=10.45	Decrease the turbidity from 13530 NTU to 12 NTU	Yang et al., 2010
Hematite <100μm	Lab	N-laure-1,3-diaminopropane as collector; Starch as depressant; pH=7.27	58.45% grade and 86.93% recovery of Fe from a 2:3 ratio of hematite: quartz mixture containing 28% grade of Fe	Liu et al., 2011

Previous investigations were focus on the physicochemical effects of concentration of sodium hydroxide on starch degradation used mostly in food or agriculture industries. Roberts and Cameron (2002) and Wootton and Ho (1989) indicated that during gelatinization of starch in the presence of sodium hydroxide it can swell rapidly at room temperature, and the granules can become smaller and more dispersed as well as homogenous with increasing the dosages of NaOH. It was observed by Maher and Peoria (1983) that the alkali/starch weight ratio can determine the degree of gelatinization. Also there are some investigations which explain chemical changes induced by NaOH-degradation of starch suspension and affected of the concentration of NaOH. Sheng et al. (2011) found that a certain amount of NaOH at 100 ^{o}C for 3 hours during starch digestion can harvest desirable water-soluble oxidized starch with carboxyl content of 3.6 g/100 g, indicating that the amount of sodium hydroxide can influence the oxidation of native starch. Niemela (1990) investigated a starch treated with 1 M and 3 M sodium hydroxide at 175 ºC and found that mixtures of carboxylic acids, up to 40-60% of the original mass of the starch, were produced. Jebber et al. (1996) reported that various carboxylic acids (formic, acetic, glycolic, lactic, 2-hydroxybutanoic, 2-hydroxy-2-methylpropanoic, and 2-hydroxypentanoic acids) were isolated from the alkali-degraded starch. Tang and Liu (2012) found that a few acidic carboxyl groups produced during alkali-degradation of starch were observed.

Although the use of alkali-gelatinized starch in mineral processing is well established, the effects of concentration of sodium hydroxide on starch adsorption on mineral surfaces are not sufficiently understood. Different concentrations of NaOH in starch digestion may lead to changes of starch granule structures, size of remnant chains and the amount of new functional groups on the chains. Those may enhance or weaken its adsorption on the surfaces of minerals. In this study, the possible functions, flocculation or dispersing, of hematite by starch digested with NaOH at different concentrations at room temperature were studied. The objective was to determine the flocculating power of caustic digested starch.

Experimental

Materials

Corn starch S-4180, containing 12.3% moisture, was purchased from Sigma-Aldrich. Sodium hydroxide S318-1, assaying 98.8%, was from Fisher Scientific. Sulfuric acid (96.8%) was used as a pH modifier and was purchased from Fisher Scientific. Iron (III) chloride hexahydrate ($FeCl_3 \cdot 6H_2O$, 99.8%), 188-510, was purchased from Fisher Scientific and used in co-precipitation tests. The powder of iron(III) oxide (hematite, CAS 1309-37-1, 99+ %, < 5 μm) was purchased from Sigma-Aldrich.

Methods

Turbidity measurement

The turbidities of starch suspensions were measured by turbidity meter 66120-200, manufactured by VWR Scientific. To prepare the starch suspensions for the turbidity measurements, 50 cm^3 of a 0.5% (5 g/dm^3) starch suspension was digested with either 50 cm^3 sodium/potassium hydroxide solutions at different concentrations or distilled water at different temperatures for 30 min, then a small volume of the digested starch suspension was diluted twice with distilled water and used for turbidity measurement.

Paste titration

The carboxyl content of caustized starch was determined according to the procedure of Mattisson et al. (1952) and Chattopadhyay et al. (1997) after slight modifications. Starch was caustized with a given concentration of sodium hydroxide and the suspension was filtered to collect the starch as a filter cake. The concentration of sodium hydroxide was chosen such that it did not cause complete digestion of the starch. Half a gram (0.5 g) of the collected starch cake was mixed with 25 cm^3 of 0.1 M HCl in a 150 cm^3 beaker at room temperature with a magnetic stirrer for 30 min. The slurry was filtered through a 150 cm^3 medium porosity fritted glass funnel and a fine stream of distilled water from a wash bottle was used to transfer the sample from the beaker. The sample was washed with 400 cm^3 of distilled water in order to completely remove the chloride ions. The starch cake was then transferred to a 500 cm^3 beaker with the aid of distilled water and the slurry was diluted to approximately 300 cm^3. The slurry was heated in a boiling water bath with continuous stirring for 15 min to ensure complete gelatinization. The hot starch solution volume was adjusted to approximately 450 cm^3 with boiling distilled water and immediately titrated to pH 8.3 with standardized 10^{-3} M sodium hydroxide with stirring. The amount of the 10^{-3} M sodium hydroxide used in cm^3 was recorded. The original untreated starch sample was used as a blank test to check potential presence of any possible inherent acidic substances in the starch. For the control blank titration, instead of stirring with 0.1 M HCl, 1 g of untreated starch or starch digested with only boiling water was stirred with 25 cm^3 of distilled water for 30 min, and the remainder of the procedures was the same as above. The acidity and carboxyl content of the starch were calculated from the following equations (Chattopadhyay et al., 1997):

$$\frac{\text{meq acidity}}{\text{100g starch}} = \frac{(\text{mL NaOH for sample} - \text{mL NaOH for blank test}) \cdot \text{Normality of NaOH} \cdot 100}{\text{Sample weight (dry basis) in g}} \quad (1)$$

$$\frac{\text{apparent \%}}{\text{Carboxyl (\% dry basis db)}} = \text{meq of acidity of 100g starch} \cdot 0.045 \quad (2)$$

Adsorption tests

To measure the adsorption density of the starch digested with sodium/potassium hydroxide or boiling distilled water on mineral surfaces, 100 cm^3 0.5% starch suspension was caustized with 100 cm^3 of a sodium hydroxide solution at a sodium hydroxide concentration of 1.5%, 1.75%, 2%, 2.25%, or 2% of potassium hydroxide, or boiling distilled water. The mixed suspension was stirred at room temperature for 30 min, and then 20 cm^3 of the suspension was withdrawn and diluted to 200 cm^3 with distilled water. Fifty cm^3 of the 0.025% starch solution was adjusted to pH 7 and mixed with 50 cm^3 2% hematite suspension (containing 1 g of hematite) that was also adjusted to pH 7. The mixture was shaken in a thermostated circular shaker for 30 min. The temperature was maintained at 25±1ºC. After reaching equilibrium, the pH of the suspension was measured again, and a small sample of the suspension was centrifuged for 10 min by Sorvall GLC-4 General Laboratory Centrifuge (G~ 325 N). The supernatant was assayed for starch following the phenol-sulfuric acid method developed by Dubois et al. (1956).

Co-precipitation tests

A certain amount of ferric chloride solution was adjusted to pH 7 to form hematite and then mixed with the caustized starch solution digested with sodium hydroxide at different concentrations which also was adjusted to pH 7 before mixing, so that the final concentration of ferric ion was 0.001 M and that of starch was 125 ppm. The mixture was shaken in a thermostated circular shaker for 30 min. The temperature was maintained at 25±1ºC. After conditioning, a small sample of the suspension was centrifuged for 10 min by Sorvall GLC-4 General Laboratory Centrifuge (G~ 325 N). The supernatant was then sampled to assay for the residual concentration of starch. Blank tests for starch were also conducted.

Settling rate measurements

To measure the settling rate of the flocs resulting from the adsorption of caustized starch on hematite, 100 cm^3 0.5% (5 g/dm^3) starch suspension was caustized with 100 cm^3 of a sodium hydroxide solution at a sodium hydroxide concentration of 1.25%, 1.5%, and 2%. The mixed suspension was stirred at room temperature for 30 min, and then 20 cm^3 of the suspension was withdrawn and diluted to 200 cm^3 with distilled water. One hundred cm^3 of the 0.025% starch solution was adjusted to pH 7 and mixed with 100 cm^3 2% hematite suspension (containing 1 g of hematite) that was also adjusted to pH 7. The mixture was shaken slightly in a thermostated circular shaker for 30 min. The temperature was maintained at 25±1ºC. After conditioning, the settling tests were performed using a 250 cm^3 graduated glass cylinder (280 mm high and 40 mm in diameter).

Flocculation/dispersion measurements

The degree of flocculation/dispersion of mineral suspension was measured by a Photometric Dispersion Analyzer (PDA2000) manufactured by Rank Brothers Inc. In the test, 0.5g hematite (-5 μm) and 50 cm^3 water were agitated using a magnetic stirrer in a 250- cm^3 beaker and circulated through the flow cell of the PDA 2000 using a peristaltic pump. The magnetic stirring bar was 50 mm long and the stirring speed was fixed at 300 rpm. The Ratio output as a function of time was recorded by a computer connected to the PDA2000. The flocculation/dispersion state of the suspension was monitored in real time following the addition of starch to the circulating suspension.

Results and discussion

Carboxyl contents of starch digested sodium hydroxide

Table 2 shows the contents of carboxyl groups generated on starch when a 0.5% starch suspension (5 g/dm^3) was digested with different concentrations of sodium hydroxide. It can be seen that with increasing concentrations of sodium hydroxide, more carboxyl groups were produced. Although the NaOH-to-starch weight ratios were less than 1, some amounts of carboxyl groups were detected. In practice, starch is usually digested with more sodium hydroxide, with NaOH-to-starch weight ratios ranging from 2 to 4. It can be expected that more carboxyl groups will be generated at these higher weight ratios. The titration tests were not performed at higher NaOH to starch weight ratios because of the difficulty in harvesting the treated starch granules for titration.

Table 2. The carboxyl content and isoelectric point of starch digested with different concentrations of sodium hydroxide

Concentration of NaOH, %	IEP of starch after digestion, pH	Acidity of carboxyl content of caustized starch, %db (dry basis)
0.075	3.80	0.0099
0.250	3.25	0.016
0.500	2.95	0.034
1.000	2.89	0.14

Flocculation/dispersion measurement with PDA

Figure 1 shows the images (1:1) of starch solution digested with 2%, 2.5% and 3% NaOH after settling. As can be seen, the size of flocs for starch remnants became smaller and smaller with increasing the concentration of NaOH, indicating that the higher concentration could lead to breakdown of the starch chain rapidly, lowering its flocculating power and playing its dispersing role on hematite to some degree. These results are in agreement with the results from flocculation/dispersion measurement with PDA as shown in Fig. 1. It can be observed that the ratio of ultra-fine hematite (-5μm) reduced significantly from 7 to 2~3, suggesting that the initial fluffy aggregated

hematite particles induced by their electrostatic attractions were not flocculated, but dispersed when adding starch digested with 2.5% NaOH.
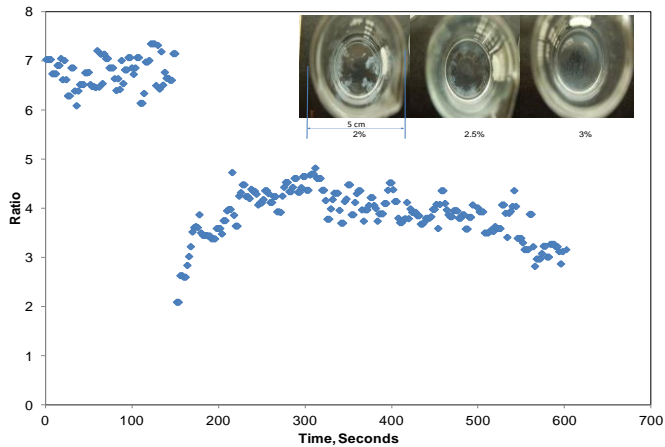

Fig. 1. Effect of starch digested with 2.5% NaOH on the flocculation/dispersion of hematite (particle size of hematite: -5μm, pulp density: 1%, pH=7, hematite: 1%, starch: 500 ppm)

Adsorption on hematite and co-precipitation with Fe (III) of caustized starch
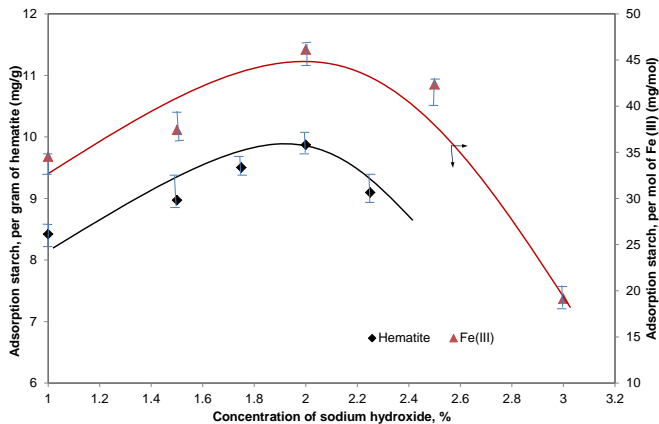
Fig. 2. Adsorption of starch on either hematite or Fe(III) for with different concentrations of sodium hydroxide used for digestion

It can be seen in Fig. 2 that there was a similar trend of adsorption of caustized starch on both co-precipitated Fe(III) and hematite for different concentrations of NaOH used for digestion. The maximum amount of starch co-precipitated with Fe(III) (46.13 mg/mol Fe(III)) and adsorbed on hematite (9.87 mg/g hematite) occurred for about 2% NaOH. The small number of carboxyl groups resulted from alkali-digestion

may help flocculation according to the results shown in Table 2. However, a decrease in the amounts of starch absorbed on either hematite or Fe (III) might be related partly to the changes of sizes of the remnants granules, inducing mostly short-chain granules from caustic starch digestion using more than 2% NaOH. This is based on the results shown in Fig. 1 and previous literature (Casu and Reggiani, 1964; Liu et al., 2002). Much smaller and homogenous short-chain granules resulted from higher concentration of NaOH used to digest starch may weaken the flocculating capacity of the caustized starch on hematite and Fe(III) leading to a decrease in the adsorption density.

Settling behaviors of -5 µm hematite treated with caustized starch by visual observations

As can be seen in Fig. 3, with increasing concentration of sodium hydroxide used to digest the starch, the settling rate of a -5 µm hematite sample was increased when it was treated with starch. The initial settling rate increased from $3.7 \cdot 10^{-5}$ m/s when the sodium hydroxide concentration was 1.25%, to $6.9 \cdot 10^{-5}$ m/s, when the sodium hydroxide concentration was 2.0%. The results are in a good agreement with the pictures taken at same time intervals during settling rate measurement of hematite treated by caustic starch, indicating that much faster settling rate was found for hematite treated by starch digested with 2.00% than with 1.25%. In view of the results shown in Fig. 1, complete digestion and dissolution of starch was achieved at a sodium hydroxide concentration of 1%. A further increase occurring for higher sodium hydroxide concentration may not be the result of better dissolution. A higher sodium hydroxide concentration induces two changes that have opposite effect on the settling behavior of hematite. On one hand, it generated acidic groups on the starch which may promote its adsorption on hematite. On the other hand, the higher concentration could lead to breakdown of the starch chain (Khosla et al., 1984), lowering its flocculation power. In the sodium hydroxide concentration range tested, it can be seen that the increasing concentration caused an increase in the settling rate. This is most likely the result of increasing adsorption density that was caused by the acidic groups of carboxylic acid. Figure 2 indicates that the adsorption density of starch was higher at higher sodium hydroxide concentrations that were used to digest starch. The acidic groups may provide more "anchor" sites for starch on the surface of hematite. It was reported by Weissenborn et al. (1995) that starch prepared with sodium hydroxide solution (weight ratio of starch/NaOH was 1: 0.4) at 85 ^{0}C could produce large and fast settling aggregates during adsorption on hematite.
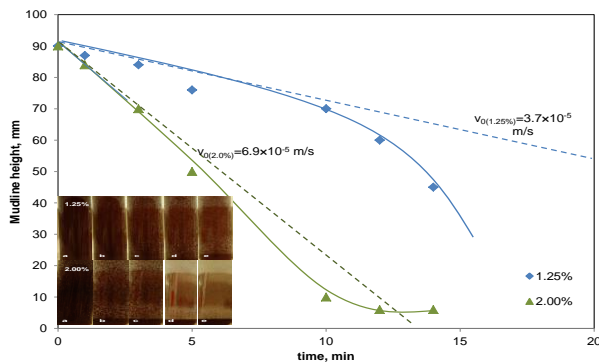
Fig. 3. Settling curves and pictures of -5 μm hematite treated by starch digested with 1.25% and 2.00% NaOH. Interval of settling pictures was: a.0 s, b. 30 s, c. 60 s, d. 120 s and e. 180 s. The two dashed lines were drawn in a tangential direction from two settling curves, respectively

FTIR spectra of starch digested sodium hydroxide

Figure 4 shows the Fourier transform infrared (FTIR) spectra of pure hematite, hematite mixed with starch digested with 2% NaOH and Fe(III) ions mixed with starch digested with 2% NaOH. It has been observed that the overtone and combination bands of Fe-O stretching vibrations near 1,110 and 1,020 cm^{-1} for pure hematite disappeared, and –CO and C-OH stretching vibrations of starch near 1,130~1,010 cm^{-1} arose when caustized starch was reacted with hematite. Those results are well in agreement with the previous research published by Tang and Liu in 2012, who found that two new small peaks, at 1,558 cm^{-1} and 1,548 cm^{-1} for the 0.3% NaOH, and 1,552 cm^{-1} and 1,544 cm^{-1} for the 0.5% NaOH, appeared for the alkali digested starch compared with the native starch, indicating the presence of carboxyl groups. However, these peaks were small meaning that the concentrations of the carboxyl groups are not very high. This is consistent with the titration results shown in Table 2. The low carboxyl contents may be a result of the relatively low NaOH to starch ratio (0.6 and 1.0). Also it can be seen that the COO$^-$ asymmetric and symmetric stretching occurred near 1,620 cm^{-1} for the caustized starch adsorbed on the hematite, and at 1,450 and 1,340 cm^{-1} in the precipitates obtained after reacting Fe(III) chloride (FeCl$_3$·6H$_2$O) with the caustized starch. Those results are in accordance with the previous literature (Gersmann et al., 1963; Casu and Reggiani, 1964; Wootton and Ho, 1989; Nakazawa and Wang, 2003; Somasundaran and Wang, 2006; Cao et al., 2009), indicating that there were indeed carboxylate groups that were involved in the interaction between the iron oxide/hydroxide species and the caustized starch.
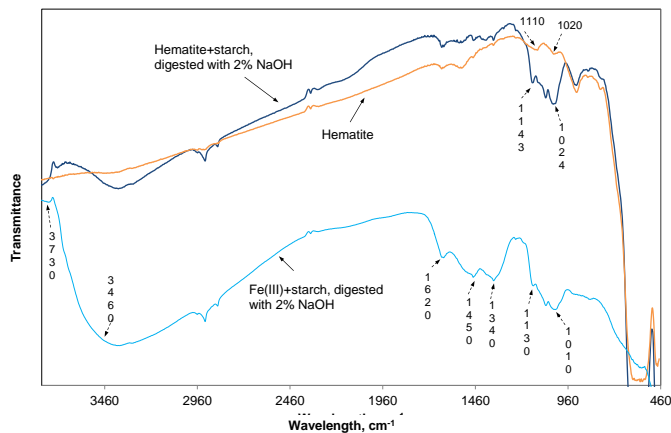
Fig. 4. FTIR spectra of starch digested with 2% sodium hydroxide adsorbed on hematite and Fe(III)

Possible model of flocculation/dispersion of caustic digested starch onto mineral surfaces

Figure 5 presents the possible model for starch, digested with NaOH of different concentrations, adsorbed on hematite. It is hypothesized that there may be four scenarios for adsorption of digested starch on mineral surfaces: no aggregation of native starch and particles, coagulation at a very low concentration, flocculation at suitable concentration, and finally dispersion at higher concentrations. Based on the data of turbidity and paste titration tests, when the weight ratio of NaOH/starch is near 4, the turbidity of the starch suspension is <10 NTU and the DS of carboxylic acids on the granules' remnants is up to 0.5/100ATU, very good gel of starch occurs which may achieve the maximum adsorption between starch and hematite due to acid-base interaction. In that case, the size of the starch remnants may provide suitable container for the flocculation of hematite. Meanwhile, the new acidic groups may provide more "anchor" sites for starch on the surfaces of minerals. However, the selective dispersion of starch occurs when the concentration of NaOH is greater than 2%. Because small short-chain starch granules cannot interact with ultra-fine particles effectively, it leads to a lower efficiency of flocculation of hematite and starts to show its dispersion to some degree. The results from Table 2 and Figs 1- 4 are in accordance with this hypothesis. Of course, the high ionic strength of the starch suspension resulting from the high concentration of NaOH during flocculation of starch and hematite cannot be ignored (Ma and Bruckard, 2010).
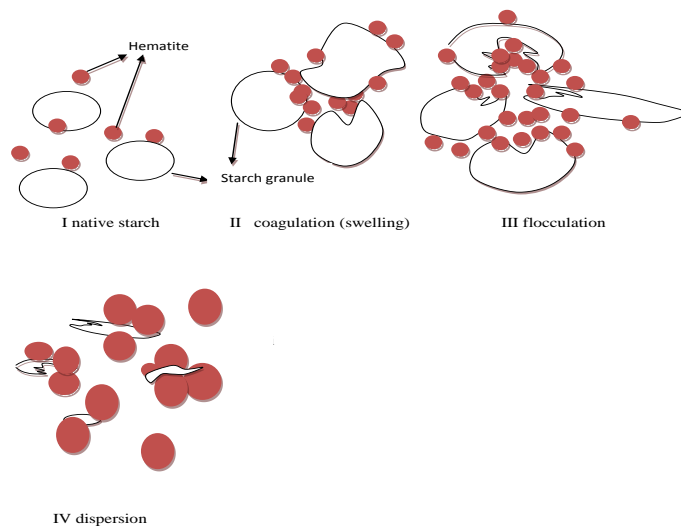
Fig. 5. Macro-model for adsorption of starch digested with increasing concentration of NaOH on hematite

Conclusions

The optimum NaOH:starch ratio equal to about 4 used for starch digestion was found to ensure maximum adsorption efficiency of 9.87 mg/g hematite on the mineral surface of hematite. It is hypothesized that there may be four possible scenarios during of starch and mineral interactions based on flocculating or dispersing mechanism. The "fluffy" flocks and open crystal areas of the granules' remnants, as well as a small amount of carboxyl groups resulting from suitable alkali-digestion, may enhance the adsorption of starch on hematite. On the other hand, too short chains of the granules may cause dispersion of hematite fines causing difficulties in settling.

Acknowledgements

References

AFENYA P.M., 1982, *Adsorption of xanthate and starch on synthetic graphite*, Int. J. Miner. Process 1, 303-319.

CAO Q., TIAN P., WU Q.L., 2009, *Modeling diameter distributions of poly (N-isopropyacrylamide-co-methacrylic acid) nanoparticles*, J. Appl. Polym. Sci. 111, 2584-2589.

CASU B., REGGIANI M., 1964, *Infrared spectra of amylose and its oligomers*, J. Polym Sci. C: 7, 171-185.

DRZYMALA J., FUERSTENAU D.W., 1981, *Selective flocculation of hematite in the hematite-quartz-ferric Ions-polyacrylic acid system: Part I. Activation and deactivation of quartz,* Int. J. Miner. Process 8, 265-277.

DUBOIS M., GILLES K.A., HAMILTON J.K., REBERS P.A., SMITH F., 1956, *Colorimetric method for determination of sugars and related substances*, Anal. Chem. 28, 350-356.

CHATTOPADHYAY S.S., SINGHAL R.S., KULKARNI P.R., *Optimization of conditions of synthesis of an oxidized starch from corn and amaranth in film-forming applications*, Carbohydr. Polym. 34, 203-212.

GERSMANN H.R., NIEUWENHUIS H.J.W., BICKEL A.F., 1963, *The mechanism of autoxidations in alkaline media*, Carbohydr. Res. 74, 1383-11385.

HOUOT R., 1983, *Beneficiation of iron ore by flotation _Review of industrial and potential applications*, Int. J. Miner. Process 10, 183-204.

IWASAKI I., LAI R.W., 1965, *Starches and starch products as depressants in soap flotation of activated silica from iron ores,* Soci. Min. Eng. Transac DEC: 364-371.

JEBBER K.A., ZHANG K., CASSADY C. J., CHUNG-PHILIPS A., 1996, *Ab Initio and Experimental Studies on the Protonation of Glucose in the Gas Phase*, J. Am. Chem. Soc. 118, 10515 - 10563.

KHOSLA N.K., BHAGAT R.P., GANDHI K.S., BISWAS A.K., 1984, *Calorimetric and other interaction studies on mineral-starch adsorption systems,* Colloids Surf. 8, 321-336.

LIU Q., CHARLET G., YELLE S., ARUL J., 2002, *Phase transition in potato starch-water system I. Starch gelatinization at high moisture level*, Food Res. Int. 35, 397-407.

LIU W., WEI D., GAO S., HAN C., 2011, *Adsorption mechanism of N-laurel-1,3-diamino propane in a hematite-quartz flotation system*, Min. Sci. Tech. (China), 21, 213-215.

MAHER G.G., PEORIA, 1983, *Alakli gelatinization of flours*, Starch/Stäkrke 35, 271-276.

MATTISSON M.F., LEGENDRE K.A., 1944, *Determination of carboxyl content of oxidized starches*, Anal. Chem. 24, 1942-1944.

MA X., BRUCKARD W.J., 2010, *The effect of pH and ionic strength on starch-kaolinite interactions*, Int. J. Miner. Process 94, 111-114.

MONTES S., ATENAS G.M., 2005, *Hematite floatability mechanism utilizing tetradecylammonium chloride collector*, Miner. Eng. 18, 1032-1036.

NAKAZAWA Y., WANG Y., 2003, *Acid hydrolysis of native and annealed starch and branch-structure of their Naegeli dextrins*, Carbohydr. Res 338, 2871-2882.

NIEMELA K., 1990, *Conversion of xylan starch, and chitin into carboxylic acids by treatment with alkali*, Carbohydr. Res. 204, 37-49.

PAVLOVIC S., BRANDAO P.R.G., 2003, *Adsorption of starch, amylose, amylopectin and glucose monomer and their effect on the flotation of hematite and quartz,* Miner. Eng. 16, 1117-1122.

PERES A.E.C., CORREA M.I., 1996, *Depression of iron oxides with corn starches,* Miner. Eng. 9, 1227-1234.

PINTO C.L.L., DE ARAUJO, A.C., PERES A.E.C., 1992, *The effect of starch, amylose and amylopectin on the depression of oxidize- minerals, Miner. Eng.* 5, 467-478.

RAO K.H., NARASIMHAN K.S., 1985, *Selective flocculation applied to Barsuan Iron ore tailings,* Int. J. Miner. Process 14, 67-75.

ROCHA L., CANCADO R.Z.L., PERES A.E.C., 2010, *Iron ore slimes flotation*, Miner. Eng. 23, 842-845.

ROBERTS S.A., CAMERON R.E., 2002, *The effects of concentration and sodium hydroxide on the rheological properties of potato starch gelatinization*, Carbohydr. Polym. 50, 133-143.

SHENG Y., WANG Q., XU X., JIANG W., GAN S., ZOU H., 2011, *Oxidation of cornstarch using oxygen as oxidant without catalyst*, LWT--Food Sci. Technol. 44,139-144.

SHIBATA J., FUERSTENAU D.W., 2003, *Flocculation and flotation characteristics of fine hematite with sodium oleate*, Int. J. Miner. Process 72, 25-32.

SOMASUNDARAN P., WANG D., 2006, *Chapter 4 Mineral-flotation reagent equilibria, in Developments in Mineral Processing*, 17, 73-141.

SUBRANMANIAN S., NATARAJAN K.A., 1988, *Some studies on the adsorption behavior of an oxidized starch on hematite*, Miner. Eng. 1, 241-254.

TANG M., LIU Q., 2012, *The acidity of caustic digested starch and its role in starch adsorption on mineral surfaces*, Int. J. Miner. Process 112-113, 94-100.

TOMASIK P., SCHILLING C.H., 2004, *Chemical modification of starch*, Adv. Carbohydr. Chem. Biochem. 59, 175-403.

WEISSENBORN P.K., WARREN L.J., DUNN J.G., 1994, *Optimisation of selective flocculation of ultrafine iron ore,* Int. J. Miner. Process 42, 191-213.

WEISSENBORN P.K., WARREN L.J., DUNN J.G., 1995, *Selective flocculation of ultrafine iron ore: 1 Mechanism of adsorption of starch onto hematite*, Colloids Surf. A: 99, 11-27.

WOOTTON M., HO P., 1989, *Alkali Gelatinisation of Wheat Starch*, Starch/Stärke 41, 261-265.

YANG Y., LI Y., ZHANG Y., LIANG D., 2010, *Applying hybrid coagulants and polyacrylamide flocculants in the treatment of high-phosphorus hematite flotation wastewater (HHFW): Optimization through response surface methodology*, Sep. Purif. Technol. 76, 72-78.

INVESTIGATION OF LEACHING KINETICS OF CERUSSITE IN SODIUM HYDROXIDE SOLUTIONS

Qicheng FENG*, Shuming WEN*, Yijie WANG*, Wenjuan ZHAO**, Jiushuai DENG*

* State Key Laboratory of Complex Nonferrous Metal Resources Clean Utilization, Kunming University of
  Science and Technology, Kunming 650093, China
**Kunming Metallurgical Research Institute, Kunming 650031, China

Abstract: The leaching kinetics of cerussite in alkaline medium was investigated with respect to experimental variables such as sodium hydroxide concentration, temperature, particle size and stirring speed. The results showed that leaching reagent concentration and reaction temperature exerted significant effects on the extraction of lead, whereas particle size and stirring speed exhibited a relatively moderate effect on the leaching rate. The leaching process followed the kinetic law of the shrinking core model, and the dissolution rates were controlled by the surface chemical reaction with an apparent activation energy value of 43.79 kJ/mol. A corresponding dissolution kinetic equation was also proposed to describe the dissolution reaction. The results indicated that sodium hydroxide could be used as an effective leaching reagent for extracting lead from cerussite.

Keywords: cerussite, sodium hydroxide, leaching, kinetics, activation energy

Introduction

Lead, as an important nonferrous metal, has been widely applied in the electric, chemical engineering, construction, atomic power filed, and other industries because of its excellent physical and chemical properties (Nowak and Laajalehto, 2007; Schroder-Wolthoorn et al., 2008; Zhu et al., 2013). Lead is mainly generated from lead-bearing minerals such as galena, cerussite and anglesite (Nikolic et al., 1996; Herrera-Urbina et al., 1998; Mikhlin et al., 2004), as well as from discarded materials containing lead such as lead-acid batteries, funnel glass and smelting slags (Yuan et al., 2012; Agrawal et al., 2004; Atanasova, 2009; Fedje et al., 2010). In the past, pyrometallurgical processes have been frequently used for smelting lead sulfide and secondary waste containing lead to obtain metallic lead (Okada et al., 2007). However, the disposal of lead using the conventional pyrometallurgical technique is associated

with undesirable emissions of harmful sulfur oxides and lead vapor or dust into the atmosphere (Ettler et al., 2005; Aydogan et al., 2007; Pan et al., 2013). Given these environmental concerns with the pyrometallurgical operation, an increasing number of studies on hydrometallurgical processes have been conducted in the recent years.

Leaching is a key step in the hydrometallurgical process, and the selection of an appropriate leaching reagent is beneficial to this process. Various leaching agents are used in hydrometallurgical processes of lead such as acids, sodium hydroxide and chloride solutions (Baba and Adekola, 2011; Lima and Bernardez, 2013; Nagib and Inoue, 2000; Liao and Deng, 2004; Qin et al., 2012). Lead-bearing minerals can be treated using acidic leaching processes. However the dissolved lead is associated with other metals such as Fe, Ca, Mg and SiO_2, which results in high acid consumption and complex purification processes (Qin et al., 2007; Feng et al., 2007; Liu et al., 2012). Therefore, a practical and selective reagent for such ores is necessary.

Sodium hydroxide is commonly used as an alkaline reagent in lead extraction. Complex ions are formed between lead cations and hydroxide ions in this leaching system. Nagib and Inoue (2000) compared acid leaching to alkaline leaching, and found that alkaline leaching has more advantages when recovering lead from fly ash generated from municipal incineration plants. In alkaline leaching, some impurities, such as Fe, Mg and Al remained in the solid residue, which facilitated the purification process. Zhao and Stanforth (2000) found that over 85% of lead could be extracted using a cost-effective alkaline leaching process through the addition of sodium sulfide, which produced less than 10% of Al impurities. Similarly, Liu et al. (2011) developed an alkaline leaching process for the production of lead concentrates from lean oxidized ores. In this process the lead concentrations were highly selectively and quantitatively produced from the leaching solution by adding sodium sulfide as precipitant. In addition, Badanoiu et al. (2013) obtained good indexes by treating PbO in waste lead-acid battery with sodium hydroxide solutions. Orhan (2005) employed sodium hydroxide as leaching agent to recover lead from electric arc furnace dust, and showed that 90% of lead was dissolved under the following optimum conditions: S/L ratio of 1/7, 95 °C, 10 M NaOH, stirred at 600 rpm for 2 h.

Given that lead resources have been continuously exploited and lead sulfide ores have gradually become depleted, oxidized lead minerals have been developed as important sources of lead metal to meet future demands. Cerussite is the most popular and common mineral among these oxidized lead minerals. Although a number of studies have indicated that alkaline leaching is a favorable method to extract lead from various lead-bearing materials, no information on alkaline leaching of cerussite and its corresponding kinetics studies has been reported so far. Therefore, this study aims to investigate the extraction of lead from pure cerussite using aqueous sodium hydroxide solutions as leaching reagents and the kinetics of this leaching process. The effect of sodium hydroxide concentration, reaction temperature, particle size and stirring speed on the dissolution ratio of cerussite are also evaluated.

Materials and methods

Materials and reagents

Samples of cerussite from the Yunnan province of China were obtained after the manual removal of gangue minerals. X-ray fluorescence (XRF) and X-ray diffraction (XRD) analyses of materials showed that the cerussite contained 76.70% Pb, 4.48% C and 18.30% O with only $PbCO_3$ crystals. The pure cerussite sample was manually ground in a mortar, and then sieved through standard test sieves to produce the desired particle sizes for the leaching experiments. Analytical-grade sodium hydroxide was used as the leaching reagent. Pure deionized water was used for all experimental works.

Leaching experiments

The leaching process was performed in a 500 cm³ three-necked flask batch reactor in a thermostatically controlled water bath, equipped with a digital mechanical stirrer, a thermometer and a condenser to prevent evaporation loss. Typically, 500 cm³ of freshly prepared sodium hydroxide solutions with various concentrations were added into the reactor and heated until the required temperature was reached. A five g sample of cerussite with the required particle size was added at a certain stirring speed, and then 5 cm³ of the resulting solutions was accurately withdrawn at specific time intervals and filtered prior to the lead concentration analysis, using an atomic absorption spectrophotometer (AAS).

Results and discussion

Cerussite can be dissolved in alkaline solution of sodium hydroxide. In this study, high concentration of aqueous sodium hydroxide was used to dissolve cerussite to form a soluble complex. The basic leaching reaction between cerussite and sodium hydroxide may be described as in Eq.(1)

$$PbCO_3 + 4OH^- = Pb(OH)_4^{2-} + CO_3^{2-}. \tag{1}$$

Effect of sodium hydroxide concentration

Several experiments, each lasting for 30 min, were carried out to investigate the effect of sodium hydroxide concentration on the dissolution of cerussite with an average particle size of 126 μm at 333 K, stirring speed of 500 rpm and solid to liquid ratio of 1/100 g/cm³. The results in Fig.1a showed a direct relationship between the lead leaching fraction and sodium hydroxide concentration. The leaching fraction of lead reached the maximum in about 15 min of dissolution when the concentration of sodium hydroxide was 5 mol/dm³, while additional leaching time was required to obtain the same leaching fraction of lead at lower sodium hydroxide concentration.
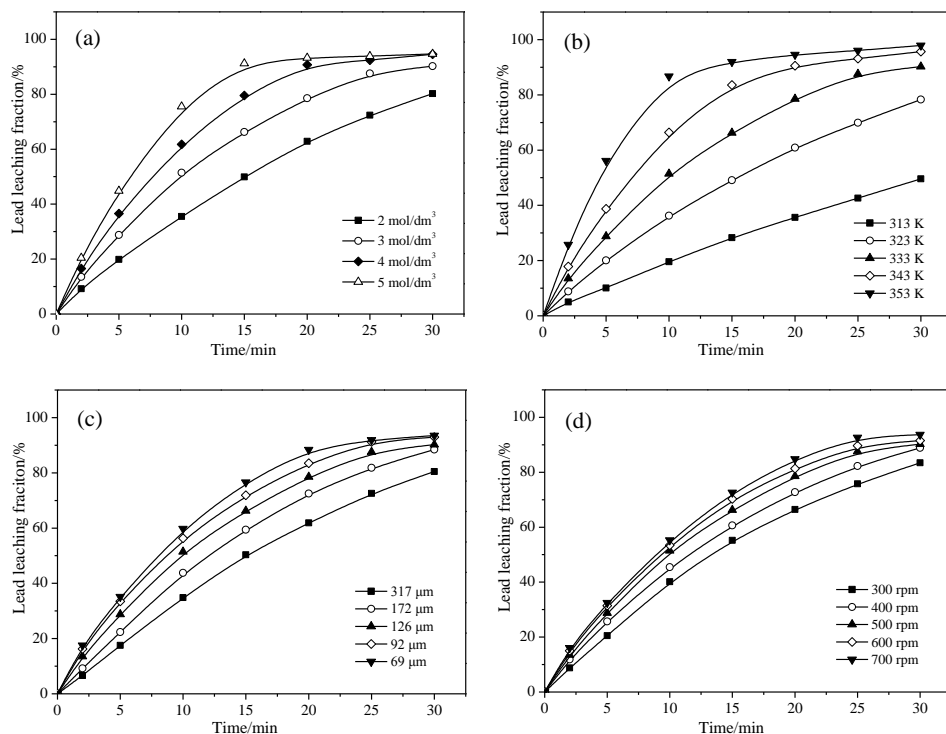
Fig.1. Effect of operation parameters on the leaching efficiency of lead: (a) sodium hydroxide concentration, (b) temperature, (c) particle size, and (d) stirring speed

3.2. Effect of temperature

Figure 1b showed the effect of temperature between 313 K and 353 K on the dissolution of cerussite. Samples with 126 μm average particle size were dissolved in 3 mol/dm^3 of sodium hydroxide. The solid to liquid ratio was kept constant at 1/100 g/cm^3 with a stirring speed of 500 rpm. The results showed that the reaction temperature clearly exerted significant effects on lead extraction. The lead leaching fraction increased with elevating temperature because of the active molecular motion. At high temperature (353 K) the leaching fraction of lead reached 86.72% in 10 min of dissolution, whereas less than 20% of lead was extracted within the same dissolution time at 313 K.

Effect of particle size

Samples with average particle sizes of 317, 172, 126, 92 and 69 μm were used in dissolution experiments at 500 rpm stirring speed, 3 mol/dm^3 sodium hydroxide, 333 K and 1/100 g/cm^3 solution. The results are given in Fig.1c. Within the coarser particle size range of 126 μm to 317 μm, the leaching fraction of lead was affected by particle size, which may be attributed to the increase in cerussite surface area. The exposure of

the sample to the solution increased with the decrease in particle size. In the finer range (69–126 µm) the difference of lead extraction was not so great that fine grinding would not be required due to the high operation cost. Based on these results, an average particle size of 126 µm was sufficient for the leaching experiments.

Effect of stirring speed

The effect of stirring speed on the dissolution performance of cerussite samples was evaluated by regulating the stirring speed to 300, 400, 500, 600 and 700 rpm. The average particle size, initial sodium hydroxide concentration, reaction temperature and solid to liquid ratio were kept constant at 126 µm, 3 mol/dm^3, 333 K and 1/100 g/cm^3, respectively. The results are given in Fig.1d. Results demonstrated that no significant impact on the leaching fraction of lead using the given stirring speed range. The stirring speed of 500 rpm was sufficient to bring mineral particles into adequate contact with leaching reagents.

Kinetics study

Leaching rate facilitates practical operation conditions and enhances the productivity of lead extraction. Thus, extracting lead economically is important. However, no information on the leaching kinetics of cerussite in sodium hydroxide solutions has been published yet. A discussion of the leaching kinetics of cerussite in sodium hydroxide solutions is necessary to investigate the reaction course and the dissolution rates.

   The dissolution of cerussite in sodium hydroxide is a heterogeneous reaction, and the relevant kinetics follows the shrinking core model which was described by Liddell (2005) in detail. According to this model, the dissolution process is controlled by either diffusion through the solution boundary, diffusion through the solid product layer, or surface chemical reaction (Liu et al., 2010; Ekmekyapar et al., 2012; Habbache et al., 2009). Assuming that the solid has a spherical appearance and the process is controlled by diffusion through the product layer, the integrated equation of the shrinking core model can be described as follows:

$$k_d t = 1-(2/3)x-(1-x)^{2/3}. \tag{2}$$

   When the process is controlled by surface chemical reaction, the integrated equation of the shrinking core model can be given as

$$k_r t = 1-(1-x)^{1/3}, \tag{3}$$

where x is the conversion fraction of solid particles, k_d is the apparent rate constant for diffusion through the product layer, k_r is the apparent rate constant for surface chemical reaction, and t is the reaction time.

Table 1. The apparent rate constants k_r and k_d for the kinetic model and their corresponding correlation coefficient values R^2

Parameter	Surface chemical reaction $1-(1-x)^{1/3}$		Diffusion through the product layer $1-(2/3)x-(1-x)^{2/3}$	
	k_r (min^{-1})	R^2	k_d (min^{-1})	R^2
Particle size (μm)				
317	0.0139	0.9992	0.0036	0.9125
172	0.0173	0.9997	0.0051	0.9350
126	0.0202	0.9988	0.0059	0.9419
92	0.0227	0.9973	0.0070	0.9550
69	0.0257	0.9991	0.0076	0.9406
Stirring speed (rpm)				
300	0.0152	0.9994	0.0041	0.9343
400	0.0175	0.9992	0.0052	0.9420
500	0.0202	0.9988	0.0059	0.9419
600	0.0216	0.9981	0.0065	0.9499
700	0.0234	0.9995	0.0073	0.9436
NaOH concentration (mol/dm^3)				
2	0.0139	0.9997	0.0036	0.9189
3	0.0202	0.9988	0.0059	0.9419
4	0.0274	0.9999	0.0084	0.9394
5	0.0371	0.9998	0.0116	0.9372
Temperature (K)				
313	0.0068	0.9994	0.0010	0.9075
323	0.0134	0.9994	0.0033	0.9255
333	0.0202	0.9988	0.0059	0.9419
343	0.0303	0.9999	0.0085	0.9309
353	0.0488	0.9998	0.0145	0.9232

Values of $1-(2/3)x-(1-x)^{2/3}$ and $1-(1-x)^{1/3}$ versus the reaction time were plotted to investigate effects of experimental variables such as sodium hydroxide concentration, temperature, particle size and stirring speed, on the dissolution kinetic model presented in Eqs. (2) and (3). The kinetics data including apparent rate constants and corresponding correlation coefficient values obtained from these two models were provided in Table 1. Low correlation coefficients were obtained for the diffusion through the product layer model, indicating that this model can not represent the rate-controlling step. Higher regression coefficient values were obtained for the surface chemical reaction model, indicating that the the surface chemical reaction acted as the rate-controlling step in this dissolution system. This hypothesis was supported by the experimental results as shown in Fig. 2, which were plots of $1-(1-x)^{1/3}$ versus time as a function of sodium hydroxide concentration, temperature, particle size and stirring

speed. In addition, it is known that if the dissolution reaction is controlled by the surface chemical reaction, then the dissolution rate should be sensitive to the reaction temperature. Combining these results as shown in Fig.1b, the dissolution rates were fairly sensitive to temperature, which further demonstrated that the dissolution process was controlled by the surface chemical reaction.
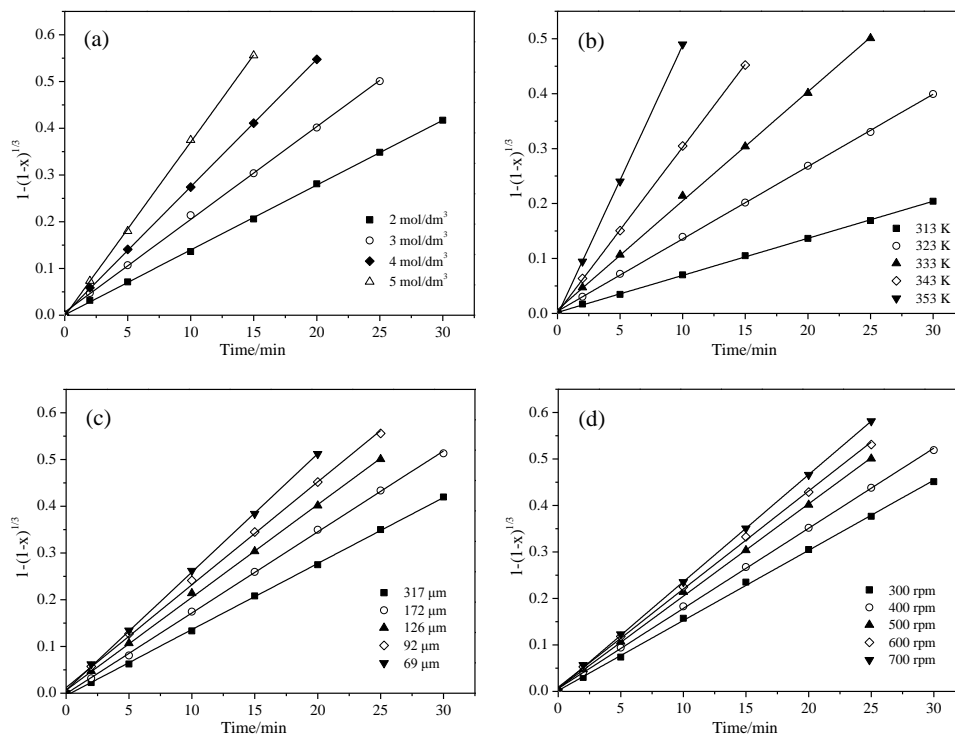

Fig. 2. Plot of $1-(1-x)^{1/3}$ versus time for different operation parameters: (a) sodium hydroxide concentration, (b) temperature, (c) particle size, and (d) stirring speed

The kinetic equation of lead extraction from cerussite can be expressed as follows:

$$1-(1-x)^{1/3}=k_0 \cdot (C)^{\alpha} \cdot (PS)^{\beta} \cdot (SS)^{\gamma} \cdot \exp(-E_a/RT) \cdot t, \qquad (4)$$

where C, PS, SS, E_a, R, and T represent the sodium hydroxide concentration, particle size, stirring speed, activation energy, universal gas constant and temperature, respectively. The constants α, β and γ are the reaction orders for the related parameters, and k_0 is the frequency or pre-exponential factor.

The values of α, β and γ were determined to be 1.0583, –0.4059 and 0.5130, respectively, according to Fig. 3a–3c. The activation energy may be calculated using the Arrhenius equation, and the Arrhenius plot of the dissolution process was shown in Fig. 3d. According to the data from Fig. 3d, the activation energy was determined to

be 43.79 kJ/mol. Substituting the value of α, β and γ and E_a into Eq.(4), the value of k_0 was calculated to be about 1.36×10^4. Thus, the equation representing the dissolution kinetics of cerussite in sodium hydroxide solutions can be expressed as follows:

$$1-(1-x)^{1/3}=1.36 \times 10^4 \cdot (C)^{1.0583} \cdot (PS)^{-0.4059} \cdot (SS)^{0.5130} \cdot \exp(-43.79/RT) \cdot t. \qquad (5)$$
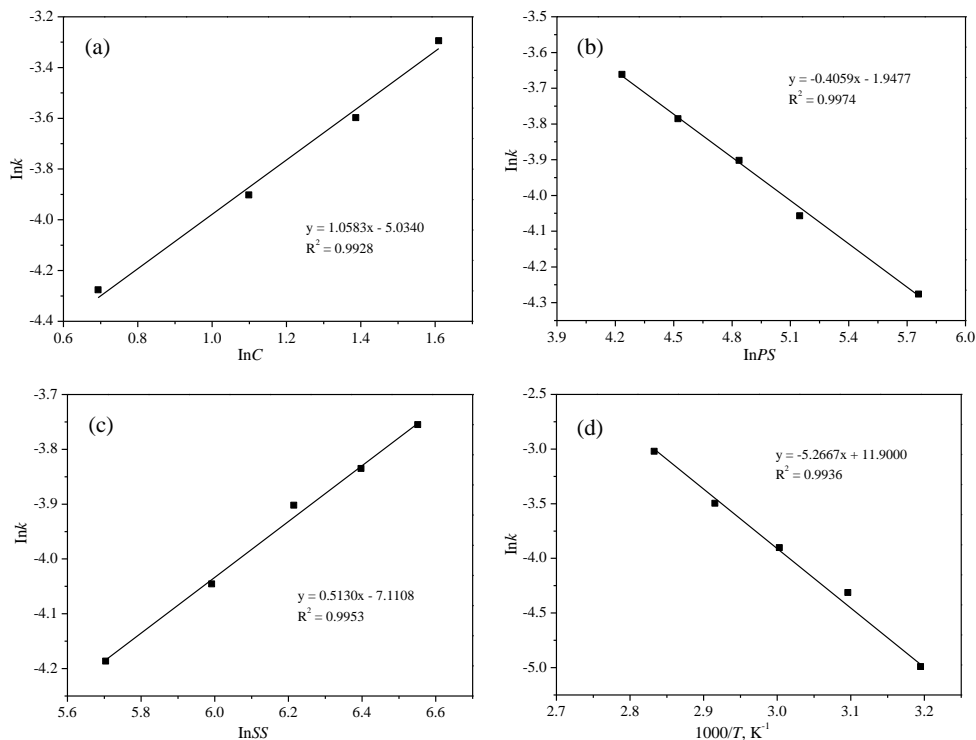

Fig.3. Plot of ln$k$ versus operation parameters: (a) sodium hydroxide concentration, (b) particle size, (c) stirring speed, and (d) temperature

Conclusions

The dissolution rate of cerussite in sodium hydroxide solutions was mainly dependent on leaching reagent concentration and reaction temperature, while particle size and stirring speed had no pronounced effect on the extraction of lead. The dissolution process followed a shrinking core model with the surface chemical reaction as the rate-controlling step. The activation energy of the dissolution reaction was 43.79 kJ/mol. The dissolution kinetics of cerussite in sodium hydroxide solutions can be expressed by the following equation:

$$1-(1-x)^{1/3}=1.36 \times 10^4 \cdot (C)^{1.0583} \cdot (PS)^{-0.4059} \cdot (SS)^{0.5130} \cdot \exp(-43.79/RT) \cdot t.$$

Acknowledgements

References

AGRAWAL, A., SAHU, K.K., PANDEY, B.D., 2004, *Recent trends and current practices for secondary processing of zinc and lead. Part I: Lead recovery from secondary sources*, Waste Management & Research 22, 240–247.

AYDOGAN, S., ERDEMOGLU, M., UCAR, G., ARAS, A., 2007, *Kinetics of galena dissolution in nitric acid solutions with hydrogen peroxide*, Hydrometallurgy 88, 52–57.

ATANASOVA, D.A., 2009, *Hydrometallurgical processing of dumped lead paste for lead acid batteries*, Bulgarian Chemical Communications 41, 285–296.

BABA, A.A., ADEKOLA, F.A., 2011, *Comparative analysis of the dissolution kinetics of galena in binary solutions of HCl/FeCl₃ and HCl/H₂O₂*, International Journal of Minerals, Metallurgy and Materials 18, 9–17.

BADANOIU, G., BUZATU, T., BUZATU, M., BUTU, M., 2013, *Study concerning PbO solubility in NaOH solution for the treatment of sulfate-oxide pastes obtained from dismantling used lead-acid batteries*, Revista de Chimie 64, 1004–1010.

ETTLER, V., JOHAN, Z., BARONNET, A., JANKOVSKY, F., GILLES, C., MIHALJEVIC, M., SEBEK, O., STRNAD, L., BEZDICKA, P., 2005, *Mineralogy of air-pollution-control residues from a secondary lead smelter: Environmental implications*. Environmental Science & Technology 39, 9309–9316.

EKMEKYAPAR, A., AKTAS, E., KUNKUL, A., DEMIRKIRAN, N., 2012, *Investigation of leaching kinetics of copper from malachite ore in ammonium nitrate solutions*, Metallurgical and Materials Transactions B 43B, 764–772.

FENG, L.Y., YANG, X.W., SHEN, Q.F., XU, M.L., JIN, B.J., 2007, *Pelletizing and alkaline leaching of powdery low grade zinc oxide ores*, Hydrometallurgy 89, 305–310.

FEDJE, K.K., EKBERG, C., SKARNEMAK, G., STEENARI, B.M., 2010, *Removal of hazardous metals from MSW fly ash-An evaluation of ash leaching methods*, Journal of Hazardous Materials 173, 310–317.

HERRERA-URBINA, R., SOTILLO, F.J., FUERSTENAU, D.W., 1998, *Amyl xanthate uptake by natural and sulfide-treated cerussite and galena*, International Journal of Mineral Processing 55, 113–128.

HABBACHE, N., ALANE, N., DJERAD, S., TIFOUTI, L., 2009, *Leaching of copper oxide with different acid solutions*, Chemical Engineering Journal 152, 503–508.

LIAO, M.X., DENG, T.L., 2004, *Zinc and lead extraction from complex raw sulfides by sequential bioleaching and acidic brine leach*, Minerals Engineering 17, 17–22.

LIDDELL, K.C., 2005, *Shrinking core models in hydrometallurgy: What students are not being told about the pseudo-steady approximation*, Hydrometallurgy 79, 62–68.

LIU, W., TANG, M.T., TANG, C.B., HE, J., YANG, S.H., YANG, J.G., 2010, *Dissolution kinetics of low grade complex copper ore in ammonia-ammonium chloride solution*, Transactions of Nonferrous Metals Society of China 20, 910–917.

LIU, Q., ZHAO, Y.C., ZHAO, G.D., 2011, *Production of zinc and lead concentrates from lean oxidized zinc ores by alkaline leaching followed by two-step precipitation using sulphides*, Hydrometallurgy 110, 79–84.

LIU, Z.X., YIN, Z.L., HU, H.P., CHEN, Q.Y., 2012, *Leaching kinetics of low-grade copper ore with high-alkality gangues in ammonia-ammonium sulphate solution*, Journal of Central South University of Technology 19, 77−84.

LIMA, L.R.P.D., BERNARDEZ, L.A., 2013, *Evaluation of the chemical stability of a landfilled primary lead smelting slag*, Environmental Earth Sciences 68, 1033–1040.

MIKHLIN, Y., KUKLINSKIY, A., MIKHLINA, E., KARGIN, V., ASANOV, I., 2004, *Electrochemical behaviour of galena (PbS) in aqueous nitric acid and perchloric acid solutions*, Journal of Applied Electrochemistry 34, 37–46.

NIKOLIC, P.M., MIHAJLOVIC, P., TODOROVIC, D.M., 1996, *Far infrared and infrared properties of single crystal anglesite*, Spectrochimica Acta Part A 52, 131–137.

NAGIB, S., INOUE, K., 2000, *Recovery of lead and zinc from fly ash generated from municipal incineration plants by means of acid and/or alkaline leaching*, Hydrometallurgy 56, 269–292.

NOWAK, P., LAAJALEHTO, K., 2007, *On the interpretation of the XPS spectra of adsorbed layers of flotation collectors-ethyl xanthate on metallic lead*, Physicochemical Problems of Mineral Processing 41, 107–116.

ORHAN, G., 2005, *Leaching and cementation of heavy metals from electric arc furnace dust in alkaline medium*, Hydrometallurgy 78, 236–245.

OKADA, T., TOJO, Y., TANAKA, N., MATSUTO, T., 2007, *Recovery of zinc and lead from fly ash from ash-melting and gasification-melting processes of MSW-Comparison and applicability of chemical leaching methods*, Waste Management 27, 69–80.

PAN, J.Q., SUN, Y.Z., LI, W., KNIGHT, J., MANTHIRAM, A., 2013, *A green lead hydrometallurgical process based on a hydrogen-lead oxide fuel cell*, Nature Communications 4, 1–6.

QIN, W.Q., LI, W.Z., LAN, Z.Y., QIU, G.Z., 2007, *Simulated small-scale pilot plant heap leaching of low-grade oxide zinc ore with integrated selective extraction of zinc*, Minerals Engineering 20, 694–700.

QIN, W.Q., JIAO, F., XU, B.J., LIU, H., 2012, *Purification of leachate from simultaneous leaching of galena concentrate and pyrolusite and preparation of $PbSO_4$ and Mn_3O_4*, Industrial & Engineering Chemistry Research 51, 5596–5607.

SCHRODER-WOLTHOORN, A., KUITERT, S., DIJKMAN, H., HUISMAN, J.L., 2008, *Application of sulfate reduction for the biological conversion of anglesite ($PbSO_4$) to galena (PbS)*, Hydrometallurgy 94, 105–109.

YUAN, W.Y., LI, J.H., ZHANG, Q.W., SAITO, F., 2012, *Mechanochemical sulfidization of lead oxides by grinding with sulphur*, Powder Technology 230, 63–66.

A FACILE APPROACH FOR FABRICATION OF SUPERHYDROPHOBIC SURFACE WITH CANDLE SMOKE PARTICLES

Dake QIN

College of Applied Technology, Soochow University, 215325, Kunshan, Suzhou, China, qindake@suda.edu.cn

Abstract: The aim of this communication is to explore a simple and efficient method for fabrication of superhydrophobic surface by candle smoke particles (CSPs). The properties of CSPs before and after the calcination process has been studied by SEM, TEM, TG-DSC, FT-IR and contact angle measurements. The results show that there is a complex mixture of elemental carbon and a variety of hydrocarbons in association with amorphous nanomaterial in CSPs, whose structure and composition leads to superhydrophobic properties. The wetting properties of CSPs can turn from superhydrophobic into superhydrophilic due to characteristic group changes by calcination process. Thus, it is a simple and efficient method to fabricate superhydrophobic or superhydrophilic surface by CSPs at low cost.

Introduction

The newly functionalized materials play an important role in interfacial engineering fields (Horiuchi et al. 2011; Yan et al. 2008), because the interaction between water and solid surface is an active research area. Especially in these years, considerable attention has been paid to the artificial superhydrophobic materials owing to its self-cleaning effect (Nishimoto et al. 2009; Goncalves et al. 2009). These studies indicate that material's surface self-cleaning properties strongly depend on the surface energy and microstructure of artificial superhydrophobic materials (Furstner et al. 2005; Jiang et al. 2004). Many naturally occurring self-cleaning surfaces such as lotus leaves suggest that a combination of low surface energy materials and a nanoscale architecture which repels water are required to create a superhydrophobic surface, which water contact angle is approximately 180° (Zhai et al. 2004). Microscale and nanoscale hierarchically structured surfaces of the materials have proven to be vital structures in generating the superhydrophobic surface properties (Han et al. 2005; Lim

et al. 2006). Hence, the construction of a nanostructure is indispensable for the design of a superhydrophobic surface.

Various methods have been proposed to fabricate superhydrophobic surface mimicking the lotus leaf surface nanostructure, including layer-by-layer assembly (Lin et al. 2006), electrodeposition (Shi et al. 2005), lithographic patterning (Furstner et al. 2005), chemical vapor deposition (Liu et al. 2004). The most of the above methods involve strict preparation conditions, high raw materials cost and low productivity. Therefore, the applications of superhydrophobic surface have been limited so far (Bao et al. 2011).

The candle is generally composed of paraffin, which is made of heavy straight-chain hydrocarbons consisting of linear n-alkane and branched iso- and cyclo-alkanes with carbon lengths ranging from $C_{16}\sim C_{30}$ and higher (Sun et al. 2006; Saber et al. 2011; Kuszlik et al. 2010; Luyt et al. 1999; Zaky et al. 2010). The candle flames present a simple example of a diffusion flame. Its burning is still complicated by the nature of its finite cylindrical wick (Sunderland et al. 2011). Some studies found the size of smoke particles produced from the candle flames, which are hydrocarbons in origin, to be around 30 nm in diameter (Pagels et al. 2009; Li et al. 1993). These candle smoke particles (CSPs) contain organic compounds and can be assembled into nanostructured superhydrophobic surface. Some studies suggest that many of the particulate organic compounds emitted in candle smoke consist of unburned wax components. The heavy alkane predominance in organic compounds of the paraffin candle smoke can be explained by volatilization of the mostly alkenes wax material and subsequent condensation into the CSPs (Fine et al. 1999).

The objective of this study is to explore a simple and efficient procedure to fabricate superhydrophobic surface through the CSPs from candle flames. Although, there have many excellent studies on the fabricate superhydrophobic surface with candle soot, some studies made the soot as a template (Deng et al. 2012; Maxime et al. 2014), other studies used paraffin wax-fixed candle soot for improving durability (Kwangseok et al. 2014) or paid attention to the optical absorption and fluorescence properties of the soot (Campbell et al. 2014). The emphasis of this work is to take advantage of the relationships before and after calcinations of CSPs, which allow the surface properties to be transformed. The proposed mechanism of observed superhydrophobicity surface properties due to calcination is discussed in detail. The paper offers a new perspective on CSPs in surface properties application.

Materials and methods

Materials

The candle used in this study was purchased from a commercial shop in Suzhou, China and used without further purification. It is a column in shape (1.5 cm in diameter ×17 cm in height) and white in color. The FT-IR results indicate that the candle is made of paraffin.

Methods

Preparation of deposition surface

The candle was placed in a simple laboratory fume cupboard. The candle is lit with a match and allowed to burn. It burns steadily about 1 min later, then a flat glass was placed above the flame of the candle to collect (by deposition) candle smoke particles (CSPs) emitted from the candle flame (the distance between the top of flame and glass is about 0.5 cm). The CSPs deposited on the glass were coded as CSPs, the deposition time was 3 min (the thickness of the CSP's layer is about 200 nm). When the CSPs have been deposited on the glass, it was placed in a muffle furnace, then heat up to 500 ^{o}C with heating rate at 10 ^{o}C/min. The resultant CSPs on the glass were coded as CSPs(500) and their color was black.

Characterization

The thermal properties of the candle smoke particles (CSPs) before and after calcination was estimated by thermogravimetric analysis (TA, Q600). The samples were heated from room temperature to 1000 ^{o}C under air atmosphere with heating rate of 10 ^{o}C/min. The wettability (water contact angle) of CSPs deposited on the glass was measured by video-based optical contact angle measuring instruments (Dataphysics, OCA-20) at ambient temperature. Water droplets of about 3.0 μL in volume were dropped carefully onto the CSPs deposition surface, and the average value of five measurements at different positions of the sample was adopted as the contact angle. The contact angle was calculated from the images by the instrument software. The morphology and size of CSPs were investigated by transmission electron microscope (FEI, TecnaiG220), and the surface morphology of CSPs and CSP's deposition layer was examined by scanning electron microscope (Hitachi, S4800).

Results and discussion

The SEM micrograph of candle smoke particles (CSPs) deposited on the glass before and after calcination process is presented in Fig. 1a and 1b. The surface morphology of the CSPs is seen to be non-uniform and extremely small with a majority of the particles about 30 nm in diameter, which were formed by burning the candle. The SEM micrograph shows that the CSPs are deposited on the glass placed above the flame of the candle. A higher magnification of the micrograph shows that the particles of matter as irregular particles, all joined together, without any carbon nanotubes or nanowires among the particles (Fig. 1a). When the CSPs are heated up to 500 ^{o}C, formation of CSPs(500), the morphology and dimension of the CSPs have not changed. The heated particles are also irregular and joined together. Furthermore, there are no carbon nanotube or nanowire forms due to calcination process (Fig. 1b).

CSPs (×30)   CSPs (×5k)   CSPs (×30k)

(a)

CSPs(500) (×30)   CSPs(500) (×5k)   CSPs(500) (×30k)
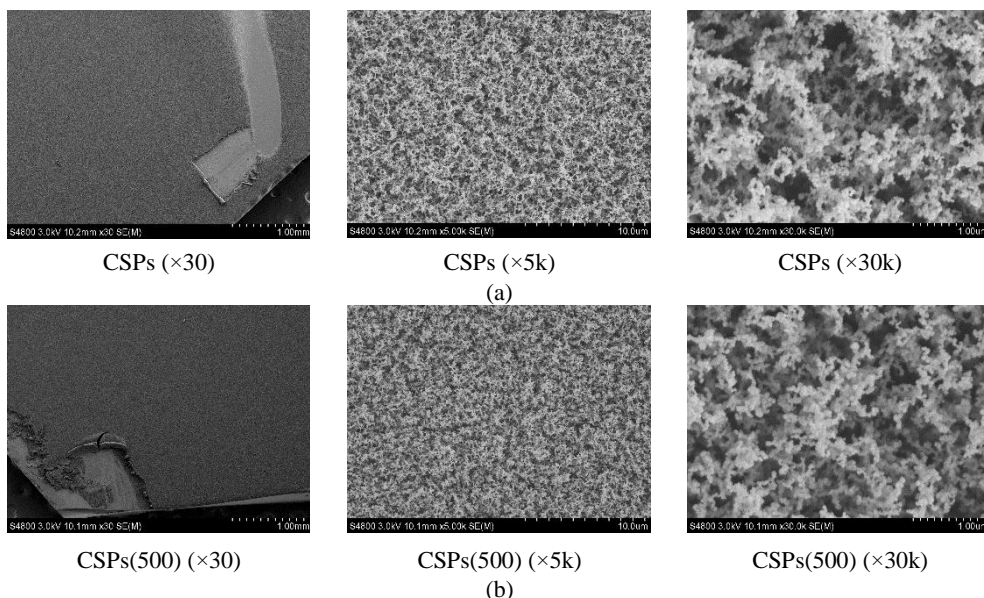
(b)

Fig. 1. The SEM micrograph of candle smoke particles deposited on the glass before and after calcination

Figure 2a is a typical TEM micrograph of the CSPs from candle flame, which is similar with the CSPs(500) (Fig. 2b). They show that the samples contain small non-uniform spherical particles. The equivalent diameter of the CSPs is about 30 nm, which is as big as the CSPs(500) samples. Meanwhile, there are not any carbon nanotubes or nanowire in the CSPs and CSPs(500) samples. The above results are all in agreement with the SEM micrograph of the CSPs. It indicates that the CSPs emitted from the candle flame are non-uniform spherical particles (about 30 nm in equivalent diameter), which maintain morphology and dimension after the calcination process at 500 $^\circ$C. The following research has focused on the chemical properties of the CSPs and CSPs (500) samples.

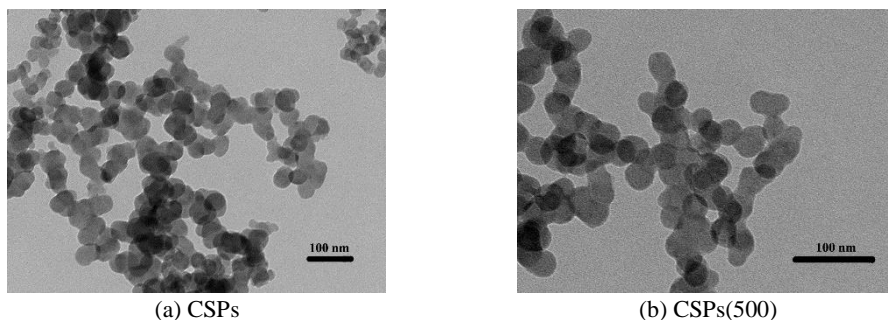(a) CSPs   (b) CSPs(500)

Fig. 2. TEM micrograph of candle smoke particles deposited on the glass before and after calcination

The 4000~400 cm^{-1} wave-number range of the FT-IR spectra measured for the CSPs and CSPs(500) samples are compared in Fig. 3. The process of burning a candle flame to obtain CSPs is a thermal decomposition process, in which the candle flame breaks up to form CSPs. The particles, formed from the atmospheric combustion of a candle flame, are a complex mixture of elemental carbon and a variety of hydrocarbons. The composition of particles has a strong impact on the chemical properties of the CSPs and CSPs(500) (Shooto et al. 2011). According to Figs 1 and 2, the equivalent diameter of the CSPs is extremely small (nanoscale) having a large surface area. The functional groups on the particle surface have an important influence on its chemical properties. As expected, the intensities of the CSPs and CSPs(500)'s FT-IR absorption bands are weak for the most of amorphous carbon is non IR-active modes. Only small features centered around 3029, 2926 and 2853 cm^{-1} are evidenced in the CSPs sample, which are attributed to the presence of stretching vibration of methylene groups. They have been identified and observed on the CSP's FT-IR spectra in comparison with the CSPs(500)'s spectra. No band in the stretching mode range of the carbonyl groups (1600~1800 cm^{-1}), and hydroxyl groups (3000~3600 cm^{-1}) was observed in the CSPs samples, indicating that the CSPs are free of usual group functionalization during the candle burning process (thermal decomposition process). A very broad and complex feature centered around 1250 cm^{-1} band is also found in the FT-IR spectrum of the CSPs, which is agreement with the large amount of amorphous carbon present in the CSPs (Bantignies et al. 2006). Interestingly, the bands with respect to the A$_{2u}$ (868 cm^{-1}) and E$_{1u}$ (1590 cm^{-1}) IR-active modes of graphite are observed in CSPs(500)'s spectra (Kuhlmann et al. 1998). Furthermore, the 1720 cm^{-1} presence stretching mode range of carbonyl groups in CSPs(500)'s spectra indicates that the methylene groups reacting with oxygen formation of carbonyl groups when the CSPs are heated up to 500 ^{o}C. At the same time, during the calcination process, complex mixture of elemental carbon and a variety of hydrocarbons in the CSPs have been transformed into polar groups or decomposed in the CSPs(500) sample. For example, the carbonyl group is strongly polar in the CSPs(500), which would lead to the CSPs deposited on the glass's surface properties turn into hydrophilic after the calcination process.

The TG and DSC curves of the CSPs and CSPs(500) samples (under air atmosphere) are presented in Fig. 4. The TG curves of the CSPs show that most the weight loss, related to the decomposition of hydrocarbons. It occurs at temperatures lower than 620 ^{o}C. During CSP's thermal decomposition processes, the disappearance of branch and backbone structure in CSPs is associated with different exothermal temperature, formation of two exothermal peaks at 593 ^{o}C and 616 ^{o}C, respectively. Interestingly, there is a little weight increasing appearance at 200~400 ^{o}C when the CSPs are heated up under air atmosphere. This phenomenon indicates that the methylene groups react with oxygen formation of carbonyl groups during the CSPs heating from 200 to 400 ^{o}C under the air atmosphere. For the CSPs(500) samples, there is no weight increase on the TG curves under the air atmosphere. It is so because

the methylene groups, reacting with oxygen formation of carbonyl groups, have been completed during preparation of the CSPs(500) by the calcination process. From a different perspective, the decomposition of carbonyl groups creates an additional exothermal peak (593 ^{o}C) in CSPs(500)'s DSC curves, which demonstrates that methylene groups were oxidized into carbonyl groups during the calcination process. From room temperature to 200 ^{o}C the weight of the CSPs(500) is decreasing slowly, which indicates that before the decomposition of backbone structure the hydroxyl groups already decompose below 200 ^{o}C.
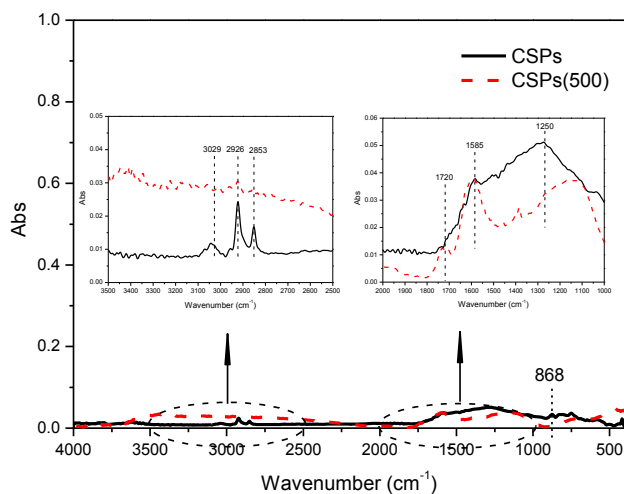

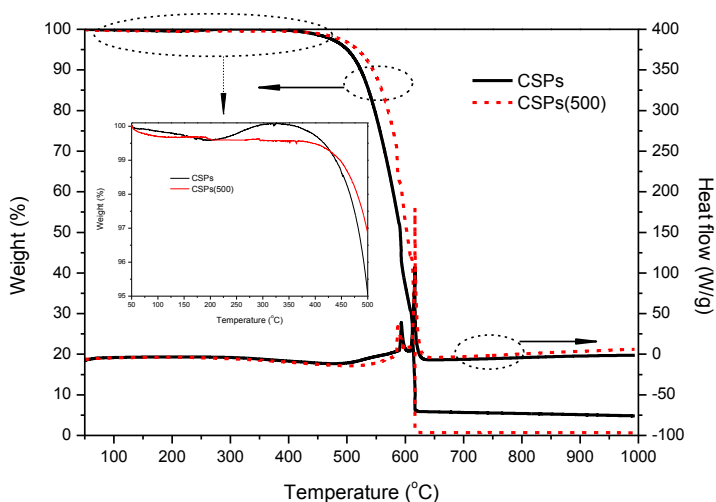Fig.3 The FT-IR spectra of candle smoke particles deposited on the glass before and after calcination

Fig. 4. TG-DSC curves of candle smoke particles deposited on the glass before and after calcination

The FT-IR spectra and TG-DSC curves reveal that the most important chemical properties' difference between CSPs and CSPs(500) samples. During the calcination process, the complex mixture of elemental carbon and a variety of hydrocarbons in the CSPs, such as methylene groups, have turned into carbonyl groups, leading to chemical properties variation. The objective of this communication is to study the surface properties of the CSPs from candle flames and to fabricate either superhydrophobic or superhydrophilic surface with a simple and efficient method. So it is interesting to investigate the wetting properties of the CSPs and CSPs(500) samples.

Wetting properties of the CSPs and CSPs(500) samples were evaluated by water contact angle measurements. The water contact angle is the average value of five measurements at different positions. Photographs of water droplets are shown in Figs 5(a-b) and the results of water contact angle measurements are 155° and 0° respectively. Interestingly, the results of the water contact angle indicate that the glass surface hydrophobic properties improved dramatically with the CSP's deposition. The water contact angle reached 155°, showing the formation of superhydrophobic surfaces from a candle flame. The method, CSP's deposition on glass surface, is very simple and of low cost. Before calcination up to 500 ^{o}C, the CSPs deposition on glass surface exhibited superhydrophobic properties accounted for their specific composition and structures. The CSPs contain a complex mixture of elemental carbon and a variety of hydrocarbons, which provide a large amount of hydrophobic groups. Based on the SEM and TEM investigation, the CSPs deposition on glass surface is expected to exhibit two types of microstructure, that is, the relatively large pores formed through the interconnection of the CSPs, and the smaller nanoscale structure within the individual nanoparticles. The above microstructures of the CSPs increase their surface roughness, which can trap air to form superhydrophobic surfaces.

The calcination of the CSPs, which forms CSPs(500) samples, led to a dramatic decrease of water contact angles from 155° to 0°. The result suggests that surface properties of the CSP's deposited on glass have been successfully converted into superhydrophilic. Given that the complex mixture of elemental carbon and a variety of hydrocarbons in the CSPs produce superhydrophobic surface, it can be removed due to calcination process. The defect sites in the carbon network of the CSPs (500) samples, which form during the calculation process, produce surface hydroxyl groups, and carbonyl groups acted as a strong adsorption site of water molecules. The carbonyl groups in the relatively large pores, which were formed through the interconnection of the CSPs, can absorb water molecule. So the water is made to spread over the surface structure of the CSPs and its aggregation, leading to water contact angles equal to 0°. The above results lead to the change of the surface properties of the CSPs from superhydrophobic to superhydrophilic by calcination at 500 ^{o}C.

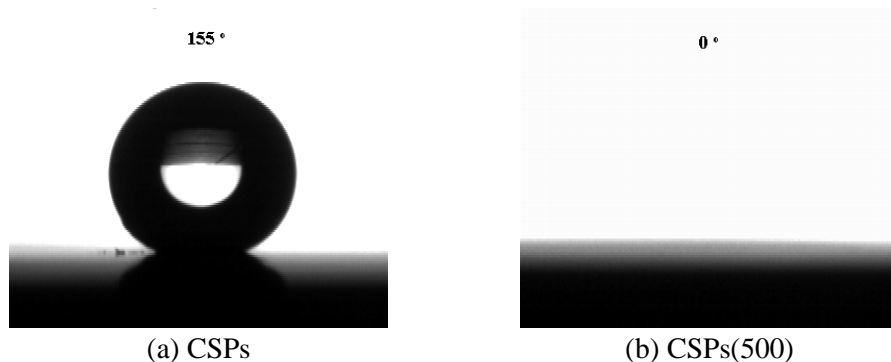(a) CSPs   (b) CSPs(500)

Fig. 5. Photographs of water droplets on candle smoke particles deposited on glass before and after calcination

Conclusion

The candle smoke particles (CSPs) emitted from the candle flame has superhydrophobic properties without any additional treatment. The special properties results from the unique structure and composition of the CSPs, for SEM and TEM micrographs provide a clear indication that the particles are nanoscale in size (about 30 nm in equivalent diameter). Furthermore, the FT-IR spectra and TG-DSC investigation show the presence of a complex mixture of elemental carbon and a variety of hydrocarbons in association with amorphous nanomaterial in the CSPs. Interestingly, the CSPs can turn into superhydrophilic after calcination at 500 ^{o}C without dramatic morphology and dimension variation, for the CSPs(500) have different functional groups compared with the CSPs. So the CSPs from the candle flames provide a simple and efficient procedure of fabrication of superhydrophobic and superhydrophilic surfaces at low cost.

Acknowledgment

References

BAO Y.B., LI Q.Y., XUE P.F., HUANG J.F., WANG J.B., GUO W.H., WU C.F., 2011, *Tailoring the morphology of raspberry-like carbon black/polystyrene composite microspheres for fabricating superhydrophobic surface*, Mater. Res. Bull, 46, 779-785.

BANTIGNIES J.L., SAUVAJOL J.L., RAHMANI A., FLAHAUT E., 2006, *Infrared-active phonons in carbon nanotubes*, Phys. Rev. B., 74, 195425.

CAMPBELL, DEAN J., ANDREWS M.J., STEVENSON K.J., 2012, *New nanotech from an ancient material: chemistry demonstrations involving carbon-based soot,* J. Chem. Educ., 89, 1280.

DENG X., MAMMEN L., BUTT H.J., VOLLMER D., 2012, *Candle soot as a template for a transparent robust superamphiphobic coating*, Science, 335, 67.

FINE P.M., CASS G.R., SIMONEIT B.R.T., 1999, *Characterization of Fine Particle Emissions from Burning Church Candles*, Environ. Sci. Technol., 33, 2352-2362.

FURSTNER R., BARTHLOTT W., NEINHUIS C., WALZEL P., 2005, *Wetting and self-cleaning properties of artificial superhydrophobic surfaces*, Langmuir, 21, 956-961.

GONCALVES G., MARQUES P.A.A.P., PINTO R.J.B., TRINDADE T., NETO C.P., 2009, *Surface modification of cellulosic fibres for multi-purpose TiO_2 based nanocomposites*, Compos. Sci. Technol., 69, 1051-1056.

HORIUCHI Y., SHIMIZU Y., KAMEGAWA T., MORI K., YAMASHITA H., 2011, *Design of superhydrophobic surfaces by synthesis of carbon nanotubes over Co-Mo nanocatalysts deposited under microwave irradiation on Ti-containing mesoporous silica thin films*, Phys. Chem. Chem. Phys., 13, 6309-6314.

HAN J.T., ZHENG Y., CHO J.H., XU X., CHO K., 2005, *Stable superhydrophobic organic-inorganic hybrid films by electrostatic self-assembly*, J. Phys. Chem. B., 109, 20773-20784.

JIANG L., ZHAO Y., ZHAI J., 2004, *A lotus leaf like superhydrophobic surface: A porous microsphere/nanofiber composite film prepared by electrohydrodynamics*, Angew. Chem., Int. Ed., 43, 4338-4341.

KWANGSEOK S., KIM M.Y., KIM D.H., 2014, *Candle-based process for creating a stable superhydrophobic surface*, Carbon, 68, 583.

KUHLMANN U., JANTOLJAK H., PFANDER N., BERNIER P., JOURNET C., THOMSEN C. 1998, *Infrared active phonons in single-walled carbon nanotubes*, Chem. Phys. Lett., 294, 237-240.

KUSZLIK A.K., MEYER G., HEEZEN P.A.M., STEPANSKI M., 2010, *Solvent-free slack wax de-oiling Physical limits*, Chem. Eng. Res. D., 88, 1279-1283.

LI W., HOPKE P.K., 1993, *Initial size distributions and hygroscopicity of indoor combustion aerosol particles*, Aero. Sci. Technol.19, 305-316.

LIM H.S., HAN J.T., KWAK D., JIN M.H., CHO K., 2006, *Photoreversibly switchable superhydrophobic surface with erasable and rewritable pattern*, J. Am. Chem. Soc., 128, 14458-14459.

LIN J.J., CHU C.C., CHIANG M.L., TSAI W.C., 2006, *Manipulating assemblies of high-aspect-ratio clays and fatty amine salts to form surfaces exhibiting a lotus effect*, Adv. Mater., 18, 3248-3252.

LIU H., FENG L., ZHAI J., JIANG L., ZHU D.B., 2004, *Reversible wettability of a chemical vapor deposition prepared ZnO film between superhydrophobicity and superhydrophilicity*, Langmuir, 20, 5659-5661.

LUYT A.S., ISHRIPERSADH K. 1999, *Comparative thermoanalytical investigation of the cross-linking behaviour of three different paraffin waxes in the presence of dicumyl peroxide*, Thermochimica acta, 333, 155-167.

MAXIME P., PAPADOPOULOS P., MAMMEN L., DENG X., SACHDEV H., VOLLMER D., BUTT H.J., 2014, *Optimization of superamphiphobic layers based on candle soot*, Pure Appl. Chem., 86, 87.

NISHIMOTO S., KUBO A., NOHARA K., ZHANG X., TANEICHI N., OKUI T., LIU Z., NAKATA K., SAKAI H., MURAKAMI T. 2009, *TiO_2 based superhydrophobic-superhydrophilic patterns: Fabrication via an ink-jet technique and application in offset printing*, Appl. Surf. Sci., 255, 6221-6225.

PAGELS J., WIERBICKA A., NILSSON E., ISAXON C., DAHL A., GUDMUNDSSON A., SWIETLICKI E., BOHGARD M. 2009, *Chemical composition and mass emission factors of candle smoke particles*, J. Aero. Sci., 40, 193-208.

SABER O., HEFNY N., AL JAAFARI A.A. 2011, *Improvement of physical characteristics of petroleum waxes by using nano-structured materials*, Fuel. Process. Technol., 92, 946-951.

SHI F., WANG Z.Q., ZHANG X. 2005, *Combining a layer-by-layer assembling technique with electrochemical deposition of gold aggregates to mimic the legs of water striders*, Adv. Mater., 17, 1005-1009.

SHOOTO D.N., DIKIO E.D. 2011, *Morphological characterization of soot from the combustion of candle wax*, Int. J. Electrochem. Sci. 6, 1269-1276.

SUN Z., HUANG Z., WANG J.S. 2006, *Studies on the size distribution, number and mass emission factors of candle particles characterized by modes of burning*, J. Aero. Sci., 37, 1484-1496.

SUNDERLAND P.B., QUINTIERE J.G., TABAKA G.A., LIAN D., CHIU C.W. 2011, *Analysis and measurement of candle flame shapes*, Proc. Combust. Inst., 33, 2489-2496.

YAN B., TAO J.G., PANG C., ZHENG Z., SHEN Z.X., HUAN C.H.A., YU T. 2008, *Reversible UV-light-induced ultrahydrophobic-to-ultrahydrophilic transition in an α-Fe$_2$O$_3$ nanoflakes film*, Langmuir, 24, 10569-10571.

ZAKY M.T., MOHAMED N.H. 2010, *Comparative study on separation and characterization of high melting point macro-and micro-crystalline waxes*, J. Taiw. Inst. Chem. Eng., 41, 360-366.

ZHAI L., CEBECI F.C., COHEN R.E., RUBNER M.F. 2004, *Stable superhydrophobic coatings from polyelectrolyte multilayers,* Nano Lett., 4, 1349-1353.

EFFECTS OF AIR-TO-PULP RATIO AND BIAS FACTOR ON FLOTATION OF COMPLEX Cu-Zn SULPHIDE ORE IN THE JAMESON CELL

Y. Hakan GURSOY, Bahri OTEYAKA

Eskişehir Osmangazi University, Mining Engineering Department, 26480 Eskişehir, Turkey,
e-mail: hgursoy@ogu.edu.tr

Abstract: The air-to-pulp ratio and bias factor are important operating parameters in the Jameson flotation cell. These parameters have significant effect on micro-events taking place between particles and bubbles in flotation, and hence on flotation performance. In this study, the possibilities of obtaining a Cu-Zn rich bulk concentrate from complex sulphide ore from the Cayeli region (Turkey) were investigated using the lab-scale Jameson cell. The effect of air-to-pulp ratio and bias factor on flotation recovery were also studied. The ore has problematic flotation behaviour due to very fine liberation size and oxidation. The results showed that the Cu-Zn rich bulk concentrate can be obtained from the ore with satisfactory grade and recovery. It was determined that the air-to-pulp ratio and bias factor have significant effect on the flotation recovery. The optimum values of air-to-pulp ratio and bias factor in flotation of rather fine sized minerals were determined to be within the range of 1-1.5 and 0.70-0.95, respectively.

Keywords: air-to-pulp ratio, bias factor, Jameson cell, flotation, hold-up

Introduction

The Jameson flotation cell, differing from other conventional flotation devices with its structural character and working principle, is an enrichment device. It was successfully used in beneficiation of difficult-to-float fine sized minerals (Jameson, 1999; Cinar et al., 2007; Sahbaz et al., 2013). The Jameson flotation cell, which first appeared in mineral processing in 1989, is used with different capacities in over 200 ore concentration plants. Nowadays, it is widely used in enrichment of fine coals and finely liberated complex sulphide ores, due to its higher flotation performance compared to other flotation devices (Evans et al, 1995; Jameson and Goel, 2012; Sahbaz et al., 2013). The most important basic reason for this is its ability to produce fine bubbles (200-1000 μm), which play an effective role in the particle-bubble collision. This feature arises from its design and its working principle.

The Jameson cell ability to create hydrophobic particle-bubble aggregates in flotation is connected initially to two separate sequential micro-events. The first one is the possibility of encountering the particle and bubble due to the gas hold-up (Oteyaka, 1993; Oteyaka and Soto, 1995), the second one is directly proportional to the particle size and inversely proportional to the bubble size (Sutherland, 1948; Gaudin, 1957; Schulze, 1993; Oteyaka, 1993; Oteyaka and Soto, 1995). The second micro-event plays an extremely important role in flotation of fine particles and directly affects the flotation recovery. The collision probability of fine particles with bubbles is related to the presence of fine bubbles in the cell. The absence of fine bubbles causes low flotation recovery (Reay and Ratcliff, 1975; Trahar and Warren, 1976; Fuerstenau, 1980; Yoon and Luttrell, 1989; Ahmed and Jameson, 1985; Miettinen at al., 2010). In conventional flotation cells, the flotation efficiency is low due to the fact that fine air bubbles cannot be produced at the appropriate size for fine particles. The Jameson flotation cell produces finer than one mm air bubbles due to its working principle. The fine bubbles cause the increase in possibility of collision, and therefore the Jameson cell is appropriate for flotation of fine size liberated ores. Furthermore, flotation in the Jameson cell is shorter than in the conventional flotation devices and hence it eliminates the number of used flotation banks (Miettinen et al., 2010).

There are important parameters that affect the flotation performance in the Jameson cell and other flotation devices. These parameters are superficial gas velocity, feed flow rate, jet length, bias factor, air-to-pulp ratio, and gas hold-up. The optimum values of these parameters change according to the particle size (Evans et al., 1995; Tasdemir, 2006; Tasdemir et al., 2007, 2011; Gursoy, 2007; Sahbaz, 2010). The air-to-pulp ratio is an important parameter, which not only determines the number and diameter of bubbles in the downcomer but also determines the flow regime (laminar or turbulent flow) and the gas hold-up value (Tasdemir, 2006; Sahbaz, 2010). Consequently, the air-to-pulp ratio is a parameter which influences the micro-events between particles and bubbles and directly affects the flotation performance. Another important operating parameter is the bias factor, which influences the concentrate grade and recovery. The bias factor (J_b) is calculated as (Mohanty and Honaker, 1999; Patwardhan and Honaker 2000; Ucar et al., 2013):

$$J_b = (Q_T - Q_F)/Q_{WW} \tag{1}$$

where, Q_T, Q_F and Q_{WW} are flow rates of tailing, feed and wash water, respectively. In general, a positive bias factor is maintained to limit entrainment of fine hydrophilic particles into the froth.

The aim of this research is to investigate the effect of air-to-pulp ratio and bias factor to obtain a bulk Cu-Zn concentrate from a fine grained complex sulphide ore by using the Jameson flotation cell.

Experimental

The ore was obtained from Cayeli Region of Turkey. Mineralogically, the ore consists of chalcopyrite, sphalerite, and pyrite, along with small quantities of bornite and tetrahedrite. The main gangue minerals are barite, quartz, cerussite and clay. The microscopically determined liberation size of chalcopyrite and sphalerite minerals from the gangue minerals is approximately 38 µm. The liberation degree for chalcopyrite and sphalerite minerals is about 75-80%. Therefore, the ore was ground down to d_{80}=38 µm in a controllable manner. The ore contains 2.75% Cu, 6.15% Zn, 24.81% Fe, and 23.33% S. The particle size analysis of the ore was carried out using a Malvern Mastersizer 2000 (Fig. 1).
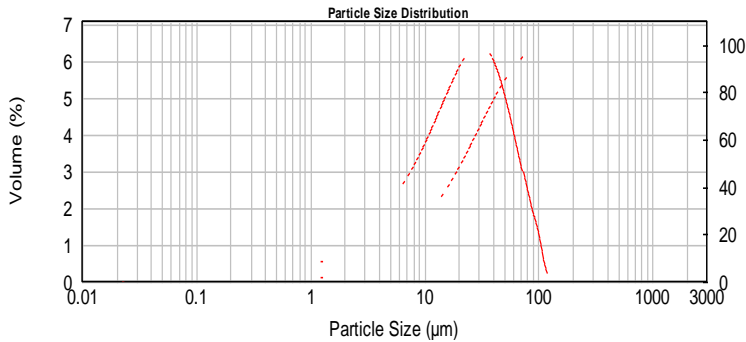

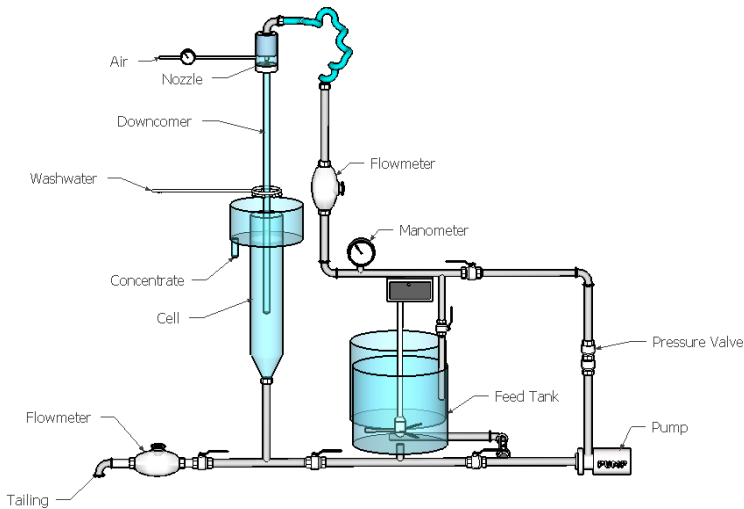Fig. 1. Distribution of particle size of ore used in experiments

Fig. 2. Jameson flotation cell (Gursoy, 2012)

A 100 g/Mg of Aerophine 3418A (produced by Cytec in the Nederland) was used as a collector, 20 g/Mg of MIBC (methyl isobuthyl carbinol) was used as a frother, and CaO was used as a pH regulator. The experiments were carried out at pH 11.8 for pyrite depression. It is known that the surface of pyrite consists of hydrophilic ferric hydroxide at high hydroxyl concentrations (pH > 11) (Goktepe, 2002; Bulatovic, 2007). The experiments were carried out using a laboratory scale Jameson flotation cell (Fig. 2).

The Jameson flotation cell is composed of 200 mm diameter cell, 26 mm diameter downcomer, and 5 mm diameter nozzle. The other flotation conditions and instrumental parameters are given as:

- Particle size : - 38 μm
- Bubble size : 0.6 – 1.0 mm
- Solid ratio : 2 %
- Frother : MIBC (20 g/Mg)
- Collector : Aerophine 3418A (100 g/Mg)
- Depressant (sphalerite) : $ZnSO_4$ (1000 g/Mg)
- pH : 11.8
- Conditioning time : 6 min
- Feed flow rate : 11.5 dm^3/min
- Waste flow rate : 14.3 dm^3/min
- Wash water flow rate : 3 dm^3/min
- Air flow rate : 9.1, 13.6, 17.5, 20.0, 21.7 dm^3/min
- Air-to-pulp ratio : 0.79, 1.18, 1.52, 1.74, 1.89
- Hold-up : 0.38, 0.44, 0.49, 0.51, 0.52
- Positive bias factor : 0.43, 0.60, 0.77, 0.93
- Feed pressure : ~110 kPa
- Separation tank diameter and height : 200 mm and 900 mm
- Downcomer diameter and length : 26 mm and 1800 mm
- Nozzle diameter : 5 mm
- Downcomer plunging depth : 60 cm.

Apart from the hold-up, values of the other parameters were directly measured from the variables given above. The hold-up value, as there was no suitable measuring apparatus, can be found by using the Tasdemir model (2006):

$$\varepsilon = 0.2183 + 0.00885V_J + 0.044\lambda - 0.0197D_N + 0.0028D_D + 0.0179L_J \text{ (for } \varepsilon \leq 0.4596),$$

$$\varepsilon = 0.2428 + 0.0031V_J + 0.066\lambda - 0.00225D_N + 0.0041D_D + 0.018L_J \text{ (for } \varepsilon > 0.4596),$$

where ε is the hold-up (%), V_J jet velocity at the end of downcomer (m/min), λ air-to-pulp ratio, D_N nozzle diameter (m), D_D downcomer diameter (m) and L_J jet length (m). In each experiment, the wash water tank (70 dm^3) and the cell were filled with tap water and then the frother was added. Then, the established study variables were set and operated with a by-pass (giving the concentrate and tailing launder back to the tank) until the pulp feed was started.

At the beginning of each experiment, the ore was conditioned in stirring tank for 6 minutes after adding the collector. The feed tank was filled with tap water and the conditioned ore was introduced to the feed tank until it reached 2% of the solid-to-liquid ratio. The pH of solid suspension in the feed tank was set to 11.8 by adding CaO. Then, the conditioned slurry was pumped (100–170 kPa) into the downcomer, which is the primary contacting zone of particles with bubbles. There is a nozzle on the top of downcomer to provide a high pressure water plunging jet. The air is drawn into the downcomer due to the Venturi effect of the plunging jet. The fine bubbles (400–700 μm) are quickly dispersed into the pulp and carried downward by the bulk fluid motion.

The three-phase mixture passed from the base of the downcomer into the separation tank, which has a much greater cross-sectional area than the downcomer. As a result, the downward superficial velocity of the mixture was reduced, allowing the hydrophobic particles–bubbles aggregate to rise to the surface and form a froth layer. Some hydrophilic particles, coming into the froth phase through hydraulic entrainment, were washed down by the addition of wash water. The concentrate product reported to launder, while the liquid phase and hydrophilic particles left through a valve at the base of the separation tank. The obtained concentrate and tailing were then dried, weighed, and chemically analysed using X-ray fluorescence spectrophotometer (XRF).

Results and discussion

The air-to-pulp ratio (ratio of the air flow rate to the feed flow rate) was obtained by keeping the pulp feed flow rate constant, while changing the vacuumed air flow rate. The speed of vacuumed air to the downcomer is measured at the start of each experiment using an air flow meter. The air flow rate entering the downcomer can be calculated (cm^3/s) from the cross-sectional area of the downcomer and air speed. The flotation experiments were carried out at the air-to-pulp ratio values of 0.79, 1.18, 1.52, 1.74, and 1.89. The flotation recovery and concentrate grade versus air-to-pulp ratio values are given in Fig. 3.
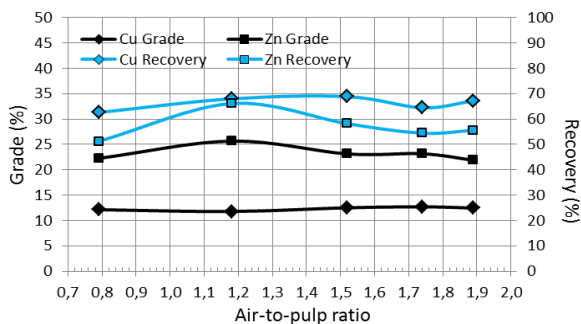

Fig. 3. Effect of air-to-pulp ratio on concentrate grade and recovery of Cu and Zn

According to the data presented in Fig. 3, the highest value of copper recovery was obtained when the air-to-pulp ratio value was 1.52. The copper content and recovery in the concentrate were respectively 12.51% and 68.83%, while the enrichment ratio was 4.55. It can also be seen that zinc also floated very easily. It could be explained by the presence of Cu ions from the oxidised copper minerals activating the sphalerite. To prove this point, the copper ore sample taken from the grinding process was filtered and NaOH was added to it. As a result a colour of solution changed to blue (turquoise) indicating the presence of Cu^{+2} ions. Next $Cu(OH)_2$ was formed (Fig. 4).

Fig. 4. Addition of NaOH to filtered pulp sample (pH 5.5)

The bias factor is one of the variables that contribute to attain optimum performance by the Jameson cell. The bias factor is defined by the fraction of wash water flowing downward and entering to the tailing stream (Eq.1). The bias factor refers to the presence or absence of froth zones. In the case of negative bias there is no froth. The bias factor is also a significant parameter determining the fine hydrophilic particles in the froth zone. With increase in the bias factor, entrainment of particles decreases and hence the concentrate grade increases (Sahbaz et.al, 2008; Tasdemir, 2006). Therefore, in this work series of flotation studies with different bias factors (0.43, 0.60, 0.77 and 0.93) were carried out to determine the effect on the concentrate grade and recovery. The results are shown in Fig. 5.

According to Fig. 5, with increasing bias factor, the concentrate grade tends to increase and conversely the recovery tends to decrease. This could be attributed to the fact of hydraulic entrainment of fine gangue particles into the concentrate decreases. However, the increase of Zn grade in the concentrate is due to the natural oxidation of the ore and no sphalerite depression. As a result, sphalerite surface is activated by Cu^{+2} ions ($ZnS + Cu^{+2} = CuS + Zn^{+2}$) and its floatability increases with collector addition.
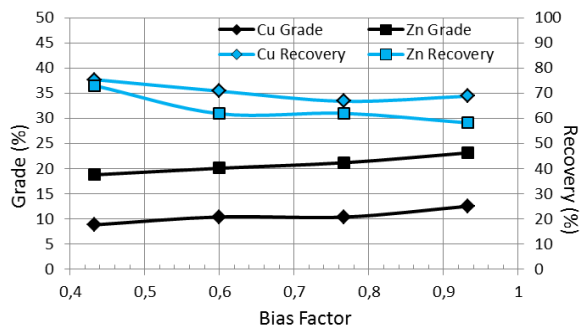
Fig. 5. Effect of bias factor on concentrate grade and recovery of Cu and Zn (for air-to-pulp ratio 1.52)

The results showed that acceptable bias factor value was 0.93 in terms of Cu grade. If cleaning stage was planned to apply after this stage, it would be performed with low bias factor in terms of recovery. As a result, greater bias factor for cleaning stage and smaller bias factor for rougher stage could be applied. The product containing 12.51% Cu, with the recovery of 68.83% was obtained by using lower bias factor, while the product of 8.80% Cu with the recovery of 75.41% was obtained with the bias factor of 0.43.

Conclusions

The effect of air-to-pulp ratio and bias factor on the Jameson cell flotation performance of fine grained complex sulphide ore was studied. It was shown that the Jameson flotation cell can be successfully used in beneficiation of fine particle size copper sulphide ores from the Cayeli region (Turkey). It was found that the air-to-pulp ratio had a significant effect on the concentrate grade and recovery. It was observed that at the air-to-pulp ratio values of between 1.18 and 1.52, provided significant improvements in the concentrate grade and recovery. The flotation performance decreased at larger values of the air-to-pulp ratio due to increased bubble sizes since the possibility of particle-bubble collision decreased.

It was also determined that a bias factor value between 0.70 and 0.95 should be chosen to obtain the concentrate with high grade and recovery as required for rougher flotation.

A further research should be performed to eliminate the negative effect of Cu^{+2} ions in the selective flotation of chalcopyrite and sphalerite.

References

AHMED, N., JAMESON, G.J., 1985, *The effect of bubble size on the rate of flotation of fine particles*, International Journal of Mineral Processing 14 (3), 195–215.

BULATOVIC, S.M., 2007, *Handbook of Flotation Reagents Chemistry, Theory and Practice: Flotation of Sulfide Ores Weiss,* ISBN: 0444530290, Publisher: Elsevier Science & Technology Books

CINAR, F., SAHBAZ, O., CINAR, M., OTEYAKA, B., KELEBEK, S., 2007, *A parametric study on Jameson cell flotation of quartz*, XII Balkan Mineral Processing Congress, Delphi, Greece.

EVANS, G.M., ATKINSON, B.W., JAMESON, G.J., 1995, *The Jameson Cell*, Flotation Science and Engineering, Edited by K.A. Matis, pp 331-363.

FUERSTENAU, D.W., 1980, *Fine particle flotation. In: Fine Particle Processing*, Proceedings International Symposium, vol. 1, pp. 669–705.

GAUDIN, A.M., 1957, *Flotation*, second ed. McGraw-Hill Book Company, New York. 560.

GOKTEPE, F., 2002, *Efect of pH on Pulp Potential and Sulphide Mineral Flotation*, Turkish J. Eng. Env. Sci. 26 (2002) , 309 – 318.

GURSOY, Y.H., 2007, *Jameson Flotasyon Hucresinde İnce Taneli Kompleks Bakir Cevherlerinin Zenginlestirilebilirliği*, Ph.D. Thesis, Eskisehir Osmangazi University, Turkey.

GURSOY,Y.H., 2012, *Determination of Collector Dosage and Conditioning Time in Jameson Cell for Cu-Zn Sulphide Ore Flotation*, Proceeding of XIIIth International Mineral Processing Symposium, Bodrum-Turkey, 409-414.

JAMESON, G.J., 1999, *Hydrophobicity and Floc Density in Induced-Air Flotation for Water Treatment*, Colloids Surfaces A: Physicochem. Eng. Asp., 151: 269-281.

JAMESON, G.J., GOEL, S., 2012, *New approaches to particle attachment and detachment in flotation*, Separation Technologies for Minerals, Coal, and Earth Resources. Society for Mining, Metallurgy, and Exploration, Englewood, Colorado, USA, 437–447.

MIETTINEN, T., RALSTON, J., FORNASIERO, D., 2010, *The limits of fine particle flotation*, Minerals Engineering, Volume 23, Issue 5, April 2010, Pages 420–437.

MOHANTY, M.K., HONAKER, R.Q., 1999, *Performance optimization of Jameson Flotation Technology for fine coal cleaning*, Minerals Engineering, vol.12, No.4, 367-381.

OTEYAKA, B., 1993, *Modelisation d'une colonne de flottation sans zone d'ecume pour la separation de particules grossieres*, Ph.D Thesis, Laval University, Canada.

OTEYAKA, B., SOTO, H., 1995, *Modelling of Negative Bias Column for Coarse Particles Flotation*, Minerals Engineering, Vol.8, 91-100.

PATWARDHAN, A., HONAKER, R.Q., 2000, *Development of a carrying-capacity model for column froth flotation*, International Journal of Mineral Processing Vol.59, Issue 4, 275-293.

REAY, D., RATCLIFF, G.A., 1975, *Experimental testing of the hydrodynamic collision model of fine particle flotation*, Canadian Journal of Chemical Engineering 53 (5), 481–486.

SAHBAZ, O., OTEYAKA, B., KELEBEK, S., UCAR A., DEMIR, U., 2008, *Separation of unburned carbonaceous matter in bottom ash using Jameson cell,* Separation and Purification Technology, 62, 103-109.

SAHBAZ, 2010, *Modification of Downcomer in Jameson Cell and Its Effect on Performance*. Ph.D. Thesis, Dumlupinar University, Department of Mining Engineering, Turkey.

SAHBAZ, O., UCAR A., OTEYAKA B., 2013, *Velocity gradient and maximum floatable particle size in the Jameson cell*, Minerals Engineering, vol 41, 79-85.

SCHULZE, H.J., 1993, *Flotation as a heterocoagulation process: possibilities of calculating the probability of flotation*, Surfactant Science Series 47, 321-353 (Coagulation and Flocculation).

SUTHERLAND, K.L., 1948, *Physical chemistry of flotation XI. Kinetics of the flotation process*, Journal of Physical and Colloid Chemistry 52, 394-425.

TASDEMIR, T., 2006, *Jameson Hucresinde Holp-Up'ın Modellenmesi ve Bazı Calışma Parametrelerinin Flotasyon Verimine Etkisi*, Ph.D Thesis, Eskisehir Osmangazi University, Turkey.

TASDEMIR, T., OTEYAKA, B., TASDEMIR, A., 2007, *Air Entrainment Rate and Holdup in the Jameson Cell*, Minerals Engineering, 20/8: 761-765.

TASDEMIR, T., OTEYAKA, B., TASDEMIR, A., 2011, *Gas entrainment rate and flow characterization in downcomer of a Jameson cell*, Physicochemical Problems of Mineral Processing, 47(2011): 61-78.

TRAHAR, W.J., WARREN, L.J., 1976, *The floatability of very fine particles- a review*. International Journal of Mineral Processing 3 (2), 103-131.

UCAR, A., SAHBAZ, O., KERENCILER, S., OTEYAKA, B., 2014, *Recycling of colemanite tailings using the Jameson flotation technology,* Physicochem. probl. miner. process. 50(2), 645−655.

YOON, R. H., LUTTRELL, G. H., 1989, *The effect of bubble size on fine particle flotation*, Miner. Process Extr. Metal. Rev., 5, 101.

RADIOACTIVITY OF DRILLING CUTTINGS FROM SHALE RESOURCES OF THE LOWER PALEOZOIC BALTIC BASIN

Anna MYKOWSKA*, Andrzej ROGALA*, Anna KALLAS*, Jakub KARCZEWSKI**, Jan HUPKA*

* Department of Chemical Technology, Faculty of Chemistry, Gdansk University of Technology, anna.mykowska@pg.gda.pl

** Department of Solid State Physics, Faculty of Applied Physics and Mathematics, Gdansk University of Technology

Abstract: Fractionated drilling wastes originating from shale gas exploration in the Baltic Basin in Polish Pomerania were subjected to measurements of mean activity concentrations of naturally occurring radioactive materials (NORMs). X-ray diffraction (XRD) and scanning electron microscopy (SEM) analyses were used to understand the rock structure and texture. The activity concentration of radionuclides in bulk wastes and fractionated samples (latter obtained through a sieve analysis) was analyzed by using a gamma-ray spectrometer. After fractionation, three different size ranges were distinguished. Radiological indices were estimated by comparison with the levels recommended by the International Association of Oil and Gas Producers (OGP) and an equivalent absorbed dose was determined with respect to appropriated disposal of cuttings. The results showed that the drilling cuttings from the Ordovician period have a natural radioactivity level comparable to other rocks with the same lithology (potassium K-40 800-992 Bq/kg and thorium Th-232 23.3-30.8 Bq/kg) and they did not exceed acceptable levels of the total absorbed dose rate. The average absorbed dose rate in outdoor air one meter above the drilling cuttings was 54.1 nGy/h. The relation between particle size and natural radioactivity indicated that the concentration of radionuclides increased as the fractions size decreased.

Introduction

Naturally occurring radioactive materials (NORM) are mostly nuclides with the half-life of hundreds millions of years and come from the Earth formation period. They are referred to as primordial (Ravisankar et al., 2014). Natural radioactivity is the major source of radiation to which humans are exposed and it represents more than 75% of all ionizing radiation (UNSCEAR, 2000). Gamma radiation is always associated with

different lithological structures and can also be the factor used to distinct one type of rock from another. Shaliness, used in formation evaluation, is a good example of this phenomenon. Elevated gamma radiation emission characterizes shales and igneous rocks (e.g. granites) as well as lower sedimentary rocks (Mykowska and Hupka, 2014). The gamma ray logging data are valuable during well logging measurement, after the borehole has been drilled and also in the stage of drilling for real-time geosteering decisions. Another aspect of NORM accumulated in rocks, regards environmental issues. The radiological hazard from drilling wastes is especially important in cuttings management.

The drilling cuttings examined in the research originated from a shale gas exploration borehole in the Baltic Basin, which is one of the three prospective regions of unconventional gas resources (Baltic, Podlasie and Lublin Basins) located in the area of the East European Platform. Silurian and Ordovician deposits in sedimentary basins of Poland often contain a relatively large proportion of organic matter, so they could be considered as unconventional hydrocarbons reservoirs (Poprawa, 2010). They contain organic matter, which is correlated with the level of natural radioactivity of rocks. In this area, the gas-bearing shales can be found most frequently in the sediments of monotonous silty-sandstone. The advantage of Paleozoic sedimentary basins, such as the Baltic Basin, is their simple structure, conducive to exploration and exploitation of unconventional resources of oil and gas (Poprawa, 2010; Kiersnowski, 2014).

The natural radioactivity of oil and gas exploration wastes was investigated in some papers (Hamlat et al., 2001; El Afifi and Awwad, 2005; Atallah et al., 2012; Hrichi et al., 2013; Hilal et al., 2014). Recently, the research was focused on the impact of particle size on gamma radiation emission. The objective of this paper is to compare activity concentrations of radionuclides, in both bulk wastes and fractioned cuttings, before and after sieve analysis, to verify the relationship between particle size and emission of natural gamma radiation. Another aspect of the research is to estimate the radiological hazard based on the absorbed dose rate.

Origin of radioactivity in oil and gas exploration and production wastes

Radioactive isotopes occur naturally in the environment but can accumulate due to industrial activities. The natural radioactivity, greater than the background radiation, has been noticed in the oil and gas recovery waste in 1930s (Otto, 1989). At the beginning of 1980's the regulatory agencies started to pay attention to the NORM associated with hydrocarbons production (Smith, 1992). Gamma radiation from the waste has a very wide range. Radium-226, which is the primary isotope of concern, has activity concentration from undetectable to 1000 kBq/kg (Smith, 1992; Hilal et al., 2014). The primordial NORMs and decay chain radioisotopes in drilling wastes are presented in Table 1 (Atallah et al., 2012). Most of discussed radionuclides emit alpha radiation (U-238, Th-232, Ra-226 and Rn-222), potassium K-40 emits electrons.

Gamma radiation accompanies both types of decay and the energy of gamma rays is between 12 keV for thorium Th-232 to 1.46 MeV for potassium K-40.

Table 1. Selected natural radionuclides associated with oil and gas production (Atallah et al., 2012)

Nuclide	Type	Half-life	Decay energy
U-238	primordial	4.47×10^9 y	α (4.2 Mev), γ (13 keV)
Th-232	primordial	1.4×10^{10} y	α (4.01 Mev), γ (12 keV)
K-40	primordial	1.28×10^9 y	β-(1.31 Mev), γ (1.46 MeV)
Ra-226	U-238 decay series	1600 y	α (4.78 Mev), γ (186 keV)
Rn-222	U-238 decay series	3.8 days	α (5.49 Mev), γ (512 keV)

The radioactivity of oil and gas waste depends on the lithology of drilled reservoir, which determines the amount of radionuclides in the subsurface and chemical composition of formation fluid. The duration of production, extraction and treatment process (also hydraulic fracturing), changes pH, pressure, temperature and causes mobilization of the NORMs (Smith, 1992; Atallah et al., 2014). The radionuclides in the drilling wastes mostly come from different types of rocks. Selected, exemplary activity concentrations of radionuclides are presented in Table 2. It shows the range of natural radioactivity levels for the same lithological types of rocks.

Potassium K-40 has higher activity concentration than uranium U-238 and thorium Th-232. Gamma-ray spectrometry during well logging shows K-40 concentration in percentiles, while U-238 and Th-232 concentration in parts per million. The concentrations of the mentioned radionuclides provide information about producible zones and reservoir characteristics. They also allow to estimate the volume and type of clays.

The solid oil and gas wastes in the form of scale and sludge, tend to accumulate in the downhole casing and tubing as well as at the surface equipment (separators, pumps, vessels, pipelines, tanks). It could present some radiological hazard (Smith, 1992; Hamlat et al., 2001; Atallah et al.,2012; Hrichi et al., 2013; Hilal et al., 2014;). Radium Ra-226 and Ra-228 can co-precipitate in the scale made of BaSO4, SrSO4 or CaCO3 (Hamlat et al., 2001). The NORM can appear also in the liquid (produced water, formation water) and gas phase. The ways of radionuclides mobilization are shown in Fig. 1. Drilling cuttings and produced water are the major source of natural radioactivity in oil and gas production, also offshore (Bakke et al., 2013).

Table 2. A comparison of activity concentrations with standard deviation [Bq/kg] of radionuclides in rocks

Lithology	Activity concentration [Bq/kg]				Rn-222 [kBq/m^3] (*)	Country	Reference
	U-238	Th-232	K-40	Ra-226			
Sandstone	34±3	53.0±4	23236±32	-	-	Nigeria	Omeje et al., 2013
Clay	23±2	32.0±3	399±51	-	-	Nigeria	Omeje et al., 2013
Gneiss	-	38.0±4	1168±42	28.4±3	-	Egypt	Harb et al., 2012
Granite	-	90.5±7	2208±91	118.0±7	-	Egypt	Harb et al., 2012
Sandstone	-	12.5±3	264±11	7.5±1.5	-	Egypt	Harb et al., 2012
Limestone	-	-	53±2	35.7±2.4	-	Poland	Malczewski et al., 2006
Limestone	-	-	473±9	43.2±6.8	-	Poland	Malczewski et al., 2006
Granite-gneiss	-	-	1177±13	49.8±6.9	-	Poland	Malczewski et al., 2004
Hornfelses	-	-	494±6	30.7±3.7	-	Poland	Malczewski et al., 2004
Granite-gneiss	-	-	-	50.4±31.4	-	Poland	Przylibski, 2004
Sandstone	-	-	-	12.8±10.7	-	Poland	Przylibski, 2004
Hornfelses	-	-	-	35.7±1.2	-	Poland	Przylibski, 2004
Shell limestone	-	-	-	-	33±4	Germany	Kemski et al., 2001
Coloured standstone	-	-	-	-	24±3	Germany	Kemski et al., 2001
Carboniferous sediments	-	-	-	-	41±3	Germany	Kemski et al., 2001
Granites		-			106±8	Germany	Kemski et al., 2001
Gneiss	-	-	-	1.0-1800	-	Mean global value	IAEA, 2010
Limestone	-	-	-	0.4-340	-	Mean global value	IAEA, 2010
Clay/shale	-	-	-	1.0-990	-	Mean global value	IAEA, 2010
Sandstone	34±3	53.0±4	23236±32	-	-	Nigeria	Omeje et al., 2013
Clay	23±2	32.0±3	399±51	-	-	Nigeria	Omeje et al., 2013
Gneiss	-	38.0±4	1168±42	28.4±3	-	Egypt	Harb et al., 2012

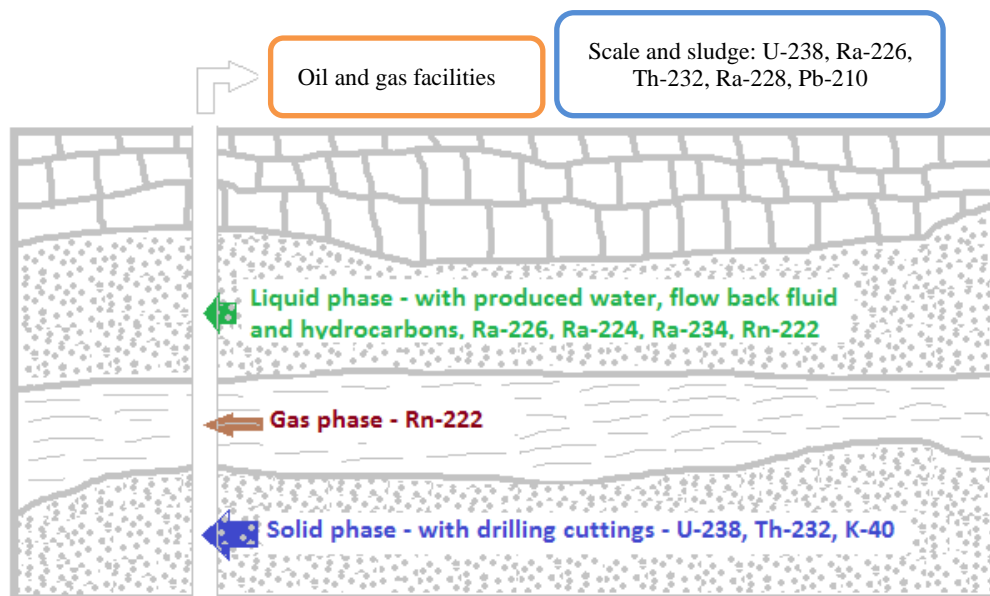(*) Radon activity concentration in soil gas above rocks

Fig. 1. NORM mobilization in oil and gas production (based on OGP, 2008)

The exemplary NORM exemptions levels taken from international regulations are provided in Table 3. The adhering to recommendations laid out in these recommendations, minimizes the risk of worker exposure to ionizing radiation.

Table 3. NORM exemption levels (OGP, 2008)

Nuclide	Type	Exemption level [Bq/kg]
U-238	primordial	5500
Pb-210	U-238 decay series	200
Po-210	U-238 decay series	200
Ra-226	U-238 decay series	1100
Ra-228	Th-232 decay series	1100

Experimental procedure

Sample preparation

The Ordovician drilling cuttings samples (Figs. 2a and 2b,) from exploration of shale gas reservoir in the Baltic Basin were collected. Two types of samples were measured: cuttings after sieve separation and centrifugation, which contain the residue drilling mud and cuttings after Dean-Stark extraction and sieve analysis. By means of sieve analysis three fractions were obtained (Fig. 2b). For activity concentration measurements 80 g of each sample was examined under the same conditions. The

samples were closed tightly and stored for 1 month to obtain equilibrium between primordial and daughters radionuclides. The drilling mud did not contain potassium ions, therefore the value of K-40 activity concentration is related only to the rocks, which is an advantage since potassium chloride is frequently added to the drilling mud, thus disturbing well logging spectrometry measurement. It can also influence the laboratory experiment when the Dean-Stark extraction is not provided.
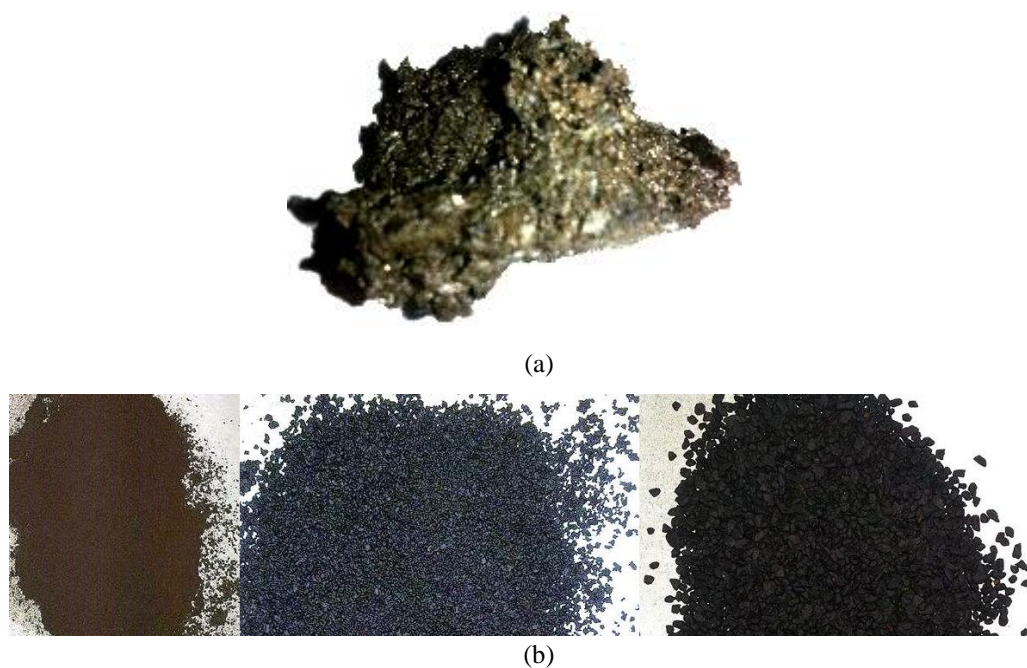

(a)

(b)

Fig. 2. Ordovician drilling cuttings. (a) original, (b) fractioned: from the left <0.425 mm, 0.425-1 mm, 1-1.6 mm

The bulk of drilling wastes originated from different depth of the borehole. One depth was chosen for a second part of experiment concerning measurement of drilling cuttings after the Dean-Stark extraction and sieve analysis.

Gamma radiation measurements

Each sample was non-destructively analyzed using a portable gamma-ray spectrometer InSpector1000 Canberra consisting of NaI(Tl), 2"x2" stabilized probe with sensitivity of Cs-137 ~3.5% and multichannel analyzer designed for environmental screening. Before measurement, the detector was calibrated using a cesium Cs-137 source. The activity concentrations were determined using decay energies provided in Table 1. The measurement was conducted in a lead shield to eliminate the influence of background radiation (Fig. 3). Each sample was measured three times. Eighty grams of drilling

cuttings were placed in a 48 mm diameter container (corresponding to probes diameter).

Fig. 3. Scintillation stabilized probe in lead shield used in the research

Absorbed dose rate (Dγ)

An absorbed dose is a dose of ionizing radiation in the outdoor air 1 m above the surface of drilling cuttings samples originating from the gamma radiation. The formula is:

$$D\gamma = 0.0417A_K + 0.462A_{Ra} + 0.604A_{Th} \tag{1}$$

where A_K, A_{Ra}, A_{Th} are the activity concentrations of K-40, Ra-226 and Th-232, respectively. According to UNSCEAR Report (UNSCEAR, 1993) the absorbed dose rate should not exceed the average global value of 55 nGy/h. The absorbed dose consists mainly of uranium, thorium and potassium radioisotopes. Others are insignificant in the gamma radiation exposure.

Results and discussion

The X-ray diffraction (XRD) showed that the major component of the studied material is quartz, sodium aluminum dioxide, aluminum silicate hydrate and wustite. To elucidate the structure of examined samples, the SEM examination was performed (Fig. 4). It confirmed the presence of quartz, silicate and sulfur in the form of pyrite

framboids. The particle size distribution after the Dean-Stark extraction and sieve analysis is provided in Table 4.

Table 4. Fractions of drilling cuttings after sieve analysis

No.	Size range [mm]	Weight percentage [%]
	Before Dean-Stark extraction	
1	<0.425	46.5
2	0.425-1.0	26.3
3	1.0-1.6	27.2
	After Dean-Stark extraction	
4	<0.425	44.9
5	0.425-1.0	28.0
6	1.0-1.6	27.1
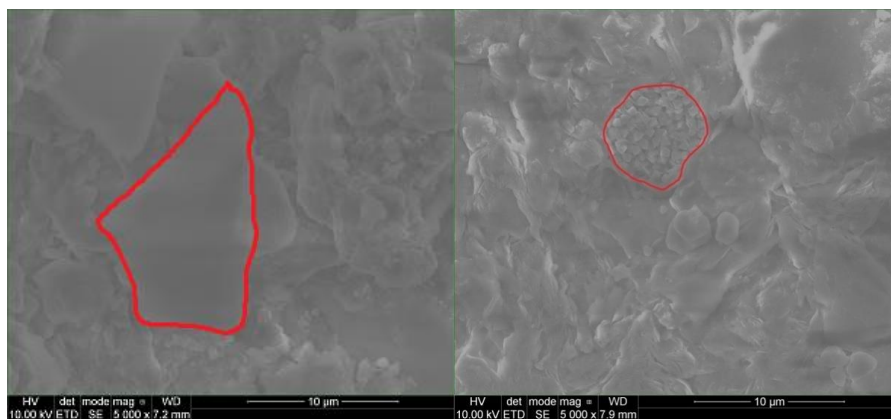
Fig. 4. SEM image of investigated material (quartz silt on the left side and pyrite framboid on the right side)

Radiation expressed in the activity concentration of radionuclides [Bq/kg] for analyzed samples is shown in Tables 5 (bulk wastes) and 6 (size fractions: BA and AA sample was also measured after sieve analysis). The average value from three measurements with standard deviation are provided. The activity concentration of Uranium U-238 was at an undetectable level, even during 24 h of exposure. Therefore, it does not pose any radiological hazard.

Table 5. Results of bulk drilling cuttings gamma radiation measurements (BX – before Dean-Stark extraction, AX – after Dean-Stark extraction, X -consecutive determination of samples SD – standard deviation)

No.	Sample	Mean concentration of K-40 [Bq/kg] with SD	Mean concentration of Th-232 [Bq/kg] with SD	Mean absorber dose rate $D\gamma$ [nGy/h]
		As received, before (B) Dean-Stark extraction		
1	BA	865±40	29.2±2.3	53.7
2	BB	838±39	29.5±2.4	52.7
3	BC	999±46	31.0±2.5	62.9
4	BD	905±42	29.2±2.3	57.0
5	BE	848±39	28.8±2.3	42.8
6	BF	680±31	28.8±2.3	53.4
		After (A) Dean-Stark extraction		
7	AA	834±38	23.3±1.9	48.9
8	AB	850±39	25.5±2.0	53.5
9	AC	867±40	26.3±2.1	54.6
10	AD	866±40	24.0±1.9	54.5

The absorbed dose associated with bulk drilling wastes was 54.1 nGy/h. Only two samples had higher absorbed dosages (BC 62.9 and BD 57.0 nGy/h) than the mean global value (55 nGy/h), however they did not constitute any radiological hazard. A diagram, comparing results from Table 5 is shown in Fig. 5. Fractioned samples are shown in Fig. 6.
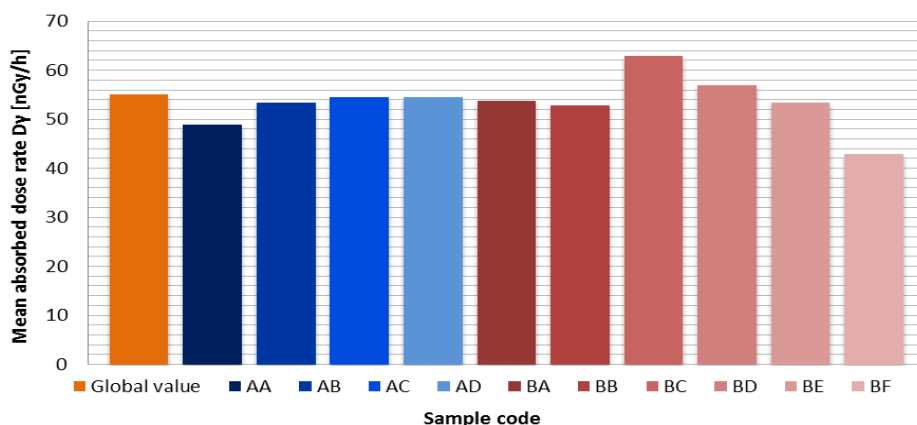

Fig. 5. Results of absorbed dose rate estimation in the bulk drilling cuttings samples (BX – before Dean-Stark extraction, AX – after Dean-Stark extraction, X -consecutive determination of samples) in relation to average global value (UNSCEAR, 1993)

The absorbed dose rate is greater for the drilling wastes before Dean-Stark extraction than after toluene extraction (53.9 nGy/h before Dean-Stark process and 53.8 nGy/h after Dean-Stark process). In the first case the sample from one depth had low level of natural radioactivity (680 Bq/kg for K-40 and 28.8 Bq/kg for Th-232). The range of activity concentration of potassium was 680-999 Bq/kg and of thorium 23.3-31.0 Bq/kg in the non-fractioned samples.

Table 6. Gamma radiation of drilling cuttings size fractions (BA before Dean-Stark extraction, AA after Dean-Stark extraction, 1-6 consecutive numbering of samples)

No.	Sample	Size range [mm]	K-40 [Bq/kg]	Th-232 [Bq/kg]	$D\gamma$ [nGy/h]
		Before (B) Dean-Stark extraction			
1	BA	-	865±40	29.2±2.3	53.7
2	BA1	<0.425	992±46	30.8±2.5	60.0
3	BA2	0.425-1.0	905±42	28.3±2.3	54.9
4	BA3	1.0-1.6	825±38	26.7±2.1	50.5
		After (A)Dean-Stark extraction			
5	AA	-	834±38	23.3±1.9	48.9
6	AA4	<0.425	852±39	24.8±2.0	50.5
7	AA5	0.425-1.0	818±38	23.8±1.9	48.5
8	AA6	1.0-1.6	800±37	23.3±1.9	47.5

Table 6 shows that the dominating gamma radiation emitter in drilling cuttings is potassium K-40 (800-992 Bq/kg), which is in line with the data provided in Table 2. Thorium Th-232 was also observed and the results (23.3-30.8 Bq/kg) are again comparable to the literature values (Table 2). There is a difference in activity concentration of radionuclides before and after Dean-Stark extraction, because some of radionuclides can be leached out from the sample, and thus the concentration of K-40 and Th-232 decreases.

The analysis of specified fractions yielded different results. The elevated radionuclides concentration in smaller size fractions was observed and both factors seem to be negatively correlated. The level of gamma radiation in bulk wastes was not greater than in the level in the individual fractions of wastes. It was observed that radionuclides can be partially redistributed in fractioned drilling cuttings. Higher absorbed dose of gamma radiation could be associated with greater specific surface area of particles, which increases gamma-ray emission. On the other hand, gamma rays can penetrate rocks and it should be researched whether this correlation exists with poor penetrating radiation such as alpha or beta particles.

The comparison of analyzed samples is presented in Fig. 6. The absorbed dose criterion was selected to inform about the radiological hazard. The average absorbed dose rate in outdoor air 1 m above the drilling cuttings was 54.9 nGy/h. This result is lower than the global value of 55 nGy/h. In this regard, the drilling cuttings did not constitute any radiological hazard and can be utilized. Only the <0.425 mm size

fraction before Dean-Stark extraction, exceeded the average global value and reached 62.4 nGy/h.
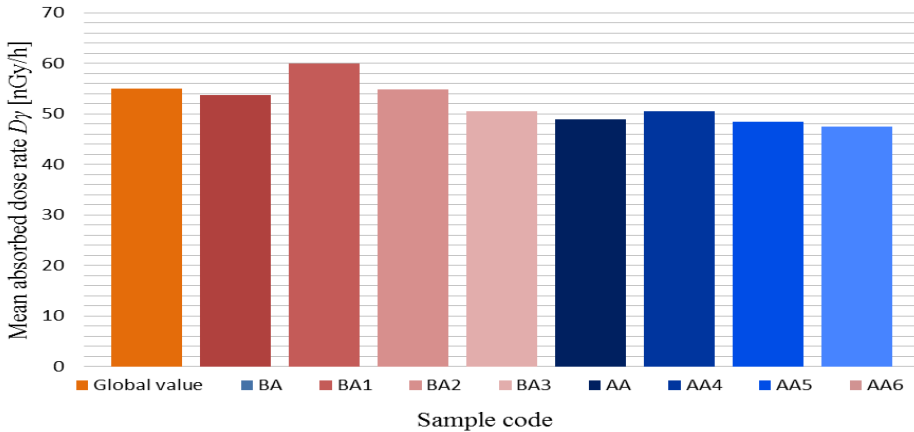

Fig. 6. Results of absorbed dose rate estimation in the fractioned drilling cuttings samples (BA – before Dean-Stark extraction, AA after Dean-Stark extraction, 1-6 consecutive numbering of samples) in relation to average global value (UNSCEAR, 1993)

The second part of the experiment aimed to check the relationship between the grain size and level of natural radioactivity. The radionuclides amount is negatively correlated with the size of grains in the drilling cuttings samples but on the other hand activity concentrations in the bulk wastes do not confirm the thesis. It can be stated with certainty, that Dean-Stark extraction leached some radioisotopes. The activity concentration and absorbed dose based on them, is higher in the samples before extraction. The difference is rather small – from a few Bq/kg for thorium to tens Bq/kg for potassium.

Final comments

The research concerned two aspects: relationship between natural radioactivity emission and grain size, and radioactivity of drilling wastes. It revealed that
1. main radiological constituent in bulk and fractionated drilling cuttings is potassium K-40,
2. activity concentration is comparable with literature values and vary from 680 to 999 Bq/kg for potassium K-40 and from 23.3 to 31.0 Bq/kg for thorium Th-232. Other radioisotopes have undetectable concentrations,
3. some of radionuclides were leached during Dean-Stark extraction,

4. examined drilling cuttings do not present any radiological hazard for humans and can be safely utilized. The absorbed dose ($D\gamma$) is 54.1 nGy/h in respect to global average value 55 nGy/h,

5. radionuclides amount in the examined fractioned drilling cuttings increased, while the size of the grains decreased.

Acknowledgements

References

ATALLAH M.F, AWWAD N.S, ALY H.F, 2012, *Environmental Radioactivity of TE-NORM Waste Produced from Petroleum Industry in Egypt: Review on Characterization and Treatment,*[Online 04.07.2014 http://dx.doi.org/10.5772/CHAPTERDOI].

EL AFIFI E.M, AWWAD N.S, 2005, *Characterization of the TE-NORM waste associated with oil and natural gas production in Abu Rudeis, Egypt,* Journal of Environmental Radioactivity, vol. 82, pp. 7–19.

BAKKE T., KLUNGSOYR J., SANNI S., 2013, *Environmental impacts of produced water and drilling waste discharges from the Norwegian offshore petroleum industry,* Marine Environmental Research, vol. 92, pp. 154-169.

HAMLAT M.S, DJEFFAL S., KADI H., 2001, *Assessment of radiation exposures from naturally occurring radioactive materials in the oil and gas industry*, Applied Radiation and Isotopes vol. 55, pp. 141–146.

HARB S., ABBADY E.B, EL-KAMEL E.H, SALEH I.I, EL-MAGEED A.I, 2012, *Natural radioactivity and their radiological effects for different types of rocks from Egypt*, Radiation Physics and Chemistry, vol. 81, pp. 221-225.

HILAL M.A., ATTALLAH M.F., MOHAMED G.Y., FAYEZ-HASSAN M., 2014, *Evaluation of radiation hazard potential of TENORM waste from oil and natural gas production*, Journal of Environmental Radioactivity, vol. 136, pp. 121-126.

HRICHI H., BACCOUCHE S., BELGAIDED J., 2013, *Evaluation of radiological impacts of tenorm in the Tunisian petroleum industry*, Journal of Environmental Radioactivity, vol. 115, pp. 107-113.

INTERNATIONAL ASSOCIATION OF OIL AND GAS PRODUCERS (OGP), 2008, *Guidelines for the management of Naturally Occurring Radioactive Material (NORM) in the oil & gas industry,* Report No: 412.

INTERNATIONAL ATOMIC ENERGY AGENCY, 2010, *Radiation protection and the management of radioactive waste in the oil and gas industry*, IAEA, Wiedeń.

KEMSKI J., SIEHL A., STEGEMANN R., VALDIVIA-MANCHEGO M., 2001, Mapping the geogenic radon potential in Germany, The Science of the Total Environment, vol. 272, pp. 21 -230.

KIERSNOWSKI H, DYRKA I., 2014, *Potencjał złożowy ordowicko-sylurskich łupków gazonośnych w Polsce: omówienie dotychczasowych raportów i propozycje udoskonalenia metodyki oceny zasobów gazu w raporcie w 2014 r.*, Przegląd Geologiczny, vol. 61, no. 6, [In Polish].

MALCZEWSKI D, BADERA J., LIZUREK G., MIRKOWSKI Z., DORDA J., 2006, *Natural radioactivity of the Paleozoic rocks from the area of Krzeszowice (southern Poland).* Przegląd Geologiczny, vol. 54, no. 9, pp. 815-822, [In Polish].

MALCZEWSKI D., TEPER L., DORDA J., 2004, *Assessment of natural and anthropogenic radioactivity levels in rocks and soils in the environs of Swieradow Zdroj in Sudetes, Poland, by in situ gamma-ray spectrometry*, Journal of Environmental Radioactivity, vol. 73, pp. 233–245.

MYKOWSKA A., HUPKA J.,2014, *Radionuclides activity and effective doses referred to geological formations*, Journal of Industrial and Intelligent Information vol. 2, no. 4, pp. 284-288.

OMEJE M., HUSIN W., NOORDDIN I., SIAK KUAN L., SOHEIL S., 2013, *Comparison of activity concentration of 238-U, 232-Th and 40-K indifferent Layers of subsurface Structures in Dei-Deiand Kubwa, Abuja, north central Nigeria*, Radiation Physics and Chemistry, vol. 91, pp. 70-80.

OTTO, G.H., 1989, *A National Survey on Naturally Occurring Radioactive Materials (NORM) in Petroleum Producing and Gas Processing Facilities. Report of the American Petroleum Institute,* Dallas, Texas, US.

POPRAWA P., 2010, *Potencjał występowania złóż gazu ziemnego w łupkach dolnego paleozoiku w basenie bałtyckim i lubelsko-podlaskim*, Przegląd Geologiczny, vol. 58, nr 3[In Polish].

PRZYLIBSKI T.A., 2004, *Concentration of Ra-226 in rocks of the southern part of Lower Silesia (SW Poland,* Journal of Environmental Radioactivity, vol. 75, pp. 171-191.

RAVISANKAR R., SIVAKUMAR S., A.CHANDRASEKARAN, PRINCE PRAKASH JEBAKUMAR J., VIJAYALAKSHMI I., VIJAYAGOPAL P., VENKATRAMAN B., 2014, *Spatial distribution of gamma radioactivity levels and radiological hazard indices in the East Coastal sediments of Tamilnadu, India with statistical approach,* Radiation Physics and Chemistry, vol. 103, pp. 89-98.

SMITH K.P.,1992, *An Overview of Naturally Occurring Radioactive Materials (NORM) in Petroleum Industry,* Argonne National Laboratory.

UNITED NATIONS SCIENTIFIC COMMITTEE ON THE EFFECTS OF ATOMIC RADIATION (UNSCEAR), 1993, *Ionizing radiations: Sources and Biological Effects of Atomic Radiation (UNSCEAR). Report to the General Assembly with annexes*, Vienna.

UNITED NATIONS SCIENTIFIC COMMITTEE ON THE EFFECTS OF ATOMIC RADIATION (UNSCEAR), 2000, *Sources and effects of ionizing radiation. Report to the United Nations General Assembly*, New York.

SELECTIVE REDUCTION OF PbSO₄ TO PbS WITH CARBON AND FLOTATION TREATMENT OF SYNTHETIC GALENA

Yong-xing ZHENG, Wei LIU, Wen-qing QIN, Jun-wei HAN, Kang YANG, Hong-lin LUO

School of Minerals Processing and Bioengineering, Central South University, Changsha, Hunan 410083, P. R. China, xyzj2013@126.com (Wei Liu), qinwenqing369@126.com (W. Qin)

Abstract: In order to recover lead from the zinc leaching residues, a new technology involving selective reduction of lead sulfate to lead sulfide with carbon followed by flotation was investigated. The reduction thermodynamics of $PbSO_4$ was discussed and the effects of molar ratio of C to $PbSO_4$, reaction temperature and time were examined by thermogravimetry (TG) and XRD. Verification tests were further carried out to prove the conclusions of thermodynamic and TG analyses, and the transformation extent could reach 86.45% under the optimal roasting conditions. The prepared galena was then subjected to micro-flotation tests, and the highest lead recovery could reach up to 75.32%.

Introduction

The recovery of lead from zinc leach residues, usually containing from 5 to 20% Pb, is of interest for the zinc plants. Nowadays, more than 70% of zinc is produced from zinc sulfide concentrates by conventional roast-leach-electrowinning processes in the world (Ozverdi and Erdem, 2010; Peng et al., 2003; Rashchi et al., 2005). Therefore, significant amounts of residues are generated during this process, which may contain mainly zinc ferrite, goethite, hematite or jarosite, depending on ways of iron elimination. Meanwhile, lead in the form of $PbSO_4$ is reported to the leach residues (Altundogan et al., 1998; Li et al., 2012). Most of the residues have to be stockpiled resulting in serious environment problems because of their heavy metal content. Currently, the concerns over these wastes are not exclusively environmental, but economic as well. In the past years, many processes have been tested for treating these

lead sulfate bearing residues, such as flotation, flotation combined with gravity concentration, pyrometallurgy and hydrometallurgy.

In term of flotation reagents of $PbSO_4$, salicylhydroxamic acid and cupferron were approved to be effective collectors (Jingyun and Jianguang, 1991; Zhu and Zhao, 1991). However, these collectors were poor in selectivity against iron compounds. Generally speaking, oxidized minerals are more difficult-to-float than their sulfide counterparts (Herrera et al., 1998; 1999). Therefore, surface modification by Na_2S or Na_2CO_3 was usually proposed to enhance its recovery (Fuerstenau et al., 1987; Herrera et al., 1998; Onal et al., 2005). However, it was still difficult to achieve a satisfactory recovery for the concentrate because the particles were extremely fine. In order to further improve this, desliming prior to flotation was proposed as a promising method (Rashchi et al., 2005). Nevertheless, the loss of lead sulfate remained unavoidable since it was partially distributed in the fine fraction.

On the other hand, the pyrometallurgical processes, such as blast furnace reduction, reverberatory and bottom blowing methods, are usually used to extract lead from the wastes, especially from the materials with lead content higher than 20% (Badanoiu and Buzatu, 2012; Peng et al., 2003; Rennerta, 2010). However, these technologies were not promising in treating the materials with a lower lead content due to the high operation cost. Chlorination and carbochlorination of $PbSO_4$, which could be performed at a relatively low temperature, were also reported for the recovery of lead from the leach residue (Menad et al., 1997). Yet the generation of Cl_2 presented another potential threat for the environment. In order to avoid these problems, a variety of hydrometallurgical processes including leaching and transformation by carbonates were introduced. In the literature available, hydrochloric acid and thiourea solution were found to be widely used (Baba et al., 2011; Qin et al., 2009; Shirchinnamjil et al., 2008; Vinals et al., 1991). However, the operating environment was usually unacceptable due to the release of various noxious gases such as HCl, H_2S and AsH_3. Generally, ammonium and sodium carbonates were usually used as transformation reagents. Gen-shou (2002) reported the preparation of tribasic lead sulfate from lead bearing ash by transformation with ammonium carbonate followed by leaching and precipitating processes. Gong et al. (1992) studied the conversion of $PbSO_4$ to $PbCO_3$ with sodium carbonate, and found that the conversion extent was improved with increasing temperature. Despite achievements made, further work was required before these technologies could be put into practice.

Recently, the transformation of $PbSO_4$ to PbS has received considerable attention as a promising method for treating the lead bearing wastes. On the one hand, the PbS obtained is less soluble than $PbSO_4$ (Appelo and Postma, 2010; Pacholewska, 2004; Weijma et al., 2002; Wolthoorn et al., 2007), which lowers the risk of pollution of the heavy metal. On the other hand, it is expected that PbS generated can be recovered by some conventional techniques. Schroder et al. (2008) applied biological reduction to convert $PbSO_4$ in the spent car batteries to PbS which was then recovered by electrochemical processes. Karnachuk et al. (2002) studied the transformation of

PbSO$_4$ in acid mine drainage to PbS with lactate bacteria, and found that the concentration of Pb^{2+} was decreased in the solution attributed to the stable precipitation of PbS formed.

The present paper focused on conversion of PbSO$_4$ to PbS by reduction roasting with carbon powder and the flotation performance of synthetic galena was also investigated. To our knowledge, there was little related work reported. The goal was to develop a new technology to enhance lead recovery from the zinc leach residues.

Experiment

Materials

The lead sulfate was of analytical grade and argon was used as a protective gas with a purity of 99.999%. The TG curves of carbon powder are shown in Fig.1, which reveals that about 23 wt% and 90 wt% of sample would be finally lost under argon and air atmosphere, respectively. It also can be seen that about 20 wt % of the sample was decreased when the temperature was increased to 650 $^{\circ}$C, indicating that mass loss of itself has little effect on the mass loss of the reduction reaction which occurred above the temperature.
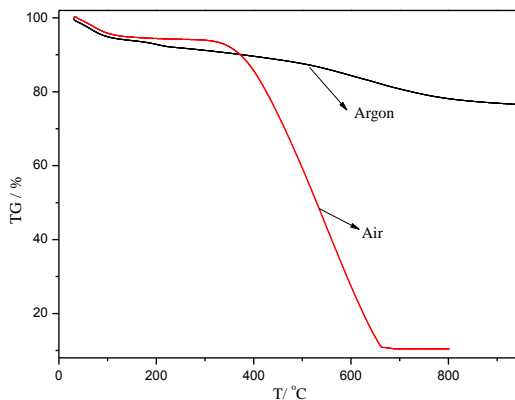

Fig.1. TG curves of the carbon powder under argon and air atmosphere

Hydrochloric acid and sodium hydroxide as pH modifiers, sodium diethyldithiocarbamate (SD) and ammonium dibutyldithiophosphate (ADD) as collectors and terpineol as frother were used in the flotation tests.

Experimental apparatus and procedure

The reaction process of PbSO$_4$ was conducted making use of a thermalanalyser (NETZSCH5, STA 449 F3) and the non-isothermal tests were carried out within 900 $^{\circ}$C at a heating rate of 10 °C/min. In the isothermal tests, sample was heated at a

heating rate of 30 °C/min to the desired temperature, and then reacted for 60 min. Samples obtained were subjected to XRD (Germany Bruker-axs D8, Cu Kα) analyses.

Verification tests were carried out in a horizontal resistance furnace under argon atmosphere. About 20 g of $PbSO_4$ was mixed with carbon powder on different molar ratio, and then loaded into an alundum crucible with a volume of 450 cm^3, which was then placed in the furnace heated. The powder samples obtained were subjected to XRD and chemical phase analyses to determine the optimal reduction conditions. The transformation extent of $PbSO_4$, which equals to the percentage of PbS accounting for total lead in this work. Micro-flotation was carried out in a cell with an effective volume of approximate 40 cm^3 and the flotation flow sheet is shown in Fig. 2. Concentrate and bottom product, after flotation, were washed with distilled water, filtered, dried, weighed and calculated.
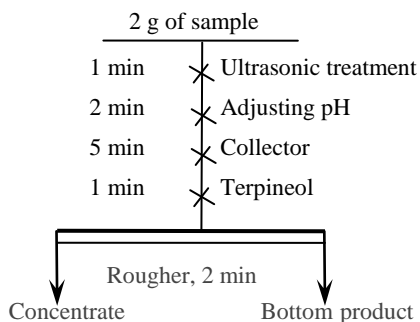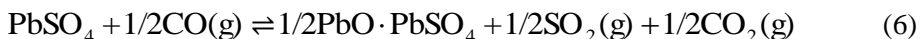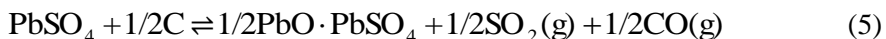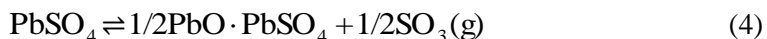

Fig. 2. Experimental schematic of the micro-flotation
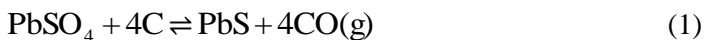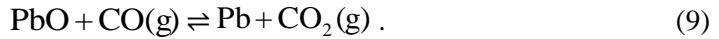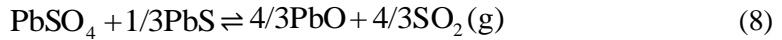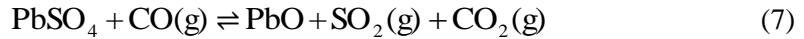
Experimental reaction mechanism

As mentioned above, the recovery of lead from zinc leach residues is of interest for the zinc plants. The present paper suggests that it should be advantageous to transform $PbSO_4$ to PbS. Therefore, selective reduction of $PbSO_4$ to PbS plays an important part in this work. The reactions that may occur are listed as follows:

$$PbSO_4 + 4C \rightleftharpoons PbS + 4CO(g) \tag{1}$$

$$PbSO_4 + 2C \rightleftharpoons PbS + 2CO_2(g) \tag{2}$$

$$PbSO_4 + 4CO(g) \rightleftharpoons PbS + 4CO_2(g) \tag{3}$$

$$PbSO_4 \rightleftharpoons 1/2PbO \cdot PbSO_4 + 1/2SO_3(g) \tag{4}$$

$$PbSO_4 + 1/2C \rightleftharpoons 1/2PbO \cdot PbSO_4 + 1/2SO_2(g) + 1/2CO(g) \tag{5}$$

$$PbSO_4 + 1/2CO(g) \rightleftharpoons 1/2PbO \cdot PbSO_4 + 1/2SO_2(g) + 1/2CO_2(g) \tag{6}$$

$$PbSO_4 + CO(g) \rightleftharpoons PbO + SO_2(g) + CO_2(g) \tag{7}$$

$$PbSO_4 + 1/3PbS \rightleftharpoons 4/3PbO + 4/3SO_2(g) \tag{8}$$

$$PbO + CO(g) \rightleftharpoons Pb + CO_2(g) \, . \tag{9}$$
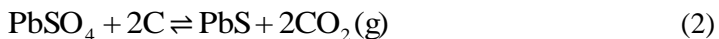
The software HSC 5.0 (Outokumpu, 2002) was used to calculate the standard Gibbs free energy changes of these reactions (Fig. 3) and the equilibrium amounts of roasted products (Fig. 4). Figure 3 presents the relationship between the standard Gibbs free energy changes and temperature. It can be seen that the decomposition of $PbSO_4$ (Eq. (4)) seems to be difficult within the temperature, but the reductions of $PbSO_4$ may be feasible (Eqs. (1)-(3)) in the presence of carbon. The selective reduction of $PbSO_4$ to PbS by carbon involves direct (Eqs. (1)and(2)) and indirect (Eq. (3)) ways. The indirect process (Eq. (3)) may be most likely attributed to the minimum of the standard free energy bellow 700 ^oC, but the direct reduction (Eqs. (1) and (2)) may prevail above this temperature. However, the PbS produced may further react with $PbSO_4$ (Eq. (8)) at temperature higher than 800 ^oC. In the meantime, the reduction of $PbSO_4$ to PbO·$PbSO_4$ or PbO (Eqs. (5)-(7)) seems also to be possible at the temperature higher than 500 ^oC and the PbO generated may be further reduced to metallic Pb (Eq. (9)). Therefore, selective transformation of $PbSO_4$ to PbS could be achieved by controlling reduction temperature.
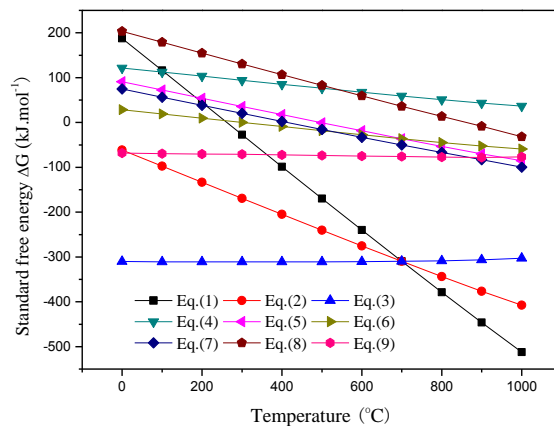

Fig. 3. Standard Gibbs free energy changes for the reduction of $PbSO_4$ in the temperature range of 0~1000 ^oC

Figure 4 shows the equilibrium amounts of roasted products as function of carbon dosage at the temperature of 700 ^oC (Fig. 4(a)) and 800 ^oC (Fig. 4(b)). The calculations were performed in 1 kmol of $PbSO_4$ under 0.1MPa (1 atm). They reveal that the amount of PbS produced was increased as the carbon dosage was increased

from 0 to 2.1 kmol. With a further increase on carbon dosage, the amount of PbS kept a constant value. However, increasing temperature is not favorable for the transformation of $PbSO_4$ to PbS at carbon dosage less than 2.1 kmol, but beneficial for the formation of PbO $PbSO_4$, PbO and even metallic Pb. Accordingly, the theoretical molar ratio of C to $PbSO_4$ was determined to be above 2.0. In order to exactly examine the factors affecting the reduction of $PbSO_4$ to PbS, TG tests were performed for the related samples.
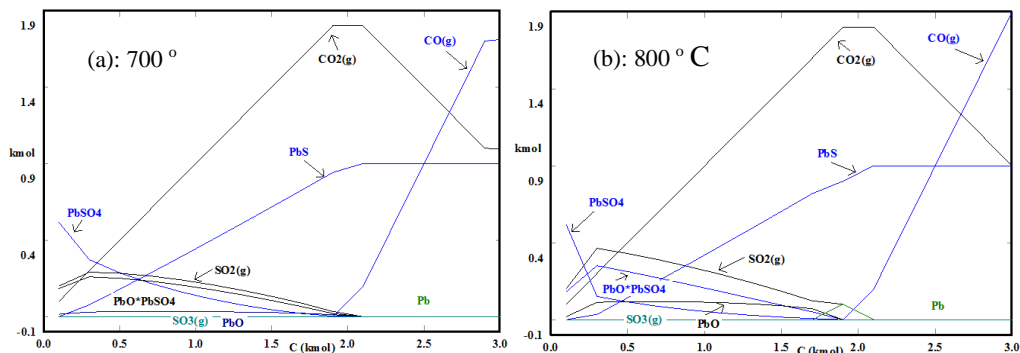

Fig. 4. Equilibrium amounts of the products as functions of carbon dosage and temperature

Results and discussion

Thermogravimetric analyses

Non-isothermal thermogravimetric tests

Figure 5 shows the TG curves (Fig. 5(a)) and derivative thermogravimetry (DTG) curves (Fig. 5(b)) with respect to temperature and different molar ratio of C to $PbSO_4$. It can be seen that sample mass was slightly decreased until the temperature was increased to 650 ^{o}C. As indicated by the TG curves of carbon powder (Fig.1), this may be accounted by the mass loss of carbon powder, which had little effect on the mass loss of reduction reaction as the temperature was increased. With a further increase on temperature, mass loss continues and their maximum rates occurred at about 700 ^{o}C. Considering the results of thermodynamic analyses, the reduction of $PbSO_4$ to PbS may be dominant around this temperature. However, for the sample with a lower carbon dosage (curve 2), DTG curve (Fig. 5(b)) shows another rate extremum at about 800 ^{o}C. As suggested by the equations (Eqs. (7)-(9)), the formation of metallic Pb may occur at this temperature. Nevertheless, these deductions needed further confirmation. Therefore, isothermal thermogravimetric tests and XRD analyses were carried out.
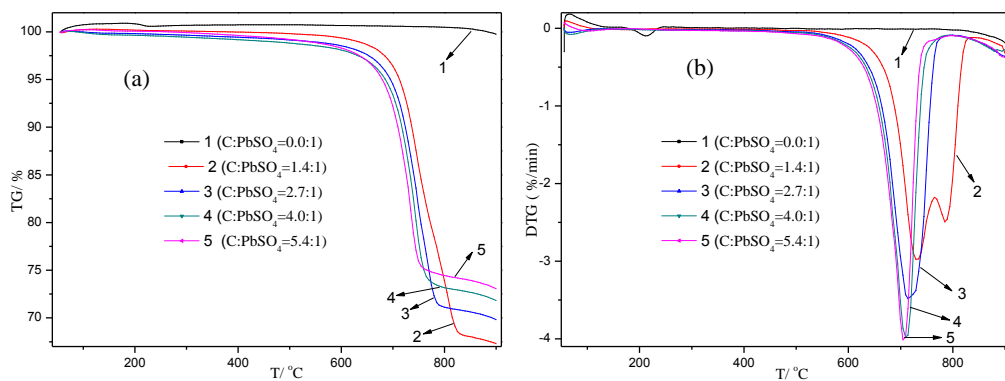
Fig. 5. TG-DTG curves of the samples with different molar ratio of C to PbSO$_4$

Isothermal thermogravimetric tests

Figure 6a presents the remaining mass as functions of time and molar ratio of C to PbSO$_4$ at 700 ^{o}C. It can be seen that the rate of mass loss was increased with increasing carbon dosage. This may be accounted by the explanation that increasing carbon dosage causes a fast de-oxidation of the PbSO$_4$. Furthermore, the reduction of PbSO$_4$ was finished within about 60 min, indicating that the transformation to PbS was highly efficient using carbon powder. The X-ray diffraction patterns of the sample obtained are shown in Fig. 6b. It can be known that the peak intensity of PbS was increased as the molar ratio of C to PbSO$_4$ was increased from 1.4 to 2.7. In the meantime, it can also be found that part of PbSO$_4$ still existed attributed to the insufficient of carbon dosage, and that small amount of metallic lead was formed ascribed to the formation of PbO (Eq. (7)) and its further reduction (Eq. (9)). However, there were no significant characteristics with a further increase on the molar ratio. Therefore, the molar ratio range of C to PbSO$_4$ was determined to be 2.7 to 4.0 as the selective reduction temperature was chosen at 700 ^{o}C.

As discussed in section 2.3, temperature plays an important part in the effective transformation of PbSO$_4$ to PbS. Figure 6c shows the effect of temperature and time on remaining mass under the maximum molar ratio (4.0) of C to PbSO$_4$. It can be seen that rate of mass loss was increased with increasing temperature, indicating that the reduction of PbSO$_4$ ran intensively at a higher temperature. The X-ray diffraction patterns of the sample obtained are shown in Fig. 6d. It was found that PbO·PbSO$_4$ was formed at 650 ^{o}C, but its peak was disappeared as the temperature was increased to 700 ^{o}C. This may be attributed to the effect of mass or heat transfer (Menad et al., 1997; Szekely, 1976).With a further increase on temperature, metallic lead was formed. These results are consistent with the thermodynamic and non-isothermal thermogravimetric analyses. Accordingly, the optimal reduction temperature was determined to be 700 ^{o}C.

Based on the above analyses, the operating process parameters for the selective transformation of $PbSO_4$ to PbS was determined as temperature of 700 ^{o}C, molar ratio of C to $PbSO_4$ ranging from 2.7 to 4.0, and reaction time within 60 min.
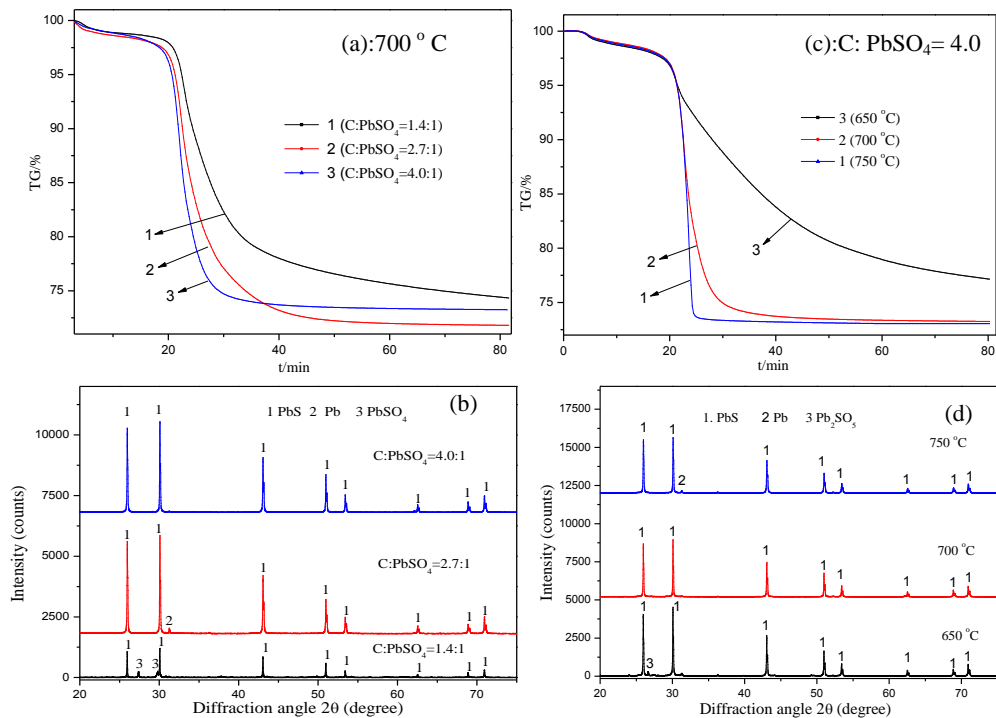

Fig. 6. Factors affecting $PbSO_4$ reduction under argon atmosphere and X-ray diffraction patterns of the roasted samples

Verification tests and micro-flotation tests

Verification tests were carried out at 700 ^{o}C and the results were shown in Figs. 7 (a) and 7(b). It can be known that the highest transformation extent reached up to 86.45% under a molar ratio of 3.5 (C: $PbSO_4$) and a reaction time of 60 min, indicating that a sample with a higher purity was prepared.

A batch of artificial galena was prepared under the optimal roasting conditions and then micro-flotation was carried out. The flotation recovery as functions of collector concentration and pH is shown in Fig. 8. Figure 8a reveals that the artificial galena could be floated and the maximum recovery of 75.32% and 62.34% were obtained at an ADD concentration of $1.4 \cdot 10^{-4}$M and a SD concentration of $1 \cdot 10^{-4}$M, respectively.

Figure 8b discloses that pH value lower than 4.0 or higher than 10.0 will not be favorable for the flotation of artificial galena. This may be accounted by the explanation that the soluble ions at a lower pH, such as Pb^{2+} from the dissolution of Pb

compounds, were reacted with the collectors and then the precipitations were formed, but at a higher pH, the galena was oxidized and the Pb(OH)$_2$ was formed on its surface (Chernyshova and Andreev, 1997; Nowak and Laajalehto, 2000). In addition, it can be seen that the lead recovery reached about 75.0% with ADD and about 62.0% with SD in the pH range of 8.0-10.0, both of which were above 50%, indicating that the galena prepared could be recovered by flotation, and it was interesting that the ADD as collector seemed more powerful than the SD. This may be ascribed to the improvement of foam properties or occurrence of hydrophobic flocculation for the flotation of fine galena in ADD solution (Song et al., 2000; Zhang et al., 2014; Zhu et al., 1996).
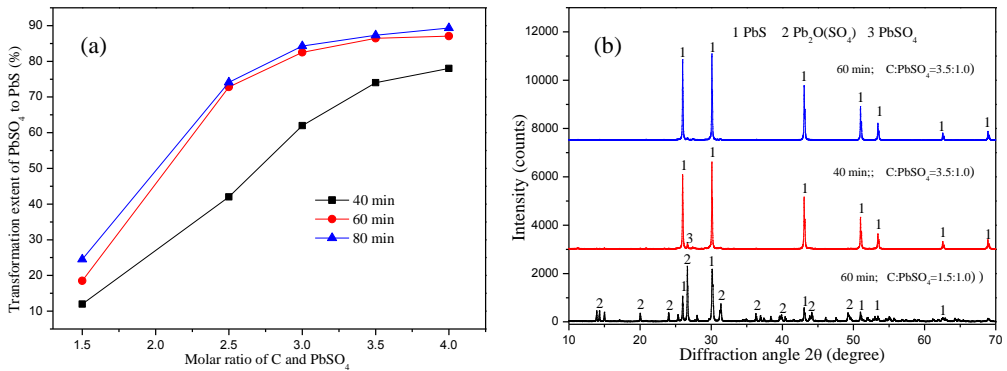

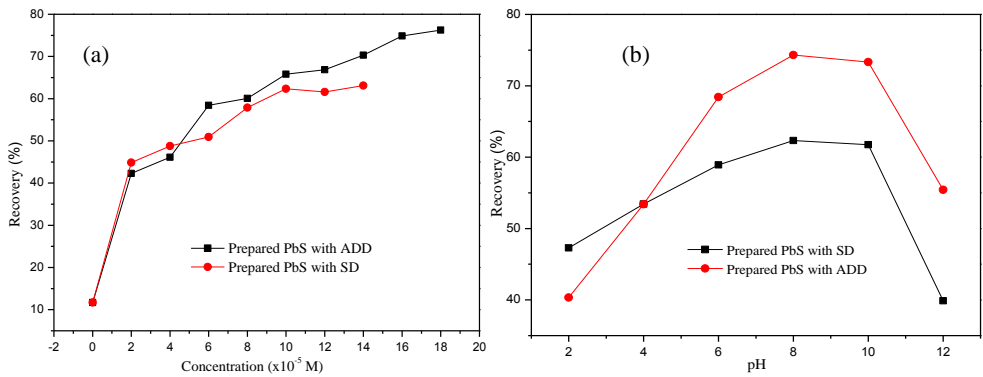Fig. 7. The transformation extent of PbSO$_4$ to PbS and XRD patterns of the sample

Fig. 8. Flotation performances of artificial galena (a, natural pH; b, ADD concentrations: 1.4·10^{-4}M, SD: 1.4·10^{-4}M; terpineol concentration.:0.065 M)

Conclusion

The results showed that PbSO$_4$ could be transformed to PbS by selective reduction roasting with carbon powder. Galena obtained could be recovered by conventional flotation technology. Accordingly, a new method to recover the PbSO$_4$ from the zinc leach residue was developed.

The parameters of selective transformation were established by thermogravimetric and XRD analyses as follows: temperature of 700 $^\mathrm{o}$C, molar ratio of C to PbSO$_4$ ranging from 2.7 to 4.0 and reaction time from 40 to 60 min. Results obtained by verification tests were consistent with the thermogravimetric analyses, and the transformation extent reached up to 86.45% under the optimal conditions. The samples of artificial galena were subjected to micro-flotation tests and the lead recovery of 75.32% and 62.34% were obtained with ADD and with SD, respectively.

Acknowledgements

References

ALTUNDOGAN H S., ERDEM M., ORHAN R., OZER A., TURNEN F., 1998, *Heavy metal pollution potential of zinc leach residues discarded in Cinkur Plant*, Tr. J. Eng. Environ. Sci., 22, 167-177.

APPELO C A J., POSTMA D., 2010, *Geochemistry, groundwater and pollution*, Taylor & Francis, 125-234.

BABA A., ADEKOLA F., FAPOJUWO D., OTOKHINA F., 2011, *Dissolution kinetics and solvent extraction of lead from anglesite ore*, Journal of Chemistry Society, 1,157-164.

BADANOIU G., BUZATU T., 2012, *Structural and physico-chemical analysis of waste from used lead-acid batteries*, UPB BuletinStiintific, Series B: Chemistry and Materials Science, 1,245-254.

CHERNYSHOVA I V., ANDREEV S I., 1997, *Spectroscopic study of galena surface oxidation in aqueous solutions I. Identification of surface species by XPS and ATR/FTIR spectroscopy*, Applied Surface Science, 108(2), 225-236.

FUERSTENAU M., OLIVAS S., HERRERA-URBINA R., HAN K., 1987, *The surface characteristics and flotation behavior of anglesite and cerussite*, International Journal of Mineral Processing, 1,73-85.

GEN-SHOU Y., 2002, *The production practice of tribasic lead sulfate from flue dust lead slag*, Hunan Nonferrous Metals(In China), 6, 8-9.

GEN-SHOU Y., DUTRIZAC J., CHEN T., 1992, *The conversion of lead sulphate to lead carbonate in sodium carbonate media*, Hydrometallurgy, 3, 399-421.

HERRERA-URBINA R., SOTILLO F., FUERSTENAU D., 1998, *Amyl xanthate uptake by natural and sulfide-treated cerussite and galena*, International Journal of Mineral Processing, 2,113-128.

HERRERA-URBINA R., SOTILLO F., FUERSTENAU D.,1999, *Effect of sodium sulfide additions on the pulp potential and amyl xanthate flotation of cerussite and galena*, International Journal of Mineral Processing, 3,157-170.

JING-YUN Z., ZHU J G., 1991, *Using salicylhroximic acid as collector in flotation of smithonite and lead sulfate*, Nonferrous Metals (in China), 4, 27-32.

KARNACHUK O., KUROCHKINA S., TUOVINEN O., 2002, *Growth of sulfate-reducing bacteria with solid-phase electron acceptors*, Applied Microbiology and Biotechnology, 4,482-486.

LEFFERTS J., MOLLOY K., ZUCKERMAN J., HAIDUC I., GUTA D., 1980, *Oxy and thio phosphorus acid derivatives of tin. 1. Triorganotin (IV) dithiophosphate esters*, Inorganic Chemistry, 6,1662-1670.

LI M., PENG B., CHAI L Y., PENG N., YAN H., HOU D., 2012, *Recovery of iron from zinc leaching residue by selective reduction roasting with carbon*, Journal of hazardous materials,6, 323-330.

MENAD N., KANARI N., GABALLAH I., 1997, *Kinetics of chlorination and carbochlorination of lead sulfate*, Thermochimica Acta, 1,61-67.

NOWAK P., LAAJALEHTO K., 2000, *Oxidation of galena surface-an XPS study of the formation of sulfoxy species*, Applied Surface Science, 157(3), 101-111.

ONAL G., BULUT G., GUL A., KANGAL O., PEREK K., ARSLAN F., 2005, *Flotation of Aladag oxide lead–zinc ores*, Minerals Engineering, 2, 279-282.

OUTOKUMPU, 2002, *Chemical Reaction and Equilibrium Software with Extensive Thermochemical Database*, HSC version 5.0. 2002.

OZVERDI A., ERDEM M., 2010, *Environmental risk assessment and stabilization/solidification of zinc extraction residue: I. Environmental risk assessment*, Hydrometallurgy, 100, 103-109.

PACHOLEWSKA, M., 2004, *Bioleaching of galena flotation concentrate*, Fizykochemiczne Problemy Mineralurgii/Physicochemical Problems of Mineral Processing, 38, 281-290.

PENG R., REN H., ZHANG X., 2003, *Metallurgy of lead and zinc*, Beijing: Science Pres,250-312.

QIN W Q.,LIU H., TANG S H., SUN W., 2009, *Preparation of lead sulfate powder directly from galena concentrates*, Transactions of Nonferrous Metals Society of China, 2,479-483.

RASHCHI F., DASHTI A., ARABPOUR-YAZDI M., ABDIZADEH H., 2005, *Anglesite flotation: a study for lead recovery from zinc leach residue*, Minerals Engineering, 18 ,205-212.

RENNERTA T.,2010, *Characterization of deposited flue-dust slurry from a former Pb-smelter site and release of inorganic contaminants, in: Proceedings of the 19th world congress of soil science: Soil solutions for a changing world[C]//Brisbane*, International Union of Soil Sciences (IUSS), Institut fur Bodenforschung: University fur Bodenkultur, 31-34.

SCHRODER-WOLTHOORN A., KUITERT S., DIJKMAN H., HUISMAN J L., 2008, *Application of sulfate reduction for the biological conversion of anglesite PbSO₄ to galena (PbS)*, Hydrometallurgy, 1,105-109.

SHIRCHINNAMJIL N., CHAO Y., FANG Z H., 2008, *Leaching of silver from Boorchi Ag-Pb ore in Mongolia with acidic thiourea solution*, Journal of Process Engineering, 4,725-730.

SONG S X., LOPEZ-VALDIVIESO A., REYES-BAHENA J L., BERMEJO-PEREZ H I., TRASS O., 2000, *Hydrophobic flocculation of galena fines in aqueous suspensions*, Journal of Colloid and Interface Science, 227(2), 272-281.

SZEKELY J.,1976, *Gas-solid reactions*, Academic Press, 324-367.

VINALS J., NUNEZ C., CARRASCO J., 1991, *Leaching of gold, silver and lead from plumbojarosite-containing hematite tailings in HCl-CaCl₂ media*, Hydrometallurgy, 2,179-199.

WEIJMA J., HOOP K., BOSMA W., DIJKMAN H., 2002, *Biological conversion of anglesite (PbSO₄) and lead waste from spent car batteries to galena (PbS)*, Biotechnology Progress, 4,770-775.

WOLTHOORN A., KUITERT S., DIJKMAN H., HUISMAN J L., 2007, *Application of sulfate reduction for the biological conversion of anglesite to galena*, Advanced Materials Research, 2,197-200.

ZHANG T., QIN W Q., YANG C Y., HUANG S P., 2014, *Floc flotation of marmatite fines in aqueous suspensions induced by butyl xanthate and ammonium dibutyldithiophosphate*, The Chinese Journal of Nonferrous Metals, 24:1578-1586.

ZHU J G., ZHAO J., 1991, *The experiments of cupferron as collector in the flotation of lead sulfate and smithsonite*, Journal of Central-South Institute of Mining and Metallurgy (in Chinese), 5, 522-528.

ZHU J G., ZHU Y S., 1996, *The chemical principle of flotation reagents*, Central South University Press (in Chinese).

INFLUENCE OF FROTHER TYPE AND DOSE ON COLLECTORLESS FLOTATION OF COPPER-BEARING SHALE IN A FLOTATION COLUMN

Przemyslaw B. KOWALCZUK, Dawid MROCZKO, Jan DRZYMALA

Wroclaw University of Technology, Division of Mineral Processing, Wybrzeze Wyspianskiego 27, 50-370 Wroclaw, przemyslaw.kowalczuk@pwr.edu.pl

Abstract: In this paper the influence of nonionic (methyl isobutyl carbinol, tri(ethylene glycol) monobutyl ether) and cationic (hexylamine) frothers on flotation of copper-bearing shale in a flotation column was investigated. It was shown that naturally hydrophobic shale did not float in pure water but it floated in the presence of the investigated frothers. The real contact angle of shale, measured by the sessile drop method, was equal to about 40°, while its effective contact angle was zero when shale was floated in a flotation column in pure water. The investigated surfactants increased the effective hydrophobicity of shale from zero to 16±1, 22±1 and 33±2° for coarse, medium and fine particles, respectively. The calculations of the effective contact angle were based on a simplified probabilistic model of flotation.

Keywords: flotation, hydrophobicity, frother, shale, flotation column

Introduction

Froth flotation is a physicochemical process widely used in a mineral processing industry. Efficiency of flotation depends on such parameters as hydrophobicity of floating particles, properties of added chemical reagents, type of flotation devices and many others (Wills and Napier-Munn, 2006). Hydrophobic particles, having the contact angle greater than zero (Nguyen and Schulze, 2004), attach to gas bubbles, form stable particle-bubble aggregates, and move upwards to the froth layer, while hydrophilic particles sink.

The role of frothers in the recovery of solid particulate matter in froth flotation was studied by many authors (Heyes and Trahar, 1977; Malysa et al., 1987; Saleh and Iskra, 1996; Pugh, 2000; Laskowski, 2001; Drzymala et al., 2007; Farrokhpay, 2011; Kowalczuk et al., 2014). It is well known that frothers reduce bubble coalescence, stabilize bubbles in the froth layer (Cho and Laskowski, 2004) and shorten the time

needed for formation of the three-phase contact (Kosior et al., 2011), leading to faster rupture of the liquid film between bubbles and solid particles. However, there is still a need to understand better the role of frothers in flotation, especially in collectorless flotation of solid materials under dynamic conditions. In this work we investigated the influence of non-ionic methyl isobutyl carbinol and tri(ethylene glycol) monobutyl ether as well as cationic hexylamine frothers on the maximum recovery, maximum size of floating particles, and effective hydrophobicity of naturally hydrophobic carbonaceous copper-bearing shale floated in a flotation column.

Experimental

The flotation experiments were carried out in a Plexiglas cylindrical flotation column having 0.82 m in height and 94 mm in diameter (Fig. 1). The column consisted of a collecting zone and a froth zone. The pulp was fed into the column near the top of the collecting zone. Starting from this point the solid particles were exposed to bubbles generated by an air sparger near the bottom of the column. The formed particle-bubble aggregates moved upwards to the froth zone and were collected as a concentrate, while the hydrophilic particles settled at the bottom of the column. The bottom part of the column was the collecting zone of non-floating particles.

A geological sample of carbonaceous copper-bearing shale originated from the Kupferschiefer stratiform copper ore mined by KGHM Polska Miedz S.A. The shale sample consisted of organic carbon, feldspar, silicates, dolomite and copper sulphide minerals. In the investigated sample the contents of Cu and total organic carbon were 7 and 8%, respectively. The density of shale was 2.5 g/dm^3, the isoelectric point of copper-bearing shale in water was pH=3.5 (Peng et al, 2014), while the point of zero charge measured by a titration method was pH=8 (Trochanowska and Kowalczuk, 2014).

The samples of carbonaceous copper-bearing shale were floated in the presence of two non-ionic (methyl isobutyl carbinol MIBC, tri(ethylene glycol) monobutyl ether C_4E_3) and one cationic (hexylamine) frothers (Table 1).

Table 1. Reagents used in flotation of investigated carbonaceous-copper bearing shale

Reagent	Molecular mass, g/mol
Methyl isobutyl carbinol (MIBC), $C_6H_{14}O$	102.2
Tri(ethylene glycol) monobutyl ether (C_4E_3), $C_4H_9O(C_2H_4O)_3H$	206.3
Hexylamine, $C_6H_{15}N$	101.2

A 6-gram sample of a narrow size fraction of shale was conditioned by stirring in a container for 5 min with either water (when floated without reagent) or aqueous solution of frother. The stirring speed was 350 rpm. Next, the mixture was pumped to the flotation column and subjected to flotation. The pumping time of the feed was 5

minutes and after this time only the aqueous solution of frother was pumped to the column. In each flotation tests the feed and aqueous solution flow rates were controlled by a peristaltic pump. The feed flow rate was 18 dm^3/h and the aqueous solution flow rate was 14 dm^3/h. The air flow rate was also controlled and kept constant at 116 dm^3/h. The floating particles were collected after 10, 30, 45 and 60 minutes of flotation as the froth products (concentrates). The non-floating particles, which assembled below the air sparger (Fig. 1) were collected after the end of flotation. The flotation products were dried at 105 °C and then weighted to determine the recovery of floating particles.
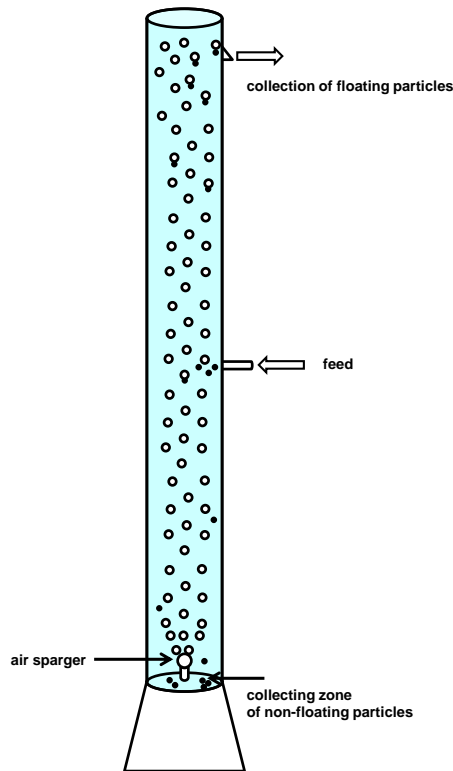
Figure 1. Scheme of flotation column used in experiments

Results and discussion

Flotation of carbonaceous copper-bearing shale was performed for three different particle sizes called coarse 100-71 µm, medium 71-40 µm and fine -40 µm fractions. Flotation was performed in pure water and in the presence of three different frothers, that is tri(ethylene glycol) monobutyl ether (C_4E_3), methyl isobutyl carbinol (MIBC) and hexylamine. When shale was floated in pure water, its recovery was zero for all

particle size fractions (Fig. 2). A lack of flotation in pure water suggests hydrophilicity of the investigated shale sample. The same observation was made in our previous works (Drzymala and Bigosinski, 1995; Kowalczuk and Drzymala, 2011), in which flotation of shale was investigated in a Hallimond tube. There was no natural flotation of shale and its so-called flotometric contact angle in water was close to zero. On the other hand Bednarek and Kowalczuk (2014) showed that the advancing and receding contact angles of the investigated shale sample in water, measured by the sessile drop method, were 43 and 24°, respectively. It means that shale is a naturally hydrophobic material but its flotation in pure water is not possible, due to a stable water film between bubbles and particles. It appears that flotation of shale can be easily initiated and its sessile drop hydrophobicity "uncovered" simply by addition of frother to the flotation system.
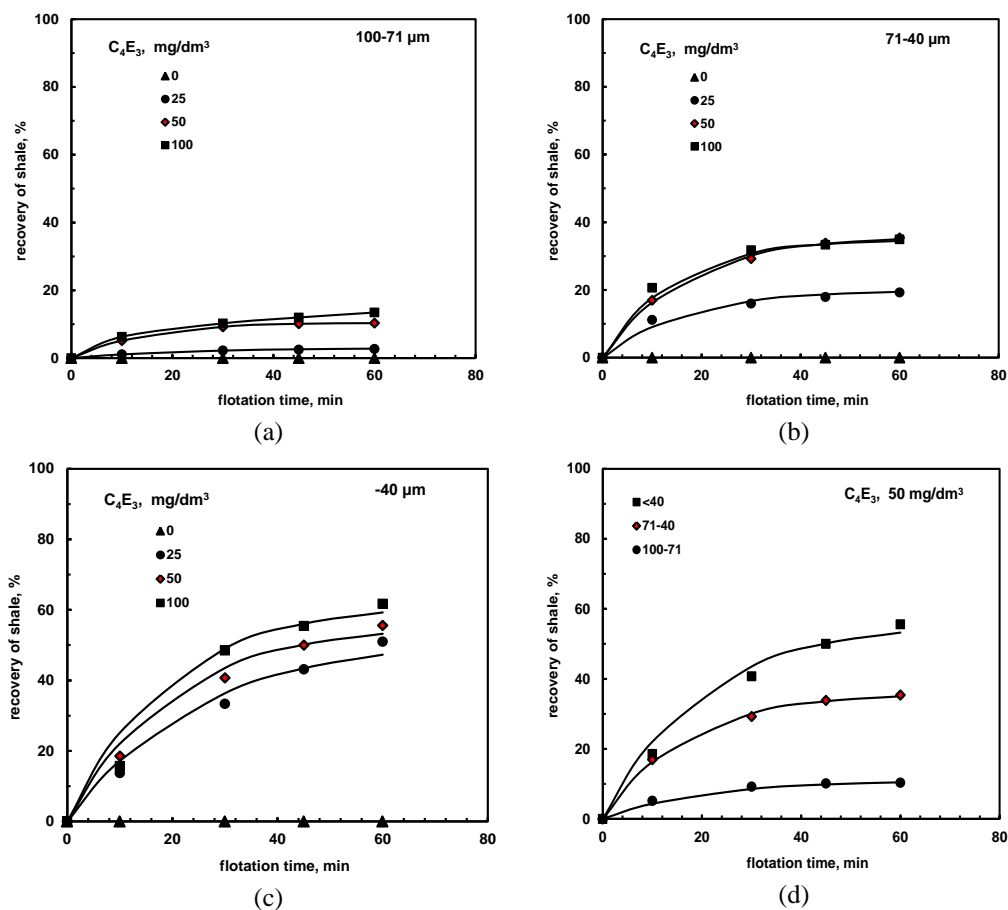

Fig. 2. Flotation kinetics of (a) coarse (100-71 µm), (b) medium (71-40 µm) and (c) fine (-40 µm) particles of carbonaceous copper-bearing shale in the presence of C_4E_3 (mg/dm^3) as well as (d) a comparison of flotation kinetics of shale in the presence of 50 mg/dm^3 of C_4E_3 for different shale size fractions

The results of flotation of investigated shale in the presence of frothers in the form of recovery of different particle size fractions and frother concentrations expressed in mg/dm^3 versus flotation time are presented in Figs. 2a-d. It can be seen that the recovery of coarse (Fig. 2a), medium (Fig. 2b) and fine (Fig. 2c) particle fractions increased with the frother concentration. The best results were obtained for the fine particles (Fig. 2d), while the lowest recovery was observed for the coarse particles in the presence of 25 mg/dm^3 of frother. The influence of frother concentration on the recovery of coarse, medium and fine samples was also observed for MIBC and hexylamine.
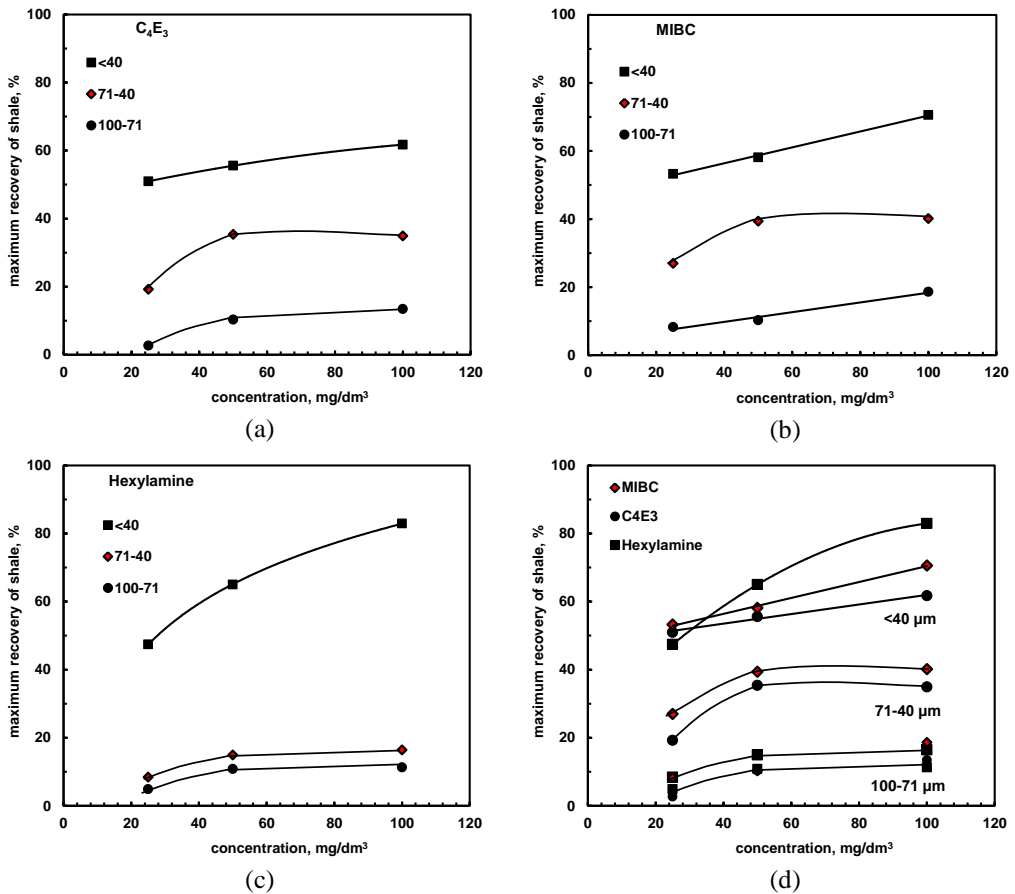

Fig. 3. Influence of frother type and dose on the maximum recovery of coarse (100-71 µm),
medium (71-40 µm) and fine (-40 µm) particles; (a) C$_4$E$_3$, (b) MIBC, (c) hexylamine,
(d) combined data taken from Figs. (a), (b) and (c)
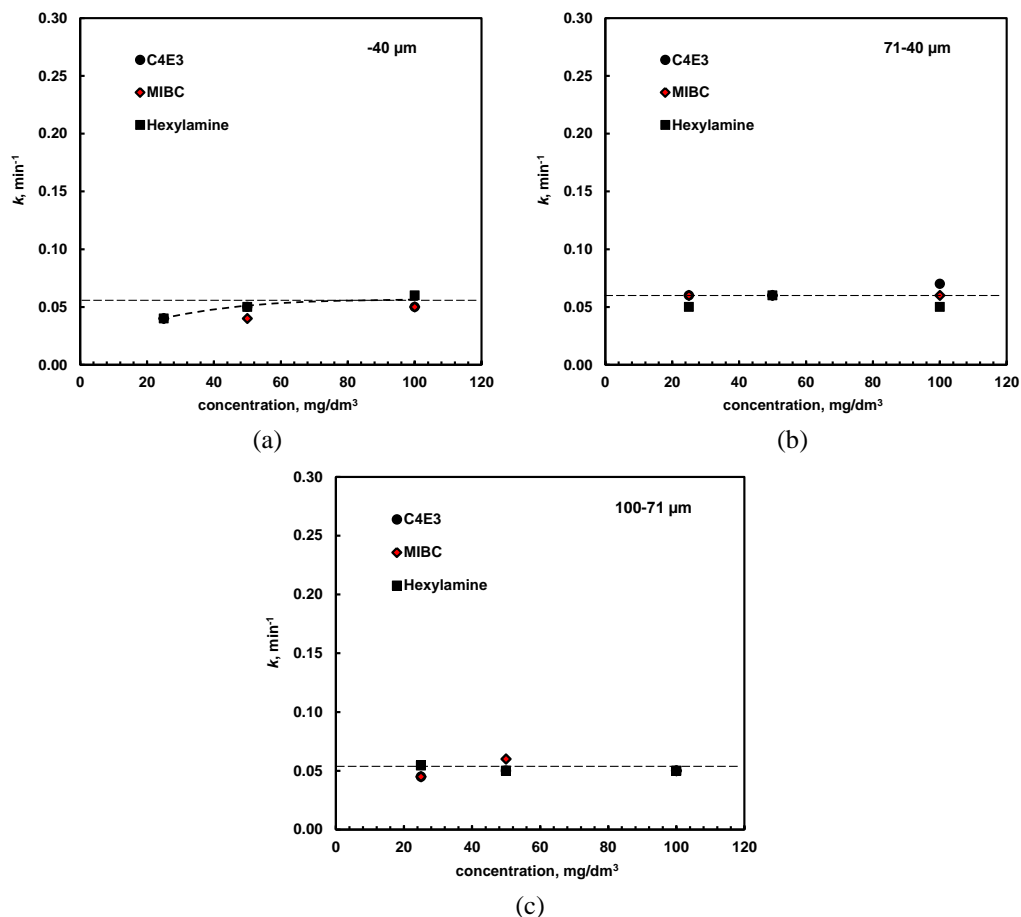
Fig. 4. Influence of frother type and dose on flotation rate constant k of (a) fine (-40 μm), (b) medium (71-40 μm) and (c) coarse (100-71 μm) particles of copper-bearing shale

Figure 3 shows the influence of frother type and its concentration on the maximum recovery of coarse, medium and fine particles of carbonaceous copper-bearing shale floated in the flotation column. It can be seen from Figs. 3a-d that the maximum recovery of fine, medium and coarse particles increases with the frother dose. It was observed for all tested in this work frothers (Figs. 3a-d). The maximum recovery of coarse and medium particles reaches a certain plateau level at concentration of about 50 mg/dm^3. A further addition of frother does not change the maximum recovery of the coarse and medium particles. A high recovery of the fine particles is only possible at high frother concentrations. Figure 3d shows that the recovery-frother dose relationship can be divided into three regions: the first one for the coarse particles, where the recovery is very low (here lower than 20%); the second one, with recovery

between 20 and 40%, for flotation of medium particles, and the third one, with the maximum recovery higher than 40%, for the fine particles.

While there is a strong influence of frother dose on the maximum recovery (R_{max}) of coarse, medium and fine particles, Figs. 4a-c show that the frother type and concentration do not change the rate constant (k) of the first-order flotation kinetics for the medium (Fig. 4b) and coarse (Fig. 4c) particles. For carbonaceous copper-bearing shale, the 1st order rate constant k (s^{-1}) was calculated from the equation:

$$R = R_{max}\left(1 - e^{-kt}\right),$$ (1)

where t denotes flotation time. From Figs. 4a-c it can be seen that the values of k (min^{-1}) for the coarse and medium particles are almost the same but their maximum recoveries are different (Figs. 3a-d). Only for fine particles (Fig. 4a) the 1st order rate constant slightly increases with frother concentration. Most likely, this is due to a lower probability of the detachment of fine particles (Jameson, 2012). Muganda et al. (2011) showed that for coarse chalcopyrite particles having contact angles lower than 50° the first-order rate constant also changed only slightly.

Having flotation data for naturally hydrophobic shale it is possible to estimate the maximum size of flotation particles. The maximum size of floating particles d_{max} can be determined from the so-called separation curves of carbonaceous copper-bearing shale flotation data gathered in the presence of C_4E_3 (Fig. 5a), MIBC (Fig. 5b) and hexylamine (Fig. 5c). There are many definitions of d_{max}. According to one of them d_{max} is the size of particles at which recovery is 50%. It is a good measure of d_{max} since, according to the theory of probability, at this point the particle has equal chance to either float or sink. Such d_{max} was previously used and discussed by Schulze (1977), Drzymala (1994), Chipfunhu et al. (2010) and Kowalczuk et al. (2011). The determined from Figs. 5a-c values of the maximum size of floating particles of shale ($d_{50}=d_{max}$) as a function of frother concentration are given in Fig. 6. It can be seen that the values of maximum size of floating particles d_{50} depend on the frother type and concentration. Figure 6 shows that at low frother concentrations the d_{50} versus concentration curve is very steep, indicating that the higher frother concentration, the coarser particles can be floated. However, it has some limitation since at high frother concentrations the maximum size of floating particles remains almost constant, what can be clearly seen for C_4E_3 and hexylamine. For these frothers a further increase in concentration does not change the value of the maximum size of floating particles expressed as d_{50}. Only for MIBC it is possible to float coarser particles.
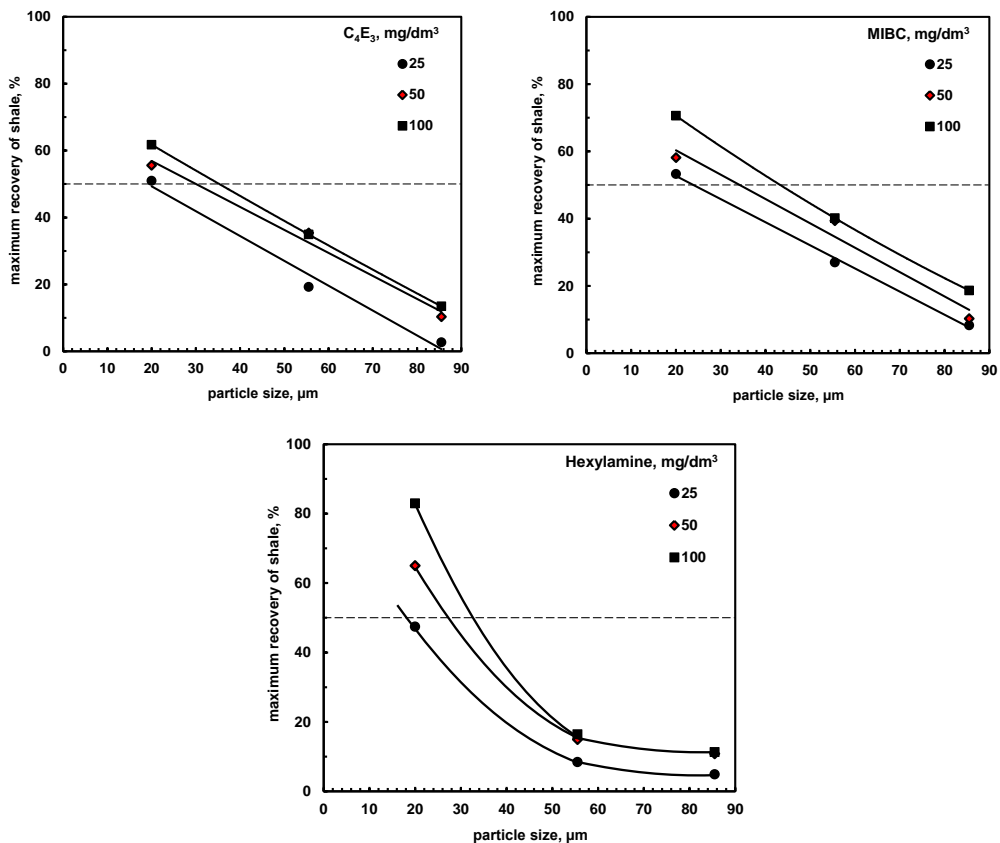
Fig. 5. Maximum recovery versus particle size of carbonaceous copper-bearing shale
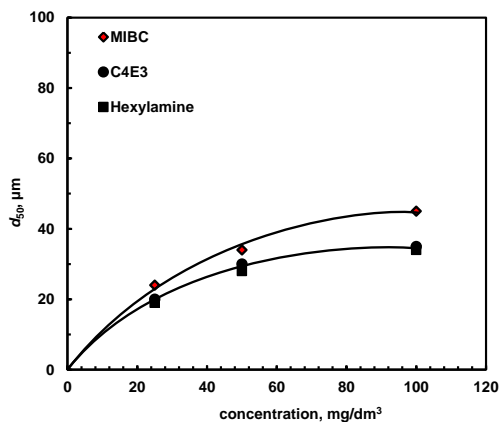in the presence of (a) C_4E_3, (b) MIBC and (c) hexylamine expressed in mg/dm^3

Fig. 6. Influence of frother type and dose on the maximum size of floating particles
of copper-bearing shale

Presented in this work results clearly indicate that the non-ionic (MIBC, C_4E_3) and cationic (hexylamine) surfactants enhance the maximum recovery and maximum size of floating particles but do not change the kinetics of the process. It can be suggested that the mechanism of flotation is the same but for increasing frother concentration there is an increase in apparent hydrophobicity of shale evidenced by the increasing maximum recovery. However, as it has been discussed, the frothers do not change the real hydrophobicity of solid materials (Heyes and Trahar, 1977; Bednarek and Kowalczuk, 2014), but they change the effective hydrophobicity from zero up to the real, measured by the sessile drop method, hydrophobicity. To calculate the effective hydrophobicity of shale, which is "uncovered" by frothers, different methods, based on flotation theories (Scheludko et al., 1976; Varbanov et al., 1993; Drzymala, 1994; Watanabe et al., 2011), can be used to evaluate the effective contact angle of shale in the presence of the investigated frothers. One of them is the formula proposed by Varbanov et al. (1993), which is based on the probabilistic model of flotation and first-order kinetic equation:

$$\theta = \arccos\left(1 - k\,\frac{2\pi d_b^2 S}{3d_p Q}\right),\qquad(2)$$

where θ is the flotometric effective contact angle (°), k rate constant (1st order, s^{-1}), S the cross-section of a flotation cell (m^2), Q air flow rate (m^3/s), d_p particle size (m), d_b bubble size (m). For the used in this work column S= 0.007 m^2, Q=3.2·10^{-5} m^3/s, d_b=3.1 mm, d_p=20, 55.5 and 85.5 µm (mean of size fractions: 100-71, 71-40, -40 µm), while values of k are given in Figs. 4a-c.

Equation 2 permits to calculate the flotometric, that is effective, contact angle, whereas the rest (Young) contact angle can be calculated using the formula proposed by Scheludko et al. (1976) and Drzymala (1994):

$$\theta_r = \arcsin\left[\frac{d_p}{d_b}\sin\left(\theta/2\right)\right] + \theta/2\;.\qquad(3)$$

The calculated values of the flotometric effective contact angle of different shale particle size fractions versus frother concentration are presented in Fig. 7. Since there was no flotation of shale in water, its effective contact angle was zero. It means that in pure water shale particles are hydrophilic (the flotometric contact angle is zero). An addition of frother initiated not only flotation of copper-bearing shale (Figs. 2-3) but also revealed its natural hydrophobicity (Fig. 7). Figure 7 shows that the effective hydrophobicity of shale does not depend on the frother type used in our investigations, including amine, which, when used with a short hydrocarbon chain (here 6 carbon atoms) works as a frother not as a collector (Ghigi, 1968). The calculated values of the maximum flotometric effective contact angles of coarse, medium and fine particles did

not change with the frother dose and were 16±1, 22±1 and 33±2°, respectively. It shows that the maximum effective contact angle increases with decreasing particle size.
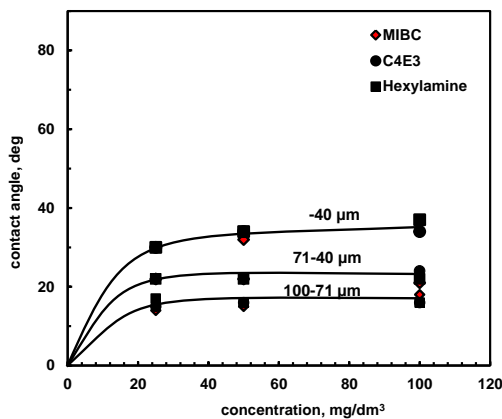

Fig. 7. Influence of frother type and dose on flotometric effective contact angle of coarse (100-71 μm), medium (71-40 μm) and fine (-41 μm) particles of copper-bearing shale

Conclusions

In this paper collectorless flotation of coarse (100-71 µm), medium (71-40 µm) and fine (-40 µm) particles of carbonaceous-copper bearing shale in the presence of non-ionic (MIBC, C_4E_3) and cationic (hexylamine) frothers was investigated. It was shown that naturally hydrophobic shale did not float in pure water. Flotation of shale was initiated by the presence of MIBC, C_4E_3 and hexylamine, which in the flotation process play the role of frothers. It was shown that the frother dose had a strong influence on the maximum recovery and maximum size of floating particles. The investigated in this work frothers enhanced flotation of shale by uncovering its natural hydrophobicity, observed by the sessile drop measurements, and being equal to about 40°. The effective hydrophobicity of the investigated shale was dependent on the frother dose, while the maximum effective hydrophobicity was only dependent on the particle size.

References

Bednarek, P., Kowalczuk, P.B., 2014, *Kąt zwilżania łupka miedzionośnego w obecności wybranych spieniaczy*, w: Łupek miedzionośny, Drzymała J., Kowalczuk P.B. (red.), WGGG PWr, Wrocław, 51–55 (in Polish, doi:10.5277/lupek1410).

Chipfunhu, D., Zanin, M., Grano, S., 2010, *The dependency of the critical contact angle for flotation on particle size–Modelling the limits of fine particle flotation*, Miner. Eng., 24(1), 50–57.

Cho, Y.S., Laskowski, J.S., 2002, *Effect of flotation frothers on bubble size and foam stability*, Int. J. Miner. Process. 64, 69–80.

Drzymala, J., 1994, *Characterization of materials by Hallimond tube flotation. Part 2: maximum size of floating particles and contact angle*, Int. J. Miner. Process., 42, 153–167 (erratum, 1995. Int. J. Miner. Process. 43, 135).

Drzymala, J., Bigosinski, J., 1995, *Collectorless flotation of sulfides occurring in the Fore-sudetic copper minerals deposit of SW Poland*, Mineralogia Polonica, 26(1), 63–73.

Drzymala J., Milczarski E., Milczarski J., 2007, *Adsorption and flotation of hydrophilic and hydrophobic materials in the presence of hydrocarbon polyethylene glycol ethers*, Colloid Surf. A: Physicochem. Eng. Asp., 308(1-3), 111–117.

Farrokhpay, S., 2011, *The significance of froth stability in mineral flotation – A review*, Adv. Colloid Interface Sci., 166, 1–7.

Ghigi, G., 1968, *Flotation of quartz with some polymer complex collectors*, Trans. IMM (London), 78, C212–C219.

Heyes, G.W., Trahar, W.J., 1976, *The natural floatability of chalcopyrite*, Int. J. Miner. Process., 4, 317–344.

Jameson, G.J., 2012, *The effect of surface liberation and particle size on flotation rate constants*, Miner. Eng., 36–38, 132–137.

Kosior, D., Zawala, J., Malysa, K., 2011, *When and how α-terpineol and n-octanol can inhibit the bubble attachment to hydrophobic surfaces*, Physicochem. Probl. Miner. Process., 47, 169–182.

Kowalczuk, P.B., Drzymala, J., 2011, *Contact angle of bubble with an immersed-in-water particle of different materials*, Ind. Eng. Chem. Res. 50(7), 4207–4211.

Kowalczuk, P.B., Sahbaz, O., Drzymala, J., 2011, *Maximum size of floating particles in different flotation cells*, Miner. Eng. 24(8), 766–771.

Kowalczuk, P.B., Buluc, B., Sahbaz, O., Drzymala, J., 2014, *In search of an efficient frother for pre-flotation of carbonaceous shale from the Kupferschiefer stratiform copper ore*, Physicochem. Probl. Miner. Process. 50(2), 835–840.

Laskowski, J S., 2001, *Coal flotation and fine coal utilization*, in Developments in mineral processing, Vol. 14, Elsevier Science Publishing, Amsterdam.

Malysa, E., Malysa, K., Czarnecki, J., 1987, *A method of comparison of the frothing and collecting properties of frothers*, Colloids and Surfaces, 23, 29–39.

Muganda, S., Zanin, M., Grano, S.R., 2011, *Influence of particle size and contact angle on the flotation of chalcopyrite in a laboratory batch flotation cell*, Int. J. Miner. Process., 98, 150–162.

Nguyen, A.V., Schulze, H.J., 2004, *Colloid science of flotation*, Marcel Dekker Inc., New York.

Peng, M., Ratajczak, T., Drzymala, J., 2014, *Zeta potential of Polish copper-bearing shale in the absence and presence of flotation frothers*, Mining Science, 21, 57–63.

Pugh, R.J., 2000, *Non-ionic polyethylene oxide frothers in graphite flotation*, Miner. Eng., 13(2), 161–162.

Saleh, A M., Iskra, J., 1996, *Effect of molecular weight of polyethylene glycol frothers in their performance in low rank coal flotation*, Physicochem. Probl. .Miner. Process., 30, 33–40.

Scheludko, A., Toshev, B.V., Bojadjiev, D.T., 1976, *Attachment of particles to a liquid surface (capillary theory of flotation)*, J. Chem. Soc., Faraday Trans. 1, 72, 2815–2828.

Schulze, H.J., 1977, *New theoretical and experimental investigations on stability of bubble/particle aggregates in flotation: A theory on the upper particle size of floatability*, Int. J. Miner. Process., 4 (3), 241–259.

Trochanowska, J., Kowalczuk, P.B., 2014, *Punkt zerowego ładunku elektrycznego powierzchni łupka miedzionośnego w roztworze wodnym*, w: Łupek miedzionośny, Drzymała J., Kowalczuk P.B. (red.), WGGG PWr, Wrocław, 61–64 (in Polish, doi:10.5277/lupek1412).

Varbanov, R., Forssberg, E., Hallin, M., 1993, *On the modelling of the flotation process*, Int. J. Miner. Process., 37, 27–43.

Watanabe, M., Kowalczuk, P.B., Drzymala, J., 2011, *Analytical solution of equation relating maximum size of floating particle and its hydrophobicity*, Physicochem. Probl. Miner. Process. 46, 13–20.

Wills, B.A., Napier-Munn, T., 2006, *Mineral processing technology. An introduction to the practical aspects of ore treatment and mineral recovery*, 7th ed., Elsevier Science & Technology Books, ISBN: 0750644508.

OPTIMUM SEPARATION ROUTE FOR SEMI-BITUMINOUS COAL USING SEMI-PILOT SCALE PNEUMATIC STRATIFICATION JIG

Feridun BOYLU[*], Tan CETINEL[**], Onur GUVEN[**], Fırat KARAKAS[*], Kenan CINKU[***], Ibrahim Ethem KARAAGACLIOGLU[*], Mehmet Sabri CELIK[*]

[*]   Istanbul Technical University, Faculty of Mines, Min. Proc. Eng. Depart., Istanbul, Turkey, karakasf@itu.edu.tr
[**]   Dumlupinar University, Engineering Faculty, Mining Eng. Depart., Kutahya, Turkey
[***] Istanbul University, Engineering Faculty, Mining Eng. Depart., Istanbul, Turkey

Abstract: Nowadays, dry beneficiation technologies with an air dense medium fluidized bed come into prominence in the field of coal preparation. In this study, the optimum conditions for different operational parameters such as discharge stargate rate, pulsation frequency, and superficial air velocity were investigated on separation of semi bituminous coal from Soma (Imbat) region using a semi pilot scale Allair jig unit. The experimental studies were carried out with two coal size fractions of -15+4 and -4+1 mm by applying rougher and scavenging stages. After the optimization of each parameter, the results for the rougher stages indicated that clean coal products could be obtained with 11.80% and 16.74% ash contents for -15+4 mm and -4+1 mm size ranges, respectively. In addition, discardable tailings with 65.44% and 60.95 % ash contents could be obtained as the result for the scavenging stages. Finally, the combination of these results for -15+1 mm size exhibited that 59.80% of the feed material with 37.70% ash content can be upgraded to clean coal products with low ash content as 19.80% while the remaining part was discarded as tailings with 68.60% ash content. These values suggested that optimizing the operational parameters of unit brings better results which are applicable in industrial application of dry processes compared to wet processes.

Keywords: semibituminous coal, dry coal cleaning, Allair jig, optimization

Introduction

In recent years, the scarcity of fresh water sources alleviated the need for coal producers to develop dry beneficiation techniques considering both technical and economic issues. It is obvious that coal will be an important energy source for many countries for many centuries. However, it is also clear that the enrichment of coal by wet methods results in drying which brings considerable cost and energy requirement.

There is a great deal of work to make dry beneficiation of coal competitive with conventional wet beneficiation processes. Some technological measures and online data collection systems along with an optimum process design for specific coal types are required to make this competition realistic since physical properties of coal and its associated minerals play a major role on separation efficiency especially for dry processing (Mohanta et al., 2013).

Dry beneficiation techniques for coal processing such as hand picking, optical or X-ray sorting (Feil et al., 2012), crushing + size classification (accelerator) (Honaker, 2007), air jigs (Honaker, 2007; Sampaio et al., 2008; Snoby et al., 2009), air tables (Patil and Parekh, 2011), FGX technologies (Zhang et al., 2011), Akaflow aerodynamic separator (Weitkaemper and Wotruba, 2010; Wotruba et al., 2010; Boylu et al., 2012; Boylu et al., 2013), tribo-electrostatic separator (Soong et al., 2001; Dwari and Rao, 2007; Tao et al., 2011), air-dense medium fluidized bed (Chen and Yang, 2003), electrostatic separation etc., exhibit many advantages over wet processes in terms of economic aspects and environmental concerns.

Among these techniques, air jigs and air-dense medium fluidized bed for pneumatic beneficiation have been commercialized and being applied in many countries. These processes are basically depending on the differences in characteristics of coal and gangue minerals such as density, particle size, and shape factors. Stratification of coal is achieved through fluidizing and pulsating air, vibration, and an oscillating deck in gravity based dry separators.

There are a number of studies which showed successful uses of gravity based dry processing for coal cleaning. These studies indicated that dry beneficiation techniques can be well adapted to coals with different characteristics (Sampaio et al., 2008; Snoby et al., 2009; Patil and Parekh, 2011).

In a recent publication Dong et al. (2015) investigated the effect of feed characteristics on the fluidization of separating fluidized bed for dry coal separation by utilizing medium sized magnetite powder (-300+100 μm) and tracer particles for simulating coals with different densities, steel balls for simulating metal products, and large glass balls for large particles in system. They examined the effect of these components on separation fluidized bed (SFB) and bubbling fluidized bed (BFB) characteristics. They found that following the addition of large glass balls, the dominant frequency varied in different layers of bed between 0.125 Hz (suitable for SFB formation) to 3.25 Hz (not exactly suitable for SFB formation). These values suggested that by introducing large particles (as 50 mm which was simulated with large glass balls) into the system would severely damage the stability of SFB as well as separation.

Zhang et al. (2014) utilized air-dense medium fluidized bed dry separating system for preparing low-ash coal. For this aim, they used fine magnetite powder and fine coal samples in order to make up the separation layer. They obtained the optimum conditions for producing clean coal products from raw coal in -80+6 mm size with 15.8% ash content. In conclusion, they obtained clean coal products with 3.71% ash

content while the yield was 67%. Meanwhile, the E_p value was as 0.055. In another study performed with a similar unit, the effect of separation density on the characteristics of the products was discussed in term of ash contents of products. It was found that clean coal with ash content of 18.21% and tailings with 63.81% ash content can be produced at a low separation density of 1.44 g/cm^3 with E_p value of 0.055. However, at high separation density value of 1.76 g/cm^3, the quality of the products increased, and clean coal and tailings with 16.35 and 67.50 % ash content values were produced (Zhenfu et al., 2001).

In addition to coal processing, these dry processing methods are also suitable for beneficiation of different minerals such as sand, ferrous minerals (Weitkaemper and Wotruba, 2010; Wotruba et al., 2010) or coal-like materials such as leonardite (Boylu et al., 2012). In some applications, gravity based dry processing methods were also developed to utilize modified systems with different dense media (Luo et al., 2007; Luo et al., 2008; Fan et al., 2009) such as sand (Kretzschmar, 2010), magnetite (Chen and Yang, 2003), magnetite+fly ash (Fan et al., 2009), magnetic pearl (Zhen-Fu et al., 2007), and paigeite (Zhao et al., 2011) for separation of both inorganics (Snoby et al., 2009), pyrite (Sampaio et al., 2008; Snoby et al., 2009), and Hg (Snoby et al., 2009). It was also reported that for proper use of air table or fluidized bed separators, optimum separation of these impurities requires the optimization of operational parameters such as vibration amplitude, frequency, air volume, superficial air velocity, transverse angle, longitudinal angle, and coal properties such as size and shape factor with careful control (Sahan and Kozanoglu, 1997; Haibin et al., 2011).

Haibin et al. (2011) examined the separation performance of 0-25 mm size South African coal while considering the effect of different parameters as vibration frequency, air volume, transverse, and longitudinal angle. Their results indicated that the optimum conditions can be listed as 3 mm of amplitude with a motor frequency, an air volume of 50%, and transverse and longitudinal angles of 7º and -2º, respectively. With the light of these findings, in this study, we investigated the effect of other operational parameters such as discharge stargate rate, pulsation frequency, and superficial air velocity for producing a clean coal concentrate and tailings.

Experimental

Material and methods

Coal sample

Semi bituminous coal from Soma (Imbat) Region, Turkey was used in the tests. According to the proximate analyses the run-of-mine (ROM) sample contains 43.00% ash, 42% volatile matter, and 10.04 MJ/kg calorific value on moisture free base. Several tests were conducted to determine the optimal feed size before optimizing the moisture effect for an effective separation. The coal samples were initially crushed to -15 mm, and classified as -15 mm, -15+4 mm, -15+1 mm, -4 mm, and -4+1 mm. Allair

jig was utilized for each fraction in two stages. During these tests, all the separation conditions were optimized manually by randomly checking the product quality and followed by fine tuning before collecting the products. The separation performance at each size fractions indicated that the coal sample should be classified into two fractions that are -15+4 mm and -4+1 mm for the optimal separation. While the separation efficiency of -15 mm fraction was 35.6%, the split fractions of -15+1 mm and -15+4 mm exhibited much higher efficiencies of 40.8% and 49.6 %, respectively. Furthermore, the ash contents of the clean products were reduced down to 17.21% from 29.69% by applying the cut size at 4 mm. On the other hand, the ash content of the clean products on these split fractions of -15+1 mm was reduced down to 16.83% from 23.36%. It was also noticed that the presence of -1 mm in the size distribution of coals significantly deteriorates the separation (Boylu et al., 2015). Therefore, the ROM coal sample was crushed into -15 mm which was also the maximum size for semi pilot scale Allair stratification jig. Based on our experience on effective dry coal processing through Allair jig, the screening was performed to classify the -15 mm coal sample to the size fractions of -15+4 mm and -4+1 mm.

Air jigging

The dry beneficiation of the coals was performed using semi pilot scale Allair Jig (Allmineral, Germany) which runs at a maximum capacity of 650 kg/h (Fig. 1). The Allair jig unit consists of feeding (Mohanta et al., 2013; Feil et al., 2012), separation (jigging) (Sampaio et al., 2008), and powder filtering units (Boylu et al., 2012) as shown in Fig. 1. In this study, discharge stargate rate, pulsation frequency, and fluidizing air rate (superficial air velocity) were the main parameters investigated. All stratification tests were performed at the fixed bed and discharging heights (in jigging cell) of 11 cm and 8.5 cm, respectively.

Fig. 1. Lab scale Allair stratification jig facility (1-feed chute, 2-belt conveyor, 3-feed chute, 4-jigging cell, 5-pulsed air production and distribution mechanism, 6-fluidized air tank, 7-dense particle discharge channel, 8-ligth particles discharge, 9-ventilation pipe, 10-filter unit)

Optimization studies were performed at two separate size fractions involving two separation stages of rougher and scavenging. The flow sheet on the optimization studies is presented in Fig. 2. The fixed and tested parameters and accompanying capacities and retention times (RT) of the -15+4 mm size fraction in jigging cell are illustrated in Table 1.
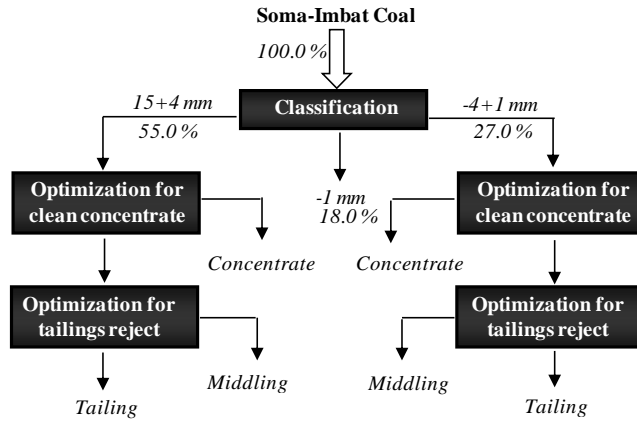

Fig. 2. Flow sheet showing percent material flow and mode of optimization studies

Table 1. The operational conditions of rougher stage separation of -15+4 mm size fraction and accompanying retention times and capacities

FSR (rpm)	DSR (rpm)	PF (s^{-1})	SAV (cm/s)	RT (min)	Capacity (kg/h)
10	14.0	3.2	1083	4.13	152.40
15	21.0	3.2	1083	2.95	213.64
20	28.0	3.2	1083	2.27	277.71
25	34.9	3.2	1083	1.89	332.82
30	44.8	3.2	1083	1.59	396.86
35	64.8	3.2	1083	1.50	420.46
20	28.0	2.8	1083	1.56	404.80
20	28.0	3.0	1083	1.78	354.38
20	28.0	3.3	1083	2.22	283.20
20	28.0	3.5	1083	2.26	278.40
20	28.0	3.7	1083	2.28	276.60
20	28.0	3.8	1083	2.23	282.77
20	28.0	3.2	1083	2.23	282.00
20	28.0	3.3	1035	2.72	231.75
20	28.0	3.3	1083	2.34	269.40
20	28.0	3.3	1131	2.33	270.90
20	28.0	3.3	1179	2.35	267.90
20	28.0	3.3	1228	2.39	264.00
20	28.0	3.3	1276	2.28	276.32

FSR: feed stargate rate, DSR: discharge stargate rate,
PF: pulsation frequency, SAV: superficial air velocity, RT: retention time

Float and sink tests

The characterization of the feed material in both size ranges (-15+4 mm and -4+1 mm) was utilized with float-sink tests. $ZnCl_2$ solutions were prepared at different densities ranging between 1.3-1.9 g/cm^3. The results were evaluated based on the degree of ash removal, combustible recovery, and separation efficiencies as calculated using Eqs. 1, 2, and 3:

$$R_{comb.}(\%) = \frac{C(100-c)}{F(100-f)} \tag{1}$$

$$R_{ash}(\%) = \frac{T\,t}{F\,f} \tag{2}$$

$$Eff_{sep.} = R_{comb.} - (100 - R_{ash}) \tag{3}$$

where R_{comb}, R_{ash}, and Eff_{sep}. are the combustible recovery, ash removal, and separation efficiency, respectively. C, T, and F represent the yields, and c, t, and f stand for the ash contents of concentrate, tailing, and feed, respectively.

Results and discussion

Effect of discharge stargate rate

The effect of discharge stargate rate values on the separation efficiency and the ash contents of the products were evaluated for the rougher and the scavenging stages. The results of these tests are shown in Figs. 3a-c. It can be clearly seen from Fig. 3a that no direct relationship was observed between the separation efficiency and the discharge stargate rate for the separation of -15+4 mm size coal to obtain a clean coal product. Nevertheless, a maximum value of 42.2% of separation efficiency was achieved at 20 rpm discharge stargate rate. In addition, any increase on this value resulted in the mixing of concentrate to the tailings stream which was formed after stratification of material inside the jig. Especially at 35 rpm, the separation efficiency decreased to a level of 22.8%. Similar behavior was also obtained for the beneficiation of -4+1 mm size coal samples where over 10 rpm discharge stargate rate, the separation efficiency decreased down to 20.4% from the peak value of 32.7%. Meanwhile, the reason for obtaining optimum separation at lower discharge stargate rates for -4+1 mm size fraction can be attributed to the lower amount of ash forming materials which in turn resulted in a thinner shale (dense ash forming particles) layer. In addition, the speed of shale particles was observed to be relatively higher in the fine fractions, and therefore lower discharge stargate rates were found sufficient for the -4+1 mm size fraction.

The effect of the discharge stargate rate on the ash contents of concentrate, middlings, and tailings are presented in Figs. 3b-c. The results revealed no significant

changes in the rougher stage for the effect of discharge stargate rate on the ash contents of concentrates. Contrary to this, the ash contents of tailings yielded distinct changes. Thus, considering different size fractions of -15+4 mm and -4+1 mm, the ash contents of concentrates were found to be varied in the range of 8.47%-12.49% and 17.45%-18.45%, respectively. However, at the optimum discharge stargate rates of 10 and 20 rpm per each fraction, the ash contents of tailings were found as 55.74% and 50.28%, respectively. It is interesting to note that these values decreased to 48.99% and 42.00% at lower discharge stargate rates, respectively.

The effect of discharge stargate rate on the separation efficiency in a series of tests for the -15+4 mm size fraction yielded no significant effect during the scavenging stages (for discharging tailings). Interestingly, under the same conditions, the experiments adopted for -4+1 mm size fraction gave high separation efficiencies at 10 rpm for both rougher (for obtaining clean coal) and scavenging stages. Evidently, the separation efficiency decreased from 28.09% to 8.7% with increasing this value to 50 rpm.

Similar dependencies for -15+4 mm size fraction for the ash contents of tailings at the scavenging stages varied in the range of 63.92%-65.46 %. On the other hand, the tests adopted for -4+1 mm sized coals resulted in 62.45% ash content with the application of optimum discharge stargate rate at 10 rpm. However, increasing this value to 50 rpm resulted in much lower ash contents of 55.00% which also gave the same trend with the concentrates.

In addition, while the ash contents of concentrate (middlings) revealed no significant effect for -15+4 mm size coals (30-35%), -4+1 mm sized coals produced a significant effect above 40 rpm because the ash content increased from 33.52% to 45.19%.

Similar studies were also reported considering the discharge stargate rate which directly controls the distribution of feed material across the bed. Weinstein and Snoby (2007) studied the effect of varying speeds of stargate rate for enrichment of bituminous coal (-4+1 mm) and obtained a clean coal product with 6.86% ash content by enriching the coal feed to 14.81% ash at a constant speed of stargate rate.

Effect of pulsation frequency

The effect of the pulsation frequency on the separation efficiency of dry process and the ash contents of concentrate and tailings are illustrated in Figs. 4a-c. As it can be seen from Fig. 4a that the optimal pulsation frequency at rougher stages was found as 3.17 s^{-1} for the separation of coal at -15+4 mm but interestingly no effective separation was found at scavenging stages and finer size fractions of -4+1 mm. Therefore, at that pulsation frequency value, these results can be explained by the coal characteristics because the samples taken from Soma-Imbat region exhibit an easy to wash character and consists of material at near gravity values. It should also be noted that the pulsation frequency varies upon the type of coal and its size distribution in feed for separation. These findings are also supported by Feil et al. (2012) who used -16+6.3

mm and -6.3+2 mm size fractions, and correlated the jig bed height with the pulsation frequency. They found that the increasing the pulsation frequency from 80 min^{-1} to 88 min^{-1} resulted in better performance when the jig bed level was ≤125 mm. Meanwhile, they also showed that this value depends on the mineral matter in the ROM coal, and can be lowered to 100 mm if there are significant amounts of mineral matter in the ROM. On the other hand, there is a critical pulsation frequency for samples exhibiting difficult to wash character and consisting of high amounts of near gravity material. Wotruba et al. (2010) reported similar dependencies, and suggested a critical pulsation frequency for coals of low washability index.
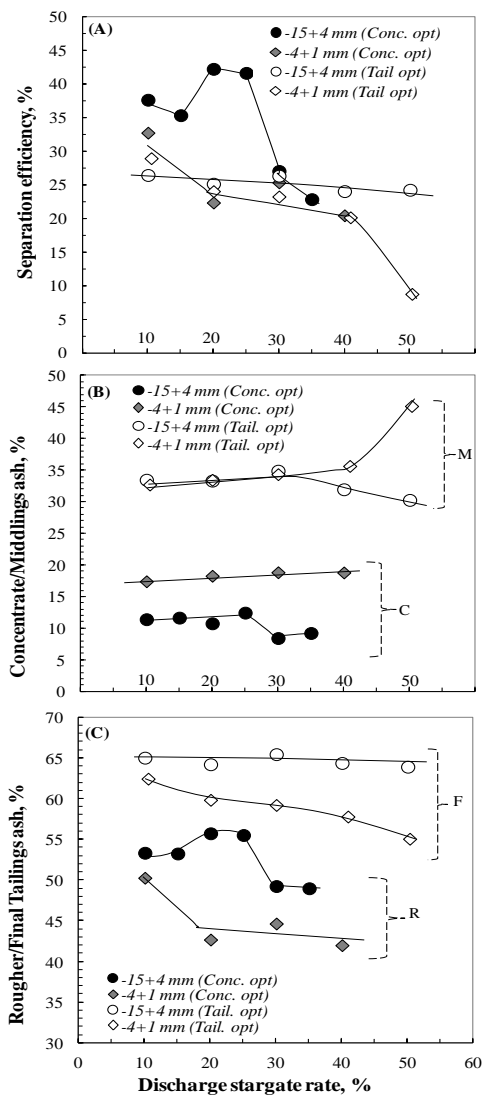

Fig. 3. Effect of discharge stargate rate on separation (M: middlings, C: concentrates, R: rougher tailings, F: final tailings)
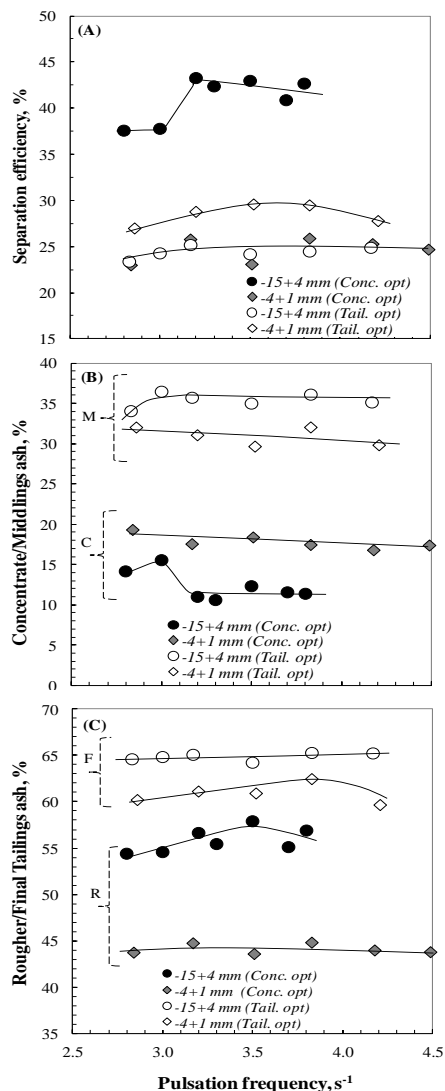
Fig. 4. Effect of pulsation frequency on separation (M: middlings, C: concentrates, R: rougher tailings, F: final tailings)

Similar results are shown in Figs. 4b-c considering the variations of the ash contents for concentrate and tailings. As mentioned before, the experimental studies at -15+4 mm size, upon increasing the pulsation frequency to 3.17 s^{-1} at the rougher stages, the ash content of concentrate decreased from 15.60% to 11.00%. However, no significant change was observed in the scavenging stages for -4+1 mm size. In summary, the tailings with highest ash content of 57.95% from the rougher stages were obtained at 3.5 s^{-1} of the pulsation frequency.

Effect of superficial air velocity

The effect of superficial air velocity on the separation efficiency and ash contents of concentrate and tailings are presented in Figs. 5a-c. Significant differences were found for optimum superficial air velocities for separation/stratification of ROM coal and tailings at both rougher and scavenging stages. Thus, it was found that while the optimum superficial air velocity was found to be >1080 cm/s at the rougher stages for the separation of -15+4 mm size fractions, it increased to >1200 cm/s at the scavenging stages. These results can be attributed to the ratio of density of feed material to the tailings (ROM/tailings) or the bulk density of stratified material. Similar results were also obtained for the tests carried out with coal samples of -4+1 mm size fraction that the optimal separation was obtained at 950 cm/s at the rougher stages where it was proportionally increased to 1030 cm/s at the scavenging stages.

Considering the specifications of the products at -15+4 mm size fraction, a concentrate with 11.00% ash content was obtained in the rougher stage whereas the tailings product with 56.90% ash content was discarded. Re-processing of the tailings taken from the rougher stage, a concentrate (middlings) assaying 33.01% ash content with the final tailings of 63.64% ash could be obtained at 1220 cm/s of the superficial air velocity (Figs. 5b-c).

Likewise, the separation tests on -4+1 mm size fraction yielded a clean coal concentrate with 16.70% ash and tailings with 46.40% ash in the rougher stage. Additionally, by re-processing of tailings taken from the rougher stage, a concentrate (middlings) and final tailings were obtained with the ash contents of 29.67% and 60.65%, respectively at 950 cm/s of the superficial air velocity (Fig. 5c).

Consequently, it can be suggested that there is an optimum superficial air velocity for each size fraction to achieve the critical onset of segregation. In this manner, the excess air produces bubbles that divide the bed into particulate and bubble phases. Thus, in the case of smaller bubble sizes, the space becomes unsufficient for particle setting in the disturbed region below the rising bubbles. Meanwhile, in the case of bigger bubble sizes, the bubble rise velocity becomes faster for providing enough time for particle setting in the disturbed region (Yang et al., 2013). He et al. (2013) investigated the separation performance of South African raw coal by dense gas-solid fluidized bed beneficiation technique. They found that depending on the increase on superficial gas velocity (0-25 cm/s), the bed pressure drop fell slowly to the stable point. Therefore, this situation indirectly gave an idea about the rising bubbles with a

well distributed size fraction to display steady conditions on the kinetic behavior of fluidization which then resulted in better density based coal beneficiation.

Similar results were obtained by Yang et al. (2013) in a vibrated gas-fluidized bed for superficial air velocity. They studied the effects of some process parameters such as vibration intensity, bed height, fluidizing time, and superficial air velocity on dry coal beneficiation. They concluded that the peak value of superficial air velocity shifted from 0.2 to 0.15 for feed size range of −6+3 mm and −3+1 mm, respectively.

Das et al. (2010) studied the hydrodynamic characteristics of dry beneficiation of iron and coal while considering the gas velocity and solids circulation rate with ash contents of the products. They used a mixture of coal samples with 43.00% ash content. In these studies, they performed separation processes by performing gas velocities of 3.55 m/s and 4.02 m/s, solids concentration rates of 9.7-11.3 $kg/m^2 s$, and 6.87-10.11 $kg/m^2 s$. As a result, they obtained clean coal products with low percentage 7-8% to the feed material. From that point of view, they suggested that increasing the gas velocity resulted in more mixing and less segregation of macerals depending on similarities in densities which in turn less beneficiation of coal.
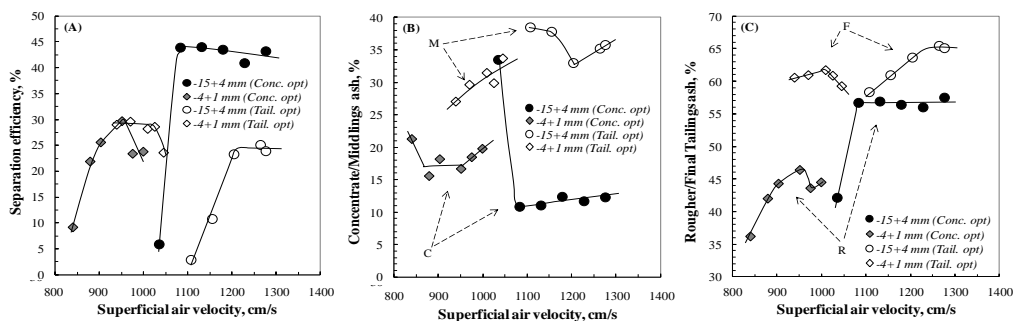

Fig. 5. Effect of superficial air velocity on separation
(M: middlings, C: concentrates, R: rougher tailings, F: final tailings)

Summary of results

Optimization of the rougher and the scavenging stages for the dry beneficiation of the Soma Imbat coal samples at two size fractions yielded the optimal conditions presented in Table 2. Additionally, the results of two-stages dry separation tests carried out at the optimum conditions are summarized in Tables 3, 4, and 5.

According to the results given in Table 3, approximately 36.9% of the feed material can be obtained as concentrate assaying 11.80% ash (25.56 MJ/kg) and 54.4% combustible recovery by performing one rougher stage for dry beneficiation of coal at -15+4 mm. In addition, the results of second stage (rougher) for the same size group showed that about 18.1% of the feed material can be obtained as middlings

assaying 35.23% ash (15.8 MJ/kg) and about 45.0% of the feed can be discarded as tailings with 65.44% ash (3.22 MJ/kg) at 73.3% ash removal rate.

Table 2. Optimal conditions for each size fraction and processing stages

Parameters	-15+4 mm		-4+1 mm	
	Rougher	Scavenging	Rougher	Scavenging
DSR (rpm)	20.0	30.0	10.0-10.2	10.2-10.5
FSR	28.0	52.0	8.4-8.5	12.0-13.3
Puls. Freq. (s^{-1})	>3.17 (3.33)	3.50	4.18	3.52
SAV (cm/s)	>1083 (1131)	>1204 (1264)	951	970

DSR: discharge stargate rate (rpm), FSR: feed stargate rate (rpm), SAV: superficial air velocity

Table 3. Summary of separation results for rougher and scavenging stages

	Products	Weight (%)	Ash (%)	Comb. Rec. (%)	Ash Rem. (%)
-15+4	*Concentrate*	36.9	11.80	54.4	10.8
	Middling	18.1	35.23	19.6	15.9
	Tailing	45.0	65.44	26.0	73.3
	Feed	100.0	40.18	100.0	100.0
-4+1	*Concentrate*	50.7	16.74	62.6	26.0
	Middling	19.0	29.67	19.8	17.3
	Tailing	30.3	60.95	17.6	56.7
	Feed	100.0	32.59	100.0	100.0

For upgrading of the samples at -4+1 mm size range, following a dry beneficiation process in two-stages, 50.7% of the feed material was obtained as concentrate assaying 16.74% ash (23.50 MJ/kg) and 62.6% combustible recovery in the rougher stage. Meanwhile, 19.0% of the feed material of this stage was obtained as middlings with 29.67% ash (18.12 MJ/kg). In addition, 30.3% of the feed material was discarded as tailings with 60.95% ash (5.09 MJ/kg) and 56.7% ash reduction ratio.

If the middlings of the dry beneficiation processes performed for each size group were added to the concentrate at -15+4 mm size, 55% of the feed material was obtained as concentrate with 19.51% ash (22.36 MJ/kg) and 74% combustible recovery while the amount, ash content, and combustible recovery of concentrate at -4+1 mm size were 69.7% of feed material, 20.27% (22.03 MJ/kg), and 82.4 %, respectively (Table 4).

Consequently, if a wide range of -15+1 mm (in the case of combination of fractions) was considered, 59.8% of the feed material having 19.80% ash (22.23 MJ/kg) and 77% combustible recovery was obtained as concentrate while 40.2% of the feed material was discarded as tailings with 64.32% ash (3.69 MJ/kg) and 68.6% ash reduction ratio.

A comparison between theoretical and experimental results (Fig. 6) carried out at two different sizes considering the amount and the ash contents of concentrate and tailings are shown in Table 5.

Table 4. Summary of separation combined results for rougher and scavenging stages

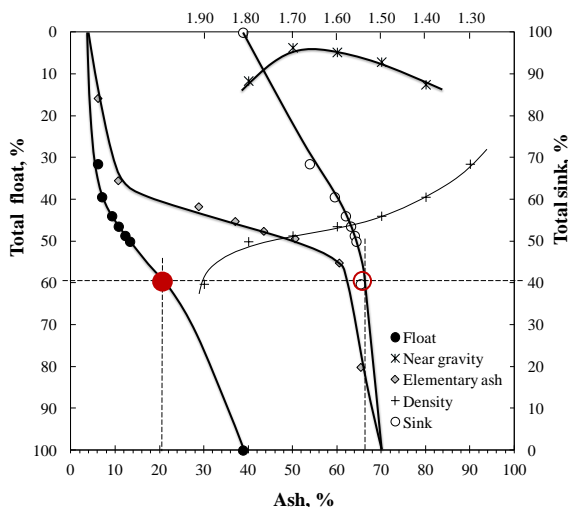| Size Fraction (mm)	Products	Weight (%)	Weight * (%)	Ash (%)	Comb. Rec. (%)	Ash Rem. (%)	Separation Efficiency (%)
-15+4	Concentrate	55.0	36.9	19.51	74.0	26.7	47.3
	Tailing	45.0	30.2	65.44	26.0	73.3	
	Feed	100.0	67.1	40.18	100.0	100.0	
-4+1	Concentrate	69.7	22.9	20.27	82.4	43.3	39.1
	Tailing	30.3	10.0	60.95	17.6	56.7	
	Feed	100.0	32.9	32.59	100.0	100.0	

*Based on the feed

Fig. 6. Washability characteristics of the tested coal and product properties after optimized separation (red filled and circled for concentrate and tailings respectively)

Table 5. Summary of combined separation results for rougher and scavenging stages at -15+1 mm

Products	Weight (%)	Ash (%)	Comb. Rec. (%)	Ash Rem. (%)	Separation Efficiency (%)
Concentrate	59.8	19.80	77.0	31.4	45.6
Tailing	40.2	64.32	23.0	68.6	
Feed	100.0	37.70	100.0	100.0	

It was clearly shown that ideal values indicated in the washability tests can be obtained by detailed optimization of parameters. This can possibly be attributed to the easy washability feature of coal. Although the performance curves for the products obtained at the optimum conditions have not been drawn, it is clear that the separation

density was about 1.9 g/cm^3 which well correlates with the concept of dry beneficiation processes.

Conclusion

Dry beneficiation process has many advantageous in terms of economic and environmental aspects. However, as revealed in this paper, there are some limitations that should be taken into account related to coal properties and process parameters. Although the tested coal sample was easily washable, at least two-stage beneficiation is required for obtaining clean coal products and tailings at an adequate quality with dry beneficiation processes. In addition, especially for that type of coals, it is important to perform beneficiation tests in two relatively narrow size ranges as -15+4 mm and -4+1 mm instead of applying one stage with a wide size range as -15+1 mm. Since the results of these tests showed that optimum discharge speed, frequency of pulsation, and fluidized air speed obtained for different sizes showed different characteristics. Even in the same size group, differences were observed for optimum values at the rougher and the scavenging stages. Finally, the processing of Soma Imbat coal on pneumatic Allair jig was found to yield products in high quality and proportional to the theoretical expectations.

Acknowledgements

References

BOYLU F., CINKU K., CETINEL T, GUVEN O., YALCIN., CELIK M.S., 2013, *Dry processing of -4 mm coal fines through air jig and aerodynamic*, XV Balkan Mineral Processing Congress, June 12-16, 2013, Sozopol, Bulgaria.

BOYLU F., TASDEMIROGLU E. V., KARAGAÇLIOGLU I. E., CETINEL T., CINKU K., 2012, *Dry processing of leonardite by air based gravity separators*, XII International Mineral Processing Symposium, October 10-12, Bodrum, Turkey.

BOYLU F., CINKU K., CETINEL T., KARAKAS F., GUVEN O., KARAAGACLIOGLU I.E., CELİK M.S., 2015, *Effect of coal moisture on the treatment of a lignitic coal through semi pilot scale pneumatıc stratıfication jig,* Coal Preparation and Utilization, in press.

CHEN, Q. AND YANG, Y., 2003, *Development of dry beneficiation of coal in China*, Coal Preparation 23: 3 -12.

DAS, M., SAHA, R. .K., MEIKAP, B.C., 2010, *Hydrodynamic characteristics of dry beneficiation of iron ore and coal in a fast fluidized bed*, World Academy of Science, Engineering and Technology 41: 658-661.

DONG L., ZHAO Y., CAI L., PENG L., ZHANG B., LUO Z., HE Y., 2015, *Effect of feed characteristics on the fluidization of separating fluidized bed for dry coal separation*, Powder Technology, 269:75-84.

DWARI, R. K., RAO, H. K., 2007, *Dry benefication of coal - a review*, Mineral Processing and Extractive Metallurgy Review, 28: 177-234.

FAN, M., LUO, Z., TAO, D., ZHAO, Y., CHEN, Q., 2009, *Dry coal separation with a vibrated air-dense medium fluidized bed,* SME Annual Meeting, Preprint 09-112, February 22-25, 1-4.

FEIL N.F., SAMPAIO C.H., WOTRUBA H., 2012, *Influence of jig frequency on the separation of coal from the Bonito seam — Santa Catarina, Brazil*, Fuel Processing Technology 96: 22–26.

HAIBIN, L., ZHENFU, L. , YUEMIN Z., WANCHANG, W., CUIYU, Z., NINGNING D., 2011, *Cleaning of South African coal using a compound dry cleaning apparatus*, Mining Science and Technology (China), 21: 117-121.

HE, J., ZHAO, Y., HE,Y., LUO,Z., DUAN, C., 2013, *Separation performance of raw coal from South Africa using the dense gas-solid fluidized bed beneficiation technique*, J. S. Afr. Inst. Min. Metall.,113,7.

HONAKER, R. Q., 2007, *Coarse dry coal cleaning, Workshop on Coal Beneficiation and Utilization of Rejects* : Initiatives, Policies and Best Practices Ranchi, India, August 22 – 24.

KRETZSCHMAR, S., 2010, *Dry beneficiation of coal using an air dense-medium fluidised bed separator*, MSc. Thesis, in Chemical Engineering, Faculty of Engineering, University of KwaZulu-Natal.

LUO Z., FAN M., ZHAO Y., TAO X., CHEN Q., CHEN Z., 2008, *Density-dependent separation of dry fine coal in a vibrated fluidized bed*, Powder Technology, 187: 119–123.

LUO, Z., ZHU, J., FAN, M., ZHAO, Y., TAO, X., 2007, *Low density dry coal beneficiation using an air dense medium fluidized bed*, Journal of China University of Mining and Technology, 17 (3): 306-309.

MOHANTA S., RAO C.S., DARAM A.B., CHAKRABORTY S., MEIKA B.C., 2013, *Air Dense Medium Fluidized Bed for Dry Beneficiation of Coal: Technological Challenges for Future*, Particulate Science and Technology, 31: 16–27.

PATIL D.P., PAREKH B.K., 2011, *Beneficiation of Fine Coal Using the Air Table*, International Journal of Coal Preparation and Utilization, 31: 203–222.

SAHAN, R. A., KOZANOGLU, B., 1997, *Use of an air fluidized bed separator in a dry coal cleaning process*, *Emg.v Corawrs. Mgmr*, 38, (3): 269-286.

SAMPAIO C.H., ALIAGAA W., PACHECOA E.T., PETTERA E., WOTRUBAB H., 2008, C*oal beneficiation of Candiota mine by dry jigging*, Fuel Processing Technology, 89: 198-202.

SNOBY, R, THOMPSON, K., MISHRA, S., SNOBY, B., 2009, *Dry jigging coal: Case History Performance,* SME Annual Meeting, Preprint 09-052, 1-4, 22-25 February, Denver, CO.

SOONG, Y., LINK, T. A., SCHOFFSTALL, M.R., GRAY, M. L., FAUTH, D. J., KNOER, J. P., JONES, J. R., AND GAMWO, I. K., 2001, *Dry beneficiation of Slovakian coal*. Fuel Processing Technology, 72, 3, 185-198.

TAO, D., SOBHY, A., LI, Q., HONAKER, R., ZHAO, Y., 2011, *Dry cleaning of pulverized coal using a novel rotary triboelectrostatic separator (RTS),* International Journal of Coal Preparation and Utilization, 31, 187-202.

WEINSTEIN, R. AND SNOBY R., 2007, *Upgrading coal quality through dry jigging*, Mining Engineer, 29-34.

WEITKAEMPER, L., WOTRUBA H., 2010, *Effective dry density beneficiation of coal*, 2010 XXV International Mineral Processing Congress (IMPC), Proceedings, September.

WOTRUBA, H., WEITKAEMPER L., STEINBERG M., 2010, *Development of a new dry density separator for fine-grained materials*, XXV International Mineral Processing Congress (IMPC), Proceedings, September.

YANG X., ZHAO Y., LUO Z., SONG S., DUAN C., DONG L., 2013, *Fine coal dry cleaning using a vibrated gas-fluidized bed,* Fuel Processing Technology, 106: 338–343.

ZHANG, H., AKBARI F., YANG, M.K. , MOHANTY, J., 2011, *Performance optimization of the FGX dry separator for cleaning high- sulfur coal*, International Journal of Coal Preparation and Utilization, 31, (3-4): 161-186.

ZHANG, B., ZHAO, Y., LUO, Z., SONG, S., LI, G., SHENG, C., 2014, *Utilizing an air-dense medium fluidized bed dry separating system for preparing a low-ash coal,* International Journal of Coal Preparation and Utilization, 34:6, 285-295.

ZHAO, Y. M., LIU, X. J., LIU, K. L., LUO, Z.F., WU, W.C., SONG, S.L., TANG, L. G., 2011, *Fluidization characteristics of a gas-paigeite-powder bed to be utilized for dry coal beneficiation*, International Journal of Coal Preparation and Utilization, 31: 149-160.

ZHEN-FU L., JIAN-FENG Z., MAO-MING F., YUE-MIN Z., XIU-XIANG, T., 2007, *Low density dry coal beneficiation using an air dense meidum fluidized bed*, Journal of China University of Mining & Technology, 17, (3): 306-309.

ZHENFU, L., QUINGRU, C., 2001, *Dry beneficiation technology of coal with an air dense-medium fluidized bed,* Int. J. Miner. Process., 63, 167-175.

SYNTHESIS AND CHARACTERIZATION
OF HYDROXYAPATITE/CHITOSAN COMPOSITES

Tomasz SZATKOWSKI[*]**, Agnieszka KOŁODZIEJCZAK-RADZIMSKA**[*]**,
Jakub ZDARTA**[*]**, Karolina SZWARC-RZEPKA**[*]**, Dominik PAUKSZTA**[*]**,
Marcin WYSOKOWSKI**[*]**, Hermann EHRLICH**[**]**, Teofil JESIONOWSKI**[*]

[*]   Poznan University of Technology, Faculty of Chemical Technology, Institute of Chemical Technology and Engineering, M. Sklodowskiej–Curie 2, PL-60965, Poznan, Poland, teofil.jesionowski@put.poznan.pl
[**]   TU Bergakademie Freiberg, Institute of Experimental Physics, Biomineralogy and Extreme Biomimetics Group, Leipziger Str. 23, 09599 Freiberg, Germany

Abstract: Hydroxyapatite (HAp)/chitosan (CS) composites were synthesized via a one-step co-precipitation method from aqueous solution, with the use of calcium chloride ($CaCl_2$) and disodium hydrogen phosphate (Na_2HPO_4). CS was obtained via partial deacetylation of chitin with the use of strong sodium hydroxide solution. Composites were prepared with various HAp/CS ratios (30/70, 50/50, 70/30, 85/15) for comprehensive comparison of their properties. Fourier Transform Infrared Spectroscopy (FT-IR) analysis showed that hydrogen bonds were formed between the organic matrix and the mineral compound, confirming a successful phase interconnection. X-ray diffraction patterns were obtained, enabling examination of the crystalline properties of the composites, including HAp identification. The porous structure parameters of the composites were investigated, and morphological analysis (SEM) was performed. Differential Thermal Gravimetry (DTG) analysis of the composites indicated that the material is thermally stable up to 200 ^{o}C. Additionally, Energy Dispersive Spectroscopy (EDS) analysis of the mineral was carried out to check the Ca/P ratio, and confirmed its similarity to pure HAp.

Introduction

Biomaterials have recently received greater widespread attention due to their increasing value in the treatment of damaged mammalian tissue, most importantly in the human body. Synthetic, inorganic materials based on calcium phosphate, in particular tricalcium phosphate (TCP, $Ca_3(PO_4)_2$) and hydroxyapatite (Hap, $Ca_{10}(PO_4)_6(OH)_2$) are extremely promising due to their outstanding biocompatibility and unique bioactivity, resulting from the high content of this compound in mammalian bones and teeth enamel (Nikpour, 2012).

Hydroxyapatite is one of the most suitable materials for hard tissue engineering applications. The mineral, both pure and in the form of a composite, not only possesses non-inflammatory, non-toxic, and non-immunogenic properties, but is also capable of forming direct bonds with living tissue, as has been proven by numerous researchers (Rupani, 2012; Jin, 2012; Bose, 2012; Ripamonti, 2012). As a result, it can be successfully employed in multiple biomedical applications, such as implant coating, dental filling, orthopedic composites or drug delivery systems. However, pure HAp in the form of powder is regarded as having poor mechanical strength, and therefore cannot be applied in load-bearing situations. Additionally, migration of HAp powder from the implanted site has been observed, which might damage the surrounding healthy tissue (Kong, 2005). These drawbacks can be minimized if the mineral is applied as a filler in a polymer matrix which has the ability to disperse stress, enhance mechanical strength, and at the same time limit the phenomenon of migration.

Few biodegradable polymers are widely used in composite preparation. These are mostly polyesters, for instance poly(lactic acid) (PLA), poly(glycolic acid) (PGA) and their copolymers (PLGA) (Wei, 2004). Chitosan (CS) has already proven to be a particularly good matrix for HAp composite (Peter, 2010; Katti, 2008). CS is a fiber-like biopolymer, which is structurally similar to cellulose and is equally abundant. The polymeric chain of chitosan is composed of D-glucosamine and N-acetyl-D-glucosamine in ß(1-4) linkage. Though chitosan possesses unique properties such as biodegradability, biocompatibility, non-toxicity and antibacterial effect, it does not reflect bone-bonding bioactivity. The bioactive properties of HAp, and the enhancement in mechanical strength of CS, offer new routes for the treatment of damaged hard tissues (Li, 2005). The composite can be prepared in various forms, including porous scaffolds (Kong, 2005), pastes (Murugan, 2004), nanofibers (Zhang, 2008), membranes (Ehrlich, 2006), and implant coatings (Pang, 2005).

During the present research, the mineral composite was prepared with the use of calcium chloride ($CaCl_2$) and disodium hydrogen phosphate (Na_2HPO_4) as sources of calcium and phosphorus, respectively. These reagents are poorly described in the literature as precursors of the mineral phase in CS composite, and therefore the results might be of significant importance.

Materials

Hydroxyapatite (HAp) was precipitated with the use of calcium chloride ($CaCl_2$) and disodium hydrogen phosphate (Na_2HPO_4). Both were purchased from Sigma-Aldrich). Chitosan (CS) was prepared via partial deacetylation of commercially available chitin (Sigma-Aldrich) according to the reaction shown in Fig. 1.
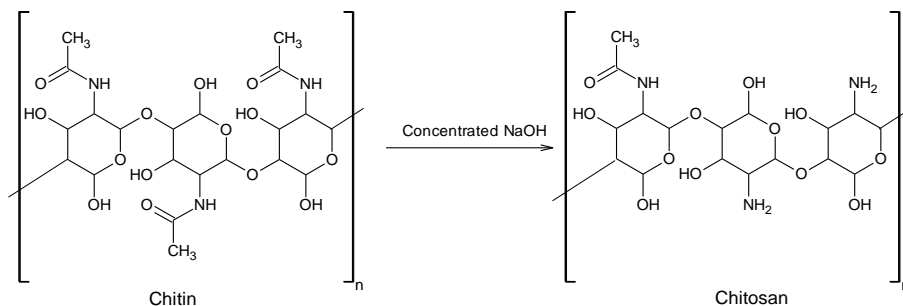
Fig. 1. Reaction of chitin deacetylation to chitosan

Synthesis of hydroxyapatite/chitosan composite via a one-step co-precipitation method

The process of one-step co-precipitation of HAp/CS composite is shown schematically in Fig. 2. A 3% chitosan solution was prepared by dispersing CS powder in a 1% aqueous solution of acetic acid, and stirring until the biopolymer fully dissolved. An appropriate amount of the prepared biomaterial solution was mixed with calcium chloride solution and stirred initially in a three-neck flask. The volumes and concentrations of the $CaCl_2$ and Na_2HPO_4 solutions were taken so as to obtain a final Ca/P ratio of 1.67, which is a characteristic value for HAp present in human hard tissue. The CS solution was introduced into the reactor in such volumes that the weight ratios of the mineral compound to the biopolymer matrix were 85/15, 70/30, 50/50, and 30/70. Na_2HPO_4 was dosed into the mixture, with vigorous stirring, causing the mineral as well as the biopolymer to precipitate gradually. The reaction proceeded in a water bath at a temperature of 40 ^{o}C. When the addition of phosphate was completed, 1M sodium hydroxide solution was added to the mixture dropwise, in order to increase its pH, and causing the CS to fully precipitate. The prepared composite was washed with distilled water, filtered off under reduced pressure, and dried in a convectional dryer at 50 ^{o}C for 24 hours.
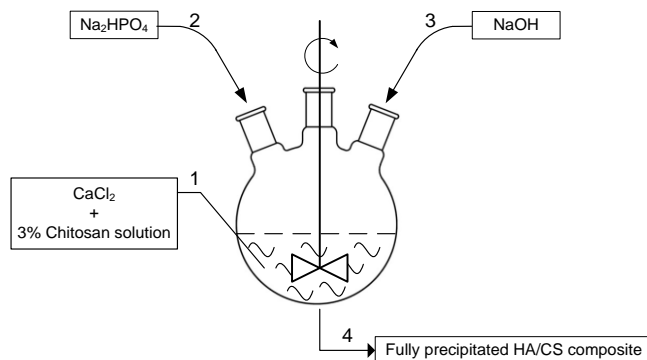

Fig. 2. Schematic diagram of preparation of HAp/CS composite via the one-step co-precipitation method

The product was subjected to numerous analyses. The presence of the expected functional groups was confirmed by FT-IR, recorded on a VERTEX 70 spectrometer (Bruker, Germany). Here the materials were analyzed in the form of tablets, made by pressing a mixture of anhydrous KBr (250 mg) and about 1.5 mg of the tested substance in a special steel ring under a pressure of approximately 10 MPa. The transparent tablet was placed in a cuvette, which was placed in the clamp of the apparatus at the focal point of the beam of radiation. The investigation was performed over a wave number range of $4000–400$ cm^{-1} (at a resolution of 0.5 cm^{-1}) with 64 scans.

Samples were also identified using the WAXS (Wide Angle X-Ray Spectroscopy) method, and elaborated with the support of X-RAYAN software. As a result of the analysis, parameters of the crystallographic structure of the composite were obtained.

Thermogravimetric analysis was performed using a Jupiter STA 449 F3 (Netzsch GmbH, Germany) unit in order to record thermal effects during heating. Samples weighing approximately 10.0 mg were placed in an Al_2O_3 crucible, and heated at a rate of 10 ºC/min from 30 ºC to 1000 ºC in a nitrogen atmosphere.

The elemental composition of the biocomposite was determined by means of EDS analysis. Characteristics of the porous structure of selected samples were acquired with use of low-temperature nitrogen sorption, recorded using an ASAP 2020 analyzer (Micromeritics Instrument Co., USA). The BET specific surface area was calculated from the BET equations and the mean pore size (S_p) as well as total pore volume (V_p) were obtained using the BJH algorithm. Description of the morphology of the samples was supported with SEM photographs, recorded from an EVO40 scanning electron microscope (Zeiss, Germany).

Results and discussion

The FT-IR spectra of pure CS and HAp and of composites with various HAp/CS ratios are shown in Fig. 3.

The FT-IR spectrum of pure CS shows a characteristic band around 3430 cm^{-1}, which corresponds to stretching vibrations of hydroxyl groups. Also visible are bands representing the $=C=O$ stretching vibrations and the $=N–H$ in-plane bending vibrations characteristic of amide I and II structures, in the wavelength number range from 1650 to 1600 cm^{-1}. Also a peak characteristic of the amide III structure is visible at 1257 cm^{-1}, whose intensity decreases with increasing HAp content in the composite. Bands visible around 2925 cm^{-1} were attributed to –CH backbone vibrations, while a peak around 1400 cm^{-1} is attributed to $–CH_3$ and $–CH_2$ in-plane deformation vibrations. A series of peaks around 1070 cm^{-1} most likely corresponds to glucosamine stretching vibrations (Zhang, 2011).

The characteristic spectrum of HAp is mainly found at lower wave numbers. Figure 3b shows characteristic bands in the ranges $1150–1000$ cm^{-1} and $500–600$ cm^{-1}, which can be associated respectively with stretching and bending vibrations of the

PO_4^{3-} group. Also identified are P=O stretching vibrations in the range 1350–1150 cm^{-1}. The peak at 3540 cm^{-1} can be attributed to stretching vibrations of free –OH groups (Danilchenko, 2009; Ehrlich, 2006). The peak is accompanied by a similar one at a lower wave number, which is characteristic of –OH groups subject to intermolecular or intramolecular hydrogen bonds.

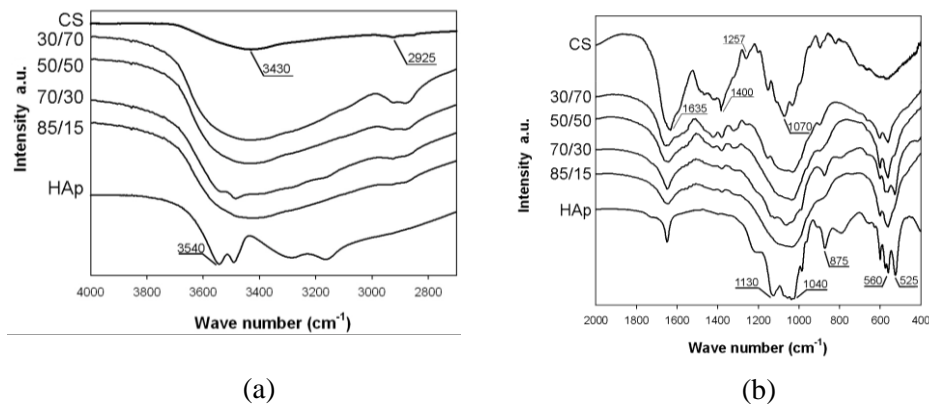(a)   (b)

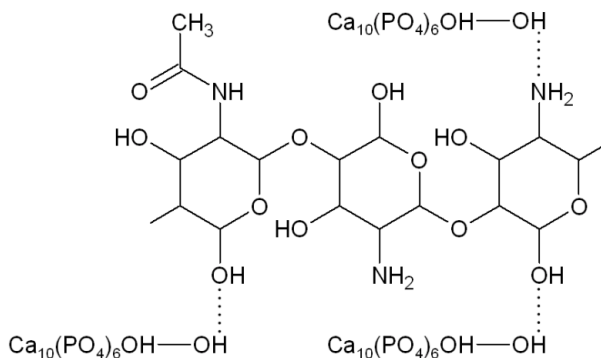Fig. 3. Comparison of FT-IR spectra of pure CS, HAp, and HAp/CS composites with various component ratios

Fig. 4. Schematic representation of hydrogen bonds between HAp and CS compounds

Comparison of the composites with various HAp/CS ratios reveals some important changes. The peak related to the –CH backbone vibrations of CS clearly decreases in intensity as HAp content increases. Strong deformations of the ß-1,4-glycosidic linkage throughout the composite setup, represented by the peak with maximum at 896 cm^{-1}, are confirmations of hydrogen interactions between HAp and CS. The disappearance/deformation of the ether bond in the pyranose ring at 1153 cm^{-1} and the amide III band at 1257 cm^{-1} serves as additional evidence for the chemical interconnection of the two phases. Moreover, the peaks attributed to stretching

vibrations of hydroxyl groups show a slight shift towards lower wavenumbers. For pure HAp the peak was recorded at 3540 cm^{-1}, while for composites it appeared at 3430 cm^{-1}. The slightly lower values of the peak for composites most likely indicate the formation of hydrogen bonds between compounds of the mineral and the biopolymer, shown schematically in Fig. 4.

X-ray diffraction patterns of the obtained composites are shown in Fig. 5. For a pure HAp sample, the existence of 2θ peaks at approximately 26.0°, 31.4°, 32.2° and 40.1° was recorded, corresponding to the diffraction planes (002), (211), (300), (310) respectively (data supported by the JCPDS database). The pattern confirms the presence of crystalline HAp obtained via the applied method. Characteristic bands for pure chitosan were located around 25° and can be assigned to chains aligned through intermolecular interactions (Zhang, 2011).
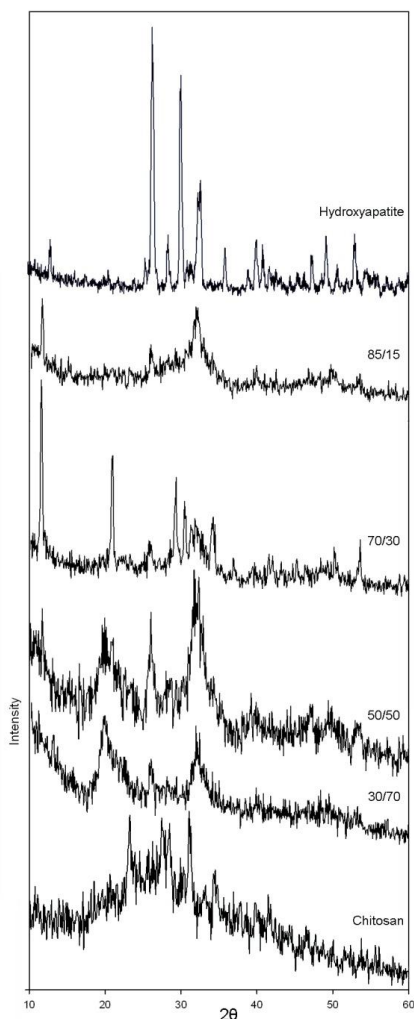
The XRD patterns for the composites suggest that HAp crystallinity decreases with increasing content of the biopolymer. There is a visible broadening of the mineral diffraction peaks with decreasing content of HAp in proportion to chitosan, suggesting diminishing size of the apatite crystals and decrease in its crystallinity (Li 2012, Nikpour 2012). Even for the composite with the lowest content of polymer matrix, it is observable that the crystallization of HAp is already altered. Broadening and weakening of the characteristic peaks of the mineral as well as of the polymer matrix after composite formation indicate bonding of the two phases.
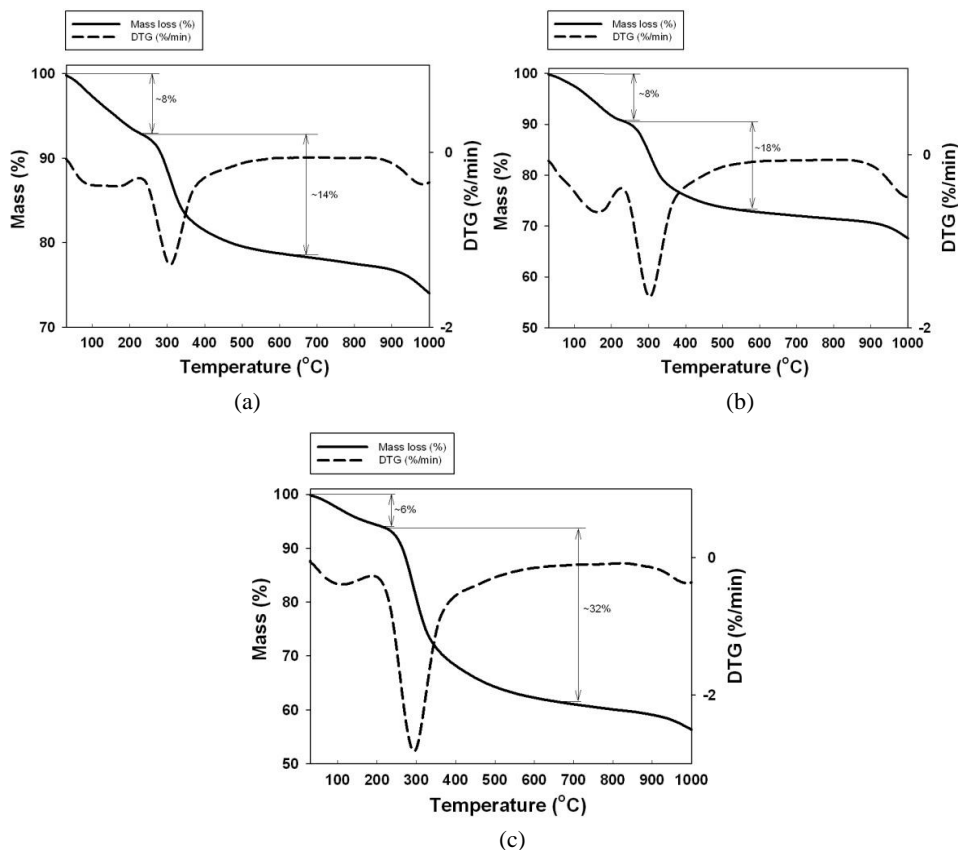
Fig. 6. Thermograms of HAp/CS composites with ratios (a) 85/15, (b) 70/30, and (c) 50/50

In graphs shown as Fig. 6. there are three significant regions visible. The first lies in a temperature range of 100–200 °C, and is most likely connected with the loss of water molecules physically and chemically bound to the CS and HAp. The quantity of water lost ranges from 6% to 8%. The second important mass loss can be observed in the temperature range 200–450 °C, and is attributed to the thermal and oxidative

decomposition of the biopolymer (Neto 2005, Ma 2009). The highest rate of decomposition, represented by the maximum peak of the DTG curve, was found to be around 300 $^{\circ}$C and is constant for all of the tested samples. From the recorded curves it can be noted that the greater the content of organic matrix, the greater the mass loss. For the sample with component ratio 50/50 the mass loss was 32% (Fig. 6c), whereas for the sample HAp/CS 85/15 (Fig. 6a) and HAp/CS 70/30 (Fig. 6b) it was 14% and 18%, respectively. The third characteristic thermal transition, which begins similarly for all samples around 850 $^{\circ}$C, reaches a maximum around 1000 $^{\circ}$C. The peak most likely corresponds to the dehydroxylation stage of the decomposition of HAp. This observation is in agreement with literature data (Wang, 2004).

Energy dispersive spectroscopy (EDS) (Fig. 7) provides important information regarding mineral composition, and can be utilized for determination of calcium and phosphorus content within a specimen. The obtained biomineral ratio of Ca/P was as high as 1.68, which is very close to the molar ratio of the elements in the HAp formula (1.67).

Element	Line	Wt%	At%
P	KA1	37.31	43.51
Ca	KA1	62.69	56.49
Total		100.00	100.00
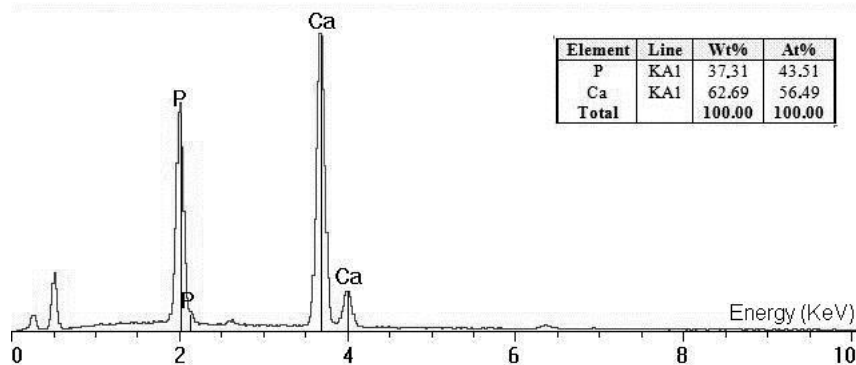
Fig. 7. EDS spectrum for pure hydroxyapatite, with a Ca/P ratio equal to 1.68

To evaluate the porous structure of the prepared biocomposites, adsorption/desorption isotherms were obtained, which were used to calculate morphological parameters. The results of the analysis are presented in Table 1.

Table 1. Parameters of the porous structure of the prepared composites

Sample name	BET surface area (m^2/g)	Total volume of pores (cm^3/g)	Mean size of pores (nm)
Pure HAp	81.0	0.370	18.2
HAp/CS 85/15	41.0	0.028	2.7
HAp/CS 70/30	23.0	0.016	2.8
HAp/CS 50/50	8.0	0.006	2.8

Values representing the porous structure properties of pure HAp are relatively high, in particular the unusually high total pore volume. The BET surface area for pure HAp is as high as 81.0 m^2/g, the measured pore volume is 0.370 cm^3/g, and the mean pore size is as high as 18.2 nm. Such high values most likely result from the crystalline nature of the prepared product. Results from nitrogen adsorption/desorption analysis clearly show a decrease in the specific surface area of the composite with increasing content of the polymer matrix. Among the prepared composites, the highest BET surface area (41.0 m^2/g) was obtained for the sample with the largest fraction of HAp (HAp/CS 85/15). The pore volume for that sample also took a relatively high value (0.028 cm^3/g). For the sample HAp/CS 70/30 a corresponding decrease in morphological parameter values was observed. The BET surface area was 23.0 m^2/g, and the pore volume also diminished, to 0.016 cm^3/g. The sample with the lowest content of mineral phase has the smallest values of BET surface area (8.0 m^2/g) and pore volume (0.006 cm^3/g) among the analyzed samples. The pore size measured for the biocomposites remained at a constant value of approximately 2.8 nm. For the composite HAp/CS 30/70 the porous structure parameters are not presented, because technical difficulties indicating that the obtained results are to be verified by further measurements. The properties of pure CS were similarly difficult to measure. It is easily noticeable that there is a decrease in specific surface area and pore volume with increasing content of organic phase. This observation suggests that the porosity of the biocomposite is mostly associated with the content of HAp in the sample.

The morphological structure of the biocomposite is supported by SEM microphotographs, as presented in Fig. 8. In this image, the plate-like shape of HAp particles incorporated into the CS matrix can be observed. The composite forms non-uniform agglomerates. The structures vary in size from about 500 nm to 5 µm.
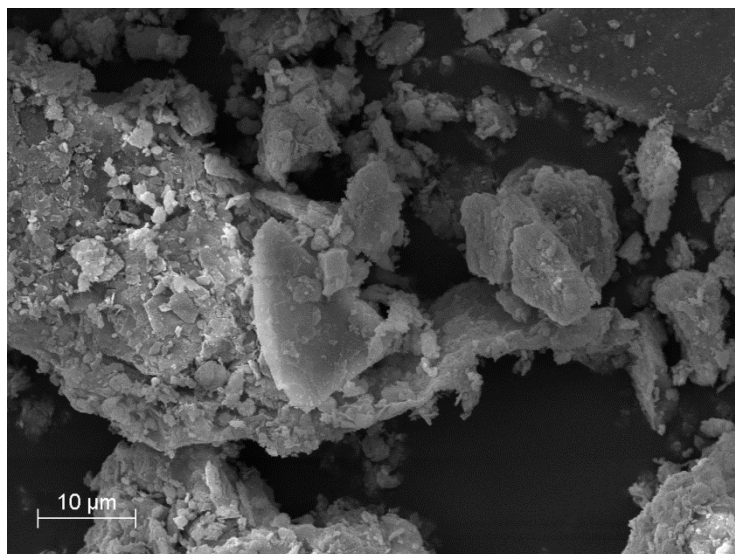
Fig. 8. SEM image of HAp/CS 50/50 composite

Conclusions

As a result of the experiment, HAp/CS composites with various component ratios were prepared via a one-step co-precipitation method, with the use of $CaCl_2$ and Na_2HPO_4 as sources of calcium and phosphorus respectively. CS was obtained through partial deacetylation of commercially available chitin.

The FT-IR spectra of the analyzed samples show that hydrogen bonds formed between the mineral and the biopolymer components, which is confirmed by the shift in the characteristic bands. The analysis provides confirmation of the success of the process of composite synthesis via the selected method. The SEM photographs support the conclusion that the components of the composite are strongly interconnected.

DTG curves show that the prepared composite is thermally stable up to about 200 ^{o}C, and two major mass losses are associated with the evaporation of adsorbed water and the degradation of chitosan. Additionally, EDS analysis shows that precipitated HAp has a calcium/phosphorus ratio similar to that of the naturally occurring mineral, thus suggesting that the biomaterial might be suitable for biomedical applications.

The biocomposite with the best morphological properties, namely high specific surface area and porosity, was found to be that with an HAp/CS ratio of 85/15, the highest ratio of mineral to organic phase. With decreasing quantities of porous inorganic mineral, the BET surface area decreases as well. Moreover the pore volume also decreases, suggesting that pores are blocked by the biopolymer.

The experimental results demonstrate the feasibility of preparation of HAp/CS biocomposites using $CaCl_2$ and Na_2HPO_4 via a one-step co-precipitation method.

References

BOSE S., TARAFDER S., 2012, *Calcium phosphate ceramic systems in growth factor and drug delivery for bone tissue engineering: A review*, Acta Biomater., 8, 1401–1421.

DANILCHENKO S. N., KALINKEVICH O. V., POGORELOV M. V., KALINKEVICH A. N., SKLYAR A. M., KALINICHENKO T. G., ILYASHENKO V. Y., STARIKOV V. V., BUMEYSTER V. I., SIKORA V. Z., SUKHODUB L. F., MAMALIS A. G., LAVRYNENKO S. N., RAMSDEN J. J., 2009, *Chitosan–hydroxyapatite composite biomaterials made by a one step co-precipitation method: preparation, characterization and in vivo tests*, J. Biol. Phys. Chem., 9, 119–126.

EHRLICH H., KRAJEWSKA B., HANKE T., BORN R., HEINEMANN S., KNIEB C., WORCH H., 2006, *Chitosan membrane as a template for hydroxyapatite crystal growth in a model dual membrane diffusion system*, J. Membr. Sci., 273, 124–128.

JIN H. H., KIM D. H., KIM T. W., SHIN K. K., JUNG J. S., PARKA H. C., YOON S. Y., 2012, *In vivo evaluation of porous hydroxyapatite/chitosan–alginate composite scaffolds for bone tissue engineering*, Int. J. Biol. Macromol., 51, 1079–1085.

KATTI K. S., KATTI D. R., DASH R., 2008, *Synthesis and characterization of a novel chitosan/montmorillonite/hydroxyapatite nanocomposite for bone tissue engineering*, Biomed. Mat., 3, 034122.

KONG L., GAO Y., CAO W., GONG Y., ZHAO N., ZHANG X., 2005, *Preparation and characterization of nano-hydroxyapatite/chitosan composite scaffolds*, J. Biomed. Mater. Res.; 75A, 275–282.

LI X.Y., NAN K.H., SHI S., CHEN H., 2012, *Preparation and characterization of nano-hydroxyapatite/chitosan cross-linking composite membrane intended for tissue engineering*, Int. J. Biol. Macromol., 50, 43–49.

LI Z., YUBAO L., AIPING Y., XUELIN P., XUEJIANG W., XIANG Z., 2005, *Preparation and in vitro investigation of chitosan/nano-hydroxyapatite composite used as bone substitute materials*, J. Mater. Sci. Mater. Med., 16, 213–219.

NARASARAJU T. S. B., PHEBE D. E., 1996, *Some physico-chemical aspects of hydroxyapatite,* J. Mat. Sci., 31, 1–21.

NETO C.G.T., GIACOMETTI J.A., JOB A.E., FERREIRA F.C., FONSECA J.L.C., PEREIRA M.R., 2005, *Thermal analysis of chitosan based networks*, Carbohydr. Polym., 62, 97–103.

NIKPOUR M.R., RABIEE S.M., JAHANSHAHI M., 2012, *Synthesis and characterization of hydroxyapatite/chitosan nanocomposite materials for medical engineering applications*, Compos.: Part B, 43, 1881–1886.

MA G., YANG D., KENNEDY J. F., NIE J., 2009, *Synthesize and characterization of organic-soluble acylated chitosan*, Carbohydr. Polym., 75, 390–394.

MURUGAN R., RAMAKRISHNA S., 2004, *Bioresorbable composite bone paste using polysaccharide based nano-hydroxyapatite*, Biomat., 25, 3829–835.

PANG X., ZHITOMIRSKY I., 2005, *Electrodeposition of composite hydroxyapatite–chitosan films*, Mater. Chem. Phys., 94, 245–251.

PETER M., BINULAL N. S., SOUMYA S., NAIR S. V., FURUIKE T., TAMURA H., JAYAKUMAR R., 2010, *Nanocomposite scaffolds of bioactive glass ceramic nanoparticles disseminated chitosan matrix for tissue engineering applications,* Carbohydr. Polym., 79, 284–289.

RIPAMONTI U., RODEN L.C., RENTON L.F., 2012, *Osteoinductive hydroxyapatite-coated titanium implants,* Biomater., 33, 3813–3823.

RUPANI A., BASTIDA L.A.H., RUTTEN F., DENT A., TURNER I., CARTMELL S., 2012, *Osteoblast activity on carbonated hydroxyapatite*, J. Biomed. Mater. Res. Part A, 100, 1089–1096.

WANG T., DORNER-REISEL A., MÜLLER E., 2004, *Thermogravimetric and thermokinetic investigation of the dehydroxylation of a hydroxyapatite powder*, J. Eur. Ceram. Soc., 24, 693–698.

WEI G., MA P.X., 2004, *Structure and properties of nano-hydroxyapatite/polymer composite scaffolds for bone tissue engineering*, Biomater., 25, 4749–4757.

ZHANG C. Y., CHEN J., ZHUANG Z., ZHANG T., WANG X. P., FANG Q. F., 2011, *In situ hybridization and characterization of fibrous hydroxyapatite/chitosan nanocomposite*, J. Appl. Polym. Sci., 124, 397–402.

ZHANG Y., VENUGOPAL J. R., EL-TURKIA., RAMAKRISHNA S., SU B., TECK LIM C., 2008, *Electrospun biomimetic nanocomposite nanofibers of hydroxyapatite/chitosan for bone tissue engineering*; Biomater., 29, 4214–4322.

CALCIUM CARBONATE MINERALIZATION. PART II: EFFECT OF POLY(ETHYLENE GLYCOL) AND BLOCK COPOLYMERS MOLECULAR WEIGHT ON FORMATION OF PRECIPITATE

Izabela POLOWCZYK[*], **Anna BASTRZYK**[*], **Tomasz KOZLECKI**[*], **Elzbieta GRZADKA**[**], **Zygmunt SADOWSKI**[*]

[*]   Wroclaw University of Technology, Faculty of Chemistry, Department of Chemical Engineering, Wybrzeze Wyspianskiego 27, 50-370 Wroclaw, Poland, izabela.polowczyk@pwr.wroc.pl
[**]   Maria Curie-Skłodowska University, Faculty of Chemistry, Department of Radiochemistry and Chemistry of Colloids, M. Skłodowskiej-Curie 3 Sq., 20-031 Lublin, Poland

Abstract: In this study the role of PEG and PEO-PPO-PEO block copolymers molecular weight in precipitation of calcium carbonate was examined. The $CaCO_3$ particles were characterized by FTIR spectroscopy, X-ray, SEM and particle size distribution analysis. In absence and presence of modifiers, mixing of the reagents led to the formation of calcite crystals. The calcium carbonate obtained with poly(ethylene glycol) and block copolymers was characterized by smaller diameter in comparison with the one without modifiers. It was observed that using compounds with different molecular weights has no obvious effect on the form and properties of precipitated calcium carbonate particles.

Introduction

It is widespread in biological systems that living organisms synthesize inorganic minerals with complex shapes, hierarchical structures and fascinating properties (Meldrum and Colfen, 2008; Zhu et al., 2013). Biomaterials are particularly promising materials, which can be environmentally friendly synthesized and possess high biocompatibility (Xu et al., 2007). These biological structures are a source of inspiration for approaching a variety of technical challenges in materials science (Ehrlich et al., 2010). The design of novel biomaterials relies on an understanding of the organic matrix proteins and templating structures in nature (Ichikawa et al., 2003; Ehrlich et al., 2010).

One of the most common biomaterial in nature is calcium carbonate. In nature, calcium carbonate is present in marine invertebrate animals such as mollusk, coral and forminifera, as well as fish otolith and animals shells (Ichikawa et al., 2003; Meldrum and Colfen, 2008; Zhu et al., 2013). This material has found abundant applications in the cosmetics, paper, paint, rubber and adhesive industries, and in biomedical application like drug delivery (Chibowski et al., 2005; Kurapati and Raichur, 2013). These applications of calcium carbonate mainly depend on parameters, such as average particle size, particle size distribution, morphology, polymorphism and chemical purity (El-Sheikh et al., 2013). Literature data revealed that to obtain the desired properties of $CaCO_3$ particles it is necessary to control pH, temperature, concentration of CO_3^{2-} and Ca^{2+} ions, the type and the concentration of additives (Kitamura, 2002; El-Sheikh et al., 2013). During the last decade most investigations have been performed by using different additives such as polymers, biopolymers, proteins, surfactants and their mixtures to guide $CaCO_3$ crystallization (Wang et al., 2009a; Wang et al., 2009b; Shestak et al., 2011; Zhao et al., 2012; Deng et al., 2013; El-Sheikh et al., 2013; Polowczyk et al., 2013; Szczes, 2013). Addition of these compounds to precipitation system led to calcium carbonate with different morphology, size and crystalline form. The most of these studies were performed using proteins, especially that present in the avian eggs shells (Hernandez-Hernandez et al., 2008; Wang et al., 2009a; Wang et al., 2009b). In literature it can be seen that not only the natural biopolymer can be used to control the properties of $CaCO_3$ but also the synthetic compounds (Xie et al., 2006; Xu et al., 2008; Ehrlich et al., 2010; Sadowski et al., 2010; Su et al., 2010; Xu et al., 2011; Deng et al., 2013, Polowczyk et al., 2013; Zhu et al., 2013). For example El-Sheikh and co-workers (2013) have done research on precipitation of $CaCO_3$ in the presence of cationic surfactant, cetyltrimethylammonium bromide, using the reaction system $Ca(OH)_2$-H_2O-CO_2. They observed that precipitate morphology was significantly changed from rombohedral to scalenohedral calcite with concentration of surfactant. Additionally, the presence of CTAB molecules influenced the properties of calcium carbonate, such as size or zeta potential. The properties of precipitate can also be influenced by the oxyethylene groups. Su and co-workers (2010) have investigated the influence of poly(ethylene glycol)-block-poly(acrylic acid)-block-poly(styrene)) polymers on the crystallization, morphology and size of $CaCO_3$. They observed that the formation of vaterite depends on the number of carboxyl groups in the copolymer and its concentration. Vaterite is the other anhydrous polymorph of calcium carbonate, and is the least stable phase since it slowly recrystallizes to become calcite in contact with water (Kim and Park, 2010). It is characterized by large specific surface and high surface activity, which can be used to improve mechanical properties of product in industry (Kim and Park, 2010). Zhao and co-workers (2012) observed that increasing the concentration of block copolymer F68, made up of symmetrical poly(ethylene oxide)-poly(propylene oxide)-poly(ethylene oxide) (PEO-PP-PEO), affected the morphology of $CaCO_3$ but has no influence on the crystalline form. The groups of EO

and EG are of particular interests because its molecules contain hydrophilic groups, which can act as a donor to metal ions to form metal complexes with diverse conformations (Xu et al., 2003; Bastrzyk et al., 2012). The effect of these type of functional groups on the properties of calcium carbonate precipitated is not well understood. This paper is a continuation of our research on this topic. In our earlier studies on precipitation of calcium carbonate it was observed that PEG 5000000 can affect the morphology of $CaCO_3$ crystals as well as a size distribution of precipitate. At a higher polymer concentration, 0.05, 0.1 and 0.5%, spherical forms of carbonates appeared in the system (Polowczyk et al., 2013). The aim of this paper is to investigate the effect of molecular weight of PEG and block copolymer (PEO-PPO-PEO) on the crystal growth of calcium carbonate.

Materials and Methods

Calcium chloride dihydrate (purity > 99%) and disodium carbonate were purchased from Sigma Aldrich. PEG 1000, PEG 6000, PEG 20000, PEG 300000 were purchased from BDH Chemicals. The following Pluronic® block copolymers: PE 3500, PE 6400, PE 6800, PE 10500 were purchased from BASF. F68 and F127 were purchased from Sigma Aldrich. All chemicals used in these syntheses were applied without further purification. The structure of all molecules of lock copolymers used in experiments are shown in Table 1.

Table 1. Structure of block copolymers

Name	Structure
PE 3500	$EO_{11}PO_{16}EO_{11}$
PE 6400	$EO_{13}PO_{30}EO_{13}$
PE 6800	$EO_{73}PO_{28}EO_{73}$
PE 10500	$EO_{37}PO_{56}EO_{37}$
F 68	$EO_{80}PO_{30}EO_{80}$
F 127	$EO_{106}PO_{70}EO_{106}$

The preparation of calcium carbonate was performed according to the method reported in our earlier paper (Sadowski et al., 2010). The solutions of sodium carbonate (0.1 M) and calcium chloride (0.1 M) with PEG or block copolymer (0.1%) were prepared one day before the calcium carbonate synthesis and have been stirred overnight. The PEG and block copolymers with different molecular weight were used. The precipitation experiments were carried out in the Erlenmeyer flasks by mixing of a sodium carbonate solution with calcium chloride one at the speed of the magnetic stirrer of 300 rpm. After 5 min or 24 h the precipitated calcium carbonate was removed from solution by centrifugation. The deposit was collected and washed twice with 100 cm^3 of deionized water and dried at 30 ºC. The experiments were conducted at ambient temperature.

The microstructure of precipitate was observed using a JSM 5800 LV scanning electron microscope (JEOL). The crystallographic structure of calcium carbonates was determined by using an D8 Advance (Bruker) X-ray powder diffractometer with CuKα radiation. Fourier transform infrared spectroscopy (FTIR) was carried out using PE 1600 FTIR spectrometer (Perkin Elmer). The samples were mixed with KBr powder. The spectra were recorded in a reflection mode from 4000 to 400 cm^{-1} at a resolution of 2 cm^{-1}. Particle size analysis was realized using a Mastersizer 2000 laser diffractometer, equipped with HydroMu dispersion unit (Malvern). In the process, about 3 cm^3 of calcium carbonates suspension were poured into 700 cm^3 of water cross-flowing through the measuring cell. The particle size measurements were carried out without and afterwards under operation of ultrasounds in the dispersion unit, so the possible agglomerates of calcium carbonate could have been broken. The surface area of the samples were measured by the BET method with helium/nitrogen mixture using a FlowSorbII apparatus (Micromeritics).
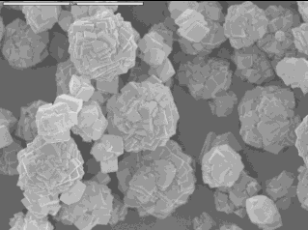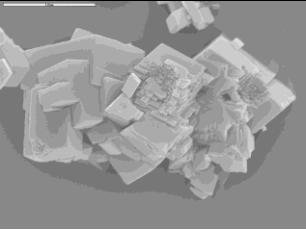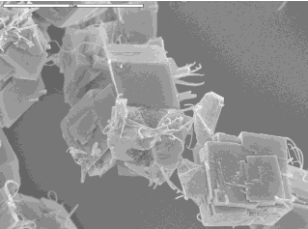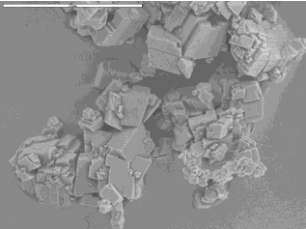
Result and discussion
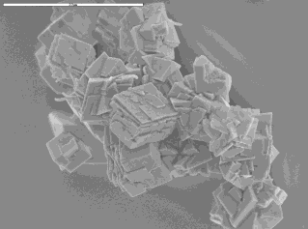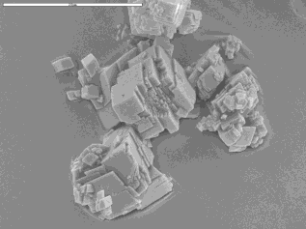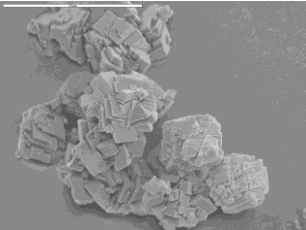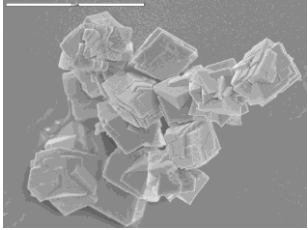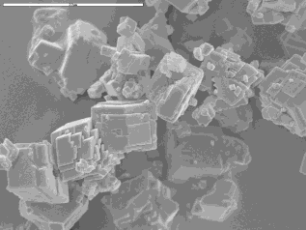
Effect of molecular weight of PEG

Table 2 shows the morphology of calcium carbonate obtained in the presence of PEG with different molecular weight at room temperature, when the concentration of Ca^{2+} and CO_3^{2-} was 50 mmol/dm^3, and the samples were collected after 5 min and 24 h of crystallization. The concentration of PEG in all investigated samples was 0.1%.

From Table 2 we can see that without any additives, calcium carbonates formed rhombohedral calcite crystals, aggregated in spherical formations after 5 min of crystallization which recrystallized in bigger non-spherical aggregates after 24 h of incubation. Addition of PEG resulted in the formation of stacked rhombohedral particles, with the ladder-like surface edges (Zhao et al., 2012). In case of low molecular weight PEG 1000 and PEG 6000 in a short time of crystallization process, whiskers-like structures are visible.

These forms were observed by Zhao and co-workers (2012) and reported as calcite. Within one day of the process, needle-like structures disappeared and the morphology of precipitate slightly differ from that without PEG and aggregates are formed of smaller crystals. From literature data, it is known that in course of crystallization the amorphous phase (ACC) is initially formed (Xu et al., 2007). Then, within very short time this phase rapidly transforms to calcite, vaterite or aragonite. The stable ACC of calcium carbonate can only be present in living organism in a 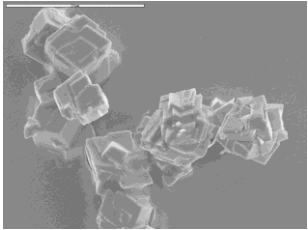form of complex matrices with macromolecules (Xu et al., 2007). Addition of soluble compounds such as polymers or surfactants led to changes in the morphology and size of crystal or various crystalline form (vaterite, aragonite or calcite) (Xu et al., 2007).

Table 2. SEM images of calcium carbonate particles precipitated in the presence of poly(ethylene glycol) with different molecular weighs. Polymer concentration was 0.1%

	5 min	24 h
without PEG		
PEG 1000		
PEG 6000		
PEG 20000		
PEG 300000		
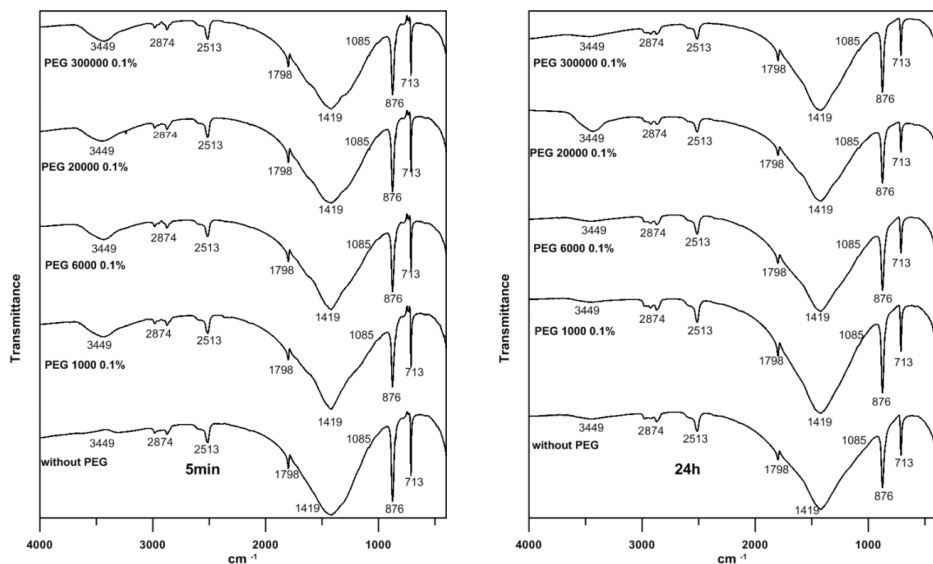
Fig. 1. FTIR spectra of calcium carbonate precipitated after 5 min and 24 h in the presence of PEG having various molecular weight

The FTIR analysis of powders obtained in the presence of PEG 1000, PEG 6000, PEG 20000 and PEG 300000 after 5 min and 24 h (Fig. 1) revealed characteristic spectra of calcite crystals based on the in-plane band and on the out-plane band at ~712 and ~875 cm^{-1} respectively, and anti-symmetry stretch at ~1420 cm^{-1} characteristic of calcite (Addadi et al., 2003; Kim and Park, 2010; Polowczyk et al., 2013). The X-ray powder diffraction patterns presented in Fig. 2 also evidenced the calcite phase creation.
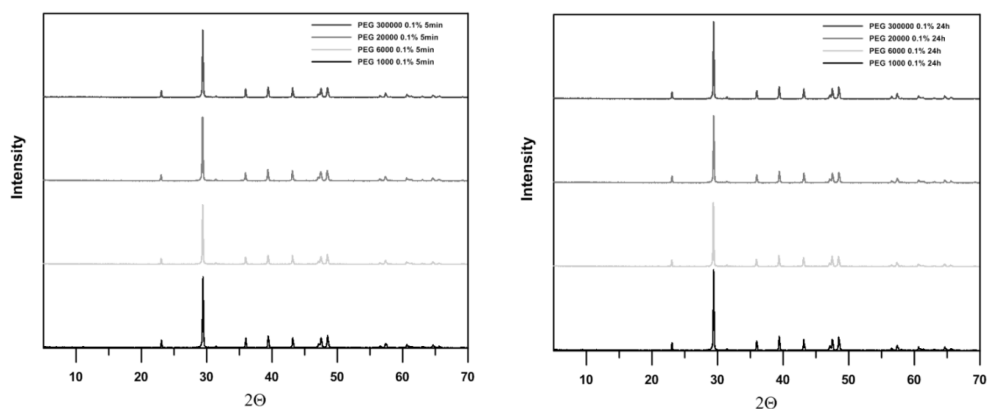

Fig. 2. XRD patterns of calcium carbonate crystals obtained in the presence of PEG, with various molecular weight after 5 minutes and 24 hours of precipitation

Presented above data revealed that particles obtained in the presence of PEG with different molecular weight are quite similar to those obtained in aqueous solution without poly(ethylene glycol), indicating that presence of this type of molecules in such concentration has no obvious influence on the crystalline form of $CaCO_3$. In the investigated systems after 5 min and 24 h only calcite crystals were formed. These data are in good agreement with data published in literature (Xie et al., 2006; Polowczyk et al., 2013). Xie and co-workers (2006) observed that PEG 6000 at concentration of 0.1% favored the precipitation of $CaCO_3$ as calcite. In our earlier studies it was observed that using PEG 5000000 at concentration of 0.1 % lead to formation of calcite after 24 h of precipitation. However, after 5 min of precipitation the spherical morphologies of calcium carbonates (vaterite, 10.6 wt.%) and calcite (89.4 wt.%) mixture was found (Polowczyk et al., 2013). On a base of this it can be supposed that poly(ethylene glycol) mostly favored the precipitation of calcite. The presence of small amount of vaterite using high molecular weight PEG polymer after short time of precipitation can result from inhibiting effect of this polymer on growth of calcite in system. Comparing the pictures of particles in Table 2 it can be said that after 24 h of crystallization the edges of crystals are more irregular in the presence of polymer than without PEG. It means that PEG has an effect on the course of calcium carbonate precipitation. The mean diameters as well as BET specific surface areas of calcite obtained with or without the polymer are presented in Table 3.

Table 3. Specific surface BET areas and diameters of calcium carbonate particles precipitated in the presence of poly(ethylene glycol) with various molecular weight. Concentration of polymer was 0.1 %

Sample name	Time	BET S.A. (m^2/g)	d_{10} (μm) no-ultrasound/ ultrasound	d_{50} (μm) no-ultrasound/ ultrasound	d_{90} (μm) no-ultrasound/ ultrasound
Without PEG	5 min	0.99	9.8/6.6	22.7/12.5	47.2/23.2
	24h	0.74	16.4/7.9	32.6/21.5	59.3/40.44
PEG 1000	5 min	0.46	12.9/10.5	23.8/17.3	43.7/28.5
	24h	0.72	9.3/6.9	19.5/14.1	44.0/24.8
PEG 6000	5 min	0.55	10.0/7.9	19.5/14.1	37.4/23.5
	24h	0.75	10.3/7.7	20.0/14.9	35.9/25.9
PEG 20000	5 min	0.65	8.5/6.9	18.4/13.4	39.7/23.7
	24h	0.81	8.9/6.7	18.9/13.1	36.1/23.9
PEG 300000	5 min	0.58	8.3/6.5	16.4/11.7	35.7/19.7
	24h	0.84	8.6/6.6	18.1/13.1	36.8/23.6

From data presented in Table 3 we can see that the specific surface area of calcium carbonate particles did not exceed one square meter per gram. Values of BET surface areas increased in the presence of PEG for the samples after 24 h of crystallization. It can be explained by the size of precipitates. Calcite obtained without polymer possesses volume median diameters, d_{50}, of 12.5 and 21.5 μm after 5 min and 24 h, respectively. The value of BET surface area of $CaCO_3$ particles was 0.99 and 0.74
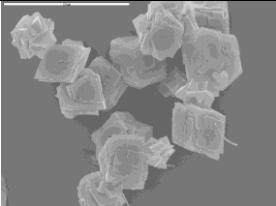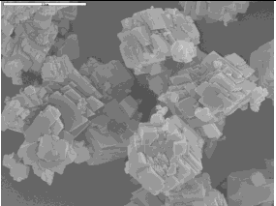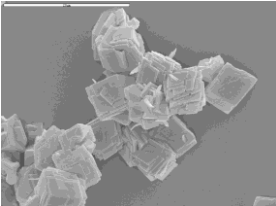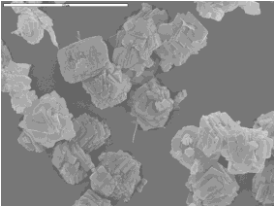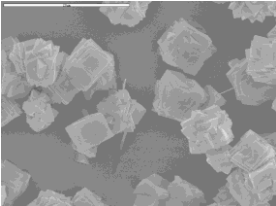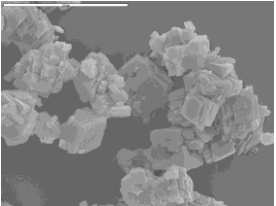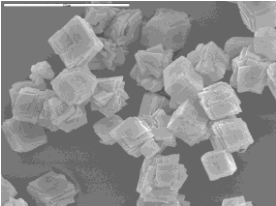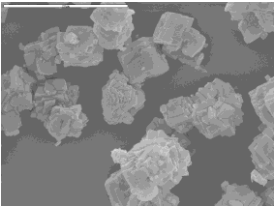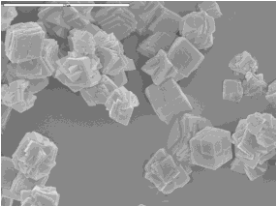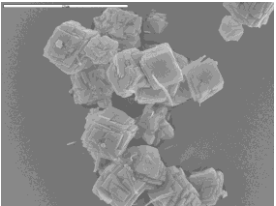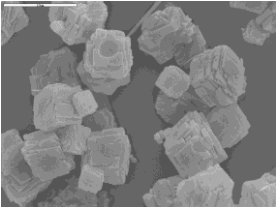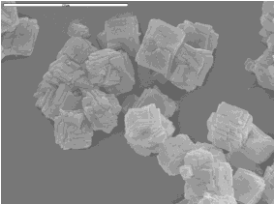
m^2/g after 5 min and 24 h of precipitation. Comparing the morphology of the samples obtained after 5 min and 24 h (Table 2) it can be seen that shape of precipitate differs significantly. The crystals obtained after 5 min had irregular sphere-like structure resulting in bigger surface BET area. Addition of poly(ethylene glycol) to system resulted in a slight changes in diameter of particles precipitated after 5 min. Furthermore, decrease of the BET surface area of crystal obtained with polymer addition after 5 min of crystallization was observed. The lower value of BET surface area in the presence of polymer for these samples can be explained by different shape of particles. More irregular shape of crystals gives a large number of edges with high surface energy (Xu et al., 2007). In contrast, the particles obtained after 24 h were characterized by smaller diameter in the presence of polymer during crystallization process. Addition of PEG 1000, PEG 6000, PEG 20000 and PEG 300000 led to production of particles with d_{50} equal 14.1, 14.9, 13.1 and 13.1 μm, respectively. Also the upper-decile, d_{90}, is much lower with PEG addition, especially after treatment of ultrasounds the aggregates were easily broken. The SEM images evidenced these results. In earlier studies it was observed that diameter of particles obtained in the presence of PEG 5000000 polymer at concentration of 0.1 wt.% was 15.7 and 15.6 μm after 5 min and 24 h of incubation, respectively (Polowczyk et al., 2013). Slight increase in a mean diameter of calcite was explained by flocculation effect (Polowczyk et al., 2013). This behavior can be explained by specific adsorption of these molecules onto calcium carbonate surface during crystallization process (Xie at al., 2006; Polowczyk et al., 2013). The poly(ethylene glycol) possesses functional groups which have ability to bind Ca^{2+} on the special face of formed $CaCO_3$, and inhibits the growth of crystals in suspension. Also, these polymers probably change the viscosity of suspension, and slow down the diffusion of ions in a system.

Effect of poly(ethylene)-poly(propylene)-poly(ethylene) block copolymers

In Table 4 the SEM images of calcium carbonates synthesized in the presence of block copolymers with different molecular weights are presented. These copolymers contain various number of EO and PO block in their structure (Table1).

It was observed that in all cases the main components of precipitate was rhombohedral calcite. The obtained forms are similar to those obtained without and with PEG polymers. For block copolymers such as PE 3500, PE 6400, PE 6800 and F 68 the needle-like structure appeared. According to data shown in Fig. 5, it can be said that addition of PEO-PPO-PEO copolymers results in calcite formation. The characteristic peaks of calcite are 712, 875 and 1420 cm^{-1}. There were no peaks of aragonite and vaterite in the obtained samples. The needle-like structure, according to literature, can occur both for aragonite and also calcite (Chen et al., 2011; Zhao et al., 2012). Zhao and co-workers (2012) observed that in the presence of F68, aggregated rod-like calcites can appear.

Table 4. SEM images of calcium carbonate particles precipitated in the presence of block copolymers with different molecular weight. The polymer concentration was 0.1 %

	5 min	24 h
PE3500		
PE6400		
PE6800		
PE10500		
F68		
F127		
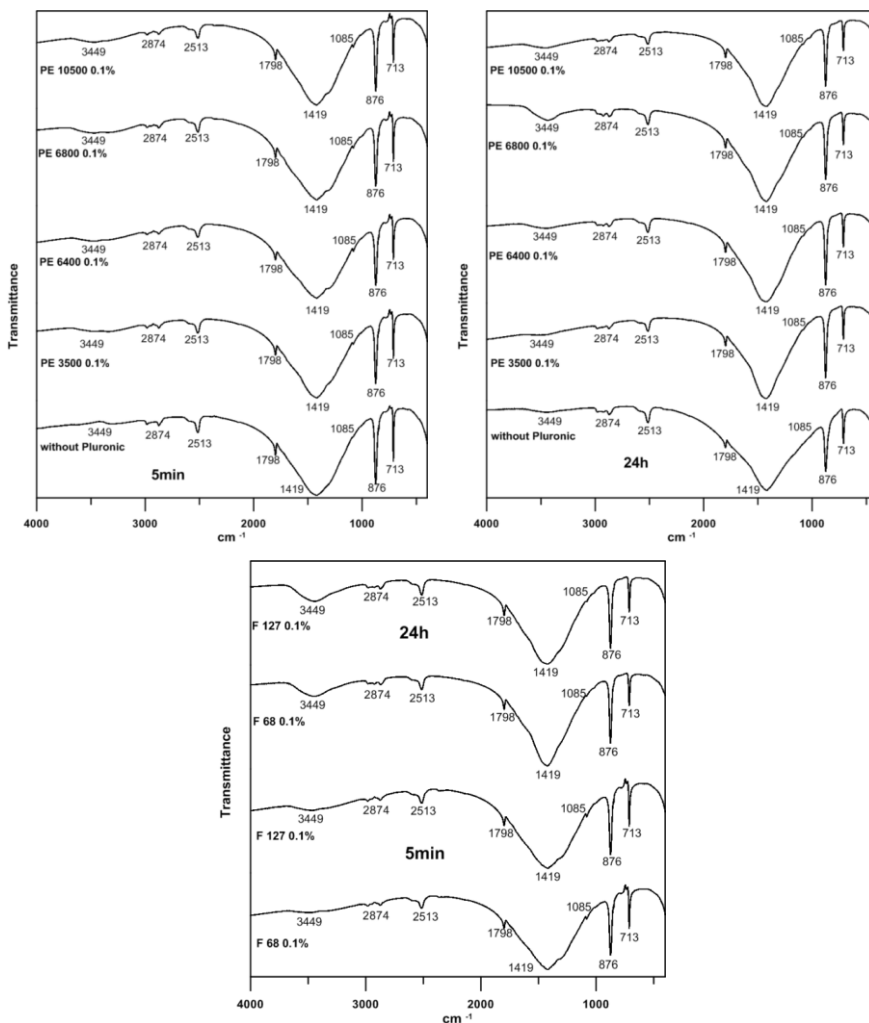
Fig. 5 FTIR spectra of calcium carbonate precipitated after 5 min and 24 h
in the presence of block copolymers with various molecular weight

Figure 6 presents XRD analysis of $CaCO_3$ obtained in the presence of block copolymers after 5 min and 24 h of precipitation. Presented data showed that the only phase of $CaCO_3$ obtained in the absence and presence of block copolymers was calcite.

The data are in good agreement with literature data. Zhao and his co-workers (2012) observed that at low concentration of F68 copolymer led to precipitation of calcite. They observed that upon increasing the concentration up to 3 g/dm^3 the mixture of calcite and spherical vaterite appeared. In our studies the concentration of block copolymers was 1 g/dm^3. There was not observed any influence of length of block PEO and PPO on crystalline form of calcite at that concentration. However, it

can be seen in Table 4, that in the presence of block copolymers the surface edges of $CaCO_3$ are irregular and rather rounded, and this results in complex morphology.
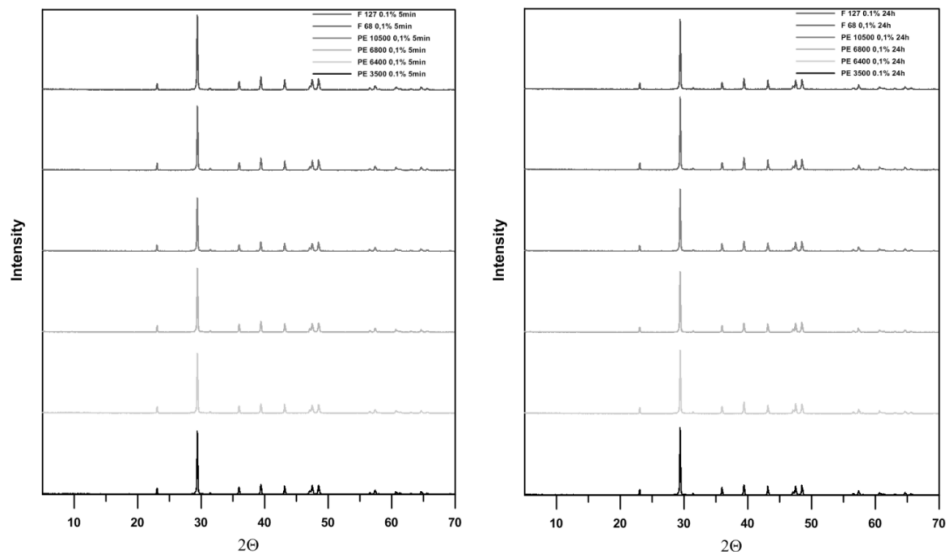
Fig. 6. XRD pattern of calcium carbonate crystals obtained in the presence of PEG with various molecular weights after 5 min and 24 h of precipitation

The BET surface areas and diameters of particles are presented in Table 5. It can be said that the block copolymers significantly influenced the size of obtained $CaCO_3$ particles as well as a specific surface area. After 24 h of precipitation and in the presence of block copolymers, the specific surface area was higher and the value was 0.95, 1.06, 0.91, 1.06, 0.88 and 0.99 for PE 3500, PE 6400, PE 6800, PE 10500, F 68 and F 127, respectively. It can be explained as a result of a morphology and size of calcite particles. After 5 min of crystallization the mean diameters of obtained precipitate was similar to those obtained without copolymers. However, the diameter d_{90} showed that the precipitate contained 90% of particles smaller than about 20 μm in the presence of copolymers. For the sample without modifiers, 90% of particles had a diameter smaller than 40 μm.

Addition of block copolymers led to a decrease in size of particles after 24 h of precipitation. The mean diameter of particle was 12.9, 12.2, 12.7, 11.9, 14.2 and 12.8 μm in the presence of PE 3500, PE 6400, PE 6800, PE 10500, F 68 and F 127, respectively. These values of diameters are similar to those obtained after 5 min of precipitation. This indicates that presence of block copolymers inhibited the growth of calcium carbonates. The molecules of block copolymers adsorb on the surface of particles. Zhao and co-workers (2012) proposed that one EO block of copolymers can adsorb on the crystal, the other is free in water. The free EO block can interact with another crystal and inhibits the growth of $CaCO_3$ in system.

Table 5. Surface areas BET and diameters of calcium carbonate particles precipitated in the presence of block copolymers with various molecular weight. Concentration of the polymer was 0.1 %

Sample name	Time	BET surface area [m^2/g]	d_{10} [μm] no-ultrasound/ ultrasound	d_{50} [μm] no-ultrasound/ ultrasound	d_{90} [μm] no-ultrasound/ ultrasound
PE 3500	5 min	0.64	8.4/7.2	16.2/12.5	28.4/21.4
	24h	0.95	7.6/6.5	15.4/12.9	29.4/22.9
PE 6400	5 min	0.66	7.5/6.4	14.6/11.6	25.6/20.7
	24h	1.06	7.7/6.0	15.6/12.2	28.3/22.3
PE 6800	5 min	0.69	6.6/5.5	13.9/10.8	26.3/19.3
	24h	0.91	8.1/6.5	16.1/12.7	29.0/22.9
PE 10500	5 min	0.73	7.1/5.4	14.5/10.8	26.0/19.5
	24h	1.06	7.4/6.0	14.6/11.9	26.6/21.9
F 68	5 min	0.65	7.4/5.7	14.6/11.5	25.4/20.2
	24h	0.88	9.0/7.2	17.6/14.2	30.9/25.6
F 127	5 min	0.66	6.8/5.4	13.5/10.8	23.7/19.1
	24h	0.99	7.0/6.2	14.7/12.8	27.1/22.8

Conclusion

Organic additives such as polymers, surfactants or low mass small molecules are known to either promote or inhibit crystal growth (Xu et al., 2007). The calcium carbonate crystals precipitated in the presence of block copolymer and poly(ethylene glycol) are calcite. It was observed that molecular mass of copolymers and PEG did not influence the crystalline form of precipitate. Two types of particles morphology was observed in the presence of block copolymers: stacked-rhombus-shaped and rod-shaped. In the case of PEG, only the rhombohedral calcite was obtained. Addition of modifiers reduced the size of crystals after 24 h and slightly increased the value of specific BET surface area. The mechanism of precipitation of calcium carbonate in the presence of PEG and PEO-PPO-PEO block copolymer are the same, because both modifiers contains in their structure EO blocks that can adsorb on the crystal surface and inhibit its growth.

Acknowledgements

References

ADDADI, L., RAZ, S., WEINER, S., 2003, *Taking advantage of disorder: Amorphous calcium carbonate and its roles of biomineralization*, Adv. Mater., 15, 959-970.

BASTRZYK, A., SZELAG, E., POLOWCZYK, I., SADOWSKI, Z., 2012, *Adsorption and co-adsorption of PEO-PPO-PEO block copolymers and surfactants and their influence on zeta potential of magnesite and dolomite*, Physicochem. Probl. Miner. Process., 48, 281-293.

CHIBOWSKI, E., SZCZES, A., HOLYSZ, L., 2005, *Influence of sodium dodecyl sulfate and static magnetic field on the properties of freshly precipitated calcium carbonate*, Langmuir, 21, 8114-8122.

CHEN, Z. Y., NAN, Z. D., 2011, *Controlling the polymorph and morphology of CaCO3 crystals using surfactant mixtures*, J. Coll. Interface Sci., 358, 416-422.

DENG, H., SHEN, X. C., WANG, X. M., DU, C., 2013, *Calcium carbonate crystallization controlled by functional groups: A mini-review*, Front. Mater. Sci. 7, 62–68.

EHRLICH, H., SIMON, P., CARRILLO-CABRERA, W., BAZHENOV, V. V., BOTTING, J. P., ILAN, M., ERESKOVSKY, A. V., MURICY, G., WORCH, H., MENSCH, A., BORN, R., SPRINGER, A., KUMMER, K., VYALIKH, D. V., MOLODTSOV, S. L., KUREK, D., KAMMER, M., PAASCH, S., BRUNNER, E., 2010, *Insights into chemistry of biological materials: Newly discovered silica-aragonite-chitin biocomposites in demosponges*, Chem. Mater., 22, 1462-1471.

EL-SHEIKH, S.M., EL-SHERBINY, S., BARHOUM, A., DENG, Y., 2013, *Effects of cationic surfactant during the precipitation of calcium carbonate nano-particles on their size, morphology, and other characteristic*, Colloids and Surfaces A: Physicochem. Eng. Aspects 422, 44-49.

HERNANDEZ-HERNANDEZ A., VIDAL, M. L., GOMEZ-MORALES, J., RODRIGUEZ-NAVARRO, A. B., LABAS, V., GAUTRON, J., NYS, Y., GARCIA RUIZ, J. M., 2008, *Influence of eggshell matrix proteins on the precipitation of calcium carbonate (CaCO₃)*, J. Cryst. Growth, 310, 1754-1759.

ICHIKAWA, K., SHIMOMURA, N., YAMADA, M., OHKUBO, N., 2003, *Control of calcium carbonate polymorphism and morphology through biomimetic mineralization by means of nanotechnology*, Chem. Eur. J., 9, 3235-3241.

KIM, S., PARK, C. B., 2010, *Dopamine-induced mineralization of calcium carbonate vaterite microspheres*, Langmuir, 26, 14730-14736.

KITAMURA, M., 2002, *Controlling factor of polymorphism in crystallization process*, J. Cryst. Growth, 237-239, 2205-2214.

KURAPATI, R., RAICHUR, A. M., 2013, *Composite cyclodextrin-calcium carbonate porous microparticles and modified multilayer capsules: novel carriers for encapsulation of hydrophobic drugs*, J. Mater. Chem. B, 1, 3175-3184.

MELDRUM, F. C., COLFEN, H., 2008, *Controlling mineral morphologies and structures in biological and synthetic systems*, Chem. Rev., 108, 4332-4432.

POLOWCZYK, I., BASTRZYK, A., KOZLECKI, T., SADOWSKI, Z., 2013, *Calcium carbonate mineralization. Part 1: Effect of poly(ethylene glycol) concentration on the formation of precipitate*, Physicochem. Probl. Miner. Process. 49, 631-639.

SADOWSKI, Z., POLOWCZYK, I., FRACKOWIAK, A., KOZLECKI, T., CHIBOWSKI, S., 2010, *Bioinspired synthesis of calcium carbonate colloid particles*, Physicochem. Probl. Miner. Process., 44, 205-214.

SHESTAK, I. V., VOROBEV, P. D., CHEREDNICHENKO, D. V., VOROBEVA, E. V., BONDAREVA, G. V., STRNADOVA, N., 2011, *Effect of polyacrylic acid and polyethylene glycol on the crystallization of calcium carbonate in the presence of magnesium ions*, Russ. J. Inorg. Chem. 56, 176-180.

SU, Y., YANG, H., SHI, W., GUO, H., ZHAO, Y., WANG, D., 2010, *Crystallization and morphological control of calcium carbonate by functionalized triblock copolymers*, Coll. Surf. A, 355, 158-162.

SZCZES, A., 2013, *Effects of DPPC/Cholesterol liposomes on the properties of freshly precipitated calcium carbonate*, Coll. Surf. B: Biointerfaces, 101, 44-48.

WANG, X., KONG, R., PAN, X., XU, H., XIA, D., SHAN, H., LU, J. R., 2009, *Lysozyme mediated calcium carbonate mineralization*, J. Colloid and Interface Sci., 322, 96-103.

WANG, X., KONG, R., PAN, X., XU, H., XIA, D., SHAN, H., LU, J. R., 2009, *Role of ovalbumin in the stabilization of metastable vaterite in calcium carbonate biomineralization*, J. Phys. Chem. B, 113, 8975-8982.

ZHAO, Y., WANG, X., JIAO, J., WANG, R., YU, L., 2012, *The preparation of calcium carbonate crystals in Pluronic® F68 solution*, J. Molecular Liquids. 169, 144-151.

ZHU, W., LIN, J., CAI, C., LU, Y., 2013, *Biomimetic mineralization of calcium carbonate mediated by a polypeptide-based copolymer*, J. Mater. Chem. B., 1, 841-849.

XIE, A. J., ZANG, C. Y., SHEN, Y. H., QIU, L. G., XIAO, P. P., HU, Z. Y., 2006, *Morphologies of calcium carbonate crystallites grown from aqueous solutions containing polyethylene glycol*, Cryst. Res. Technol., 41, 967-971.

XU, F., XIE, Y., ZHANG, X., WU, C. Z., XI, W., HONG, J., TIAN, X., 2003, *From polymer-metal complex framework to 3D architectures: growth, characterization and formation mechanism of micrometersized α-NiS*, New J. Chem., 11, 1331-1335.

XU, A. W., MA, Y., COLFEN, H., 2007, *Biomimetic mineralization,* J. Mater. Chem., 17, 415-449.

XU, X. R., CAI, A. H., LIU, R., PAN, H. H., TANG, R. K., CHO, K., 2008, *The roles of water and polyelectrolytes in the phase transformation of amorphous calcium carbonate*, J. Cryst. Growth, 310, 3779-3787.

XU, X., ZHAO, Y., LAI, Q., HAO, Y., 2011, *Effect of polyethylene glycol on phase and morphology of calcium carbonate*, J. Appl. Polym. Sci., 119, 319-324.

THIOSULFATE LEACHING OF SILVER FROM A SOLID RESIDUE AFTER PRESSURE LEACHING OF INDUSTRIAL COPPER SULFIDES FLOTATION CONCENTRATES

Katarzyna WEJMAN-GIBAS, Tomasz CHMIELEWSKI, Kamil BOROWSKI, Krzysztof GIBAS, Magdalena JEZIOREK, Jerzy WODKA

Wroclaw University of Technology, Faculty of Chemistry, Division of Analytical Chemistry and Chemical Metallurgy, Wybrzeże Wyspiańskiego 27, 50-370 Wrocław, Poland (tomasz.chmielewski@pwr.edu.pl)

Abstract: Hydrometallurgical recovery of silver from a solid residue after pressure leaching of a flotation copper concentrate from the Lubin Concentrator (KGHM Polska Miedz S.A.) was investigated. Thiosulphate leaching was examined with regard to the highest possible leaching efficiency and optimization process parameters. The effect of thiosulfate ions concentration within the range from 0.25 to 1.00 mol/dm^3 at a constant ammonia concentration, and ammonia concentration within the range from 0.40 to 1.00 mol/dm^3 at a constant thiosulfate concentration on leaching recovery of selected metals were examined. Moreover, the effect of copper(II) ions addition on silver leaching was studied. It was shown that the leaching recovery of silver increased with increasing thiosulfate and ammonia concentration. At the highest thiosulfate ions concentration, the observed silver leaching recovery was 60%. The best results were obtained at an ammonia concentration of 0.80 mol/dm^3, where the leaching recovery of Ag reached 75%. It was established that addition of Cu(II) did not affect silver leaching. Nearly 100% efficiency of thioslulohate silver leaching was achieved by pretreatment of the solid residue after pressure leaching with NaOH solutions.

Introduction

Noble metals such as silver, platinum group metals (PGM) and gold are recovered from primary and secondary resources by means of leaching. The richest sources of these metals, being a feed for leaching, are noble metals ores, by-products of nonferrous metals processing, anodic slimes from copper electroraffination and solid residues from hydrometallurgical circuits. The basic sources of silver are concentrates, scraps, anodic slimes, photographic films, ashes after thermal treatment, jewelry, coins

and metal alloys. The growing silver demand has resulted in an intense development of research for improving existing hydrometallurgical methods of noble metals production (Fleming, 1992; Orab et al., 2014).

Either significant or dominating role of hydrometallurgical unit operations both in production of numerous non-ferrous (Al, Ni, Co, Cu, Zn) and precious metals (Ag, Au, PGE) is an evidence of the essential position and important meaning of chemical methods of metals manufacturing in modern extractive metallurgy (Gupta and Mukherjee, 1990; Habashi, 1999; Chmielewski, 2012; Agacayak, 2014).

The most important operation in hydrometallurgy is leaching of properly prepared raw material by means of a specific chemical compound – leaching agent. Usually the leaching agents and process conditions are selected depending on the type of material and mineralization, in order to selectively and effectively extract the valuable elements to a solution and to avoid emission of dangerous and toxic gases to the atmosphere. Ores and concentrates have different mineralogical and metallic compositions. Zinc, copper, cobalt, nickel, silver, gold and platinum group metals, as valuable metals, are economically important components of polymetallic sulphide materials (Marsden et al., 2003; Ochromowicz and Chmielewski, 2011). The leaching experiments (Everett and Moyes, 1992; Chmielewski, 2009) showed that a shale by-products from the Lubin Concentrator (ZWR Lubin) can be effectively processed using hydrometallurgical methods (thiosulfate atmospheric leaching) in order to recover silver and other accompanying metals.

Leaching of noble metals using oxygenated sodium cyanide solutions was patented in 1887. The major benefit of this method is high selectivity of silver versus gold extraction and very high stability of noble metal-cyanide complexes (Sayiner 2014; Aromaa, 2015). Despite many benefits of cyanide leaching, there is a continuous quest for an alternative method of noble metals recovery, which is characterized by high recovery, selectivity and non-toxicity (Fleming, 2007). Thiosulfate leaching is one of the promising alternative to the cyanide leaching method, with regard to its low toxicity and high efficiency of ores and concentrates leaching. Another benefit of this method is relatively low price of chemical agents used as the leaching medium in the process (Briones and Lapidus, 1998; Mahmoud 2015).

Berezowsky and Sefton (1979) investigated silver recoveries from oxidation leach residues of copper sulfide concentrates in different leaching systems, including cyanide, thiourea, chloride and thiosulfate solutions. The results of thiosulfate leaching showed that the presence of copper in the solution enhanced silver extraction and the chemical behavior of copper ions in this system is very complex (Kerley, 1981). Li et al. (1995) found that thiosulfate ions stabilized silver in the soluble form in the solution, while ammonia and copper accelerated the leaching reaction. The oxidation state of copper in the thiosulfate leaching solutions are of the critical importance for the silver leaching process. Moreover, it is necessary to keep the proper molar ratio of ammonia to thiosulfate to enhance the leaching. To the contrary, the copper might be stabilized in Cu(I) and Cu(II) oxidation states, reducing its ability to

catalyze the silver leaching reaction. Research priorities should be focused on the detailed description of reactions involved and should determine the role of different copper complexes in establishing the optimum molar ratio between ammonia, thiosulfate and copper complexes (Flett et al., 1983; Wassink, 2011; Deutsch and Dreisinger, 2013).

The objective of this study was to examine the thiosulfate leaching recovery of silver from a solid residue after pressure leaching of the copper flotation concentrate from Lubin Concentrator (KGHM Polska Miedz S.A.). Effect of the dose of ammonia, copper and thiosulfate ions on silver recovery was investigated.

Experimental

The leaching feed in the study was a commercial flotation copper sulfide concentrate produced at the Lubin Concentrator (KGHM Polska Miedz S.A.). The concentrate contained copper and other metals, such as Zn, Co, Ni, Ag, V, and Mo, which significantly increase the value of this material. A continuously decreasing copper concentrate grade, high content of organic carbon, presence of lead and arsenic, make the concentrate a potential and suitable feed for hydrometallurgical treatment. The Lubin concentrate is a polymetallic and polymineral material (Grotowski, 2007; Chmielewski, 2012). The chemical composition of Lubin flotation concentrate (KLE) is presented in Table 1. The concentrate has a unique mineralogy. Copper is mainly present in two easy-to-leach sulfides, that is bornite and chalcocite. Furthermore, a significant amount of pyrite additionally enhances the copper leaching rate by galvanic effects (Chmielewski, 2012).

A series of thiosulphate leaching experiments was conducted. The effect of thiosulfate ammonia copper ions concentration on silver leaching efficiency was examined. In addition, the effect of solid residue modification in NaOH solutions was investigated. The leaching experiments were conducted in a stirred glass reactor immersed in a water bath with controlled temperature. The agitation rate of 400 min^{-1} was kept in all experiments. All experiments were carried out at room temperature. The leaching reactor was equipped with a condenser, to avoid rapid vaporization of the leaching agent. The density of the leaching slurry was expressed as a solid-to-liquid phase ratio (g/cm^3).

During each leaching experiment, samples of the slurry were taken from the reactor and filtered for analysis of metals concentration, using the Atomic Absorption Spectroscopy (AAS) technique. The leaching efficiency was evaluated by determining metals recoveries according to the formula:

$$R_{\%} = \frac{c \cdot V}{m \cdot \alpha} \cdot 100\% , \qquad (1)$$

where:

$R_{\%}$ metal leaching recovery, %
C metal concentration in the solution, g/dm^3 (mg/dm^3)
V leaching solution volume, dm^3
M mass of the concentrate, g
A metal content in the concentrate, % (g/Mg).

The subject of this study was a solid residue after pressure leaching of the commercial flotation sulfide concentrate produced at the Lubin Concentrator (KGHM Polska Miedz S.A.). To obtain the solid residue, the KLE sample of the concentrate was initially leached with sulfuric acidic under hydrothermal oxygenated conditions. The parameters of pressure leaching process were: time 2 hours, O$_2$ partial pressure 0.75 MPa, solid-to-liquid ratio (s/l) 1:10, temperature 140 °C, agitation rate 400 min^{-1}, and H$_2$SO$_4$ initial concentration of 120 g/dm^3. Table 2 presents the chemical composition of the solid residue after pressure leaching.

In the final step of thiosulfate leaching experiments, the recovery of silver and accompanying metals were evaluated for leaching of solid residue previously pretreated with NaOH solution. The pretreatment process parameters were: temperature 95 ºC, time 3 hours, NaOH concentration of 100 g/dm^3, solid-to-liquid ratio 1:6. The chemical composition of solid residue was presented in Table 3.

Table 1. Chemical composition of a commercial Lubin flotation concentrate (KLE)

Cu %	Zn %	Ni g/Mg	Co g/Mg	Fe %	Pb %	Ag g/Mg	As %	V g/Mg	Mo g/Mg	S %	C $_{org}$ %
12.9	0.74	49	148	7.6	5.42	455	0.165	657	272	13.34	9.44

Table 2. Chemical composition of solid residue after pressure leaching of Lubin concentrate KLE

Cu %	Zn %	Ni g/Mg	Co g/Mg	Fe %	Pb %	Ag g/Mg
1.44	0.092	178	345	0.92	8.00	380

Table 3. Chemical composition of solid residue after pressure leaching of Lubin concentrate followed by pretreatment with NaOH

Cu %	Zn %	Ni g/Mg	Co g/Mg	Fe %	Pb %	Ag g/Mg
2.22	0.14	5.31	274	1.43	12.30	585

Results and discussion

The effect of thiosulfate ions concentration on Ag and Cu leaching was investigated for four different thiosulfate concentrations (0.25, 0.50, 0.75 and 1.00 mol/dm^3). The leaching experiments were conducted at 25 ^{o}C and the leaching time was 6 hours. Figures 1 and 2 show the changes in Ag and Cu leaching recovery during the leaching process at various thiosulphate concentrations.
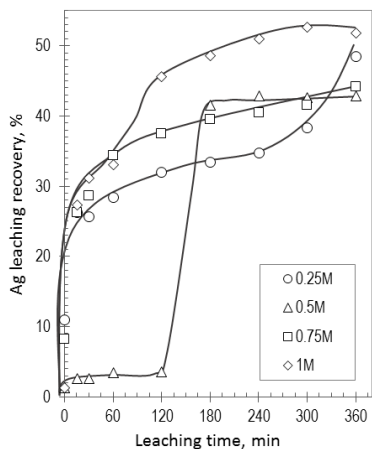
Fig. 1. Effect of thiosulfate ions concentration on Ag recovery; s/l = 1:10, initial NH$_3$ concentration 0.6 mol/dm^3, temperature 25 ^{o}C
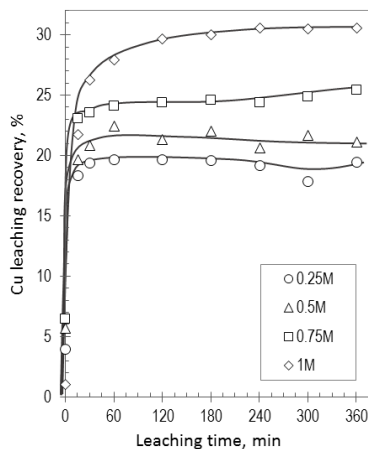
Fig. 2. Effect of thiosulfate ions concentration on Cu recovery; s/l = 1:10, initial NH$_3$ concentration 0.6 mol/dm^3, temperature 25 ^{o}C
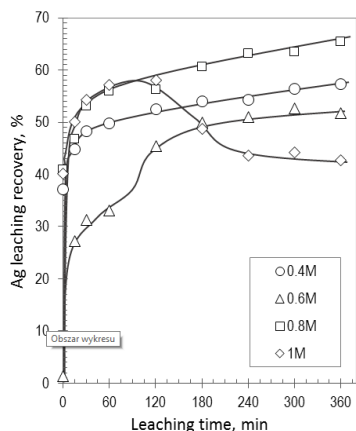
Fig. 3. Effect of ammonia ions concentration on Ag recovery; s/l = 1:10, initial S$_2$O$_3^{2-}$ concentration 1.0 mol/dm^3, temperature 25 ^{o}C
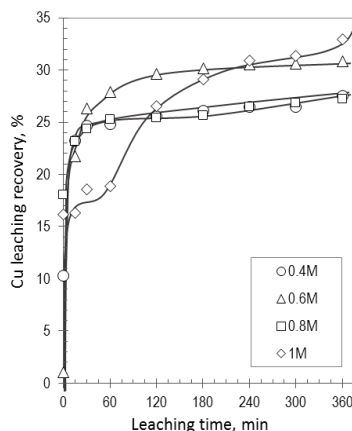
Fig. 4. Effect of ammonia ions concentration on Cu recovery; s/l = 1:10, initial S$_2$O$_3^{2-}$ concentration 1.0 mol/dm^3, temperature 25 ^{o}C

The observed leaching results show that with increasing thiosulfate ions concentration the leaching efficiency increases for both Ag and Cu. At the highest thiosulfate ions concentration the leaching recoveries of Ag and Cu were 60 and 35%, respectively. It confirms the possibility of thiosulfate leaching application for silver extraction.

The effect of Cu(II) ions addition on silver leaching from solid residue after pressure leaching was investigated at thiosulfate and ammonia concentrations of 0.5 and 0.6 mol/dm^3, respectively. The concentration of Cu(II) was 0.1 mol/dm^3. The leaching was conducted at 25°C for 6 hours. The results are presented in Figs. 5-7. The aim of the experiment was to investigate the possibility of enhancing the leaching efficiency of silver by copper(II) ions addition to the leaching solution.
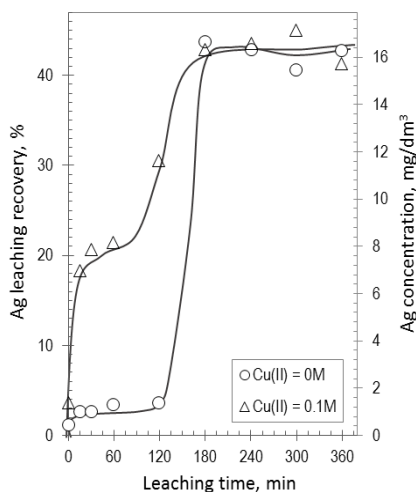
Fig. 5. Effect of addition of Cu(II) on Ag recovery; s/l = 1:10, initial NH$_3$ concentration 0.6 mol/dm^3, initial S$_2$O$_3$$^{2-}$ concentration 0.5 mol/dm^3, temperature 25 ^{o}C

The obtained results show that the addition of Cu(II) did not affect the final silver concentration and recovery. However it had a significant effect on the initial silver leaching rate. It can be concluded that Cu(II) is not needed in the process.

In the leaching experiments conducted with thiosulfate ions, the course of the process was investigated under the most optimum conditions, determined from the previous investigation of solid phase pretreated with NaOH. The parameters of modification process were as follows: NaOH concentration of 2.5 mol/dm^3, temperature 95°C, time 3 hours, s/l ratio 1:6. The purpose of this process was to liberate the silver-bearing grains by dissolution of argentojarosites (Patino et al., 2010). The process occurs according to the following reaction:

$$AgFe_3(SO_4)_2(OH)_{6(s)} + 4OH^- \rightarrow Ag(OH)_{(s)} + 3Fe(OH)_{3(s)} + 2SO_4^{2-}{}_{(aq)} . \qquad (1)$$
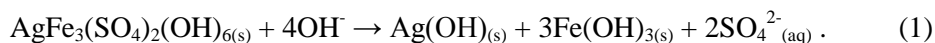
It was expected, that silver liberation from argentojarosites would allow to maximize the leaching recovery of metal in thiosulfate leaching. The mass decrease of a solid after chemical modification with NaOH was about 35%.
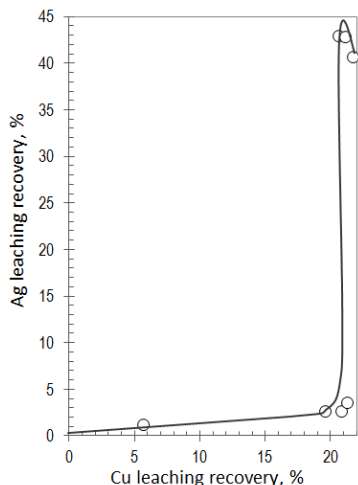
Fig. 6. Ag recovery vs. Cu recovery in thiosulfate leaching without addition of Cu(II) ions; s/l = 1:10, initial NH_3 concentration 0.6 mol/dm^3, initial $S_2O_3^{2-}$ concentration 0.5 mol/dm^3, temperature 25 ^{o}C
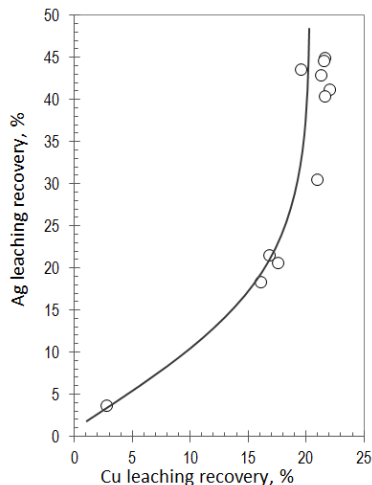
Fig. 7. Ag recovery vs. Cu recovery in thiosulfate leaching with addition of 0.1 mol/dm^3 Cu(II) ions; s/l = 1:10, initial NH_3 concentration 0.6 mol/dm^3, initial $S_2O_3^{2-}$ concentration 0.5 mol/dm^3, temperature 25 ^{o}C

In the closing stage of the experiments regarding thiosulfate leaching, the leaching recovery of silver and copper from pretreated solid residue were determined. The leaching experiments were conducted at the optimum parameters, which were: thiosulfate ions concentration 1.0 mol/dm^3, ammonia concentration 0.8 mol/dm^3, temperature 25°C, time 6 hours. Figures 6 and 7 present the results.

From Figures 8-10 it is clearly seen that solid residue modification with NaOH allowed to extract almost 100% of silver in thiosulfate leaching after 4 hours. It proves the hypothesis that silver is locked inside the jarosites structure in the solid residue after pressure leaching. The leaching recovery of copper reached 20 % after 6 hours, while other accompanying metals such as Ni and Co did not leach into the solution. The leaching curves of Ni and Co are not given in the paper, as the efficiency was close to 0%. The chemical composition of solid residue after thiosulfate leaching was presented in Table 4.
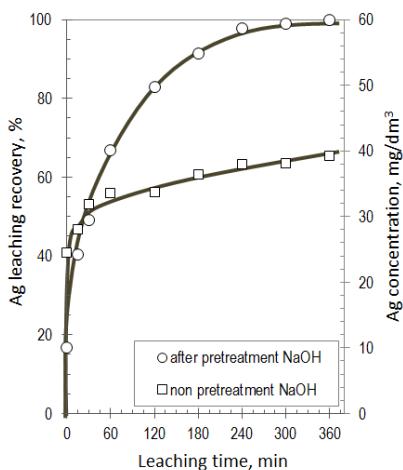
Fig. 8. Effect of NaOH modification on Ag recovery; s/l = 1:10, initial NH_3 concentration 0.8 mol/dm^3, initial $S_2O_3^{2-}$ concentration 1.0 mol/dm^3, temperature 25 ^{o}C
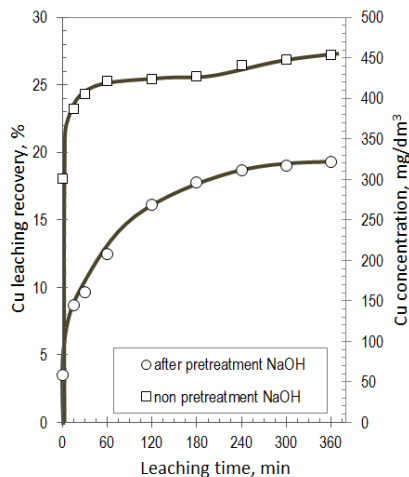
Fig. 9. Effect of NaOH modification on Cu recovery; s/l = 1:10, initial NH_3 concentration 0.8 mol/dm^3, initial $S_2O_3^{2-}$ concentration 1.0 mol/dm^3, temperature 25 ^{o}C
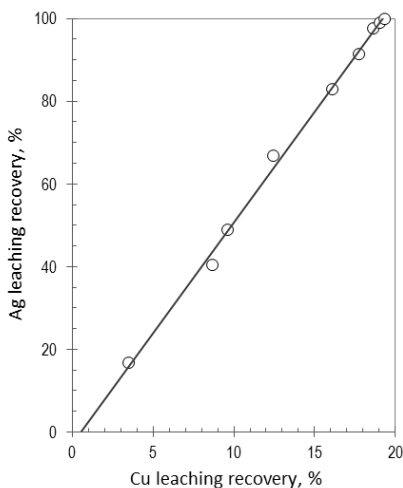
Fig. 10. Ag recovery vs. Cu recovery in thiosulfate leaching after modification with NaOH; s/l = 1:10, initial NH_3 concentration 0.8 mol/dm^3, initial $S_2O_3^{2-}$ concentration 1.0 mol/dm^3, temperature 25 ^{o}C

Table 4. Chemical composition of solid residue after thiosulfate leaching

Cu %	Zn %	Ni g/Mg	Co g/Mg	Fe %	Pb %	Ag g/Mg
1.96	0.12	4.65	233	1.25	6.34	5.15

Conclusions

The results of silver and accompanying metals leaching from a solid residue after pressure leaching of the Lubin flotation concentrate (KGHM Polska Miedz S.A.), with concentrated thiosulfate solutions, indicate the possibility of effective silver extraction into the solution. The leaching efficiency of other metals (Cu, Ni, Co) in thiosulfate solutions is relatively low, resulting in poor leaching recoveries.

The results of leaching experiments of solid residue from pressure leaching pretreated with NaOH solutions show, that thiosulfate is very efficient in silver leaching from modified solid residues from pressure leaching with oxygenated sulfuric acid. The leaching recovery of silver reached nearly 100% after 4 hours of thiosulfate leaching at 25 ºC. However, the pretreatment process with NaOH resulted in poor copper leaching efficiency and caused total inhibition of Ni and Co leaching.

Acknowledgements

References

AGACAYAK T., ARAS A., AYDOGAN S., ERDEMOGLU M., 2014. *Leaching of chalcopyrite concentrate in hydrogen peroxide solution*, Physicochemical Problems of Minerals Processing 50(2), 657-666.

AROMAA J., RINTALA L, KAHARI M., FORSEN O, 2015. *Dissolution of gold with cyanide replacing reagents*, Physicochemical Problems of Minerals Processing 51(1), 269-279.

BACHOWSKI C., STASZAK J., BYSZYŃSKI L., BOCZAR W., TEODORSKI D., 2003. *Search for alternative methods of processing of copper ores in KGHM „ Polska Miedz'' S.A. – hydrometallurgical technologies,* VIII Seminar „Hydrometallurgy of Sulphide Copper Resources'', Lubin, June 26. 2003: 125, (In Polish).

BEREZOWSKY R.M.G.S., SEFTON V.B., 1979. *Recovery of Gold and Silver from Oxidized Leach Residues by Ammonia Thiosulfate Leaching*, paper presented at the 108th AIME Annual Meeting, New Orleans, LA, Feb. 18–22.

BRIONES R., LAPIDUS G.T., 1998. *The leaching of silver sulfide with the thiosulfate–ammonia–cupric ion system*, Hydrometallurgy 50, 243–260.

CHMIELEWSKI T., 2007. *Atmospheric leaching of shale by-product from Lubin Concentrator,* Physicochemical Problems of Minerals Processing 41, 337-348.

CHMIELEWSKI T., 2012. *Hydrometallurgy in KGHM Polska Miedź SA – Circumstances, Needs and Perspectives of Application*, Separation Science and Technology 47, 9, 1264-1277.

DEUTSCH J.L., DREISINGER D.B., 2013. *Silver sulfide leaching with thiosulfate in the present of additives Part I: Copper-ammonia leaching*, Hydrometallurgy 137, 156-164.

EVERETT P.K., MOYES A.J, 1992. *The Intec Copper Process, Extractive Metallurgy of Gold and Base Metals*, 26–28 Oct. 1992, 287–292.

FLEMING C.A., 1992. *Hydrometallurgy of precious metal recovery*, Hydrometallurgy 30, 127–162.

FLEMING C.A., 2007. *The Leaching and Recovery of Gold from Ores and Concentrates Section 3 Gold and Silver Recovery*, Lakefield Research Ltd., 20-32.

FLETT D.S., DERRY R., WILSON J.C., 1983. *Chemical study of thiosulfate leaching of silver sulfide*, Trans. Inst. Min. Metall. 92, C216–C223.

GROTOWSKI A., 2007. *Possibilities and perspectives for implementation of hydrometallurgical methods in KGHM Polska Miedz S.A*., Proc.VIII International Conference on Non-ferrous Ore Processing, Wojcieszyce (Poland), May 21–23, KGHM Cuprum Wroclaw 2007: 29.

GUPTA C.K., MUKHERJEE T.K, 1990. *Hydrometallurgy in Extraction Processes, Vol. I and II,* CRC Press: Boca Raton, FL.

HABASHI F., 1999. *Textbook of Hydrometallurgy*, Metall. Extract. Quebec.

KERLEY B.J. JR.., 1981. *Recovery of Precious Metals from Difficult Ores*, U.S. Pat. 4, 269, 622.

LI J., MILLER J.D., WAN R.Y., LE VIER K.M., 1995. *The ammoniacal thiosulfate system for precious metal recovery*, Proceedings of XIX International Mineral Processing Congress 7, 37–42.

MAHMOUD M.H.H., AWAD H.M., ELHABIB O.A., 2015. *Gold leaching from a Saudi ore by the nonpolluting thiosulfate process* Mahmoud, Physicochemical Problems of Minerals Processing 51(1), 59-72.

MARSDEN J., BREWER B., HAZEN N., 2003. *Copper Concentrate Leaching Developments by Phelps Dodge Corporation*, TMS Warrendale, 1429–1446.

OCHROMOWICZ K., CHMIELEWSKI T., 2011. *Solvent extraction in hydrometallurgical processing of Polish copper concentrates*, Physicochemical Problems of Minerals Processing 46, 207-218.

ORABY E. A., BROWNER R. E., NIKRAZ H. R., 2014. *Effect of silver in thiosulfate leaching of gold-silver alloys in the presence of copper and ammonia relative to pure gold and silver*, Mineral Processing & Extractive Metall. Rev., 35: 136–147.

PATINO F., ROCA A., REYES M., CRULLS M., RIVERA I., HERNANDEZ E.H., 2010. *Kinetic modeling of the decomposition and cyanidation of argentojarosite*, Journal of the Mexican Chemical Society 54(4), 216-222.

SAYINER B., 2014. *Influence of lead nitrate on cyanide leaching of gold and silver from Turkish gold ores,* Physicochemical Problems of Minerals Processing 50(2), 507-513.

WASSINK B., 2011. *Analysis for Thiosulfate in the Presence of Sulfite, Sulfate, Copper(II) and Ammonia-Ammonium Buffer*, University of British Columbia, 19-25.

ANALYSIS OF PROCESS OF REMOVING IMPURITIES FROM CALCIUM CARBONATE

Damjan HANN, Joze KORTNIK

University of Ljubljana, Faculty of Natural Sciences and Engineering, Department of Geotechnology and Mining, Askerceva 12, 1000 Ljubljana, joze.kortnik@guest.arnes.si

Abstract: Calcium carbonate is used as an additive in the production of paper and some other production processes. The aim of this study was to determine the chances of the calcite sample to be mechanically cleaned of impurities, so that the material can become commercially interesting, primarily to be sold to the paper and other-related industries. A mineralogical petrographic investigation carried out on a sample of calcite showed that an unfavorable impurity is, in particular, graphite – which is otherwise fairly easily to remove by flotation. Flotation was performed with samples of different particle size. The purpose of this was to find an optimal particle size for carrying out the flotation. In order to achieve an effective flotation results it is first necessary to achieve a proper liberation of grains. The second part of the study was to explore the optimal sequence of treatment procedures for tested calcite, using milling, flotation, and sedimentation.

Keywords: calcium carbonate, flotation of graphite, ISO brightness

Introduction

Some of the minerals are used as additives in the production of paper and other production processes. For instance, in paper industry some raw materials are used for coatings and as fillers. Fillers are the most significant portion of additives in this industry, in terms of percentage of weight (Gaudreault et al., 2009). Typical filler additions range from 3% to 30 % (Scott, 1996). One of these is calcium carbonate (Gronfors, 2010), which has been eagerly researched as an essential material used for industrial products over the past years (Kadota et al., 2014; Chikazawa and Fuji, 2001). White inorganic materials are added to paper to improve the printability of the surface, opacity, brightness, and the smoothness of paper (Kirwan, 2013).

Mineral resources extracted from deposits usually do not occur alone, but contain impurities in variable proportions. Impurities may affect the color of raw material, so

it is usually necessary to mechanically and chemically remove impurities before the application of useful substances.

The chemical treatment is often an environmentally unfriendly process, resulting in various unfavorable effects on the product, e.g. an unpleasant smell. Thus, it is desirable for the mineral raw material to be as mechanically cleaned of impurities as possible before going through the optional chemical treatment.

Due to differences in the composition of ore in different seams with the same mineral resource, and also because of such differences within a given deposit, it is necessary to adapt an ore preparation procedure to meet the specific requirements. We therefore need to optimize already in practice well-known technological processes, depending on the type and proportion of useful substances and impurities. This practically means that procedure, adapted to the specific requirements of the mineral resource, is original.

The aim of this study was to determine the possibility of removing some of the impurities from calcite samples with the use of mechanical cleaning methods. We were especially focused on removing graphite (Wakamatsu and Numata, 1991) in order to make the final product useful for the paper, paint, adhesives, sealants and similar industries. Other authors also acknowledge the problem of graphite occurrence in raw materials, especially its negative impact on the color of useful substances and write about ways for its removal in their articles. Raghavan et al. (1992), for instance, in the article on processing kaolin contaminated with small amounts (0.1-0.3%) of graphitic impurities, reported that the beneficiation technique based on froth flotation was successfully used for the removal of ultrafine graphite particles.

Material and experimental procedures

A mineralogical and petrographic investigation was carried out on a sample of calcite, the purpose of which was to determine mineral composition of the calcite sample, with a focus on determining the presence of undesirable impurities.

The sample was used for making a standard petrographic thin section for optical microscopic analysis. The analysis of impurities was made with a scanning electron microscope (SEM) with backscattered electrons (BSE) in a high vacuum. For this purpose the surface of the sample was smooth yet not polished. A semi-quantitative chemical composition was determined on the basis of the X-ray spectra of characteristic Kα radiation at 20 kV accelerating energy (EDS-Energy Dispersive System).

The sample was homogeneous, with a uniform light gray color. Microscopic analysis showed that it was a calcite marble. The visual assessment of the quantity of non-carbonate inclusions was 2%. Practice shows that the color of the marble depends on impurities; the more impurities, the more colored they are.

The following impurities were determined in the calcite (listed with decreasing frequency): opaque minerals, especially graphite (Fig. 1), quartz, white mica,

feldspars, dolomite, titanite, chlorite, and biotite. Grains of pyrite and iron oxides were also present. Quartz, mica, iron oxides and pyrite appeared in approximately equal ratios. In the process of obtaining a suitable calcite flour it was necessary to remove the graphite, as well as Fe-oxides, and pyrite, which slightly color flour to gray when milling.
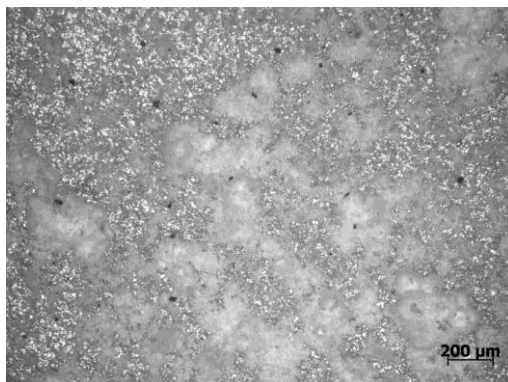
Fig. 1. Black graphite particles in calcite marble

The mineralogical petrographic analysis of the sample of calcite showed that it is necessary to pay particular attention to the removal of graphite components in calcite, as their effect on the color of calcite flour according to the properties of graphite itself and its share in the sample is dominant. Due to the fact that graphite has electrostatic properties (Taylor, 1988) the first association was electrostatic separation of graphite from the other components in the corona field.

The sample for the test with electrostatic separator mark "Krupp" was prepared in an appropriate particle size range: 0.1 to 3 mm as required by the manufacturer of the device in order to achieve the proper results. The separator should have separated the electrically conductive components of the sample from the electrical non-conductive, but we did not get the desired result. The reason for this was that the graphite particles had a diameter of only a few micrometers, and were thus at the particle size at which we wanted to separate them, still joined together with calcite. The electrostatic separator recognized most of the particles as electrically non-conductive, therefore we did not carry out further research with this equipment.

The next procedure with which we wanted to remove the graphite components out of calcite marble was flotation. This physicochemical process of separation of various minerals exploits the hydrophobic and hydrophilic properties of the separated components and is among beneficiation methods the most often used because of its superior efficiency (Drzymala, 2007; Ahmed et al., 2013). Graphite is quite hydrophobic (Du, 2008), and relatively easy to separate with the flotation. Naturally hydrophobic minerals are not easily wetted with water due to the low polarity of their

surfaces. With the appropriate reagents added the efficiency of the procedure only increases.

Before carrying out the flotation we crushed and milled calcite sample. Then analyses (Table 1) of the particle size with a Sympatec Helos H2070 particle size analyzer as well as analyses of the ISO brightness R_{457} of the samples with a Datacolor Elrepho SF450X spectrophotometer were performed.

Table 1. Particle size and ISO brightness R_{457} of the samples before the flotation

Sample	d_{50}/d_{98} (μm)	R_{457} (%)
Sample 1 (basic milling)	41.52/211.50	76.95
Sample 2 (1 min of additional milling)	26.61/189.50	76.36
Sample 3 (5 min of additional milling)	5.99/51.48	78.13
Sample 4 (15 min of additional milling)	3.69/46.92	77.42
Sample 5 (30 min of additional milling)	2.74/33.51	75.95

The flotation of graphite was carried out with the flotation cell of the type "Denver" (Fig. 2). 1.2 dm^3 of water with a pH value between 7.5 and 8 was poured in the flotation cell container. An adequate pH was achieved by the stepwise addition of NaOH and stirring. Kerosene (500 g/Mg) was added as a collector in the slightly alkaline water (Kaya and Canbazoglu, 2007). The kerosene and water solution was stirred for about 1 minute at 1,300 rpm, and then 150g of calcite was added. Also, a frother was added - pine oil (100 g/Mg) before the air vane was opened. The relatively high hydrophobicity of graphite made it possible to begin flotation immediately. Graphite particles were raised by the air bubbles to the surface and ended up in the overflow. With a frother added we achieved stable froth, eliminated the additional amount of graphite, and thus increased the efficiency of flotation.

Fig. 2. Flotation of graphite with the flotation cell "Denver"

The flotation process was performed using samples of different particle size. The purpose of this was to find the optimal particle size for carrying out the flotation. For effective flotation it is first, as in all other cases of mineral dressing, necessary to achieve the proper liberation of grains by crushing and milling. However, when the material is crushed and milled two problems arise. First, the milling of the material results in attrition between the calcite and graphite particles which consequently leads to undesired coloring of the calcite surfaces. Another problem is linked to the flotation process, more precisely to the flotation of fine grains. When floating extremely small grains the ratio between the number of air bubbles and the number of particles of the floated component is markedly in favor of the latter, and so the flotation process may not be effective. The problem of the fine particles flotation is also weak collision of the fine particles with bubbles (Sahbaz et al., 2012).

Results and discussion

After the flotation process was carried out, the samples were dried, and re-analysis of the ISO brightness followed. Before carrying out the flotation, the initial samples had the R_{457} values in the range between 76% and 78%, and the minimum value was found in Sample 5 (Table 1).

Table 2. ISO brightness R_{457} of the samples after flotation

Sample	R_{457} (%)	ΔR_{457} before and after flotation (%)
Sample 1	81.81	4.86
Sample 2	82.66	6.30
Sample 3	84.94	6.81
Sample 4	86.04	8.62
Sample 5	83.97	8.02

The highest value and the greatest progress of ISO brightness R_{457} after the flotation were found in Sample 4 (Table 2). This sample had a mean particle size prior to flotation of $d_{50} = 3.69$ μm. From the ISO brightness R_{457} of samples after flotation it can be assumed that with Sample 4 an adequate liberation of grains was achieved and separating process was successfully carried out. At the same time milling was not so long-lasting that would result in excessive attrition between graphite and calcite grains and coloring of the latter.

Considering that, usually one and the same material has different optical properties with different grain sizes, flotation products were milled to a comparable size. Sample 5 with the median particle size $d_{50} = 2.74$ μm, represented the reference point and was

not milled further. Other samples were milled in two stages. The first stage lasted for 12 min and the second stage an additional 30 min.

After the first stage of milling ISO brightness improved somewhat for most samples (Table 3), which can be attributed to the emergence of new calcite surfaces. After the final milling to a comparable size, the ISO brightness had somewhat deteriorated (Table 4). The milling does, however, still open new surfaces of calcite, which improves optical properties. At the same time the liberated graphite grains cause the calcite surfaces to re-color due to attrition.

Table 3. Particle size and ISO brightness R_{457} of the samples after the first stage of additional milling (12 min)

Sample	d_{50}/d_{98} (μm)	R_{457} (%)
Sample 1	9.53/51.51	83.38
Sample 2	6.37/54.70	85.87
Sample 3	4.29/53.98	86.10
Sample 4	3.44/42.22	85.82

Table 4. Particle size and ISO brightness R_{457} of the samples after the second stage of additional milling (30 minutes, Sample 5 – no additional milling)

Sample	d_{50}/d_{98} (μm)	R_{457} (%)
Sample 1	2.85/49.31	81.33
Sample 2	2.85/51.83	80.06
Sample 3	2.55/44.72	84.02
Sample 4	2.52/42.70	83.86
Sample 5	2.74/33.51	83.97

After completing the optimization, the purpose of which was to find a suitable particle size to carry out the flotation, we wanted to check the optimal sequencing of treatment procedures for calcite sample. As shown in Fig. 3, the procedures consisted of milling, flotation, and sedimentation followed by centrifugation. Sedimentation was performed with the sample manually mixed in the water. The heavier grains first sediment to the bottom of the vessel, after that the water was removed by a centrifuge. For the further process only the top – the clean part of the sample was used, while the lower part with heavier grains such as pyrite and other iron minerals was discarded. The clean part of the sample represented approximately 80% of the initial sample. As can be seen from the scheme we also tried with a two-stage flotation.
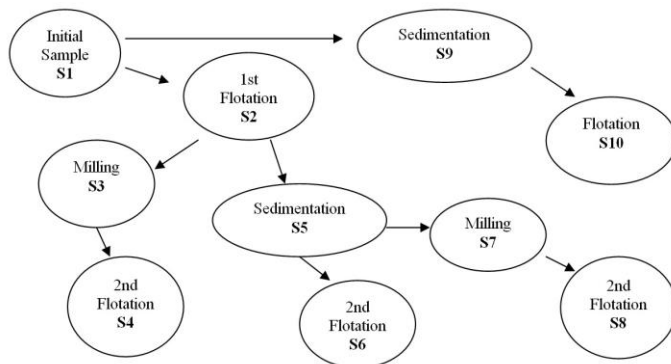
Fig. 3. Sequencing of treatment procedures

Sample S1: initial sample
Sample S2: floated
Sample S3: floated, milled
Sample S4: floated, milled, again floated
Sample S5: floated, sedimented
Sample S6: floated, sedimented, again floated
Sample S7: floated, sedimented, milled
Sample S8: floated, sedimented, milled, again floated
Sample S9: sedimented
Sample S10: sedimented, floated

Table 5. Particle size and ISO brightness R_{457} after completion of the cleaning procedures

	Sample									
	S1	S2	S3	S4	S5	S6	S7	S8	S9	S10
d_{50} (µm)	4.16	-	2.46	-	-	-	2.56	-	-	-
d_{98} (µm)	83.74	-	29.55	-	-	-	26.87	-	-	-
R_{457} (%)	75.57	80.9	81.98	81.59	82.05	81.26	82.82	82.33	76.05	82.46

The results of the analysis (Table 5) indicate that a multi-stage flotation did not bring the desired progress of the ISO brightness of the samples. Twicely floated Sample S4 didn't have higher ISO brightness than the once floated Sample S2. After the second flotation the samples had actually lower values of ISO brightness than after the first flotation. This is partly due to the impact of the reagents used for the flotation. As has already been stated, the most problematic mineral with regard to the optical properties in the tested material was graphite, so that the removal of heavy minerals with sedimentation presented much smaller progress compared to the flotation process. Sample S9 with ISO brightness $R_{457} = 76.05\%$ showed only a minor improvement in regard to the measured parameter in comparison to initial Sample S1

with $R_{457} = 75.57\%$. In the case of different sequencing of the same procedures, sedimentation prior to flotation proved to be the better option – once heavy particles are eliminated, flotation is more effective than with the presence of heavy particles.

Conclusions

We wanted to clean calcite sample from impurities, particularly graphite, which was exposed in the test material as the main cause of the coloring of the calcite. The aim was examining the potential use of the tested calcite in the paper industry, as well as in industries like the paint, adhesive, and sealant. In doing so, we tried to get the highest possible level of ISO brightness, while the recovery has not been a priority concern.

At first, due to electrical conductivity of graphite, the electrostatic separation of graphite from other material was used. However, the process was not successful, because on one hand the lower limit of separating with the equipment that we have is about 100 μm, and on the other hand graphite particles in the tested material had a diameter of only a few microns.

Removal of the graphite was then undertaken using the flotation process, in which ore is separated on the basis of the hydrophobicity and hydrophilicity of the separated components. Graphite is a naturally hydrophobic, and with the addition of suitable reagents the efficiency of the process can be additionally increased.

Monitoring the process of separation of impurities from calcite was carried out by determining the ISO brightness R_{457}. The initial values of R_{457} were between 76% and 78%, while the required minimum value in the paper industry is about 94%. For the production of paints the minimum limit is approximately 90%.

Samples prepared with the different particle size were first floated, and then milled in two stages. ISO brightness R_{457} was determined for the initial sample and for the products, respectively.

The maximum value of ISO brightness R_{457} was measured in Sample 3 after flotation and the first stage of additional milling (initial $d_{50} = 6$ μm, $R_{457} = 86.10\%$, final $d_{50} = 4.3$ μm) as well in Sample 4 after flotation ($d_{50} = 3.7$ μm, $R_{457} = 86.04\%$). The maximum value of ISO brightness R_{457} among the samples, which were milled to a comparable size (about 2.7 μm), was found in "Sample 3" ($d_{50} = 2.55$ μm, $R_{457} = 84.02\%$).

The optimum particle size for carrying out the flotation with the tested material, therefore, was determined, but it may not be equal to the required particle size, which of course, depends on the intended use of material tested.

With the procedures applied we came fairly close to the minimum requirements concerning optical qualities in the aforementioned industries. Further progress in the corresponding values would be possible with the use of chemical procedures.

For comparison, Raghavan et al. (1992) in their article on processing kaolin contaminated with small amounts (0.1-0.3%) of graphitic impurities stated that the beneficiation technique based on froth flotation was successfully used for the removal

of ultrafine graphite particles. The process removed around 70% of graphite, which in the case of ultra-fine particles can be considered a success.

In regards to the most economical and effective sequence of treatment procedures for the tested material, the process in which the material is first treated by the gravitational process − sedimentation and followed by the single-stage flotation proved to be most efficient. Flotation in two stages has not proven particularly effective because the graphite was already fairly well removed in the first stage of flotation.

References

AHMED, A. M. H., ALJUHANI, S. M., DRZYMALA, J., 2013, *Flotation after a direct contact of flotation reagents with carbonate particles, Part 1. Model investigations*, Physicochem. Probl. Miner. Proc., 49(2), 713−723.

CHIKAZAWA, M., FUJI, M., 2001, *Nanoparticles of lime and calcium carbonate*, J. Soc. Inorganic Mater., 8, 507-514.

DRZYMALA, J., 2007, *Mineral Processing. Foundations of Theory and Practice of Minerallurgy*, Oficyna Wydawnicza PWr., Wroclaw, http://www.dbc.wroc.pl/Content/2070/Drzymala.pdf.

DU, H., 2008, *Flotation chemistry of selected alkali halide salts and naturally hydrophobic minerals: a molecular dynamics simulation study*, PhD. Thesis. University of Utah, http://books.google.si/books?id=wG2thJzLnfQC&printsec=frontcover&hl=sl&source=gbs_ge_summ ary_r&cad=0#v=onepage&q&f=false.

GAUDREAULT, R., CESARE, N. D., WEITZ, D.,VEN, T. G. M., 2009, *Flocculation kinetics of precipitated calcium carbonate*, Coll. Surf. A: Physicochem. Eng. Aspects, 340, 56-65.

GRONFORS, J., 2010, *Use of fillers in paper and paperboard grades*, http://urn.fi/URN:NBN:fi:amk-2010060811766.

KADOTA, K., FURUKAWA, R., TOZUKA, Y., SHIMOSAKA, A., SHIRAKAWA, Y., HIDAKA, J., 2014, *Formation mechanism of non-spherical calcium carbonate particles in the solution using cluster-moving Monte Carlo simulation*, J .Mol. Liq., 194, 115-120.

KAYA, O., CANBAZOGLU, M., 2007, *A study on the floatability of graphite ore from yozgat akdagmadeni (Turkey)*, http://www.oredressing.net/download.aspx?T=DOC&ID=83.

KIRWAN, M. J., 2013, *Handbook of paper and paperboard packaging technology*, John Wiley & Sons, Bognor Regis, 432 pp.

RAGHAVAN, P., SIVAM, C., LALITHAMBIKA, M., DAMODARAN, A. D., 1992, *Removal of ultrafine graphite impurities from China clay by floc- flotation*, Int. J. Min. Proc., 36, 51-61.

SAHBAZ, O., ERCETIN, U., OTEYAKA, B., 2012, *Determination of turbulence and upper size limit in Jameson flotation cell by the use of computational fluid dynamic modelling*, Physicochem. Probl. Miner. Proc., 48, 533-544.

SCOTT, W. E., 1996, *Principles of wet end chemistry*, Tappi Press, Atlanta.

TAYLOR, J. B., 1988, *Dry electrostatic separation of granular materials*, http://ieeexplore.ieee.org/stamp/stamp.jsp?tp=&arnumber=25295.

WAKAMATSU, T., NUMATA, Y., 1991, *Flotation of graphite*, Min. Eng., 4, 975-982.

REMOVAL OF PALLADIUM(II) FROM AQUEOUS CHLORIDE SOLUTIONS WITH CYPHOS PHOSPHONIUM IONIC LIQUIDS AS METAL ION CARRIERS FOR LIQUID-LIQUID EXTRACTION AND TRANSPORT ACROSS POLYMER INCLUSION MEMBRANES

Magdalena REGEL-ROSOCKA, Martyna RZELEWSKA, Monika BACZYNSKA, Marta JANUS, Maciej WISNIEWSKI

Poznan University of Technology, Institute of Chemical Technology and Engineering, Berdychowo 4, 60-965 Poznan, Poland, magdalena.regel-rosocka@put.poznan.pl

Abstract: This paper presents an application of three phosphonium ionic liquids for removal of Pd(II) ions from aqueous chloride solutions with liquid-liquid extraction and transport across polymer inclusion membranes (PIM). Trihexyl(tetradecyl)phosphonium chloride and bromide (Cyphos IL 101 and 102) and bis-(2,4,4-trimethylpentyl)phosphinate (Cyphos IL 104) were investigated as carriers of Pd(II) from aqueous chloride media. Extraction of Pd(II) with Cyphos IL 102 has not been previously described in the literature. Cyphos IL 102 used for the first time as metal ion carrier, efficiently extracts palladium(II) ions both with liquid-liquid extraction and PIM. NaCl concentration does not affect Pd(II) extraction with Cyphos IL 102, while increasing HCl content in the feed aqueous phase causes decrease in extraction efficiency. Stripping of Pd(II) with 0.5 M NH_4OH is efficient (84 to 90%) and the organic phase after stripping could be reused for extraction. For PIM transport the highest values of the normalized initial flux are obtained for CTA membrane containing Cyphos IL 101 and a receiving phase: mixture 0.1 thiourea + 0.5 M HCl. It is indicated that initial flux does not determine the final result of the transport through the membranes because from the separation point of view, the most important is a complete transport of the solute to the receiving phase, described by the Pd(II) recovery factor.

Introduction

Platinum group metals (PGMs) form a group of precious metals consisting of six elements: ruthenium, rhodium, palladium, platinum, osmium, and iridium. Palladium is a heavy metal, and its extraction from various industrial solid wastes is important

from an economical and environmental point of view. Palladium is a valuable element (888 $/oz, July 2014) and has wide applications in the manufacturing of catalysts in oil refineries, petrochemical industry, jewelry and electronics (Najafi et al., 2013; Swain et al., 2010). An important way to obtain noble metals (e.g. palladium) is to recover them from sources such as used catalysts, electronic scraps, anodic mud, etc. Pyrometallurgical methods have always been used for PGMs separation. However, recently growing popularity of hydrometallurgical methods is noticed for recovery of noble metals, mainly from aqueous chloride solutions (Willner and Fornalczyk, 2012). Moreover, hydrometallurgical processes are preferred as energy-saving ones (Akita et al., 1996; Kargari et al., 2006).

Solvent extraction (SX) is a favorable method for removal of PGMs from sources containing low concentrations of these metals, because it offers a number of advantages such as high selectivity and metal purity. Among conventionally used PGMs extractants are alkyl derivatives of aliphatic amines and quaternary ammonium salts (Lee et al., 2009; Najafi et al., 2013), pyridine derivatives (e.g. ACORGA CLX 50) (Regel-Rosocka et al., 2007), phosphoroorganic extractants (e.g. Cyanex 921 or 923) (Gupta and Singh, 2013; Nowottny et al., 1997) and hydroxyoximes (Reddy et al., 2010). Moreover, some acyclic analogues of thiacalix[4]arenes (Torgov et al., 2013), malonamide derivative (e.g. DMDOHEMA) (Poirot et al., 2014), thiodiglycolamide derivative (Paiva et al., 2014) and phosphonium ionic liquids (Cieszynska and Wisniewski, 2010) were investigated. Phosphonium ionic liquids (IL) have been proposed as a new group of solvents for separation processes both in extraction and adsorption systems (Cieszynska and Wisniewski, 2011; Guibal et al., 2008; de los Rios et al., 2012).

Looking for environmentally friendly separation techniques, many researchers have proposed transport across polymer inclusion membranes (PIMs) for separation of metal ions and small organic compounds as an alternative to SX (Kogelnig et al., 2011; Martak and Schlosser, 2006; Regel-Rosocka et al., 2012). PIMs are formed by casting a solution containing an extractant, a plasticizer and a base polymer (Ines et al., 2012; Nghiem et al., 2006). Up to now, PIMs are reported to be applied for separation processes including transport of precious metals, lanthanides, alkali metals, heavy metals such as Pb(II), Zn(II) or Cd(II) (Ines et al., 2012; Nghiem et al., 2006; Pospiech, 2013; Ulewicz and Radziminska-Lenarcik, 2012).

The aim of this work is to compare three phosphonium ionic liquids, for the first time tributyl(tetradecyl)phosphonium bromide (Cyphos IL 102), for the removal of Pd(II) from aqueous chloride solutions with liquid-liquid extraction and transport across polymer inclusion membranes.

Experimental

Materials

Three phosphonium ionic liquids, i.e. trihexyl(tetradecyl)phosphonium chloride and bromide (Cyphos IL 101 and 102) and bis-(2,4,4-trimethylpentyl)phosphinate (Cyphos IL 104) supplied by Cytec Industry Inc. (USA) were used as extractants or carriers for SX or PIM separations. Other organic compounds, i.e. cellulose triacetate (CTA), o-nitrophenyloctyl ether (NPOE), dichloromethane (DCM) were of analytical grade and used without further purification.

Liquid-liquid extraction procedure

The model aqueous solutions for extraction contained: $1 \cdot 10^{-3} - 5 \cdot 10^{-3}$ M Pd(II) in 0.1 M HCl with and without NaCl, $2.5 \cdot 10^{-3}$ M Pd(II) in 0.1; 1; 3 or 5 M HCl (ionic strength I = 5 M), $2.5 \cdot 10^{-3}$ M Pd(II) in 0.1 M HCl with 1; 3 or 5 M NaCl. $5 \cdot 10^{-3}$ M solution of extractant (Cyphos IL 102) in toluene was used as the organic phase.

Extraction has been carried out in a typical way: equimolar aqueous feeds containing metal ions added as chlorides were mechanically shaken with IL phase (volume ratio w/o = 1) for 20 min at 22 ± 2 ºC in glass separation funnels and then allowed to stand for phase separation. Studies of extraction time were carried out in the time range from 1 to 60 min. Stripping of metal ions from the loaded organic phases was carried out with 0.5 M NH$_4$OH solution, at volume ratio w/o = 1 for 10 minutes at 22 ± 2 ºC in glass separation funnels.

Transport across polymer inclusion membranes

Model aqueous feed contained $5 \cdot 10^{-3}$ M PdCl$_2$ in 0.1 M HCl, while 0.5 M NH$_4$OH, 1 and 3 M HCl or mixture of 0.1 M thiourea and 0.5 M HCl were used as the receiving phases.

PIMs were prepared from three basic substrates: polymeric matrix (CTA), carrier (phosphonium ILs), plasticizer (ONPOE). A portion of three-substrate solution in solvent (DCM) was casted on a 7.0 cm diameter Petri dish. The organic solvent was allowed to evaporate overnight and the resultant membrane (flexible, transparent, homogenous and strong thin film) was separated from a glass plate. Before membranes were fixed in the sandwich-type membrane module, presented in the previous paper (Regel-Rosocka et al., 2012), the membranes were soaked for 24 h in distilled water to achieve their homogeneity. The membrane thickness was measured by digital ultrameter (MG-401, ELMETRON, Poland) in at least 15 different sites of the membrane surface.

Pd(II) determination

Atomic absorption spectrometer (Hitachi Z-8200) was used for Pd(II) determination in the aqueous solutions before and after extraction and in the feed aqueous phase and receiving phases during PIM separation at 247.6 nm in the air-acetylene flame.

Results and discussion

Extraction and stripping of Pd(II) with Cyphos IL 102

As SX of Pd(II) with Cyphos IL 101 and 104 was presented elsewhere (Cieszynska and Wisniewski, 2011) in the paragraph referring to liquid-liquid extraction there are presented data only on Cyphos IL 102.

As shown in Fig. 1, extraction equilibrium state was established quickly with Cyphos IL 102 as an extractant. After 1 min of shaking constant values of $E_{Pd(II)}$ were obtained. This fast extraction kinetics with IL 102 is in accordance with the results obtained in our team for the other phosphonium ILs (Cieszynska et. al., 2007; Cieszynska and Wisniewski, 2011). Moreover, extraction efficiency of Pd(II) with Cyphos IL 102 was high; almost 100% Pd(II) was extracted from 0.1 M HCl which was confirmed by change in color of the aqueous phase. All feeds were orange before extraction, but after extraction from 0.1 M HCl solutions were discolored. The initial rate of metal ion transfer to the organic phase containing $5 \cdot 10^{-3}$ M Cyphos IL 102 in toluene was equal to $4 \cdot 10^{-5}$ mol/dm$^3 \cdot$s.
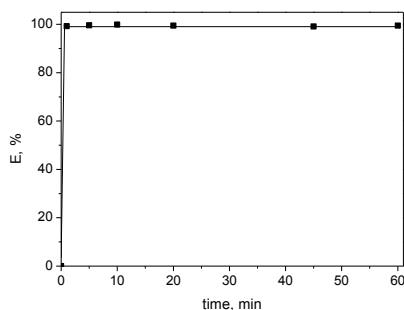
Fig. 1. Extraction of Pd(II) from 0.1 M HCl with $5 \cdot 10^{-3}$ M Cyphos IL 102 (feed: $2.5 \cdot 10^{-3}$ M Pd(II))
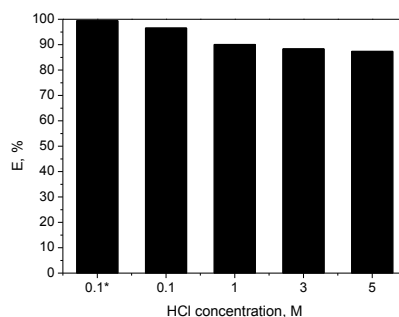
Fig. 2. Effect of HCl concentration on the efficiency of Pd(II) extraction with $5 \cdot 10^{-3}$ M Cyphos IL 102 (feed: $2.5 \cdot 10^{-3}$ M Pd(II)), 0.1; 1; 3 or 5 M HCl; *without NaCl; I = 5 M)

After the organic phases were loaded with metal ions, Pd(II) was stripped with 0.5 M NH$_4$OH. This stripping of Pd(II) was rapid and steady state of the process was obtained in the period from 1 to 5 min. As a result of extraction the organic phase was loaded with Pd(II) up to 260 mg/dm^3, and stripping with 0.5 M NH$_4$OH solution allowed it to recover 220 - 230 mg/dm^3 Pd(II). It means that the Pd(II) transport from the organic to the stripping phase is efficient (84 to 90%) and the organic phase after stripping could be reused for extraction.

As Pd(II) forms anionic chlorocomplexes, its extraction depends on the concentration of HCl and chloride anions in the aqueous feed. Therefore, an effect of HCl concentration in the feed aqueous phase on Pd(II) extraction has been investigated and the results are shown in Fig. 2. With the increase in HCl

concentration in feed phase, the extraction efficiency slightly decreased, which was consistent with the results for Cyphos IL 101 and IL 104. The highest percentage extraction (about 100%) was achieved without NaCl addition.

The effect of ionic strength (*I*) on Pd(II) extraction was also verified. The Pd(II) extraction efficiency to the IL phase was equal to 99.5; 99.7; 97.5 and 98.5% from feed solutions containing 0.1; 1; 3 and 5 M NaCl, respectively (*I* = 0.11; 1.11; 3.11 and 5.11 M, respectively). Extraction efficiency with and without NaCl was almost at the same level. Percentage extraction of Pd(II) at 3 M chloride concentration was about 3% lower (which is within error limits) than at the other concentrations. It means that Pd(II) extraction with Cyphos IL 102 was not affected by NaCl concentration. NaCl presence in the aqueous phase is advantageous because of an improvement of phase separation after extraction.

Pd(II) extraction isotherms

Finally, the equilibrium of Pd(II) extraction has been investigated. The extraction isotherms of Pd(II) with Cyphos IL102 are presented in Fig. 3.

Pd(II) extraction isotherms shown in Fig. 3 are not linear and both reach plateau. It means that this organic phase could be loaded up to 300, 350 mg/dm^3 (2.8 - 3.3$\cdot$10^{-3} M) depending on the NaCl content in the feed aqueous phase. As in the previous cases, extraction occurred slightly better without the addition of NaCl than in the presence of the salt.

Positive results of Pd(II) extraction with the phosphonium ILs studied encouraged the authors to apply the phosphonium ILs as metal ion carriers in transport across polymer inclusion membranes.
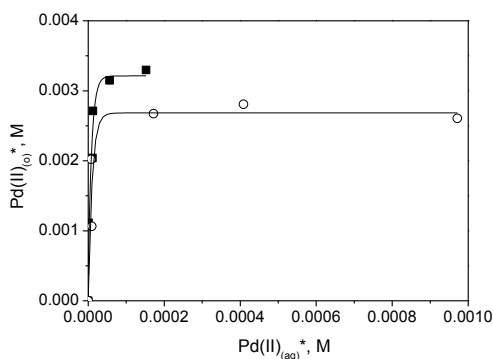
Fig. 3. Isotherms of Pd(II) extraction from the feed 1$\cdot$10^{-3} - 5$\cdot$10^{-3} M Pd(II) in 0.1 M HCl without NaCl (■) and with 1 M NaCl (○); the organic phase 5$\cdot$10^{-3} M IL102 (* denotes equilibrium concentrations)

Pd(II) transport across PIMs

Transport of metal ions through PIM can be described by initial flux (J_0, mol/s·m^2), defined in detail elsewhere (Resina et al., 2008). Depending on the amount of the membrane constituents casted on a glass dish, thickness of the membranes formed ranged from 29 to 56 μm. As the membranes differed with the thickness that might affect the transport resistance and cause decrease in metal ion flux. Therefore a normalized initial fluxes (J_N) were calculated (Regel-Rosocka et al., 2012). The thinnest CTA membrane containing Cyphos IL 102 was chosen as a reference and metal ion fluxes were calculated as follows:

$$J_N = J_0 \cdot \frac{d_M}{d_R} \tag{1}$$

where d_R was the reference membrane thickness (equal 29 μm), d_M corresponded to the thickness of the membrane which flux was normalized.

a) IL 101, receiving phase: 1 M HCl

b) IL 102 , receiving phase: 3 M HCl

c) IL 104, receiving phase: 3 M HCl
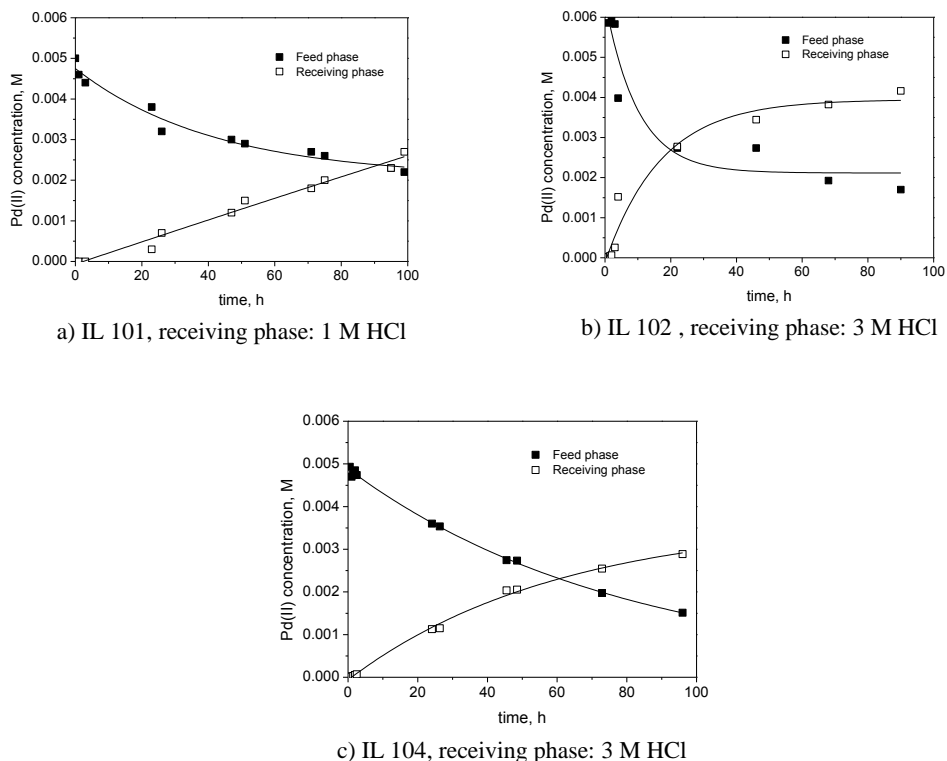
Fig. 4. Pd(II) concentration profiles in the feed aqueous phase and receiving phases vs. time of PIM process

Transport of Pd(II) profiles through PIMs containing CTA, and various Cyphos ILs (that differ with an anion) are shown in Fig. 4. For membrane containing Cyphos IL 101 1 M HCl was used as a receiving phase because 3 M HCl solution was too acidic, and caused damage of the membrane. It should be noticed that the mass transfer across membranes was rather slow due to small membrane area. Thus, significant increase in Pd(II) concentration in the receiving phase was reported after 60 - 70 h of transport process.

Pd(II) concentration in the feed aqueous phase decreased faster for membrane containing Cyphos IL 102 as a carrier and 3 M HCl as receiving phase, and finally reached lower values compared to membrane containing Cyphos IL 104 and the same receiving phase.

Extraction efficiency of palladium(II) was calculated using Eq. 2:

$$E = \frac{c_0 - c}{c_0} \cdot 100\% \qquad (2)$$

where c_0 and c are Pd(II) concentrations in the feed aqueous phase and in the aqueous phase after 90 h and normalized initial flux of palladium(II) are compared in Fig. 5 for different receiving phases.
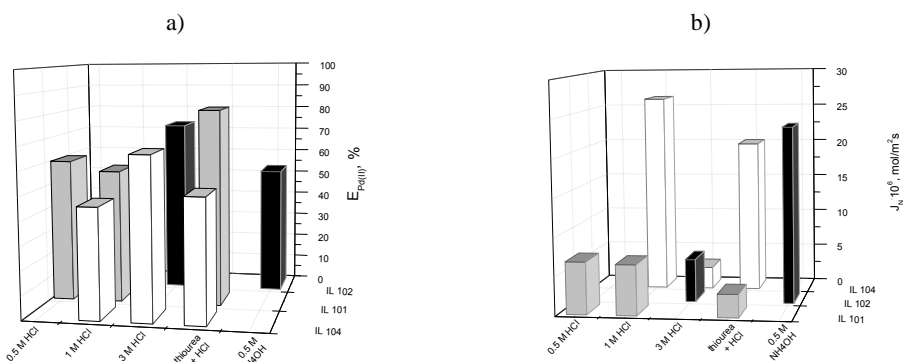
Fig. 5. Percentage extraction of Pd(II): (a) in the end of the process and normalized initial flux of Pd(II) (b) from the feed aqueous phase to the various receiving phases

It is noticeable that with increasing HCl concentration for membranes with IL 101 $E_{Pd(II)}$ decreased, only mixture of thiourea and HCl was almost twice as efficient as HCl solutions. On the other hand, Pd(II) transport through membranes containing IL 104 increased with increasing HCl content in the receiving phase. It is also noteworthy that initial fluxes for two processes with IL 104 carrier were high, while finally $E_{Pd(II)}$ values were not so significant. On the contrary, initial flux for IL 101 carrier and 0.1 M thiourea + 0.5 M HCl receiving phase was rather low, while Pd(II) extraction at the end of the process amounted to 80%. The J_N values were low for Cyphos IL 104 and 3 M HCl as receiving phase and Cyphos IL 101 (receiving phase mixture thiourea and

HCl, Fig. 5b). It can be stated that initial flux did not determine the final result of the transport through the membranes. The highest values of the normalized initial flux were obtained for CTA membrane containing Cyphos IL 101 and the receiving phase: mixture 0.1 thiourea + 0.5 M HCl. Since receiving phase containing thiourea and HCl caused formation of thin layer of precipitation at the end of the process, for Cyphos IL 102 membranes ammonium solution was applied to strip Pd(II) from the membrane and was found to be effective. However, from the point of view of further processing of the receiving phase, chloride receiving phase is more advantageous. Thus, ammonium solution was not used as stripping phase for other membranes.

The highest values of extraction efficiency were obtained for CTA membranes containing Cyphos IL 102, Cyphos IL 104 and 3 M HCl as receiving phase and also Cyphos IL 101 and mixture 0.1 M thiourea + 0.5 M HCl (Fig. 5a).

Another issue to be emphasized is the difference between $E_{Pd(II)}$ and recovery factor (RF) values. RF was defined, following equation 3, as the ratio of Pd(II) transferred to the receiving phase (c_s) after 90 h of the process and the initial Pd(II) content in the feed aqueous phase (c_0):

$$RF = \frac{c_s}{c_0} \cdot 100\% .$$ (3)

The RF values for two different receiving phases are shown in Fig. 6.
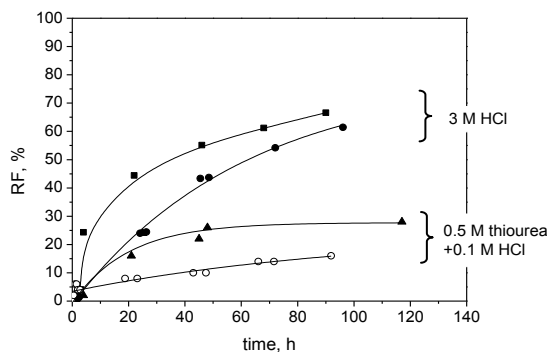
Fig. 6. Pd(II) recovery factor vs. time of transport through PIMs containing Cyphos IL 102 (■), Cyphos IL 104 (●, ○), Cyphos IL 101 (▲) as the ion carriers

From the separation point of view, the most important is a complete transport of the solute to the receiving phase, described by RF. However, not always RF of Pd(II) was equal to percentage extraction. In most cases more Pd(II) was extracted to the membrane (e.g. 73% for IL 102) than was recovered to the receiving phase (66% for IL 102). The values of $E_{Pd(II)}$ and RF strongly depended on the type of carrier and the receiving phase. For instance, the recovery factor values of Pd(II) were significantly higher when 3 M HCl was used as the receiving phase than thiourea + HCl mixture.

Conclusions

Generally, Cyphos IL 102 is an efficient extractant of Pd(II) from aqueous chloride solutions. Addition of NaCl and increasing HCl content in the feed aqueous phase slightly reduces the efficiency of Pd(II) extraction. Comparing with previous research of our team it can be stated that anion type of the phosphonium ILs studied has no influence on liquid-liquid extraction efficiency.

The results of the studies have also shown that the efficiency of PIMs containing phosphonium ILs depends mainly on the type of receiving phase. Phosphonium ILs studied, especially Cyphos IL 102, used for the first time as a metal ion carrier – efficiently extract Pd(II) both in liquid-liquid extraction and transports across polymer inclusion membranes. Transport of Pd(II) ions is better for carriers with small anion (Cyphos IL 101 and IL 102) than with carrier with big anion (Cyphos IL 104). The highest extraction efficiency was obtained for Cyphos IL 101 carrier and receiving phase composed of thiourea + HCl. 3 M HCl efficiently strips Pd(II) from PIMs containing Cyphos IL 102 and Cyphos IL 104. Though the greatest initial normalized flux values are obtained for the membranes containing Cyphos IL 101 (receiving phase: mixture 0.1 M thiourea + 0.5 M HCl) and Cyphos IL 102 (receiving phase: 0.5 M NH_4OH) Pd(II) recovery factors obtain the highest values (above 60%) for Cyphos IL 102 and 104 and 3 M HCl receiving phase.

Acknowledgments

References

AKITA, M., YANG, L., TAKEUCHI, H., 1996, *Solvent extraction of gold(III) from hydrochloric acid media by non-ionic surfactants*, Hydrometal., 43, 37-46.

CIESZYNSKA, A., REGEL-ROSOCKA, M., WISNIEWSKI, M., 2007, *Extraction of palladium(II) ions from aqueous chloride solutions with phosphonium ionic liquid Cyphos IL 101*, Pol. J. Chem. Technol., 2, 99-101.

CIESZYNSKA, A., WISNIEWSKI, M., 2010, *Extraction of palladium(II) from aqueous chloride solutions with Cyphos®IL 101/toluene mixtures as novel extractant*, Sep. Purif. Technol., 73, 202-207.

CIESZYNSKA, A., WISNIEWSKI, M., 2011, *Selective extraction of palladium(II) from hydrochloric acid solutions with phosphonium extractants,* Sep. Purif. Technol., 80, 385-389.

GUIBAL, E.; GAVILAN, CAMPOS, K.; BUNIO, P.; VINCENT, T. & TROCHIMCZUK, A., 2008, *CYPHOS IL 101 (Tetradecyl(trihexyl)phosphonium chloride) immobilized in biopolymer capsules for Hg(II) recovery from HCl solutions*, Sep. Sci. Technol., 43, 2406-2433.

GUPTA, B., SINGH, I., 2013, *Extraction and separation of platinum, palladium and rhodium using Cyanex 923 and their recovery from real samples*, Hydrometal., 134-135, 11-18.

INES, M., ALMEIDA, G. S., CATRALL, R. W., KOLEV, S. D., 2012, *Recent trends in extraction and transport of metal ion using polymer inclusion membrane (PIMs)*, J. Membr. Sci., 415, 9-23.

KARGARI, A., KAGHAZCHI, T., MARDANGAHI, B., SOLEIMANI, L., 2006, *Experimental and modeling of selective separation of gold(III) ions from aqueous solutions by emulsion liquid membrane system*, J. Membr. Sci., 279, 389-393.

KOGELNIG, D., REGELSBERGER, A., STOJANOWIC, A., JIRSA, F., KRACHLER, R., KEPPLER, B.K., 2011, *A polymer inclusion membrane based on the ionic liquid trihexyl(tetradecyl)phosphonium chloride and PVC for solid-liquid extraction of Zn(II) from hydrochloric acid solution,* Monatsh. Chem., 142, 769-772.

LEE, J. Y., KUMAR, J. R., KIM, J. S., PARK, H. K., YOON, H. S., 2009, *Liquid-liquid extraction/separation of platinum(IV) and rhodium(III) from acidic aqueous chloride solutions using tri-iso-octylamine*, J. Hazard. Mater., 168, 424-429.

MARTAK, J., SCHLOSSER, S., 2006, *Phosphonium ionic liquids as new reactive extractants of lactic acid*, Chem. Pap., 60, 395-398.

NAJAFI, A., KARGARI, A., SOLEIMANI, M., 2013, *Extraction of palladium from aqueous wastewaters using Alamine 300 as extractant*, Desalin. Water Treat., 51, 958-968.

NGHIEM, L. D., MORNANE, P., POTTER, I. D., PERERA, J. M., CATRALL, R. W., KOLEV, S. D., 2006, *Extraction and transport of metal ions and small organic compounds using polymer inclusion membranes (PIMs)*, J. Membr. Sci., 281, 7-41.

NOWOTTNY, C., HALWACHS, W., SCHUGERL, K., 1997, *Recovery of platinum, palladium and rhodium from industrial process leaching solutions by reactive extraction*, Sep. Purif. Technol., 12, 135-144.

PAIVA, A. P., CARVALHO G. I., COSTA, M. C., ROSA A. M., NOGUEIRA, C., 2014, *Recovery of platinum and palladium from aqueous chloride solutions by a thiodiglycolamide derivative*, Solvent Extr. Ion Exch., 32, 78-94.

POIROT, R., BOURGEOIS, D., MEYER D., 2014, *Palladium extraction by a malonamide derivative (DMDOHEMA) from nitrate media: extraction behavior and third phase characterization*, Solvent Extr. Ion Exch., 32, 529-542.

POSPIECH, B., 2013, *Hydrometallurgical recovery of cobalt(II)from aqueous chloride solutions by transport through polymer inclusion membranes*, Physicochem. Probl. Miner. Process., 49, 641-649.

REDDY B.R., RAJUA B., LEE J. Y., PARK H. K., 2010, *Process for the separation and recovery of palladium and platinum from spent automobile catalyst leach liquor using LIX 84I and Alamine 336*, J. Hazard. Mater., 180, 253-258.

REGEL-ROSOCKA M., WISNIEWSKI M., BOROWIAK-RESTERNA A., CIESZYNSKA A., SASTRE A.M., 2007, *Selective extraction of palladium(II) from hydrochloric acid solutions with pyridinecarboxamides and ACORGA®CLX50*, Sep. Purif. Technol., 53, 337-341.

REGEL-ROSOCKA, M., NOWAK, L., WISNIEWSKI, M., 2012, *Removal of Zn(II) and iron ions from aqueous chloride solutions with phosphonium ionic liquids*, Sep. Purif. Technol., 97, 158-163.

RESINA, M., FONTAS, C., PALET, C., MUNOZ, M.., 2008, *Comparative study of hybrid and activated composite membranes containing Aliquat 336 for the transport of Pt(IV)*, J. Membr. Sci., 311, 235-242.

DE LOS RIOS, A. P., HERNANDEZ-FERNANDEZ, F. J., ALGUACIL, F. J., LOZANO, L. J., GINESTA, A., GARCIA-DIAZ, I., SANCHEZ-SEGADO, S., LOPEZ, F. A., GODINEZ, C., 2012, *On the use of imidazolium and ammonium-based ionic liquids as green solvents for the selective recovery of Zn(II), Cd(II), Cu(II) and Fe(III) from hydrochloride aqueous solutions,* Sep. Purif. Technol., 97, 150-157.

SWAIN, B., JELONG, J., KIM, S. K., 2010, *Separation of platinum and palladium from chloride solution by solvent extraction using Alamine 300*, Hydrometal., 104, 1-7.

TORGOV, V.G., US, T.V., KORDA, T.M., KOSTIN, G.A., TKACHEV, S.V., DRAPAILO, A.B., 2013, *Extraction of palladium with acyclic analogs of thiacalix[4]arenes from nitric acid solutions*, Russ. J. Inorg. Chem., 58, 1383-1389.

ULEWICZ, M., RADZYMINSKA-LENARCIK, E., 2012, *Application of supported and polymer inclusion membrane with 1-decyl-2-methylimidazole for separation of transition metal ions*, Physicochem. Probl. Miner. Process. 58,, 91-102.

WILLNER, J., FORNALCZYK, A., 2012, *Electronic scraps as a source of precious metals*, Przem. Chem., 91, 517-522.

HYDROXYAPATITE AS A SUPPORT IN PROTEASE IMMOBILIZATION PROCESS

Jakub ZDARTA[*]**, Katarzyna BUDZINSKA**[*]**, Agnieszka KOLODZIEJCZAK-RADZIMSKA**[*]**, Lukasz KLAPISZEWSKI**[*]**, Katarzyna SIWINSKA-STEFANSKA**[*]**, Przemyslaw BARTCZAK**[*]**, Adam PIASECKI**[**]**, Hieronim MACIEJEWSKI**[***]**,**[****]** ,Teofil JESIONOWSKI**[*]

[*] Poznan University of Technology, Faculty of Chemical Technology, Institute of Chemical Technology and Engineering, Berdychowo 4, PL-60965, Poznan, Poland, teofil.jesionowski@put.poznan.pl

[**] Poznan University of Technology, Faculty of Mechanical Engineering and Management, Institute of Materials Science and Engineering, Jana Pawla II 24, PL-60965, Poznan, Poland

***Adam Mickiewicz University in Poznan, Faculty of Chemistry, Umultowska 89b, PL-61614 Poznan, Poland

****Poznan Science and Technology Park, A. Mickiewicz University Foundation, Rubiez 46, Poznan, Poland

Abstract: Hydroxyapatite is used as a matrix for immobilization of protease from *Aspergillus oryzae* by a process of adsorption. The matrix obtained has the surface area of 26 m^2/g and particles in the shape of flakes of diameters no greater than 650 nm. The efficiency of the proposed method was confirmed by the Fourier transform infrared spectroscopy, elemental analysis and by analysis of parameters of the pore structure of matrix and products after immobilization. On the basis of the Bradford method it was found that the greatest amount of enzyme (132 mg/g) was immobilized from a solution of initial enzyme concentration of 7 mg/cm^3 after 24 h of the process.

Keywords: hydroxyapatite, enzyme immobilization, protease, physicochemical characteristic

Introduction

Proteases (also termed peptidases) make a well-known group of enzymes responsible for division of long chains of amino acids into shorter fragments through a process of hydrolysis of peptide bonds. The biocatalysts are characterized by high activity in a wide range of temperatures (30-80 ^{o}C) and pH (5-10), with the maximum activity at 40 ^{o}C and at pH 8 (Li et al., 2011). Enzymes from this group are produced by many micro-organisms such as bacteria, yeast, fungi, but their industrial production is based on the use of two fungi species from families of *Aspergillus* and *Bacillus* (Sharma et al., 2013). Peptidases have been applied in pharmaceutical industry, leather industry as

well as in production of food and detergents (Sarker et al., 2013). They have been also added to fodder (Dragomirescu et al., 2012). Recently, they have been increasingly used for bioremediation of water and sewage (Padmapriya et al., 2012). Similar use have ureases, enzymes of a hydrolase class, that are used in wastewater treatment (Krajewska 2009 a, b). A very good support for this group of enzymes is hydroxyapatite (HA) ($Ca_{10}(PO_4)_6(OH)_2$) (Jesionowski et al., 2014), which is inorganic and water insoluble mineral belonging to the family of calcium phosphates. The most important advantages of HA are biocompatibility, bioactivity, non-toxicity and immunogenic properties (Pahm et al., 2013). The application of hydroxyapatite is limited because of its low mechanical strength (Liu et al., 2014).

In nature, hydroxyapatite (HA) occurs as mineral and it also makes about 80% wt. of bones (Daniels et al., 2010, Xing et al., 2014). Because of its properties, hydroxyapatite is a very good substitute of bones and has been of great interest in tissue engineering (Alves Cardoso et al., 2012). In pharmaceutics it has been used as a support of drugs (Zhang et al., 2012), and after introduction of titanium ions into its structure, it has been used for decomposition of pathogens in a blood purification therapy upon UV irradiation (Kandori et al., 2013). Hydroxyapatite is also able to bind metal ions from water solutions, especially if it is a component of composite materials. Thus, hydroxyapatite is applied for removal of toxic metal ions from wastewater and soil (Carro et al., 2013). HA has been also proved, to be an effective adsorbent of lead ions (Ramesh et al., 2013, Cui et al., 2013), and when modified with lead ions, it shows high ability to remove uranium ions (Popa 2013). Besides the application in medicine and for remediation of natural environment, hydroxyapatite is also used in electrochemistry for production of biological sensors (Ma et al., 2009). Another application of hydroxyapatite is in packing of chromatographic columns used for separation of proteins, enzymes or DNA (Dancu et al., 2011).

This study was undertaken to check a possibility of using hydroxyapatite as a support for enzyme immobilization. The method proposed permits stabilization of enzyme structure and improvement in its properties (Rodrigues et al., 2013).

Salman et al. (2008) used the HA matrix for multiple enzyme immobilization in biodetectors for calorimetric evaluation of glucose and urea content. The results proved that the method and established parameters of reaction are suitable for the regular analysis of reversible adsorption *in situ*, for the same biosensors. An attempt was also made to immobilize the recombined human morphogenetic bone protein (rhBMP-2) on the surface of unmodified and modified hydroxyapatite. Adsorption of the protein growth agent was confirmed. These data may be used as the basis for formulation of theoretical description for delivery of drugs that increase the rate of bone growth and osteointegration of implants (Zurlinden et al., 2005). Hydroxyapatite was also tested for applications in encapsulation of alkaline phosphatase. The analysis of results confirmed immobilization of enzyme and preservation of the biocatalyst activity. This protein takes part in mineralization of new bones as they form. Thus, an attempt was made to evaluate the efficiency of substance obtained during the process

of stimulated bone formation (Jiang et al., 2010). The subject of other papers involved the binding of fusion protein FN_{RGD}/OC onto the surface of hydroxyapatite. The results illustrated the advantage of immobilized FN_{RGD}/OC over the native FN, which manifested as intensification in osteoblasts proliferation. Therefore, the strategy for designing multifunctional proteins integrated into the hydroxyapatite matrix can be used for bone regeneration (Kang et al., 2011). During immobilization, it is important to ensure the possibility of repeated use of enzyme. The method of repeatable adsorption and total removal of protein from the hydroxyapatite surface has been presented. The ability to reuse the HA support for adsorption of fibrinogen and FBS proteins has been proved (Tagaya et al., 2010).

The hitherto results have brought a substantial contribution to dynamic development of immobilization of enzymes on the surface of hydroxyapatite. However, there are still many problems that need detailed solutions, which have prompted us to undertake the study reported in this work. The aim of our study was immobilization of *Aspergillus oryzae* protease by adsorption on the surface of hydroxyapatite. A comprehensive physicochemical analysis of the support was made and the effectiveness of proposed procedure of enzyme immobilization was evaluated. The amount of adsorbed protein and changes in the content of particular elements in the products after immobilization were established. The changes in the porous structure of the support after immobilization additionally confirmed the process efficiency.

Experimental

Materials

Ethyl alcohol (purity 96%), phosphoric acid (purity 85%) and calcium chloride were purchased from Chempur Company (Poland). Phosphate buffer of pH=7 was obtained from Amresco Company (USA). Protease (PRT) from *Aspergillus oryzae*, sodium phosphate dibasic and Coomassie Brilliant Blue were purchased from Sigma–Aldrich (Germany).

Preparation of hydroxyapatite

The procedure for obtaining hydroxyapatite was as follows. A proper volume of 1 M calcium chloride solution was placed in a reactor equipped with a high-speed stirrer (ca. 900 rpm) mounted in a water bath of 40 ºC. To the reactor a 100 cm^3 of 0.6 M sodium phosphate dibasic solution dissolved in ethyl alcohol was dosed. Then, the mixture was stirred for about 15 min, filtered off under reduced pressure on a Sartorius AG set (Germany) and washed with water. A scheme of HA preparation is shown in Fig. 1. The product was dried at 120 ºC in a Memmert dryer (Germany) and subjected to calcination at 600 ºC in a Nabertherm furnace (Germany). Finally, obtained hydroxyapatite was ground and sieved through sieve of 63 μm.
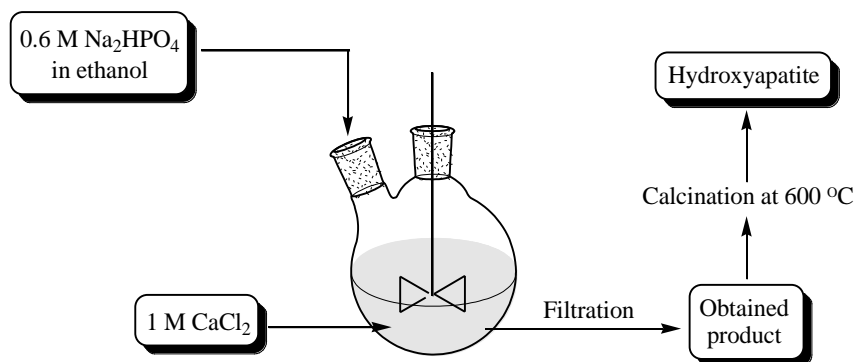
Fig. 1. Schematic diagram of hydroxyapatite preparation

Immobilization of protease onto hydroxyapatite surface

To each of three conical flasks a portion of 500 mg hydroxyapatite was introduced and then 15 cm^3 of the enzyme solution with concentrations of 3, 5 and 7 mg/cm^3 at phosphate buffer of pH=7 was added. The process of immobilization was performed in different times, from 1 min to 96 h, at ambient temperature. After completion of the process, the mixtures were filtered off under reduced pressure and the obtained products were dried in air at room temperature for 24 h.

Evaluation of physicochemical properties

The dispersive characteristics of hydroxyapatite were determined using a Zetasizer Nano ZS apparatus made by Malvern Instruments Ltd. (UK), operating on the non-invasive back-scattering method and measuring particles with sizes between 0.6 to 6000 nm.

On the basis of SEM image recorded by an EVO40 scanning electron microscope (Zeiss, Germany), the surface morphology and microstructure of hydroxyapatite was examined.

Fourier transform infrared spectroscopy (FTIR), recorded by an Vertex 70 spectrometer (Bruker, Germany) was used to obtain the presence of functional groups. The investigation was performed at a resolution of 0.5 cm^{-1}.

The elemental contents of carbon, hydrogen and nitrogen were established by using a Vario EL Cube instrument made by Elementar Analysensysteme GmbH (Germany)

The surface composition of hydroxyapatite (contents of Ca and P) was analysed by energy dispersive X-ray spectroscopy (EDX) using a Princeton Gamma-Tech unit equipped with a prism digital spectrometer (Germany). EDX technique is based on analysis of X-ray energy values using a semiconductor. Before the analysis, samples were placed on a special carbon tape. The presence of carbon materials is needed to create a conductive layer which ensures delivery of electric charge from the sample. Representative parts (500 μm^2) were analyzed for proper evaluation of surface composition.

Hydroxyapatite was also subjected to crystalline structure determination using the WAXS method (wide-angle X-ray scattering). X-ray diffraction measurements were performed using CuK$_\alpha$ (λ = 0.15418 nm) radiation. The accelerating voltage and applied current were 30 kV and 25 mA, respectively. The other measurement parameters were as follows: 2Θ angle range 5–60º, counting step (2Θ) 0.04º, counting time 3 s.

In order to characterize the porous structure of the examined substances, their surface area, pore volume and average pore size were determined using an ASAP 2020 instrument, Micromeritics Instrument Co. (USA). All samples were degassed at 120 °C for 4 h in a vacuum chamber prior to measurement. The surface area was determined by the multipoint Brunauer–Emmett–Teller (BET) method (Sing et al., 1985, Foo et al., 2010). The Barrett–Joyner–Halenda (BJH) method was applied to determine the pore volume and average pore size (Barrett et al., 1951).

The amount of enzyme adsorbed and immobilization yield was determined according to the Bradford method using bovine serum albumin as a standard (Bradford, 1976). Spectrophotometric measurements needed for the calculations were made by using a UV-1601 PC Shimadzu spectrophotometer (Japan) at 595 nm. Prior to measurements, a reagent composed of Coomassie Brilliant Blue G-250, 85% phosphoric acid and 96% ethyl alcohol was made and added to the albumin solution. It was also used as a reference substance.

During evaluation of efficiency of the process, the amount of enzyme adsorbed per a time unit q_t was determined using the formula:

$$q_t = \frac{(C_0 - C_t) \cdot V}{m} \tag{1}$$

where C_0 and C_t *denote* concentrations of enzyme (mg/cm^3) in the solution before and after adsorption, respectively; V is volume of solution (cm^3), and m is the mass of the hydroxyapatite support (g).

Results and discussion

Hydroxyapatite characterization

Morphology of obtained hydroxyapatite was characterized using scanning electron microscope images presented in Fig. 2. The SEM images show that hydroxyapatite particles are in the form of flakes, which tend to form aggregates. Hydroxyapatite characterized in earlier works (Bardhan, 2011) had similar morphology. To supplement the data from SEM, the particle size distribution was determined and the obtained results are presented in Fig. 3. Figure 3 shows that obtained hydroxyapatite has a monomodal particle size distribution in the range of 396-615 nm, corresponding to primary particles showing a tendency to aggregate. Over 70% of the volume

contribution is taken by the particles of 531 nm (39.3%) and 459 nm (35.7%). The particle size distribution is in agreement with that reported by Earl et al. (2006).

At the next step the crystalline structure of hydroxyapatite obtained was resolved. It was shown that the proposed in this work procedure leads to formation of crystalline hydroxyapatite, which is confirmed by the presence of diffraction maxima for 2Θ of 26, 32, 33, 34, 40, 47, 49 and 54 in the X-ray diffractogram (Fig. 4) (Kolodziejczak-Radzimska et al., 2014). To confirm the presence of elemental characteristic of hydroxyapatite, the EDX analysis as well as the elemental analysis were made. According to the results, the content of calcium in the obtained material is higher than that of phosphorus and the mass ratio of Ca/P is close to 1.5. Based on elemental analysis, the presence of carbon and hydrogen was noted as 22% of C and 1.07% of H).
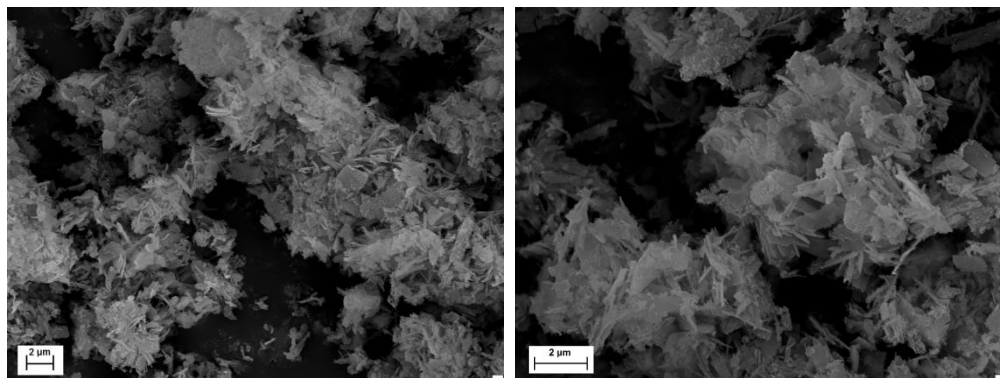
Fig. 2. SEM images of obtained hydroxyapatite (at different magnifications)
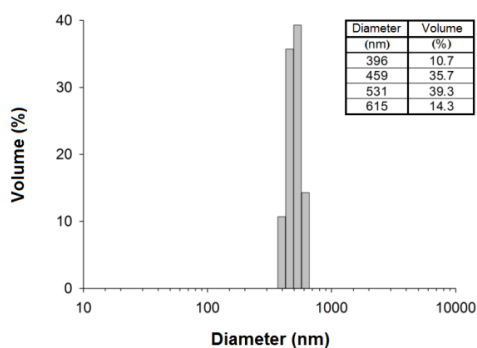
Fig. 3. Particle size distribution of obtained hydroxyapatite support
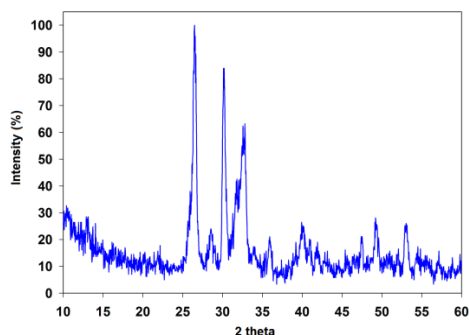
Fig. 4. XRD pattern of hydroxyapatite support

Characterization of products after protease immobilization

To verify enzyme immobilization on the hydroxyapatite surface, the FTIR spectra of samples were recorded and analyzed. Figure 5 presents results of spectroscopic study of hydroxyapatite and products after 24 h of immobilization from the solutions with different concentrations. The most important fragment of the spectra, from 1700 to 1200 cm^{-1}, was magnified. The spectrum of hydroxyapatite shows a broad signal between wavenumbers 3550 and 3200 cm^{-1} generated by the stretching vibrations of hydroxyl groups, while the signal with the maximum at 1630 cm^{-1} is assigned to physically adsorbed water. The bands at 1200, 1050 and 600 cm^{-1}, a very characteristic of hydroxyapatite, are assigned to the stretching vibrations of phosphate groups (PO$_4^{3-}$) (Uddin, 2010). The band at 800 cm^{-1} is assigned to the hydrophosphate ions (HPO$_4^{2-}$) (Uddin, 2010).
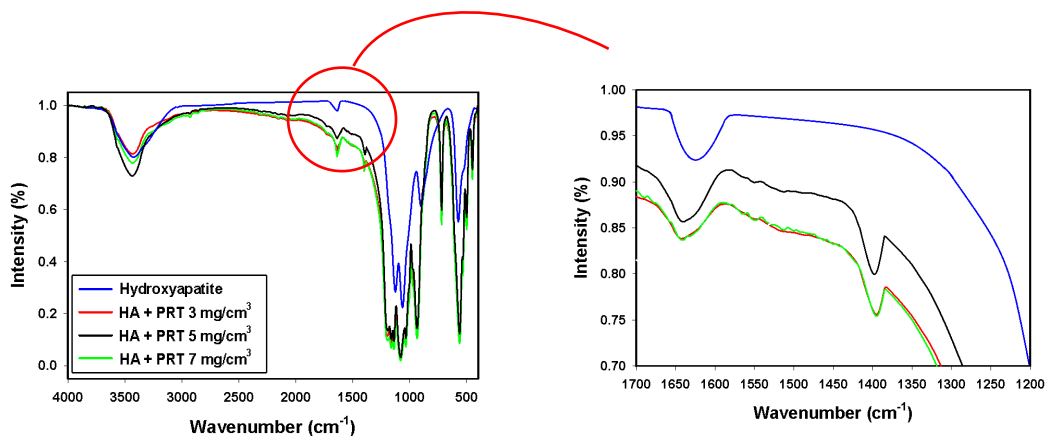
Fig. 5. FTIR spectra of hydroxyapatite and products after protease immobilization for 24 h from enzyme solution with various concentration

The characteristic bands of protease appear at the wavenumber of 2900 cm^{-1}, and in the range of 1700–1200 cm^{-1}. Their presence confirms immobilization of protease on the support. The band about 2900 cm^{-1} is assigned to the stretching vibrations of methyl and methylene groups (–CH$_2$ and –CH$_3$). The signal at about 1650 cm^{-1} corresponds to the stretching vibrations of C=C bonds (Ozsagiroglu, 2012). The band at about 1400 cm^{-1} is generated by the vibrations of –C–N bonds in the protease molecule (Singh, 2011). The FTIR spectra after immobilization of the biocatalyst also show the signals at 700 cm^{-1} and 490 cm^{-1}, and their presence is assigned to the wagging vibrations and out-of-plane vibrations of C–H bonds in protease (Zhang, 2006). Moreover, the spectra show the bands at the same wavenumbers, at which the hydroxyapatite bands occur but of higher intensity than in the spectra of hydroxyapatite. It is a result of the presence of –C–O bonds in the protease molecule, which vibrations are manifested as the signals at 1150 cm^{-1} and 1050 cm^{-1}. A similar situation takes place for the signals assigned to the vibrations of hydroxyl groups, they also become more intense after immobilization.

The spectrophotometric analysis performed on the basis of the Bradford method (Bradford, 1976), permits estimation of the amount of enzyme adsorbed on the support surface per 1 g of the matrix. The relevant data are presented in Table 1.

Table 1. Amount of immobilized enzyme

Immobilization time	Enzyme concentration (mg/cm^3)		
	3	5	7
	Amount of immobilized enzyme (mg/g)		
1 (min)	52	70	76
5 (min)	53	73	96
10 (min)	58	75	108
30 (min)	59	78	115
60 (min)	60	80	118
120 (min)	63	82	123
24 (h)	67	91	132
96 (h)	68	91	132

The analysis of the data from Table 1 shows that with increasing initial concentration of enzyme in solution, the amount of protease immobilized on the hydroxyapatite matrix increases. The greatest amount of protease (132 mg) per gram of the matrix was immobilized from the protease solution of 7 mg/cm^3 after 24 h of the process. Immobilization is the most effective in the first minutes of the adsorption process. The rate of adsorption decreases with time and after 24 h the increase in the mass of protease is no longer detectable. The time of 24 h was found to be the optimum for immobilization by adsorption of protease onto the hydroxyapatite surface. Based on the increase of amount of immobilized enzyme, which raises with

raise of initial concentration of peptide solution, curves presenting dependence of q_t on time were evaluated (Fig. 6).
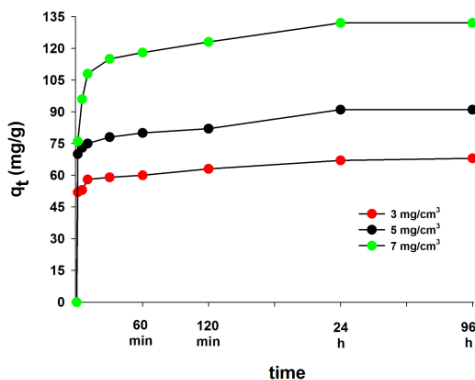
Fig. 6. Effect of contact time on enzyme adsorbed by HA
(enzyme concentration 3, 5 and 7 mg/cm^3, HA dose 0.5 g)

Figure 6 shows a plot of the amount of enzyme adsorbed (mg/g) versus contact time for different initial enzyme concentrations of 1, 5 and 7 mg/cm^3. Noteworthy, for each model concentration of enzyme in solution (3-7 mg/cm^3) the adsorption equilibrium is reached after 24 h. The equilibrium concentration (q_e) was equal to 68, 91, 132 mg/g for 1, 5 and 7 mg/cm^3, respectively.

Based on the data from Table 1, the effectiveness of proposed method was calculated and the results are presented in Table 2. The immobilization yield (%) was calculated basing on the following equation:

$$I_y = \frac{A_I \cdot 100\%}{A_T} \tag{2}$$

where I_y is immobilization yield (%), A_I amount of immobilized enzyme and A_T is amount of immobilized enzyme with 100% yield.

Tables 1 and 2 show that the yield of the process is not correlated with the amount of immobilized enzyme. The highest yield of 75.6 % was obtained for adsorption from the initial enzyme solution of concentration 3 mg/cm^3 for the reaction time of 96 h. The lowest yield of about 60% was obtained for the process performed from the initial enzyme concentration of 5 mg/cm^3. It should be noted that for each initial enzyme concentration the yield after one minute of the process is higher than half of its maximum value, what means that over half of the enzyme amount gets immobilized at the beginning of the process. This observation can be explained by the fact that most of the active sites of the hydroxyapatite matrix saturated at the beginning of adsorption because of a high concentration of protease in the initial solutions.

Table 2. Protease immobilization yield

Immobilization time	Enzyme concentration (mg/cm^3)		
	3	5	7
	Immobilization yield (%)		
1 (min)	57.8	46.7	36.2
5 (min)	58.9	48.7	45.7
10 (min)	64.4	50.0	51.4
30 (min)	65.6	52.0	54.8
60 (min)	66.7	53.3	56.2
120 (min)	70.0	54.7	58.6
24 (h)	74.4	60.7	62.9
96 (h)	75.6	60.8	63.0

Effective immobilization of protease on the surface of hydroxyapatite is also confirmed by the results of elemental analysis. The results revealed changes in the contents of the most important elements (N, C, H) in the samples after immobilization. The changes dependent on time of adsorption and concentration of enzyme solution. The results are shown in Table 3. The hydroxyapatite used contained 1.07% of hydrogen and 0.22% of carbon. After enzyme immobilization, the samples revealed increase in contents of hydrogen and carbon, but also in content of nitrogen coming from enzyme (Xiaochun, 2013). The elemental analysis showed the increase in the content of C, H, N elements in the samples after immobilization, irrespective of adsorption time. The most pronounced changes were noted in the content of carbon. In the samples after immobilization lasting for 96 h from the solution of initial concentration of 7 mg/cm^3, the content of carbon increased over twice with respect to

Table 3. Results of elemental analysis for hydroxyapatite matrix and products

Enzyme concentration (mg/cm^3)	Immobilization time	Elemental analysis (%)		
		N	C	H
Hydroxyapatite (HA)		-	0.22	1.07
3	60 (min)	0.10	0.32	1.13
	24 (h)	0.11	0.33	1.14
	96 (h)	0.11	0.34	1.14
5	60 (min)	0.10	0.37	1.14
	24 (h)	0.12	0.38	1.15
	96 (h)	0.12	0.39	1.15
7	60 (min)	0.12	0.41	1.16
	24 (h)	0.13	0.44	1.19
	96 (h)	0.13	0.44	1.19

that in the hydroxyapatite matrix. The increase in the content of hydrogen and nitrogen was not so great, but with increasing the initial enzyme concentration and time of immobilization process, the percentage contribution of these elements in the samples increased.

In the next step, the parameters of porous structure of hydroxyapatite matrix and samples after immobilization were determined to analyse the effect of immobilization on the surface area, pore size and pore volume. The results for selected times of immobilization are presented in Table 4. Hydroxyapatite has BET surface area of 26 m^2/g, which decreases as a result of immobilization. The changes are most pronounced in the samples obtained after adsorption lasting 96 h, irrespective of the enzyme concentration in the initial solution. The smallest surface area was determined for the sample after immobilization from the solution of the highest concentration. Similar tendencies were observed for the pore size and total pore volume. The hydroxyapatite matrix contained pores of 2.7 nm in diameter (on average) and total volume of 0.018 cm^3/g. The changes in the porous structure observed after the process of immobilization, i.e. decreased surface area, average pore diameter and total pore volume, evidence the effectiveness of the process (Gustafsson et al., 2012). With increasing time of the process and initial concentration of enzyme solution, a significant decrease in the values of above mentioned parameters was observed (Table 4). The smallest average pore diameter and total pore volume were found in the sample after immobilization of protease for 96 h from the enzyme solution of initial concentration 7 mg/cm^3 (pore size 1.3 nm and pore volume 0.005 cm^3/g). It should be added that the results obtained for the samples after immobilization lasting for 24 h and 96 h did not differ much, what suggests on small changes in the hydroxyapatite structure taking place after 24 h of immobilization.

Table 4. Porous structure parameters of obtained HA and products after immobilization

Enzyme concentration (mg/cm^3)	Immobilization time	BET surface area (m^2/g)	Pore volume (cm^3/g)	Pore size (nm)
Hydroxyapatite (HA)		26	0.018	2.7
3	60 (min)	17	0.011	2.1
	24 (h)	15	0.009	1.7
	96 (h)	15	0.008	1.7
5	60 (min)	15	0.010	1.7
	24 (h)	13	0.007	1.5
	96 (h)	13	0.006	1.5
7	60 (min)	14	0.008	1.5
	24 (h)	12	0.005	1.3
	96 (h)	11	0.005	1.3

Conclusions

The proposed in this work method for synthesis of hydroxyapatite gave a product made of particles in the shape of flakes of sizes not exceeding 650 nm. The obtained matrix had well-developed crystalline structure characteristic of hydroxyapatite and the Ca/P mass ratio of about 1.5. The obtained data showed that the method proposed for immobilization of protease is effective and leads to immobilization of enzyme on the matrix surface. The evidence of successful immobilization was provided by the FTIR study, Bradford method measurements, elemental analysis and character of porous structure of products after immobilization, with respect to those of the initial matrix. The process of immobilization on the hydroxyapatite surface was performed for different times, where the optimum duration was 24 h since after this time no significant increase in the amount of enzyme was noted. The greatest amount of enzyme (132 mg/g) was immobilized from the solution of initial concentration of 7 mg/cm^3, however, the highest yield of the process (over 75%) was obtained from the solution of initial enzyme concentration of 3 mg/cm^3.

Acknowledgements

References

ALVES CARDOSO D., JANSEN J.A., LEEUWENBURGH S.C.G., 2012, *Synthesis and application of nanostructured calcium phosphate ceramics for bone regeneration*, Journal of Biomedical Materials Research B: Applied Biomaterials*, 100, 2316–2326.

BARDHAN R., MAHATA S., MONDAL B., 2011, *Processing of natural resourced hydroxyapatite from eggshell waste by wet precipitation method*, Advances in Applied Ceramics, 110, 80−86.

BARRETT E.P., JOYNER L.G., HALENDA P.H., 1951, *The determination of pore volume and area distributions in porous substances. I. Computations from nitrogen isotherms*, Journal of the American Chemical Society, 73, 373–380.

BRADFORD M.M., 1976, *A rapid and sensitive method for the quantitation of microgram quantities of protein utilizing the principle of protein-dye binding,* Analytical Biochemistry, 72, 248−254.

CARRO L., HABLOT E., CORADIN T., 2013, *Hybrids and biohybrids as green materials for a blue planet,* Journal of Sol-Gel Science and Technology, 70, 263–271.

CUI H., ZHOU J., ZHAO Q., SI Y., MAO J., FANG G., LIANG J., 2013, *Fractions of Cu, Cd, and enzyme activities in a contaminated soil as affected by applications of micro- and nanohydroxyapatite*, Journal of Soils and Sediments, 13, 742–752.

DANCU A.-C., BARABAS R., BOGYA E.-S., 2011, *Adsorption of nicotinic acid on the surface of nanosized hydroxyapatite and structurally modified hydroxyapatite*, Central European Journal of Chemistry, 9, 660–669.

DANIELS Y., ALEXANDRATOS S.D., 2010, *Design and synthesis of hydroxyapatite with organic modifiers for application to environmental remediation*, Waste Biomass Valor, 1, 157–162.

DRAGOMIRESCU M., PREDA G., VINTILA T., VLAD-OROS B., BORDEAN D., SAVII C., 2012, *The effect of immobilization on activity and stability of a protease preparation obtained by an indigenous strain, Bacillus licheniformis B 40,* Revue Roumaine de Chimie, 57, 77–84.

EARL J.S., WOOD D.J., MILNE S.J., 2006, *Hydrothermal synthesis of hydroxyapatite*, Journal of Physics: Conference Series, 26, 268−271.

FOO K.Y., HAMEED B.H., 2010, *Insights into the modeling of adsorption isotherm systems*, Chemical Engineering Journal, 156, 2–10.

GUSTAFSSON H., JOHANSSON E., BARRABINO A., ODEN M., HOLMBERG K., 2012, *Immobilization of lipase from Mucor miehei and Rhizopus oryzae into mesoporous silica*, Colloids and Surfaces B: Biointerfaces, 100, 22−30.

JIANG P.J., WYNN-JONES G., GROVER L.M., 2010, *A calcium phosphate cryogel for alkaline phosphatase encapsulation*, Journal of Materials Science, 45, 5257–5263.

JESIONOWSKI T., ZDARTA J., KRAJEWSKA B., 2014, *Enzymes immobilization by adsorption: A review,* Adsorption, 20, 801–821.

KANDORI K., OKETANI M., WAKAMURA M., 2013, *Effects of Ti(IV) substitution on protein adsorption behaviors of calcium hydroxyapatite particles*, Colloids and Surfaces B: Biointerfaces, 101, 38–73.

KANG W., KIM T.-I., YUN Y., KIM H.-W., JANG J.-H., 2011, *Engineering of a multi-functional extracellular matrix protein for immobilization to bone mineral hydroxyapatite*, Biotechnology Letters, 33, 199–204.

KOLODZIEJCZAK-RADZIMSKA A., SAMUEL M., PAUKSZTA D., PIASECKI A., JESIONOWSKI T., 2014, *Synthesis of hydroxyapatite in the presence of anionic surfactant*, Physicochemical Problems of Mineral Processing 50, 225−236.

KRAJEWSKA, B., 2009 a, *Ureases I. Functional, catalytic and kinetic properties: A review*, Journal of Molecular Catalysis B: Enzymatic 56, 9–21.

KRAJEWSKA, B., 2009 b, *Ureases. II. Properties and their customizing by enzyme immobilizations: A review*, Journal of Molecular Catalysis B: Enzymatic 59, 22–40.

LI G.Y., CAI Y.J., LIAO X.R., YIN J., 2011, *A novel nonionic surfactant- and solvent-stable alkaline serine protease from Serratia sp. SYBC H with duckweed as nitrogen source: Production, purification, characteristics and applications*, Journal of Industrial Microbiology and Biotechnology, 38, 845–853.

LIU Y., HUANG J., LI H., 2014, *Nanostructural characteristics of vacuum cold-sprayed hydroxyapatite /graphene-nanosheet coatings for biomedical applications*, Journal of Thermal Spray Technology, 23(7), 1149-1156.

MA R., WANG B., LIU Y., LI J., ZHAO Q., WANG G., JIA W., WANG H., 2009, *Direct electrochemistry of glucose oxidase on the hydroxyapatite/Nafion composite film modified electrode and its application for glucose biosensing*, Science in China Series B: Chemistry, 52, 2013–2019.

OZSAGIROGLU E., IYISAN B., GUVENILIR Y.A., 2012, *Biodegradation and characterization studies of different kinds of polyurethanes with several enzyme solutions*, Polish Journal of Environmental Studies, 21, 1777−1782.

PADMAPRIYA M., WILLIAMS B.C., 2012, *Purification and characterization of neutral protease enzyme from Bacillus subtilis,* Journal of Microbiology and Biotechnology Research, 2, 612–618.

PHAM T.T.T., NGUYEN T.P., PHAM T.N., VU T.P., TRAN D.L., TAHI H., DINH T.M.T., 2013, *Impact of physical and chemical parameters on the hydroxyapatite nanopowder synthesized by chemical precipitation method*, Advances in Natural Sciences: Nanoscience and Nanotechnology, 4, 1–9.

POPA K., 2013, *Sorption of uranium on lead hydroxyapatite*, Journal of Radioanalytical and Nuclear Chemistry, 298, 1527–1532.

RAMESH S.T., RAMESHBABU N., GANDHIMATHI R., KUMAR M.S., NIDHEESH P.V., 2013, *Adsorptive removal of Pb(II) from aqueous solution using nano-sized hydroxyapatite*, Applied Water Science, 3, 105–113.

RODRIGUES R.C., ORTIZ C., BERENGUER-MURCIA A., TORRES R., FERNANDEZ-LAFUENTE R., 2013, *Modifying enzyme activity and selectivity by immobilization*, Chemical Society Reviews, 42, 6290–6307.

SALMAN S., SOUNDARARAJAN S., SAFINA G., SATOH I., DANIELSSON B., 2008, *Hydroxyapatite as a novel reversible in situ adsorption matrix for enzyme thermistor-based FIA*, Talanta, 77, 490–493.

SARKER P.K., TALUKDAR S.A., DEB P., SAYEM S.M.A., MOHSINA K., 2013, *Optimization and partial characterization of culture conditions for the production of alkaline protease from Bacillus licheniformis P003*, Springer Plus, 2, 506–517.

SHARMA N., TRIPATHI S., 2013, *Kinetic study of free and immobilized protease from Aspergillus sp.*, Journal of Pharmacy and Biological Sciences, 7, 86–96.

SING K.S.W., EVERETT D.H., HAUL R.A.W., MOSCOU L., PIEROTTI R.A., ROUQUEROL J., SIEMIENIEWSKA T., 1985, *Reporting physisorption data for gas/solid systems with special reference to the determination of surface area and porosity,* Pure and Applied Chemistry, 57, 603–619.

SINGH A.N., SINGH S., SUTHAR N., DUBEY V.K., 2011, *Glutaraldehyde-activated chitosan matrix for immobilization of a novel cysteine protease, Procerain B*, Journal of Agricultural and Food Chemistry, 59, 6256–6262.

TAGAYA M., IKOMA T., HANAGATA N., CHAKAROV D., KASEMO B., TANAKA J., 2010, *Reusable hydroxyapatite nanocrystal sensors for protein adsorption*, Science and Technology of Advanced Materials, 11, 1–8.

UDDIN M.H., MATSUMOTO T., ISHIHARA A., OKAZAKI M., SOHUMURA T, 2010, *Apatite containing aspartic for selective protein loadin*g, Journal of Dental Research, 89, 488−492.

XIAOCHUN L., SHANGYU D., CHUANGYE Y., XINGI G., JIAWEI W., YIGONG S., 2013, *Structure of a presenilin family intramembrane aspartate protease*, Nature, 493, 56–61.

XING Z.-C., CHANG H.-W., CHUN S., KIM S., KANG I.-K., 2014, *Immobilization of collagen on hydroxyapatite discs by covalent bonding and physical adsorption and their interaction with MC3T3-E1 osteoblasts*, Tissue Engineering and Regenerative Medicine, 11, 1–7.

ZHANG L.-X., WANG J., WEN J.-Q., LIANG H.-G., DU L.-F., 2006, *Purification and partial characterization of a protease associated with photosystem II particles*, Physiologia Plantarum, 95, 591−595.

ZHANG X., ZHANG W., YANG Z., ZHANG Z., 2012*, Nanostructured hollow spheres of hydroxyapatite: preparation and potential application in drug delivery*, Frontiers of Chemical Science and Engineering, 6, 246–252.

ZURLINDEN K., LAUB M., JENNISSEN H.P., 2005, *Chemical functionalization of a hydroxyapatite based bone replacement material for the immobilization of proteins*, Materialwissenschaft und Werkstofftechnik, 36, 820–827.

INFLUENCE OF PRE-AERATION ON CYANIDE LEACHING OF A NON-REFRACTORY SULPHIDE GOLD AND SILVER ORE

Beste AYDIN, Huseyin BASTURKCU, Alim GUL

Mineral Processing Department, Faculty of Mines, Istanbul Technical University, Istanbul, Turkey
even@itu.edu.tr

Abstract: The leaching behaviour of a sulphide gold-silver ore was investigated in terms of a relationship between gold and silver extractions and cyanide consumption. Ninity five Au % and 88.0% Ag extractions were obtained under the determined conditions of 24 h leaching duration, -74 μm particle size, 40% solids ratio, 4 g/dm^3 NaCN concentration, and 450 rpm stirring speed with NaCN consumption of 3.35 g/dm^3. Since the NaCN consumption was higher than in industrial applications, $Pb(NO_3)_2$ and H_2O_2 additions and aeration using an air pump were tested during leaching in order to decrease the consumption. While $Pb(NO_3)_2$ addition with aeration caused a decrease in the metal extractions, the individual or combined additions of H_2O_2 and aeration could not provide a reduction in the cyanide consumption. Therefore, the effect of the pre-aeration followed by cyanidation was tested. Eventually, applying 4 h of pre-aeration before a shorter leaching duration of 12 h provided 92.0% Au and 90.5% Ag extractions with a reduced NaCN consumption of 2.44 g/dm^3.

Keywords: nonrefractory sulphide gold–silver, cyanidation, lead nitrate, hydrogen peroxide, aeration

Introduction

Cyanidation has been in use for recovering gold for almost a century due to its advantages such as simplicity and feasibility (Yang et al*., * 2010a,b,c). The improvement in leaching kinetics, leaching agent costs, and environmental issues are the major challenges (Liu and Yen, 1995).

The leaching behaviour of gold in the presence of sulphide minerals depends strongly on both the amount of dissolved sulphur and the oxygen concentration in solution (Dai and Jeffrey, 2006). Since the dissolution of sulphide minerals consumes oxygen, a reduction in the gold-leaching rate occurred associated with low dissolved oxygen in the pulp. The equations related to cyanide consumption and passivation of gold with sulphide is as follows (Deschenes, 2005):

$$2MS + 2(x + 1)CN^- + O_2 + 2H_2O \rightarrow 2M(CN)_x^{(2-x)} + 2CNS^- + 4OH^- \qquad (1)$$

$$MS + 2OH^- \rightarrow M(OH)_2 + S^{2-} \qquad (2)$$

$$2M(OH)_2 + 1/2O_2 + H_2O \rightarrow 2M(OH)_3 \qquad (3)$$

$$2S^{-2} + 2O_2 + H_2O \rightarrow S_2O_3^{2-} + 2OH^- \qquad (4)$$
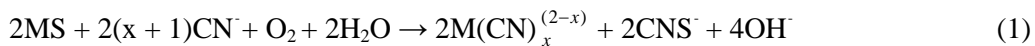
(x = 1, 2, 3..).

The effect of a higher oxygen level in the pulp containing sulphide minerals and their dissolved ions was investigated by Yen and Aghamiran (2002). They suggested that gold-bearing sulphide minerals could be divided into three groups based on their effect on gold leaching. The first group has a negative effect (stibnite, chalcocite, and pyrrhotite). The second group neither seriously reduces nor greatly enhances gold-leaching (pyrite, chalcopyrite, arsenopyrite, and sphalerite) while the third group that improves gold leaching (galena).

According to Weichselbaum et al. (1989), with the addition of trace amounts of sodium sulphide to the cyanide solution, gold leaching is prevented because of the formation of a passive layer of Au_2S on the gold surface. Similar results were obtained by Lorenzen and Van Deventer (1992) on gold leaching with reactive sulphide minerals like pyrrhotite. In another study, Jeffrey and Breuer (2000) investigated the effect of sulphur species using gold containing 5% silver instead of high purity gold. They suggested that dissolved sulphide reduces the rate of gold leaching by forming a monolayer of sulphur species.

The concentration of cyanide used varies depending on the mineralogical structure of the ore. Generally, the cyanide concentration practiced industrially is in the range of 0.15 to 0.5 g/dm^3. However, the feed material may contain significant amounts of cyanide consumers and/or high silver content (*i.e.*, >20 g/Mg). In such cases, higher cyanide concentrations, in the range of 2 to10 g/dm^3 NaCN, are needed. For those ores, gold recoveries may be reached above 90% indicating that the ore is non-refractory (Marsden and House, 2006). Although acceptable extractions can be obtained with those types of nonrefractory ores, cyanide consumption remains high, and it needs to be reduced. Therefore, many studies have been carried out on the basis of cyanide-oxygen interaction, which is described for alkaline cyanide solutions in the Bodlander equations:

$$2Au + 4NaCN + O_2 + 2H_2O \Leftrightarrow 2NaAu(CN)_2 + 2NaOH + H_2O_2 \qquad (5)$$

$$2Au + 4NaCN + H_2O_2 \Leftrightarrow 2NaAu(CN)_2 + 2NaOH. \qquad (6)$$
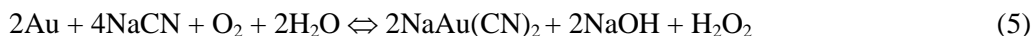
In order to speed up the gold and silver dissolution, higher oxygen and cyanide concentrations should be provided but high cyanide concentrations also increase cyanide consumption (Ellis and Senanayake, 2004). The use of oxygen or auxiliary

oxidizing reagents such as sodium peroxide, potassium permanganate, bromine, and chlorine are essential for the dissolution of gold under normal conditions. However, these auxiliary oxidants are not used anymore due to their cost and complications involved in their handling (Yannopoulos, 1991; Guzman et al., 1999; Cruells et al., 2000; Nugenta et al., 1991; Xie and Dreisinger, 2009).

The effect of hydrogen peroxide on gold leaching is a controversy subject. According to Zurilla et al. (1978) and Kirk et al. (1978), the dissolution rate of gold in oxygen–free solutions containing hydrogen peroxide is very slow, and the oxide layer formation on gold surface prevents gold leaching to take place. Other studies showed that the amount of hydrogen peroxide can be significant parameter on gold leaching. The gold leaching rate increased using a concentration of 0.015 mol/dm^3 H_2O_2 in a solution of 0.01 mol/dm^3 NaCN at pH 10. On the other hand, the same studies demonstrated that smaller quantities of hydrogen peroxide (*i.e.*, < 0.0025 mol/dm^3) prevented the gold dissolution rates at higher pH such as >11 (Guzman et al., 1999). Although hydrogen peroxide seems to be the most suitable alternative to atmospheric oxygen, its industrial use is questioned since it has a potential to oxidize cyanide resulting in high cyanide and peroxide consumptions and passivates the gold surface (Knorre et al., 1993; Ball et al., 1989; Habashi, 1967).

On the other hand, gold surfaces can be passivated by sulphide minerals bearing Cu, Fe, and Zn. In the literature, advantages of oxygen and $Pb(NO_3)_2$ for the kinetics of gold dissolution and/or cyanide consumption during the leaching of ores containing sulphide minerals was reported (Weichselbaum et al., 1989; Dufresne et al., 1994; Deschenes and Wallingford, 1995). Deschenes et al. (2002) indicated that lead nitrate addition increases gold leaching kinetics by reducing the detrimental effect of metallic sulphides, and decreases cyanide consumption. Morrison (1994) explained the role of lead nitrate as a catalyst at the surface of the gold preventing passivation. It also inhibits the dissolution of metallic sulphides providing a decline in cyanide consumption. On the contrary, it was found that lead nitrate is detrimental to the cyanidation when not added properly. It can prevent the dissolution of gold and increase cyanide consumption (Deschenes and Prud'homme 1997; Dufresne et al., 1994; Deschenes and Fulton, 1998). It has also been reported that the effect of lead nitrate was especially noticeable at low cyanide concentrations while there was no advantage at high cyanide concentrations (Weichselbaum et al., 1989).

The present research work aims at evaluating the leaching behaviour of non-refractory sulphide gold-silver ore. First, the characterization of the ore sample was initially accomplished by mineralogical analysis. Then, fundamental industrial cyanidation parameters such as leaching duration, cyanide concentration, particle size, and solids ratio were tested. After the optimising the experimental conditions, other parameters such as $Pb(NO_3)_2$ addition, use of oxidizing reagents, and aeration were tested in order to increase gold and silver recoveries and decrease cyanide consumption.

Experimental

Material and methods

Materials

The gold ore sample used in the present study was obtained from Canakkale Region of Turkey. The sample was crushed below 2 mm using jaw, cone, and roll crushers in turn. A representative sample was taken from the crushed ore for the chemical and mineralogical analyses. The chemical analysis of the gold ore sample is given in Table 1. According to the result of the chemical analysis, the sample assays 18.85 mg/dm^3 Au and 120 mg/dm^3 Ag.

Table 1. Chemical analysis of the gold ore sample

Element	Content (mg/dm^3)	Element	Content (%)
Au	18.85	Al	1.04
Ag	120	Ca	0.05
As	137.5	Fe	3.51
Bi	511	K	0.03
Zn	79	Mg	0.02
Co	41.8	Na	0.01
Cu	182	S	0.8
Se	51	Si	41

Mineralogical analyses were performed on polished section samples employing QEMSCAN (Quantitative Evaluation of Minerals by Scanning Electron Microscopy). The gold ore sample is dominated by pyrite and quartz, and the remainder is kaolinite. Other minerals are negligible, and including trace amounts of tetrahedrite, tennantite, sulphides, and sulpho-salts. The sample contains particles of well liberated pyrite, moderately inter-grown tetrahedrite, and minor sulphides/sulpho-salts. Sulphides are liberated from non-sulphide phases. Quartz and kaolinite are highly liberated but retain mutual intergrowths. Gold exists in clusters of native gold grains inter-grown with silver sulpho-salts. A significant amount of gold is contained in liberated particles of electrum. The remaining gold occurs as small and encapsulated grains of native gold, electrum, and calaverite. Silver primarily occurs as large chlorargyrite grains and some relic argentite. The association of Au and Ag minerals with pyrite is dominant. Pyrite contains most of the accounted iron, and the remaining iron is mainly locked in Fe-Ti oxides and steel contamination. Almost all the sulphur (99%) comes from pyrite and the remaining sulphur is locked in minor sulphides and some sulphates. Au-Ag occurrences in the sample were observed as native gold (95-100% Au and 0-5% Ag), argentian native gold (80-95% Au and 5-15% Ag), electrum (20-

80% Au and 20-80% Ag), calaverite ($AuTe_2$, ~37% Au), chlorargyrite (AgCl), argentite (Ag_2S), and jalpaite-proustite (Ag_3CuS_2-Ag_3AsS_3). SEM images of the samples are shown in Figs. 1a-d.
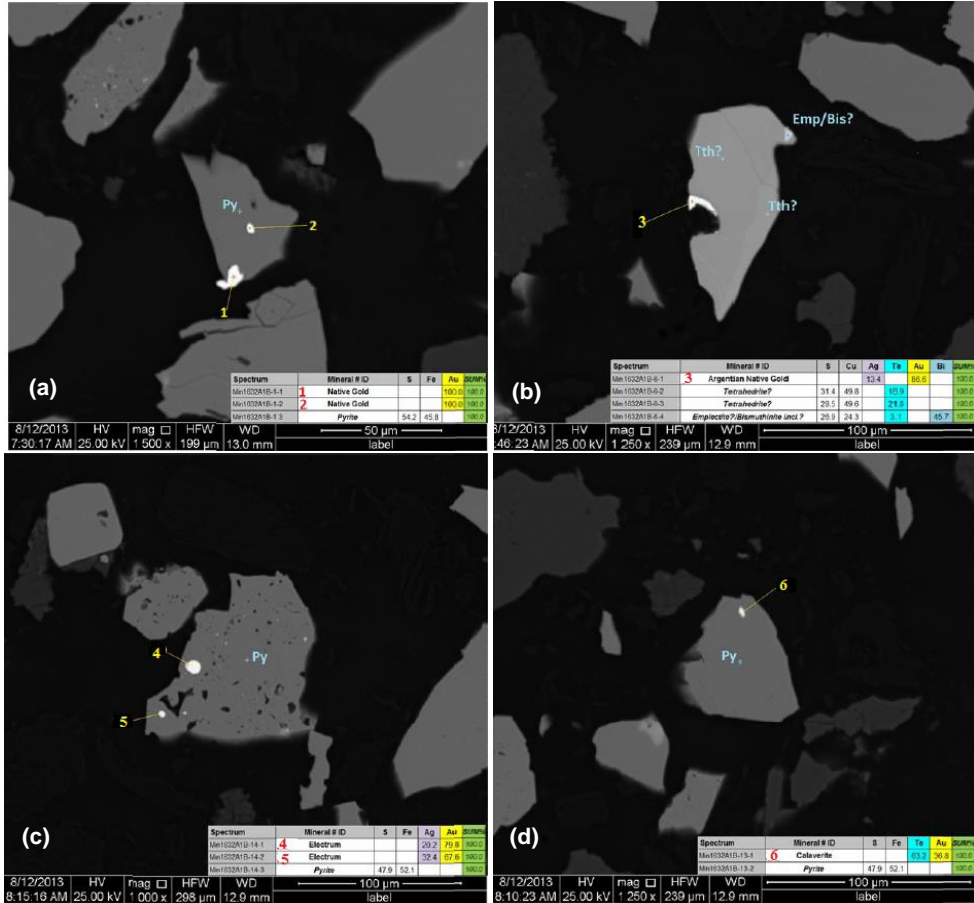
Fig. 1. SEM images of the ore sample (a) 1-native gold, 2-native gold (b) 3-argentian native gold (c) 4-electrum, 5-electrum (d) 6-calaverite

Methods

The representative sample was ground below 100 μm using a ring mill for the agitation leaching tests, which are conducted in a beaker employing a mechanical mixer (IKA RW20) with teflon coated impeller speed at 450 rpm. Analytical grade NaCN (Merck) was used for the cyanidation process, where lime was used as a pH regulator to keep pH (WTW 3401 pH meter) between 10.5 and 11. After the leaching was complete, the solid-liquid separation was performed with a vacuum filter. In order to determine free cyanide concentration in the pregnant solution, the titration process was performed using standard silver nitrate (0.02 mol/dm^3) solution and rhodamine as

indicator. The dried leach cake was assayed for Au and Ag employing fire assay method.

In the cyanidation tests, parameters such as leaching duration, cyanide concentration, particle size, and solids ratio were tested. After the conditions were optimized, the effect of $Pb(NO_3)_2$ was investigated in the presence of hydrogen peroxide and aeration. Furthermore, pre-aeration tests were carried out as there is sulphide minerals present.

Results and discussion

Effect of leaching time

To investigate the effect of leaching time, the experiments were carried out at different leaching durations (12, 24, 48, and 96 h). All experiments were accomplished with 1 g/dm^3 NaCN concentration at 10% solids ratio, at room temperature, and -100 μm particle size. The results presented in Fig. 2 show that the optimum leaching time is 24 h where the extractions of gold and silver are 95.89% and 90.35%, respectively. As seen in Fig. 2, leaching time of 24 h was found to be a critical value since Ag recovery decreased beyond this leaching time. Despite long leaching durations are preferred for silver extraction; probably because of relatively low NaCN concentration it did not increase in this case.

The highest silver recoveries were obtained at leaching times of 12 and 24 h. However, the increasing the leaching time beyond 24 h had a negative effect on Ag extraction. The reason for that situation was thought to be the precipitation of silver sulphide compounds. The silver sulphide layer formed particularly on the surface of electrum could not be oxidized due to the deficiency of dissolved oxygen in pulp. Marsden and House (2006) reported that a silver sulphide layer of 1 to 2 μm thickness forms on the surface of electrum in the presence of sulphide ions. The consisted layer prevents the reaction of electrum with sodium cyanide, and decreases dissolution kinetics of silver.

Effect of NaCN concentration

NaCN concentrations of 0.5, 1.0, and 2.0 g/dm^3 were tested to examine the effect of cyanide concentration on the dissolution of Au and Ag. As it can be seen from Fig. 3, 95.9% Au and 90.35% Ag recoveries were achieved at 1 g/dm^3 NaCN concentration. When 2 g/dm^3 NaCN was used, a minor increase in the recoveries was obtained for both metals. Since the increase in the recoveries was not significant, it was decided to conduct test at 1 g/dm^3 NaCN concentration in further studies.

Effect of particle size

The effect of particle size on the dissolution of Au and Ag was investigated with different particle sizes below 150, 100, 74, 53, and 38 μm. According to the results given in Fig. 4, the metal recoveries increased as the particle size decreased. It is known that the dissolution rate of Au and Ag generally increases as the particles size decreases due to an increase in gold liberation and/or surface area of gold particles as

the result of flattening or physical breakage during grinding except ores containing cyanides (Marsden and House, 2006). As seen from Fig. 4 leaching of the -74 μm particle size fraction yielded recoveries above 90%, and an increase in the recovery of the finer particle is marginal.
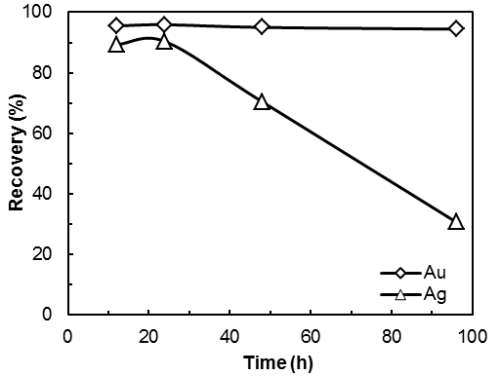
Fig. 2. Effect of leaching time on gold and silver recoveries (1 g/dm^3 NaCN concentration, 10% solids ratio, -100 μm particle size, and 450 rpm stirring speed at room temperature)
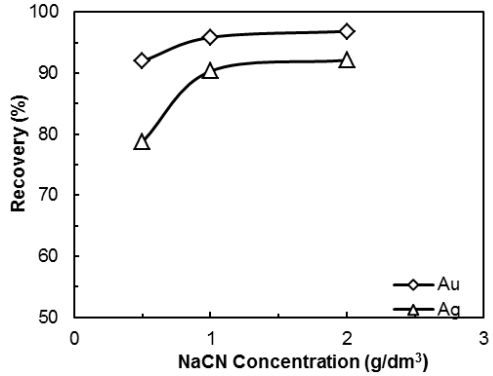
Fig. 3. Effect of NaCN concentration on gold and silver recoveries (10% solids ratio, 24 h cyanidation time, -100 μm particle size, and 450 rpm agitation speed at room temperature)
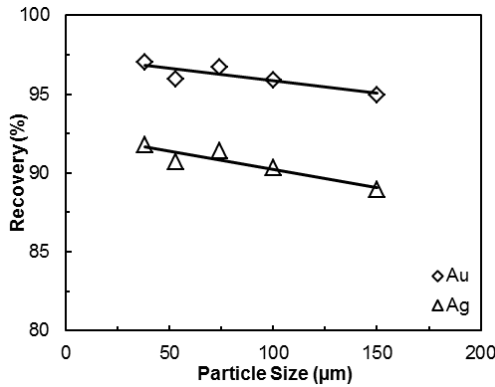
Fig. 4. Effect of particle size on gold and silver recoveries
(10% solids ratio, 1 g/dm^3 NaCN concentration, 24 h cyanidation time,
and 450 rpm stirring speed at room temperature)

Effect of solids ratio

The effect of different solids ratios such as 10, 20, 30, 40, 50% (w/w) on the cyanidation were tested at varying NaCN concentrations under the optimum conditions determined from the previous experiments. According to the results demonstrated in Fig. 5, the highest Au and Ag recoveries were achieved as 98.26% and 95.22%, respectively, at 10% solids ratio and 4 g/dm^3 NaCN concentration.

Even though the highest recoveries were obtained at 10% solids ratio, the leaching is usually performed at higher solids ratios, that is between 35% and 50%, in industrial applications. Therefore, 40% solids ratio with the same NaCN concentration was chosen for the following tests. The optimum leaching parameters at 40% solids ratio were 24 h cyanidation time, -74 μm particle size, 4 g/dm^3 NaCN concentration, and 450 rpm stirring speed under atmospheric conditions. Under these conditions, the NaCN consumption was 3.35 g/dm^3.

A concentration of 4 g/dm^3 NaCN seems to be too high compared to the concentration used in industrial applications, which is around 0.5 g/dm^3. However, Marsden and House (2006) reported that cyanide concentrations from 2 to 10 g/dm^3 in the presence of silver contents may be above 20 g/Mg. Since the ore sample used in this study contains 120 mg/dm^3 Ag, the use of 4 g/dm^3 NaCN concentration would be suitable. On the other hand, the reason for relatively high NaCN consumption may be attributed to the presence of sulphur species, which reacts with cyanide to form thiocyanite, sulphate, sulphide, and polysulphide ions or leads to sulphur coatings on the gold surface. Thiocyanite increases NaCN consumption as seen in the following reactions (Marsden and House, 2006):

$$S^0 + CN^- \Leftrightarrow SCN^- \tag{7}$$

$$S^{2-} + CN^- \Leftrightarrow SCN^- + 2e \tag{8}$$

$$S_2O_3^{2-} + CN^- \Leftrightarrow SO_3^{2-} + SCN^-. \tag{9}$$

The adverse effect of sulphur species on cyanide consumption may be prevented by using Pb(NO$_3$)$_2$, oxidizing reagents, and aeration individually or in combination.

Fig. 5. Effect of solids ratio in the presence of 1-2-4 g/dm^3 NaCN (24 h cyanidation time, -74 μm particle size, and 450 rpm stirring speed at room temperature) on recovery
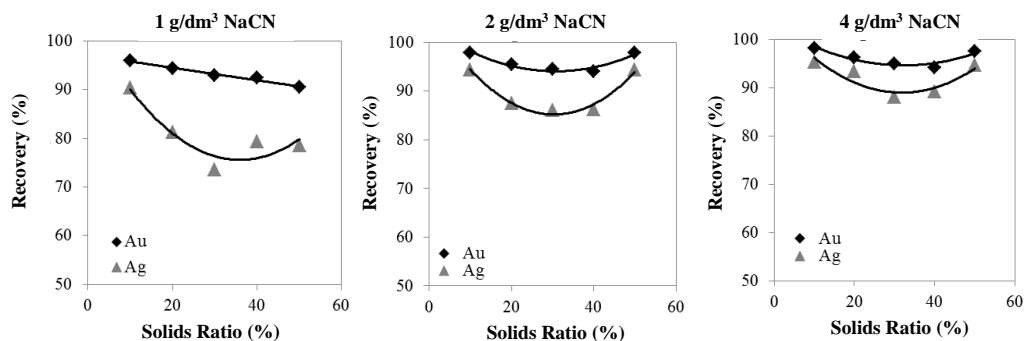
Effect of lead nitrate

The effect of lead nitrate was investigated in order to improve gold extraction and minimize the cyanide consumption. Different amounts of lead nitrate (100, 200, and

400 g/Mg) were used at a 6 dm^3/min aeration rate. The leaching conditions were 4 g/dm^3 NaCN concentration, 40% solids ratio, pH 10.5-11.0, and 24 h stirring duration. As it is seen from Table 2, the addition of lead nitrate did not provide any beneficial effect on gold-silver recovery nor cyanide consumption, whereas the lead nitrate addition caused a significant decrease in gold and particularly silver recoveries.

The lead forms an insoluble hydroxide and possibly some lead sulphate depending on pH and sulphate concentration in solution. It is known that in the presence of sulphide minerals, lead nitrate precipitates sulphides. Therefore, formation of a sulphide film on the gold surface is prevented (Breuer et al., 2008, Deschenes et al., 2000; Hedley and Tabachnick , 1968). In the presence of cyanide, thiocyanate is formed due to the oxidation of lead sulphide (Breuer et al., 2008):

$$PbS + CN^- + 1/2\ O_2 + H_2O \rightarrow Pb^{2+} + SCN^- + 2OH^-. \tag{10}$$
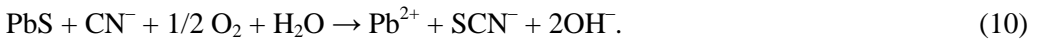
In the presence of excess amounts of sulphide species in the leaching solution, sulphide ions react with oxygen much faster to form polysulphides. At that point, oxidation of sulphide ions is accelerated with the existence of lead sulphide in the absence of cyanide in leach medium. As seen from the following reactions, lead sulphide acts as a catalyst in the oxidation reactions (Breuer et al., 2008):

$$2S^{2-} + 1/2\ O_2 + H_2O \xrightarrow{\ PbS\ } S_2^{2-} + 2OH\text{-} \tag{11}$$

$$S_{x-1}^{2-} + S^{2-} + 1/2\ O_2 + H_2O \xrightarrow{\ PbS\ } S_x^{2-} + 2OH^-. \tag{12}$$

Table 2. Effect of lead nitrate on gold-silver recovery and NaCN consumption
(40% solids ratio, 4 g/dm^3 NaCN concentration, 24 h leaching time,
-74 µm particle size, and 450 rpm stirring speed at room temperature)

Amount of lead nitrate (g/Mg)	Gold recovery (%)	Silver recovery (%)	NaCN consumption (g/dm^3)
0	95.03	87.99	3.35
100	62.69	79.30	3.88
200	52.97	44.46	3.88
400	65.93	25.59	3.83

It has been reported by many researchers that the addition of lead nitrate improves the rate of gold dissolution and NaCN consumption due to the presence of excess amounts of sulphur species in their leach slurries. Considering the high NaCN consumption values obtained, it is seen that the dissolved lead(II) ions precipitated sulphur ions to form lead sulphide. However, in the presence of air and cyanide, lead sulphide oxidized leading to thiocyanate formation, and thus leaving little amount of dissolved sulphur species in the leach solutions. Therefore, the use of lead nitrate did not provide any improvement in the results.

Effect of oxygen

Liu and Yen (1995) reported that the effect of sulphide minerals on the dissolution of gold and silver depended on the sulphide mineral and oxygen contents in solution. Yen and Aghamiran (1998) suggested that oxygenation of the pulp had a positive effect on gold leaching in the presence of pyrrhotite, pyrite, sphalerite, and chalcopyrite. Therefore, the relationship between NaCN consumption, gold-silver recoveries and oxygen addition to the pulp was investigated.

The introduction of oxygen as hydrogen peroxide (H_2O_2), at different dosages during leaching was investigated under optimum conditions obtained previously. The results are demonstrated in Table 3. According to the repeated experiment results, it is seen that the test results slightly improved at 0.005 mol/dm^3 H_2O_2 concentration where Au-Ag recoveries were 95.15% and 92.44%, respectively, with 3.90 g/dm^3 NaCN consumption. When H_2O_2 concentration increased to 0.020 mol/dm^3, Au and Ag extractions were obtained as 96.64% and 90.35%, respectively, with 3.64 g/dm^3 NaCN consumption. The reason for relatively higher cyanide consumption can be attributed to the oxidation of NaCN by H_2O_2. It seems that H_2O_2 acted as an oxidizing agent rather than an oxygen source.

The leaching tests performed at 4 g/dm^3 NaCN concentration resulted in high NaCN consumptions. Also, the effect of H_2O_2 addition on lower (1 g/dm^3) NaCN concentration was investigated. However, the tests showed that metal extraction values remained below 70%.
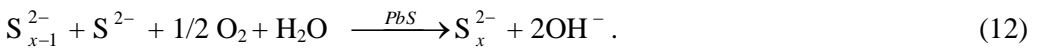
Table 3. Effect of H_2O_2 addition on gold-silver recovery and NaCN consumption
(40% solids ratio, 4 g/dm^3 NaCN concentration, 24 h leaching time,
-74 μm particle size, and 450 rpm stirring speed at room temperature)

Amount of H_2O_2 (mol/dm^3)	Gold Recovery (%)	Silver Recovery (%)	NaCN Consumption (g/dm^3)
0	95.03	87.99	3.35
0.005	95.15	92.44	3.90
0.010	95.29	91.27	3.80
0.015	96.05	90.93	3.75
0.020	96.64	90.35	3.64

According to Habashi (1967) cyanide concentration and dissolved oxygen directly influence the rate of gold dissolution. The dissolution rate depends on the cyanide concentration at low cyanide concentrations, and it is related to the oxygen concentration at high cyanide concentration:

$$v = 0.5_{CN^-} \, \delta^{-1} \, [CN^-] \tag{13}$$

$$v = 2AD_{O_2} \, \delta^{-1} [O_2] \tag{14}$$

where A is gold surface, D is diffusion coefficient, and δ is thickness of the boundary layer (Deschenes and Wallingford, 1995).

Oxygen can be introduced into solution by bubbling air into the slurry. It was done at a rate of a 6 dm^3/min capacity. According to the results given in Table 4, Au and Ag recoveries reached up to 96% and 92%, respectively, in the case of bubbling air only. When the results are compared, the addition of 0.005 mol/dm^3 H$_2$O$_2$ and bubbling air provided similar recoveries. However, a simultaneous usage of air and peroxide caused a detrimental effect on Ag recovery. The reason for that was thought to be the presence of excess oxygen in the medium, which prevented Ag dissolution as in the case of increased amounts of H$_2$O$_2$. It it known that the dissolved oxygen is appears when hydrogen peroxide decomposes into oxygen and water in solution as follows:

$$2H_2O_2 \rightleftharpoons O_2 + 2H_2O. \tag{15}$$

It has been suggested that high dissolved oxygen concentrations may cause passivation of the gold-silver surface due to an oxide layer formation (Cathro et al., 1961).

Table 4. Effect of oxidant types on gold and silver recoveries and NaCN consumption
(40% solids ratio, 4 g/dm^3 NaCN concentration, 24 h leaching time,
-74 μm particle size, and 450 rpm stirring speed at room temperature)

Oxidant Type	Gold Recovery (%)	Silver Recovery (%)	NaCN Consumption (g/dm^3)
–	95.03	87.99	3.35
0.005M H$_2$O$_2$	95.15	92.44	3.90
Air + 0.005M H$_2$O$_2$	96.07	70.25	3.95
Air	96.36	91.80	3.98

On the other hand, NaCN consumptions had a parallel trend to Au recoveries. The main objective of studying the effect of oxygen enriched medium was to reduce NaCN consumption. However, the results obtained showed that introducing oxygen into the solution during leaching process caused an increase in NaCN consumption and improvement of Au and Ag extractions. Therefore, the effect of pre-aeration was studied to increase further the Au and Ag dissolution.

Effect of pre-aeration

The pre-aeration was carried out by bubbling air into the slurry for 4 h at 40% solids ratio. In the course of pre-aeration, NaCN was not added. However, the pH value was kept constant around 10.5-11.0. After finishing the pre-aeration operation, 4 g/dm^3 NaCN was added, and leaching was accomplished for 12, 18, and 24 h periods. The results are presented in Table 5. According to the test results, 12 h of leaching time was found to be sufficient, which provided 92% Au and 90.5% Ag recoveries. Furthermore, NaCN consumption decreased to 2.44 g/dm^3 (Fig. 6). Therefore, the

effect of pre-aeration time as 2 and 8 h followed by a 12 h leaching process was investigated. In the case of 2 and 8 h pre-aeration times, Au and Ag extractions were obtained at 4 h pre-aeration time considerably reduced, with smaller NaCN consumption equal to 2.04 g/dm^3 and 1.51 g/dm^3, respectively.

Table 5. Effect of pre-aeration on gold and silver recoveries and NaCN consumption
(40% solids ratio, 4 g/dm^3 NaCN concentration, 4 h pre-aeration time,
-74 μm particle size, and 450 rpm stirring speed at room temperature)

Leaching Duration (h)	Gold Recovery (%)	Silver Recovery (%)	NaCN Consumption (g/dm^3)
12	92.04	90.52	2.44
18	85.28	89.78	3.41
24	71.39	91.52	3.45

It can be suggested that pre-aeration made the leaching environment rich in oxygen and oxidized sulphide species, allowing the gold and silver particles to be exposed. During pre-aeration, NaCN was not introduced into the leaching to prevent NaCN to oxidise. As long as pre-aeration time increased, the oxygen concentration in the leach medium also increased as expected. However, longer pre-aeration times than 4 h had a negative effect on gold dissolution while silver dissolution was not affected. The reason for that the result was thought to be oxide layer formation which caused passivation of the gold surface and inhibited gold leach solution.
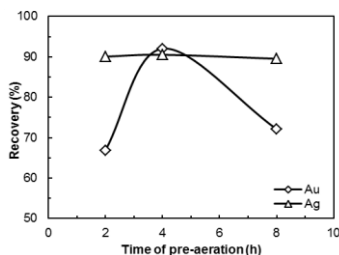
Fig. 6. Effect of time of pre-aeration (40% solids ratio, 4 g/dm^3 NaCN concentration,
12 h cyanidation time after pre-aeration time of 2, 4, and 8 h, -74 μm particle size,
and 450 rpm stirring speed at room temperature)

Conclusions

This investigation has characterized non-refractory sulphide gold-silver ore and presented its leaching behaviour under oxidizing conditions. During leaching of the sulphide ores, sulphur species react with sodium cyanide and prevent the formation of a film layer on gold and silver surfaces. Since it was reported in the literature that lead nitrate prevents the formation of a sulphide film on gold and silver surfaces and decreases NaCN consumption, different dosages of lead nitrate were used in this

study. Nevertheless, the dissolved lead(II) ions precipitated sulphur ions and formed lead sulphide, while in the presence of air and cyanide, lead sulphide oxidized simultaneously leading to thiocyanate formation.

Although slight improvements were observed in the gold and silver extractions with H_2O_2 addition, air injection, and the combination of air/peroxide, NaCN consumption did not reduce because of the oxidation of cyanide by the severe oxidizing conditions. Therefore, an alternative way of aeration prior to cyanidation was performed, which provided the oxidation of sulphide ions rather than cyanide. Accordingly, cyanidation following pre-aeration of the leach slurry for 4 h resulted in above 90% Au and Ag recoveries. NaCN consumption was reduced to 2.44 g/dm^3 from 3.35 g/dm^3, and the leaching time was reduced from 24 h to 12 h.

Acknowledgments

References

BALL, S.P., MONHEMIUS, A.J., WYBORN, P.J., 1989, *The use of inorganic peroxides as accelerators for gold heap leaching*, Precious Metals '89, 149–162.

BREUER, P.L., JEFFREY, M.I., HEWITT, D.M., 2008, *Mechanisms of sulfide ion oxidation during cyanidation. Part I: The effect of lead(II) ions,* Minerals Engineering, 22, 579-586.

CATHRO, K.J., WALKLEY, A., 1961, *The cyanidation of gold*, CSIRO Publication Melbourne, Australia: CSIRO.

CRUELLS, M., ROCA, A., PATINO, F., SALINAS, E., and RIVERA, I., 2000, *Cyanidation kinetics of argentian jarosite in alkaline media*, Hydrometallurgy, 55(2), 153-165.

DAI, X. and JEFFREY, M.I., 2006, *The effect of sulfide minerals on the leaching of gold in aerated cyanide solutions*, Hydrometallurgy, 82, 118–125.

DESCHENES, G. WALLINGFORD, G., 1995, *Effect of oxygen and lead nitrate on the cyanidation of a sulfide-bearing gold ore*, Minerals Engineering, 8, 923-931.

DESCHENES, G. PRUD'HOMME, P.J.H., 1997, *Cyanidation of a copper-gold ore*, International Journal of Mineral Processing, 50, 127-141.

DESCHENES, G., FULTON, M., 1998, *Improving cyanidation of a sulfide ore by using an efficient pre-leaching*, Proceedings of the Int. Symp. on the Recovery of Gold, Montreal, 4–7 May.

DESCHENES, G., LASTRA, R., FULTON, M., 2002, *Effect of the mineralogy of sulfide-bearing gold ores on the performance of cyanidation and its control variables*, In Proceeding of the Annual Meeting of the Canadian Mineral Processors CIM, Ottawa, 325–338.

DESCHENES, G., 2005, *Advances in the cyanidation of gold*, Advances in Gold Ore Processing, published by Elsevier.

DUFRESNE, C., DESCHENES, G., CIMON, D., 1994, *Control of cyanidation at the Yvan Vezina plant*, Minerals Engineering, 7 (11), 1427-1434.

ELLIS, S. SENANAYAKE, G., 2004, *The effects of dissolved oxygen and cyanide dosage on gold extraction from a pyrrhotite-rich ore*, Hydrometallurgy, 72, 39–50.

GUZMAN, L., SEGARRA, M., CHIMENOS, J.M., FERNANDEZ M.A., ESPIELL, F., 1999, *Gold cyanidation using hydrogen peroxide*, Hydrometallurgy, 52, 21–35.

HABASHI, F., 1967, *Kinetics and mechanism of gold and silver dissolution in cyanide solution*, Montana Bureau of Mines Geological Bulletin, 59, 42.

HEDLEY, N., TABACHNICK, H., 1968, *Mineral dressing notes No 23*, Chemistry of Cyanidation, American Cyanamid Company, New Jersey, USA.

JEFFREY, M.I., BREUER, P.L., 2000, *The cyanide leaching of gold in solutions containing sulfide*, Minerals Engineering, 13 (10-11), 1097-1106.

KIRK, D.W., FOULKES, F.R., GRAYDON, W.F., 1978, *A study of anodic dissolution of gold in aqueous alkaline cyanide*, Journal of Electrochemical Society, 125, 1436-1443.

KNORRE, H., LOROESCH, J., GOS, S., STOLL, M., ZIEGLER, A., 1993. *Process for leaching precious metals with hydrogen peroxide and cyanide leaching solution*, US Patent No. 5250272.

LIU, G.Q., YEN, W.T., 1995, *Effects of sulfide minerals and dissolved oxygen on the gold and silver dissolution in cyanide solution*, Minerals Engineering, 8, 111-123.

LORENZEN, L., VAN DEVENTER, J.S.J., 1992, *The mechanism of leaching of gold from refractory ores*, Minerals Engineering, 5 (10-12), 1377-1387.

MARSDEN, J.O., HOUSE, I.C., 2006, *The chemistry of gold extraction*, published by the SME Inc., 2nd Edition.

MORRISON, R.M., 1994, *Factors impacting on lead nitrate additions to cyanidation circuits*, MSL Report 94-42 (CR).

NUGENT, A., BRACKENBURY, K., KINNER, J., 1991, *AuPLUS systems for the treatment of gold ores using hydrogen peroxide and calcium peroxide*, World Gold'91 Queensland: AIMMEM, 173-176.

YANG, X., MOATS, M.S., MILLER, J.D., 2010a, *Gold dissolution in acidic thiourea and thiocyanate solutions*, Electrochimica Acta, 55, 3643–3649.

YANG, X., MOATS, M.S., MILLER, J.D., 2010b, *The interaction of thiourea and formamidine disulfide in the dissolution of gold in sulfuric acid solutions*, Minerals Engineering, 23 (9), 698–704.

YANG, X., MOATS, M.S., MILLER, J.D., 2010c, *Using electrochemical impedance spectroscopy to investigate gold dissolution in thiourea and thiocyanate acid solutions*, ECS Tran, 28(6), 213–222.

YANG, X., MOATS, M.S., MILLER, J.D., WANG, X., SHI, X., XU, H., 2011, *Thiourea–thiocyanate leaching system for gold*, Hydrometallurgy, 106 (1–2), 58–63.

YANNOPOULOS, J.C., 1991, *The Extractive Metallurgy of Gold*. Van Norstand Rainhold, Newyork.

YEN, W. T., AGHAMIRIAN, M. M., 1998, *Effect of sulfide minerals and dissolved ions on gold dissolution rate in oxygenated cyanide solution*, Proceedings of the International Symposium on Gold Recovery, 79-86.

YEN, W. T., AGHAMIRIAN, M. M., 2002, *Effect of sulfide minerals and dissolved ions on gold dissolution*, In: Laptante, A. (Ed.), CIM General Annual Meeting, Special Vol.51. CMP/CIM, Canadian Institute of Mining, Metallurgy and Petroleum, Montreal, 79-86.

XIE, F. and DREISINGER D.B., 2009, *Use of ferricyanide for gold and silver cyanidation*, Transaction of Nonferrous Metals Society of China 19, 714-718.

WEICHSELBAUM, J., TUMILTY, J.A., SCHMIDT, C.G., 1989, *Improved gold recovery by cyanidation - a kinetic problem*, Processing. Extraction Metallurgy '89. I.M.M., London, 679-690.

ZURILLA, R.W., SEN R.K., and YEAGER E., 1978, *The kinetics of oxygen reduction reaction on gold in alkaline solution*, Journal of Electrochemical Society, 125, 1103-1109.

MINERAL PRECONCENTRATION
USING NEAR INFRARED SENSOR-BASED SORTING

Shekwonyadu IYAKWARI, Hylke J. GLASS

Camborne School of Mines, University of Exeter, Penryn Campus, Cornwall, TR10 9FE, UK
si233@exeter.ac.uk (S. Iyakwari), h.j.glass@exeter.ac.uk (H. J. Glass)

Abstract: This paper predicts qualitatively and quantitatively the near infrared activity of individual minerals in simple and complex mineral associations using mixtures of common alteration minerals found in a copper ore. It was found that spectra dominance in most cases is dependent on any or combination of mineral composition, relative proportion or concentration and/or mineral accessibility or sensitivity to near infrared radiation. The analysis of results also indicated that, in most cases, only freely occurring waste, such as clays (kaolinite and/or muscovite) and calcite, can be targeted for discrimination. In this paper, a strategy for the application of near infrared for preconcentration of copper bearing minerals like chrysocolla and malachite from coarse ore particles was proposed. Other applications also considered in this paper include preconcentration of hematite from associated clays and carbonate waste, and the determination of moisture content in kaolinitic clays.

Keywords: near infrared, copper, hematite, preconcentration, strategy, intimate mixtures, moisture

Introduction

The main goal of near infrared (NIR) application in a mineral processing operation is to accurately classify the composition of individual spectra obtained by scanning and classifying ore particles according to their value. This is complicated by the fact that most spectra are influenced by a complex mixture of minerals. Hence, a number of minerals could exist within the range in varying compositions and arrangements among other modes of occurrence. In order to develop an efficient sensor-based sorting process, determination of the point of dominance of individual minerals and ratio at which spectral mixing is reached is important.

In the longer wavelength region of NIR (1300 to 2500 nm), a few functional groups (-OH, H_2O and or CO_3^{2-}) dominate spectra due to vibrational processes (Clark, 1995). Based on the presence or absence of these functional groups, minerals can be classified into three major groups: a) NIR-active minerals which display absorption

features, b) NIR-active minerals which do not display absorption features, and c) non-active minerals. Note that NIR-active minerals without distinctive absorption features are highly absorbing throughout the longer wavelength region of NIR, with the ability of masking feature of other minerals (Iyakwari and Glass, 2014). Even when present in combination with other minerals, non-active minerals do not influence NIR spectra either by absorbing or displaying absorption features. In some instances the NIR features in non-active minerals are a result of either impurities (fluid inclusions) or external environmental interference (moisture) (Aines and Rossman, 1984; Pommerol and Schmitt, 2008; Iyakwari et al., 2013).

This paper aims to predict individual NIR-active minerals exerting a dominant influence over other mineral responses within the same NIR spectral range. Mineral associations as present in a hydrothermally-formed supergene-enriched copper deposit found in the Atacama district in Northern Chile (Daroch and Barton, 2011) are used in this paper. From the modal mineralogy, chrysocolla and malachite are the copper-bearing minerals in the ore. Both minerals are absorption features displaying NIR-active minerals (Iyakwari et al., 2013). Associated NIR-active waste minerals in the ore include kaolinite, calcite, muscovite, chlorite, biotite and hematite (Iyakwari et al., 2013; Iyakwari and Glass, 2014). Hence, chrysocolla and malachite preconcentration is scoped from these associated NIR-active waste minerals in the ore. Preconcentration of iron oxide ore (hematite) from clay and/or carbonate gangue minerals and the potential for using NIR for determination of moisture content of kaolinitic clays are also considered.

According to Clark et al. (1999), there are four types of complex mixtures or associations of materials: intimate, linear or areal, coatings, and molecular mixtures. With respect to current research, only intimate mixtures consisting of two or more minerals were investigated. This research aims to further study intimate mixtures of NIR-active minerals and explore strategies of applications in complex ore preconcentration.

According to Iyakwari and Glass (2014), the NIR feature depth and reflectance are affected by variation in the particle size. Hence, to avoid the influence of varying particle size, similar particle sizes were used in this study. Pure minerals were mixed with the sole aim of quantitatively and qualitatively classifying or defining them based on their best diagnostic absorption features in NIR (Iyakwari and Glass, 2014), and developing discrimination strategies from associated waste. This study is intended to reveal the degree of sensitivity of these minerals individually in the mixtures. The investigation also aims to establish whether minerals can be individually identified and classified relative to one another, and at what ratio spectra appear mixed, showing features relating to all minerals in concentration, or when one mineral relative to the other(s) becomes invisible (masked or replaced) in a spectrum.

Material and methods

Eight NIR-active minerals with expected association in a copper ore were selected: calcite and malachite (carbonate-bearing), kaolinite, muscovite, chrysocolla, chlorite (clinochlore), biotite (hydroxyl- and water-bearing) and hematite. Minerals were crushed and ground to -45 µm particle size fraction. The ground samples were first analysed for purity using X-Ray Diffraction (XRD, Siemens/Bruker D5000). XRD measurements were matched with known mineral signatures using EVA software. Results of XRD indicate that the samples were of high purity.

Table 1 presents NIR-active minerals in the ore, indicating their diagnostic feature(s) wavelength absorption position between 1300 and 2500 nm, and the functional groups responsible for their absorption. Ground minerals (-45 µm) were intimately mixed according to prescribed ratios of mass. While simple mixtures involving two minerals were only prepared for a series of mass ratios, complex mixtures involving three or more minerals were only created with equal mass of each mineral. Each mixture was homogenised using a Grant-bio PTR-60 end-to-end shaker. The end-to-end shaker was set to rotate at 30 rpm for eighteen hours. Following this treatment, the mixtures appeared to be homogeneous. In order to achieve the desired objectives, the investigation was broken down into four parts:

a) minerals with similar functional groups,
b) minerals with dissimilar functional groups,
c) influence of hematite on NIR-active feature displaying minerals,
d) complex mixture or associations.

The spectra were generated by a NIR line scanner, which measures on a succession of adjacent areas across the mineral surface, each with a size of 2.9 mm by 9 mm. The measured NIR signal was converted to a reflectance by first measuring the upper and lower signal values. For the upper limit, denoted I_{light}, a highly-reflective board made of aluminium was scanned. For the lower limit, denoted I_{dark}, a scan was made in the absence of near infrared illumination. The NIR signal, I, was then converted into a reflectance, R, as follows (Iyakwari et al., 2013):

$$R = \frac{I - I_{\text{dark}}}{I_{\text{light}} - I_{\text{dark}}} \ . \tag{1}$$

Field data are often accompanied by noise self-generated by the sensor and/or the result of physical fluctuations in surrounding environment (Stark and Lutcher, 2005). All spectra were smoothed using OriginPro 9.0 software with the Savitzky–Golay method (Savitzky and Golay, 1964), applying a polynomial of order 2 to a frame size of 9 points.

Table 1. Absorption features of NIR-active minerals (between 1300 nm and 2500 nm) in copper ore (after Iyakwari et al., 2013; Iyakwari and Glass, 2014)

Group	Mineral	Molecule absorption feature, nm		
		–OH	H_2O	CO_3^{2-}
Silicate	chrysocolla	1415, 2270	1415, 1915	–
	muscovite	1415, 2205, 2350	1415, 1840, 1915	–
	kaolinite	1400, 1415, 2160, 2200	1415, 1840, 1915	–
	biotite	2255, 2370	1920	–
	chlorite	1415, 2265, 2360	–	–
Carbonate	calcite	–	–	1920, 2000, 2150, 2340
	malachite	2360	–	2275, 2360
Oxide	hematite	non–feature displaying NIR–active mineral		

Results and discussion

NIR spectra of intimate mixtures (Tables 2 and 3) revealed that when a particle contains mixtures of minerals, the visibility of absorption features of individual minerals in its NIR spectrum or spectra may depend on any or the combination of these mineralogical factors:
1) NIR-active mineralogical composition,
2) relative proportion or concentration, or
3) relative mineral accessibility or sensitivity to NIR radiation.

Other factors may include instrumental parameters, such as the spatial and spectral resolution (the narrowest spectral feature that can be resolved by a spectrometer) of the sensor, as well as the sensor sensitivity and mode of scanning. For some intimate mixtures, spectra dominance depends on concentration and mineral accessibility to NIR radiation. An example of concentration-dependent mixture (association) is chrysocolla and muscovite (Fig. 1 and Table 2). The mineral with higher concentration will dominate the spectrum of mixture. The mixture of muscovite and chlorite (Fig. 2 and Table 2) is a good example of mineral accessibility-dependent association. Here, muscovite dominates spectra even at lower concentration relative to chlorite, implying that muscovite is more readily accessible to NIR radiation than chlorite.

In other instances, spectral dominance depends on the NIR-active mineral composition, with minerals behaving differently in different mixtures. For example, weak mineral in one mixture may be strong when mixed with another mineral. An example is chlorite: the spectrum of both minerals mixed with chrysocolla (Fig. 3)

shows features of the minerals side-by-side. The visibility of features of either mineral is concentration-independent as both minerals are equally NIR-sensitive. In chrysocolla-malachite mixtures, chrysocolla shows more spectral dominance. This is not observed for chlorite mixed with malachite. When mixed with malachite, chlorite features are captured, meaning that malachite is more readily accessible to NIR than chlorite.

Fig. 1. NIR spectra of chrysocolla-muscovite mixtures. Bottom and top spectra
are reference for chrysocolla and muscovite, respectively

Fig. 2. NIR spectra of chlorite-muscovite mixtures. Bottom and top spectra
are reference for chlorite and muscovite, respectively

Apart from the weakness of malachite in chrysocolla mixtures and the complete spectral mixing of malachite and kaolinite (Fig. 4), only the effect of malachite and hematite is fairly consistent across range of mixtures. The consistency of both minerals may be due to their colour (Clark, et al., 1999). Malachite may also have additional influence due to its -OH and CO_3^{2-} combination chemical structure, making it strong enough to display its absorption feature (2275 nm) even at higher hematite concentration when both are mixed together (Fig. 5).

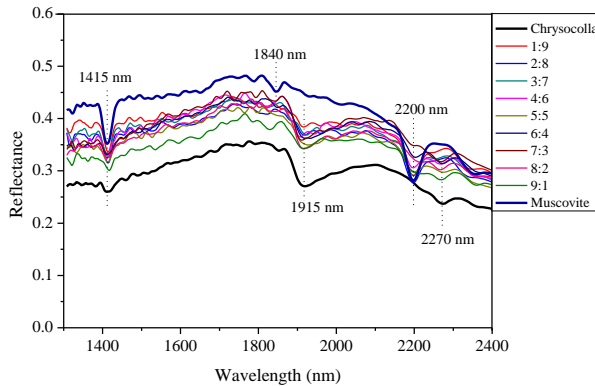Fig. 3. NIR spectra of chrysocolla-chlorite mixtures. Bottom and top spectra
are reference for chrysocolla and chlorite, respectively

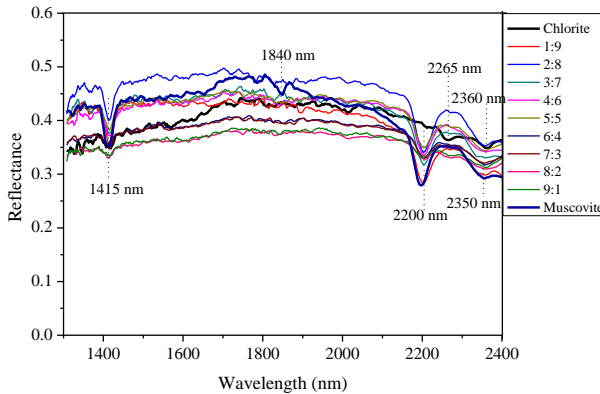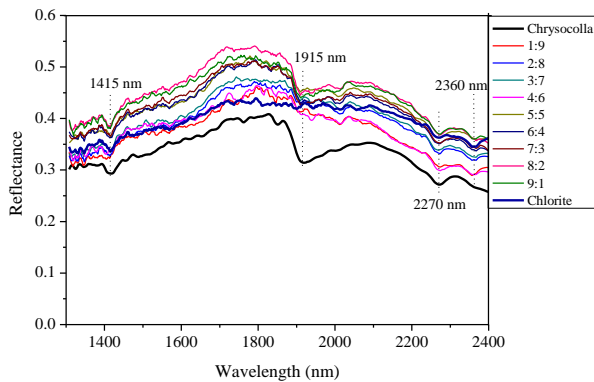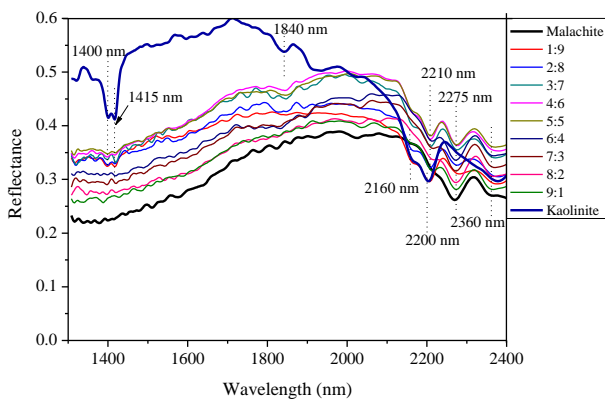Fig. 4. NIR spectra of malachite-kaolinite mixtures. Bottom and top spectra
are reference for malachite and kaolinite, respectively
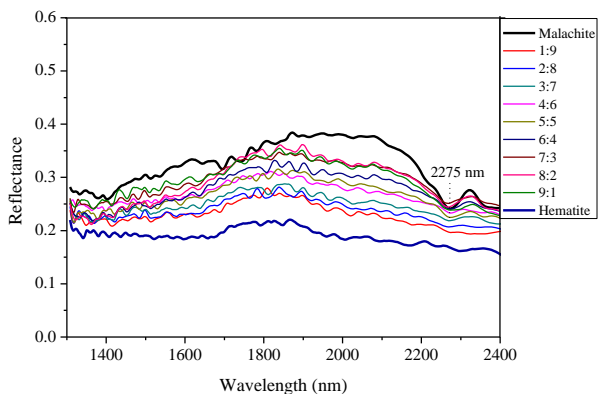
Fig. 5. NIR spectra of malachite- hematite mixtures. Bottom and top spectra
are reference for hematite and malachite, respectively

Table 2. Spectral dominance in intimate mixture of minerals

Mineral 1	Mineral 2	Mass ratios of minerals (mineral 1: mineral 2)								
		1:9	2:8	3:7	4:6	5:5	6:4	7:3	8:2	9:1
Minerals with similar functional groups										
chrysocolla	muscovite	Muscovite			mixed spectra			chrysocolla		
chrysocolla	kaolinite	Kaolinite				mixed spectra				
chrysocolla	chlorite	mixed spectra								
chlorite	muscovite	muscovite								
kaolinite	muscovite	muscovite						kaolinite		
chrysocolla	biotite	featureless spectra								
kaolinite	chlorite	kaolinite								
chlorite	biotite	featureless spectra								
biotite	muscovite	muscovite								featureless spectra
malachite	calcite	malachite								
Minerals with dissimilar functional groups										
chrysocolla	calcite	broad spectra					chrysocolla			
muscovite	calcite	mixed spectra				displaced muscovite (2350 nm) features		muscovite		
kaolinite	calcite	mixed spectra					kaolinite			
chlorite	calcite	broad spectra			chlorite					
malachite	chlorite	malachite								
malachite	kaolinite	mixed spectra								
chrysocolla	malachite	mixed spectra					chrysocolla			
biotite	calcite	calcite								
malachite	biotite	broad spectra	malachite							
malachite	muscovite	mixed spectra					malachite			
Influence of hematite on NIR-active features displaying minerals										
chrysocolla	hematite	hematite (featureless spectra)								chrysocolla
malachite	hematite	hematite (featureless spectra)		malachite						
calcite	hematite	hematite (featureless spectra)								
muscovite	hematite	hematite (featureless spectra)		muscovite						
kaolinite	hematite	hematite (featureless spectra)						kaolinite		
chlorite	hematite	hematite (featureless spectra)								
biotite	hematite	hematite (featureless spectra)								

Table 3. Spectral dominance in intimate mixture of complex mineral associations

Complex mixture or associations											
Mineral 1	Mineral 2	Mineral 3	Mineral 4	Mineral 5	Mineral 6	Mass ratios of minerals					
						1	1	1	1	1	1
hematite	chrysocolla	muscovite	–	–	–	hematite (featureless spectra)					
hematite	chrysocolla	kaolinite	–	–	–	kaolinite					
hematite	malachite	calcite	–	–	–	malachite					
muscovite	biotite	chlorite	–	–	–	muscovite					
hematite	malachite	kaolinite	–	–	–	malachite/kaolinite					
malachite	muscovite	hematite	–	–	–	malachite/muscovite					
chlorite	biotite	calcite	–	–	–	chlorite					
calcite	hematite	muscovite	–	–	–	muscovite/calcite					
chrysocolla	biotite	hematite	–	–	–	hematite (featureless spectra)					
biotite	hematite	chlorite	–	–	–	hematite (featureless spectra)					
biotite	muscovite	calcite	–	–	–	muscovite/calcite					
kaolinite	calcite	hematite	–	–	–	kaolinite					
muscovite	hematite	kaolinite	–	–	–	muscovite/kaolinite					
chlorite	biotite	calcite	hematite	–	–	chlorite/calcite					
chlorite	biotite	calcite	muscovite	–	–	muscovite/calcite					
kaolinite	calcite	hematite	muscovite	–	–	muscovite/kaolinite					
hematite	biotite	muscovite	chlorite	calcite	–	hematite (featureless spectra)					
malachite	calcite	hematite	muscovite	kaolinite	chrysocolla	hematite (featureless spectra)					

Implication to ore sorting and strategy development

The main objective of this research is to understand whether individual minerals can be identified when they occur together and are scanned within the same spectral range, and if their preconcentration is feasible. From analysis of spectra of various mixtures, the following observations were made: hematite drowns out chlorite, biotite and calcite features for all realistic proportions of these minerals. Hence, where absorption feature of any of these minerals is visible, the spectra will indicate almost complete absence of hematite. Chrysocolla is only visible in hematite at 90% concentration relative to hematite. At equal concentration, malachite and muscovite dominate hematite by showing their best diagnostic absorption feature near 2275 nm for malachite and 2200 nm for muscovite.

Both chrysocolla and malachite, which are the copper-bearing NIR-active minerals, can be targeted together by selecting the best diagnostic absorption feature of chrysocolla near 2270 nm. This is true since the feature is common at any given ratio

of their mixtures. Chrysocolla is more NIR-active than calcite, while muscovite spectral dominance over chrysocolla and vice versa is concentration dependent. Kaolinite is more readily accessible to NIR radiation than chrysocolla across all mixing ranges, with spectra appearing mixed at higher chrysocolla concentration. Chrysocolla, chlorite, hematite and/or biotite are better preconcentrated together. While chrysocolla and chlorite show absorption features side-by-side in a spectrum, chrysocolla in concentration with biotite display featureless spectra across the mixing range. This is similar to spectra of chlorite and biotite mixtures.

Malachite dominates both chlorite and calcite features at any given ratio. Malachite is relatively more NIR-active than hematite, as it shows one of its features at relatively higher hematite concentration (from ratio 4:6, malachite-hematite), while malachite features appear mixed with kaolinite. For malachite and biotite, at higher biotite concentration (90%), spectra appear featureless. Malachite dominates muscovite at higher concentration relative to muscovite, while their spectra appear mixed at higher muscovite concentration.

The spectral analysis of calcite mixed with malachite, chrysocolla, chlorite or hematite suggests that identification of calcite in such mixtures is only feasible for freely occurring calcite. Calcite dominates biotite across the mixing range. At higher calcite concentration, calcite shows features side-by-side those of kaolinite and muscovite but calcite is completely masked in the spectra from equal ratios. Hence, all three minerals can be preconcentrated together by either selecting 2200 nm feature to discriminate high -OH -low calcite or 2340 nm to discriminate high calcite -low -OH.

Though kaolinite is differentiated from muscovite by its double absorption features as against muscovite single feature (Hunt, 1979; Hunt and Hall, 1981), complete discrimination between both minerals cannot be achieved. This is true since both minerals share the same wavelength position (2200 nm) as their best diagnostic absorption feature position (Iyakwari et al., 2013). The visibility of the double kaolinite features in the mixtures with muscovite is concentration dependent. Both muscovite and kaolinite dominate chlorite and biotite.

Chlorite, apart from showing features side-by-side with chrysocolla and dominating calcite, is weak in mixtures with other NIR-active minerals. The NIR spectra of mixtures of chlorite and biotite are featureless and hence display a combined sensitivity. Where mineralogy is unknown, the spectra can be misinterpreted to represent a strongly absorbing NIR-active mineral without features. This is also true for the chrysocolla-biotite mixtures. Therefore, except in the biotite mixtures with chrysocolla and chlorite, biotite does not show its absorption features or any spectral influence in any mixture. Hence, of all minerals and mixtures investigated in this work, the spectral analysis indicates that biotite is the weakest of all the NIR-active minerals. According to Clark (1995), the iron content in biotite is responsible for masking the -OH absorption feature at shorter wavelengths near 1400 nm. Therefore, the weakness or absence of biotite features in the spectra of biotite mixed with other iron bearing minerals is ascribed to increasing iron concentration.

In general, calcite features are also invisible in the complex mixtures involving three or more minerals, where hematite, malachite or chrysocolla are present in concentration. The mixtures of strongly absorbing hematite and strongly reflecting muscovite or kaolinite indicate that at equal proportions or ratios the highly reflective hydroxyl minerals show their best diagnostic absorption feature near 2200 nm. The spectral analysis also confirms strong hematite absorption at longer NIR wavelengths (1300 to 2500 nm), reducing the overall level of reflectance and possibly masking or drowning features of other NIR-active feature displaying minerals (Bishop and Dummel, 1996; Iyakwari and Glass, 2014).

Copper-bearing minerals preconcentration

For preconcentration of copper-bearing minerals such as malachite and chrysocolla, the fact that spectra appear mixed and in some instance featureless implies that only freely occurring calcite, muscovite and/or kaolinite spectrum can be targeted for removal/reduction as a waste. Therefore, four options based on associations of the copper-bearing minerals with or without high iron bearing minerals (non-feature displaying NIR-active minerals) using NIR are developed in Fig. 6.

The first option (Fig. 6) considers silicate copper bearing minerals (chrysocolla) occurring without high iron-rich minerals (hematite). Because chrysocolla shows features side-by-side to those of kaolinite and muscovite when these occur in isolation of hematite, the spectrum displaying features diagnostic of chrysocolla (2270 nm), with or without kaolinite (2160 and 2200 nm) or muscovite (2200 nm) features, is considered as a product. Hence, the spectrum showing the calcite feature (2340 nm) is classified as a waste, since calcite displaying spectrum in chrysocolla particles indicates high grade calcite (approximately 100%). Where the spectrum appears showing features of calcite in addition to kaolinite or muscovite, given that chrysocolla has more features drowning ability on calcite even at higher calcite concentration, the spectrum shall be classified as the waste.

The second option (Fig. 6) considers copper carbonate-bearing minerals (malachite) when occurring without iron-rich minerals. Since malachite shows features side-by-side those of kaolinite and muscovite, NIR spectrum showing features near 2275 nm with or without 1415, 2200 and 2360 nm will be classified as the product. While the spectrum showing exclusively features near 2340 nm diagnostic of calcite are targeted as the waste. This is so because calcite (2340 nm) is completely masked or displaced by malachite. Therefore, similar to chrysocolla, only freely occurring CO_3^{2-} features near 2340 nm shall be considered as the waste, as any spectrum showing calcite features indicate absence of malachite. The third option (Fig. 6) considers both copper-bearing minerals (chrysocolla and/or malachite) occurring in association with high iron-bearing minerals (hematite). Since high iron-rich minerals with either chrysocolla or malachite may result in a featureless spectrum, featureless spectra may indicate the product for relatively high concentrations of hematite. This also applies to biotite occurring with chrysocolla and/or chlorite. Therefore, in

addition to the featureless spectra, the spectra showing features diagnostic of either or both chrysocolla or malachite near 2270 nm and 2275 nm respectively, with or without 1415, 1915 or 2360 nm, shall also be considered as the product. Hence, only spectra showing features near 2200 nm (muscovite and kaolinite) or 2160 nm (kaolinite only) and 2340 nm (calcite) are classified as the waste. This option is targeted at removing (reducing) both calcite and clay minerals. Note that the choice of only the 2340 nm feature may also target low-grade clays (kaolinite and muscovite), selecting both feature (2200 and 2340 nm) will target both low-grade and high-grade calcite and clays minerals. This option should only be chosen if high purity of minerals fractions is more important than a high recovery: low-grade but valuable minerals (malachite or chrysocolla) are likely to be locked in muscovite or kaolinite.

Finally, when spectra appear to be similar, being either featureless or showing diagnostic features of all NIR-active minerals, the ore will not be sortable using a NIR sensor.
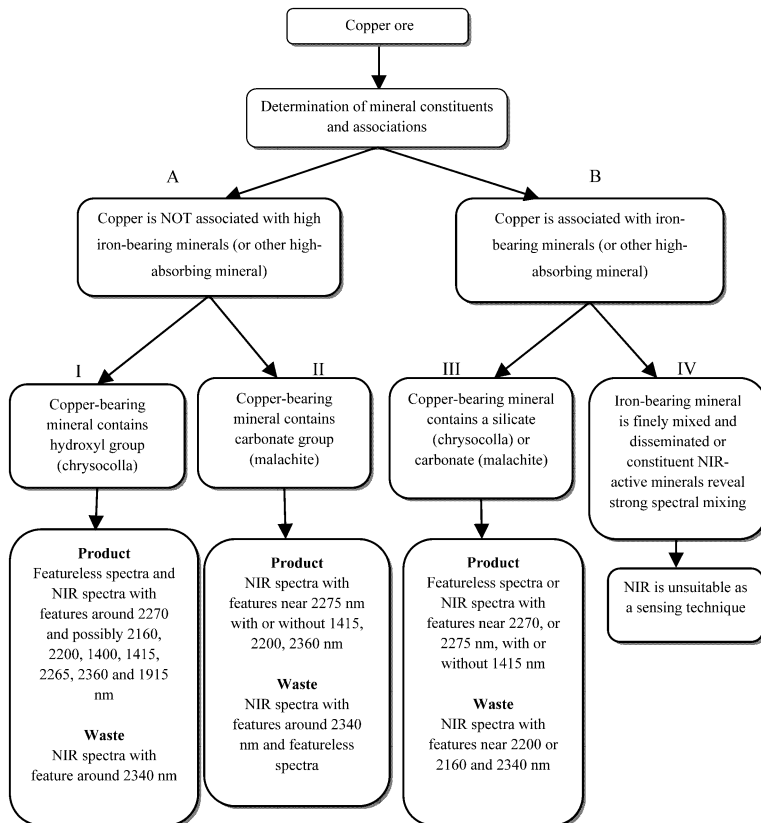

Fig. 6. Framework for NIR sorting for copper ore, based on the characteristics
of an individual spectrum (modified from Iyakwari et al., 2013)

Hematite preconcentration

For preconcentration of hematite from clay (e.g. muscovite, kaolinite) and/or carbonate (calcite) minerals, the absence of absorption features (2200 nm) will indicate the dominance and purity of hematite particle. Hence, preconcentration can be achieved by upgrading hematite and reducing water consumption during washing. Though the absence of 2200 nm absorption features is indicative of product (hematite) and the presence of the absorption features indicative of presence of clay minerals (waste), the waste fraction of this preconcentration strategy shall require washing instead of disposal. Discarding either muscovite or kaolinite bearing mineral may lead to valuables sent to waste, when the clay absorption feature (2200 nm) is present in spectra at equal hematite-muscovite or hematite-kaolinite concentration.
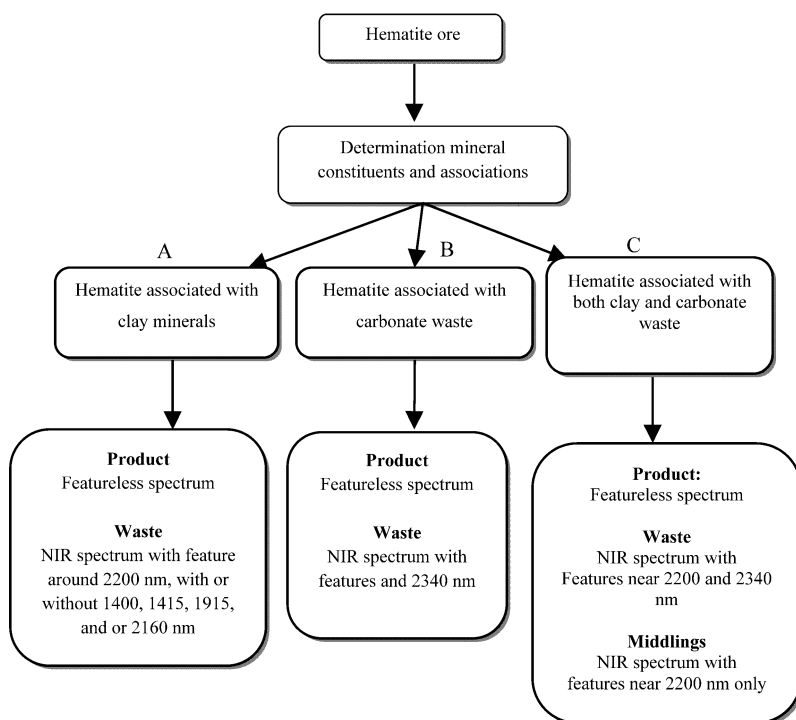
Fig. 7. Framework for NIR sorting for hematite ore using characteristics of individual spectra

In the case of carbonate (calcite) removal, particles displaying calcite feature (2340 nm) shall be classified as waste not requiring further treatment, since calcite does not show features in the presence of hematite. It should also be noted that spectra not displaying calcite features does not mean the absence of calcite. Therefore, while preconcentration of hematite from calcite may give high recovery, the grade of ore is likely to be low due to dilution. Hence, the product fraction will require further upgrading. A strategy is presented in Fig. 7.

For the determination of moisture content in kaolinitic clays containing either hematite minerals or other NIR-active minerals without absorption features, the presence of hematite is likely to mask the water features (1915 or 1840 nm and/or 1415 nm), creating the impression that clay samples are moisture free (dry). As an indirect way of determining the moisture content in kaolinitic clay sample, the presence of hematite or any high spectral absorbing mineral in concentration could also indicate the presence of moisture, as the absence of water features does not necessarily imply a dry sample.

Conclusion

The strategies outlined depend upon the ore type, constituent NIR-active mineralogy and character, as such may need to be either calibrated or modified for specific ore type to achieve optimal results. Therefore, in order to scope an application, a good understanding of constituent minerals, minerals associations and diagnostic features locations of the NIR-active minerals in the ore is essential. The aim of using NIR as a preconcentration method is to upgrade an ore by either eliminating or reducing the quantity of overall waste material reporting to the next processing stage. Using the NIR, this can only be achieved by reducing the waste fraction, since most minerals are dominated by others. In this investigation carbonate (calcite) and/or clay (muscovite/kaolinite) rich particles are the only groups of waste minerals that can be targeted by NIR, since other non-copper-bearing minerals like chlorite, biotite and hematite cannot be effectively discriminated from chrysocolla or malachite. The same is true for hematite ores, as only clay and carbonate minerals can be reduced from a feed.

The absence of water (or moisture) features in the NIR spectra does not imply that the moisture content of kaolinite bearing sample is zero. Hence, NIR is not recommended for direct moisture content determination in clays known to contain either hematite or other NIR-active mineral without diagnostic absorption features.

Acknowledgements

Reference

AINES R.D., ROSSMAN G.R., 1984, *Water in minerals? A peak in the infrared*, J. Geophys. Res. 89(B6), 4059.

BISHOP J.L., DUMMEL A., 1996, *The influence of fine-grained hematite powder on the spectral properties of Mars soil analogs; VIS-NIR bi-directional reflectance spectroscopy of mixtures*. Lunar and Planetary Institute Science Conference Abstracts. Vol. 27.

CLARK R.N., 1995, *Reflectance spectra*. In: Ahrens, T.J. (Ed.), *Rock Physics and Phase: A Handbook of Physical Constants*, Washington, American Geophysical Union, 178–188.

CLARK R.N., 1999, *Spectroscopy of rocks and minerals, and principles of spectroscopy*, P3–52. In N Rencz (ed.). *Remote sensing for the earth sciences: Manual of remote sensing*. Vol. 3. John Wiley & Sons, New York.

DAROCH G.A., BARTON M.D., 2011, *Hydrothermal alteration and mineralization in Santo Domingo Sur iron oxide (-Cu-Au) (IOCG) deposit, Atacama Region, Chile*. 11th SGA Biennial meeting "Let talk ore deposits".

HUNT G.R., 1979, *Near-infrared (1.3-2.4 μm) spectra of alteration minerals; potential for use in remote-sensing*, Geophys, 44 (12) 1974-1986.

HUNT G.R., HALL R.B., 1981, Identification of kaolins and associated minerals in altered volcanic rocks by infrared spectroscopy. Clay miner, 29(1) 76-78.

IYAKWARI S., GLASS H.J., 2014, *Influence of mineral particle size and choice of suitable parameters for ore sorting using near infrared sensors*. Miner Eng, 69, 102-106.

IYAKWARI S., GLASS H.J., KOWALCZUK P.B., 2013, *Potential for near infrared sensor-based sorting of hydrothermally-formed minerals*. J Near Infrared Spec, 21 (3) 223–229.

POMMEROL A., SCHMITT B., 2008, *Strength of H2O near infrared absorption bands in hydrated minerals: Effects of particle size and correlation with albedo*, J. Geophys. Res., 113, E100009, doi10.1029/2007JE003069.

STARK E., LUCHTER K., 2005, *NIR instrumentation technology*, NIR news 16, (7), 13-16.

SAVITZKY A., GOLAY M.J.E., 1964, *Smoothing and differentiation of data by simplified least squares procedures*, Anal. Chem. 36, 1627-1639.

COMPARISON OF FLOAT-SINK AND PROGRESSIVE RELEASE FLOTATION OF GROUND PRODUCTS OF COAL MIDDLINGS

Weining XIE[*], **Yaqun HE**[*,**], **Cheng LUO**[*], **Xia ZHANG**[*], **Hong LI**[*], **Jiadong YU**[*], **Haifeng WANG**[*], **Fengnian SHI**[***]

[*] School of Chemical Engineering and Technology, China University of Mining and Technology, Xuzhou, Jiangsu 221116, China, yqhe@cumt.edu.cn

[**] Advanced Analysis and Computation Center, China University of Mining and Technology, Xuzhou, Jiangsu 221116, China

[***] University of Queensland, Sustainable Minerals Institute, Julius Kruttschnitt Mineral Research Centre

Abstract: An additional recovery of coking coal middlings can be utilized for increasing of the concentrate yield of coking coal. A combined flow sheet of comminution and flotation can realize this target. To investigate the effect of grinding process on further flotation of ground products, progressive release flotation tests were used to compare with the float-sink tests, which were regarded as a criterion. Coal middlings were ground by wet-milling with iron balls to <0.5 mm. Curves of ash vs. cumulative yields of sized products indicated that the concentrate yield of coal separated by progressive release flotation was lower than that of coal benefited by the float-sink test, with the same ash for four size fractions (0.5-0.25 mm, 0.25-0.125 mm, 0.125-0.074 mm and <0.074 mm). Distributions of elements conducted by energy disperse spectroscopy (EDX) showed that associated kaolinite was liberated and exposed on the surface. It led to the shift of local surface property from hydrophobicity to hydrophilicity. Meanwhile, analyses of chemical property performed by an X-Ray photoelectron spectrometer (XPS) depicted that the hydrophilic mineral FeOOH, which generated in the grinding process, was adsorbed on the coal surface. Flotation of the ground products were worsened due to the increase of hydrophilicity of the coal surface.

Keywords: coal middlings, float-sink, progressive release flotation, XPS, EDX

Introduction

Nowadays, a grinding process has become an important method in utilization of coal by areas of gasification, liquification and combustion (Zuo et al., 2013; Elham et al., 2013; Shi and Zuo, 2014). For coal beneficiation, comminution was proposed especially for the recovery of coal middlings, which are associated with ash minerals (Lytle et al., 1983; Bokanyi and Csoke, 2003; Cui et al., 2007). The liberated ground products can be

re-separated by either gravity concentration or flotation, according to differences in either density or surface wettability of coals.

Comminution of coal can not only realize size reduction and mineral liberation, but also exposes the inner interface (Xia et al., 2013). In this case, Xie et al. (2013) studied the liberation characteristics of coal middlings comminuted by a jaw crusher and ball mill, respectively. Based on liberation of minerals during grinding, ultra clean coal was produced by flotation (Bokanyi and Csoke, 2003; Fu and Shan, 2006). Despite these, changes in surface properties also occur because of the exposure of inner surface. Recently, Sokolovic et al. (2012) introduced the methods of attrition to improve floatability of oxidized anthracite waste coal. Xia et al. (2013) found the changes of amounts functional groups of Taixi coal ground by a dry rod mill, and the flotation behavior of coals treated by this method was improved. The objects of these studies are coals with the size below 0.5 mm, which are suitable to be separated by flotation. The purpose is to liberate macerals from minerals. A number of studies of combined flow sheet of comminution and flotation for lump coal is relatively low. Nevertheless, this technique is utilized for beneficiation of metallic ores (Moslemi et al., 2011; Miettunen et al., 2012). Bruckard and Sparrow (2011) found that abrasion of media in the grinding process can influence the selective attachment of reagent to the mineral surface. Goncalves et al. (2011) evaluated the effect of availability of iron oxide and newly generated hydroxide compounds on flotation of sulphide copper ore ground by wet-milling with different media. A method of X-ray photoelectron spectrometer (XPS) analysis was also utilized by mineral processing researchers to evaluate the effect of grinding on further flotation (Liu et al., 2011). In this regard, in our studies the sampled coking coal middlings were firstly ground by wet-milling in a ball mill with iron balls. Progressive release flotation tests of sized products (0.5-0.25, 0.25-0.125, 0.125-0.074 and <0.074 mm) were performed in comparison to the float-sink tests. Simultaneously, distributions of elements and chemical composition of ground products were analyzed by energy disperse spectroscopy (EDX) and XPS, respectively. Meanwhile, the maceral composition of sized ground products was also determined. Combination of various analyses of properties of ground products were used to explain the difference of cumulative yields of clean coal with the same ash between these two methods. The reason of changes in the surface properties of coal was also discussed in this paper.

Materials and methods

The coking coal middlings, which were sampled from a coal preparation plant, were chosen as the experimental materials. The content of ash and sulfur was 29.84 and 1.5%, respectively. Before the wet-milling process, the investigated samples were firstly crushed to size of 3-0.5 mm by a jaw crusher. The wet-milling process was conducted to reduce the size to <0.5 mm. Then, the slimes were filtrated and dried at the room temperature. The ground products were sieved into four size fractions, with a series of stainless steel sieves with sizes of 0.25, 0.125 and 0.074 mm.

The float-sink tests were conducted according to the GB/T 478-2008 standard. Densities used in the float-sink tests were 1.3, 1.4, 1.5, 1.6, 1.8 and 2.0 kg/dm^3. For the tests of coal middlings, heavy media of different densities were prepared by using different amount of $ZnCl_2$ in water. As the $ZnCl_2$ was not easy to dissolve, hot water was firstly used and the float-sink tests were conducted after the temperature of a medium decreased to the room temperature. For the tests of the ground products, the heavy media of different densities were obtained by adjusting the proportions of benzene (0.88 kg/dm^3), CCl_4 (1.55 kg/dm^3) and $CHBr_3$ (2.89 kg/dm^3).

In the progressive release flotation tests, n-dodecane and 2-octanol were used as the collector and frother, respectively. As the flotation selectivity of ground coal was poor, flotation tailings were separated with relatively low ash and high yield. In this case, a flotation flow sheet was optimized to improve the quality of flotation tailings. The optimized timed-release flotation flow sheet is shown as Fig. 1. Herein, dosages of n-dodecane and 2-octanol were 1.0 and 0.1 kg/Mg at the stage of roughing stage, respectively. For the scavenging, the dosages of n-dodecane and 2-octanol decreased to 0.35 and 0.04 kg/Mg.
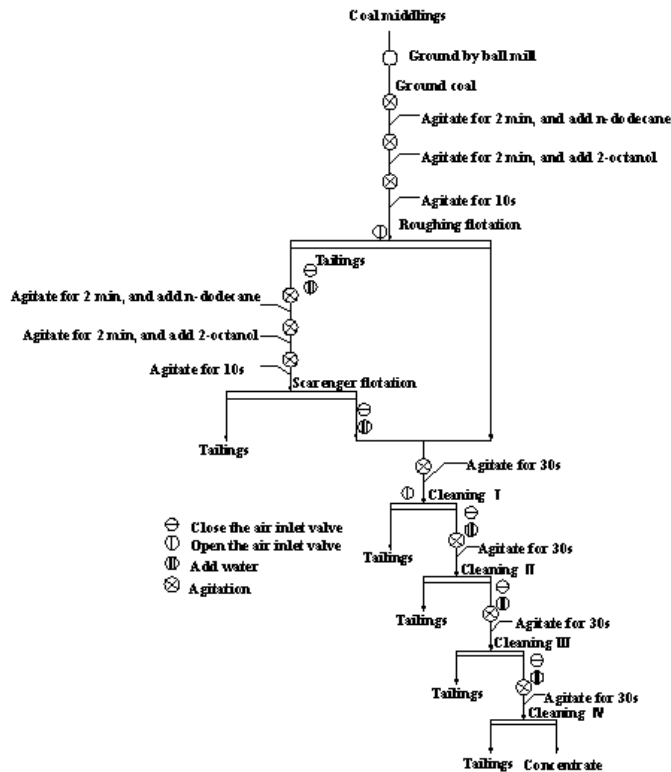

Fig. 1. Flow sheet of optimized progressive release flotation

A mineral composition of the original coal was investigated by a D8 Advance X-ray Diffractometer (XRD) made by BRUKER AXS. Cu-Kα radiation was generated at a tube voltage of 40 kV and a tube current of 30 mA. The incident beam was focused onto a beam spot of 250 um in a diameter by a collimeter. A scanning velocity was 0.1 sec/step and a sampling interval was 0.01945^0.

A distribution analysis of elements on the surface of ground products was conducted by EDX. In the first procedure, the unsized ground products were solidified in the mixture of epothin epoxy resin (20-8140-128) and epothin epoxy hardener (20-8142-064) with the proportion of 5 to 2 for more than 48 h (Xie et al., 2013). An EDX instrument, namely Bruker Quantax400-10, was utilized. Operating parameters for elemental analysis were as follows: Target: Rh anode, operating voltage: 25 kV, X-ray path: vacuum, ketector: Si (Li), measurement time: 300 s.

After the investigation of distribution of elements, maceral compositions of the sized ground products were analyzed with a the polarizing microscope. Over 500 points were observed for each sample. A content of each maceral was determined.

The ground products with the size below 74 μm were sieved and pressed into a pellet for XPS analysis. High resolution spectra were obtained by XPS at the room temperature in an ultra-high vacuum, with the surface analysis system (THERMO ESCALAB 250Xi, America). Passing energy was 20 eV and step size of energy was 0.05 eV. Scan numbers of high resolution spectra for different elements were ranged from 5 to 20. Binding energies were corrected by setting the C 1s hydrocarbon ($-CH_2-CH_2-$bonds) peak at 284.8 eV (Becker and Cherkashinin, 2013).

Results

Analyses of mineral and maceral compositions

The mineral composition of coal middlings is shown in Fig. 2. About 8 kinds of associated minerals were found in the sample. A relative content of kaolinite is the
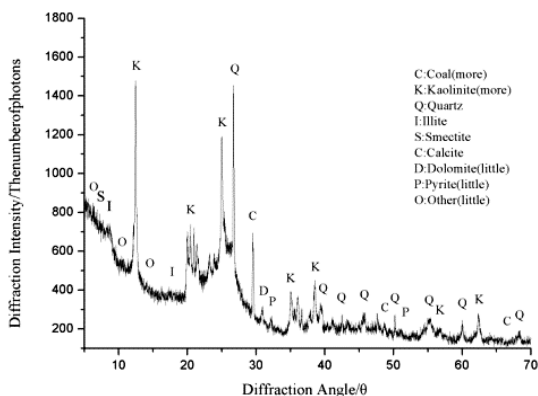

Fig. 2. Phase composition of coal middlings investigated by XRD

highest in all minerals. As kaolinite is hydrophilic, the flotation behavior of the ground products may be worsened if kaolinite is present on the surface. The contents of quartz, illite, smectite, dolomite and pyrite are relatively low.

The maceral composition of the sized ground products are shown in Table 1. The contents of exinite in these four sized products is less than 4%. It indicates that this maceral nearly has no effect on the total flotation behavior of coal. In the case of other two macerals, the content of vitrinite increases with the particle size, while inertinite shows an opposite trend. Images, which were observed with a polarizing microscope, are shown in Fig. 3. Figure 3 shows that liberation of different macerals was not significant. Vitrinite was liberated from inertinite but still they were associated with each other. These two main macerals are easy-to-float and flotation of vitrinite is a little better than that of inertinite (Zhao., 2010; Guo et al., 2013). Although, Bokanyi and Csoke (2003) showed for Mecsek coal that flotation of vitrinite is usual better than that of exiuite, and flotation of inertinite is poor. From this view of point the difference of flotation of the sized ground products might be relatively small.

Table 1. Maceral composition of sized ground products

Size fraction, mm	Vitrinite	Inertinite	Exinite
0.5-0.25	58.47	39.35	2.18
0.25-0.125	54.19	42.17	3.64
0.125-0.074	48.55	48.66	2.79
<0.074	46.08	52.31	1.61

The difference between the sized ground products and original coal is relatively small and is less than 3%. The float-sink curves of the four samples are nearly the same. Simultaneously, associated minerals found in original coal were also investigated in the ground products. The results of investigations indicate that no selective grinding occurs during comminution of coal middlings in the ball mill.
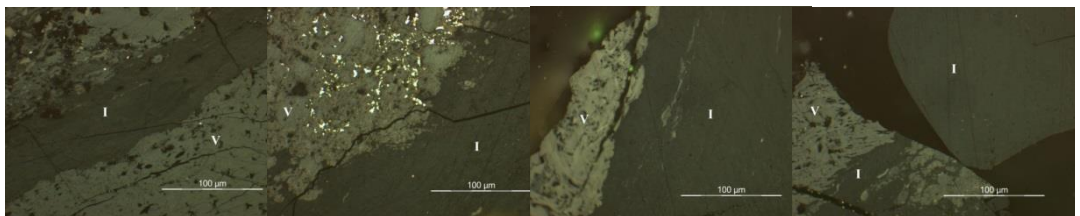
(a)　　　　　　(b)　　　　　　(c)　　　　　　(d)
Fig. 3. Imagines of macerals of ground products

Liberation of coal middlings by grinding

Usually, the wet-milling process cannot only reduce the size, but also promote liberation of associated minerals from coal particles. The float-sink tests of the ground

products can illustrate the results of liberation. Figure 4 shows the density vs. cumulative yield of coking coal middlings and ground products, respectively. The cumulative yields of the ground products with lower density are obviously higher than those of coal middlings. At the density of 1.5 kg/dm^3, the difference of cumulative yield is nearly 20%. In comparison to the original coal, the grinding process of coal middlings increases the yield of coal with small or large density at the same time. Thus, the potential of beneficiation is improved. Meanwhile, the difference in the surface wettabilities between liberated coals and minerals is relatively high. Thus, the ground products can be efficiently processed by flotation.
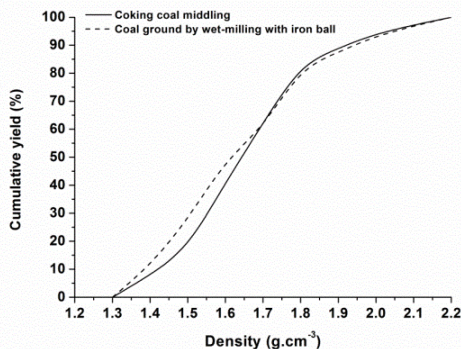
Fig. 4. Cumulative yield vs. density of coking coal middlings and ground products

Comparison between float-sink and progressive release flotation of the sized coal

Figure 5 presents the cumulative yield vs. ash of the sized ground coals separated by float-sink and progressive release flotation tests. The results of the float-sink tests indicate that the difference in the cumulative yield of these four sized products is not significant, except for the 0.5-0.25 mm size fraction of coals. If comparing the cumulative yield of clean coal with ash of 10%, the results for the 0.5-0.25 mm size fraction of coal are better. The flotation results for the 0.125-0.074 mm and <0.074 mm coals are better than those for the other two fractions. In comparison to the results of the float-sink tests of the sized coals, the yield of flotation concentrate with a low ash content for each sized ground products are worse, since flotation of liberated coal and gangue is different. Especially for coals of 0.5-0.25 mm and 0.25-0.125 mm in size, the difference increases to nearly 15%, if the ash is 10%. The changes in the surface properties of ground products during the wet-milling process may be the reason of the difference between the results obtained by these two methods.
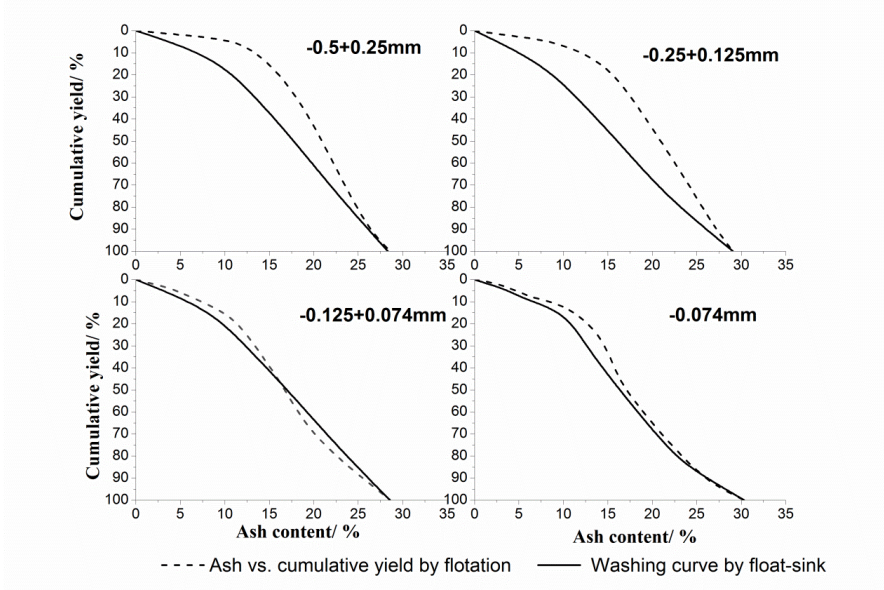
Fig. 5. Cumulative yield vs. ash of ground products separated by float-sink
and progressive release flotation

Discussion

Distributions of elements on the newly generated surface

Just as mentioned above, kaolinite was the main associated mineral. This mineral is hydrophilic and it has a negative influence on the flotation of ground products. Therefore, the microscopic image and distribution relationship of elements on the new surface were measured by SEM and EDX. The results are shown in Fig. 6. The figures show that in the selected areas the distribution character of Al and Si are the same. This indicates that kaolinite is present on the surface. Figure 6 also shows that the particles,
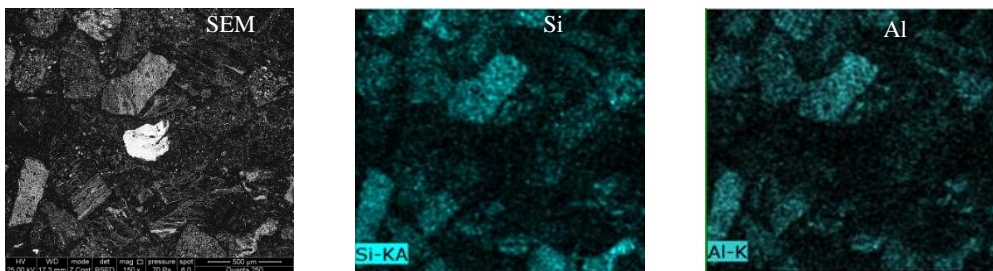
Fig. 6. Distributions of Si and Al on the newly generated surface

which are covered by kaolinite, occupy a relatively high portion of the surface. As kaolinite is hydrophilic, the flotation of the ground products is reduced.

XPS analyses of the ground products

Chemical properties of coals were analyzed by XPS. The high resolution spectra of C, O, H, Fe, S, Al, Si and Ca in samples were recorded to investigate the possible changes of chemical valances during grinding. As a result, a new compound was found on the surface. Figures 7 and 8 depict the Fe 2p and O 1s signals of ground products, respectively. Peaks with binding energies of 711.50 eV of Fe and 531.20 eV of O in Figs. 7 and 8 are consistent with FeOOH. Thus, a part of the surface of ground products was covered by FeOOH.
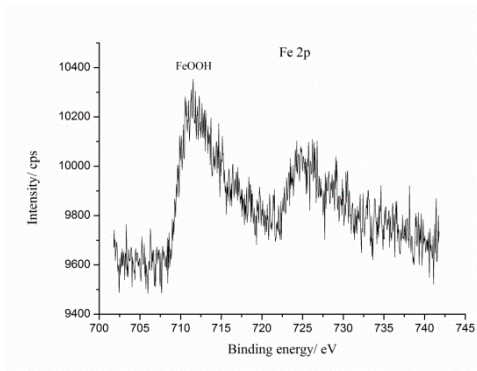
Fig. 7. Fe 2p signal of ground products   Fig. 8. O 1s signal of ground products
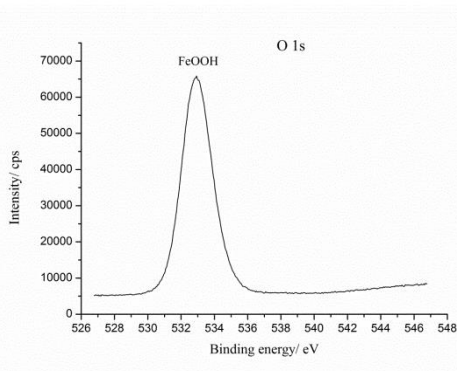
The chemical analysis also shows the presence of pyrite. During the wet-milling process with iron balls, the galvanic coupling phenomenon existed between the grinding medium and liberated pyrite. Due to galvanic coupling, oxidation occurs on the surface of iron ball and reduction reaction occurres on pyrite. The oxidative products of Fe^{3+} react with OH^{-1} to form a compound of hydroxide of Fe (Gu and Zhong, 2011). The results of XPS indicated that the new compound was FeOOH. FeOOH is hydrophilic. It is adsorbed on the surface of ground products. In this case, the surface of the ground products locally becomes hydrophilic. The changes in the surface properties reduce flotation. The cumulative yield of ground coals performed by progressive release flotation dropped in comparison with the results of the float-sink tests at the same ash for the sized products.

Conclusions

A grinding process of coal middlings leads to liberation of coal macerals from associated minerals. The float-sink tests of ground products indicated the increase of

separation potential in comparison to the original coal. The differences between mineral and maceral compositions of the four sized ground products were relatively small. The property of the newly produced surface changed during the grinding process. The cumulative yields of the sized coals separated by using progressive release flotation were obviously lower those of coals beneficiated by float-sink, at the same ash content. The distributions of elements analyzed by EDX indicated the presence of hydrophilic kaolinite on the surface of the ground products. This leads to a change of local surface property from hydrophobic to hydrophilic and a decrease of flotation of the ground products. Meanwhile, the newly generated FeOOH was adsorbed on the local new surface having a weak negative effect on the flotation of coal. It was evident that these changes led to a decrease in the cumulative yield.

Acknowledgements

References

BECKER D., CHERKASHININ G., HAUSBRAND G., JAEGERMANN W., 2013, *XPS study of diethyl carbonate adsorption on LiCoO2 thin films*. Solid State Ionics 230: 83-85.

BOKANYI L., CSOKE B., 2003, *Preparation of clean coal by flotation following ultrafine liberation*. Appl. Energ. 74: 349-358.

Bruckard W.J., Sparrow G.J., Woodcock J.T., 2011, *A review of the effects of the grinding environment on the flotation of copper sulphides*. Int. J. Miner. Process. 100: 1-13.

CUI L., AN L., GONG W., JIANG H., 2007, *A novel process for preparation of ultra-clean micronized coal by high pressure water jet comminution technique*. Fuel 86: 750-757.

ELHAM D., HADI Z., BEHDAD M., 2013, *A combined experimental and theoretical study on aboratory-scale comminution of coal and biomass blends*. Powder Technol. 235:412-421.

FU X., SHAN X., JIANG H., 2006, *Study on the flotation technology for deep-cleaning of coal slime*. J. China Coal Soc. 31:90-93.

GONCALVES K.L.C., ANDRADE V.L.L., PERES A.E.C., 2003, *The effect of grinding conditions on the flotation of a sulphide copper ore*. Miner. Eng. 16: 1213-1216.

GU G., ZHONG Z., 2008, *Electrochemical properties on surface of galena in grinding system and its influence on flotation*. J. Central South Univer. (Sci. Technol.) 9: 54-58.

GUO Y., TANG Y., WANG S., LI W., JIA L., 2013, *Maceral separation of bark liptobiolite and molecular structure study through high resolution TEM images.* J. China Coal Soc. 38:1021-1024.

LIU F., LI W., GUO H., ET AL., 2011, *XPS study on the change of carbon-containing groups and sulfur transformation on coal surface*. J. Fuel Chem. Technol. 39: 81-84.

LYTLE J.M., DANIEL J.L., TINGEY G.L., 1983, *Concentration of sulphur and mineral rich components in particle classes during coal comminution*. Fuel 61:1299-1303.

MIETTUNEN H., KAUKONEN R., CORIN K., OJALA S., 2012, *Effect of reducing grinding conditions on the flotation behaviour of low-S content PGE ores*. Miner. Eng. 36:195-203.

MOSLEMI H., SHAMSI P., HABASHI F., 2011, *Pyrite and pyrrhotite open circuit potentials study: Effects on flotation*. Miner. Eng. 24: 1038-1045.

SHI F., ZUO W., 2014, *Coal breakage characterization-Part 1: Breakage testing with the JKFBC.* Fuel 117: B: 1148-1155.

SOKOLOVIC J., STANOJLOVIC R., MARKOVIC Z., 2012, *Activation of oxidized surface of anthracite waste coal by attrition*. Physicochem. Probl. Miner. Process. 48: 5-18.

XIA W., YANG J., ZHAO Y., ET AL., 2012, *Improving floatability of taixi anthracite 176 coal of mild oxidation by grinding*. Physicochem. Probl. Miner. Process. 48: 393-401.

XIA W., YANG J., LIANG C., 2013, *Effect of microwave pretreatment on oxidized coal flotation*. Powder Technol. 233: 186-189.

XIE W., HE Y., ZHU X., ET AL, 2013, *Liberation characteristics of coal middlings comminuted by jaw crusher and ball mill*. Int. J. Min. Sci. Technol. 23: 669-674.

ZHAO W., 2010, *Study on modification of macerals in Shenfu coals and its flotability.* Master thesis Xidian University.

ZUO W., ZHAO Y., HE Y., ET AL., 2012, *Relationship between coal size reduction and energy input in Hardgrove mill*. Int. J. Min. Sci. Technol. 22: 121-124.

HYDROTHERMAL SYNTHESIS OF LITHIUM SILICATE FROM WASTE GLASS. A PRELIMINARY STUDY

Nichola J. COLEMAN, Andrew P. HURT, Atiya RAZA

School of Science, University of Greenwich, Chatham Maritime, Kent, ME4 4TB, United Kingdom
nj_coleman@yahoo.co.uk

Abstract: Current environmental directives to conserve resources and to divert waste streams have generated significant interest in mineral recycling. In this respect, this preliminary study has demonstrated that lithium metasilicate can be prepared by hydrothermal reaction between waste container glass and lithium hydroxide solutions at 100 °C. Minor proportions of calcium hydroxide, calcite, lithium carbonate and tobermorite were also produced during the reaction. Percentage crystallinity and proportion of lithium metasilicate in the reaction product were found to increase as functions of lithium hydroxide concentration (between 1 and 4 M). This research has also shown that the lithium metasilicate phase can take up 6.4 mmol/g of Zn^{2+} ions after 24 h during batch sorption. Further work to optimise the yield and to appraise the antimicrobial properties of Zn^{2+}-bearing lithium metasilicate is now warranted.

Introduction

During the past decade, a number of research projects has been carried out to "up-cycle" surplus soda-lime-silica glass from the municipal waste-stream. Potential value-added applications for waste glass include the production of ion-exchange and water filtration media, lightweight aggregates and ceramics (Ayadi et al., 2011; Coleman et al., 2014; Korkosz et al., 2012; Matteucci et al., 2002; Velis et al., 2014).

Lithium metasilicate, Li_2SiO_3, is a synthetic alkaline inosilicate comprising Q^2 silicate chains and charge-balancing lithium ions which crystallises in the orthorhombic system (Pfeifer et al., 1998). The current technological significance of lithium metasilicate arises from its potential applications as a breeder material for tritium, ionic conductor, gas-sensor and CO_2-sorbent (Ortiz-Landeros et al., 2011). This material can be obtained *via* a range of synthetic routes including: solid state reaction (Ortiz-Landeros et al., 2011; Pfeifer et al., 1998); modified combustion (Cruz and Bulbulian, 2003); sol-gel synthesis (Pfeifer et al., 1998; Zhang et al., 2008);

hydrothermal processing (Ortiz-Landeros et al., 2011) and mechanical milling (Yang et al., 2012). To date, the reported preparations of lithium metasilicate have been carried out using refined silicate reagents such as colloidal silica, tetraethoxysilane, amorphous silica gel and silicic acid.

This preliminary study explores the possibility of using waste container glass as a reactive silicate source for the hydrothermal synthesis of lithium metasilicate at 100 °C in the presence of 1 M, 2 M and 4 M lithium hydroxide solutions. The reaction products were characterised by powder X-ray diffraction analysis (XRD) and the sample prepared with 4 M lithium hydroxide solution was also analysed by ^{29}Si magic angle spinning nuclear magnetic resonance spectroscopy (MAS NMR) and Fourier transform infrared spectroscopy (FTIR). The potential of this material to be used as a carrier for antimicrobial zinc ions was also considered.

Materials and methods

Materials, synthesis and characterisation

Lithium hydroxide, LiOH·H$_2$O, was obtained from Sigma-Aldrich UK and used as-received. Colourless soda-lime-silica glass containers were collected from the municipal waste stream in Rochester, Kent, UK, and ground to pass 125 µm. An oxide analysis of the glass, obtained by X-ray fluorescence spectroscopy at the Materials Research Institute, Sheffield Hallam University, Sheffield, UK, is given in Table 1.

Table 1. Composition of waste glass

Oxide Component	Mass %
SiO$_2$	72.1
Na$_2$O	13.4
CaO	11.3
MgO	1.30
Al$_2$O$_3$	1.14
K$_2$O	0.39
SO$_3$	0.21
Fe$_2$O$_3$	0.08
TiO$_2$	0.05
Mn$_3$O$_4$	0.03
Loss on ignition	Nil

The syntheses of lithium metasilicate were attempted by heating of 3.0 g of waste glass and 60 cm^3 of either 1 M, 2 M or 4 M LiOH$_{(aq)}$ at 100 ºC in hermetically sealed

PTFE reaction vessels for 5 days. The syntheses were carried out in triplicate and the reaction products were washed with deionised water to pH ~ 7 and dried to constant mass in air at 40 ºC. Specimens produced in 1 M, 2 M and 4 M LiOH$_{(aq)}$ were labelled LS-1, LS-2 and LS-4, respectively.

The reaction products were analysed by powder XRD using a Bruker D8 diffractometer with Cu Kα = 0.15406 nm, a step size of 0.019 ° in the 2θ range from 5 to 60 ° and a measuring time of 1 s *per* step. X-ray diffraction data were compared with JCPDS files using DIFFRAC.EVA software (supplied by Bruker, Germany). Quantitative XRD analysis and crystallite size calculations were carried out by Rietveld refinement using a fundamental parameters approach with full axial model (Cheary and Coelho, 1992) on TOPAS version 4.2 structure analysis software (Bruker, Germany). The lithium metasilicate structure used for the quantitative analysis was described by Tang et al. (2012) and all other structures were selected from the TOPAS structure database.

Secondary electron images of the LS-4 products were obtained from uncoated samples attached to carbon tabs on an Hitachi SU8030 scanning electron microscope with an accelerating voltage of 1 kV. The ^{29}Si MAS NMR spectrum of the LS-4 reaction products was recorded on a JEOL JNM-ECX 300 MHz spectrometer using a pulse delay of 60 s, an acquisition time of 0.02048 s and 20000 scans. ^{29}Si chemical shifts were referenced to tetramethylsilane (TMS). The FTIR spectrum was obtained using a Perkin Elmer Paragon spectrometer in transmission mode on a pressed KBr disc between 500 and 4000 cm^{-1} wavenumbers.

Zn^{2+}-uptake

The uptake of Zn^{2+} ions by the LS-4 reaction products was determined by batch sorption at 25 °C by contacting 50 mg of material with 200 cm^3 of 0.5 mM zinc nitrate solution in a screw-capped polypropylene bottle for up to 24 h. At various intervals the supernatant liquors were recovered and analysed for zinc by inductively coupled plasma spectroscopy (using a Perkin-Elmer Optima 4300DV spectrometer). Each batch sorption experiment was carried out in triplicate.

Results and discussion

Characterisation

The powder XRD patterns of the hydrothermal reaction products of waste container glass and 1 M, 2 M or 4 M aqueous lithium hydroxide solutions are shown in Fig. 1. These data confirm that the principal reaction product in each case is orthorhombic lithium metasilicate (which matches JCPDS file 29-0828), and that minor quantities of calcium hydroxide, calcite, lithium carbonate and tobermorite are also present in varying proportions.

An example of the experimental and calculated XRD patterns for LS-4 and the residual difference between the two sets of data are shown in Fig. 2. The small residual difference indicates that the fitting is satisfactory.

The relative proportions of the components (by mass) of each of the samples and the calculated lattice parameters for the lithium metasilicate phase are listed in Table 2. In each case, weighted profile R-factors (R_{wp}) below 10% demonstrate that the fittings are satisfactory. These data indicate that percentage crystallinity and proportion of lithium metasilicate present in the product increase with increasing concentration of lithium hydroxide in the reaction mixture. The proportions of calcite, lithium carbonate and calcium hydroxide in the product also increase as functions of lithium hydroxide concentration. Additionally, the poorly crystalline calcium silicate hydrate mineral, tobermorite ($Ca_5Si_6O_{16}(OH)_2 \cdot 4H_2O$), is found to be present in specimens LS-1 and LS-2 at 5.6% and 3.8%, respectively; although, this phase is absent in sample LS-4.
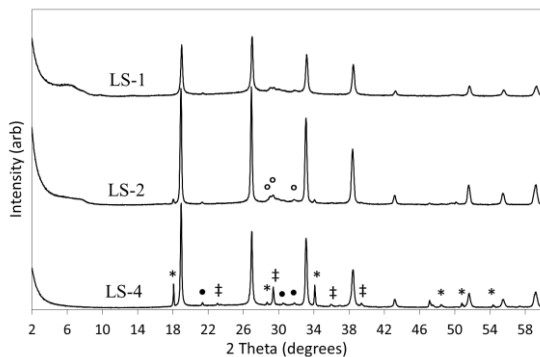

Fig. 1. Powder XRD data for the hydrothermal reaction products of waste glass and aqueous lithium hydroxide (key: Li_2SiO_3 – unmarked; $Ca(OH)_2$ – *; $CaCO_3$ – ‡; Li_2CO_3 – •; $Ca_5Si_6O_{16}(OH)_2 \cdot 4H_2O$ – °)
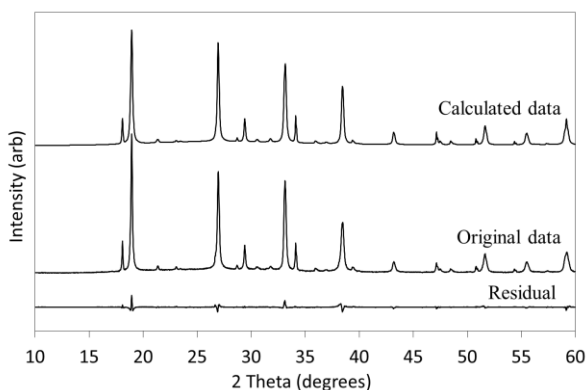

Fig. 2. Experimental and calculated powder XRD patterns for LS-4
and the residual difference between the two data sets

These findings indicate that high concentrations of lithium hydroxide facilitate the breakdown of the silicate network of the glass and promote the crystallisation of the lithium metasilicate product. High concentrations of lithium hydroxide also suppress the solubility of calcium ions leached from the glass network which precipitate out as calcium hydroxide and calcite (*via* atmospheric carbonation). The solubility of calcium ions increases as the concentration of lithium hydroxide is reduced, thus enabling the through-solution formation of the by-product calcium silicate hydrate phase, tobermorite in samples LS-1 and LS-2.

Mean crystallite sizes of the lithium metasilicate phases in each of the products are given in Table 2. These data show that the crystallite sizes are in the region of 40 to 60 nm and that the lithium hydroxide concentration of the reaction mixture has no specific impact on the size of the crystals produced.

Table 2. Composition, Li_2SiO_3 lattice parameters and crystal size of hydrothermal reaction products

Property	LS-1	LS-2	LS-4
Li_2SiO_3 (wt%)	47.3	58.2	67.9
Amorphous phase (wt%)	45.3	33.0	20.0
$Ca_5Si_6O_{16}(OH)_2.4H_2O$ (wt%)	5.6	3.8	0
$CaCO_3$ (wt%)	1.1	1.9	3.8
Li_2CO_3 (wt%)	0.7	2.6	4.9
$Ca(OH)_2$ (wt%)	0	0.5	3.4
Weighted profile R-factor (R_{wp})	6.1	9.5	8.9
Lattice parameters (Å)	$a = 9.386$ $b = 5.401$ $c = 4.688$	$a = 9.393$ $b = 5.401$ $c = 4.688$	$a = 9.392$ $b = 5.404$ $c = 4.684$
Crystal size (nm)	40 ± 6	60 ± 15	55 ± 7

The most highly crystalline specimen (80% crystallinity) comprising the highest proportion of lithium metasilicate (68% Li_2SiO_3), LS-4, was selected for further analysis by SEM, NMR and FTIR. Scanning electron micrographs of LS-4 are presented in Fig. 3 and indicate that the material is principally composed of granules in the size range 50 to 100 μm comprising ~400 nm blocky interlocking particles.

The ^{29}Si MAS NMR spectrum of LS-4 is given in Fig. 4 and comprises a single Q^2 resonance at-– 75.5 ppm and a low-intensity Q^1 signal at – 72 ppm in the ratio 65:1. A very broad weak signal also appears in the spectrum at approximately – 110 ppm. The Q^2 mid-chain silicate resonance is consistent with those reported in the literature for phase-pure lithium metasilicate (Pfeifer et al., 1983; Zhang et al., 2008). However, the NMR data presented by Zhang et al. (2008) consists of an asymmetrical Q^2 signal with additional downfield intensity in the Q^1 region which may arise from chain-end silicate species. It is on this basis that the discrete Q^1 resonance observed in this study is tentatively assigned to the terminal groups of the silicate chains; although, the

possible presence of a minor sorosilicate phase cannot be dismissed. The very broad signal centred around −110 ppm arises from Q^4 amorphous silica.
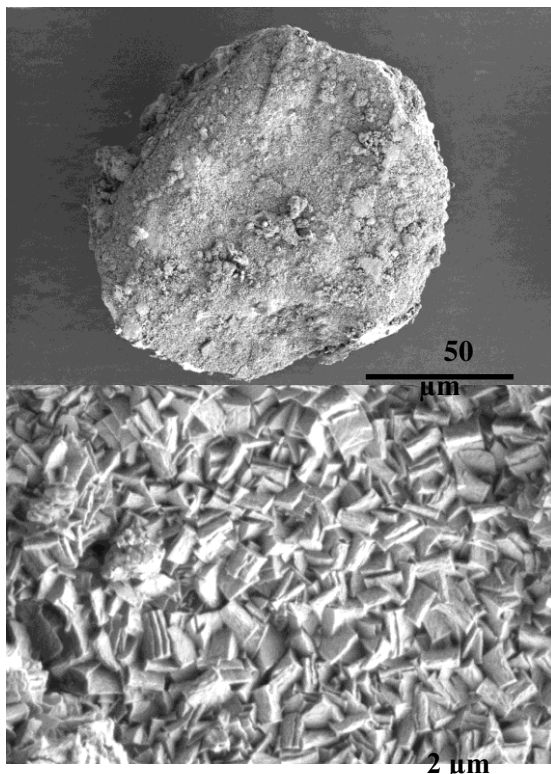
Fig. 3. SEM micrographs of sample LS-4
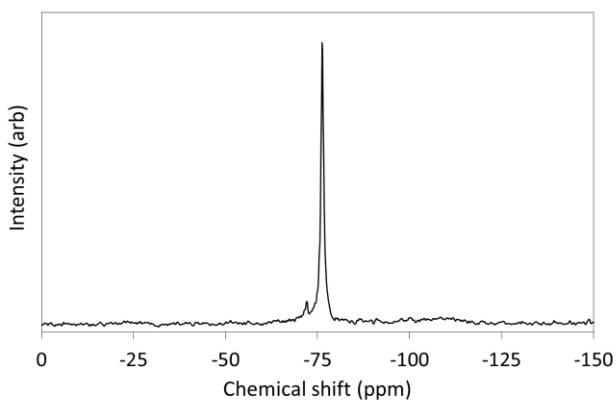
Fig. 4. ^{29}Si MAS NMR spectrum of the hydrothermal reaction products
of waste glass and aqueous lithium hydroxide

The FTIR spectrum of LS-4 is presented in Fig. 5 and closely resembles those of lithium metasilicate reported in the literature (Yang et al., 2012; Zhang et al., 2008). Bands at 1043, 983, 736 and 619 cm^{-1} arise from Si-O-Si vibrations. The signal at 523 cm^{-1} is assigned to Si-O-Li deformations and O-Si-O vibrations give rise to the bands at 945 and 863 cm^{-1}. Stretching vibrations of adsorbed water and hydroxide groups appear at 3440 cm^{-1} and the bands at 1500 and 1440 cm^{-1} are attributed to carbonate stretching modes of calcite and lithium carbonate.
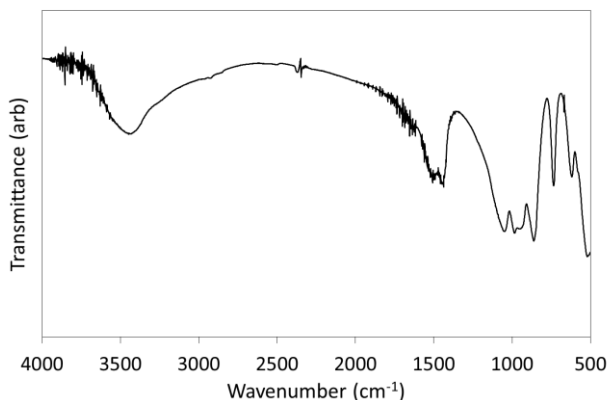
Fig. 5. FTIR spectrum of the hydrothermal reaction products
of waste glass and aqueous lithium hydroxide

Zn^{2+}-uptake

Zinc is an essential antioxidant and anti-inflammatory agent in the human body, which also possesses antimicrobial properties by inhibiting nutrient uptake and interfering with proton transfer processes in bacteria. The sorption characteristics of numerous Zn^{2+}-bearing zeolites, clays and synthetic silicates have been investigated with a view to these materials being incorporated into polymer blends, food packaging, pharmaceutical formulations and biomedical devices (Coleman, 2009; Coleman et al., 2010; El-Kamash et al., 2005; Purna Chandra Rao et al., 2006; Qui and Zheng, 2009).

The uptake of zinc ions by sample LS-4 as a function of time is plotted in Fig. 6. Within 24 h, the uptake of zinc ions is 6.4 mmol/g. The extent of zinc-loading far exceeds those of other synthetic silicates such as tobermorite, $Ca_5Si_6O_{16}(OH)_2 \cdot 4H_2O$, (1.6 mmol/g) and umbite, $K_2ZrSi_3O_9 \cdot H_2O$, (0.6 mmol/g) whose zinc-bearing phases have been shown to possess antimicrobial action against *Staphylococcus aureus, Pseudomonas aeruginosa* and *Escherichia coli* (Coleman et al. 2009, Coleman, 2010).
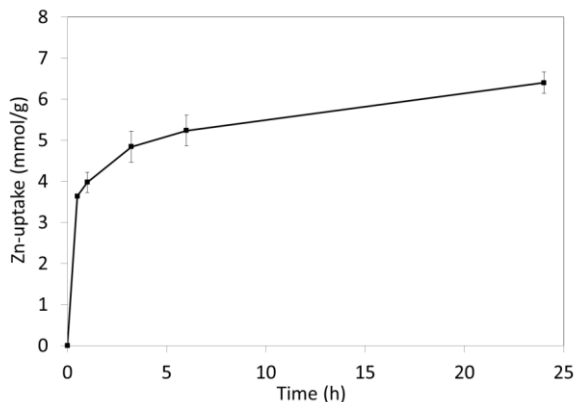
Fig. 6. Uptake of zinc ions by LS-4

The powder XRD pattern of the LS-4 sample after Zn^{2+} batch sorption is shown in Fig. 7. The small quantity of sample present after ion exchange (~100 mg recovered) compromises the signal-to-background ratio of these data; nonetheless, it is evident that a proportion of the lithium metasilicate has become amorphised during the Zn^{2+}-uptake process and that the relative intensities of the reflections of lithium metasilicate have altered. This indicates that, despite the similar size of the lithium Li^+ and zinc Zn^{2+} cations, 90 and 88 pm, respectively, significant structural disruption occurs during the Zn^{2+}-uptake process. This may to arise from the more specific co-ordination requirements of zinc compared with those of lithium, although further work would be required to confirm the specific mechanism of interaction between the Zn^{2+} ions and the lithium metasilicate phase.
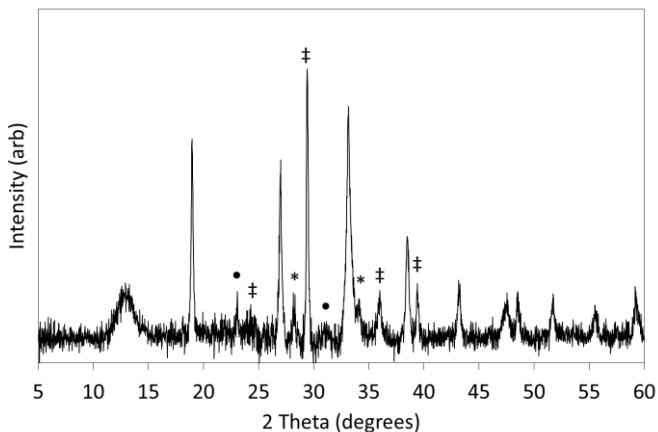
Fig. 7. Powder XRD pattern of zinc-exchanged LS-4
(key: Li_2SiO_3 – unmarked; $Ca(OH)_2$ – *; $CaCO_3$ – ‡; Li_2CO_3 – •)

Waste glass as a feedstock for lithium metasilicate

Current environmental directives to preserve resources and divert waste streams have stimulated significant interest in mineral recycling and 'up-cycling' in added-value applications. Poor collection facilities and colour mismatch limit the supply of suitable glass cullet that can be effectively recycled as new container glass. In addition, large quantities of recycled cullet can alter the feedstock during glass manufacture causing variations in composition and redox chemistry, which can compromise the quality of the finished glass (Karamberi and Moutsatsou, 2005).

This preliminary study has demonstrated that lithium metasilicate can be prepared by hydrothermal reaction between waste container glass and lithium hydroxide solution at 100 °C. Minor proportions of calcium hydroxide, calcite, and lithium carbonate were also produced during the reaction. Percentage crystallinity and proportion of lithium metasilicate in the product both increased as functions of lithium hydroxide concentration. Lower concentrations of lithium hydroxide also promoted the formation of poorly crystalline tobermorite by increasing the solubility of calcium ions released from the glass. A previous study indicated that tobermorite, an ion-exchanger, can be synthesised from waste glass under similar hydrothermal conditions in 1, 2 and 4 M sodium hydroxide solution (Coleman et al., 2013). These studies have demonstrated that waste glass is a potentially versatile feedstock for a range of technologically significant silicate phases.

This research has also shown that Zn^{2+} ions can be taken up by lithium metasilicate, and that the extent of Zn^{2+}-uptake after 24 h by the waste glass-derived lithium metasilicate exceeds those of other synthetic silicate minerals reported in the literature (Coleman et al. 2009, Coleman 2010). These initial results indicate that the Zn^{2+}-bearing lithium metasilicate may be a suitable filler material for antimicrobial polymer composites. Further research is now underway to optimise the yield of the lithium metasilicate product phase and to evaluate the antimicrobial properties of its Zn^{2+}-bearing counterpart.

Conclusions

A novel hydrothermal route to the formation of a mixed product, principally comprising lithium metasilicate, from waste container glass has been demonstrated. Percentage crystallinity and proportion of lithium metasilicate in the reaction product were found to increase as functions of lithium hydroxide concentration. This research has also shown the lithium metasilicate phase can take up 6.4 mmol/g of Zn^{2+} ions after 24 h during batch sorption. Further work to optimise the yield and to appraise the antimicrobial properties of Zn^{2+}-bearing lithium metasilicate is now warranted.

References

AYADI, A., STITI, N., BOUMCHEDDA, K., RENNAI, H., LERARI, Y., 2011, *Elaboration and characterization of porous granules based on waste glass*, Powder Technol. 208, 423-426.

CHEARY, R.W., COELHO, A.A., 1992, *A fundamental parameters approach to X-ray line-profile fitting*, J. Appl. Cryst. 25, 109-121.

COLEMAN, N.J., 2009, *Aspects of the in vitro bioactivity and antimicrobial properties of Ag^+- and Zn^{2+}-exchanged 11 Å tobermorites* J. Mater. Sci.: Mater. Med. 20, 1347-1355.

COLEMAN, N.J., LEWIS, S.P., MENDHAM, A.P., TRIVEDI, V., 2010, *Zn^{2+}-exchange kinetics and antimicrobial properties of synthetic zirconium umbite ($K_2ZrSi_3O_9{\cdot}H_2O$)*, J. Porous Mater. 17, 747-757.

COLEMAN, N.J., LI, Q., RAZA, A., 2014, *Synthesis, structure and performance of calcium silicate ion exchangers from recycled container glass*, Physicochem. Probl. Miner. Process. 50, 5-16.

CRUZ, D., BULBULIAN, S., 2003, *Synthesis of lithium silicate tritium breeder powders by a modified combustion method*, J. Nucl. Mater. 312, 262–265.

EL-KAMASH, A.M., ZAKI, A.A., ABED EL GELEEL, M., 2005, *Modeling batch kinetics and thermodynamics of zinc and cadmium ions removal from waste solutions using synthetic zeolite A*, Hazard. Mater. B127, 211-220.

KARAMBERI, A, MOUTSATSOU A., 2005, *Participation of coloured glass cullet in cementitious materials*, Cem. Concr. Compos. 27, 319-327.

KORKOSZ, A., PTASZYNSKA, A., HANEL, A., NIEWIADOMSKI, M., 2012, *Cullet as a filter medium for swimming pool water treatment*, Physicochem. Probl. Miner. Process. 48, 295-301.

MATTEUCCI, F., DONDI, M., GUARINI, G., 2002, *Effect of soda-lime glass on sintering and technological properties of porcelain stoneware tiles*, Ceram. Int. 28, 873-880.

ORTIZ-LANDEROS, J., CONTRERAS-GARCÍA, M.E., GÓMEZ-YÁÑEZ, C., PFEIFER, H., 2011, *Surfactant-assisted hydrothermal crystallization of nanostructured lithium metasilicate (Li_2SiO_3) hollow spheres: (I) synthesis, structural and microstructural characterization*, J. Solid State Chem., 184, 1304-1311.

PFEIFER, H., MEILER, W., DEININGER, D., 1983, *NMR of organic compounds adsorbed on porous solids*, Annu. Rep. NMR Spectrosc. 15, 291-356.

PFEIFER, H., BOSCH, P., BULBULIAN, S., 1998, *Synthesis of lithium silicates*, J. Nucl. Mater. 257, 309-317.

PURNA CHANDRA RAO, G., SATYAVENI, S., RAMESH, A., A., SESHAIAH, K., MURTHY, K.S.N., CHOUDARY, N.V., 2006, *Sorption of cadmium and zinc from aqueous solutions by zeolite 4A, zeolite 13X and bentonite*, J. Environ. Manag. 81, 265-272.

QUI, W., ZHENG, Y., 2009, *Removal of lead, copper, nickel, cobalt, and zinc from water by a cancrinite-type zeolite synthesized from fly ash*, Chem. Eng. J. 145, 483-488.

TANG, T., CHEN, P., LUO, W., LUO, D., WANG, Y., 2012, *Crystalline and electronic structures of lithium silicates: A density functional theory study*, J. Nucl. Mater. 420, 31-38.

VELIS, C.A., FRANCO-SALINAS, C., O'SULLIVAN, C., NAJORKA, J., BOCCACCINI, A.R., CHEESEMAN, C.R., 2014, *Up-cycling waste glass to minimal water adsorption/absorption lightweight aggregate by rapid low temperature sintering: optimization by dual process-mixture response surface methodology*, Environ. Sci. Technol. 48, 7527-7535.

YANG, A., WANG, H., LI, W., SHI, J., 2012, *Synthesis of lithium metasilicate powders at low temperature via mechanical milling*, J. Am. Ceram. Soc. 95, 1818-1821.

ZHANG, B., NIEUWOUDT, M., EASTEAL, A.J., 2008, *Sol–gel route to nanocrystalline lithium metasilicate particles*, J. Am. Ceram. Soc. 91, 1927-1932.

LIGNITE CLEANING IN NaCl SOLUTIONS BY A REVERSE FLOTATION TECHNIQUE

Haijun ZHANG[*], Qingxia LIU[**],[***]

[*] National Engineering Research Center for Coal Processing and Purification, China University of Mining and Technology, Xuzhou 221116, China, zhjcumt@163.com
[**] Low Carbon Energy Institute, China University of Mining and Technology, Xuzhou 221116, China
[***] Department of Chemical and Materials Engineering, University of Ualberta, Edmonton T6G 2R3, Canada, qingxia2@ualberta.ca

Abstract: A cleaning possibility of low (BD) and high ash content (IM) lignites in NaCl solutions using a reverse flotation technique was studied. Preliminary test results indicated that BD lignite cannot be cleaned effectively in the traditional manner because gangue was floated first rather than a combustible material. Further studies indicated that the lignite cleaning in NaCl solutions using the reverse flotation technique is possible. However, a large quantity of dodecyl amine hydrochloride (DAH) was required. A lower ash content in a concentrate can be obtained by addition of NaCl. A concentrate yield can be improved by addition of starch. Under the test conditions, for BD lignite with the ash content in the feed 15.19%, the ash content in the concentrate 11.44% and the concentrate yield 67.38% were obtained. Similarly, for IM lignite with the ash content in the feed 57.40%, the ash content in the concentrate 32.90% and the concentrate yield 25.08% were obtained. The flotation rate constant k and maximum ash recovery ε_∞ significantly increased with the NaCl concentration.

Keywords: lignite, reverse flotation, NaCl, kinetics, coal preparation

Introduction

Flotation, an important and versatile mineral processing technique, is a selective separation process for which the separation efficiency depends primarily on differences in surface properties of various mineral particles (Anderson, 1916; Taggart, 1920; Subrahmanyam and Forssberg, 1988; Nguyen et al., 1998). Lower rank coals (e.g. lignite) are more hydrophilic, and therefore difficult to float in the traditional manner, even using a high reagent dosage. It is due to the presence of higher oxygen functional groups, such as hydroxyl, carbonyl and carboxyl (Arnold and Aplan, 1989; Atesok and Celik, 2000; Jia et al., 2000; Cebeci, 2002; Zhang and Tang, 2014).

In contrast to traditional flotation, previous studies have reported that a reverse flotation technique can be used for coal separation, whereby gangue moves to the flotation froth and a combustible material does not (Stonestreet and Franzidis, 1988, 1989, 1992; Pawlik and Laskowski, 2003). In many studies of coal reverse flotation, cationic amine surfactants were used to float gangue since these surfactants act as ash collectors, coal depressants and frothers (Dey, 2012). Ding and Laskowski (2006) investigated reverse flotation of subbituminous coal. In their study, the ash content decreased from 34.6 to 16.7% for a concentrate yield of 50.4%. In addition, Patil and Laskowski (2008) for bituminous coal using reverse flotation obtained the concentrated ash content of 16.5% and 55% concentrate yield for a feed ash content of 34.7%. In this case, the reverse flotation technique is most likely better suited for lignite flotation because of its strongly hydrophilic character compared with a higher rank coal.

There is a correlation between the flotation recovery, kinetics, bubble size distribution and stability profile of froth with addition of salt solutions (Marrucci and Nicodemo, 1967; Weissenborn and Pugh, 1996; Pugh et al., 1997; Harvey et al., 2002; Marcelja, 2006). Many studies have demonstrated that electrolyte ions can enhance the flotation performance (Klassen and Mokrousov, 1963; Laskowski, 1965; Yoon, 1982; Hampton and Nguyen, 2009; Ozdemir et al., 2009, 2013). Paulson and Pugh (1996) found that the ionic strength is an important factor in scaling the overall recovery of graphite, which was linked to the dissolved gas concentration gradients in the electrolyte solutions. Bournival et al. (2012) investigated the stability of bubbles through measurements of coalescence time between bubble at the tip of capillary using high-speed video imaging. They demonstrated that the bubble became more stable as the salt concentration increased in the solution. The results also suggested that a relatively larger concentration of salt was required to achieve stability in the froth zone.

In this study, to evaluate the possibility of lignite cleaning in NaCl solutions using the reverse flotation technique, two lignites (BD with low ash content and IM with high ash content) were selected as raw samples. The effect of NaCl, dodecyl amine hydrochloride (DAH) and starch on the reverse flotation performance was investigated. In addition, the flotation performance, as a function of NaCl, was estimated by analysing the flotation kinetics.

Experimental

Two lignite samples were used as flotation feed: BD lignite with low ash content (15.19%) and IM lignite with high ash content (57.40%) on a dry basis. The BD and IM lignite samples were obtained from Alberta (Canada) and Inner Mongolia (China), respectively. The as-received samples were crushed to −2 mm. Next, the crushed samples were ground to −425 μm using a ball mill (ADVAN-TEC, No. 5C). The analysis and particle size distribution of lignite samples on a dry basis are presented in Tables 1 and 2.

Dodecyl amine hydrochloride (DAH, $C_{12}H_{28}ClN$, $\geq 99\%$) was used as a surfactant in preliminary tests (traditional flotation tests). DAH which is known for its beneficial role in flotation of low-rank coal at a small dosage (Kelebek et al., 2008). DAH in large dosages is also used as a collector for gangue in the reverse flotation tests (Stonestreet and Franzidis, 1988; Pawlik and Laskowski, 2003). In this paper kerosene was used as a collector, corn starch $((C_3H_{10}O_5)_n$, MW=162.15 g/mol, laboratory grade) as a coal depressant, 4-methyl-2-pentanol (MIBC, laboratory grade) as a frother and sodium chloride (NaCl, laboratory grade) was used as a soluble salt. To increase the solubility of corn starch, 1% causticised corn starch solution was prepared (corn starch-to-NaOH = 4:1, wt.%). All experiments were conducted in distilled water.

The reverse flotation tests were performed in a 1 dm^3 Denver flotation cell. All tests were performed at room temperature. For each test, 50 g of lignite sample on a dry basis was first mixed with 500 cm^3 desired salt solution in the cell, and then agitated for 5 min at an impeller rotation speed of 1600 rpm. Next, starch, DAH and MIBC were added to a slurry. The condition time for starch, DAH, and MIBC was 3, 2, and 1 min, respectively. After conditioning, the desired salt solution was added again to increase the volume of slurry in the cell to 1 dm^3, and then, the slurry was stirred for additional 4 min. Subsequently, air was introduced into the cell at a flow rate of 1.35 dm^3/min. Either distilled water or desired salt solution was added during the tests to maintain a constant pulp level, and then, the slurry was floated for 20 min. The froth was collected after 2, 6, 12 and 20 min. Finally, the flotation concentrate (combustible material which did not report to the flotation froth) and tailings (gangue which reported to the flotation froth) were filtered, dried, weighed, and then the ash content was determined by applying the ASTM procedure. The ash and combustible recoveries were calculated using equations:

$$\text{Ash recovery (\%)} = [M_T A_T / M_F (100 - A_F)] \times 100 \tag{1}$$

$$\text{Combustible Recovery (\%)} = [M_C (100 - A_C)/M_F (100 - A_F)] \times 100 \tag{2}$$

where M_C, M_T, M_F are concentrate, tailings feed masses (%), respectively, A_C, A_T, A_F are ash contents in concentrate, tailings and feed (%), respectively. The ash contents in the concentrate and tailing were on a dry basis.

The cumulative ash recoveries after 2, 6, 12 and 20 min of flotation time were fitted to the first-order rate equation:

$$\varepsilon = \varepsilon_\infty [1 - \exp(-kt)], \tag{3}$$

where ε is cumulative ash recovery at time t, ε_∞ the maximum ash recovery and k is the first-order rate constant. The non-linear regression software 1stOpt (http://www.7d-soft.com) was used to simulate the flotation rate constant (k), maximum ash recovery (ε_∞) and correlation coefficient (R^2).

Table 1. Analysis of −2 mm lignite samples on dry basis

Samples	Inherent moisture (wt.%)		Ash (wt.%)		Volatile matter (wt.%)		Fixed carbon (wt.%)	
	As received	Dry basis	As received	Dry basis	As received	Dry basis	As received	Dry basis
BD lignite	22.46	−	11.78	15.19	45.86	59.14	19.90	25.67
IM lignite	20.16	−	45.83	57.40	19.48	24.40	14.53	18.20

Table 2. Size and ash content of −425 μm lignite samples on dry basis

Size fraction (μm)	BD lignite				IM lignite			
	Weight (%)	Ash (%)	Cumulative weight (%) finer than size	Cumulative ash (%) finer than size	Weight (%)	Ash (%)	Cumulative weight (%) finer than size	Cumulative ash (%) finer than size
−425+250	16.15	11.49	100.00	15.19	22.7	48.64	100	57.40
−250+150	21.58	11.94	83.85	15.90	21.85	55.27	77.3	59.97
−150+75	21.80	12.80	62.27	17.27	23.86	59.05	55.45	61.82
−75+45	11.91	14.55	40.47	19.68	15.11	62.00	31.59	63.92
−45	28.56	21.82	28.56	21.82	16.48	65.68	16.48	65.68
Total	100.00	15.19			100	57.40		

Results and discussion

Lignite characterisation

The particle size and ash distribution BD and IM lignite samples presented in Table 2 indicate that the ash content of both lignite samples increased as the particle size decreased. The yield of -45 μm size fraction is 28.56%, with ash content of 21.82% for the BD lignite sample, whereas for the IM lignite sample the yield of the -45-μm size fraction is 16.48%, with ash content of 65.68%. The significant increase in the ash content for fine particles (-45 μm) can be explained by a fragile characteristics of lignite, which causes a decrease in the selectivity in froth flotation. In addition, fine lignite particles are easy to slime during the flotation process. Therefore, separation of fine particles is crucial to enhance the flotation performance of lignite samples.

To understand the hydrophilic properties of lignite samples, Fourier transform infrared spectroscopy FTIR (ABB MB3000) was used to analyse the oxygen functional groups. A high rank coal with ash content of 10.89% was selected as a reference sample. For all tests, three samples were ground to −45 μm using a ball mill. The spectra were collected in the range of 500 to 4,000 cm^{-1} at a spectral resolution of 2 cm^{-1}. The FTIR spectra of three samples are presented in Fig. 1. It can be seen that the oxygen

functional groups were abundant in the IM lignite sample, whereas they were scarcely present in high rank coal. The increase in the oxygen functional groups implied the increase in hydrophilicity. The FTIR analysis indicated that BD and IM lignite samples were more hydrophilic than high rank coal.
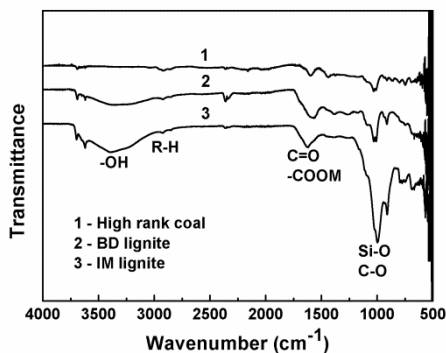
Fig. 1. FTIR spectra of high rank coal (1), BD (2) and IM (3) lignite samples

Preliminary tests

A sample of BD lignite was selected for preliminary tests in the traditional manner. DAH was used as surfactant, kerosene as collector, MIBC as frother, and NaCl as soluble salt. The test conditions were the same as previously described. The preliminary tests were first performed in NaCl solutions without any flotation reagents. Table 3 shows the effect of NaCl concentration on the BD lignite flotation performance. From Table 3 it can be seen that the ash content in the froth products was higher than for the feed and decreased with flotation time, that indicates on the reverse flotation process.

To improve floatability of BD lignite, DAH, which is the cationic amine surfactant, was added together with kerosene and MIBC. Tables 4 and 5 show the effect of DAH and kerosene on the BD lignite flotation performance, respectively. It can be seen that a similar flotation response was reported when compared with that of NaCl solutions, even in the absence of DAH. DAH improved the reverse flotation performance compared with kerosene, and the ash content decreased with increase in the DAH dosage. In the preliminary tests, the ash of BD lignite decreased from 15.19 to 13.71% for the concentrate yield of 54.05% after 20 min of flotation. The preliminary test results suggest that BD lignite cannot be cleaned effectively in the traditional manner and that gangue was floated first rather than the combustible material. Based on the preliminary tests, batch reverse flotation tests of BD and IM lignite were performed in a subsequent experiment to further evaluate the possibility of lignite cleaning in the NaCl solutions by the reverse flotation technique.

Table 3. Flotation results for BD lignite as a function of NaCl without flotation reagents

NaCl concentration	0.1 M		0.3 M		0.5 M		1.0 M		2.0 M	
Flotation time (min)	Yield (%)	Ash (%)	Yield (%)	Ash (%)	Yield (%)	Ash (%)	Yield (%)	Ash (%)	Yield (%)	Ash (%)
2	5.97	19.71	10.26	18.54	8.94	18.18	9.07	18.50	10.71	18.81
6	7.01	18.22	11.47	14.45	12.66	15.95	14.40	16.46	17.22	14.90
12	9.31	17.96	13.43	16.23	11.32	13.26	13.13	13.97	15.49	15.73
20	9.90	16.67	9.85	13.91	11.41	13.77	10.61	13.00	13.55	14.46
Sink	67.81	13.88	54.99	14.69	55.67	15.22	52.78	15.02	43.03	14.44
Total	100.00	15.19	100.00	15.19	100.00	15.19	100.00	15.19	100.00	15.19

Table 4. Flotation results for BD lignite as a function of DAH (kerosene 3000 g/Mg, MIBC 800 g/Mg)

DAH dosage	0 g/Mg		100 g/Mg		300 g/Mg		500 g/Mg		700 g/Mg	
Flotation time (min)	Yield (%)	Ash (%)	Yield (%)	Ash (%)	Yield (%)	Ash (%)	Yield (%)	Ash (%)	Yield (%)	Ash (%)
2	32.50	15.90	30.72	16.44	22.56	17.41	27.43	17.49	29.21	17.84
6	9.38	16.40	7.87	16.51	6.81	17.39	7.38	16.15	6.82	16.20
12	4.28	15.78	4.03	15.26	4.97	15.75	3.51	15.34	3.71	14.91
20	4.33	15.31	5.35	14.76	3.15	15.50	6.04	14.91	6.21	14.68
Sink	49.51	14.43	52.03	14.29	62.51	14.09	55.64	13.95	54.05	13.71
Total	100.00	15.19	100.00	15.19	100.00	15.19	100.00	15.19	100.00	15.19

Table 5. Flotation results for BD lignite as a function of kerosene (DAH 300 g/Mg, MIBC 800 g/Mg)

Kerosene dosage	1000 g/Mg		2000 g/Mg		3000 g/Mg		4000 g/Mg		5000 g/Mg	
Flotation time (min)	Yield (%)	Ash (%)	Yield (%)	Ash (%)	Yield (%)	Ash (%)	Yield (%)	Ash (%)	Yield (%)	Ash (%)
2	18.73	18.84	20.11	17.99	22.56	17.41	23.63	17.29	32.37	16.60
6	10.61	16.77	9.28	16.74	6.81	17.39	8.58	16.66	7.33	16.21
12	4.56	15.64	5.68	15.55	4.97	15.75	4.73	15.22	4.57	15.60
20	3.65	15.32	2.07	14.88	3.15	15.50	4.13	15.23	3.29	15.21
Sink	62.44	13.79	62.85	14.04	62.51	14.09	58.93	14.13	52.43	14.14
Total	100.00	15.19	100.00	15.19	100.00	15.19	100.00	15.19	100.00	15.19

Batch reverse flotation tests

The previous studies indicated that inorganic electrolytes can generate abundant smaller bubbles and that the charge of gas bubbles in the aqueous solution can be re-

duced and even reversed by the addition of multivalent inorganic salts (Li and Somasundaran, 1991; Ozdemir et al., 2009). In this case, inorganic electrolytes may improve floatability of fine particles with a high ash content in the reverse flotation process. The effect of NaCl on lignite reverse flotation was tested in the presence of DAH, starch and MIBC. The results for BD and IM lignite samples are shown in Figs. 2 and 3, respectively. Figures 2 and 3 show that the ash content in concentrate decreased with addition of NaCl for both lignite samples. The concentration of NaCl had only a little effect on the yield of the products of BD lignite, while for IM lignite, the concentrate yield decreased with addition of NaCl. However, it is difficult to explain the effect of NaCl concentration on the product yield and ash contents because of the presence of other chemical additives in the process. This difficulty is attributed to the possibility that the flotation behaviour of either gangue or combustible material frequently varies in the presence of NaCl and DAH during the flotation process. Yoon and Yordan, (1991) investigated the bubble-particle attachment time for the quartz-amine flotation system as a function of KCl concentration at pH 6.75. The induction time was found to decrease with increase of KCl concentration at low DAH concentration ($5 \cdot 10^{-6}$ M). In contrast, the induction time was found to increase with increase in KCl concentration at higher DAH concentration ($5 \cdot 10^{-4}$ M), particularly when KCl concentration was higher than 10^{-1} M.

The mechanism of action in NaCl solutions using the reverse flotation technique requires further investigation, particularly the interactions in this system, which were implemented with the simultaneous addition of NaCl, DAH, starch and MIBC. Under the test conditions, although for IM lignite the concentrate yield decreased by addition of NaCl, lower ash content is obtained, which can be substantially reduced from 57.40 to 28.82% by adding 0.4 M NaCl.

Fig. 2. Effect of NaCl on reverse flotation of BD lignite (DAH 5000 g/Mg, starch 2500 g/Mg, MIBC 200 g/Mg)

Fig. 3. Effect of NaCl on reverse flotation of IM lignite (DAH 5000 g/Mg, starch 3000 g/Mg, MIBC 200 g/Mg)

The excellent ash-collecting ability of quaternary amines in coal reverse flotation has been reported by Stonestreet and Franzidis (1988, 1989, 1992). The effect of DAH on reverse flotation of lignite is shown in Figs. 4 and 5. Figures 4–5 show that for BD

and IM lignite samples, both concentrate yield and ash content decreased with increasing DAH dosages. The ash content in the concentrate for BD lignite decreased slightly from 12.56 to 11.26% while for IM lignite the ash content decreased from 42.45 to 27.68%, when the DAH dosage increased from 2000 to 6000 g/Mg. The results clearly indicate that BD lignite was difficult to clean.
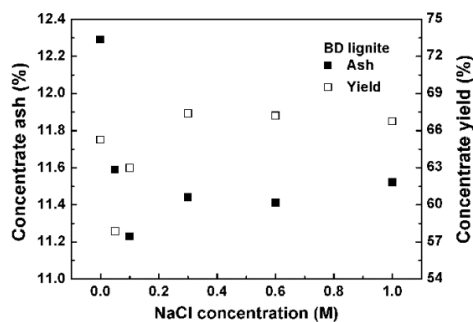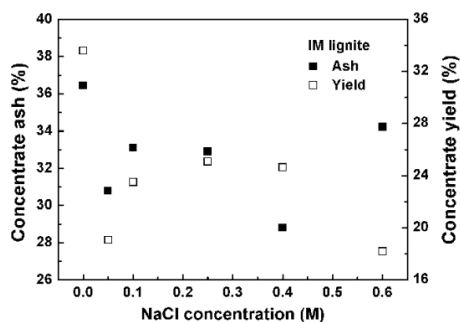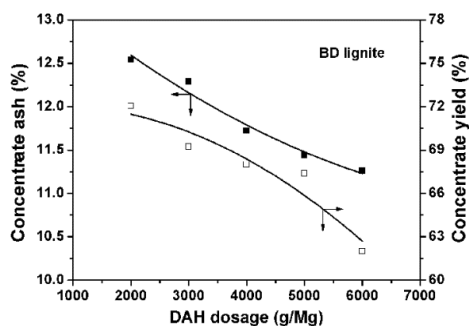

Fig. 4. Effect of DAH on reverse flotation of BD lignite (NaCl 0.3 M, starch 2500 g/Mg, MIBC 200 g/Mg)
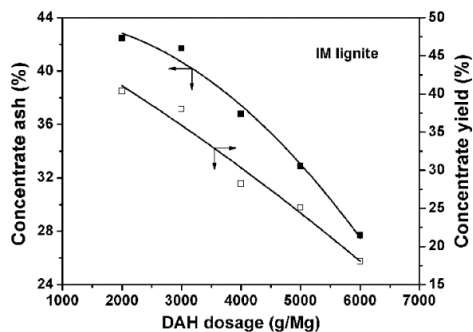
Fig. 5. Effect of DAH on reverse flotation of IM lignite (NaCl 0.25 M, starch 3000 g/Mg, MIBC 200 g/Mg)

The ash content in the concentrate decreased with DAH concentration. It result was observed by Ding and Laskowski (2006) and Kelebek (2008) for coal reverse flotation. It could be explained by the effect of adsorption density of amine on coal and gangue. Pawlik and Laskowski (2003) reported that the adsorption density of amine on hydrophilic-oxidised and subbituminous coals was much higher than on bituminous coal and silica. Yoon and Yordan (1991), who studied the induction time and the flotation recovery of quartz particles at pH 6.6, found that the induction time first decreased and then increased with the increase in DAH concentration, whereas the flotation recovery first decreased and then increased concomitantly. The shortest induction time and the highest flotation recovery were obtained at approximately 10^{-3} M DAH concentration, which was largely consistent with the investigated range of DAH dosage (which corresponds to $4.5\cdot10^{-4}$ M $-$ $1.4\cdot10^{-3}$ M) in this study. The results supported the hypothesis that cationic amine surfactants can be used as collectors for ash and as depressants for coal (Dey, 2012).

The effect of starch on reverse flotation of lignite is shown in Figs. 6 and 7. It can be seen that the increase in starch dosage increased the concentrate yield and ash content for BD and IM lignite. The results indicate that addition of starch cannot improve the selectivity in this process, however improves the concentrate yield.

Fig. 6. Effect of starch on reverse flotation of BD lignite (NaCl 0.3 M, DAH 5000 g/Mg, MIBC 200 g/Mg)
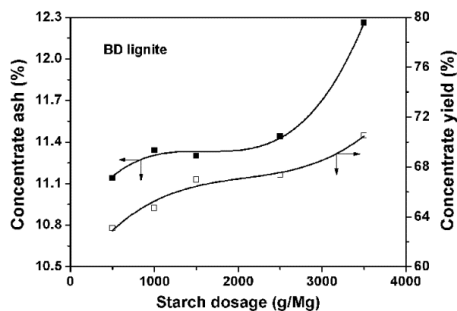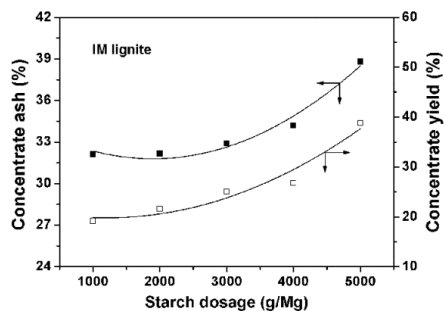
Fig. 7. Effect of starch on reverse flotation of IM lignite (NaCl 0.25 M, DAH 5000 g/Mg, MIBC 200 g/Mg)

Kinetics of lignite reverse flotation as a function of NaCl solutions

The results clearly indicate that cleaning of BD and IM lignite samples is possible by using the reverse flotation technique with the ambient pH value in NaCl solutions. For BD lignite with the ash content in the feed of 15.19%, the ash content in the concentrate 11.44% and the concentrate yield 67.38% were obtained, whereas for IM lignite with the ash content in the feed of 57.40% the ash content in the concentrate and yield were 32.90 and 25.08%, respectively.

Sodium chloride influences the kinetics of flotation (Table 6). It is evident that the flotation rate constant k and maximum ash recovery ε_∞ significantly increased with NaCl concentration. The flotation rate constant k for BD lignite increased from 0.15 $\min^{-1}$ (in distilled water) to 0.62 $\min^{-1}$ in 0.01 M NaCl solution.

Table 6. Flotation kinetic parameters for BD and IM lignite as a function of NaCl

NaCl Concentration	BD lignite			NaCl Concentration	IM lignite		
	K (min^{-1})	ε_∞ (%)	R^2		K (min^{-1})	ε_∞ (%)	R^2
0.00 M	0.15	48.43	0.9943	0.00 M	0.30	77.60	0.9992
0.05 M	0.51	51.85	0.9788	0.05 M	0.31	90.80	0.9970
0.10 M	0.62	51.74	0.9959	0.10 M	0.55	83.41	0.9920
0.30 M	0.35	47.70	0.9950	0.25 M	0.54	83.19	0.9978
0.60 M	0.42	48.24	0.9962	0.40 M	0.63	90.18	0.9984
1.00 M	0.50	47.36	0.9934	0.60 M	0.78	87.58	0.9988

For IM lignite the maximum ash recovery ε_∞ increased from 77.60% (in distilled water) to 90.80% in 0.05 M NaCl solution. It can be explained by differences in the bubble size and bubble coalescence. As shown in Fig. 8, abundant smaller bubbles

were generated as the NaCl concentration increased. This phenomenon was consistent with the findings of Craig et al. (1993), who showed that the bubble coalescence was inhibited in certain salt solutions and that a number of smaller bubbles was generated. In addition, Ozdemir et al. (2009) reported that the flotation efficiency of fine particles increased in bore water because of the high number of bubbles in the flotation system.
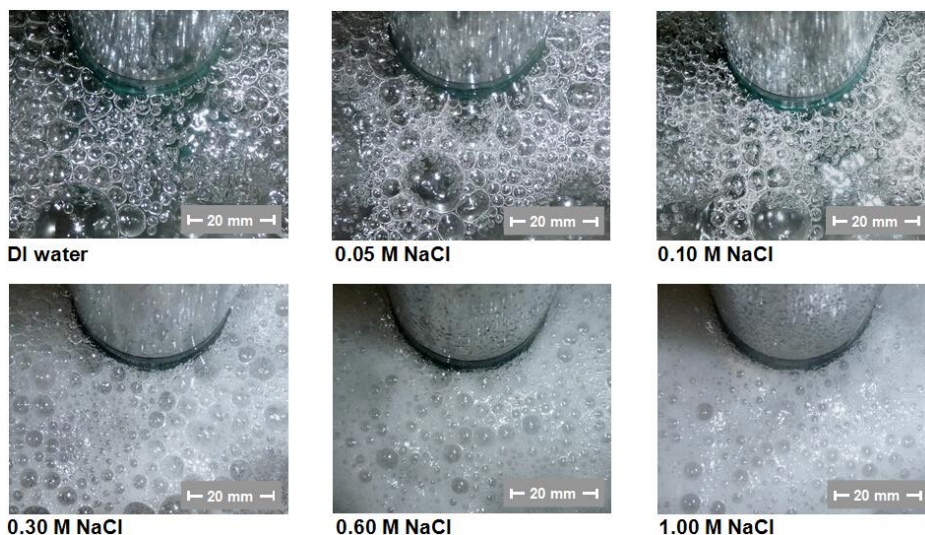
Fig. 8. Bubbles in distilled water (DI) and NaCl solutions
(1 dm^3 Denver cell, impeller speed of 1600 rpm, air flow rate of 1.35 dm^3/min)

Conclusions

This study investigated the flotation performance of low (BD) high (IM) ash content lignite samples in NaCl solutions using the reverse flotation technique. Based on the results, the following conclusions can be presented.

1. FTIR spectra indicated that BD and IM lignite samples were more hydrophilic than high rank coal. A sample of BD lignite cannot be cleaned effectively in the traditional manner since gangue was floated first rather than the combustible material.

2. Cleaning of lignite in NaCl solutions using the reverse flotation technique is possible. A high concentration of dodecyl amine hydrochloride (DAH) was required to float gangue from lignite by reverse flotation. Lower ash content in the concentrate can be obtained by addition of NaCl. The concentrate yield can be improved by addition of starch. Under the ambient pH value in NaCl solutions in the reverse flotation technique, for BD lignite with the ash content in the feed of 15.19%, the ash content in the concentrate 11.44% and the concentrate yield 67.38% were obtained, whereas for IM lignite with the ash content in the feed of 57.40% the ash content in the concentrate and yield were 32.90 and 25.08%, respectively.

3. The flotation rate constant k and maximum ash recovery ε_∞ significantly increased with the increase in the NaCl concentration primarily because of abundant smaller bubbles generated by presence of NaCl.

Acknowledgments

References

ANDERSON R.J., 1916. *Recent progress in flotation*. Journal of the Franklin Institute, 181(5), 643-657.

ARNOLD B.J., APLAN F.F., 1989. *The hydrophobicity of coal macerals*. Fuel, 68(5), 651–658.

ATEŞOK G., ÇELIK M.S., 2000. *A new flotation scheme for a difficult-to-float coal using pitch additive in dry grinding*. Fuel, 79(12), 1509–1513.

BOURNIVAL G., PUGH R.J., ATA S., 2012. *Examination of NaCl and MIBC as bubble coalescence inhibitor in relation to froth flotation*. Minerals Engineering, 25(1), 47–53.

CEBECI Y., 2002. *The investigation of the floatability improvement of Yozgat Ayridam lignite using various collectors*. Fuel, 81(3), 281–289.

CRAIG V.S.J., NINHAM B.W., PASHLEY R.M., 1993. *Effect of electrolytes on bubble coalescence*. Nature, 364, 317–319.

DEY S., 2012. *Enhancement in hydrophobicity of low rank coal by surfactants—A critical overview*. Fuel Processing Technology, 94(1), 151–158.

DING K.J., LASKOWSKI J.S., 2006. *Coal reverse flotation. Part II: Cleaning of a subbituminous coal*. Minerals Engineering, 19(1), 79–86.

HAMPTON M.A., NGUYEN A.V., 2009. *Accumulation of dissolved gases at hydrophobic surfaces in water and sodium chloride solutions: Implications for coal flotation*. Minerals Engineering, 22, 786–792.

HARVEY P.A., NGUYEN A.V., EVANS G.M., 2002. *Influence of electrical double-layer interaction on coal flotation*. Journal of Colloid and Interface Science, 250, 337–343.

JIA R., HARRIS G.H., FUERSTENAU D.W., 2000. *An improved class of universal collectors for the flotation of oxidized and low–rank coal*. International Journal of Mineral Processing, 58, 99–118.

KELEBEK S., DEMI U.R., SAHBAZ O., UCAR A., CINAR M., KARAGUZEL C., OTEYAKA B., 2008. *The effects of dodecylamine, kerosene and pH on batch flotation of Turkey's Tuncbilek coal*. International Journal of Mineral Processing, 88, 65–71.

KLASSEN V.I., MOKROUSOV V.A., 1963. *An introduction to the theory of flotation*. Butterwords, London, 338-342.

LASKOWSKI J., 1965. Coal flotation in solutions with raised concentration of inorganic salts. Colliery Guardian, 361–365.

LI C., SOMASUNDARAN P., 1991. *Reversal of bubble charge in multivalent inorganic salt solutions—effect of magnesium*. Journal of Colloid and Interface Science, 146(1), 215–218.

MARCELJA S., 2006. *Selective coalescence of bubbles in simple electrolytes*. The Journal of Physical Chemistry, 110(26), 13062–13067.

MARRUCCI G., NICODEMO L., 1967. *Coalescence of gas bubbles in aqueous solutions of inorganic electrolytes*. Chemical Engineering Science, 22(9), 1257–1265.

NGUYEN A.V., RALSTON J., SCHULZE H.J., 1998. *On modelling of bubble–particle attachment probability in flotation*. International Journal of Mineral Processing, 53(4), 225–249.

OZDEMIR O., TARAN E., HAMPTON M.A., KARAKASHEV S. I., NGUYEN A.V., 2009. *Surface chemistry aspects of coal flotation in bore water*. International Journal of Mineral Processing, 92, 177–183.

OZDEMIR O., 2013. *Specific ion effect of chloride salts on collectorless flotation of coal*. Physicochemical Problems of Mineral Processing, 49(2), 511–524.

PATIL D.P., LASKOWSKI J.S., 2008. *Development of zero conditioning procedure for coal reverse flotation*. Minerals Engineering, 21(5), 373–379.

PUGH R.J., WEISSENBORN P., PAULSON O., 1997. *Flotation in inorganic electrolytes; the relationship between recovery of hydrophobic particles, surface tension, bubble coalescence and gas solubility*. International Journal of Mineral Processing, 51, 125–138.

PAULSON O., PUGH R. J., 1996. *Flotation of inherently hydrophobic particles in aqueous solutions of inorganic electrolytes*. Langmuir, 12, 4808–4813.

PAWLIK M., LASKOWSKI J.S., 2003. *Coal reverse flotation, Part I*. Coal Preparation, 23, 91–112.

PAWLIK M., LASKOWSKI J.S., 2003. *Coal reverse flotation, Part II*. Coal Preparation, 23, 113–127.

STONESTREET P., FRANZIDIS J.P., 1988. *Reverse flotation of coal—A novel way for the beneficiation of coal fines*. Minerals Engineering, 1(4), 343–349.

STONESTREET P., FRANZIDIS J.P., 1989. *Development of the reverse coal flotation process: Depression of coal in the concentrates*. Minerals Engineering, 2(3), 393–402.

STONESTREET P., FRANZIDIS J.P., 1992. *Development of the reverse coal flotation process: Application to column cells*. Minerals Engineering, 5(9), 1041–1051.

SUBRAHMANYAM T.V., FORSSBERG E., 1988. *Froth stability, particle entrainment and drainage in flotation—A review*. International Journal of Mineral Processing, 23, 33–53.

TAGGART A. F., 1920. Flotation. Journal of the Franklin Institute, 189(4), 485-498.

WEISSENBORN P.K., PUGH R.J., 1996. *Surface tension of aqueous solutions of electrolytes: relationship with ion hydration, oxygen solubility, and bubble coalescence*. Journal of Colloid and Interface Science, 184, 550–563.

YOON R.H., 1982. *Flotation of coal using micro-bubbles and inorganic salts*. Mining Congress Journal, 68(12), 76–80.

YOON R.H., YORDAN J.L., 1991. *Induction time measurements for the quartz-amine flotation system*. Journal of Colloid and Interface Science, 141, 374–383.

ZHANG W.J., TANG X.Y., 2014. *Flotation of lignite pretreated by sorbitan monooleate*. Physicochemical Problems of Mineral Processing, 50(2), 759–766.

APPLICABILITY OF PUBLISHED EXPERIMENTAL WORKS AS A KNOWLEDGE SOURCE IN RECOMMENDATION OF GOLD ORE PROCESSING WORKFLOWS

Lotta RINTALA, Jari AROMAA, Olof FORSEN

Department of Materials Science and Engineering, Aalto University, PO Box 16200, 00076 Aalto, Helsinki, Finland, lotta.rintala@aalto.fi, jari.aromaa@aalto.fi, olof.forsen@aalto.fi

Abstract: The experimental work is the most time consuming and expensive part of the process design. A case-based reasoning (CBR) methodology can be used to assist in the process design. *Auric Adviser* is a CBR system under development for recommendation of gold ore processing workflows. In *Auric Adviser* the knowledge in gold ore processing is represented in two models. The first model holds the knowledge needed to recommend process chains already used in industry. The second knowledge model is intended to recommend the most efficient unit processes based on research results. The objective of this study was to analyse the information richness of journal articles and other publications concerning single process steps of gold extraction. The aim was to study the applicability of these publications as a source for the second *Auric Adviser* knowledge model. In this study, 25 publications concerning leaching of gold were analysed and information was extracted in a case base. The case base was taken as either a process or experimental description with clearly defined differences to other descriptions. In total, 218 cases that described results of gold leaching were extracted from the sources. The analysis of descriptions showed that the knowledge necessary for design the second *Auric Adviser* model can be elicited from journal articles and other publications concerning single process steps. The trends in the case description were that the gold content and process outcome were usually well described. Nevertheless, the information richness varied in descriptions of raw materials, experimental arrangements but the results were often missing details. The incompleteness of information causes challenges in the process comparison although it does not prevent the CBR system to work.

Keywords: gold ore, leaching, case-based reasoning, process development

Introduction

The availability of knowledge is not an issue for today's expert designing gold ore processes as the amount of knowledge available in forms of journal articles and indus-trial reports is large and increasing continuously. It can be seen from Tables 1 and 2,

where the numbers of publications found in the Scopus data base (scopus.com) by several search terms are listed. The terms were searched within article title, abstract and keywords. A selected subject area was Physical Sciences and all document types were included. From Table 1 it can be seen that half of publications concerning gold ores are published within last 14 years.

Table 1. Number of publications about gold ore processing (source: scopus.com, accessed: 10.10.2014)

Terms used in the search	Published in years	
	1960-2014	2000-2014
gold AND ore	11978	6561
"gold ore"	3715	1563
gold AND refractory	998	533
gold AND refractory AND pretreatment	153	97
gold AND refractory AND preoxidation	11	6

Table 2 shows the increasing rate of research on treatment of refractory gold ores. Instead of the availability of knowledge, the facing challenge for each expert is to remember, classify and perform the comparative analysis of available knowledge.

Table 2. Number of publications about refractory gold ore processing (source: scopus.com, accessed: 10.10.2014)

Terms used in the search	Published in years	
	1960-2014	2000-2014
gold AND refractory AND roasting	118	51
gold AND refractory AND bioleaching	112	63
gold AND refractory AND oxidation	390	211
gold AND refractory AND oxidation AND sulfide	205	110
gold AND refractory AND oxidation AND oxygen	65	36
gold AND refractory AND oxidation AND "nitric acid"	8	16
gold AND refractory AND oxidation AND chlorine	18	6

Development of new hydrometallurgical processes requires extensive, time consuming and often expensive experimental work. To enhance the development phase utilisation of existing information is important. The published sources can provide anything from large reviews to minute details and the challenge is how to use this information most effectively. Efficient exploitation of the existing knowledge helps to select needed experiments for specific processes precisely. A case-based reasoning (CBR) methodology has been tested and found to be suitable for recommendation of gold ore processing workflows (Rintala et al., 2011a, 2011b; Sauer et al., 2013, 2014).

It can help to assist with the tasks to remember, classify, recommend and perform the comparative analysis of the knowledge on gold ore processing. It is a decision support method, which is very similar to the way human reach decisions or solve problems. It solves new problems by using previously successful solutions to similar problems and adapting proven solutions to a current problem based on the knowledge stored in previous cases (Aamodt and Plaza, 1994; Lenz et al., 1998). The main benefit of CBR over other decision support methods is its ability to work with incomplete and fuzzy data (Rintala et al. 2011a, 2011b; Sauer et al., 2013).

In this work we extracted over 200 descriptions of experimental work about gold dissolution and processing of gold ore or concentrate from various sources. The information content of these descriptions was analysed and applicability of published experimental work as a knowledge source in the recommendation of gold ore processing workflows by the CBR methodology was studied.

Auric Adviser – a CBR system for recommendation of gold ore processing workflows

The CBR system under development is called *Auric Adviser* (Sauer et al., 2013, 2014). In *Auric Adviser* the knowledge in gold ore processing is represented as a two-stage approach. Two knowledge models serve each of two aspects of the approach. The first model presented by Sauer et al. (2013, 2014) holds the knowledge needed to recommend process chains already used in the industry. The second knowledge model is intended to recommend the most efficient unit processes based on research results. The suitable cases are retrieved from the case base using a similarity between new (query) and existing cases. The similarity between query q and case c is calculated as (Stahl and Roth-Berghofer, 2008):

$$Sim\ (q,c) = \sum_{i=1}^{n} \omega_i\, sim_i(q_i, c_i) \tag{1}$$

where sim_i and ω_i denote local similarity measure and weight of attribute i, respectively, Sim represents the global similarity measure. The similarity is computed in an interval between 0 and 1 [0,1], which represent most dissimilar and identical values, respectively.

The knowledge for the first *Auric Adviser* model was formalised using the open source similarity-based retrieval tool myCBR in its latest version 3.0 (myCBR, 2012). After knowledge formalisation 25 cases were extracted from descriptions of existing gold mines (Marsden and House, 2006). A test run of the retrieval of cases from the first knowledge model is shown in Table 3.

Table 3. The best (1–3) and the worst (lowest Sim) matching cases retrieved
from the *Auric Adviser* case base

Attribute	Query	1st	2nd	3rd	Lowest Sim (q,c)
Gold ore grade	12 g/Mg	8.5	4.7	5.0	70.0
Ore type	refractory iron sulphide	refractory iron sulphide	refractory iron sulphide	refractory iron sulphide	silver-rich
Gold distribution	grain enclosed in mineral	colloidal particles in solution	grain enclosed in mineral	grain enclosed in mineral	Unknown
Gold grain size	submicron sized	submicron sized	fine	submicron sized	Unknown
Iron sulphide	Pyrite	pyrite	pyrite	pyrite	Pyrite
Clay present	Yes	yes	yes	unknown	No
Sim (q,c)		0.86	0.85	0.82	0.20

When a process is designed for either a new gold ore or concentrate the expert can post a query to *Auric Adviser* for searching the existing process designs for similar raw materials. Several attributes can be used to characterise the raw material in the study. The test query consisted of the following attributes: gold ore grade is 12 g/Mg, ore type is refractory iron sulphide, gold distribution is grain enclosed in mineral, gold grain size is submicron sized and iron sulphide is pyrite. Table 3 shows how *Auric Adviser* retrieves the best matching cases according to the query from the case base by using the similarity (Eq. 1).

The best matching case is the Goldstrike mine in Nevada, United States. Gold is present primarily in the colloidal form within pyrite and marcasite mineral grains as submicron sized inclusions. The ore contains some clay minerals. The ore is processed by pressure oxidation. After crushing, grinding and thickening slurry is pretreated using an acidification process. Then, the slurry is heated using two stages of splash heating and fed into six autoclaves. Leaching is performed by agitated cyanide leaching and carbon-in-leach (CIL) and gold is recovered from the carbon eluate solution by electrowinning (Marsden and House, 2006).

The second best matching case is the McLaughlin mine in California, United States that was closed in 2002. Fine-grained gold was associated with fine-grained sulphide minerals. Among other reasons refractory properties of the ore were caused by presence of clays. The process applied was acidic pressure oxidation. Leaching was performed by agitated cyanide leaching and carbon-in-pulp (CIP) and gold was recovered from the carbon eluate solution by electrowinning (Marsden and House, 2006).

The third best matching case is the Lihir project that consists of two deposits in Lihir Island, Papua New Guinea. Gold is locked as submicron particles within a pyrite matrix. Also in this case ore is treated by pressure oxidation, followed by agitated cyanide leaching and CIL. Then gold is recovered from the carbon eluate solution by electrowinning (Marsden and House, 2006).

After analysis of the cases the next step is to test a new raw material under process conditions that are used in the retrieved cases, beginning from conditions of the best matching case and if the process performance is not acceptable, tests are performed in decreasing order of similarities of the retrieved cases. Here almost the same process was applied for three most similar cases to the query. This indicates that the relevant first experiments for the new raw material are pressure oxidation test by parameters used in three best matching cases. The second *Auric Adviser* model can be used to define the experimental design, as it is intended to hold the knowledge of the specific treatments.

Material and methods

The aim of this paper was to study the applicability of scientific publications as knowledge source for the second *Auric Adviser* model. The target of knowledge formalisation for *Auric Adviser* is to efficiently exploit the knowledge from journal articles and other publications to propose and develop process steps for gold processing.

As described earlier, in *Auric Adviser* the knowledge of gold ore processing is represented as a two-stage approach. The first knowledge model recommends process chains already used in the industry. The second knowledge model is intended to recommend the best treatments based on research results. The cases are represented as treatments on either specific raw material or processing stage. The treatments are unit processes that are seen as actions that change the system state. For example, leaching is a treatment that takes solid raw material and leachate as the input and results in pregnant solution and residue as the output. The treatments are defined by listing the preconditions and effects of the unit processes. The treatment cases are stored in the case base and the case-based reasoning methodology is used for the case retrieval according to the user query (Fig. 1).
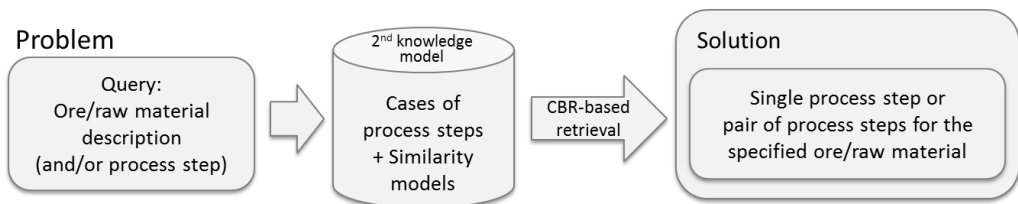
Figure 1. Operation of second *Auric Adviser* model

The process of encoding knowledge of CBR system in case representation and in global and local similarity measure is called knowledge formalisation. First, relevant categories in a domain and their relationships with each other are identified. Then, characteristics and important attributes are established for each category and the form of case representation is determined. After the relevant entities are identified, the next step is to find suitable data types and value ranges to represent these attributes. Then,

the similarities between attributes are modelled by taxonomies, comparative tables and mathematical functions (Aamodt and Plaza, 1994). The case-based reasoning is heavily dependent on the structure and content of its collection of cases. It must be decided what to store in the case and how the case memory should be organised and indexed for effective retrieval and reuse. An appropriate structure for describing the case contents can be also found. There are the central questions to be answered in order to use published hydrometallurgical experiments as the cases in the CBR application. In this study, the case was expected to include description of raw material that was studied and description of the solution chemistry and experimental arrangements that were used, as well as process outcomes.

To analyse how detailed the experiments about gold extraction were published, 17 journal articles and 8 other publications were chosen to be analysed and the information of used process and its details were collected in a case base.

Table 4. Analysed publications and amount of cases extracted

Journal articles/ Other publications	Number of analysed publications	Amount of cases extracted	References
Hydrometallurgy	6	47	Crundwell and Godorr, 1997; Breuer and Jeffrey, 2002; Chandra and Jeffrey 2004; Breuer et al., 2005, Dai and Feffrey, 2006; Feng and van Deventer, 2007
Minerals Engineering	2	31	Groudev et al., 1996; Aylmore and Muir, 2001
Mining informational and analytical bulletin (scientific and technical journal)	6	69	Vorobjev et al., 2003; Zuboreva, 2006; Gurman and Jatlukova, 2007; Rubcov, 2007; Zuboreva, 2007; Gurman, 2009
Doklady akademii nauk respubliki Tadzhikistan	1	12	Zinchenko et al., 2010
Vestnik KRSU	1	3	Vorobjev et al., 2010
Izvestiya Chelyabinskogo Nauchnogo Tsentra (UrO RAN)	1	1	Chekushin and Oljnikova, 2005
Master thesis	1	20	Fairley, 1998
Books	3	31	Chernjak, 1987; Chungaev, 1987; Meretukov, 2008
Bulletin	4	4	Demetjev et al., 2000, 2005; Emeljanov, 2004; Haavanlammi et al., 2010
TOTAL	25	218	

The publications were collected by using publication databases, such as Science Direct, Scopus and Google Scholar. In the initial search round words "leaching" and "gold" were used, and in the second search round words "refractory" and "ore" were added. The analysed publications and amount of cases extracted are listed in Table 4.

The information given for one case was evaluated and stored using as many categories and details as possible. It was often possible to extract several cases for analysis from one publication. The case was taken as either process or experiment description with clearly defined differences to other descriptions. In total 218 cases were extracted, which included 40 cases, where either gold or gold containing alloy was leached and 178 cases which described leaching of either ore or concentrate. From the latter ones, 86 cases were described as leaching of the refractory gold ore. To determine the attributes that were used to describe the cases in publications the information given for one case was stored using as many details as possible.

Results and discussion

The attributes that were used to describe the case in the analysed publications were arranged in four categories: raw material, solution, process parameters and process performance. The found attributes are presented in Table 5. Table 5 shows that there is varying number of attributes used to describe these four categories. These attributes can be used in the similarity calculation of the CBR system recommending gold ore processing workflows although none of the cases covered information on every attribute presented in Table 5. Especially the attributes describing the raw material were often missing details.

Table 5. Attributes that were used to describe cases in analysed publications

Raw material	Solution	Process parameters	Process performance
Minerals	Ligand	Pumping rate	Reaction rate
Pre-treatments	Stabilisator	Solids in slurry	Recovery
Pre-treatment period	Oxidant	Solid-to-liquid ratio	Reagent consumption
Particle size	Catalyst	Reactor volume	
Au concentration		Solution volume	
Other valuable metals		Agitation method	
Other elements		Stirring speed	
		Gas bubbling	
		Dissolved oxygen	
		Temperature	
		pH	
		Oxygen partial pressure	
		Retention time	

The most important attributes for the second *Auric Adviser* model were: gold concentration, solution chemistry in details, temperature, pH, reagent consumption and process outcome. The percentages of cases covering information of these attributes are shown in Table 6. The gold concentration of studied sample was usually reported. The

process outcome, like either reaction rate or recovery of gold, was described in the majority of cases as well. The journal articles very often contained information on the solution chemistry and pH than other publications. The temperature and reagent consumption were sparsely reported in all sources.

Table 6. Analysed cases covering information of listed attributes

Attribute	Journal articles, %	Other publications, %	All publications, %
Au concentration	83	62	80
Solution chemistry in details	71	47	65
Temperature	49	47	49
pH	67	38	60
Reagent consumption	20	24	19
Outcome of the process	82	98	86

In the analysis of cases concerning either ore or concentrate a higher number of attributes, such as origin and chemical analysis of the studied sample are important. The results are presented in Table 7. The gold concentration of studied sample was usually described as well as the process outcome, temperature and reagent consumption were sparsely reported in all sources.

Table 7. Cases concerning either ore or concentrate covering information of listed attributes

Attribute	Journal articles, %	Other publications, %	All publications, %
Au concentration	95	56	84
Origin of the ore/concentrate (deposit etc.)	62	46	57
Chemical analysis of the studied sample	12	42	20
Solution chemistry in details	65	48	61
Temperature	40	44	41
pH	70	42	62
Reagent consumption	25	19	23
Outcome of the process	98	98	98

The experimental arrangements were usually well described in the journal articles. However, the chemical analyses of studied samples were described more often in other publications than journal articles. In the journal articles the material description was frequently limited to reporting the origin of either ore or concentrate. This is problematic from perspective of knowledge applicability in recommendation of gold ore processing workflows as well as from perspective of repeatability of the study. In some cases it may be possible to estimate the character of ore on the basis of geology of the ore region by using available ore and mineral databases (Pietarsaari 2011). The information on geology of the area, such as analyses of bore samples can be found from

these databases. However, the information may not be up to date. Old drill samples may not represent the ore mined from the site today. The analysis of the existing information sources showed that the knowledge necessary to design the second *Auric Adviser* model can be elicited from the journal articles and other publications concerning single process steps. The attribute sets, such as shown in Table 5, can be used to describe the treatment performance. However, in some cases the sources did not contain enough information to create a well-defined case. In the next phase of the research the second *Auric Adviser* model will be formalised using the open source similarity-based retrieval tool myCBR. After that, the applicable cases from this study can be transferred to the case base of *Auric Adviser*.

Conclusions

The *Auric Adviser* model helps to select starting point for experiments. The first *Auric Adviser* knowledge model can be used to give ideas of existing process designs for similar raw materials. The second *Auric Adviser* knowledge model is intended to be used to define the experimental design. After initial tests the factorial design can be used to design full set of experiments. In this research the applicability of scientific publications as a source for the second *Auric Adviser* model was studied. To analyse how detailed the experiments about gold extraction are published, 17 journal articles and 8 other publications were chosen to be analysed and the information of used process and its details were collected in the case base. In total, 218 cases were extracted from various publications. To determine the attributes that are used to describe cases in publications the information given in a single case was collected using as many details as possible. The analysis of the case descriptions showed that gold content and outcome of the process were usually well describe, whereas the process details were not.

Acknowledgements

References

AAMODT A., PLAZA E., 1994. *Case-based reasoning: Foundational issues, methodological variations and system approaches*. AI Communications, 7 (1), 39–59.

AYLMORE M.G., MUIR D.M., 2001. *Thiosulfate leaching of gold – A review*, Minerals Eng., 14(2): 135–174.

BREUER P.L., DAI X., JEFFREY M.I., 2005. *Leaching of gold and copper minerals in cyanide deficient copper solutions*, Hydrometallurgy, 78(3–4), 156–165.

BREUER P.L., JEFFREY M.I., 2002. *An electrochemical study of gold leaching in thiosulfate solutions containing copper and ammonia*, Hydrometallurgy, 65(2–3), 145–157.

CHANDRA I., JEFFREY M.I., 2004. *An electrochemical study of the effect of additives and electrolyte on the dissolution of gold in thiosulfate solution*, Hydrometallurgy, 73(3–4), 305–312.

CHEKUSHIN V.S., OLJENIKOVA N.V., 2005. *Pererabotka zolotosoderzhashih rudnyh koncentratov (obzor metodov) – Processing of the auriferous ore concentrates (the review of methods)*, Izvestiya Chelyabinskogo Nauchnogo Tsentra Proceedings of the Chelyabinsk Scientific Center – Proceedings of the Chelyabinsk Scientific Center, 30(4), 95–102.

CRUNDWELL F.K., GODORR S.A., 1997. A mathematical model of the leaching of gold in cyanide solutions, Hydrometallurgy, 44(1–2), 147–162.

CHERNJAK A.S., 1987. *Himicheskoje obogashenie rud*, 224 p., Nedra: Moscow.

CHUGAEV L.V., 1987. *Metallurgija blagorodnyh metallov*, 431 p., Metallurgija: Moscow.

DAI X., JEFFREY M.I., 2006. *The effect of sulfide minerals on the leaching of gold in aerated cyanide solutions*, Hydrometallurgy, 82(3–4), 118–125.

DEMENTJEV V.E., LOCEJSHIKOV V.V., EMELJANOV Ju.E., KOBOLOV A.Ju., 2005. *Biogidro-metallurgicheskaja pererabotka neobogashennyh zolotosoderzhashih rud*, Zolotodobycha, No. 81, Online: http://zolotodb.ru/articles/placer/factory/495.

DEMENTJEV V.E., TATARINOV A.P., GUDKOV S.S., GRIGORYEV S.G., RJAZANOVA I.I., 2000. *Perspektivy izvlechenija zolota metodom kuchnogo vyshelachivanija v holodnyh klimaticheskih regionah Rossii*, Zolotodobycha, No. 23, Online: http://zolotodb.ru/articles/ technical/374.

EMELJANOV E.J., 2004. *Opyt bakterialnogo vyshelachivanija zolotosoderzhashih rud v KNR*, Zolotodobycha, No. 63, Online: http://zolotodb.ru/articles/foreign/669.

FAIRLEY L.M., 1998. *A survey of conventional and novel processes for the treatment of refractory gold*. Master thesis, The University of British Columbia, Vancouver.

FENG D., van DEVENTER J.S.J., 2007. *The role of oxygen in thiosulphate leaching of gold*. Hydrometallurgy, 85(2–4), 193–202.

GROUDEV S.N., SPASOVA I.I., IVANOV I.M., 1996. Two-stage microbial leaching of a refractory gold-bearing pyrite ore. Minerals Engineering, 9(7), 707–713.

GURMAN M.A., JATLUKOVA N.G., 2007. *Testovye issledovanija kuchnogo vyshelachivanija prob zolotosoderzhashej rudy*. Mining informational and analytical bulletin scientific and technical journal, No. 12, 6 p.

GURMAN M.A., ALEKSANDROVA T.A., 2009. *Rezultaty issledovanij po ugolno-sorbcionnomu vyshe-lachivaniju zolota*. Mining informational and analytical bulletin scientific and technical journal, No. 12, 320–328.

HAAVANLAMMI L., HIETALA K., KARONEN J., 2010. *Hydrocopper® – for treating variable copper concentrates* [online], Available from: <http://www.outotec.com/37061.epibrw> [Accessed: 20th March 2010].

LENZ M., BARTSCH-SPÖRL B., BURKHARD H.-D., WESS S. (Eds.) 1998. *Case-Based Reasoning Technology, From Foundations to Applications*. Lecture Notes in Artificial Intelligence, XIV, 405 p. ISBN 3-540-64572-1.

MARSDEN J, HOUSE C.I., 2006, *Chemistry of Gold Extraction* (2nd Edition), 682 p, Society for Mining Metallurgy and Exploration: Littleton.

MERETUKOV M.A., 2008. *Zoloto: Himija, mineralogija, metallurgija*, 526 p Ruda i metally: Moscow.

myCBR 3. 2012. Retrieved March 1, 2013, from http://www.mycbr-project.net/.

PIETARSAARI S., 2010, *The application of public geological data in description of raw material for hydrometallurgical processes*. M.Sc. Thesis, Aalto University, 80 p.

RINTALA L., AROMAA J., FORSÉN O., 2011a. *The Use of Decision Methods in the Selection of Leaching Alternatives*, in: Proceedings of European Metallurgical Conference EMC 201, Vol. 5, 1659–1671 (GDMB: Düsseldorf).

RINTALA L., LILLKUNG K., AROMAA J., 2011b. *The use of decision and optimization methods in selection of hydrometallurgical unit process alternatives*. Physiochemical Problems of Mineral Processing, 46, 229– 242.

RUBCOV I.J., 2007. *Razrabotka principialnoj tehnologicheskoj shemy skorostnogo kuchnogo vyshelachivanija zolota*. Mining informational and analytical bulletin scientific and technical journal, No 1, 301–308.

SAUER C.S., RINTALA L., ROTH-BERGHOFER T., 2013. *Research and Development in Intelligent Systems XXX*, BRAMER M., PETRIDIS M., (Eds.) *Knowledge Formalisation for Hydrometallurgical Gold Ore Processing*. Springer International Publishing. p. 291–304.

SAUER C.S., RINTALA L., ROTH-BERGHOFER T., 2014. *Two-phased Knowledge Formalisation for Hydrometallurgical Gold Ore process recommendation and validation*. Künstliche Intelligenz, 28, 283–295.

STAHL A., ROTH-BERGHOFER T., 2008. *Rapid Prototyping of CBR Applications with the Open Source Tool myCBR. Advances in Case-Based Reasoning*. Lecture Notes in Computer Science, 5239, 615–629. DOI: 10.1007/978-3-540-85502-6_42

VOROBJEV A.E., KARGINOV K.G., SHELKIN A.A., TSHEKUSHINA T.B., 2003. *Praktika primenenija tiosulfatnogo vyshelachivanija blagorodnyh metallov iz prirodnyh materialov*. Mining informational and analytical bulletin scientific and technical journal, No 7, 2 p.

VOROBJEV A.E., TURSUNBAEVA A.K., MALJUKOVA N.N., 2010. *Vyshelachivanie zolota iz pervichnyh rud v perkoljatorah*. Vestnik KRSU, 10(10), 154-158. Online: http://www.krsu.edu.kg/vestnik/2010/v10/a38.pdf.

ZINCHENKO Z.A., SAMIHOV Sh.R., BOBOHONOV B.A., 2010. *Issledovanija po kolonnomu vyshelachivaniju zolotosoderzhashih rud razlichnyh mestorozhdenij*. Doklady akademii nauk respubliki Tadzhikistan, 53(7), 553–556.

ZUBOREVA N.A., 2006. *Ekologo-ekonomicheskoe obosnovanie effektivnosti izvlechenija zolota iz upornyh rud metodom bakterialnogo vyshelachivanija*. Mining informational and analytical bulletin scientific and technical journal, No 6, 164–166.

ZUBOREVA N.A., 2007. *Biovyshelachivanie kak odin iz metodov ekonomicheskogo stimulirovanija izvlechenija zolota iz upornyh rud*. Mining informational and analytical bulletin scientific and technical journal, No. 10, 147–151. Online: http://www.giab-online.ru/files/Data/2007/10/9_Zuboreva9.pdf.

INVESTIGATION OF KINETICS AND MECHANISM OF PRICEITE LEACHING IN SULPHURIC ACID SOLUTIONS

Aycan GUR

Department of Chemistry, Science Faculty, Yuzuncu Yil University, 65100, Van, Turkey
aycangurbor@yahoo.com

Abstract: The leaching kinetics and mechanism of priceite having the formula of $4CaO \cdot 5B_2O_3 \cdot 7H_2O$ was investigated in sulphuric acid solutions. For the dissolution process, the effects of reaction temperature, sulphuric acid solution concentration, solid/liquid ratio, particle size, and stirring speed were investigated as effective parameters for the experiments. The experimental data indicated that the dissolution rate increased with the increasing reaction temperature, the decreasing particle size, and the solid/liquid ratio. The conversion rate increased up to 1.0 mol/dm^3 with the increasing acid concentration, and then decreased with the increasing acid concentration over concentrations of 1 mol/dm^3. It was also determined that the stirring speed had no significant effect on the dissolution rate. The dissolution process of priceite in sulphuric acid solution was tested with regard to heterogeneous and homogeneous reaction models, and it was found that the dissolution rate was controlled by first order pseudo-homogeneous reaction model. The activation energy of the dissolution process was determined as 26.07 kJ·mol^{-1}. The results were evaluated graphically and statistically. The experimental data were found to fit well with the mathematical model.

Keywords: boron minerals, priceite, sulphuric acid, leaching kinetics, boric acid

Introduction

Boron and its compounds today are used in many different applications and processes. Boron salt production has significantly increased due to demand by the nuclear industry for heat-resistant materials, ceramics, high quality steel, polymers, etc. (Nemodruk and Karalova, 1965). There have been many studies examining the kinetics of boron ores leaching including leaching kinetics of inderite and inyoite in water saturated with CO_2 (Alkan et al., 1991), colemanite in ammonium nitrate (Gur, 2008), in perchloric acid solutions (Gur, 2008), in potassium hydrogen sulphate solutions (Guliyev et al., 2012), in citric acid solution assisted by mechanic agitation and microwaves (Cavus and Kuslu, 2005), and ulexite in borax pentahydrate solutions

saturated with CO_2 (Kuslu et al., 2010). Gur (2006) studied the leaching kinetics of calcined ulexite in ammonium chloride solutions at a high solid/liquid ratio revealing that the dissolution rate increased with the increase of the calcination temperature, solution concentration, and reaction temperature. However, it was not affected by pre-hydration. Additionally, graphical and statistical methods were employed in the leaching process. The results showed that the dissolution based on a homogeneous reaction model can be shown as $[1-X(B_2O_3)]-1-1 = k(c(NH_4Cl))^{1.982} \cdot t$ where X is the conversion factor (X=amount of dissolved B_2O_3 in the solution/amount of B_2O_3 in the original sample), k is the rate constant, and c is the solution concentration.

Gulensoy and Kocakerim (1978) investigated the solubility of ulexite mineral in water saturated with CO_2 in natural and calcined samples at different temperatures. They found that the calcination process and the solution pH had a positive effect on the leaching rate. Davies et al. (1991) performed the thermally decomposed powdered colemanite as enlarging the extraction ratio of boric acid in acid solutions for calcined mineral samples, and they found the optimal calcination temperature was 600 °C. At higher temperature, flash calcinations produced vitrified cenospheres becoming highly resistant to acidic dissolution. The 600 °C flash calcinations could make calcined samples dissolving as efficiently as the calcined produced by ordinary soak calcinations for a longer time. Alkan et al. (1991) investigated the leaching kinetics of colemanite samples in water saturated with CO_2 changing particle size, pre-heating temperature of mineral, and reaction temperature. They determined that the leaching process was controlled chemically. In another work by Ozmetin et al. (1996) examining the leaching kinetics of colemanite in acetic acid solutions, the conversion factor was found to be increasing with the increasing temperatures and decreasing particle sizes. It was also observed that the dissolution rate was unaffected by the stirring speed to any significant extent. Meanwhile, some researchers carried out the leaching of boron minerals in nitric acid (Imamutdinova and Bickhurova, 1967), in hydrochloric acid (Zdanovskii and Imamutdinova, 1963), and in ammonium chloride (Gur and Kandilcik, 2009). Kunkul et al. (1997) studied the leaching kinetics of ulexite in ammonia solutions saturated with CO_2 and determined that the leaching rate increased with the increasing the ammonia solution concentrations, reaction temperatures and calcination temperatures. It was also detected that the leaching process can be showed by a first-order pseudo homogeneous kinetic reaction model. Kunkul et al. (2003) carried out ulexite leaching in an ammonium sulfate solution and found that the dissolution rate rose with increasing ammonium sulfate concentrations, mixing speed and reaction temperatures. They also indicated that the diffusion controlled ash or product layer defined and fitted the process.

Priceite is first in rank boron mineral mined in Turkey and is an important source for boric acid production. There are few studies into the leaching of priceite in literature, and there has to date been no study analyzing the kinetics of priceite in sulphuric acid solutions. Filling this gap in literature is the objective of this work, in which it is aimed both to contribute to literature, and to emphasize the importance of

the leaching kinetics of priceite. In this regard, the goal of this study is to clarify the dissolution mechanism of priceite in sulphuric acid solutions, and to indicate the effects of the designed experimental parameters in regards to acid concentration, solid/liquid ratio, particle size, stirring speed, and reaction temperature on the dissolution rate.

Experimental

Preparation of materials

The priceite samples used in this study originated from the Sultancayiri region in Balikesir, Turkey. First, the visible impurities were separated manually from the mineral, then ground, crushed, and sieved using ASTM standard sieves to obtain particle sizes in the range of -1.4+1 mm, -1+0.6 mm, -0.6+0.4 mm, and -0.4+0.225 mm. The sample used in the experimental section was analyzed, and the mineral content was 47.72% B_2O_3, 31.54% CaO, 17.74% H_2O, and 3% insoluble matter.

Apparatus and procedure

In the experimental section, the leaching rate of the priceite sample was determined as a function of time by changing the sulphuric acid solution concentration, particle size, solid/liquid ratio, stirring speed, and reaction temperature. The dissolution experiments were performed in a 250 cm^3 glass reactor at atmospheric pressure. A mechanic mixer was employed for mixing reaction medium, and a thermostat was used to maintain a constant reaction temperature. Then, 50 cm^3 of a sulphuric acid solution was added the reactor. When the desire reaction temperature was reached, a given quantity of priceite was put into the solution, and stirring was started at a constant speed. As soon as the reaction time was finished at a certain time period, the solution content was filtered. The quantity of B_2O_3 in the filtrate was measured using a volumetric method (Scott, 1963), and the results were plotted as a function of conversion factor, and defined as: X=amount of dissolved B_2O_3 in the solution/amount of B_2O_3 in the original sample, versus time. The variables thought to affect the dissolution rate were selected as particle size, acid concentration, solid/liquid ratio, reaction temperature and stirring speed. The experimental design for the dissolution process is presented in Table 1.

Table 1. Parameters used in the experiments

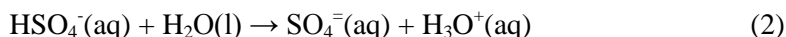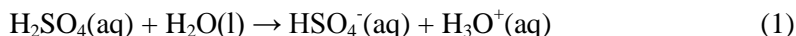| Particle size (mm)	-1.4+1	-1+0.6 *	-0.6+0.4	-0.4+0.25
Acid concentration (mol/dm^3):	0.5	1*	1.5	2
Solid/ liquid ratio (g/cm^3):	0.01*	0.02	0.04	0.06
Reaction temperature (K):	293	303	313*	323
Stirring speed (rpm):	400*		500	600

*values shown with asterisks were used when one of the parameters was studied

Results and discussion

Firstly, the effect of stirring speed on dissolution rate was investigated. The experiments were carried out at stirring speeds of 400, 500, and 600 rpm. In these experiments, the sulphuric acid solution concentration, particle size, solid/liquid ratio, and reaction temperature were kept at 1 mol/dm^3, -1+0.6 mm, 1/50 g/cm^3, and 313 K, respectively. It was determined from the experimental results that 64.85% of XB_2O_3 at 400 rpm, 65.32% of XB_2O_3 at 500 rpm, and 65.48% of XB_2O_3 at 600 rpm were obtained for a 10 min leaching time. It can be understood from these results that the reagent amounts of grains were completely suspended in the medium, and further, it can be inferred that stirring speed had no significant impact on the leaching, according to which, stirring speed was omitted from the analysis (Gur and Kandilcik, 2009).

Reaction occurring during dissolution

In aqueous medium sulphuric acid dissociates according to the following reactions:

$$H_2SO_4(aq) + H_2O(l) \rightarrow HSO_4^-(aq) + H_3O^+(aq) \tag{1}$$

$$HSO_4^-(aq) + H_2O(l) \rightarrow SO_4^=(aq) + H_3O^+(aq) \tag{2}$$

and the equilibrium constant of reaction (2) is $K_a = 0.012$. When priceite is placed in a sulfuric acid solution, the following reaction occurs:

$$4CaO \cdot 5B_2O_3 \cdot 7H_2O(s) + 8H_3O^+(aq) \rightarrow 4Ca^{2+}(aq) + 10H_3BO_3(aq) + 4H_2O(l). \tag{3}$$

When Ca^{2+} concentration reaches a limiting value in the sulfuric acid solution, Ca^{2+} and SO_4^{2-} ions form a solid $CaSO_4(s)$ that restricts the dissolution of priceite according to Eqs. (4) and (5):

$$[Ca^{2+}] \cdot [SO_4^{2-}] = K_{sp} \tag{4}$$

$$Ca^{2+}(aq) + SO_4^{2-}(aq) \rightarrow CaSO_4(s). \tag{5}$$
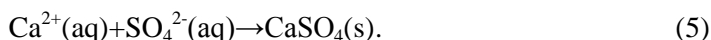
Thus, the leaching reaction of priceite in sulfuric acid solutions can be defined with the following reaction:

$$4CaO \cdot 5B_2O_3 \cdot 7H_2O(s) + 4H_2SO_4(aq) + 4H_2O(l) \rightarrow 4CaSO_4(s) + 10H_3BO_3(aq). \tag{6}$$
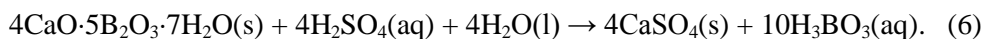
Effects of parameters

The parameters affecting the dissolution rate of priceite in sulfuric acid solutions were carried out for each parameter using the values indicated in Table 1. While the effect of one parameter was done, the other parameters value indicated with asterisks in Table 1 were kept constant.

Effect of particle size

The experiments focusing on the particle size were carried out with 1.4+1 mm, -1+0.6 mm, -0.6+0.4 mm, and -0.4+0.25 mm size fractions. The experimental data showed in Fig. 1 indicate that particle size had a reasonable effect on the leaching of priceite in sulphuric acid solutions. According to Fig. 1, the conversion factor increased as the particle size decreased. The increasing dissolution rate with the decreasing particle size resulted in the growth of the contact surface of the mineral with volume (in cm^3) of the acid solution (Gur and Kandilcik, 2009).
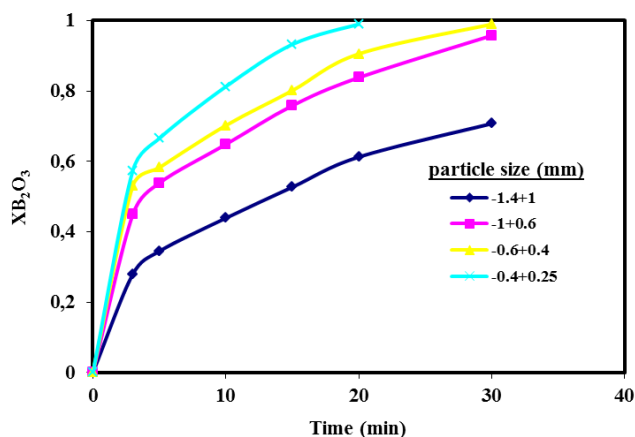

Fig. 1. Effect of particle size on dissolution rate (T 313 K; C 1 mol/dm^3; S/L 0.5/50 g/cm^3, SS 400 rpm)

Effect of sulphuric acid concentration

The effect of H_2SO_4 concentration on the dissolution rate was studied at different H_2SO_4 concentrations of 0.50, 1, 1.50, and 2.0 mol/dm^3. In the experiments, the dissolved amount of mineral was measured at reaction temperature of 40 ^{o}C, solid/liquid ratio of 1/50 (g/cm^3), and the stirring speed of 400 rpm. The experimental data seen in Fig. 2 indicate that leaching degree decreased with the increasing H_2SO_4 concentrations. This evidence can be elucidated the increasing SO_4^{2-} ion per unit volume by the increasing H_2SO_4 concentration. This caused the appearance of reaction (5), being the precipitation of solid $CaSO_4$ and $CaSO_4.2H_2O$ on the mineral surfaces. This solid by-product layer generates obstacle for H_3O^+ ion to diffuse to the mineral, and causes a decrease in the dissolution rate on the mineral surface (Tunc et al., 1999).
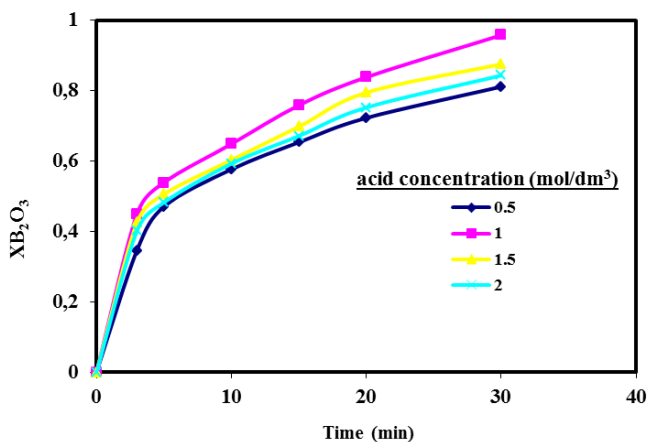
Fig. 2. Effect of H$_2$SO$_4$ concentration on dissolution rate (*T* 313 K, *PS* -1+0.6 mm, *S/L* 0.5/50 g/cm^3, *SS* 400 rpm)

Effect of solid/liquid ratio

In order to determine the effect of the solid/liquid ratio on the dissolution of priceite, the experiments were carried out with different solid/liquid ratios in the range of 0.5/50 to 3/50 g/cm^3. The results presented in Fig. 3 show the effect of this parameter, and indicating that the conversion factor of priceite decreased as the solid/liquid ratio increased, which can be expressed in terms of the decreasing ratio of solids per quantity of the reagent in the suspension media (Gur and Kandilcik, 2009).
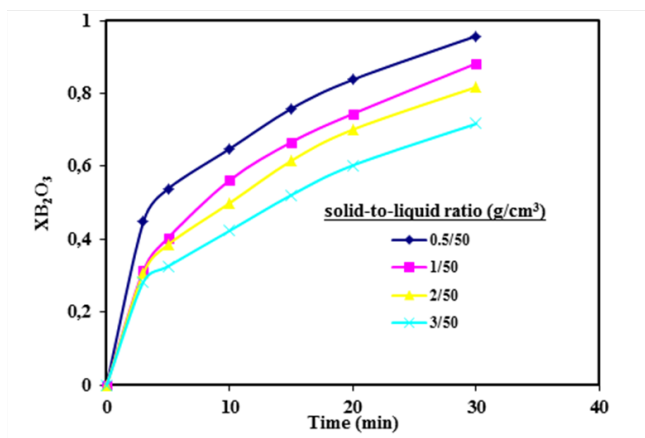

Fig. 3. Effect of solid/liquid ratio on dissolution rate (*T* 313 K, *PS* -1+0.6 mm, *C* 1 mol/ dm^3, *SS* 400 rpm)

Effect of reaction temperature

The effect of temperature on the dissolution rate was investigated at the temperatures of 293, 303, 313, and 323 K, and the results are presented in Fig. 4. According to the experimental data presented in Fig. 4, increasing reaction temperatures resulted in an increased dissolution of priceite owing to the exponential dependency of the rate constant in the Arrhenius equation.
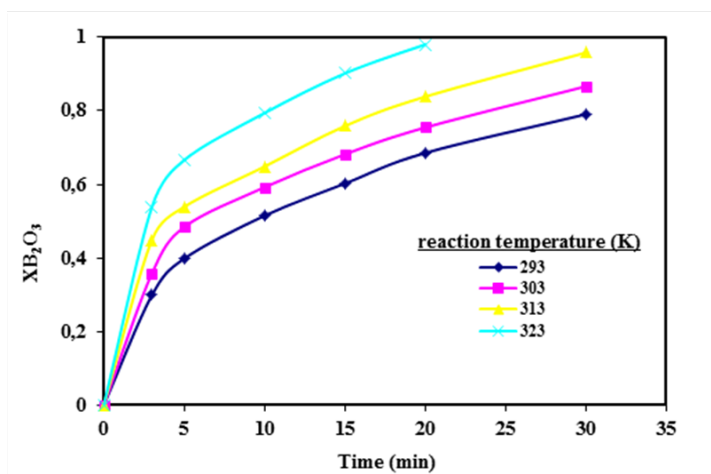

Fig. 4. Effect of reaction temperature on dissolution rate (PS -1+0.6 mm, C 1 mol/dm^3. S/L 0.5 g/50 cm^3, SS 400 rpm)

Kinetic analysis

The reaction between a solid and liquid can be represented using heterogeneous and homogeneous control models. A diffusion film control, surface chemical reactions control and product layer control models were used as heterogeneous reaction control models in this study. A first-order pseudo reaction control and a second-order pseudo reaction control model were used as homogenous models in this study.

Heterogeneous reaction models

Fluid solid heterogeneous reactions have important applications in chemical and metallurgical processes. A prosperous reactor plan for these processes relies chiefly upon kinetic results. The reactions taking place between a fluid and spherical solid particle are:

$$A \text{ (f)} + b\, B \text{ (s)} \rightarrow \text{products.} \tag{7}$$

The following models are proposed.

Diffusion film control model

The kinetics of a diffusion film control model are indicated through Eq. 8 (Levenspiel, 1972):

$$k_1 \cdot t = X \tag{8}$$

where k_1 is the reaction rate constant (min^{-1}), t reaction time (min), X conversion factor, and Eq. 9:

$$k_a = k_1 \rho R / 3Bc \tag{9}$$

where k_a is the mass transfer coefficient between fluid and solid particle (cm.min^{-1}), C is the concentration of sulphuric acid (mol/cm^3), R is the radius of particle (cm), ρ is the density of mineral (mol/cm^3), and b is the stoichiometric coefficient of the solid.

Surface chemical reactions control model

The kinetics of the chemical reaction control model are shown through Eq. 10 (Levenspiel, 1972):

$$k_2 \cdot t = 1 - (1-X)1/3 \tag{10}$$

where k_2 is the reaction rate constant (min^{-1}), t time (min), X conversion factor, and Eq.11:

$$k_b = k_2 \rho R_o / bC \tag{11}$$

where k_b is the rate constant (cm.min^{-1}), C is the concentration of sulphuric acid (mol/cm^3), R_o is the radius of the particle (cm), ρ is the density of mineral (mol/cm^3), and b is the stoichiometric coefficient of the solid.

Product layer diffusion control model

The kinetics of the product layer diffusion control model are shown through Eq. 12 (Levenspiel, 1972)

$$k_3 \cdot t = [1 - 3(1-X)2/3 - 2(1-X)] \tag{12}$$

where k_3 is reaction rate constant (min^{-1}), t time (min), X conversion factor, and Eq.13

$$k_c = k_3 \rho R_o 2 / 6bC \tag{13}$$

where k_c is the determinant diffusion factor of gaseous reactant in the ash layer (cm.min^{-1}), C is the concentration of sulphuric acid (mol/cm^3), R_o is the radius of the particle (cm), ρ is the density of the mineral (mol/cm^3), and b is the stoichiometric coefficient of the solid.

Homogeneous reaction models

In homogeneous reactions all reacting materials are found in a single phase of either gas, liquid, or solid. Though there are several of ways explaining the rate of reaction, the potent estimate, dependent on the unit volume of reacting fluid, is used almost for homogeneous system.

First order pseudo homogenous reaction control

The kinetics of the product layer diffusion control model are indicated through Eq. 14 (Levenspiel, 1972).

$$k_4.t = -\ln(1-X) \tag{14}$$

where k_4 is the reaction rate constant (min^{-1}), t is the time (min), and X is the conversion factor.

Second order pseudo homogenous reaction control

The kinetics of the product layer diffusion control model are indicated through Eq. 15 (Levenspiel, 1972):

$$k_5.t = [X(1-X)-1] \tag{15}$$

where k_5 is the reaction rate constant (min^{-1}), t is the time (min), and X is the conversion factor.

The experimental data in this investigation were analyzed according to both heterogeneous and homogeneous reaction models using graphical and statistical methods. When the results were analyzed graphically and statistically using the non-catalytic heterogeneous reaction models, it was determined that the results fitted well with none of the heterogeneous reaction kinetic models. The results were then tested with the homogeneous models, and it was determined that the process could be stated by a first-order pseudo homogeneous reaction kinetics model (Gur and Kandilcik, 2009).

As can be seen graphically in Fig. 5, fine linear agreements exist between the formula of the first-order pseudo homogeneous reaction kinetic model and time for various reaction temperatures. Imamutdinova and Bikchurova (1967) revealed the salting out of particles from the solution. The dissolving is a very complex structure containing gradual dissolution of likely boric acid film and diffusion of the reacting reagent via this film besides the other steps. The process can be indicated by a first-order pseudo homogeneous reaction model. The concentrations of reagent types do not lower in the film. It can be taken to be constant in every part. The reaction occurring in the reaction area is rapid enough, while the total system may be shown by a pseudo homogeneous first-order reaction model (Gur and Kandilcik, 2009; Tunc et al., 1999).
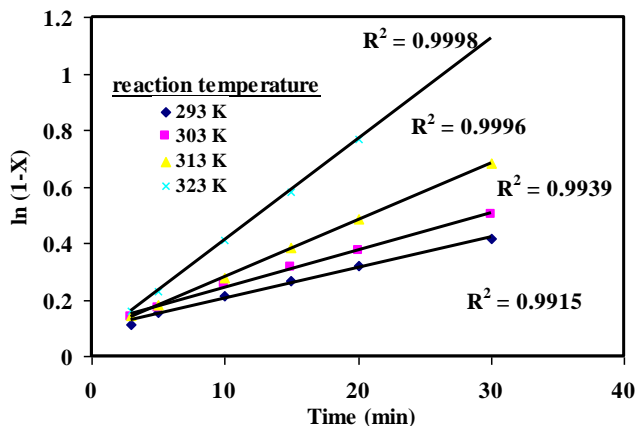
Aycan Gur

Fig. 5. Conformity of experimental results with ln (1-*X*) versus time for reaction temperature

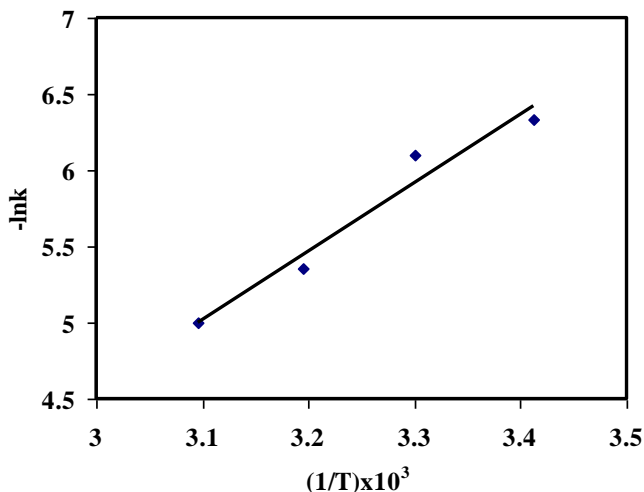
Fig. 6. Arrhenius plot for dissolution process

For this process, the rate expression can be written as follows:

$$\ln(1-X)=kt. \tag{16}$$

To contain the effect of the parameters on the rate constant, the reaction model can be shown as follows:

$$k=k_o(D)a(C)b(S/L)cexp(-E_a/RT). \tag{17}$$

Combining Eqs. (16) and (17), Eq. 18 gives

$$\ln(1-X) = k_o \, (D) \, a \, (C) \, b \, (S/L) \, c \, exp \, (-E_a/RT) \, t. \tag{18}$$

The constant values of *a*, *b*, *c* (in Eqs. (17) and (18)) were calculated as -0.8822, 0.7090, and -0.3436, respectively. The Arrhenius equation was used to calculate the leaching activation energy. The dependency of the reaction temperature on the chemical reactions is described by the Arrhenius equation. For this process, the Arrhenius plot is shown in Fig. 6, and the activation energy of the dissolution process can be calculated from this equation. From the slope of this line, the activation energy of process was found to be 26.07 kJ.mol^{-1}, and the intercept was calculated as 1.04.102.

In conclusion, the kinetic statement containing the parameters used in this leaching process can be described as follows:

$$\ln(1-X)=1.04 \times 102(D)\text{-}0.8822(C)0.7090 \ (S/L)\text{-}0.3436 \exp(-3130/T)t. \qquad (19)$$

Conclusions

The leaching kinetics of priceite was investigated in sulphuric acid solutions. The dissolution rate increased with the sulphuric acid concentrations up to 1 mol/dm^3, and then decreased with the increasing sulphuric acid concentrations over 1 mol/dm^3. The increase in the reaction temperature, decrease in the particle size and solid/liquid ratio increased the dissolution rate. The present study has also explained the dissolution process of priceite in H_2SO_4 solutions. According to the data obtained from the experiments, increasing H_3O^+ ion concentrations increased the dissolution, while increasing SO_4^{2-} ion concentrations decreased the dissolution due to the formation of $CaSO_4$ and/or $CaSO_4.2H_2O$ which substantially restricted the diffusion of H_3O^+ ions the mineral surface. The graphical and statistical methods employed in the kinetic models provided leaching kinetics of priceite in sulphuric acid solutions which was described by the first-order pseudo homogenous reaction control model. The activation energy for leaching process of priceite in sulphuric acid solutions was established to be 26.07 kJ/mol. A semi empirical mathematical model was constructed.

References

ALKAN, M., KOCAKERIM, M.M., COLAK, S., 1985, *Dissolution kinetics of colemanite in water saturated by carbon dioxide*, Journal of Chemical Technology and Biotechnology, 35A, 382–386.

ALKAN, M., OKTAY M., KOCAKERIM, M.M., KARAGOLGE, Z., 1991, *Dissolution kinetics of some borate minerals in CO_2 saturated water*, Hydrometallurgy, 26, 255–262.

CAVUS, F., KUSLU, S., 2005, *Dissolution kinetics of colemanite in citric acid solutions assisted by mechanical agitation and microwaves*, Industrial and Engineering Chemistry Research, 44, 8164-8170.

DAVIES, T.W., ÇOLAK, S., HOOPER, R.M., 1991, *Boric acid production by the calcination and leaching of powdered colemanite*, Powder Technology, 65, 433-440.

GULENSOY, H., KOCAKERIM, M.M., 1978, *Solubility of ulexite mineral in CO_2-containing water and geololojical formation of this mineral*, Bulletin of the Mineral Research and Exploration Institute of Turkey, 90, 1–19.

GULIYEV, R., KUSLU, S., CALBAN, T., ÇOLAK, S., 2012, *Leaching kinetics of colemanite in potassium hydrogen sulphate solutions*, Industrial and Engineering Chemistry Research, 18, 38-44.

GUR, A., 2006, *Dissolution kinetics of calcined ulexite in ammonium chloride solutions at high solid-to-liquid ratios*, Acta Physico-chimica Sinica, 22, 1287-1290.

GUR, A., 2008, *A kinetic study on leaching kinetics of colemanite in ammonium nitrate solutions*, Chineese Journal of Inorganic Chemistry, 24, 467–473.

GUR, A., ALKAN, E., 2008, *Leaching kinetics of colemanite in perchloric acid solutions*, Journal of Chemical Engineering of Japan, 41, 354–360.

GUR, A., KANDILCIK, M., 2009, *Leaching kinetics of tincal in ammonium chloride solutions*, Chinese Journal of Inorganic Chemistry, 25, 767–773.

IMAMUTDINOVA, V.M, BIKCHUROVA, A., 1967, *Kinetics of dissolving borates in HNO_3 solutions*, Zhurnal Prikladnoi Khimii, 40, 1616–1618.

KUNKUL, A., YAPICI, S., KOCAKERIM, M.M., COPUR, M., 1997, *Dissolution kinetics of ulexite in ammonia solutions saturated with CO_2*, Hydrometallurgy, 44, 135-145.

KUNKUL, A., DEMIRKIRAN, N., BAYSAR A., 2003, *Dissolution kinetics of ulexite in ammonium sulfate solutions*, Industrial and Engineering Chemistry Research, 42: 982–986.

KUSLU, S., DISLI F.T., COLAK S., 2010, *Leaching kinetics of ulexite in borax pentahydrate solutions saturated with carbon dioxide*, Industrial and Engineering Chemistry Research, 16, 673-678.

LEVENSPIEL, O., *Chemical Reaction Engineering*, 2nd ed., Wiley, New York, 1972.

NEMODRUK, A.A., KARALOVA, Z.K., 1965, *Analytical Chemistry of Boron*, Kondor, R., Translator; Israel Program for Scientific Translations: Jerusalem, 1-2.

OZMETIN, C., KOCAKERIM, M.M., YAPICI, S, YARTASI, A., 1996, *A semiemprical kinetic model for dissolution of colemanite in aqueous acetic acid solutions*, Industrial and Engineering Chemistry Research, 35, 2355-2359.

SCOTT W.W., MCBROOM, RB, *Standard Methods of Chemical Analysis*, Vol. 1, D. Van Nostrand, New York, 1963.

TUNC, M., KOCAKERIM, M.M., GUR, A., YARTASI, A., 1999, *A semi-empirical kinetic model for dissolution of ulexite in aqueous acetic acid solutions*, Energy, Education, Science and Technology, 3, 32-37.

ZDONOVSKII A.B., IMAMUTDINOVA V.M., 1963, *Kinetics of solution of native borates in HCl solutions*, Zhurnal Prikladnoi Khimii, 36, 1675–1680.

SPECIES FORMED ON IRON SURFACE DURING REMOVAL OF COPPER IONS FROM AQUEOUS SOLUTIONS

Tomasz SUPONIK, Antoni WINIARSKI, Jacek SZADE

Silesian University of Technology, Akademicka 2, 44-100 Gliwice, Poland, tomasz.suponik@polsl.pl

Abstract: The subject of the research covered in this paper is the removal of copper (Cu^{2+}) cations from water at low pH (initial values of pH 3 and 6) by means of zero-valent iron. The chemical states and atomic concentrations of solids formed on the surface of zero-valent iron, and the type of deposited polycrystalline substances have been analyzed with the use of XPS and XRD. The type of process causing the copper removal from water at low pH, corresponding to the effect of acid mine drainage, has been identified by analyzing the changes of physicochemical parameters and specified chemicals content in water. Cu^{2+} was removed from water for the initial pH of 6 was much more effective than at lower pH. The formation of $Cu_xFe_{3-x}O_4$, where $x \leq 1$, and to a lesser degree Cu_2O, Cu^0 and/or CuO and/or Cu_2S, were the basic processes of the removal of copper at almost neutral pH of water (pH about 6), while the formation of copper in metallic form and Cu_2O, as well as probably CuO, were the basic processes for lower pH (pH about 3). The adsorption of Cu^{2+} on the surface of shell covering square-shaped cold-rolled steel sheet cell was an additional process causing the removal of copper from water at almost neutral pH.

Keywords: water, zero-valent iron, copper, x-ray photoelectron spectroscopy, diffraction

Introduction

The waste material from mine waste disposal sites may contain large amounts of sulphide minerals. The leachate from these objects may be characterized by low concentration of dissolved oxygen (DO), low pH values (about 2 to 5), high total dissolved solids (TDS) and high concentration of metals in ionic form as well as sulphates. These leachates are called acid mine drainage (AMD). The leachate may contain different kinds of contaminants. Copper released from mine waste disposal sites as a result of AMD possesses a danger to ground and surface water. This element is an essential trace element for living organisms, but its intake at high levels can cause detrimental health effects (Rangsivek and Jekel, 2005). When addressing

groundwater contaminated by waste disposal sites the copper in cationic form should be ranked in priority based on their toxicity and persistent characteristics.

In order to protect groundwater in the vicinity of mine waste disposal sites, the permeable reactive barrier (PRB) technology may be applied. Zero-valent iron (ZVI, Fe^0) has been used as a reactive material in the presented tests.

The possibility of removing copper cations (Cu^{2+}) from water using ZVI has been considered for many years. Despite that, the type of products generated on the surface of this material in case of low pH values of water (and in specified chemical conditions) and the type of processes that cause the purification of the water may be interesting in the view of effective application of ZVI in PRBT. The main objectives of the paper, thus, are the identification of the products formed on the surface of ZVI as a result of the purification of water and the identification of the predominant processes which result in the removal of Cu^{2+}. The latter shall be performed by means of an analysis of the changes of physicochemical parameters and some chemicals in low pH water, and based on the products formed on the surface of ZVI and their properties.

Materials and method

Although the cells used in the batch tests were called ZVI, they were made of steel (in accordance with EN 10131:2006, this was "cold rolled uncoated and zinc or zinc-nickel electrolytically coated low carbon and high yield strength steel flat products for cold forming"). The cells were square-shaped, made of cold-rolled steel sheet (0.5 mm thickness), and their dimensions and masses amounted to 5x5 mm and 0.1 g, respectively. Just before their use, the cells were immersed in concentrated nitric acid for ca. 120 s and in demineralised water for about 120 s. Subsequently, they were immediately used in the batch tests. The tests were conducted in a programmable MULTI BIO RS-24 BIOSAN rotator equipped with plastic tubes filled with synthetic AMD solutions (to eliminate the headspace, a gaseous phase above the solutions, the volume of the solution was 58 cm^3) with the initial pH of 3.0 and 6.0 and with iron cells. Only one iron cell was applied in each plastic tube. The pH of the solutions was adjusted by a slow titration with a ultra-pure sulphuric acid solution (0.1 mol/dm^3) or with ultra-pure sodium hydroxide solution (0.1 mol/dm^3). Copper ion solutions were prepared by adding desired amounts of metal salt ($CuSO_4 \cdot 5H_2O$) into bottles and pouring distilled water. The concentration of copper in solutions at pH 3 and 6 amounted to 3.51 mg/dm^3 and 2.96 mg/dm^3, respectively. The intention of the authors was to exceed several times the allowable concentration of copper within the meaning of legal regulations available in the Journal of Laws (2014, item 1800).

The groundwater contaminated by mine waste disposal sites is characterized by high concentration of sulphates and low values of pH. These two parameters have a great impact on the concentration of oxygen in water. The concentration of dissolved oxygen in groundwater (in unconfined aquifer) located next to coal mine waste

disposal sites in the south of Poland amounted, based on own research, to about 6 mg/dm^3. In order to reduce the concentration of oxygen in the samples of water and to adjust their condition to the that of a contaminated aquifer, the solutions were heated to 35 ^{o}C before using them in the batch tests. This way, the initial concentration of DO amounted to about 6 mg/dm^3. The ambient air temperature in the laboratory was about 22 ^{o}C.

After filling, the plastic tubes they were closed with corks. Each sample had to undergo five minutes of orbital rotation in a programmable rotator with a speed range of 20 rpm. After that, a 6 second reciprocal motion (with a turning angle of 90°) with vibration motion followed. This sequence of shaking was repeatedly reiterated. The sequence continued for 24 hours and after this time a constant values were achieved. After shaking the samples, the solutions were passed through thick filters and subjected to chemical analysis. The quantitative analysis of chemicals in solutions was carried out for Cu_{tot}, Fe^{2+}, Fe_{total} with the use of UV-Vis Spectrophotometer DR5000 HachLange. The concentration of copper in the solutions was measured as a total value (Cu_{to}). Since, at the beginning there were no copper species in the solutions other than Cu^{2+}, the removal of the copper in the second oxidation state has been assessed in the article. The concentration of dissolved Fe^{3+} was calculated as a difference between Fe_{total} and Fe^{2+}. The pH, oxidation-reduction potential (ORP), dissolved oxygen and conductivity were measured with the Knick PORTAMESS meters.

The measurements were carried out twice. The results, shown in Table 1, were calculated using the arithmetic mean.

In order to verify the identity of products created on the surface of iron cells and to assess the mechanisms of the water purification using ZVI, the following tests were conducted on iron cells before and after the batch tests.

1. Identification of elements and determination of atomic concentrations of solids located on the surface of the iron cells before and formed after the batch tests. These measurements were carried out with the use of X-ray Photoelectron Spectroscopy (XPS). Measurements were performed using a PHI 5700/660 Multipurpose Electron Spectrometer based on two separate test chambers joined by an UHV transfer system by Physical Electronics using monochromatized Al$_{K\alpha}$ radiation (hν = 1486.6 eV). The energy resolution of the spectrometer equipped with a hemispherical energy analyzer was about 0.3 eV. The anode was operated at 15 kV and 225 W. Survey and multiplex high-resolution spectra (HRES) were measured in ultrahigh vacuum. HRES were fitted using mixed Gaussian and Lorentzian functions and Shirley background with the application of MultiPak program. The range in survey mode was from –2 to 1400 eV. The measurement parameters for survey mode and HRES were respectively: pass energy 187.85 and 23.50; step 0.800 eV and 0.100 eV; time per step 20 ms and 100 ms. The size of the analyzed area (in HRES) was 1.0–1.5 × 2.0–2.5 mm.

2. Determination of polycrystalline substances located on the surface of iron cells before and after the batch tests. These measurements were carried out with the use of

x-ray diffraction (XRD). X-ray Multipurpose Diffractometer EMPYREAN by PANalytical was used for the analysis of solid objects. The diffractometer was equipped with PreFIX (pre-aligned, fast interchangeable X-ray) modules making a change in the optical path effortless for the user. The PDF4+ database was used for identification of chemical compounds. Crystal lattice parameters were measured.

Results

The applicability of ZVI in PRB in the treatment of AMD is well established. The research concerning the removal of metals using this material has been conducted for several years (Wilkin and McNeil, 2003; Rangsivek and Jekel, 2005; Li and Zhang, 2007; Fiore and Zanetti, 2009; Puls et al., 1998; Groudev et al., 2007, Klimkova et al., 2011). The literature, however, includes conflicting reports on the mechanism for individual metals. For instance according to Wilkin and McNeil (2003), when the value of pH is lower than 7, the process causing the removal of metals in the cationic form is adsorption onto either the iron surface or the iron corrosion products. In the research presented by Li and Zhang (2007), the predominant removal mechanism for metals with a much more positive and slightly more positive standard electrode potential than that of iron, is respectively the reductive precipitation and the sorption and/or reductive precipitation. The authors referred to above state that the sorption/surface complex formation is the removal mechanism for metal ions with a standard potential very close to or more negative than that of iron. At this point it should be made clear that the type of process obviously depends on the chemical and physicochemical composition of the solution. In general, sorption as a removal mechanism is not preferred because soluble copper (Cu^{2+}) remains in its more soluble oxidation state, and in the case of change in the physicochemical conditions it may be released back to the environment.

Karrabelli et al. (2008) claimed that up to the pH value of 6.5, copper exists in solution mainly in the form of Cu^{2+}. In the pH range between 7 and 9.5, cationic species like $Cu(OH)^+$, $Cu_2(OH)_2^{2+}$, and $Cu_3(OH)_4^{2+}$ are dominant. Beyond these values, $Cu(OH)_2$ and the anionic species $Cu(OH)_3^-$ and $Cu(OH)_4^{2-}$ become increasingly effective. In the presented study, due to their pH values, copper ions are expected to occur in a divalent form during the experiments.

In accordance with the results presented in Table 1, the iron cell had the ability to remove copper (Cu^{2+}) from synthetic water when the pH was low and almost neutral. The lower the pH values in copper solutions, the slower the observed decrease of Cu^{2+} concentrations. Moreover, more Fe^{2+} appeared in water with a lower initial pH value, than in high pH water. Thus, it has been concluded that the oxidation of ZVI proceeds faster at low pH, which has been confirmed by other researchers, e.g. Kowal and Swiderska-Broz (1996). Similar variations and a faster decrease of ORP for lower values of pH in the tests have been observed in research presented by Suponik (2015).

Table 1. Physicochemical parameters and concentrations of chemicals
in solution used in batch test for initial pH of 3 and 6

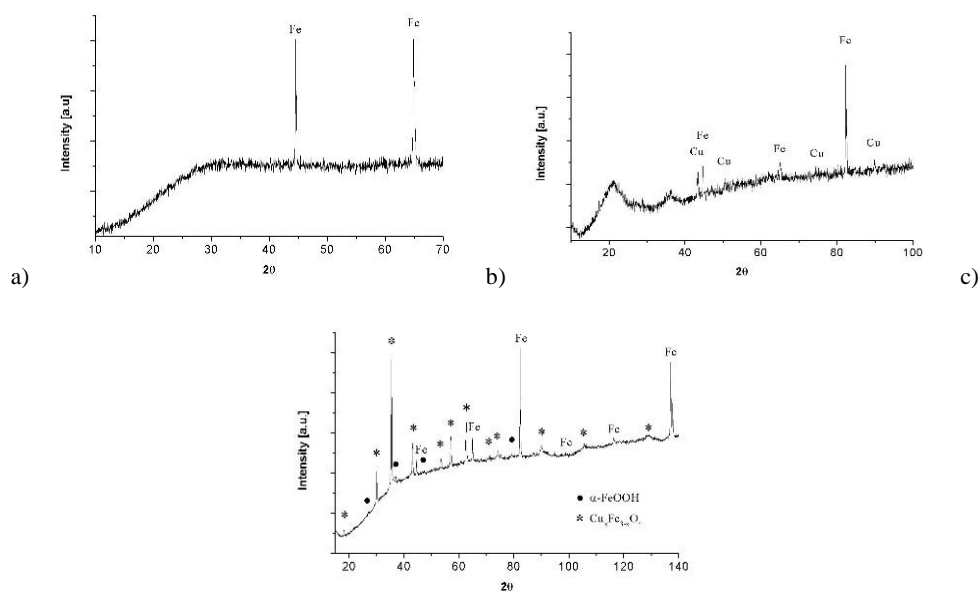| Stage of the batch test	pH	Cond., µS/cm	ORP mV	DO mg/dm^3	Cu^{2+} mg/dm^3	Fe^{2+} mg/dm^3	Fe^{3+} mg/dm^3
Parameters for initial pH = 3							
initial values	3.00	1068	441	5.9	3.51	BDL	0.08
values after 24 hrs of shaking	4.82	407	144	5.0	1.54	6.68	9.65
Parameters for initial pH = 6							
initial values	6.00	182	354	6.3	2.96	BDL	0.09
values after 24 hrs of shaking	6.39	228	148	5.5	0.67	0.22	4.26

BDL – below detection limit

Fig. 1. XRD graph of iron cell: a) before the batch test; b) after the batch test for initial pH
of the solution amounting to 3; c) after the batch test for initial pH of the solution amounting to 6.
Fe – iron in metallic form; Cu – copper in metallic form

Figure 1 presents the diffraction patterns after X-rays interacted with crystalline substances on iron cells before and after the batch tests. Based on Fig. 1a it can be claimed that iron is found on the surface of iron cell assessed before the batch tests (as might be expected). The lattice parameters of pure iron are similar to the parameters of many alloys in which the main component is iron. According to the XRD graphs

obtained after the batch tests (Fig. 1b and 1c) it can be concluded that copper and iron in metallic forms are present on the cell surfaces in case of the initial pH of the solution of 3 (Fig. 1b). In case of the initial pH of 6 (Fig. 1c) it can be concluded that α-FeOOH, magnetite in the form of $Cu_xFe_{3-x}O_4$ (where $x \leq 1$) and metallic iron are present. In both cases iron comes from the substrate (is located under the first atomic layers). The formation of magnetite was also investigated by Grosvenor et al. (2004) and Karrabelli et al. (2008). The latter noticed (on the basis of XRD analyses) a slow development of iron oxides, primarily in the forms of Fe_3O_4 and γ-Fe_2O_3.

A protective "passivating" magnetite layer on Fe^0 surface is formed due to low oxygen Fe^0 corrosion (Furukawa et al., 2002). It may mask the redox active sites and, as other corrosion products, reduce the barrier permeability by occupying available pore space. On the other hand, the formation of these products on large surfaces may be beneficial for the immobilization of metals in ionic forms by means of sorption (Rangsivek and Jekel, 2005).

Table 2. Atomic concentrations of elements (expressed as percentages) on iron cells before and after batch tests for initial pH of solutions amounting to 3 and 6 – on the basis of XPS measurements

elements	values before the batch tests, in atom %	values after 24 hrs of shaking for initial pH = 3, in atom %		values after 24 hrs of shaking for initial pH = 6, in atom %	
	XPS - survey mode	XPS - survey mode	XPS - HRES	XPS - survey mode	XPS - HRES
C	62.64	26.32	26.38	34.65	37.41
N	0.99			0.67	
O	29.30	55.71	52.55	46.54	43.54
Na	0.25				
P				2.61	3.47
S		1.12	0.97	0.79	0.96
Cl				0.22	
Ca				0.98	0.97
Fe	6.81	15.59	18.76	10.38	10.21
Cu		1.26	1.35	3.16	3.44

The atomic concentration of elements on the iron cells before and after the batch tests are presented in Table 2. Depending on the type of samples the measurements were performed several times. Since the results of the tests were similar the values for one chosen measurement were presented in Table 2. Each assessed sample contained carbon and oxygen. The presence of these elements and nitrogen has been explained by contamination of the samples (by atmospheric air and other factors) in their transport for the measurements. For that reason, these results have not been taken into consideration in further analysis (except for carbon and oxygen contained in

carbonates and oxygen contained in metal oxides). Calcium (which the presence in the solution is explained by incorrect distillation) has probably formed (with sulphur and carbon) $CaSO_4$ and/or $CaCO_3$, where the calcium carbonate is more likely due to the fact that Ca was only present on the iron cell when the pH was higher (Table 2).

Due to the importance of the main problems raised in this article, the further part of the analysis in this paragraph takes into account only iron and copper. In this case, the atomic concentrations of iron and copper on iron cells for initial pH of solution equal to 3 and 6 amounted respectively to 93.69% and 74.83% for iron and 6.31% and 25.17% for copper. This means that copper was better removed from the solution at a higher initial value of pH, which was to be expected and was also presented in a paper by Suponik (2015).

The HRES spectrums for C1s, S2p, Ca2p, O1s, Fe2p and Cu2p are shown in Fig. 2. The binding energy of the XPS lines was normalized to the binding energy of C1s = 285eV. The lines were standardized to the same height.
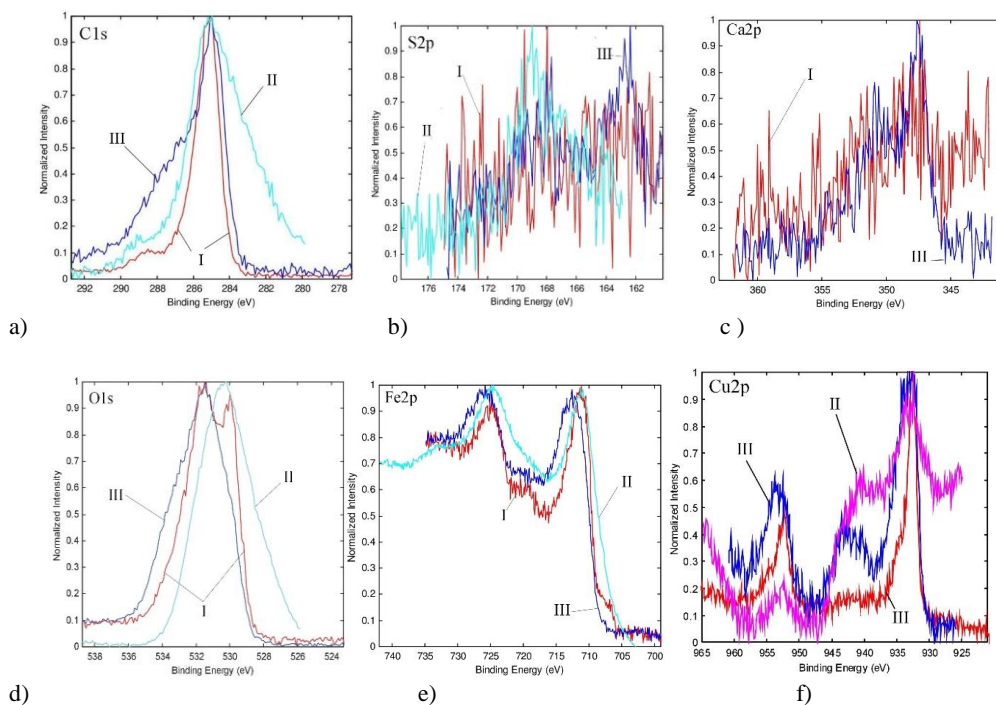

Fig. 2. High resolution a) C1s; b) S2p; c) Ca2p; d) Os1; e) Fe2p; f) Cu2p spectrum for iron cells before and after batch test. Binding energy of XPS lines normalized to binding energy of C1s = 285 eV; lines standardized to the same height; I – cell before the test, II – cell after the test, initial pH = 3, III – cell after the test, initial pH = 6

Based on the C1s spectrum (Fig. 2a) obtained from the iron cell batch test with the initial pH of solution amounting to 6, it can be said that carbonate has probably

formed on the surface of the cell (e.g. C1s 289.6 eV - $CaCO_3$). At the same time, the Ca2p spectrum shows that both $CaCO_3$ ($Ca2p_{3/2}$ 346.9 eV - $CaCO_3$) and $CaSO_4$ ($Ca2p_{3/2}$ 348.0 eV - $CaSO_4$) can be generated under these conditions (Fig. 2c). The S2p spectrum presented in Fig. 2b confirms the presence of sulphates on the cell but for the initial pH of the solution amounting to 3 it is $CaSO_4$ (S2p 169.0 eV and 169.3 eV), while for the initial pH of 6 it is rather $FeSO_4x7H_2O$ (S2p 168.0 eV). Furthermore, in case of the initial solution pH of 6, Cu_2S (S2p 162.4 eV - Cu_2S) and/or FeS_2 (S2p 162.9 eV - FeS_2) may also be formed but in very small quantities (Fig. 2b) because the photoelectric lines corresponded to the sulfides are very week. In addition, it is a lack of evidence for the presence of FeS_2 and Cu_2S in the crystalline form on X-ray diffractograms (Fig. 1). Main contribution to the C1s line comes from hydrocarbons deposited on the surface. It always happens when a sample is stored in air atmosphere. The binding energy of the C1s line coming from hydrocarbons is 285.0 eV. Deflection of the C1s spectrum to the right to the value about 283 eV for the initial pH = 3 is explained by the effect of loading. In the case of the iron cell immersed in a solution of pH = 3, the surface of the sample was heterogeneous. This caused various parts of the sample to be charged in various degrees. The correct neutralization of the entire surface was impossible, as evidenced by a shift towards lower binding energy of other lines (e.g. O1s, Fe2p in Fig.2), including the line C1s.

In the O1s spectrum for the cell before the batch test (Fig. 2d), two peaks are noticeable. The binding energy that corresponds to the peaks amounts to 530.4 eV and 531.4 eV, indicating that respectively iron oxides (e.g. Fe_2O_3 - O1s 529.9 eV) and hydroxides (O1s from min 530.9 to max 532.0 eV – hydroxides) – mainly iron hydroxides (because iron is the main element presented on the surface of cell, see Table 2), are probably generated on the surface of the iron cell. Although in case of the second peak (i.e. for 531.4 eV) carbonates (O1s from min 530.5 to max 531.5 eV – carbonates) and sulphates (O1s from min 531.5 to max 532.5 eV – sulphates) might also be formed, Figs. 2a and 2b do not indicate the presence of these compounds. These compounds, and also other than iron metal oxides (O1s from min 528.1 to max 531.1 eV – metal oxides), as well as hydroxides (O1s from min 530.9 to max 532.0 eV - hydroxides) may be formed on the iron cell in case of the initial pH amounting to 6, while for the initial pH = 3, less sulphates, carbonates and hydroxides are likely to form, in comparison with metal oxides causing a shift in the peak to the right.

The spectrums of Fe2p (Fig. 2e) obtained from cells before and after the test for initial pH of solution amounting to 3, indicate the presence of Fe_2O_3 (Fe2p 710.9 eV - Fe_2O_3) and/or Fe_3O_4 (Fe2p 710.8 eV – Fe_3O_4) and iron in the metallic form (Fe2p 707.0 eV). The spectrum for initial pH = 6, on the other hand, indicates the presence of $FeSO_4$ (Fe2p 712.1 eV – $FeSO_4$) and/or α-FeOOH (Fe2p 711.8 eV – α-FeOOH) as well as Fe_3O_4 and Fe_2O_3. Iron hydroxides can form a passivation layer of increasing thickness on the surface of ZVI, with the progress of corrosion. This reduces its reactivity.

The binding energy (Cu2p) that corresponds to the compounds formed on the surface of iron cells for both initial pHs are 932.5 eV and 934.0 eV, which means that the following copper compounds may be formed:

- for binding energy 932.5 eV: copper in metallic form (Cu2p 932.6 eV – Cu_{metal}), Cu_2S (Cu2p 932.5 eV), Cu_2O (Cu2p 932.5 eV – although this is unlikely because Cu_2O is formed in oxygen-containing environment), $CuFeO_2$ (Cu2p 932.6 eV) – generally Cu in metallic form and in first oxidation state,
- for binding energy 934.0 eV: $CuFe_2O_4$ (Cu2p 933.8 eV), CuO (Cu2p 933.7 eV – although this is unlikely because CuO is formed in an oxygen-containing environment) – generally Cu in second oxidation state.

The peaks, that correspond to the binding energy of 940.5 eV, result from the fact that the surface of the cells was heterogeneous.

Discussion

Based on the present research, it may be stated that iron oxides and iron in metallic form have been found on the surface of iron cell before the batch tests.

In the case of a cell applied in the solution, pH of which was 3, Cu^0 has formed, causing the removal of copper from the solution. Furthermore, Cu_2O, CuO and Fe_2O_3 were probably formed on the surface of the iron cell as well, but to a lesser degree, as these compounds are formed in an oxygen-containing environment. In the substrate of created layers, Fe^o has also been identified.

Pure magnetite and magnetite, in which copper replaces iron creating $Cu_xFe_{3-x}O_4$ that is mainly $CuFe_2O_4$ and $Cu_{0.5}Fe_{2.5}O_4$, have formed on the surface of the iron cell for initial pH of the solution amounting to 6. The lattice parameters of pure magnetite are similar to the parameters of this mineral, in which iron was substituted by copper. Copper can replace iron in every structure. The XRD diffraction pattern of Fe_3O_4 is very similar to the $CuFe_2O_4$ and $Cu_{0.5}Fe_{2.5}O_4$ ones. Magnetite is present in regular structures as well as in orthorhombic, tetragonal, rhombohedral and monoclinic structures and the XRD diffraction pattern for these are similar. Due to very similar ionic radii of copper and iron, the differences in the diffraction pattern can be only observed in the intensities.

Copper, in this case, could have also created other forms, mainly Cu^0, Cu_2S, Cu_2O and CuO, while (as for pH = 3) there is no clear evidence which one was the main compound and if they are formed they have non-crystalline forms. The iron compounds such as $FeSO_4$ and/or Fe_2O_3, but mainly α-FeOOH, were also generated in these conditions. Since the distilled water was probably prepared incorrectly, $CaCO_3$ has also been created on the surface of the cell.

Upon visual inspection, the surface of iron cells used in the tests was covered tightly with black film for initial pH of 6 and with black-brown film for pH 3. Oxidation of copper usually takes place from Cu_2O to CuO, which is characterized by black color – just as magnetite, hematite (which is may also be deep red) and goethite

(which may also be brown). Cu_2O is red in color. This fact indicates either a lack or a small amount of this compound on the surface of the iron cells used in the tests. Rangsivek and Jekel (2005) and Uzum et al. (2009) claim that in the case of deoxygenated acidic conditions in water and for nano-scale ZVI in the presence of kaolinite clay, Cu^0 and Cu_2O have been formed on the surface of iron. Karabelli et al. (2008) have confirmed these results for pure nano ZVI in their studies and claimed that Cu^{2+} ions were removed primarily via a redox mechanism that resulted in the formation of Cu_2O and Cu^0. Both of these compounds were also detected in the XPS presented in the article (for pH = 3 and 6; see Fig. 2f). Yet only Cu^0 was confirmed by the XRD, but only for pH = 3 (see Fig. 1b). In general, it can be concluded that small amount of Cu_2O (red) and Cu^0 (orange-red color) were dominated by the black compounds. However, larger amount of Cu_2O and Cu^0 was formed for the cell submerged in a solution of pH = 3 (cell was black-brown), and smaller for pH=6 (cell was black).

Li and Zhang (2007) report that ions with standard electrode potential larger than that of Fe^{2+} are bound to nano ZVI as a result of redox reaction. The value of standard electrode potential for Cu^{2+} is higher than that of Fe^{2+} and the following reaction proceeds:

$$Fe^0 + Cu^{2+} \rightarrow Fe^{2+} + Cu^0. \tag{1}$$
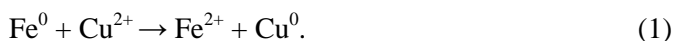
Considering the conclusions presented by Karabelli et al. (2008), Rangsivek and Jekel (2005) and Uzum et al. (2009), and the fact that the binding energy (in XPS) reported for metallic copper is very similar to Cu^+ in Cu_2O (Fig. 2f), it can be claimed that this compound appears also as a result of purification of water contaminated by copper ions, but more for initial pH of solutions 3 rather than 6. According to Karabelli et al. (2008), the redox reaction then might be written as follows:
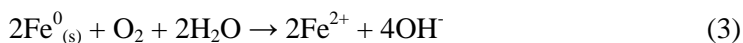
$$Fe^0 + 2Cu^{2+} + H_2O \rightarrow Fe^{2+} + Cu_2O + 2H^+. \tag{2}$$
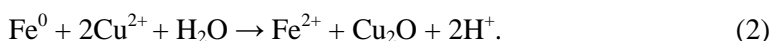
As provided by Furukawa et al. (2002), Roh et al. (2000), Rangsivek and Jekel (2005) and Uzum et al. (2009), the secondary minerals typically formed on the surface of ZVI as a result of purification of groundwater contaminated by metals in ionic forms are Fe_3O_4, $CaCO_3$, α-Fe_2O_3, α-$FeOOH$. These compounds were confirmed in the research presented in the article. Other compounds, not identified in the research, are: γ-$FeOOH$, $Fe(OH)_2$, $Fe_2O_3 \cdot 0.5H_2O$, $FeCO_3$, FeS_2, Fe_3S_4, mackinawite ($(FeNi)_{1+x}S$, where x is from 0 to 0.11), and green rust ($[Fe_{1-x}^{2+} Fe_x^{3+}(OH)_2]^{x+}$ $[x/n\ A^{n-} \cdot mH_2O]^{x-}$, where x is the Fe^{3+}/Fe_{tot} ratio), which is usually created under neutral pH conditions. Although, according to Wilkin and McNeil (2003), green rust is a primary corrosion product formed on ZVI in sulphate rich solutions, it has not been observed by visual inspection on the surface of the iron cell and there has been no evidence of it in the presented results. This is probably due to the "pure" conditions of purification. As provided by Cornell and Schwertmann (1996), green rust is stable only at low grades
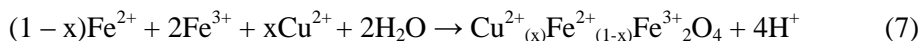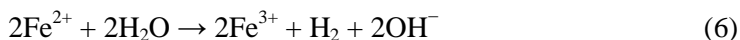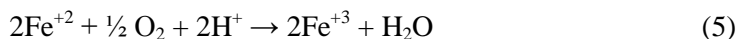
of oxide reduction and its oxidation usually leads to the formation of Fe_2O_3 or γ-FeOOH. Roh et al. (2000) also reported that green rust is an intermediate stage and is finally transformed into α-FeOOH, γ-FeOOH, Fe_3O_4, and Fe_2O_3.

In general, more chemical compounds were formed on the surface of the iron cell for higher initial pH of the solution. These conditions result in a much larger specific surface area. According to the research of Suponik (2015b) which was conducted using the same shaking methodology as shown in the presented article, the specific surface (obtained by Multi-point BET method) of cells increased from the value of 0.0312 m^2/g (for a cell which has not been used in the batch test) to 0.1206 m^2/g for initial pH of solution amounting to 3 and to 0.3354 m^2/g for initial pH = 6.

The affinity of Cu^{2+} sorption is generally determined by pH at the point of zero charge (pH_{PZC}). This parameter describes the condition (pH value) in which the electrical charge on the surface of ZVI is zero. If the ZVI surface is positively charged with respect to the PZC (under an acidic condition or pH below pH_{PZC} protons are sorbed on the functional group which results in the surface of cell having a net positive charge), the Cu^{2+} is not adsorbed on the ZVI surface. If the ZVI surface would be negatively charged with respect to the PZC (at above pH_{PZC} the oxygen atom stays deprotonated and the surface tends to have a net negative charge), the Cu^{2+} sorption would be directly adsorbed on the ZVI surface. The point of zero charge for most iron oxides is typically in the range of pH about 6 to 8 (for instance for Fe_3O_4 from 3.8 to 8.2; for α-FeOOH from 6.7 to 9.2) (Kosmulski, 2011), while for CuO and Cu_2S it is 6.9, 7.6 (Gonzalez and Laskowski, 1974) and <2 (He at al. 2009), respectively. In accordance with the research presented by Suponik (2015b), the pH_{PZC} of iron cells submerged in solutions, for the initial pH of 3 and 6 with the same shaking method used as in the present article, was about 6.2 in both cases. Thus, in the first case (initial pH = 3), the sorption of Cu^{2+} on the surface of cells is not possible, while it may occur in the second case – in the experiment in which the initial pH of the solution was 6 and the final pH was 6.39. The shell coating the cell following the test is characterized by roughly equal amounts of negative and positive charges, as the pH of the solution (6.39) is close to the pzc of the compounds formed on the surface of ZVI. Since both charges exist on the shell coating cell at this pH, the sorption of Cu^{2+}, as well as the negatively charged ions which are present in the solution, can occur at the cell surface.

As it has been said, except for the formation of Cu^0 and Cu_2O (emerging mainly for initial pH of the solution amounting to 3), the $Cu_xFe_{3-x}O_4$ is the main compound generated as a result of water purification from copper in ionic form, for initial pH of the solution amounting to 6. Ferrous and ferric ions created as a result of reactions 3, 4, 5, 6 (based on Puls et al., 1998) form $Cu^{2+}_{(x)}Fe^{2+}_{(1-x)}Fe^{3+}_2O_4$ in accordance with equation 7:

$$2Fe^0_{(s)} + O_2 + 2H_2O \rightarrow 2Fe^{2+} + 4OH^- \tag{3}$$

$$Fe^0_{(s)} + 2H_2O \rightarrow Fe^{2+} + H_2 + 2OH^- \tag{4}$$

$$2Fe^{+2} + \tfrac{1}{2} O_2 + 2H^+ \rightarrow 2Fe^{+3} + H_2O \tag{5}$$

$$2Fe^{2+} + 2H_2O \rightarrow 2Fe^{3+} + H_2 + 2OH^- \tag{6}$$

$$(1 - x)Fe^{2+} + 2Fe^{3+} + xCu^{2+} + 2H_2O \rightarrow Cu^{2+}_{(x)}Fe^{2+}_{(1-x)}Fe^{3+}_2O_4 + 4H^+ \tag{7}$$

where $x \leq 1$.

Conclusions

Copper released from mine waste disposal sites as a result of acid mine drainage poses a danger to ground and surface water. To protect water, ZVI might be used. Under these conditions and at reduced oxygen content in water, copper in the second oxidation step was removed at the initial pH of 6 much more effectively than at lower pHs. The formation of magnetite (in which copper replaces iron), and to a lesser degree Cu_2O, Cu^0 and/or CuO and/or Cu_2S, were the basic processes in the removal of copper for almost neutral pH of the aqueous solution (pH about 6), while the formation of copper in metallic form and Cu_2O, as well as probably CuO, were the basic processes for lower pHs (pH about 3).

Since more chemical compounds, that is α-FeOOH, $CaCO_3$, Fe_2O_3 and $FeSO_4$ were formed on the surface of ZVI for almost neutral pH of aqueous solution (larger specific surface than for lower initial pH of solution was created) and the pH at the point of zero charge for shells coating ZVI was about 6.2 (the final pH for almost neutral pH of solution amounted to 6.39) the adsorption of Cu^{2+} on the surface of shells were additional process causing copper removal from water in these conditions.

References

CORNELL R.M., SCHWERTMANN U., 1996, *The iron oxides*, VCH Publishers: New York.

FURUKAWA Y., KIM J.W., WATKINS J., WILKIN R.T., 2002, *Formation of ferrihydrite and associated iron corrosion products in permeable reactive barriers of zero-valent iron*, Environmental Science and Technology 36.24, 5469-5475.

GONZALEZ G., LASKOWSKI J., 1974, *The point of zero charge of oxidized copper minerals: tenorite, malachite and chrysocolla*, Journal of Electroanalytical Chemistry and Interfacial Electrochemistry 53.3: 452-456.

GROSVENOR A.P., KOBE B.A., BIESINGER M.C., MCINTYRE N.S., 2004, *Investigation of multiplet splitting of Fe 2p XPS spectra and bonding in iron compounds,* Surface and Interface Analysis, 36: 1564-1574.

HE F., ADDAI-MENSAH J., BEATTIE D., 2009, *Sericite–chalcocite mineral particle interactions and hetero-aggregation (sliming) mechanism in aqueous media*, Chemical Engineering Science 64.13: 3083-3093.

FIORE S., ZANETTI M.C., 2009, *Preliminary Tests Concerning Zero-Valent Iron Efficiency in Inorganic Pollutants Remediation*, American Journal of Environmental Sciences 5.4: 556–561.

GROUDEV S., SPASOVA I., NICOLOVA M., GEORGIEV P., 2007, *Acid Mine drainage cleanup in a uranium deposit by means of a passive treatment system*, Physicochemical Problems of Mineral Processing, 41: 265-274.

KARABELLI D., UZUM C., SHAHWAN T., EROGLU A.E., SCOTT T.B., HALLAM K.R., LIEBERWIRTH I., 2008, *Batch removal of aqueous Cu^{2+} ions using nanoparticles of zero-valent iron: a study of the capacity and mechanisms of uptake*, Ind. Eng. Chem. Res. 47: 4758-4764.

KOSMULSKI M., 2011, *The pH-dependent surface charging and points of zero charge: V. Update*, Journal of colloid and interface science 353.1: 1-15.

KLIMKOVA S., CERNIK M., LACINOVA L., FILIP J., JANCIK D., ZBORIL R., 2011, *Zero-valent iron nanoparticles in treatment of acid mine water from in situ uranium leaching.* Chemosphere, 82. 8: 1178-1184.

KOWAL L.A., ŚWIDERSKA-BRÓŻ M., 1996, *Oczyszczanie wody,* PWN, Warszawa-Wrocław.

LI X.Q., ZHANG W.X., 2007, *Sequestration of Metal Cations with Zerovalent Iron Nanoparticles: A Study with High Resolution X-Ray Photoelectron Spectroscopy (HRXPS),* Journal of Physical Chemistry 111.19: 6939–6946.

PULS R.W., POWELL M.R., BLOWES D.W., GILLHAM R.W., SCHULTZ D., SIVAVEC T., VOGAN J.L., POWELL P.D., 1998, *Permeable reactive barrier technologies for contaminant remediation*, Washington: United States Environmental Protection Agency.

RANGSIVEK R., JEKEL M.R., 2005, *Removal of Dissolved Metals by Zero-Valent Iron (ZVI): Kinetics, Equilibria, Processes and Implications for Stormwater Runoff Treatment,* Water Research 39: 4153–4163.

ROH Y., LEE S.Y., ELLESS M.P., 2000, *Characterization of corrosion products in the permeable reactive barriers*, Environmental Geology, 40: 184-194.

SUPONIK T., 2015, *Zero-valent iron for inorganic contaminants removal from low pH water,* Environment Protection Engineering, vol.41, no.1.

SUPONIK T., 2015b. *Study of precipitates formed on the iron reactors following the removal of copper from water,* accepted for publication in Environment Protection Engineering (2014), DOI: EPE_260214.

UZUM C., SHAHWAN T., EROGLU A.E., HALLAM K.R., SCOTT T.B., LIEBERWIRTH I., 2009, *Synthesis and characterization of kaolinite-supported zero-valent iron nanoparticles and their application for the removal of aqueous Cu^{2+} and Co^{2+} ions,* Applied Clay Science, 43:172-181.

WILKIN R.T., MCNEIL M.S., 2003, *Laboratory evaluation of zero-valent iron to treat water impacted by acid mine drainage,* Chemosphere 53: 715-725.

EFFECT OF SPODUMENE LEACHING WITH SODIUM HYDROXIDE ON ITS FLOTATION

Fushun YU[*, **], **Yuhua WANG**[**], **Lei ZHANG**[**]

[*] School of Resources and Environmental Engineering, Shandong University of Technology, Zibo 255049, China

[**] School of Minerals Processing and Bioengineering, Central South University, Changsha 410083, China, csuwangyh@163.com

Abstract: Effects of NaOH on flotation of spodumene, quartz and feldspar using oleic acid as a collector were investigated through microflotation and bench scale flotation tests. It was determined that NaOH acted more than a pH regulator in the tests. The X-ray photoelectron spectroscopy revealed that spodumene was preferentially leached by conditioning with high concentration of NaOH in the solution and exposed more Li positive sites on the mineral surface leading to an improved flotation.

Keywords: spodumene, flotation, preferential leaching, XPS analysis

Introduction

Spodumene (LiAl[SiO$_3$]$_2$) is a typical monoclinic pyroxene mineral (Krause, 1968; Moon and Fuerstenau, 2003) with a theoretical Li$_2$O grade of 8.07%. As the richest lithium bearing minerals in nature, spodumene is one of the main mineral resources of lithium (Rai et al., 2011). The major consumer of spodumene was the aluminum and ceramics industry (Wendt, 1971; Nicholson, 1978). However, a great number of applications of spodumene and lithium compounds were being developed rapidly in the battery and fuel cell industry in recent years (Lu et al., 2013; Thomas, 2009; Whittingham, 2004). Lithium has become a precious commodity, since the application of lithium ion batteries is considered to be the preferred technology for the next generation of electric vehicles.

Spodumene exists generally in granite pegmatite deposits, which contain quartz, feldspar, muscovite as well as some tantalite and niobite. Flotation is the most important process to selective separate spodumene from other aluminosilicates (Jie et al., 2014). Since many investigations on flotation of spodumene have been conducted (Moon, 1985; Menendez et al., 2004; Yi, 2011; Zhong et al., 2012), there is a

consensus that conditioning in highly alkaline solutions prior to flotation improves spodumene separation effectiveness. However, research on the mechanism of alkali role is insufficient and the effects of alkali on flotation of spodumene have not been clear yet. In the present study, the effects of NaOH on flotation of spodumene, quartz, and feldspar have been investigated, and the mechanisms of NaOH reactions with the minerals were envisaged by X-ray photoelectron spectroscopy (XPS) as well.

Materials and methods

Material of single minerals

Pegmatitic spodumene, quartz and feldspar were obtained from the Koktokay Rare Metal Mine located in Xinjiang Altay district in China. The hand-picked crystals were ground in a porcelain mill with agate balls in it to an appropriate particle size, and then screened by means of stainless steel screens. The samples with the desired size were filtered, vacuum-dried and stored in glass bottles for the use of single mineral flotation tests and measurements. The chemical compositions of the obtained samples are presented in Table 1. It illustrates that the samples were all of high grade, satisfying the requirement for flotation tests.

Table 1. Chemical analysis of three mineral samples (%)

Mineral	Al_2O_3	SiO_2	Li_2O	K_2O	Na_2O	Fe_2O_3	CaO	MnO	Cr_2O_3
Spodumene	28.43	62.09	7.81	0.22	0.32	0.94	0.15	0.16	0.05
Quartz	1.01	98.28	-	0.11	0.14	0.13	0.37	-	0.13
Feldspar	18.86	65.78	-	10.41	2.89	0.13	0.36	-	-

Material of actual ores

Actual spodumene ores from Kangding county in Sichuan, China, were crushed to minus 3 mm by a jaw crusher and a double roll crusher. Based on the X-ray diffraction (XRD) analysis, the mineral constituents of the ores were mainly spodumene (19.97%), quartz (29.50%), feldspar (29.41%), albite (10.81%) and muscovite (6.76%), as shown in Table 2. The chemical compositions of the spodumene ores by chemical assay are given in Table 3.

Table 2. Mineral constituents of spodumene ore (%)

Mineral	Spodumene	Quartz	Feldspar	Albite	Muscovite	Chlorite	Biotite	Others
Constituent	19.97	29.50	29.41	10.81	6.76	0.79	0.25	2.51

Microflotation

Microflotation tests were performed in a laboratory flotation apparatus using -0.105 + 0.038 mm size of single mineral samples as a feed. For each test, 2 g of sample was

placed in a plexiglass cell (40 cm^3), which was then filled with ultra-pure water. The sample was conditioned for 3 min after each reagent addition, and the flotation time was 5 min. All flotation tests were carried out at a room temperature of about 25 °C. The concentrates and tailings were filtered, dried, and weighed to calculate the flotation recovery under various flotation conditions.

Table 3. Multi-elements analysis of spodumene ore

Element	Percentage (%)	Element	Percentage (%)
Li_2O	1.48	CaO	0.21
Al_2O_3	14.43	MgO	0.13
SiO_2	73.29	S	0.096
K_2O	4.41	BeO	0.01
Na_2O	1.72	Nb_2O_5	0.011
Fe_2O_3	2.01	Ta_2O_5	0.009
C	0.35	Loss on ignition	0.43

Bench scale flotation

A 500 g sample of spodumene ores was ground to 70% passing 0.074 mm in a Φ200×400mm XMB-type steel mill at a pulp density of 60% (by weight). The pulp was transferred to a 1.5 L XFD-type flotation cell and diluted to a density of about 30%. Following the given flowsheet, various reagents were added successively, and the pulp was conditioned for a settled time. The froth product was gathered for 5 min. The concentrates and tailings were separately dried, weighed and assayed to calculate the yield and recovery of Li_2O.

Reagents

Oleic acid was used as the collector for the flotation tests. HCl and NaOH were used for the pH adjustment in the experiments. Na_2CO_3 and $CaCl_2$ were used as a modifier in the flotation of spodumene actual ores. All the reagents were of analytical grade, water used in micro flotation was ultra-pure water (18.25 MΩ·cm), and water used in actual ores was tap-water of the Changsha city.

XPS analysis

Dry powder samples of three minerals at a particle size of minus 2 μm were used for the XPS analysis, which was performed using an X-ray photoelectron spectrometer (Thermo Fisher, ESCALAB 250Xi, England) with a mono-chromatic Al X-ray source at 150 W to study the distribution density and binding energy of the elements on the mineral surface. The vacuum pressure was approximately 10^{-9} mbar. Each analysis started with a survey scan from 0 to 1200 eV with pass energy of 200 eV at steps of 1 eV with 1 sweep. For each element appearing on the full spectrum scan, fine spectrum scans (resolution of 0.1 eV) were carried out with pass energy of 30 eV at

steps of 0.1 eV. Relative proportions of all the elements on mineral surfaces were calculated by the ratios of the normalized peak areas on the intensity vs binding energy curve.

Results and discussion

Microflotation tests

Microflotation of spodumene, quartz and feldspar as a function of pH using oleic acid as the collector has been conducted and the results shown in Figure 1. It can be seen that flotation of spodumene is much better than that of quartz and feldspar, especially in the weak alkaline pH range. The maximum recovery of spodumene reaches approximately 80% at pH 8.7, while in the entire pH range, feldspar and quartz minerals float poorly with maximum recoveries of about 20%. It can be noticed that the recovery of spodumene turns good again at highly alkaline pH of 12.5. The tendency of spodumene recovery at still higher pH is of great interest to be investigated.
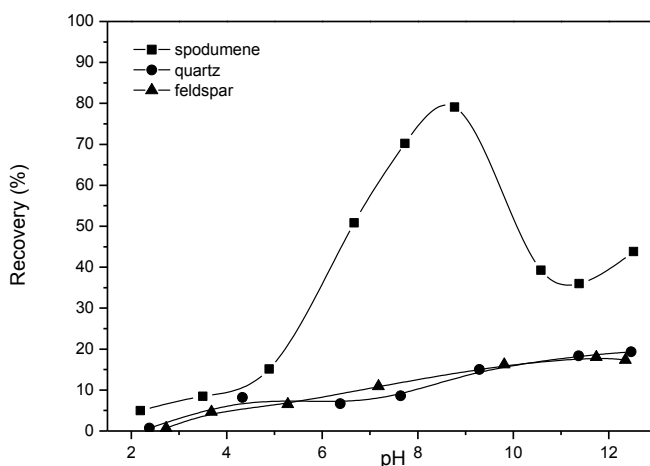
Fig. 1. Flotation recoveries of single minerals as a function of pH using 6.0×10^{-4} M oleic acid

   Figure 2 illustrates that the flotation recovery of three minerals vs. NaOH dosage, with the oleic acid concentration of 6.0×10^{-4} M. Since it is hard to measure precisely the pH values in extremely alkaline solutions, the horizontal ordinate in Figure 2 reflects NaOH dosages instead of pH values. The solution with the dosage of NaOH 250 mg·dm^{-3} agrees with the measured pH value of about 11.8. Figure 2 indicates that the flotation recovery of spodumene increases as the dosage of NaOH in solution increases, while the quartz recovery remains nearly stable and the feldspar recovery decreases gradually. It can be concluded that NaOH has a considerable effect on the flotation of spodumene.
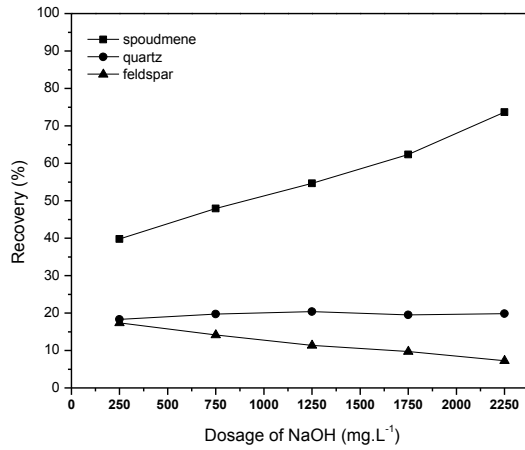
Fig. 2. Effect of NaOH dosage on the recovery of investigated minerals
at oleic acid concentration of $6.0 \cdot 10^{-4}$ M

The effects of NaOH solution leaching of the minerals prior to their flotation were investigated in the next tests. The mineral pulps were conditioned for 10 min in alkaline solution with various NaOH dosages, then filtered and water-washed to neutral pH. The flotation recoveries of the prepared minerals at pH 8.70 ± 0.20, using oleic acid at a concentration of $6.0 \cdot 10^{-4}$ M are demonstrated in Figure 3. It is shown there, that the flotation recovery of spodumene increases after leaching treatment in NaOH solution. It can be seen that the bigger of the NaOH dosage, the higher recovery is achieved. The maximum recovery of spodumene is up to 94% as the NaOH dosage is at 2250 mg·dm^{-3}. The flotation recovery of quartz remains approximately constant while feldspar recovery declines slowly with the increase of NaOH dosage.
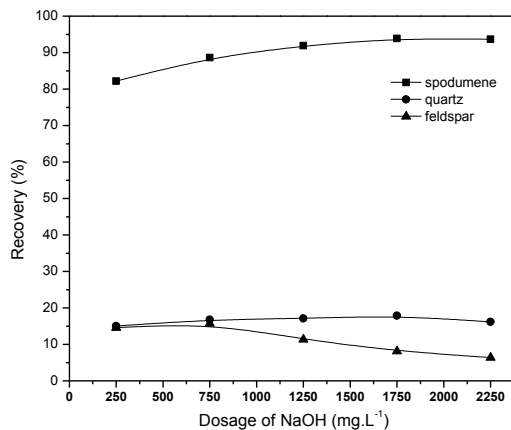
Fig. 3. Effects of NaOH leaching on flotation recovery
of three investigated minerals

Bench scale tests

Bench scale tests were carried out for the actual ore to investigate the effects of NaOH on the flotation of spodumene ore. Figure 4 shows the flowsheet of tests for exploring the effects of NaOH dosage on spodumene flotation, and Figure 5 presents the grade and recovery of spodumene concentrates as a function of NaOH dosage. It can be seen from Figure 5 that the grades of the concentrates decrease and the recoveries increase as the dosage of NaOH increases. This could be attributed to the fact that highly alkaline pH improves not only the flotation of spodumene, but also the gangue minerals, using $CaCl_2$ as activating agent (Fuerstenau and Pradip, 2005; Yu et al., 2014). NaOH acts as pH regulator only in this set of tests.
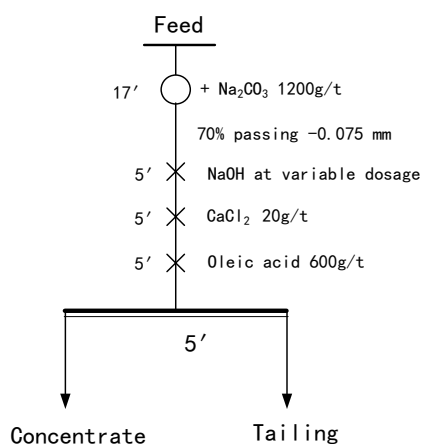
Fig. 4. Flowsheet of tests to explore
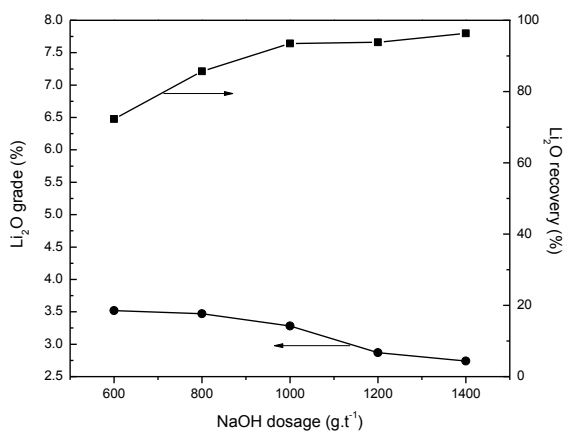the effects of NaOH dosage
on spodumene flotation

Fig. 5. Effects of NaOH dosage on the grade
and recovery of spodumene concentrates

The NaOH dosage of 1 kg/Mg was adopted in the next tests to inspect the effects of conditioning time of NaOH solution on spodumene flotation. Figure 6 illustrates the tests flowsheet and Figure 7 shows the tests results. The results demonstrate that the conditioning time of NaOH solution has an obvious impact on the flotation of spodumene ore. The grades of the concentrates increase and the recoveries decrease as the conditioning time goes up. It could be deduced that the effects of NaOH on the flotation of spodumene are greater than expected from NaOH acting as the pH regulator.
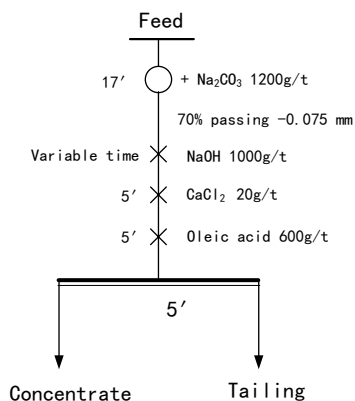
Fig. 6. Flowsheet of tests to explore effects of conditioning time of NaOH on spodumene flotation
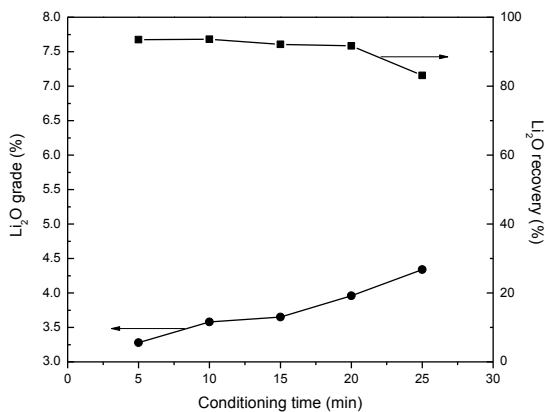
Fig. 7. Effects of conditioning time of NaOH solution on grade and recovery of spodumene concentrates

XPS analysis results

Based on the results of micro-flotation and bench scale flotation tests, it can be concluded that NaOH could change the flotation behavior of spodumene significantly. Since flotation behavior is determined by the mineral surface characteristics, the X-ray photoelectron spectroscopy (XPS) technique was applied to get information on elements of the sample surface layers. For the purpose of comparing the state of the surface before and after NaOH leaching, both samples, untreated and treated in NaOH solution, were investigated. Samples of the latter were stirred in NaOH solution at a concentration of 2250 mg·dm^{-3} for 10 min, which were then filtered and water-washed to a neutral pH. The vacuum-dried samples were sent for the XPS measurements.

The XPS spectra of spodumene, quartz and feldspar before and after NaOH leaching are shown in Fig. 8. The XPS spectral results are summarized in Table 4. It should be noted that the C (1s) detected in the samples is impurity, which was adsorbed at the surface inevitably during the sample preparation and XPS testing process (Liu et al., 1988). Table 4 demonstrates that no significant chemical shifts in the binding energy of the elements in three mineral samples are observed after NaOH leaching treatment. For the relative percentages of elements on mineral surfaces, the most obvious change occurs on Li (1s) element on spodumene surface, which increases from 6.63% to 7.35% after leaching in NaOH solution. The 0.72% percentage change of Li (1s) is big enough to eliminate the errors caused by the irreproducibility of XPS measurements.
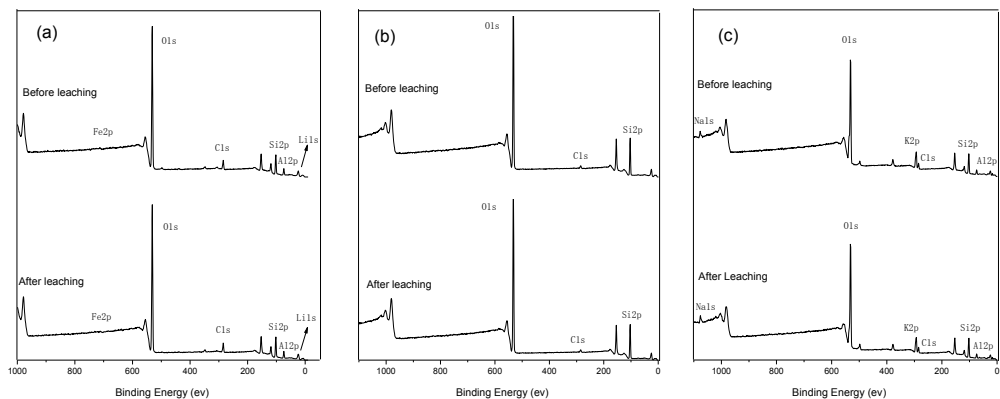
Fig. 8. XPS spectra of minerals before and after leaching in NaOH solution,
(a) spodumene; (b) quartz; (c) feldspar

Table 4. XPS analysis of three minerals before and after leaching in NaOH solution

Mineral	Element	Valence	Binding energy (eV)		Relative percentage (%)	
			Before leaching	After leaching	Before leaching	After leaching
	Li 1s	1	56.05	56.07	6.63	7.35
	Al 2p	3	74.58	74.61	9.65	9.74
Spodumene	Si 2p	4	102.45	102.49	19.79	19.76
LiAl[Si$_2$O$_6$]	O 1s	-2	531.72	531.72	53.73	53.24
	Fe 2p	3	712.17	712.26	0.37	0.27
	C 1s	4	284.80	284.84	9.83	9.64
Quartz	Si 2p	4	103.26	103.31	34.90	34.94
SiO$_2$	O 1s	-2	532.43	532.49	61.74	61.88
	C 1s	4	284.79	284.80	3.35	3.18
	Al 2p	3	74.51	74.41	7.17	7.33
	Si 2p	4	102.91	102.80	24.06	23.87
Feldspar	O 1s	-2	532.00	531.95	54.94	54.83
KAl[Si$_3$O$_8$]	K 2p	1	293.27	293.21	5.90	5.70
	Na 1s	1	1075.97	1076.01	1.58	2.36
	C 1s	4	284.84	284.77	6.35	5.91

The surface of spodumene exposes more Li positive sites after NaOH solution leaching. This increases adsorption of the anionic collector. Accordingly, the flotation of spodumene improves after leaching in the NaOH solution. This conclusion coincides well with the previous microflotation tests results and bench scale tests. It is also worth to note that flotation of quartz stays the same and flotation of feldspar declines slightly after NaOH leaching. The percentages of Si (2p) and O (1s) on quartz

surface changes rarely after NaOH leaching, which leads to a stabilized flotation of quartz. For feldspar mineral, the generation of Na_2SiO_3 may be the reason for the decline of feldspar recovery. Since the Si (2p) percentage on feldspar surface decreases from 24.06% to 23.87% after leaching, the dissolved Si transfers to Na_2SiO_3 in NaOH solution by chemical reaction. Na_2SiO_3 is a depressant which can depress the flotation of gangue minerals significantly (Chulhyun and Hoseok, 2010; Rao, 2010). In the bench scale flotation tests, the grade of concentrate increases and the recovery decreases as the conditioning time of NaOH solution goes up. The possible explanations for this phenomenon may also contribute to the spontaneous sodium silicate generated in the alkaline pulp after conditioning for adequate time, which depresses the flotation of the minerals selectively.

Conclusions

The microflotation tests revealed that the flotation recovery of spodumene increases at extremely alkaline pH while for quartz it remains nearly constant and decreases slightly for feldspar, as the dosage of NaOH increases. The flotation of spodumene is enhanced by leaching at high concentrations of NaOH solution before flotation. For quartz and feldspar NaOH leaching does not promote their flotation and the recovery of feldspar even declines. The grades of the concentrates decrease and the recoveries increase with the increase of the NaOH dosage in bench scale tests. Moreover, conditioning time of NaOH solution has a significant impact on the flotation of the spodumene ore. The grades of the concentrates increase and the recoveries decrease as the conditioning time goes up. It is concluded that NaOH acts more than a pH regulator in these tests.

The XPS analysis revealed that spodumene was preferentially leached by conditioning at high concentrations of NaOH and exposed more Li positive sites on the mineral surface. The percentages of Si and O on quartz surface do not change after NaOH leaching. The generation of Na_2SiO_3 may be the reason for the decline of the feldspar recovery. Because the Si percentage on feldspar surface decreases after NaOH leaching treatment and the dissolved Si in NaOH solution can be transferred to Na_2SiO_3 it leads to depression of aluminosilicate minerals flotation. The spontaneously generated sodium silicate in the alkaline pulp after conditioning for adequate time is the possible explanation for the fact that the grades of concentrates increase and the recoveries decrease as the conditioning time of NaOH solution rises.

Acknowledgements

References

CHULHYUN P., HOSEOK J., 2010, *The effect of sodium silicate as pH modifier and depressant in the froth flotation of molybdenite ores*, Mater. Trans., 51, 1367-1369.

FUERSTENAU D.W., PRADIP 2005, *Zeta potentials in the flotation of oxide and silicate minerals*, Adv. Colloid Interface Sci., 114-115, 9-26.

JIE Z., WEIQING W., JING L., YANG H., QIMING F., HONG Z., 2014, *Fe(III) as an activator for the flotation of spodumene, albite, and quartz minerals*, Miner. Eng., 61, 16-22.

KRAUSE J.T., 1968, *Internal friction of twinned spodumene*, J. Appl. Phys., 58, 4472-4473.

LIU S., WANG D., PAN C., 1988, *Analysis on X-ray photoelectron spectroscopy*, Science Press, Beijing.

LU L., HAN X., LI J., HUA J., OUYANG M., 2013, *A review on the key issues for lithium-ion battery management in electric vehicles*, J. Power Sources, 226, 272-288.

MENENDEZ M., VIDAL A., TORANO J., GENT M., 2004, *Optimisation of spodumene flotation*, Eur. J. Miner. Process. Environ. Protec., 4, 130-135.

MOON K.S., 1985, *Surface and crystal chemistry of spodumene and its flotation behavior*, University of California, Berkeley, Vol. Ph. D.

MOON K.S., FUERSTENAU D.W., 2003, *Surface crystal chemistry in selective flotation of spodumene $(LiAl[SiO_3]_2)$ from other aluminosilicates*, Int. J. Miner. Process., 72, 11–24.

NICHOLSON, P., 1978, *Past and future development of the market for lithium in the world aluminum industry*, Int. J. Energy, 235-413.

RAI B., SATHISH P., TANWAR J., PRADIP, MOON K.S., FUERSTENAU D.W., 2011, *A molecular dynamics study of the interaction of oleate and dodecylammonium chloride surfactants with complex aluminosilicate minerals*, J. Colloid Interface Sci., 362, 510–516.

RAO D.S., 2010, *Effects of modulus and dosage of sodium silicate on limestone flotation*, Maejo Int. J. Sci. Technol., 4, 397–404.

THOMAS C.E., 2009, *Fuel cell and battery electric vehicles compared*, Int. J. Hydrogen Energ., 34, 6005–6020.

WENDT G., 1971, *Operating experiences with electrolytes containing lithium fluoride*, Metall. Trans., 2, 155–161.

WHITTINGHAM M.S., 2004, *Lithium batteries and cathode materials*, Chem. Rev., 104, 4271–4301.

YI X., 2011, *Test study on low temperature flotation of spodumene*, Chin. Mine Eng., 40, 20–43.

YU F., WANG Y., WANG J., XIE Z., 2014, *Investigation on different behavior and mechanism of Ca^{2+}, Fe3+ adsorption on spodumene surface*, Physicochem. Probl. Miner. Process., 50, 535–550.

ZHONG H., LEI M., LV L., LUO L., 2012, *Study on beneficiation process of low grade refractory spodumene ore*, Non-Metallic Mines, 35, 28–65.

INVESTIGATION OF QUARTZ FLOTATION FROM DECARBURIZED VANADIUM-BEARING COAL

Liuyi REN, Yimin ZHANG, Ying BIAN, Xiang LIU, Chun LIU

College of Resources and Environment Engineering, Wuhan University of Technology, Wuhan 430070, China, rly1015@163.com (Liuyi Ren)

Abstract: Ether diamine (Fm 2835-2L) was used as a collector for flotation of quartz. It allows flotation of quartz from mica and calcite. The adsorption mechanism of Fm 2835-2L on quartz was investigated by flotation tests, zeta-potential measurements and infra-red (FTIR) spectra measurements. Results show that Fm 2835-2L adsorbs on the quartz surface in physical adsorption with no new products, changing its zeta potentials, and increasing its hydrophobicity. The effect of calcium ions on flotation of quartz was investigated by flotation tests and zeta-potential measurements. Results show that under neutral or weakly acidic conditions calcium cation can adsorb onto the surfaces of quartz, increase the zeta potential of quartz particles, which in turn causes weaker aggregation of quartz particles and lower flotation recovery of quartz. Under the alkaline conditions the hydrolytic components of calcium are also adsorbed on the quartz surface and increase the zeta potential of quartz particles, which causes stronger aggregation of quartz particles and higher flotation recovery of quartz. However, the hydrolytic components such as $CaOH^+$, $Ca(OH)_{2(aq)}$ and $Ca(OH)_{2(s)}$ were not formed in significant amounts in the best flotation tests.

Introduction

In recent years, the enrichment of vanadium-bearing coal has becoming an important issue (Ni et al., 2010; Wu et al., 2008). Many studies have been devoted to reduce the cost of vanadium extraction from coal and to facilitate utilization of resources below cut-off grade (Zhao et al., 2013a; Zhao et al., 2013b). However, there a limited number of papers on mechanism of the vanadium materials enrichment process. Therefore, it is necessary to study the effect of various parameters on enrichment process.

In the vanadium-bearing coals, about 90% vanadium occurs in muscovite. Quartz is the main gangue mineral in the muscovite ores, which results in a low purity of muscovite and limits its wide applications. Therefore, there is an urgent need for

improvement of beneficiation of low grade muscovite ores. In many studies quartz is removed by screening and gravity separation due to differences in shape, hardness and density of ore components. However, these methods provide poor efficiency in case of particles below 50 µm in size (Wang et al., 2014).

Ether monoamine and ether diamine are used as the collectors for flotation of silicate gangue minerals in the iron ore industry. It is known that diamines are strong collectors for quartz in comparison to monoamines with comparable chain length (Ma et al., 2009; Smith and Scott, 1990; Scott and Smith, 1991). This is due to smaller pK_a values of diamines in comparison to monoamines and the doubly charged amine species of the diamines promoting stronger flotation of quartz (Scott and Smith, 1991).

In practical mineral separations, unavoidable metal ions such as Fe(III), Mg (II), and Ca (II) can profoundly affect the flotation of minerals (Fan and Rowson, 2000; Zhu et al., 2012). These ions can activate the gangue minerals, thereby increasing their flotation by promoting collector adsorption (Ejtemaeia et al., 2012). Wang and Yu (2007) investigated the effects of metal ions on the flotation of spodumene and beryl sand and found that Fe(III) and Ca(II) ions improved flotation. However, it largely depends on the type of collector used (i.e. anionic, cationic, or amphoteric). In most cases, metal ions are highly detrimental to the process during flotation of the oxide minerals. The activation of the silicates by metallic cations impairs the selectivity of the separation of the oxides and silicates such as beryllium minerals from quartz (Ejtemaeia et al., 2012). Fornasiero and Ralston (2005) studied the Cu(II) and Ni(II) activation in the flotation of quartz, lizardite and chlorite minerals. They found that quartz can be activated by these metal ions to float with xanthate at pH 7–10. Since the copper and nickel hydroxides are stable species, their adsorption/precipitation on the mineral surface improves the flotation of these minerals. All metal ions such as Fe(III), Mg(II), Ca(II), Cu(II), and Ni(II), may have potential as activators in the flotation of albite, spodumene, and quartz minerals.

The objective of the present investigation is to improve understanding of the effect of metal ions on quartz flotation and the underlying adsorption mechanism of ether diamine as collector in flotation of quartz from vanadium-bearing mica present in coal. Flotation performance of Fm 2835-2L as the collector was assessed by flotation tests using single minerals and a decarburized sample of vanadium-bearing coal. Their adsorption on minerals was analyzed by zeta-potential measurement and the Fourier transform infrared (FTIR) spectroscopy. The effect of ion dissolution in flotation system on the quartz flotation during enrichment process of vanadium-bearing coal was studied by different flotation technology and ion dissolution. In this paper, the results of these investigations were discussed and the role of ether diamine collector and calcium ion dissolution in quartz flotation is delineated.

Materials and methods

Materials

The vanadium-bearing stone coal was collected from Teng-da Mining and Metallurgy Co. Ltd., Hubei, PR China. Around 200 kg of representative ore samples were crushed to below 2 mm size with two-stage jaw crusher and one-stage roll crusher. The materials were then well mixed and divided into 2 kg samples for mineralogical and pre-concentration studies. Quartz was obtained from the mineral processing laboratory of Wuhan University of Technology. The chemical analysis showed that it contained more than 99% SiO_2 and was sufficiently pure for research purposes. Ether diamine (Flotigam 2835-2L from Clariant) was used as collector for quartz. The 2# oil, also known as terpenic oil, a mixture of higher alcohols, widely used as foaming agent or collector in the non-ferrous metal flotation was also used. Other chemicals employed in the test were of A.R. grade. Single mineral experiments were carried out with distilled water only.

Methods

The crushed materials were firstly decarburized in a SXZ-10-B muffle furnace at 700 °C for 90 min. The loss on ignition was between 12 and 13%. Then, the decarburized sample was mixed and divided into 200 g samples for quartz flotation. In the flotation NaOH and H_2SO_4 were used as modifiers, sodium silicate as inhibitor, Fm 2835-2L as collector, and oil as foaming agent. The flotation of decarburized sample was conducted in a single XFDⅡ0.5 flotation cell at the pulp density of 50%.

Single quartz flotation tests were conducted in a flotation cell having 40 cm^3 in volume. In each test, the mineral sample of 2 g was placed into flotation cell to disperse for 3 min, followed by adjusting the pH value for 3 min, and then mixed with the collector Fm 2835-2L for 5 min, floated for 5 min. Finally, the product was filtered, dried, weighed and analyzed.

The determination of vanadium, silicon and calcium content was performed in accordance with test Methods of Vanadium in Coal Standard (GB/T19226-2003) and by the potassium dichromate volumetric method. Others analyses were performed with the Xios advanced X-ray fluorescence (XRF) analyzer.

X-ray diffraction (XRD) analysis was conducted with a D/Max-IIIA X-ray diffractometer using Cu-Kα radiation, voltage 40 kV, current 30 mA at the scanning rate of 15°/min from 3° to 70°. The phases were identified by comparison of the peak positions and *d* values with the data published by the International Centre for Diffraction Data (ICDD).

Detailed mineralogy on the head ore and decarburization samples were done using a Leica DMLP polarization microscope while the quantitative evaluation of minerals by scanning electronic microscopy (QEMSCAN).

In order to characterize the nature of the interactions between the collector and quartz particles, the infrared spectra of collector as well as the samples with or without

collectors pretreated were measured by the KBr technique. Fourier transform infrared (FTIR) spectra of the samples were recorded with a Nicolet Model Nexus 670 (USA) instrument using KBr pellets at a resolution of 4 cm^{-1}.

Zeta potential of quartz was determined with a Coulter Delsa440sx Instrument (Beckmen-Coulter/USA). The measurements were conducted by inserting 0.5 g of mineral into 100 cm^3 of surfactant solution. NaOH (1%, mass fraction) and H_2SO_4 (1%, mass fraction) solutions were used for adjusting pulp pH. An average of six measurements was performed for each mobility point.

Results and discussions

Mineralogy of decarburization

Roasting decarburization was employed to eliminate the effect of carbon on mineral separation. The roasting temperature was 700 °C due to beneficial effect of this temperature on the subsequent leaching process and mineral surface property. The decarburized sample was analyzed using the quantitative evaluation of minerals approach by scanning electron microscopy (see Fig. 1). The chemical and mineral compositions of the decarburized samples are shown in Tables 1 and 2, respectively. The grade of V_2O_5 after roasting increased from 0.71% to 0.82%, pyrite was converted to hematite, and calcite was decomposed into CaO and CO_2 because of the local overheating of muffle. Silicate minerals were mainly in the form of amphibole and olivine, whereas sulfate minerals were primarily composed of calcium, sulfur, and other elements. The calorific value produced in the roasting process can be used for a subsequent leaching.
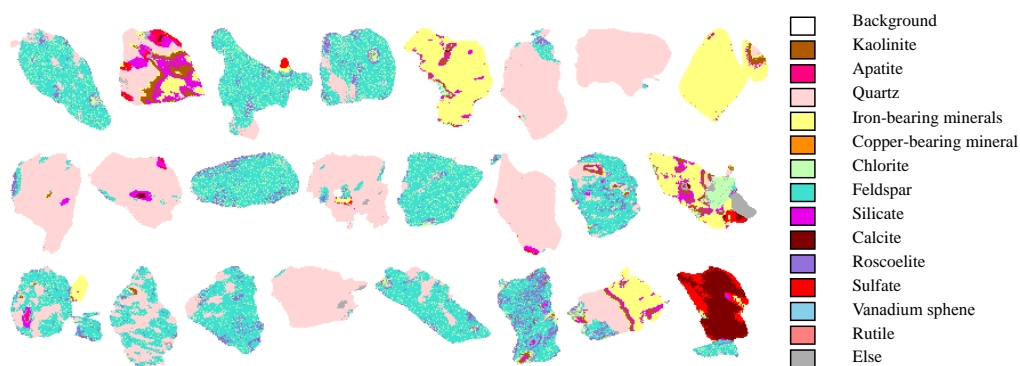

Fig. 1. Mineralogical phase of decarburization sample (-150 +75 μm)

Table 1. Chemical composition of decarburized sample (%)

Element	V_2O_5	SiO_2	Al_2O_3	Fe_2O_3	K_2O	Na_2O	CaO	MgO	S	C
Content	0.82	54.31	10.59	5.67	4.90	0.35	7.35	3.13	1.90	2.72

Table 2. Mineral composition of decarburized sample (%)

Mineral	Quartz	Calcite	Muscovite	Feldspar	Iron mineral	Kaolinite	Silicate	Sulfate	Other
Content	34.21	5.97	12.81	12.72	12.88	5.00	3.52	3.60	9.29

Single mineral flotation

To investigate the flotation of quartz alone, the Fm 2835-2L collector was used. The results are summarized in Fig. 2. The recovery of quartz increases with the concentration of Fm 2835-2L. When the concentration is greater than 50 mg/dm^3, the recovery reaches a plateau. The effect of the pH on the flotation of quartz in the presence and absence of Fm 2835-2L is shown in Fig. 2 b. The results indicate that the recovery changes a little with the pH value from 5.0 to 9.0 (±0.2) in the presence of Fm 2835-2L. The recovery decreases sharply to 84.8% at about pH 10.0. The highest recovery at pH 7.1 is below 30% in the absence of collector. This result indicates that quartz does not have natural floatability. It also corresponds with the results of other invetsigations.
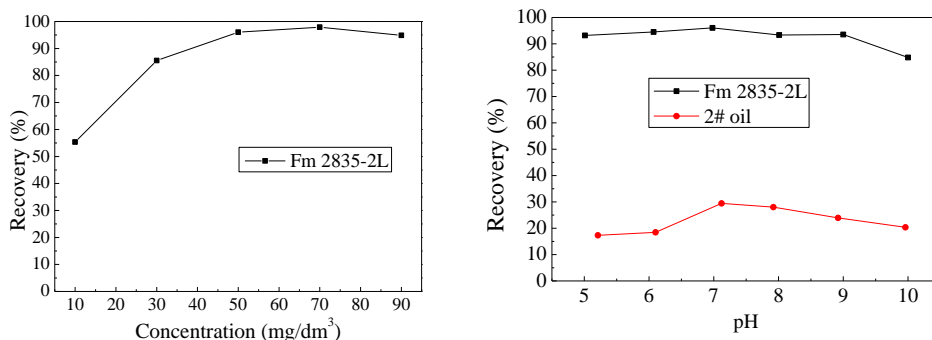

Fig. 2. Effect of pH and collector concentration on quartz flotation, a) relation between recovery and collector concentration at pH 7.1 , b) relation between recovery and pH with and without collector (2# oil content was 30 mg/dm^3 while Fm 2835-2L was 50 mg/dm^3

The adsorption mechanism of collector on quartz was investigated using the infrared analysis and zeta potential, as shown in Figs 3 and 4. The IR spectra of quartz, Fm 2835-2L, and the interaction product are given in Fig. 3. The IR spectrum of quartz (see Fig. 3 curve 1) agrees well with the standard spectrum of SiO2. It exhibits two strong Si—O absorption band at about 1100 cm^{-1} and 500 cm^{-1}. The Si—O and Si—O—Si stretching band can be seen in the wavenumber range of 1081.87−1170.58 and 779.10−796.46 cm^{-1} respectively. After the interaction with Fm 2835-2L, the IR spectrum of quartz (see Fig. 3 curve 2) gives no other characteristic absorption peaks showing that the adsorption on the surface of the quartz is physical.
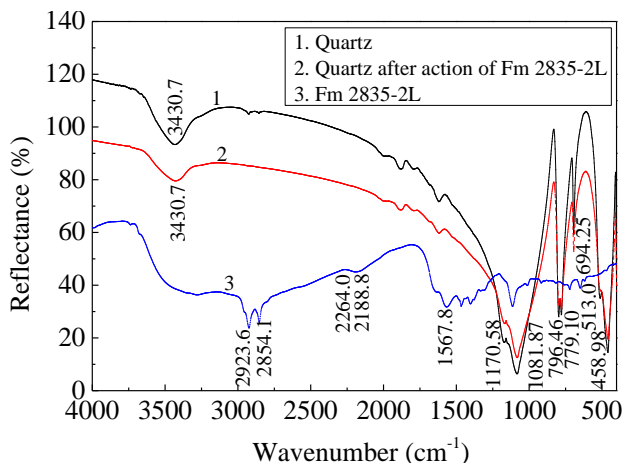
Fig. 3. Infrared spectra of quartz, quartz after action of Fm 2835-2L and pure Fm 2835-2L
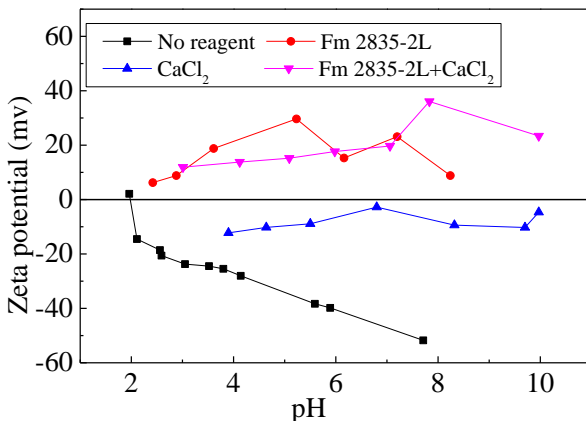

Fig. 4. Relationship between zeta potential of quartz and pulp pH
with or without collector and regulator

Zeta-potential of quartz in the presence of no reagent, Fm 2835-2L, $CaCl_2$ and mixed Fm 2835-2L and $CaCl_2$ as a function of pH are illustrated in Fig. 4. The quartz iso-electric point (iep) is about 2.0. The results indicates that the ether diamine (Fm 2835-2L) has a strong influence on the quartz zeta-potential and increases the charge on quartz at all pH values. Quartz is negatively charged when the pH exceeds 2.0. The positively charged Fm 2835-2L absorbs on the quartz surface through electrostatic interactions. However, when the pH of the solution is less than 2.0, quartz is positively charged.

$CaCl_2$ also has a strong influence on the quartz zeta-potential and increases the charge of quartz at all pH values but surface is negatively charged up to pH 10. Figure 4 also indicated that when both Fm 2835-2L and $CaCl_2$ interact with quartz, the zeta-

potential of quartz increases only in the alkaline solutions. The reason may be that when calcium cations are present in the flotation pulp, under neutral or weak acidic conditions, these cations decrease aggregation of quartz particles by increasing the zeta potential of the quartz particles. Therefore, the flotation recovery of quartz declines in the presence of calcium ions, while under the alkaline conditions, the adsorption of other components of calcium increases the zeta potential of quartz particles and improve its recovery.

Quartz flotation from decarburized vanadium-bearing coal

According to the flowsheet of the process shown in Fig. 5, the flotation of quartz from the decarburized sample of vanadium-bearing coal was studied using Fm 2835-2L as collectors in the presence of Ca (II). Based on the results of single quartz flotation, 50g/Mg of Fm 2835-2L was used at pH 7.0 in the absence of additives and in the presence of Ca (II) which was leached out from the decarburization sample. The results in Table 3 indicate that concentrate grade was 51.13% SiO_2 and it was lower than that in the feed (54.31%). Thus, quartz was not enriched by flotation with Fm 2835-2L. However, the minerals containing vanadium were slightly better recovered than quartz because V_2O_5 content increased to 1.04% from 0.82%. It is known that all the amines are relatively strong collectors for quartz (Wang et al., 2014; Liu et al., 2011; Vidyadhar and Hanumantha, 2007) and it has been confirmed in the single quartz flotation. However, the obtained results (Table 3) contradict this fact when flotation is performed for the decarburized sample of vanadium-bearing coal. Probable surface chemical phenomena giving rise to the observed experimental results will be discussed in the following section.

Table 3. Results of removing quartz from decarburized coal without pre-desliming. Numbers in %

Production	Yield	V_2O_5		CaO		SiO_2	
		Grade	Recovery	Grade	Recovery	Grade	Recovery
Concentrate	34.67	1.04	43.97	2.01	9.48	51.13	32.64
Tailing	65.33	0.70	55.77	10.18	90.52	56.00	67.36
Feeding	100.00	0.82	100.00	7.35	100.00	54.31	100.00

It was known that pre-desliming improves vanadium enrichment (Bian, 2014). In this part of investigations, classification by sedimentation was used to remove slimes below 0.04 mm in size and the coarse grains above 0.04 mm. Next, to further remove the slimes, flotation at pH 9.4 with 2# oil was performed, followed by a second flotation to remove quartz at about pH 7.0 with Fm 2835-2L as the collector. The results of the process are shown in Fig. 6 and Table 4.
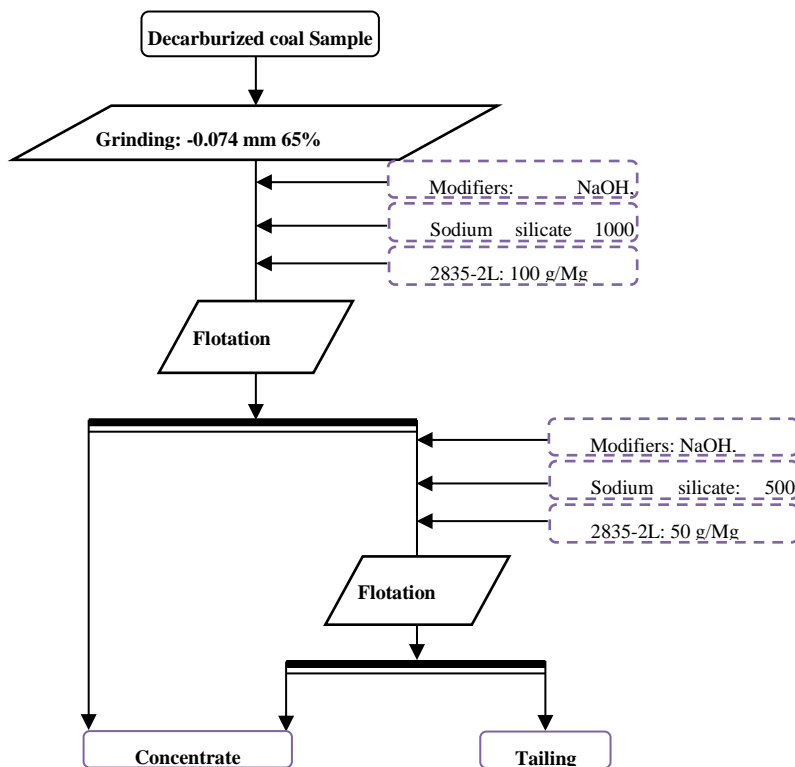
Fig. 5. Flowsheet for removing quartz from coal

Table 4. Results of removing quartz from decarburized coal after pre-desliming (%)

Production	Yield	V$_2$O$_5$		CaO		SiO$_2$	
		Grade	Recovery	Grade	Recovery	Grade	Recovery
Slime	22.22	0.84	22.76	7.01	21.19	62.62	25.62
Slime	12.69	0.92	14.24	5.68	9.81	36.62	8.56
Concentrate	33.02	0.67	26.98	1.52	6.83	75.00	45.60
Tailing	32.07	0.93	36.37	14.25	62.17	34.25	20.22
Feeding	100.00	0.82	100.00	7.35	100.00	54.31	100.00

As Table 4 demonstrates, quartz was enriched in concentrate to 75% of SiO$_2$ through classification and flotation desliming. The 2# flotation product (slime) contained fine grains also noticed by Bian (2014). One reason of better separation results may be that the pre-desliming process removed the detrimental ions from the flotation system. The addition of Fe^{3+} may be another reason of improvement of quartz recovery. Zhang et al. (2014) proved that Fe(III) was an activator for the flotation of

quartz. To discuss this issue, ion dissolution would be studied in the following part of paper.
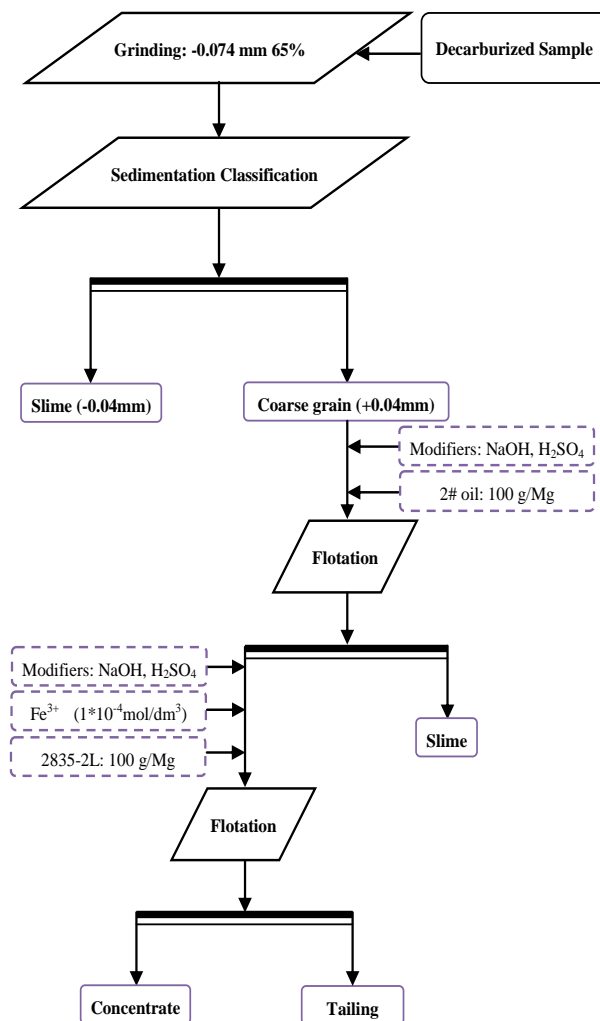

Fig. 6. Flowsheet for removing quartz from coal after pre-desliming

Influence of roasting on ion dissolution in flotation process

In flotation process, separation can be affected by polyvalent metal cation present in the slurry. The reason may be that the change of mineral composition and crystal structure after roasting lead to dissolution of ion. Therefore, polyvalent metal cations concentration in three kinds of slurry was determined by ICP and the results were shown in Table 7. Coal and decarburized coal were milled to -0.074 mm 63% and then mixed with aqueous solution and stirred for 10 min. The supernatant of the mixture

was used for ion concentration determination by means of ICP. The ion concentration of the flotation slurry of decarburized and deslimed stone coal was also tested by the same method. Otherwise, the ion concentrations of the three kinds of slurry were tested at the same slurry concentration, stirred for the same time (10 min), rest for 5 min to produce the supernatant.
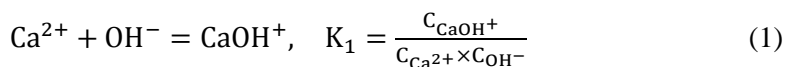
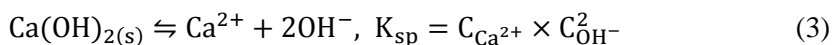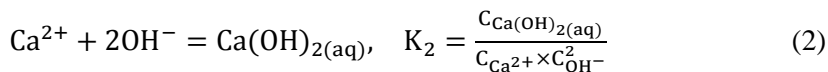Table 5. Polyvalent metal cation ion concentration in slurry (mg/dm^3)

Sample	Si^{4+}	Al^{3+}	Fe^{3+}	Mg^{2+}	Ca^{2+}	Ba^{2+}
The head ore of coal	2.153	1.169	3.286	24.41	418.900	0.127
Decarburized coal	5.040	0.304	0.234	30.56	1267.000	0.874
Decarburized and deslimed coal	1.317	0.164	0.004	1.278	425.500	0.235

As shown in Table 5, the iron concentration in slurry changes sharply after the roasting decarburization of the stone coal. The concentration of Al^{3+} and Fe^{3+} ion decreased, while the concentration of Si^{4+}, Mg^{2+}, Ca^{2+} and Ba^{2+} increased. However, the ion concentration in solution after desliming decreased sharply. Studies of Ejtemaeia et al., 2012; Fornasiero and Ralston, 2005; Lev et al., 2012; Xu et al. 2013 have shown that in the sodium oleate flotation system and pH 8~10 the ions of Al^{3+}, Fe^{3+} and Ca^{2+} strongly activate the phyllosilicates minerals, while in dodecylamine flotation system, those ions have a strong suppression of the phyllosilicate minerals, while higher valence ions have a stronger suppression. Hence, most of polyvalent metal ions in the slurry can decrease the separation of calcite and mica. Roasting decreased Al and Fe content in the trivalent state, increased significantly Mg, Ca and Ba content in the divalent state. Roasting process resulted in the change of ion concentration in slurry, which is unfavorable for flotation.

Solution chemistry of Ca^{2+} in quartz flotation

The adsorption of calcium ions on quartz was influenced by the pulp pH significantly. The results of previous research on the relationship between pH and calcium ions adsorption on the quartz indicated that calcium ions are adsorbed on the surface of the quartz when the pH value was above 10.7 and the adsorption reached the peak when pH was 12.3 (Wang and Hu, 1987). It was known that metal ions activation of mineral was mainly due to the formation of hydroxy complexes, which required strict pH conditions. Therefore, the dissolved calcium species were studied. The following equilibrium equations can be considered:

$$Ca^{2+} + OH^- = CaOH^+, \quad K_1 = \frac{c_{CaOH^+}}{c_{Ca^{2+}} \times c_{OH^-}} \tag{1}$$

$$Ca^{2+} + 2OH^- = Ca(OH)_{2(aq)}, \quad K_2 = \frac{C_{Ca(OH)_{2(aq)}}}{C_{Ca^{2+}} \times C_{OH^-}^2} \tag{2}$$

$$Ca(OH)_{2(s)} \leftrightharpoons Ca^{2+} + 2OH^-, \quad K_{sp} = C_{Ca^{2+}} \times C_{OH^-}^2 \tag{3}$$

The balance for Ca is:

$$C_{Ca} = C_{Ca^{2+}} + C_{CaOH^+} + C_{Ca(OH)_{2(aq)}} \tag{4}$$

Taking the logarithm of Eqs. (1), (2) and (3) yields:

$$\lg K_1 = \lg C_{CaOH^+} - \lg C_{Ca^{2+}} - \lg C_{OH^-}, \tag{5}$$

$$\lg K_2 = \lg C_{Ca(OH)_{2(aq)}} - \lg C_{Ca^{2+}} - \lg C_{OH^-}, \tag{6}$$

$$\lg Ca(OH)_{2(s)} = \lg C_{Ca^{2+}} + \lg C_{OH^-} \tag{7}$$

For $\lg K_1 = 1.4$, $\lg K_2 = 2.77$, $pK_{sp} = 5.22$ the calcium ion concentration in the decarburized coal flotation system is 1267.000 mg/dm^3, thus $C_{Ca} = 3.168 \times 10^{-2}$ mol/dm^3. Solving Eqs. (4) to (7), the relation between $C_{Ca^{2+}}$, C_{CaOH^+}, $C_{Ca(OH)_{2(aq)}}$ and pH can be represented by Eqs. (8) to (11):

$$\lg C_{Ca^{2+}} = -1.5 - \lg(1 + 25.12 \times 10^{pH-14} + 588.84 \times 10^{pH-14}), \tag{8}$$

$$\lg C_{CaOH^+} = pH - 14.1 - \lg(1 + 25.12 \times 10^{pH-14} + 588.84 \times 10^{pH-14}), \tag{9}$$

$$\lg Ca(OH)_{2(aq)} = 2pH - 26.73 - \lg(1 + 25.12 \times 10^{pH-14} + 588.84 \times 10^{pH-14}), \tag{10}$$

$$\lg Ca(OH)_{2(s)} = 2pH - 29.75 - \lg(1 + 25.12 \times 10^{pH-14} + 588.84 \times 10^{pH-14}). \tag{11}$$

The log c-pH diagram is illustrated in Fig. 7. The results of Fig. 7 indicated that hydroxy complex of Ca are formed when pH value is above 9.1. It can activate quartz and improve its recovery (Xie, 2011). However, the best pH condition for Fm 2835-2L flotation of quartz is about 7.0. The hydrolytic components (CaOH$^+$, Ca(OH)$_{2(aq)}$, Ca(OH)$_{2(s)}$) are not formed in insignificant amounts, and only Ca^{2+} can be adsorbed on the surface of quartz and influence its recovery. Based on the available data (Xie, 2011; Fuerstenau and Han, 2002), Ca(OH)$_{2(aq)}$ is not formed at pH values lower than 12.0, until the calcium ion concentration exceeds $5 \cdot 10^{-2}$ mol/dm^3, higher than 3.168×10^{-2} mol/dm^3 in this study. Thus, Ca(OH)$_{2(aq)}$ was not considered in this analysis. Also, at this calcium concentration, Ca(OH)$_{2(s)}$ forms when pH exceeds 12.3. Therefore, Ca(OH)$_{2(s)}$ precipitate was not considered here. Solution chemistry analysis of Ca^{2+} agree with the data of Wang and Hu (1987), Xie (2011) and Fuerstenau and

Han (2002) and the zeta potential measurement already presented in this study. Thus Ca must be eliminated to improve the quartz floatability when Fm 2835-2L is used as the collector.
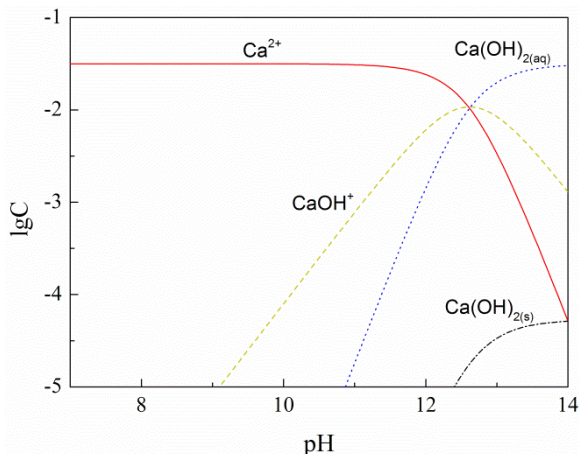

Fig. 7. Relation between log c and pH for Ca^{2+}, $CaOH^{+}$, $Ca(OH)_{2(aq)}$, $Ca(OH)_{2(s)}$ in decarburized coal pulp

Conclusions

Ether diamine collector (Fm 2835-2L) adsorbs on the quartz surface by physical adsorption changing its zeta potentials significantly increasing its flotation. Under neutral or weakly acidic conditions calcium cation can adsorb onto the surfaces of quartz, increase the zeta potential of quartz particles, which in turn causes weaker aggregation of quartz particles and lower flotation recovery of quartz, and the hydrolytic components such as $CaOH^{+}$, $Ca(OH)_{2(aq)}$ and $Ca(OH)_{2(s)}$ are not formed in significant amounts in the best flotation tests. Ca must be eliminated in quartz flotation from decarburized vanadium bearing coal when Fm 2835-2L is used as the collector.

Acknowledgments

References

BIAN, Y., 2014, *Mineralogy Process and Pre-concentration Technology of Mica-type Vanadium-bearing Stone Coal*, *Wuhan University of Technology*, Thesis, pp56.

EJTEMAEIA, M., IRANNAJAD, M., GHARABAGHI, M, 2012, *Role of dissolved mineral species in selective flotation of smithsonite from quartz using oleate as collector*, Int. J.Miner. Process. 114–117, 40–47.

FAN, X.; ROWSON, N. A., 2000, *The effect of Pb(NO3)2 on ilmenite flotation*, Miner. Eng. 13, 105–115.

FORMASIERO, D., RALSTON, J., 2005, *Cu(II) and Ni(II) activation in the flotation of quartz, lizardite and chlorite*. Int. J. Miner. Process. 76, 75–81.

FUERSTENAU, M. C., Han, K. N., 2002, *Metal–Surfactant Precipitation and Adsorption in Froth Flotation*, J. Colloid Interface Sci. 256, 175–182.

LEV, O. F., AGATHE, D., INNA, V. F., 2012, *Selective flotation of silicates and Ca-bearing minerals: the role of non-ionic reagent on cationic flotation*, Int. J. Miner. Process. 314–323.

LIU, W. G., WEI, D. Z., CUI, B. Y., 2011, *Collecting performances of N-dodecylethylene-diamine and its adsorption mechanism on mineral surface*, Trans. Nonferrous Met. Soc. China 21, 1155-1160.

MA, M., BRUCKARD W. J., HOLMES, R., 2009, *Effect of collector, pH and ionic strength on the cationic flotation of kaolinite*, Int. J. Miner. Process. 93, 54–58.

NI, H., HUANG, G., YUAN, A. W., WANG, X., ZHOU, X. Y., 2010, *Comprehensive utilization technology for low grade stone coal containing vanadium*, Chin. J. Nonferrous Met. 62, 92–95.

SCOTT, J. L., SMITH, R. W., 1991, *Diamine flotation of quartz*, Miner. Eng. 4, 141–150.

SMITH, R. W., SCOTT, J. L., 1990, *Mechanisms of dodecylamine flotation of quartz*, Miner. Process. Extr. Metall. Rev. 7, 81–94.

VIDYADHAR, A., HANUMANTHA RAO, K., 2007, *Adsorption mechanism of mixed cationic/anionic collectors in feldspar-quartz flotation system*, J. Colloid Interface Sci. 306, 195–204.

WANG, D. Z., HU, Y. H., 1987, *Solution chemistry of flotation*, Hunan Science and Technology Press, 134–143.

WANG, L., SUN, W., HU, Y. H., XU, L. H., 2014, *Adsorption mechanism of mixed anionic/cationic collectors in Muscovite-Quartz flotation system*, Miner. Eng. 64, 44–50.

WANG, Y. H., YU, F. S., 2007, *Effects of metallic ions on the flotation of spodumene and beryl,* J. China Univ. Min. Technol. 17, 0035–0039.

WU, H. L., ZHAO, W., LI, M. T., DENG, Z. G., GE, H. W., WEI, C., 2008, *New craft study on enriching vanadium by means of priority coal flotation from high carbon stone coal*, J. Chin. Rare Earth Soc. 26, 530–533.

XIE, X. Z., 2011, *Study on the Separation of Limonite from Gangues by Flotation and Its Mechanisms*, Central South University, Thesis, pp39–43.

XU, L. H., WU, H. Q., DONG, F. Q., 2013, *Flotation and adsorption of mixed cationic/anionic collectors on muscovite mica*, Miner. Eng. 41–45.

ZHAO, Y. L., ZHANG, Y. M., LIU, T., CHEN, T. J., BIAN, Y., BAO, S. X., 2013, *Pre-concentration of vanadium from stone coal by gravity separation*, Int. J. Miner. Process. 121, 1–5.

ZHAO, Y. L., ZHANG, Y. M., BAO, S. X., LIU, T., BIAN, Y., LIU, X., JIANG, M. F., 2013, *Separation factor of shaking table for vanadium pre-concentration from stone coal*, Sep. Purif. Technol. 115, 92–99.

ZHU, Y. G., ZHANG, G. F., FENG, Q. M., YAN, D. C., WANG, W. Q., 2012, *Effect of surface dissolution on flotation separation of fine ilmenite from titanaugite*, Trans.Nonferrous Met. Soc. China 21, 1149–1154.

ZHANG, J., WANG, W. Q., LIU, J., HUANG, Y., FENG, Q. M., ZHAO, H., 2014, *Fe(III) as an activator for the flotation of spodumene, albite, and quartz minerals*, Miner. Eng. 61, 16–22.

COMPARISON OF SELECTED METHODS OF MULTI-PARAMETER DATA VISUALIZATION USED FOR CLASSIFICATION OF COALS

Dariusz JAMROZ*, Tomasz NIEDOBA**

* AGH University of Science and Technology, Faculty of Electrical Engineering, Automatics, Computer Science and Biomedical Engineering, Department of Applied Computer Science, al. Mickiewicza 30, 30-059 Krakow, Poland, jamroz@agh.edu.pl
** AGH University of Science and Technology, Faculty of Mining and Geoengineering, Department of Environmental Engineering and Mineral Processing, al. Mickiewicza 30, 30-059 Krakow, tniedoba@agh.edu.pl

Abstract: Methods of multi-parameter data visualization through the transformation of multidimensional space into two-dimensional one allow to present multidimensional data on computer screen, thus making it possible to conduct a qualitative analysis of this data in the most natural way for human – by a sense of sight. In the paper a comparison was made to show the efficiency of selected seven methods of multidimensional visualization and further, to analyze data describing various coal type samples. Each of the methods was verified by checking how precisely a coal type can be classified when a given method is applied. For this purpose, a special criterion was designed to allow an evaluation of the results obtained by means of each of these methods. Detailed information included presentation of methods, elaborated algorithms, accepted parameters for best results as well the results. The framework for the comparison of the analyzed multi-parameter visualization methods includes: observational tunnels method multidimensional scaling MDS, principal component analysis PCA, relevance maps, autoassociative neural networks, Kohonen maps and parallel coordinates method.

Introduction

Multidimensional analysis of data is becoming an increasingly efficient statistical tool of data analysis. There are several methods of such approach which are being used much more often than in the past because of natural development of informatics. Modern statistical software allows the operator to analyze even huge sets of data

relatively fast and with adequate precision. There are many books and articles in the field of mineral processing concerning such problems in many aspects such as (Ahmed and Drzymala, 2005; Gawenda et al., 2005; Brozek and Surowiak, 2005; 2007; 2010; Lyman, 1993; Niedoba 2009; 2011; 2013b; Niedoba and Surowiak, 2012; Saramak, 2011; 2013; Snopkowski and Napieraj, 2012; Tumidajski and Saramak, 2009). The precise description of processes and their characteristics may be found in (Drzymala, 2007; 2009). Among multidimensional statistical analysis methods, special attention should be given to multidimensional visualization methods which are the subject of this paper.

Owing to the methods of multidimensional data visualization through the transformation of multidimensional space into two-dimensional, it is possible to show multidimensional data on the computer screen, thus making it possible to carry out a qualitative data analysis in the most natural way for a human being – by a sense of sight. Many methods had been used previously for analyzing multidimensional coal data, i.e. observational tunnels method (Niedoba and Jamroz, 2013; Jamroz and Niedoba, 2014), Kohonen network (Jamroz and Niedoba, 2015), multidimensional scaling (Jamroz, 2014b), relevance maps (Niedoba, 2015), PCA (Niedoba, 2014), autoassociative neural networks (Jamroz, 2014c) and parallel coordinates (Niedoba and Jamroz, 2013). Thanks to the above methods, results have been obtained for coal and they have been described in several papers. This paper presents a comparison of the above-mentioned multi-parameter visualization methods.

Apart from multi-parameter methods, there are also several other methods which can be applied to many purposes. These include: grand-tour method (Asimov, 1985), method of principal component analysis (Hotelling, 1933; Jolliffe, 2002), use of neural networks for data visualization (Aldrich, 1998; Jain and Mao, 1992; Kohonen, 1989), parallel coordinates method (Inselberg, 2009), multidimensional scaling (Kruskal, 1964), the scatter-plot matrices method (Cleveland, 1984), method using the so-called relevance maps (Assa et al., 1999), method of observational tunnels (Jamroz, 2001; 2014a). Furthermore, the visualization of multidimensional solids is also possible (Jamroz, 2001; 2009).

Experiment

Three types of coal, 31 (energetic coal), 34.2 (semi-coking coal) and 35 (coking coal) according to the Polish classification, were used in the investigation (Olejnik et al., 2010). Seven-parameter data consisted of 205 samples, including 72 samples of the coal type 31, 61 samples of the coal type 34.2 and 72 samples of the coal type 35. The whole set of data used in this paper can be found in Niedoba (2013a). They were obtained from three different Polish coal mines. Subsequently, all of them were initially screened on a set of sieves of the following sizes: –1.00, –3.15, –6.30, –8.00, –10.00, –12,50, –14.00, –16.00 and –20.00 mm. Then, the size fractions were additionally separated into density fractions by separation in dense media using zinc

chloride aqueous solution of various densities (1.3, 1.4, 1.5, 1.6, 1.7, 1.8 and 1.9 g/cm^3). The fractions were used as a basis for further consideration and additional coal features were determined by means of chemical analysis. For each density-size fraction such parameters as combustion heat, ash contents, sulfur contents, volatile parts contents and analytical moisture were determined, making up, together with the mass of these fractions, seven various features for each coal type.

Methods

Observational tunnels method

Theoretical grounds of observational tunnels method were described in paper by Jamroz (2001). Intuitively, it may be said that the method of observational tunnels makes use of a parallel projection with a local orthogonal projection of an extent limited by the maximal radius of the tunnel. This solution makes it possible to observe selected parts of a space bearing important information, which, for example, is not possible using an orthogonal projection. Detailed information concerning observation tunnels method, applied algorithm and obtained results for visualization of 7-parameter data describing three coal types were presented in paper by Niedoba and Jamroz (2013).

Multidimensional scaling

Multidimensional scaling (MDS) is the method based on mapping of n-dimensional space into m-dimensional space. It is based on calculation of a distance between each pair of n-dimensional points. On the basis of these distances the considered method determines mutual location of these points images in destined m-dimensional space. Let d_{ij} mean distance between n-dimensional points of no. i and j. Multidimensional scaling is based on such location of points in m-dimensional space that distance D_{ij} calculated in this space between mapped points of no. i and j is possibly closest to d_{ij}. The operation of algorithm MDS can be based on iterative change of location of randomly (initially) located points in m-dimensional space in the way assuring the function $S = \sqrt{\sum_{i>j}\left(D_{ij} - d_{ij}\right)^2}$ achieving the smallest possible value. For $m=2$ this method allows to watch multidimensional data directly on two-dimensional computer screen. Detailed information concerning MDS method, applied algorithm and obtained results for visualization of 7-parameter data describing three coal types were presented in paper by Jamroz (2014b).

Principal Component Analysis

PCA method is one of the statistical methods of factor analysis. It consists of perpendicular projection of multidimensional data on the plane represented by properly selected eigenvectors V_1 and V_2, which are related to the highest eigenvalues

of covariance matrix of observational set. The selection of vectors V_1 and V_2 allows to obtain an image on plane representing the biggest number of data changes whose mutual distance is the biggest. Detailed information concerning PCA method, applied algorithm and obtained results for visualization of 7-parameter data describing three coal types were presented in paper by Niedoba (2014).

Relevance maps

Relevance maps method on plane serving for data visualization is based on placing special points called relevance points which represent individual features of the considered object (Assa, 1999). For each feature (coordinate) the relevance point representing this feature is assigned. That means that by seven-dimensional data set 7 such points are placed on plane which represent individual coordinates. The distribution of the points representing presented multidimensional data shows relations between these data and features. The more i^{th} feature is present in a certain object (which means that i^{th} coordinate is higher), the closest the point representing certain object according to relevance representing i^{th} feature (coordinate) should be. Thus, each relevance point representing a certain feature divides the plane into areas more or less dependent on i^{th} feature (more or less distanced from relevance point representing the ith feature). Detailed information concerning relevance maps method, applied algorithm and obtained results for visualization of 7-parameter data describing three coal types were presented in paper by Niedoba (2015).

Autoassociative neural networks

Autoassociative neural networks are an example of self-organizing neural networks whose learning process occurs without the teacher. When applied to visualization of multi-parameter data, the network has n inputs, one of indirect layers consisting of 2 neurons and n outputs. The number of network inputs and outputs is equal to the number of parameters of the analyzed data. The network is learnt by error backward propagation method. As a result of learning process, the same signals should impact both the outputs and inputs of neural networks. The described network is based on a change of input n-dimensional space B into two-dimensional space Y and then back into n-dimensional space B^* in the most similar way to B. The data going through the layer of two neurons which outputs represent two-dimensional space Y, are compressed by network. Thus, resulting in a two-dimensional preservation of certain individual features of original data from space B, which allows for reconstruction of the data.

When the learning process is over, the data visualization can start. It consists in providing input to each data vector x on the neural network and projecting two-dimensional point representing it (on the basis of data from hidden layer consisting of two neurons). The location of this point is determined by two coordinates taken directly from the outputs of two neurons which constitute indirect layer and represent (in a compressed way) space B. Detailed information concerning autoassociative

neural networks method, applied algorithm and obtained results for visualization of 7-parameter data describing three coal types were presented in paper by Jamroz (2014c).

Kohonen maps

Kohonen maps are an example of self-organizing neural networks in which the learning process occurs without the teacher. They are one-layer networks with competitive learning rules to which the term of neighborhood was introduced. Each network input is connected to each neuron. During the learning process the weights are modified for the neuron – winner, whose output signal that is a response to part of teaching series is the biggest, and, to a lesser degree, for the weights neighboring the neuron winners. The modification of weights occurs in a way so that the neuron response (winner and winner's neighbors) to a given part of teaching series is even bigger.

By accepting the two-dimensional neighborhood (neurons positioned in lines and web columns), it is possible to represent network output directly on the screen in a way that a signal of neuron located in i^{th} line and j^{th} column is shown on the screen as a point of coordinates (i, j). Detailed information concerning Kohonen maps method, applied algorithm and obtained results for visualization of 7-parameter data describing three coal types were presented in paper by Jamroz and Niedoba (2015).

Parallel Coordinates

In parallel coordinates method, there are n parallel axes located on plane, related to n dimensions of space. One point of space is represented by broken curve. This curve is passing through each ith axis in place related to value of ith coordinate of the point. Detailed information concerning parallel coordinates method, applied algorithm and obtained results for visualization of 7-parameter data describing three coal types were presented in paper by Niedoba and Jamroz (2013).

Results and discussion

As part of previous works, for each of the compared methods a computer program was created to obtain views of analyzed multidimensional data. In this way, seven systems were created. All of them were created by means of C++ language with application of Microsoft Visual Studio. All these methods were described in detail in the authors' previous papers, including detailed information about individual methods, elaborated algorithms and accepted parameters allowing to obtain best results. For the purpose of obtaining clear results, the data representing various coal types were analyzed in pairs. Such an approach made it possible to state if images of points representing various coal samples were located in easily separated areas of the figure or otherwise.

Having results obtained in the previous works, it is possible to compare multidimensional data visualization methods in this paper. For evaluation purposes, it

is necessary to test each of the methods by verifying how clearly they allow to state if the amount of information contained in seven coal features is sufficient to classify coal types properly. For this purpose a special criterion must be determined allowing to evaluate the transparency of results. The definition of appropriate criterion is not a simple task. The result of each working program is a view (two-dimensional one) of seven-parameter data describing coal. Here is where the most difficult thing occurs: how to evaluate separated areas of the particular figure when compared to others. Therefore, let us assume that areas of the figure occupied by points representing various coal types will be separated by curve. Furthermore, let us assume that the parameter evaluating the level of complexity of the curve is the number of inflection points. Curve consists of arcs, where arc is the fragment of curve turning in the same direction. Curvature within one arc can change even by transferring into a fragment of straight line. The inflection points are the points connecting arcs turning in various directions. For inflection points determined in this way the second differential is equal to zero. It is assumed that part of the straight line is treated as inflection point only if it connects arcs turning in various directions (although, the second differential for the whole part of line is equal to zero).

The following criterion is accepted: result obtained as the effect of visualization is clearer if the separating curve consists of a lower number of inflection points.

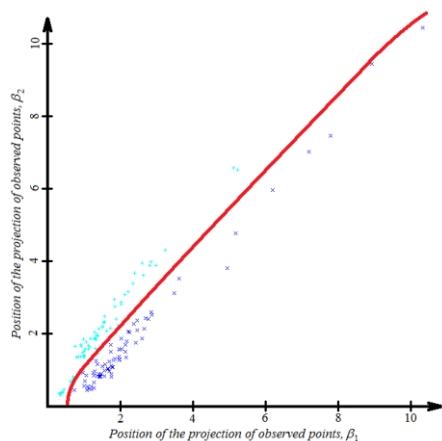On all figures black spots on curves represent inflection points.

Fig. 1. Curve which separates points representing coal type 31 (x) and coal type 34.2 (+) with application of observational tunnels method. The curve has no inflection points
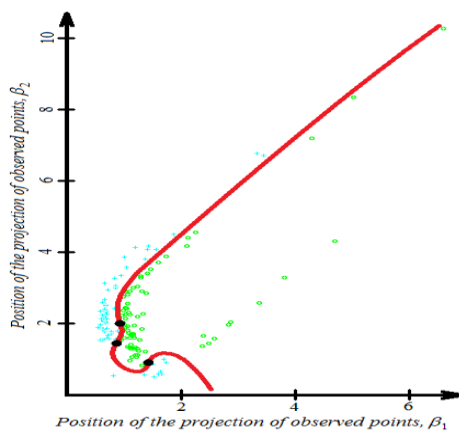
Fig. 2. Curve which separates points representing coal type 34.2 (+) and coal type 35 (o) with application of observational tunnels method. The curve has three inflection points

Figures 1-3 present the views of curves obtained for observational tunnels method. These curves separate areas of the figures occupied by images of points representing various coal types. Figure 1 shows that curve separating points of coal type 31 from coal type 34.2 has no inflection points. This is an example of the least complicated

curve (best separated areas) for the accepted criterion. Figure 2. shows a situation in which curve separating coal type 34.2 and coal type 35 had 3 inflection points. From Fig. 3 it can be observed that curve separating coal type 31 from coal type 35 has only one inflection point. It means that four inflection points were used to obtain three views allowing to state that each coal type can be separated from each other. This value will be the evaluation of observational tunnels method used to create Figs. 1–3.
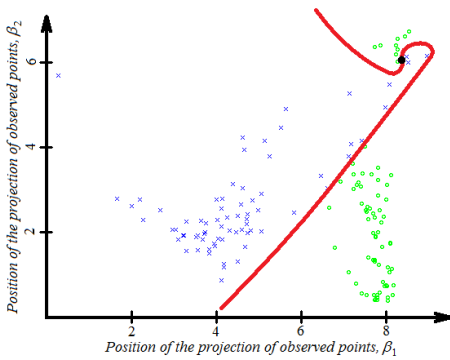

Fig. 3. Curve which separates points representing coal type 31 (x) and coal type 35 (o) with application of observational tunnels method. The curve has one inflection point
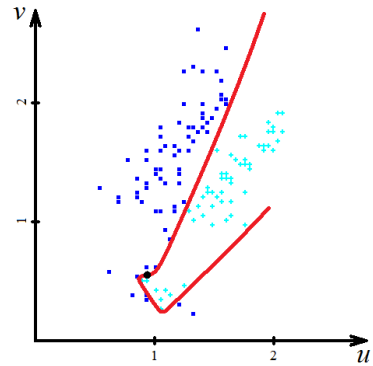

Fig. 4. Curve which separates points representing coal type 31 (■) and coal type 34.2 (+) with application of multidimensional scaling. The curve has one inflection point
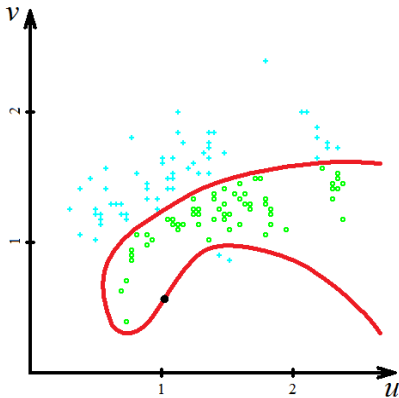

Fig. 5. Curve which separates points representing coal type 34.2 (+) and coal type 35 (o) with application of multidimensional scaling. The curve has one inflection point
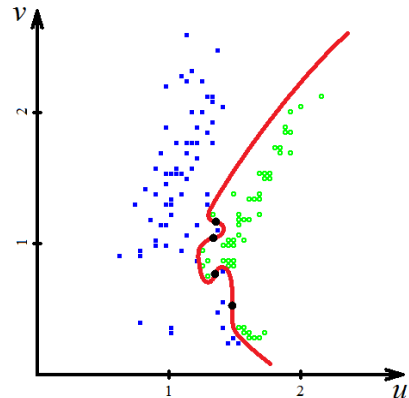

Fig. 6. Curve which separates points representing coal type 31 (■) and coal type 35 (o) with application of multidimensional scaling. Curve has four inflection points

Figures 4–6 present views of curves obtained for multidimensional scaling. Figure 4 shows that curve separating points of coal type 31 from coal type 34.2 has only one

inflection point. Figure 5 shows a situation in which curve separating coal type 34.2 and coal type 35 has also 1 inflection point. From Fig. 6 it can be observed that curve separating coal type 31 from coal type 35 has four inflection points. This is an example of a complicated curve for the accepted criterion. It can be noticed that in this case the possibility of separating points which represent various coal types is not so clear as in the case of, for example, Fig. 1. To use multidimensional scaling for obtaining three views that allow to state that each coal type can be separated from others, curves with 6 inflection points have to be used.

Figures from 7 to 9 present views of curves obtained for PCA method. Figure 7 shows that curve separating points of coal type 31 from coal type 34.2 has even five inflection points. Fig. 8 shows a situation in which curve separating coal type 34.2 and coal type 35 had four inflection points. From Fig. 9 it can be observed that curve separating coal type 31 from coal type 35 had also 4 inflection points. To obtain three views allowing to state that each coal type can be separated from others with the use of PCA method, curves containing a total of 13 inflection points were used.
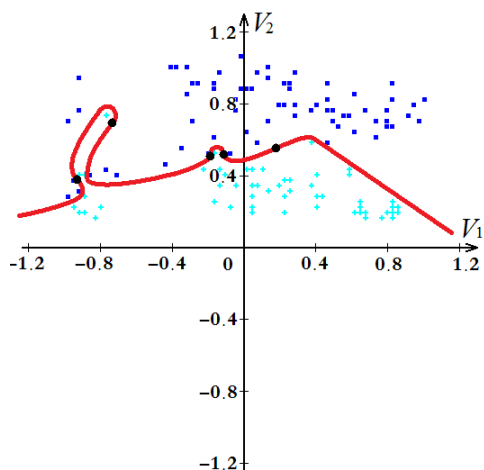

Fig. 7. Curve which separates points representing coal type 31 (■) and coal type 34.2 (+) with application of PCA method. The curve has five inflection points
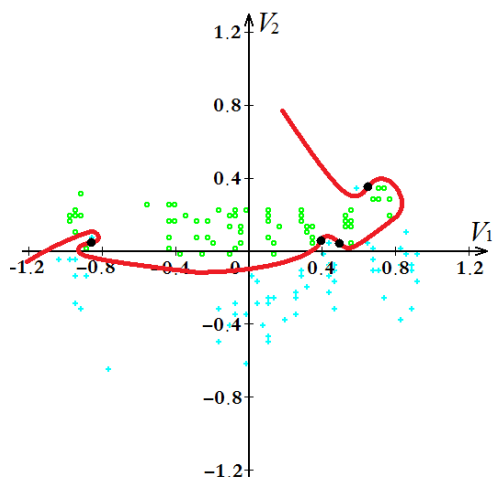
Fig. 8. Curve which separates points representing coal type 34.2 (+) and coal type 35 (o) with application of PCA method. The curve has four inflection points

Figure 10 presents, only for additional information, graph with sorted absolute values of covariance matrix eigenvalues. Eigenvectors related to the largest eigenvalues were used to construct Figs. 7, 8 and 9. In general case, it is possible to evaluate efficiency of PCA method on the basis of these eigenvalues distributions – how much information would be preserved during n-dimensional space mapping into the space determined by k eigenvectors related to k biggest absolute values of covariance matrix eigenvalues obtained by means of PCA method. As it can be seen in the Fig. 10 two first eigenvalues for all three coal pairs are much bigger than the

others. So, it can be stated that majority of the information is mapped on two-dimensional figures presented above which were created as the result of projecting data on two appropriate eigenvectors.
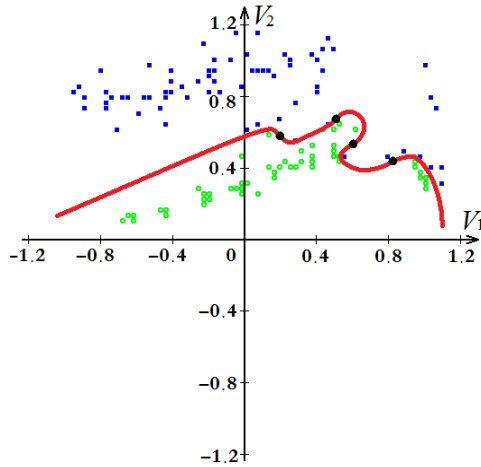

Fig. 9. Curve which separates points representing coal type 31 (■) and coal type 35 (o) with application of PCA method. The curve has four inflection points
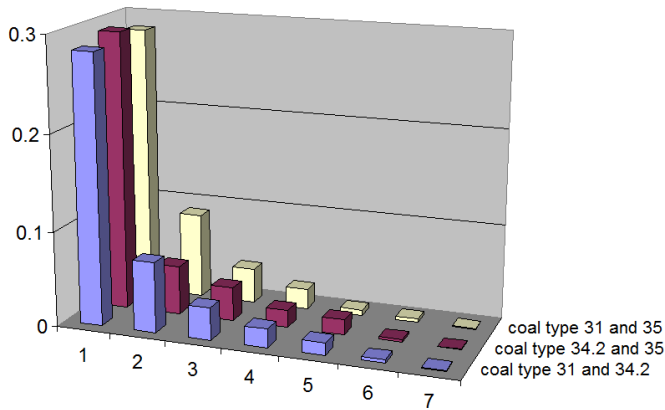
Fig. 10. Sorted absolute values of covariance matrix eigenvalues calculated for data being source for Figs 7-9

Figures 11–13 present views of curves obtained for the relevance maps method. Figure 11 shows that curve separating points of coal type 31 from coal type 34.2 has three inflection points. Figure 12 shows a situation in which curve separating coal type 34.2 and coal type 35 has four inflection points. From Fig. 13 it can be observed that curve separating coal type 31 from coal type 35 has four inflection points. To obtain

three views allowing to state that each coal type can be separated from others with the use of relevance maps, curves containing a total of 11 inflection points were used.

Fig. 11. Curve which separates points representing coal type 31 (■) and coal type 34.2 (+) with application of relevance maps. The curve has three inflection points

Fig. 12. Curve which separates points representing coal type 34.2 (+) and coal type 35 (o) with application of relevance maps. The curve has four inflection points

Fig. 13. Curve which separates points representing coal type 31 (■) and coal type 35 (o) with application of relevance maps. The curve has four inflection points
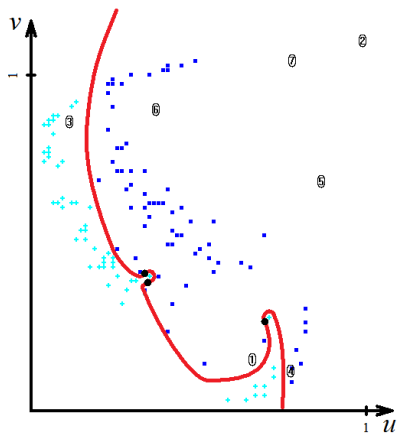

Fig. 14. Curve which separates points representing coal type 31 (■) and coal type 34.2 (+) with application of autoassociative neural networks. The curve has one inflection point

Figures 14–16 present views of curves obtained for autoassociative neural networks. Figure 14 shows that curve separating points of coal type 31 from coal type 34.2 has only one inflection point. Figure 15 shows a situation in which curve separating coal type 34.2 from coal type 35 has no inflection points. From Fig. 16 it

can be observed that curve separating coal type 31 and coal type 35 has 2 inflection points. To obtain three views allowing to state that each coal type can be separated from others with the use of autoassociative neural networks, curves containing a total of 3 inflection points were used. These curves gave the best result. Visualization by means of autoassociative neural networks allows to obtain the clearest results.

Fig. 15. Curve which separates points representing coal type 34.2 (+) and coal type 35 (o) with application of autoassociative neural networks. The curve has no inflection points

Fig. 16. Curve which separates points representing coal type 31 (■) and coal type 35 (o) with application of autoassociative neural networks. The curve has two inflection points

Fig. 17. Curve which separates points representing coal type 31 (x) and coal type 34.2 (+) with application of Kohonen maps. The curve has one inflection point
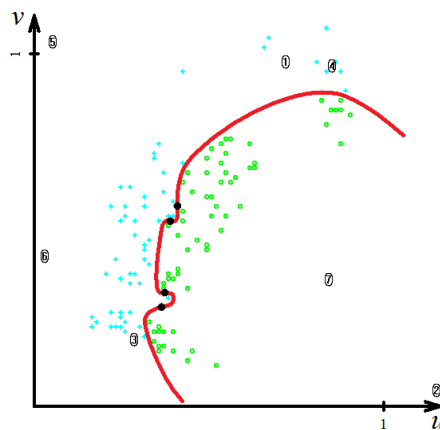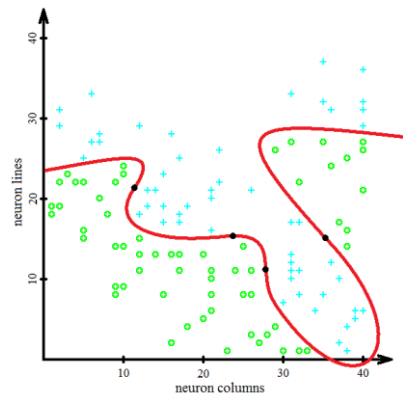

Fig. 18. Curve which separates points representing coal type 34.2 (+) and coal type 35 (o) with application of Kohonen maps. The curve has four inflection points
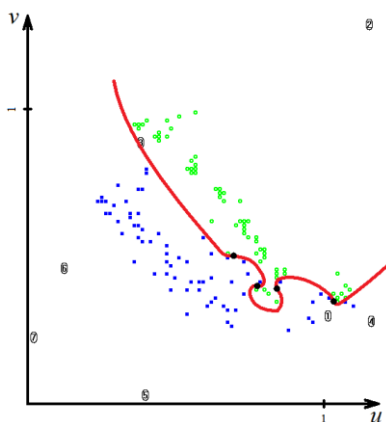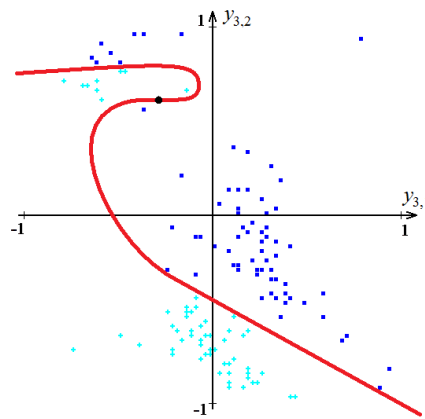
Figures 17–19 present views of curves obtained for Kohonen maps. Figure 17 shows that curve separating points of coal type 31 from coal type 34.2 has only one inflection point. Figure 18 presents a situation in which curve separating coal type

34.2 and coal type 35 has 4 inflection points. From Fig. 19 it can be observed that curve separating coal type 31 from coal type 35 has three inflection points. To obtain three views allowing to state that each coal type can be separated from others with the use of Kohonen maps, curves containing a total of 8 inflection points were used.
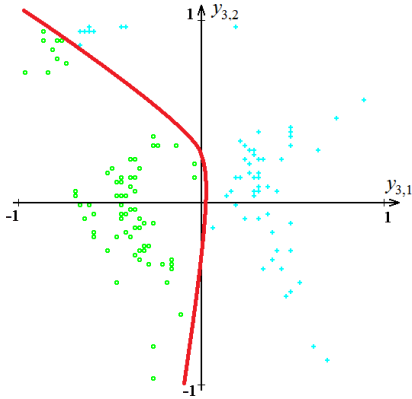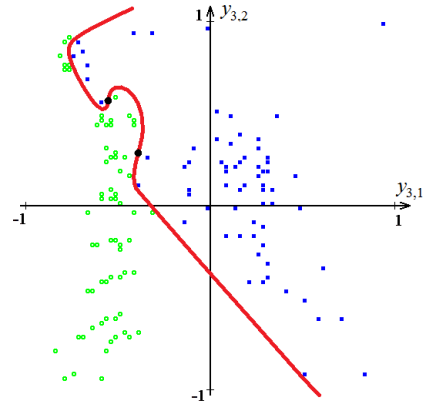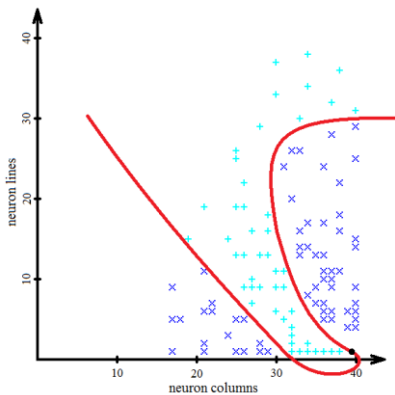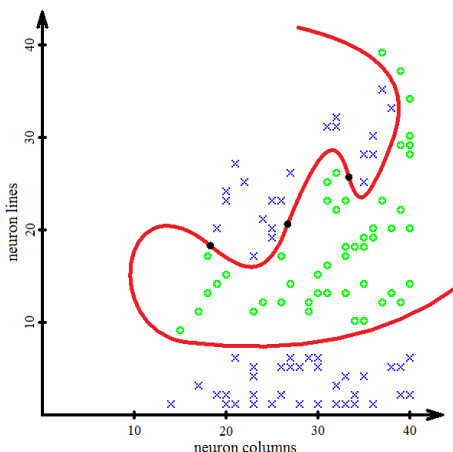

Fig. 19. Curve which separates points representing coal type 31 (x) and coal type 35 (o) with application of Kohonen maps. The curve has three inflection points

The visualization of analyzed coal samples by means of parallel coordinates method did not allow to conclude that 7-parameter data, the subject of analysis, was sufficient to classify coal types properly (Niedoba and Jamroz, 2013). It means that this method cannot be used efficiently for analyses concerning coal samples.

Table 1 contains the juxtaposition of obtained results for the seven analyzed methods of multidimensional visualization. Column "View 31/34.2" presents a number of inflection points for curves separating images of points representing coal types 31 and 34.2. The clearest result for these two coal types was obtained by means of observational tunnels method (no inflection points). Column "View 34.2/35" presents a number of inflection points for curves separating images of points representing coal types 34.2 and 35. The clearest view in this case was obtained by means of autoassociative neural networks (no inflection points). Column "View 31/35" presents a number of inflection points for curves separating images of points representing coal types 31 and 35. The clearest result comparing these two types of coal was obtained by means of observational tunnels method (one inflection point). The last column shows the sum of inflection points indicated in the previous columns.

Finally, the autoassociative neural networks method with result of only 3 inflection points gives the best outcome. The worst outcome gave parallel coordinates method – on the basis of obtained views it was not possible to separate analyzed points representing various coal types. That is why this method was rejected from further

analyses. Among methods allowing to obtain appropriate results, the worst was PCA method with the result of 13 inflection points all together.

Table 1. Final ranking of the compared multi-parameter visualization methods. For each method, a number of inflection points was indicated for curves separating images of points representing various coal types. Additionally, the sum of curves' inflection points from three views was presented

Location	Method	View 31/34.2	View 34.2/35	View 31/35	Sum
1	Autoassociative neural networks	1	0	2	3
2	Observational tunnels	0	3	1	4
3	Multidimensional scaling	1	1	4	6
4	Kohonen maps	1	4	3	8
5	Relevance maps	3	4	4	11
6	Principal component analysis	5	4	4	13
7	Parallel coordinates	Inefficient method			

While comparing visualization methods it is worth mentioning an additional fact. Almost all of the analyzed methods required a personal interference of the operator in the process of obtaining the clearest views. Particularly, it was based on the choice of appropriate parameters, randomization of initial random values and stopping algorithm when clear results were obtained. The exception was PCA method which does not require any interference of the operator during creation of multi-parameter data view.

Additionally, two of the described methods should be highlighted as the most efficients ones –these are autoassociative neural networks and Kohonen maps. Only these two methods allowed to obtain clear results showing on one figure the possibility of separating all three analyzed coal types (Jamroz, 2014c; Jamroz and Niedoba, 2015). In such cases views for pairs of coal types were given for better transparency.

Worth paying attention is the fact that multidimensional visualization can be used in 3D (Bondarev et al., 2011). However, in this case to observe data on the screen it is necessary to make projection from 3D into 2D (even three-dimensional screen is always flat). Thus, it requires additional observation of the obtained 3D data from various sides which are not always clear for each observation angle. The methods presented in the paper allow directly to notice some important features without any additional analysis by 2D projections – all what is needed is to observe and get result. It happens because the observer uses his most natural mechanism – sense of sight. Indeed, it is then connection between visualization methods creating two-dimensional figures and human personal neural network – brain, which analyzes this figures by sense of sight.

The criterion accepted in the paper which determines clearness of space division by samples representing various coal types is not the only possible one. Authors considered also possibility of evaluating clearness of figure division by means of

broken line constructed from intervals. However, in this case there were situations which require complicated broken line, constructed from many intervals to obtain visually clear results. The interesting alternative could be also division of space with application of principal curves (Einbeck et al., 2007). The efficiency of such approach in practice should be verified.

Conclusions

As a result of conducted analysis of seven methods of multidimensional visualization used for evaluating the possibility of efficient classification of 7-parameter coal samples, the following conclusions can be drawn.

1. The criterion introduced to analysis allowed to evaluate the transparency of obtained results by individual methods of multidimensional visualization.

2. The autoassociative neural networks method turned out to be the best. Furthermore, this method showed in the most effective manner the possibility of separating points representing coal type 34.2 and coal type 35.

3. The clearest possibility of separating points representing coal type 31 and coal type 34.2 was presented by observational tunnels method. Also, this method presented in the most effective manner the possibility of separating points representing coal type 31 and coal type 35.

4. The worst method was parallel coordinates method – on the basis of obtained views, it was impossible to state whether the separation of points representing individual coal types is possible or not.

5. Among methods which allowed to obtain appropriate results the worst was PCA method.

6. Only the PCA method did not require any interference of the operator during creation of multidimensional data view. The other methods required such interference by choosing appropriate parameters, randomization of initial random values and stopping algorithm when clear results were obtained.

7. Only two of the tested methods: autoassociative neural networks and Kohonen maps allowed to obtain clear views, showing the possibility of separating all three coal types on one figure (Jamroz, 2014c; Jamroz and Niedoba, 2015). In such cases, views for pairs of coal types were obtained additionally only to increase the image quality.

References

AHMED H.A.M., DRZYMALA J. (2005), *Two-dimensional fractal linearization of distribution curves*, Physicochemical Problems of Mineral Processing, 39, 129-139.

ALDRICH C. (1998), *Visualization of transformed multivariate data sets with autoassociative neural networks*, Pattern Recognition Letters, 19(8), 749-764.

ASIMOV D. (1985), *The Grand Tour: A Tool for Viewing Multidimensional Data,* SIAM Journal of Scientific and Statistical Computing, 6, 128-143.

ASSA J., COHEN-OR D., MILO T. (1999), *RMAP: a system for visualizing data in multidimensional relevance space,* Visual Computer, 15(5), 217-234.

BONDAREV A.E., GALAKTIONOV V.A., CHECHETKIN V.M. (2011), *Analysis of the development concepts and methods of visual data representation in computational physics*, Computational Mathematics and Mathematical Physics, 51(4), 624-636.

BROZEK M., SUROWIAK A. (2010), *Argument of Separation at Upgrading in the Jig*, Archives of Mining Sciences, 55(1), 21-40.

BROZEK M., SUROWIAK A. (2007), *Effect of Particle Shape on Jig Separation Efficiency*, Physicochemical Problems of Mineral Processing, 41, 397-413.

BROZEK M., SUROWIAK A. (2005), *The Dependence of Distribution of Settling Velocity of Spherical Particles on the Distribution of Particle Sizes and Densities*, Physicochemical Problems of Mineral Processing, 39, 199-210.

CLEVELAND W.S., MCGILL R. (1984), *The many faces of a scatterplot*, Journal of the American Statistical Association, 79, 807-822.

DRZYMALA J. (2009), *Basics of minerallurgy,* Oficyna Wydawnicza Politechniki Wroclawskiej, Wroclaw. [in Polish]

DRZYMALA J. (2007), *Mineral processing: foundations of theory and practice of minerallurgy,* Oficyna Wydawnicza Politechniki Wroclawskiej, Wroclaw.

GAWENDA T., SARAMAK D., TUMIDAJSKI T. (2005), *Regression models of rock materials crushing in jaw crushers*, Scientific Issues of Civil Engineering and Environmental Engineering Faculty of Koszalin University of Science and Technology, series: Environmental Engineering, 22, 659-670. [in Polish]

EINBECK J., EVERS L., BAILER-JONES C. (2007), *Representing Complex Data Using Localized Principal Components with Application to Astronomical Data*, in GORBAN A., KEGL B., WUNSCH D., ZINOVYEV A. (eds.), *Principal Manifolds for Data Visualisation and Dimension Reduction*, LNCSE 58, Springer, Berlin – Heidelberg – New York, 180-204.

HOTELLING H. (1933), *Analysis of a complex of statistical variables into principal components*, Journal of Educational Psychology, 24, 417-441 and 498-520.

INSELBERG A. (2009), *Parallel Coordinates: VISUAL Multidimensional Geometry and its Applications*, Springer.

JAIN A.K., MAO J. (1992), *Artificial neural network for non-linear projection of multivariate data*, in: Proc. IEEE Internat. Joint Conf. On Neural Networks, Baltimore, MD, 3, 335-340.

JAMROZ D. (2014a), *Application of Multidimensional Data Visualization in Creation of Pattern Recognition Systems*, in GRUCA A., CZACHORSKI T., KOZIELSKI S. (eds.),, *Man-Machine, Interactions 3*, AISC, Switzerland, Springer International Publishing, 242, 443-450.

JAMROZ D. (2014b), *Application of multidimensional scaling to classification of various types of coal*, Archives of Mining Sciences, 59(2), 413-425.

JAMROZ D. (2014c), *Application of multi-parameter data visualization by means of autoassociative neural networks to evaluate classification possibilities of various coal types*, Physicochemical Problems of Mineral Processing, 50(2), 719-734.

JAMROZ D. (2009), *Multidimensional labyrinth - multidimensional virtual reality*, in CYRAN K., KOZIELSKI S., PETERS J., STANCZYK U., WAKULICZ-DEJA A. (eds.),, Man-Machine, Interactions, AISC, Heidelberg, Springer-Verlag, 59, 445–450.

JAMROZ D., NIEDOBA T. (2015), *Application of multidimensional data visualization by means of self-organizing Kohonen maps to evaluate classification possibilities of various coal types*, Archives of Mining Sciences, 60(1), 39-50.

JAMROZ D., NIEDOBA T. (2014), *Application of Observational Tunnels Method to Select Set of Features Sufficient to Identify a Type of Coal*, Physicochemical Problems of Mineral Processing, 50(1), 185-202.

JAMROZ D. (2001), *Visualization of objects in multidimensional spaces*, Doctoral Thesis, AGH, Krakow. [in Polish]

JOLLIFFE I.T. (2002), *Principal Component Analysis*, Springer Series in Statistics, 2nd ed., Springer, NY.

KOHONEN T. (1989), *Self Organization and Associative Memory*, Springer-Verlag.

KRUSKAL J. B. (1964), *Multidimensional scaling by optimizing goodness of fit to a nonmetric hypothesis*, Psychometrika, 29, 1–27.

LYMAN G. J. (1993), *Application of Line-Length Related Interpolation Methods to Problems in Coal Preparation – III: Two dimensional Washability Data Interpolation*, Coal Preparation, 13, 179-195.

NIEDOBA T., JAMROZ D. (2013), *Visualization of multidimensional data in purpose of qualitative classification of various types of coal*, Archives of Mining Sciences, 58(4), 1317-1333.

NIEDOBA T. (2013a), *Multidimensional characteristics of random variables in description of grained materials and their separation processes,* Wydawnictwo Instytutu Gospodarki Surowcami Mineralnymi i Energia PAN, Krakow. [in Polish].

NIEDOBA T. (2009), *Multidimensional distributions of grained materials characteristics by means of non-parametric approximation of marginal statistical density function*, AGH Journal of Mining and Geoengineering, 33(4), 235-244. [in Polish].

NIEDOBA T. (2014), *Multi-parameter data visualization by means of principal component analysis (PCA), in qualitative evaluation of various coal types*, Physicochemical Problems of Mineral Processing, 50(2), 575-589.

NIEDOBA T. (2015), *Application of relevance maps in multidimensional classification of coal types*, Archives of Mining Sciences, vol. 60(1), 93-106.

NIEDOBA T. (2013b), *Statistical analysis of the relationship between particle size and particle density of raw coal*, Physicochemical Problems of Mineral Processing, 49(1), 175-188.

NIEDOBA T., SUROWIAK A. (2012), *Type of coal and multidimensional description of its composition with density and ash contents taken into consideration*, in Proceedings of the XXVI International Mineral Processing Congress, 1, 3844-3854.

NIEDOBA T. (2011), *Three-dimensional distribution of grained materials characteristics*, in Proceedings of the XIV Balkan Mineral Processing Congress, Tuzla, Bosnia and Herzegovina, 1, 57-59.

OLEJNIK T., SUROWIAK A., GAWENDA T., NIEDOBA T., TUMIDAJSKI T. (2010), *Multidimensional coal characteristics as basis for evaluation and adjustment of its beneficiation technology*, AGH Journal of Mining and Geoengineering, 34(4/1), 207-216. [in Polish]

SARAMAK D. (2013), *Mathematical models of particle size distribution in simulation analysis of High-pressure grinding rolls operation*, Physicochemical Problems of Mineral Processing, 49(1), 495–512.

SARAMAK D. (2011), *Technological Issues Of High-Pressure Grinding Rolls Operation In Ore Comminution Processes*, Archives of Mining Sciences, 56(3), 517-526.

SNOPKOWSKI R., NAPIERAJ A. (2012), *Method Of The Production Cycle Duration Time Modeling Within Hard Coal Longwall Faces*, Archives of Mining Sciences, 57(1), 121-138.

TUMIDAJSKI T., SARAMAK D. (2009), *Methods and models of mathematical statistics in mineral processing*, Wydawnictwo AGH, Krakow. [in Polish]

TUMIDAJSKI T. (1997), *Stochastic analysis of grained materials properties and their separation processes*, Wydawnictwo AGH, Krakow. [in Polish]

Professor Andrzej Luszczkiewicz, Ph.D., D.Sc.
a tribute on his 70th birthday

Professor Andrzej Luszczkiewicz received his master and engineer degrees from the Faculty of Mining Engineering of the Silesian University of Technology in 1969 in Gliwice. Soon after graduation he participated in internships at the Institute of Mineral Processing of the Silesian University of Technlogy and next the Institute of Mining Engineering of the Wroclaw University of Technology. This was the moment when he decided to devote his future to teaching, science, and technology. In 1970 he participated in a year-long industrial training at the Mineral Processing Division of KGHM. This helped him to get understanding and knowledge on technology of beneficiation of all Polish copper enrichment plants. It gave him a good base to start scientific works for improvement of efficiency of industrial processing of copper ores, especially by flotation. At the same time he was promoted to assistant and next to senior assistant positions at the Mining Engineering Institute of the Wroclaw University of Technology. In 1973 Professor Luszczkiewicz was hired as an assistant professor in a newly created Mineral Processing Group at the Institute of Inorganic Chemistry and Metallurgy of Rare Elements of the Chemistry Faculty of the Wroclaw University headed by Professor Janusz Laskowski. He was teaching theoretical basis and technology of mineral processing at the Department of Mining and at the Department of Chemistry of the Wroclaw University of Technology. In addition to that, he was teaching at the Faculty of Earth Sciences of the University of Wroclaw. The accomplishments of his research on novel methods of evaluation of industrial processes were summarized in his Ph.D. thesis entitled *Evaluation of copper ore processing technologies in the light of statistical investigation*, defended in March 1976 at the Institute of Mining Engineering of the Wroclaw University of Technology. The supervisor of his doctoral thesis was Marek Stefański, professor of the Main Mining Institute in Katowice. The remaining part of the year 1976 he spent as a postdoctoral fellow at the University of

Belgrade in the former Yugoslavia. He was also a postdoc at the University of British Columbia in Vancouver working for Professor Jan Leja from 1978 to 79.

At the beginning of 1982 his Mineral Processing Group was moved to the Institute of Mining Engineering of the Wroclaw University of Technology. Soon after he started cooperation with Professor K. Kovacev of the University of Mining and Geology in Sofia on copper ores processing. The cooperation was very intensive from 1984 to 1990. In 1979, soon after emigration of Professor Janusz Laskowski to USA and next to Canada, Professor Luszczkiewicz, after a short period of time of heading the Mineral Processing Group by Dr. Janusz Lekki (✝2014) and Professor Jerzy Malewski, he became the leader of the Group, later renamed Group of Minerals and Wastes Processing. He has been the leader until now, with a break between 1997 and 2003 to be a deputy Director of the Institute of Mining, responsible for Teaching and Cooperation with Foreign Countries.

In 2002 he obtained his Doctor of Science (habilitation) degree from the Mining and Geoengineering Department of the AGH University of Science and Technology in Kraków. Since then, he has been a member of the Faculty Council of the Geoengineering, Mining and Geology Department of the Wroclaw University of Technology. In 2008 he was appointed associate professor of the Wroclaw University of Technology.

His research interest is very broad. Initially, working under the supervision of Professor Janusz Laskowski, he took part in the research on development of enrichment methods of the ore from the Lubin-Glogow Copper Basin in Poland. A special emphasis was put on metals present in copper ores and their recovery in the course of processing of various mineral raw materials of primary and secondary origin. This has become the main theme of his research interests and activities in the future.

From 1976 to 1987 he headed a research project on flotation of titanium-magnetite-vanadium (Ti-Fe-V) ore from Suwalki (NE Poland). The project carried out at the Wroclaw University of Technology involved separation and processing of ilmenite and sulphide minerals from the Ti-Fe-V ores. The project was a part of program on the Ti-Fe-V ore beneficiation which was co-ordinated by the Institute of Metallurgy of Iron in Gliwice, Poland. The goal was to develop a technology for production of commercial ilmenite and obtaining nickel-copper sulphide concentrates. The technology of desulfurization of the Ti-Fe-V ore was based on separation of sulphide minerals by flotation followed by hydrometallurgical recovery of accompanying metals and included not only nickel and copper but also cobalt and silver. This technology was developed in cooperation with metallurgists from the Institute of Ferrous Metallurgy in Gliwice.

Parallel to research on the Ti-Fe-V ore, Professor Luszczkiewicz has spent many years investigating rare earth elements (REE) minerals. It was initiated due to two international research programs devoted to a search for new sources of REE for the Polish industry. The program was implemented and coordinated by the Technical University of Wroclaw at the beginning 1970 and '80. The goal of the programs was to find national and foreign sources of REE including the use of fluorocarbonate ores

from Vietnam and Mongolia, basing on scientific and technical cooperation of both countries with Poland. He took part in the development of a beneficiation technology of the Vietnamese bastnaesite ore from Nam-Nam-Xe and the Mongolian synchisite ore from Lugin Gol in Gobi Desert. The processing was launched first in the late 1970s and next 80s as a pilot plant operated by the Wroclaw University of Technology in Kowary. This technology was also implemented in industrial enrichment plants in Vietnam and Mongolia.

In 1989 Professor Luszczkiewicz's interest turned to alternative sources of titanium and other metals including zirconium as well as REE, associated with sands of the South Baltic Sea and gravel aggregate sands of Lower Silesia. He proposed a concept of ilmenite, zirconium and REE concentrates production by domestic industry from Polish sources which was at that time cost-effective. It was verified on a semi-industrial scale using send wastes processed in Mietkow and Proszkowice near Sobotka, glass sands from Osiecznica near Boleslawiec and glass sands from Biala Gora near Tomaszów Mazowiecki. Under the supervision of Professor Luszczkiewicz at the end of 1980s and early 90s, the presence of heavy minerals and their content in 35 natural aggregates deposits of Lower Silesia were documented.

Changes in the Polish political system and industry ownership structure in 1990s resulted in a cease of research and industrial production of REE and heavy minerals from sands from the domestic sources. It was a good time for Professor Luszczkiewicz to summarize his the knowledge and experience on REE and heavy minerals. He co-authored a monograph devoted to REE. It was the first and the only book on REE in Polish. In addition to that, later in 2002, he wrote a monograph entitled *Scientific and technological aspects of the occurrence of heavy minerals in detrital raw materials*ʼ which was the basis for his D.Sc. dissertation (habilitation).

In the 1990s Professor Luszczkiewicz has been working on beneficiation of molibdenum-copper-tungsten ore from Myszków (in cooperation with the Upper Silesia Division of the State Geological Institute), recovery of valuable components from mining waste of former mining and metallurgical plant in Zloty Stok, and from barite mine wastes in Boguszow.

Lead removal from copper flotation concentrates was investigated by Professor Luszczkiewicz from 1992 to 1994. Lead, next to silver, is one of the most important component of the Polish copper ores. He made a detailed analysis of mineralogical forms of lead in the copper concentrates from Lubin mine and showed a possibility of partial separation of galena using thioglyclic compounds used as flotation depressors.

In late the 1990s, together with Dr. T. Chmielewski from the Department of Chemistry of the Technical University of Wroclaw, he has developed a unique process of treating byproducts of copper ore flotation with sulfuric acid. This process releases sulphide minerals from the carbonate rock matrix much better than grinding. The method was tested on a semi-industrial scale and implemented in the Polkowice concentrator between 2003 and 2006. It was documented that the recovery of copper in the final concentrates, after applying the modification, increased by 3 to 4%, while the

increase in the quality of the concentrates was from 1 to 2% Cu. This resulted in a significant reduction of copper losses to the flotation tailing. In the history of KGHM, no other technology provided such a significant increase in the efficiency of copper ore flotation.

The black shale fraction of the LGOM copper ore is an interesting and important material. Professor Luszczkiewicz created and participated in many research projects involving copper-bearing shale, including a project within the 6th Framework Programme of the European Union (FP6 European Project Bioshale, 2004-2008) on a *Search for a sustainable way of exploiting black shale ores using biotechnology*. This project was carried out by an international team of more than a dozen research centers, from 8 European countries. New solutions of the copper shale processing, including bioleaching, were proposed and developed.

An interesting project was conducted by Professor Luszczkiewicz in 1999-2000 dealing with platinum and gold recovery from special materials of LGOM, particularly from a part of the copper deposit called Western Polkowice. The upgradeability tests of the ore provided by geologists allowed to worked out a process based on flotation leading to 95-98% recovery of gold in concentrates containing up to 150 ppm of gold. However, such an excellent flotation of gold was not followed by the platinum group metals and the reason for that is still unknown.

In the years 2000-2010 he participated in Professor A. Ciesla's projects devoted to separation of copper ore components using strong magnetic fields produce by super-conducting separators owned by the Department of Electrical Engineering, AGH, Krakow.

Being all the time interested in research on heavy minerals he has been involved in various projects, initiated either by himself or by industrial partners, dealing with processing of raw materials from rocks of SKSM Sobotka and DSS Pilawa, glass sands of KiZPPS Osiecznica and KGHM flotation tailings from Lubin.

His scientific activity in the last years is related mainly to the research on various technological problems of Polish copper industry. Led by him research projects included technological improvements, research towards reduction of metals losses in the flotation tailings, testing new flotation reagents, improvement of copper ore beneficiation tests and finding methods for evaluation of effectiveness of enrichment processes.

Despite his time-consuming research and administrative duties Professor Luszczkiewicz is a full-time teacher delivering lectures and conducting laboratories exercises with students of the Faculty of Geoengineering, Mining and Geology of the Wroclaw University of Technology. He has supervised more than 50 master thesis and engineering projects in mineral process engineering and land use of mineral wastes. He also supervised four Ph.D. students and currently he is involved in two Ph.D. theses. He was also serving several time as a reviewer of doctoral theses. For his accomplishments he obtained several special awards granted by the Rector of the Wroclaw University of Technology. He also achieved the prize of the Senate of the Wroclaw University of Technology. He holds a prestigious title of the General Director of Min-

ing. The Mineral Processing Laboratory, which currently he is the head, has a professionally equipped laboratory to conduct all kind of research.

Professor Luszczkiewicz has been a member of the Editorial Board of Physicochemical Problems of Mineral Processing journal with which he is associated almost from the beginning of nearly 50 year long history of this journal. He is also a founder and member of the Editorial Board of the Journal of the Polish Mineral Engineering Society as well as a member of two committees of the Polish Academy of Science: Mining Committee (Section of Mineral Processing) and Committee for Sustainable Management of Mineral Resources.

Currently the members of this research and teaching team are: Dr. Alicja Bakalarz, Dr. Magdalena Duchnowska, Dr. Zaklina Konopacka, Dr. Przemyslaw. B. Kowalczuk, Dr. Danuta Szyszka, Piotr Karwowski (M.Sc.) and full professor Jan Drzymała (Ph.D., D.Sc.).

Professor Luszczkiewicz has published over 100 papers and nearly 150 reports of investigations. In 1977, together with Professor Janusz Laskowski of the University of British Columbia and Professor Jerzy Malewski of Wroclaw Univeristy of Technology, and in 1989 together with Professor Janusz Laskowski, he wrote monographs on mineral processing.

Prof. Luszczkiewicz is married with Elzbieta. He is a father of one son, Witold, and a grandfather of two grandsons: Blazej and Ziemowit. He likes classical music, in particular, J.S. Bach and W.A. Mozart. He and his wife like bike trips and they toured a large part of Europe. His hobbies include traveling and classic black-and-white film photography as well digital photography. His passion is also collecting and using herbs.

The list of his publications is printed below.

1. Laskowski J., Iskra J., Łuszczkiewicz A., *Flotacja piaskowcowej rudy miedzi związkami krzemoorganicznymi*. Rudy i Metale Nieżelazne, R.14, 1969, Nr. 12, 681–684.

2. Łuszczkiewicz A., *Niektóre problemy automatyzacji procesów przeróbczych*. Prace Naukowe Instytutu Górnictwa Politechniki Wrocławskiej, nr 11, 1974, 74–93.

3. Łuszczkiewicz A., Korelacje pomiędzy podstawowymi wskaźnikami przemysłowego procesu flotacji rud miedzi w świetle laboratoryjnych wskaźników wzbogacalności, Fizykochemiczne Problemy Przeróbki Kopalin, nr 9, 1975, 121–131.

4. Łuszczkiewicz A., Sak A., Laskowski J., *Badania flokulacji adsorpcji flokulanta na ziarnach mineralnych*. Materiały sympozjum: Fizykochemia układów silnie rozdrobnionych, Baranów Sandomierski, Wyd. PAN, Kraków, 1976.

5. Łuszczkiewicz A., Sak A., Laskowski J., *Flokulacja wodnych zawiesin mułów węglowych*. Chemia Stosowana, vol. XXI, Nr 3–4, 1977, 389–403.

6. Łuszczkiewicz A., Mager J., Laskowski J., *Badania wpływu zmian w technologii zakładu flotacyjnego na wyniki wzbogacania przy pomocy analizy korelacyjnej*. Materiały sesji naukowej; Rozwój nowoczesnych technologii w przemyśle metali nieżelaznych, tom 1, 115–126, Wyd. Instytutu Metali Nieżelaznych, Gliwice, 1977.

7. Łuszczkiewicz A., Lekki J., Laskowski J., *Badania współdziałania odczynników i ocena przemysłowego procesu flotacji rud miedzi*. Materiały konferencji: Przeróbka Mechaniczna Kopalin, Wyd. Separator, Katowice, vol.4, 1977, 3–13.

8. Luszczkiewicz A., Lekki J, Laskowski J., *Floatability of ilmenite*. Proceedings of the XXII International Mineral Processing Congress, Second Round Table Seminar, Warsaw, 1979, 163–182,.

9. Grygorcewicz E., Łuszczkiewicz A., Przykłady zastosowań metod statystycznych i elektronicznej techniki obliczeniowej w zakładzie wzbogacania rud. Rudy i Metale Nieżelazne, R. 25, Nr 6, 1980, 263–267.

10. Łuszczkiewicz A., *Piaski morskie południowego Bałtyku jako źródło ilmenitu i cyrkonu*. Materiały XVI Krakowskiej Konferencji Naukowo Technicznej Przeróbki Kopalin, Wyd. AGH, 1982, 21–27.

11. Drzymala J., Luszczkiewicz A., Simiczyjew P., *Hercynite – pleonaste from ilmenite – magnetite rocks of Krzemianka (NE Poland)*. Mineralogia Polonica, vol.13, 1982, No.2, 33–42.

12. Łuszczkiewicz A., Próby wydzielania koncentratów ilmenitu i cyrkonu z piasków morskich południowego Bałtyku. Fizykochemiczne Problemy Mineralurgii, nr 15, 1983, 55–63.

13. Drzymala J., Luszczkiewicz A., Simiczyjew P., *Flotation study on high–hercynite ilmenite ores*. International Journal of Mineral Processing, vol. 10, No. 4, 1983, 289–296.

14. Łuszczkiewicz A., Lekki, Drzymała J., *Problemy wzbogacania rudy tytanomagnetytowej*. Prace Instytutu Metalurgii Żelaza, No. 3–4 (35), 1983, 119–124.

15. Łuszczkiewicz A., *Flotacja cyrkonu z półproduktów wzbogacania piasków*. Fizykochemiczne Problemy Mineralurgii, nr 16, 1984, 64–70.

16. Łuszczkiewicz A., *Technologiczna ocena możliwości wzbogacania piasków morskich Bałtyku*. Materiały konferencji: Eksploatacja złóż minerałów ciężkich południowego Bałtyku. Prace Naukowe Instytutu Chemii Nieorganicznej i Metalurgii Pierwiastków Rzadkich Politechniki Wrocławskiej, nr 51, 1984, 107–116.

17. Drzymała J., Łuszczkiewicz A., Lekki J., *Wzbogacanie zaolejonych szlamów szlifierskich zawierających stal stopową oraz ścierniwo*. Fizykochemiczne Problemy Mineralurgii, nr 16, 1984, 11–16.

18. Drzymala J., Luszczkiewicz A., Microlaboratory study on magnetic, gravity and high tension separation of hercynite and pleonaste from low–grade ilmenite concentrates. International Journal of Mineral Processing, vol.14, 1985, 233–238.

19. Łuszczkiewicz A., Lekki J., Chmielewski T., *Odsiarczanie rudy tytanomagnetytowej. Technologia i podstawy procesu*. Materiały XIX Krakowskiej Konferencji Naukowo–Technicznej Przeróbki Kopalin, Wyd. AGH, Kraków, 1985, 61–74.

20. Łuszczkiewicz A., Simiczyjew P., Świderski J., *Laboratoryjne próby flotacji skaleni ze zwietrzelinowego złoża w rejonie Karpnik*. Materiały konferencji: Surowce skaleniowe Dolnego Śląska, Wyd. Komitet Naukowo–Techniczny NOT ds. Polityki Surowcowej, 1985, 119–131.

21. Łuszczkiewicz A., Glapa W., *Koncepcja otrzymywania koncentratów minerałów ciężkich z piasków ławic bałtyckich*. Fizykochemiczne Problemy Mineralurgii, nr 17, 1985, 205–218.

22. Lekki J., Kiełkowska M., Łuszczkiewicz A., *Oddziaływanie oleinianu z hercynitem zachodzące w czasie flotacji ilmenitu z rud tytanomagnetytowych*. Fizykochemiczne Problemy Mineralurgii, nr 17, 77–88, 1985.

23. Łuszczkiewicz A., Kurzyca M. *Wydzielanie ilmenitu z półproduktów przeróbki piasków drogą wzbogacania elektrycznego*. Fizykochemiczne Problemy Mineralurgii, nr 18, 1986, 179–191.

24. Łuszczkiewicz A., *Odzysk minerałów ciężkich z piasków szklarskich Kopalni „Osiecznica”*. Fizykochemiczne Problemy Mineralurgii, nr 19, 1987, 309–319.

25. Luszczkiewicz A., Wierzbicki Z., *Relationship between radioactivity and rare earth elements content in bastnaesite ore flotation products*. Proceedings XIX Conference of Mining and Metallurgy, Bor, Yugoslavia, vol.1, 1987, 293–297.

26. Glapa W., Łuszczkiewicz A., *Możliwości eksploatacji minerałów ciężkich z Ławicy Odrzanej i Słupskiej*. Górnictwo Odkrywkowe, vol. XXX, 1988, nr 1, (197), 34–49.

27. Łuszczkiewicz A., *Odpady z płukania żwirów jako znaczące źródło minerałów ciężkich*. Materiały sympozjum Optymalizacja Wykorzystania Surowców Mineralnych w Procesach Przeróbki i Przetwórstwa, PAN, Centrum Podstawowych Problemów Gospodarki Surowcami Mineralnymi i Energią, Kraków, 1988, 154–165.

28. Łuszczkiewicz A., Kowalczyk J., Mazanek C., *Możliwości zaspokojenia krajowego zapotrzebowania na ziemie rzadkie*. Materiały sympozjum Optymalizacja Wykorzystania Surowców Mineralnych w Procesach Przeróbki i Przetwórstwa, Wydawnictwa Centrum Podstawowych Problemów Gospodarki Surowcami Mineralnymi i Energią PAN, Kraków, 1988, 141–153.

29. Łuszczkiewicz A., Wierzbicki Z., *Badania flotowalności fluorowęglanowych rud pierwiastków ziem rzadkich*. Prace Naukowe Instytutu Chemii Nieorganicznej i Metalurgii Pierwiastków rzadkich Politechniki Wrocławskiej, nr 57, 1988, 77–86.

30. Łuszczkiewicz A., Mazanek C., Wierzbicki Z., *Rudy fluorowęglanowe jako źródło ziem rzadkich dla przemysłu karajowego*. Rudy i Metale Nieżelazne, R. 34, 1989, No.12, 438–443.

31. Luszczkiewicz A., Kowalczyk J., Mazanek C., 1989, Rohstoffe der Seltenen Erden und ichre Aufbereitungsmethoden in Polen (Sources and processing methods of rare earths in Poland). Erzmetall, Vol. 42, 1989, No. 12, 570–573.

32. Łuszczkiewicz A., Kurzyca M., Steinhoff J., Świerkot–Kapała A., *Ocena możliwości pozyskiwania minerałów ciężkich z piasków Ławic Słupskiej i Odrzanej*. Przegląd Górniczy, tom 44, 1988, nr 10, 12–18.

33. Łuszczkiewicz A., Nawrocki J., *Surowce okruchowe, charakterystyka, technologie pozyskiwania minerałów ciężkich*. Fizykochemiczne Problemy Mineralurgii, nr 23, 1990, 7–17.

34. Łuszczkiewicz A., *Minerały ciężkie w żwirach i piaskach eksploatowanych na Dolnym Śląsku*. Fizykochemiczne Problemy Mineralurgii, nr 23, 1990, 27–39.

35. Łuszczkiewicz A., Mazanek C., 1990, Pozyskiwanie koncentratów minerałów ciężkich z aluwiów przedsudeckich na przykładzie złoża Proszkowice. Fizykochemiczne Problemy Mineralurgii, nr 23, 1990, 41–58.

36. Łuszczkiewicz A., *Właściwości minerałów pierwiastków ziem rzadkich decydujące o technologii ich wzbogacania*. [W:] Pierwiastki ziem rzadkich, surowce, technologie, zastosowania, Praca zbior. pod red. W. Charewicza, Wydawnictwa Naukowo-Techniczne, Warszawa, 1990, 94–108.

37. Łuszczkiewicz A., Mazanek C., *Technologie wzbogacania surowców pierwotnych*. [W:] Pierwiastki ziem rzadkich, surowce, technologie, zastosowania, Praca zbior. pod red. W. Charewicza, Wydawnictwa Naukowo–Techniczne, Warszawa, 1990, 108–119.

38. Łuszczkiewicz A, *Technologie pozyskiwania pierwiastków ziem rzadkich z surowców okruchowych (rozsypiskowych)*. [W:] Pierwiastki ziem rzadkich, surowce, technologie, zastosowania, Praca zbior. pod red. W. Charewicza, Wydawnictwa Naukowo–Techniczne, Warszawa, 1990, 119–132.

39. Łuszczkiewicz A., Kaczmarek B., *Ocena możliwości wydzielania minerałów ciężkich z piasków szklarskich z rejonu Białej Góry*. Fizykochemiczne Problemy Mineralurgii, Nr 25, 1992, 123–132.

40. Kaczmarek B., Łuszczkiewicz A., *Minerały ciężkie w piaskach szklarskich z "Białej Góry". Cz.I.* Szkło i Ceramika, Nr 3, 1992, 16–21.

41. Drzymała J., Szulmanowicz A., Łuszczkiewicz A., Chmielewski T., *Bezkolektorowa flotowalność siarczków z Lubińsko-Głogowskiego Zagłębia Miedziowego*. Materiały XXV Krakowskiej Konferencji Naukowo-Technicznej Przeróbki Kopalin, Centrum Podstawowych Problemów Gospodarki Surowcami Mineralnymi i Energią PAN, Kraków, 1993, Seria Sympozja i Konferencje Nr 8, 133–142.

42. Łuszczkiewicz A., Czechowski F., Wydzielanie koncentratów łupkowych z lubińskich rud miedzi i zachowanie się pierwiastków towarzyszących w procesie termicznej obróbki tych koncentratów. Polskie Towarzystwo Mineralogiczne – Prace Specjalne Nr 3, Kraków, 1993, 33–46.

43. Łuszczkiewicz A. Badania wzbogacalności rud molibdenowo–wolframowo–miedziowych z rejonu Myszkowa. Fizykochemiczne Problemy Mineralurgii, Nr 27, 1993, 55–68.

44. Łuszczkiewicz A., Sztaba K., *Wykorzystanie odpadów flotacyjnych powstających przy przeróbce krajowych rud miedzi.* Materiały XI Gliwickiego Sympozjum Naukowo-Techniczne Przeróbki Kopalin. Politechnika Śląska, Gliwice 1994.

45. Łuszczkiewicz A., Drzymała J., Grotowski A., *Problemy flotacyjnego rozdziału siarczków miedzi i ołowiu.* Rudy i Metale Nieżelazne, R. 40, 1995, Nr 8, 315–318.

46. Luszczkiewicz A., Sztaba K.S., *Beneficiation of flotation tailing from Polish copper sulfide ores.* Proceedings, XIX International Mineral Processing Congress, San Francisco 1995, SME, vol.4, 121–124.

47. Drzymała J., Chmielewski J., Luszczkiewicz A., Difficulties in separating copper and lead sulphides by xanthate flotation: negative role of contact of particles in the presence of depresants. [In]: Changing Scopes in Mineral Processing, M. Kemal, V. Arslan, A. Akar, (editors), Balkema, Rotterdam, 1996, 225–228.

48. Łuszczkiewicz A., Muszer A., *Złoto w odpadach górniczych z okolic Złotego Stoku*. Fizykochemiczne Problemy Mineralurgii, nr 31, 1997, 197–209.

49. Muszer A., Łuszczkiewicz A., *Wstępne wyniki wzbogacania odpadów górniczo–hutniczych z okolic Złotego Stoku*. W: Metale szlachetne w NE części Masywu Czeskiego i w obszarach przyległych, geneza, występowanie, perspektywy. Wydawnictwa Instytutu Nauk Geologicznych Uniwersytetu Wrocławskiego, Wrocław, 1997, 34–41.

50. Muszer A., Łuszczkiewicz A., *Występowanie złota w osadach Białej Głuchołaskiej i Złotego Potoku (Głuchołazy–Jarnołtówek)*. W: Metale szlachetne w NE części Masywu Czeskiego i w obszarach przyległych, geneza, występowanie, perspektywy. Wydawnictwa Instytutu Nauk Geologicznych Uniwersytetu Wrocławskiego, Wrocław, 1997, 133–141.

51. Drzymała J., Bigosiński J., Łuszczkiewicz A., Malewski J., Mikołajczuk R., Pietrzyk G., Pradel K., Szulmanowicz A., Wojtaszek T., *Tomas Alva Edison i jego wkład w rozwoju przeróbki kopalin.* W: Prace Naukowe Instytutu Górnictwa Politechniki Wrocławskiej, Nr 85, Studia i Materiały Nr 27, 1998, 13 – 20.

52. Łuszczkiewicz A., *Perspektywy wykorzystania składowisk odpadów flotacyjnych z przeróbki rud miedzi w regionie legnickim.* Materiały konferencji: Proekologiczna rekonwersja przemysłu w województwie legnickim, Polanica, 30–31 lipca 1998, Wyd. Wojewoda Legnicki, CBPM Cuprum, Wrocław, Akademia Rolnicza we Wrocławiu, 1998, 117–137.

53. Łuszczkiewicz A. *Wydzielanie koncentratów złota i platynowców z pozabilansowej rudy miedzi.* Polskie Towarzystwo Mineralogiczne–Prace Specjalne, Nr 12, Kraków, 1998, 41–62.

54. Łuszczkiewicz A., Muszer A., Gold from Rakowice placer deposit near Lwowek Slaski, SW Poland (Złoto ze złoża kruszyw naturalnych Rakowice koło Lwówka Śląskiego). Physicochemical Problems of Mineral Processing, No. 33, 115–122, 1999.

55. Łuszczkiewicz A., *Ocena flotowalności złotonośnej pozabilansowej rudy miedzi.* Gospodarka Surowcami Mineralnymi, Tom 15, 1999, Zeszyt Specjalny, 197–209.

56. Łuszczkiewicz A., *Odzysk fluorytu z barytowych odpadów flotacyjnych kopalni Boguszów*. Gospodarka Surowcami Mineralnymi, Tom 15, 1999, Zeszyt Specjalny, 211–220.

57. Luszczkiewicz A., Chmielewski T., *Acid treatment of copper sulfide concentrate in the flotation circuit of carbonaceous ores.* Proceedings of the 6–th International Conference on Mining, Petroleum and Metallurgy, Cairo University, Vol.1–B, 1999, 85–91.

58. Łuszczkiewicz A., Chmielewski T., *Acid treatment of copper sulfide concentrate in the flotation circuit.* Materiały V Międzynarodowej Konferencji Przeróbki Rud Metali Nieżelaznych, Szklarska Poręba, 25–27.10.1999, KGHM Polska Miedź S.A., Wyd. CBPM Cuprum, IMN, 1999, 59–66.

59. Łuszczkiewicz A., *Minerały ciężkie ze złoża kruszyw naturalnych w Rakowicach koło Lwówka Śląskiego.* Prace Naukowe Instytutu Górnictwa Politechniki Wrocławskiej, Nr 87, Studia i Materiały, Nr 28, 2000, 27 – 38.

60. Łuszczkiewicz A., *Technologiczna ocena minerałów ciężkich w surowcach rozsypiskowych Dolnego Śląska.* Materiały Międzynarod. Konf. Nauk.–Techn. KOMEKO 2000, Production of minerals and environmental protection, Szczyrk 14–16 marca 2000, wyd. Centr. Mechaniz. Górn. KOMAG, ref. nr 16, 2000, 1–9.

61. Muszer A., Łuszczkiewicz A., *Węglik tytanu w żelazie rodzimym z Gór Bardzkich na Dolnym Śląsku.* . Prace Naukowe Instytutu Górnictwa Politechniki Wrocławskiej, Nr 88, Studia i Materiały, Nr 28, 2000, 53 – 63.

62. Łuszczkiewicz A., Koncepcje wykorzystania odpadów flotacyjnych z przeróbki rud miedzi w regionie legnicko–głogowskim. Inżynieria Mineralna, Nr 1, vol. 1, 2000, 25–35.

63. Łuszczkiewicz A., *Wykorzystanie frakcji czarnych łupków miedzionośnych z rud z rejonu lubińsko–głogowskiego.* W: Współczesne problemy przeróbki rud miedzi w Polsce, Polkowice, 16 listopad 2000, Wyd. Komitet Górnictwa PAN i KGHM Polska Miedź S.A., 2000, 137–156.

64. Łuszczkiewicz A., *Uwarunkowania kompleksowego wykorzystania pospolitych surowców okruchowych.* W: Przeróbka i wykorzystanie surowców skalnych, Wydawnictwo Instytutu Gospodarki Surowcami Mineralnymi i Energią PAN, Kraków, 2002, 77–87.

65. Łuszczkiewicz A., *Próby wydzielania flotowalnych składników użytecznych z odpadów flotacyjnych z przeróbki rud miedzi.* W: Nowoczesne technologie i systemy mechanizacyjne do przeróbki surowców mineralnych. Biblioteka KOMEKO 2002, Gliwice, 2002, 199–213

66. Łuszczkiewicz A., *Ocena skuteczności wydzielania wieloskładnikowych koncentratów pierwiastków rozproszonych.* Prace Naukowe Instytutu Górnictwa Politechniki Wrocławskiej, Nr 102, 2002, Konferencje, Nr 33, 85–103.

67. Łuszczkiewicz A., Znaczenie gospodarcze i technologie pozyskiwania surowców rozproszonych. Inżynieria Mineralna, Nr S.1 (7), 2002, 61–77.

68. Łuszczkiewicz A., *Chemiczna modyfikacja produktów pośrednich w układach technologicznych flotacji rud miedzi.* W: „Możliwości poprawy jakości koncentratu miedziowego w procesie przeróbki rud miedzi w KGHM Polska Miedź S.A.", Materiały Sympozjum, Fundacja Nauka i Tradycje Górnicze, AGH, KGHM Polska Miedź S.A., Kraków, 2002, 29–42.

69. Cieśla A., Łuszczkiewicz A. Próby wydzielenia składników śladowych z niektórych odpadach mineralnych przy użyciu nadprzewodnikowego separatora matrycowego. Inżynieria Mineralna, vol. 4, 2003, Nr S.3(10), 41–48.

70. Łuszczkiewicz A., *Możliwości ceny skuteczności wydzielania składników rozproszonych.* Rozdz. W: „Identyfikacja i ocena wybranych właściwości surowców mineralnych oraz procesów ich przeróbki". Pr. zbior. pod red. K. Sztaby, Wyd. Inst.Gosp.Sur.Min. PAN, Kraków 2003, 128–143.

71. Łuszczkiewicz A., *Odpady z przeróbki pospolitych surowców okruchowych jako źródło cennych minerałów ciężkich.* Zeszyty Naukowe Wydziału Budownictwa i Inżynierii Srodowiska Politechniki Koszalińskiej, Seria: Inżynieria Środowiska, r 22, 2005. 586–600.

72. Łuszczkiewicz A., Chmielewski T., Technologia chemicznej modyfikacji produktów pośrednich w układach flotacji siarczkowych rud miedzi. Rudy i Metale Nieżelazne, R. 51, 2006, Nr 1, 2–10

73. Łuszczkiewicz A., Konopacka Ż., Drzymała J., *Flotacja czarnych łupków z lubińskich rud miedzi.* W: Mat. Konfer. „Perspektywy zastosowania technologii biołdugowania do przerobu rud miedzi zawierających łupki", BIOPPROCOP '06, Lubin, 19 czerwca 2006, Wyd. KGHM Cuprum Sp. z O.O., Wrocław 2006, 29–47

74. Łuszczkiewicz A., *Badania odpadów technologicznych z dawnej działalności górniczej i hutniczej w rejonie Złotego Stoku*. Prace Naukowe Instytutu Górnictwa Politechniki Wrocławskiej, Nr 117, 2006, Seria: Studia i Materiały 32, 178–191

75. Łuszczkiewicz A., Wieniewski A., *Kierunki rozwoju technologii wzbogacania rud w krajowym przemyśle miedziowym*. Górnictwo i Geoinżynieria, Rok 30, 2006, Zeszyt 3/1, 181–196.

76. Muszer A., Luszczkiewicz A., *Mineralogical characteristic of accessory minerals from Osiecznica deposit, SW Poland*. Physicochemical Problems of Mineral Processing, No. 40, 2006, 77–88.

77. Łuszczkiewicz A., *Rozkłady pierwiastków ziem rzadkich (REE) w wybranych kaolinach Dolnego Śląska*. Czasopismo Techniczne Nr 1328, R. 126, Kraków 2006, 23–29.

78. Łuszczkiewicz A., *Wstępne próby pozyskiwania produktów skaleniowych z odpadów granitowych z rejonu Gniewkowa na Dolnym Śląsku*. Zeszyty Naukowe Wydziału Budownictwa i Inżynierii Środowiska Politechniki Koszalińskiej, Seria: Inżynieria Środowiska, Nr 23, 2007, 445–454.

79. Luszczkiewicz A., Chmielewski T., Konieczny A., Kowalska M., *Non–oxidative acidic treatment of copper sulfide concentrates in the flotation circuit.* In: Mineral Processing Vol. II (Proceedings of the Sixth International Copper–Cobre Conference, Aug. 25–27, 2007, Toronto, Ontario, Canada, Eds: R. del Villar, J.E. Nesset, C.O. Gomez, A.W. Stradling), 53–62

80. Chmielewski T, Łuszczkiewicz A. Konopacka Ż., Wydzielanie i koncepcja przeróbki czarnych łupków z lubińskich rud miedzi. (Separation and concept of processing of black shale copper ore from Lubin mine), Materiały VIII Międzynarodowej Konferencji Przeróbki Rud Metali Nieżelaznych ICNOP'07, Wojcieszyce, 21–23.05.2007, Wyd. KGHM Cuprum CBR, 2007,171–184.

81. Konopacka Z., Luszczkiewicz A., Chmielewski T. *Effect of non–oxidative leaching on flotation efficiency of Lubin middlings*. Physicochemical Problems of Mineral Processing, No. 41, 2007, 275–289.

82. Groudev S., Spasova I., Nicolova M., Chmielewski T., Luszczkiewicz A., *Recovery of copper by flotation of microcially pretreated black shales*, Proceedings: Bio- and Hydrometallurgy'07, Falmuth, UK, 1–2 May 2007 (published in the form of CD)

83. d'Hugues P., Norris P.R., Johnson B., Grotowski A., Chmielewski T., Luszczkiewicz A., Sadowski Z., Skłodowska A., Farbiszewska T, *Presentation of the FP6 European Project Bioshale. Exploitation of black shale ores using biotechnologies – Polish case studies*, Physicochemical Problems of Mineral Processing, No. 41, 2007, 373–386.

84. d'Hugues P., Grotowski A., Luszczkiewicz A., Sadowski Z., Fabiszewska T., Skłodowska A., Loukola–Ruskeeniemi K., Langwaldt J., Palma J., Norris P., Glombitza F., Grudev S., Pasava J., Johnson B., *The Bioshale project: search for a sustainable way of exploiting black shale ores using biotechnology*, , 17th International Biohydrometallurgy Symposium, *Frankfurt am Main, Germany 2–5 September 2007*. Biohydrometallurgy : from the single cell to the environment (IBS 2007). Ed. by Axel Schippers [i in.]. Stafa-Zurich: Trans Tech Publ., 2007, 42–45.

85. Chmielewski T., Łuszczkiewicz A., *Hydrometalurgia dla półproduktu łupkowego ZG Lubin – potrzeba zmian technologicznych*. Mat. Konf. Metale Towarzyszące w Przemyśle Metali Nieżelaznych, Wrocław, 9 – 11 kwietnia 2008, 1–16.

86. Luszczkiewicz A.; Chmielewski T., *Acid treatment of copper sulfide middlings and rougher concentrates in the flotation circuit of carbonate ores*. International Journal of Mineral Processing, Volume: 88, No. 1–2, 2008, 45–52.

87. Chmielewski T., Luszczkiewicz A., Konopacka Z., *Acidic pretreatment of hard–to–tread copper ore flotation middlings to facilitate flotation efficiency.* Proceedings of XXIV International Mineral Processing Congress, Beijing 24–28 Sept. 2008, Vol. 3, Wang D.D., Sun C.Y., Wang F.L., Zhang L.C., Han L. (Eds), Science Press, 2008, 1189–1200.

88. Chmielewski T., A. Łuszczkiewicz A., *Koncepcja zmian technologicznych w ZWR Lubin – założenia techniczne.* W: Metody hydrometalurgiczne a rozwój produkcji w KGHM „Polska Miedź" S.A. Lubin 17 lutego 2009 r.

89. Bakalarz A., Łuszczkiewicz A.: *Flotacja rudy miedzi z użyciem n–dodekanu jako odczynnika zbierającego*. W: Materiały Krakowskiej Konferencji Młodych Uczonych 2009, Kraków, 17–19 września 2009. Kraków : [Fundacja Studentów i Absolwentów Akademii Górniczo–Hutniczej "Academica"], 2009, 13–20.

90. Bakalarz A., Łuszczkiewicz A.: *Flotacja rudy miedzi z rejonu Rudnej przy użyciu n–heptanu jako odczynnika zbierającego*. Górnictwo i Geologia. Prace Naukowe Instytutu Górnictwa Politechniki Wrocławskiej, nr 126, 2009, 5–17.

91. Drzymała J., Foszcz D., Łuszczkiewicz A.: *Ocena przemysłowego wzbogacania rud.* Cuprum Czasopismo Naukowo–Techniczne Górnictwa Rud, 2009, nr 1/2, 75–90.

92. Chmielewski T., Luszczkiewicz A., *Leaching of gangue in technological flotation circuits of Polish copper ores*. Proceedings of the 7th International Copper Conference COPPER 2010, Hamburg, June 6–10, 2010,Vol. 7, GDMB Clausthal–Zellerfeld 2010, 2655–2672.

93. Konieczny A., Grotowski A., Wieniewski A., Łuszczkiewicz A., Trybalski K., *Postęp w przeróbce rud miedzi – wyzwania dla KGHM Polska Miedź S.A*. Mat. Międzynarodowego Kongresu Górnictwa Rud Miedzi, Lubin 2009, Tom 2, 31–44.

94. DrzymaLa J., Luszczkiewicz A., Foszcz D., *Application of Upgrading Curves for Evaluation of Past, Present, and Future Performance of a Separation Plant*. Mineral Processing and Extractive Metallurgy Review, Vol. 31, 2010, No. 3, 165–175.

95. Chmielewski T., Luszczkiewicz A., Konieczny A., *Processing of hard–to–treat copper ore and flotation middlings using chemical treatment.* Proceedings of XXV International Mineral Processing Congress, Brisbane QLD, Australia, 6–10 September 2010, The Australasian Institute of Mining and Metallurgy, 2010, 1799–1806.

96. Konopacka Z., Rajczakowska D., Kruczek J., Łuszczkiewicz A., *Wzbogacanie grawitacyjne mączki skaleniowo–kwarcowej ze Strzeblowa na Dolnym Śląsku.* Prace Naukowe Instytutu Górnictwa Politechniki Wrocławskiej, Vol. 131, 2010, nr 38, 101–112.

97. Drzymała J., Łuszczkiewicz A., *Zalety krzywej uzysk–uzysk (Fuerstenaua) do technologicznej analizy i oceny wzbogacania surowców*. Przegląd Górniczy, 2011, Vol. 67, No. 7–8, 122–128.

98. Duchnowska M., Łuszczkiewicz A., *Ocena wzbogacania rud wieloskładnikowych na przykładzie wzbogacania rudy miedzi z rejonu Lubina*. Interdyscyplinarne zagadnienia w górnictwie i geologii. T. 2, pod red. Jana Drzymały i Wojciecha Ciężkowskiego. Wrocław, Oficyna Wydawnicza Politechniki Wrocławskiej, 2011. 213–221.

99. Luszczkiewicz A., Chmielewski T., Konieczny A., *Leaching and Flotation of Concentrate and Middligs in Flotation Circuits of Carbonate–Shale Copper Ores*. Proceedings of XXVI International Mineral Processing Congress, New Delhi, Institute of Minerals & Materials Technology (IMMT), Indian Institute of Mineral Engineers, 2012, 3067–3075.

100. Drzymala J., Kowalczuk P.B., Foszcz D., Muszer A., Henc T., Luszczkiewicz A., *Analysis of separation results by means of the grade–recovery Halbich upgrading curve.* Proceedings of XXVI International Mineral Processing Congress 2012, New Delhi, Institute of Minerals & Materials Technology (IMMT), Indian Institute of Mineral Engineers, 1239–1249.

101. Drzymala J., Kowalczuk P.B., Oteng–Peprah M., Foszcz D., Muszer A., Henc T., Luszczkiewicz A., *Application of the grade–recovery curve in the batch flotation of Polish copper ore* MINERALS ENGINEERING Vol. 49, No. 8, 2013, 17–23

102. Bakalarz A., Luszczkiewicz A., *Flotation of sulfide minerals from copper ores in the presence of either nonpolar or thiol collectors*. Proceedings XXVII International Mineral Processing Congress,

J. Yianatos, A. Doll, C. Gomez, R. Kuyvenhoven (eds), Santiago, Chile 20–24 Oct. 2014, Chapter 3, 47–56.

103. Chmielewski T., Konieczny A., Drzymala J., Kaleta R., Luszczkiewicz, *Development concepts for processing of Lubin–Glogow complex sedimentary copper ore.* Proceedings XXVII International Mineral Processing Congress, J. Yianatos, A. Doll, C. Gomez, R. Kuyvenhoven (eds), Santiago, Chile 20–24 Oct. 2014, Chapter 11, 10–19.

104. Duchnowska M., Luszczkiewicz A., Drzymala J., *Comparison of effectiveness of working in parallel streams industrial flotation machines*. Proceedings XXVII International Mineral Processing Congress, J. Yianatos, A. Doll, C. Gomez, R. Kuyvenhoven (eds), Santiago, Chile 20–24 Oct. 2014, Chapter 5, 28–37.

105. Bakalarz A., Gloy G., Luszczkiewicz A., *Flotation of Sulfide Components of Copper Ore in theP-resence of n–Dodecane*, Mineral Processing and Extractive Metallurgy Review, 2014, Vol. 36, No 2, 103–111.

106. Potulska A., Luszczkiewicz A., *Effect of particle size on flotation of polysulphide copper sedimentary ore*. Proceedings XXVII International Mineral Processing Congress, J. Yianatos, A. Doll, C. Gomez, R. Kuyvenhoven (eds), Santiago, Chile 20–24 Oct. 2014, Chapter 5, 184–193.

Jan Drzymala